Université de Strasbourg

UNIVERSITÉ DE STRASBOURG

École Doctorale des Sciences de la Vie et de la Santé STRASBOURG

ÉCOLE DOCTORALE des Sciences de la Vie et de la Santé

UMR7156 : Génétique Moléculaire, Génomique, Microbiologie

THÈSE présentée par :

Natalia NIKITCHINA

soutenue le : **26 octobre 2023**

pour obtenir le grade de : **Docteur de l'université de Strasbourg**

Discipline/ Spécialité : Aspects moléculaires et cellulaires de la biologie

Mise au point d'un système CRISPR-Cas12a ciblant l'ADN mitochondrial humain

THÈSE dirigée par :

Dr. ENTELIS Nina	Directeur de recherche, UMR7156, IPCB, Strasbourg, France

EXAMINATEUR :

Prof. DUCHÊNE Anne-Marie	Professeur, IBMP, Strasbourg, France

RAPPORTEURS :

Prof. Dr. KUNZ Wolfram S.	Professeur, Université de Bonn, Bonn, Allemagne
Dr. MIREAU Hakim	Directeur de recherche, UMR1318, Université Paris-Saclay, Versailles, France

---

AUTRES MEMBRES DU JURY :

Invité	**Dr. TARASSOV Ivan**	Directeur de recherche, UMR7156, Strasbourg, France
Invité	**Dr. MAZUNIN Ilya**	Directeur de recherche, Institut des sciences et technologies de Skolkovo, Moscou, Russie

Université de Strasbourg

UNIVERSITY OF STRASBOURG

École Doctorale des Sciences de la Vie et de la Santé STRASBOURG

DOCOTRAL SCHOOL of Life Sciences and Health

UMR7156 : Molecular Genetics, Genomics, Microbiology

THESIS presented by :

Natalia NIKITCHINA

defended on : **26 octobre 2023**

to obtain the degree of : **Doctor of the University of Strasbourg**

Discipline/ Speciality : Molecular and cellular aspects of biology

Development of a CRISPR-Cas12a system targeting human mitochondrial DNA

THESIS supervised by :

Dr. ENTELIS Nina	Research director, UMR7156, IPCB, Strasbourg, France

EXAMINATOR :

Prof. DUCHÊNE Anne-Marie	Professor, IBMP, Strasbourg, France

EXTERNAL JURY MEMBERS :

Prof. Dr. KUNZ Wolfram S.	Professor, University of Bonn, Bonn, Germany
Dr. MIREAU Hakim	Research director, UMR1318, University of Paris-Saclay, Versailles, France

---

ADDITIONAL JURY MEMBERS :

Invited	**Dr. TARASSOV Ivan**	Research director, UMR7156, Strasbourg, France
Invited	**Dr. MAZUNIN Ilya**	Research director, Skolkovo Institute of Science and Technology, Moscow, Russia

ACKNOLEDGMENT

First of all, I would like to express my gratitude to the esteemed members of the jury: Prof. Anne-Marie Duchêne, Prof. Wolfram Kunz, and Dr. Hakim Mireau, for generously dedicating their valuable time and expertise to evaluate my thesis. Your willingness to contribute your insights, despite your demanding schedules, is sincerely appreciated.

To my supervisors, Nina and Ivan,

I find myself echoing the sentiments of a certain old wizard, Albus Dumbledore, who once said, "Words are, in my not-so-humble opinion, our most inexhaustible source of magic." I truly cannot express all the gratitude I feel for both of you, as doing so would result in a volume thicker than my current PhD thesis!

Nina, I want to begin by thanking you for writing that grant which gave me the opportunity to join your lab in France and be involved in such amazing research. I vividly recall the moment you told me you wanted me as your PhD student; my heart skipped a beat, and I almost dropped everything I was holding. You've not only been the best supervisor I've ever encountered (seriously, Nina, how do you remember the details of my experiments better than I do after all these years?), but you've also provided invaluable support during my time here. Moving to a new country can be daunting, but thanks to you, I always knew there were people who cared about me and were willing to lend a helping hand. I cannot overstate how much I've gained from working with you. You've shown me what it means to be responsible, possess a critical mind, have confidence, and yet, not lose oneself in the relentless pursuit of research. Thank you, Nina, for sending me to discuss cloning design with Guillaume – thanks to you, I'm now married!

Both of you are incredible scientists, and I'm honored to have had the chance to learn from you and gain from your experience. While I may not have been the one to arrive at the lab at 9 AM (or ever, really), I hope that you both have nothing but fond memories of our time together.

I would like to express my gratitude to my first supervisor, Ilya Mazunin, with whom my scientific journey began at the Immanuel Kant Baltic Federal University in Kaliningrad. In your lab, I handled a pipette for the first time. On my first day, you provided me with some reagents and instructed me to conduct a PCR, without much explanation. It took me half a day just to dilute the primers. Perhaps your teaching methods were a bit unconventional, but you certainly encouraged us to think for ourselves and not fear making mistakes, even if it meant using extra reagents. I am truly grateful to you for fostering my independence and pushing me beyond my comfort zone. Thanks to you, I crossed paths with Nina and Ivan, and together, we tackled our challenging project.

I would like to extend my heartfelt thanks to all the members of "Trafic intracellulaire d'ARN et maladies mitochondriales".

Anne-Marie, I'm truly at a loss for words – you are simply the best! You're not only the most wonderful and kind person I've ever met, but you've also become a cherished friend. I feel happy and honored to have you in my life. Our unforgettable trip to Austria will forever hold a special

place in my heart, and your endless kindness is something I can never repay. Remember when you babysat me during my first days in the lab? You were the best teacher! Your guidance and support mean a lot to me.

I want to express my thanks to Anna for her wonderful sense of humor and daily kindness. I can't count how many microscopies experiments you generously helped me to conduct! You are the true guru of microscopy! I also want to extend my gratitude to Sacha for the fruitful discussions and scientific advice. I genuinely believe that I've had the privilege of meeting one of the most talented researchers with the best memory!

I want to thank Nikita. My goodness, how many years have we known each other? Throughout all this time, I've always known that I could count on you. You've been not only a good friend but also a fantastic coworker. I wish you the best of luck as you continue your research. I have every confidence that you'll successfully complete our great project!

I would like to extend my heartfelt appreciation to Joseph Schacherer and Anne-Marie Duchêne for their invaluable contributions to the insightful discussions that took place during my annual progress review.

I would like to express my gratitude to our collaborators for their invaluable contributions:

Firstly, a huge thank to Vadim Shmanai for his exceptional skills as a chemist, which have allowed him to synthesize not only the possible but also the seemingly impossible.

I also extend my thanks to our collaborators from Skolkovo Institute of Science and Technology and Rutgers University for our collaborative work on a joint article.

To Sam Das from John Hopkins, I want to express my appreciation for your assistance in realizing the NGS experiment and for our insightful discussions.

Last but not least, a special thanks to Gábor Zsurka for his invaluable help and insights in analyzing NGS data.

Your contributions have been instrumental in our research journey, and I'm truly grateful for your expertise and collaboration.

I would like to express my gratitude to the students I had the privilege of supervising during my work – Patrick Bertrand, Jules Rigal, and Cindy Arias. You three have been exceptional! Working with you has not only been a pleasure but also incredibly fun. I have no doubt that each of you will find your way to a bright future. Thank you for your dedication and enthusiasm.

I would like to thank all the members of UMR7156 GMGM for your help and support during my PhD. The collaborative atmosphere, guidance, and new friendships have been invaluable in my research journey.

I would like to express my deepest gratitude to my dearest best friend Aline. Even though we're miles apart, you've been my rock through this PhD journey and all the ups and downs in my life. Seriously, your advice on things like sequencing has been a lifesaver – you should be charging for it! But jokes aside, I genuinely don't think I could have made it through this without your support. Your friendship means the world to me.

I want to thank my amazing Guillaume, who not only endured my PhD rants but also became a master of home duties. You're my superhero! Your unwavering support, late-night thesis discussions and your genuine sense of humor have made this journey both bearable and memorable. I'm so incredibly grateful that I met you during my PhD. This is for sure, the best outcome one can get during the PhD :D

I won't have enough words to thank my family, despite the physical distance that separates us, you've been unwavering support not only throughout my PhD journey but throughout my entire life. Your belief in me and your continuous encouragement mean so much to me. I couldn't have asked for better people by my side. I hope I've made you proud.

Reflecting on the past four years, I can truly say that this journey has been a transformative and fulfilling experience. The challenges and triumphs have contributed significantly to my personal and academic growth, and I am indebted to all those who played a role in this endeavor.

Thank you all for your invaluable support, belief in my capabilities, and the countless ways you made this academic journey more meaningful and enriching.

With heartfelt gratitude,
Natalia

TABLE OF CONTENTS

Acknoledgment 4

TABLE OF CONTENTS 7

List of abreviations 11

1. INTRODUCTION 21

1.1. Mitochondria are essential organelles 23

1.1.1. Mitochondria structure and dynamics 23

1.1.2. Mitochondrial functions 26

1.2. Features of mitochondrial DNA organization 29

1.2.1. Human mitochondrial DNA organization 29

1.2.2. Human mitochondrial DNA replication 34

1.2.3. Human mitochondrial DNA transcription 38

1.2.4. Human mitochondrial DNA translation 40

1.2.5. Reparation of human mitochondrial DNA 42

1.3. Import of macromolecules into human mitochondria 46

1.3.1. Protein import 46

1.3.2. RNA import 49

1.4. Human mtDNA mutations and their role in pathogenesis 53

1.4.1. Mitochondrial mutations. Heteroplasmy effect and its dynamic 53

1.4.2. mtDNA mutations and mitochondrial disorders 57

1.5. Therapeutic strategies for mitochondrial disorders 62

1.5.1. Standard therapeutical treatment 62

1.5.2. Mitochondrial replacement therapy 62

1.5.3. Allotopic strategy 64

1.5.4. Anti-replicative strategy 65
1.5.5. Anti-genomic approaches 66
1.5.6. mtDNA base editing technologies 79
1.5.7. mitoCRISPR 81

2. MATERIALS AND METHODS 87

2.1. Materials 89
2.1.1. Mammalian cell lines used in the study 89
2.1.2. Bacterial strains used in the study 89
2.1.3. Oligonucleotides used in the study 90
2.1.4. Antibodies used in the study 93
2.1.5. Sequences of hybridization probes used in the study 94
2.1.6. Sequences of crRNAs used in the study 95

2.2. Methods 96
2.2.1. Cell culture conditions and mycoplasma screening 96
2.2.2. Gibson assembly 97
2.2.3. Subcellular fractionation to test the protein localization 98
2.2.4. Western blot hybridization 99
2.2.5. Flp-In T-REx monoclonal stable cell line generation 100
2.2.6. Isolation of crude mitochondria 101
2.2.7. Submitochondrial fractionation to test the protein localization 102
2.2.8. Immunofluorescent staining and confocal laser scanning microscopy 102
2.2.9. Site-directed mutagenesis 103
2.2.10. Design of AsCas12a crRNAs 105
2.2.11. *In vitro* transcription of AsCas12a crRNAs bearing import determinants 105
2.2.12. Chemical synthesis of AsCas12a crRNAs 105
2.2.13. *In vitro* cleavage in cell lysate 106
2.2.14. Oxygen Consumption measurement 107

2.2.15. RNA transfections for mitochondrial import evaluation 108
2.2.16. RNA isolation from mitochondria..... 108
2.2.17. Submitochondrial fractionation of RNA 109
2.2.18. Northern blot analysis..... 109
2.2.19. Quantitative analysis of RNA import..... 110
2.2.20. Expression and purification of recombinant AsCas12a nuclease 110
2.2.21. *In vitro* cleavage with the recombinant AsCas12a..... 112
2.2.22. Total DNA isolation..... 113
2.2.23. qPCR to determine mtDNA copy number..... 113
2.2.24. Knockdown of MGME1 with siRNA..... 114
2.2.25. mtDNA isolation for NGS 114
2.2.26. NGS of linker-ligated mtDNA..... 116
2.2.27. LM-PCR..... 117
2.2.28. Southern blot analysis 119
2.2.29. *In vitro* cleavage with the commercial AsCas12a protein 120
2.2.30. NGS of PCR/LM-PCR products..... 120
2.2.31. Nested PCR..... 121

3. Results..... 123

3.1. Import of AsCas12a nuclease into human mitochondria..... 125
3.1.1. Fusion of AsCas12a nuclease with COX8A MTS..... 125
3.1.2. Improvement of AsCas12a mitochondrial localization..... 129
3.1.3. Su9-AsCas12a stable cell line 133
3.1.4. Impact of the Su9-AsCas12a nuclease expression on mitochondrial respiration, protein synthesis and mitophagy in the stable cell line 137

3.2. Import of AsCas12a crRNA into human mitochondria..... 141
3.2.1. Fusion of AsCas12a crRNA with hairpin import determinants 170
3.2.2. Possibility to shorten or split AsCas12a crRNA 170
3.2.3. AsCas12a crRNA conjugation with chemical residues 194

3.3. Functional assessment of the mitoAsCas12a system functionality *in vivo* 196
3.3.1. Analysis of the Su9-AsCas12a cleavage activity and mtDNA levels in cultured human cells 196
3.3.2. mtDNA free ends detection after the mitoCRISPR system exposure ... 200
3.4. Use of the Type V CRISPR-Cas system to induce a deletion in human mitochondrial DNA 205
3.4.1. *In vitro* cleavage programmed by two crRNAs 206
3.4.2. Detection of AsCas12a-crRNAs mtDNA specific cleavage by linker-mediated PCR and NGS 208
3.4.3. PCR amplification of mtDNA molecules bearing the induced deletion 211
3.4.4. NGS validation of the deletion boundaries 215
4. Conclusions and perspectives 223
4.1. Import of AsCas12a nuclease into human mitochondria 225
4.2. Import of AsCas12a crRNA into human mitochondria 227
4.3. Functional assessment of the mitoAsCas12a system functionality *in vivo* 228
5. Bibliography 235
6. Annexes 269

LIST OF ABREVIATIONS

% – percentage

°C – degrees **C**elsius

***µ*g** – **m**icro**g**ram

***µ*L** – **m**icro**l**itre

2'-O-Me – **2'-O-Me**thyl

a. u. – **a**rbitrary **u**nits

AAV – **a**deno-**a**ssociated **v**irus

ABE – **a**denine **b**ase **e**ditor

AcCoA – **ac**etyl-**co**enzyme **A**

ADP – **a**denosine **di**phosphate

ANT – **a**denine **n**ucleotide **t**ranslocator

ART – **a**ssisted **r**eproductive **t**echniques

AsCas12a – *Acidominococcus* **s**pecies **Cas12a**

ATG4D – **a**utopha**g**y-related cysteine peptidase **4D**

ATP – **a**denosine **tri**phosphate

BER – **b**ase **e**xcision **r**epair

bp – **b**ase **p**are

BSA – **b**ovine **s**erum **a**lbumin

Cas – **C**RISPR **as**sociated (Protein)

CBE – **c**ytosine **b**ase **e**ditor

cm^2 – **square c**enti**m**eter

CO_2 – carbon dioxide

COX8A – **c**ytochrome C **ox**idase subunit **8a** (MTS)

Cpf – **C**RISPR **p**utative **e**ffector **1**

CRISPR – **c**lustered **r**egularly **i**nterspaced **s**hort **p**alindromic **r**epeats

crRNA – **CR**ISPR **RNA**

CRT – **c**ytoplasmic **r**eplacement **t**herapy

CSB – **c**onserved **s**equence **b**lock

DAPI – 4′,6-**dia**midino-2-**p**heny**l**indole

DMEM – **D**ulbecco's **m**odified **E**agle **m**edium

DMSO – **dim**ethyl **s**ulph**o**xide

DNA – **d**eoxyribo**n**ucleic **a**cid

Drpl – **d**ynamin-**r**elated **p**rotein **l**

DSB – **d**ouble-**s**tranded **b**reak

dsDNA – double-stranded DNA

ECM – encephalomyopathy

EMEM – **e**ssential **m**odified **E**agle's **m**edium

ER – **e**ndoplasmic **r**eticulum

EtBr – **et**hidium **br**omide

ETC – **e**lectron **t**ransport **c**hain

$FADH_2$ – **f**lavin **a**denine **d**inucleotide (**h**ydroquinone form)

FBSN – **f**amilial **b**ilateral **s**triatal **n**ecrosis

FCCP – **c**arbonyl **c**yanide **p**-(tri-**f**luromethoxy)phenyl-hydrazone

g – **g**ram

GA – **G**ibson **a**ssembly

GAPDH – **g**lycer**a**ldehyde 3-**p**hosphate **de**h**y**drogenase

GFP – **g**reen **f**luorescent **p**rotein

GQ – **G**-**q**uadruplex

GRAVY – **gr**and **av**erage of h**y**dropathicity

GTP – **g**uanosine **t**ri**p**hosphate

HDR – **h**omology-**d**irected **r**epair

HEK – **h**uman **e**mbryonic **k**idney

HRP – **h**orse**r**adish **p**eroxidase

HSP – **h**eavy **s**trand **p**romoter

Hz – **H**ertz

IM – **i**nner **m**embrane (mitochondrial)

IMAC – **i**mmobilized **m**etal **a**ffinity **c**hromatography

IMS – **i**nter**m**embrane **s**pace (mitochondrial)

IPTG – **i**so**p**ropyl-β-D-1-**t**hio**g**alactopyranoside

J – **J**oule

kb – **k**ilo**b**ase (1000 bp)

KSS – **K**earns-**S**ayre **s**yndrome

L – **l**itre

LB – **L**uria-**B**ertani broth

LC3 – microtubule-associated protein 1A/1B-**l**ight **c**hain **3**

LHON – **L**eber's **h**ereditary **o**ptic **n**europathy

LM-PCR – **l**inker-**m**ediated **PCR**

lncRNA – **l**ong **n**on**c**oding **RNA**

LS – **L**eigh **s**yndrome

LSP – **l**ight **s**trand **p**romoter

M – **m**ol

MAM – **m**itochondria-**a**ssociated **m**embranes

MCU – **m**itochondrial **c**alcium **u**niporter

MELAS – **m**itochondrial **e**ncephalomyopathy, **l**actic **a**cidosis, **s**troke-like episodes

MERRF – **m**yoclonic **e**pilepsy with **r**agged **r**ed **f**ibers

Mfn – **m**ito**f**usi**n**

MGME1 – **m**itochondrial **g**enome **m**aintenance **e**xonuclease **1**

MILS – **m**aternally **i**nherited **L**eigh **s**yndrome

mL – **m**illi**l**itre

MLS – **m**itochondrial **l**ocalization **s**equence

MMEJ – **m**icrohomology-**m**ediated **e**nd **j**oining

MMR – **m**is**m**atch **r**epair

MOMP – **m**itochondrial **o**uter **m**embrane **p**ermeabilization

MPP – **m**itochondrial **p**rocessing **p**eptidase

MRGs – **m**itochondrial **R**NA **g**ranule**s**

mRNA – **m**essenger **RNA**

MRPL4 – **m**itochondrial **r**ibosomal **p**rotein **L4**

MRT – **m**itochondrial **r**eplacement therapy

mtDNA – **m**itochondrial **DNA**

MTERF1 – **m**itochondrial **ter**mination **factor 1**

mtPAP – **mit**ochondrial **p**oly-**A** **p**olymerase

MTS – **m**itochondrial **t**argeting **s**equence/**s**ignal

NADH – **n**icotinamide **a**denine **d**inucleotide (NAD) + **h**ydrogen (H)

NARP – **n**europathy, **a**taxia, and **r**etinitis **p**igmentosa

ng – **n**ano**g**ram

NGS – **n**ext **g**eneration **s**equencing

NHEJ – **n**on-**h**omologous **e**nd-**j**oining

NUMTS – **nu**clear **mit**ochondria DNA **s**egment

O_2 – oxygen

OCR – **o**xygen **c**onsumption **r**ate

O_H – **h**eavy strand **o**rigin of replication

O_L – **l**ight strand **o**rigin of replication

OM – **o**uter **m**embrane (mitochondrial)

OPA1 – **o**ptic **a**trophy **p**rotein **1**

PBS – **p**hosphate **b**uffer **s**aline

PCR – **p**olymerase **c**hain **r**eaction

PEO – **p**rogressive **e**xternal **o**phthalmoplegia

pH – **p**otential of **h**ydrogen

Pi – **i**norganic **p**hosphate

pI – **i**soelectric **p**oint

PINK1 – **P**TEN-**in**duced putative **k**inase **1**

PMSF – **p**henyl**m**ethyl**s**ulfonyl **f**luoride

PNAs – **p**eptide **n**ucleic **a**cids

Pol γ – mitochondrial DNA **pol**ymerase **gamma**

POLRMT – **mit**ochondrial **R**NA **pol**ymerase

PPK – **p**almo**p**lantar **k**eratoderma

PS – **p**hos**s**phorothioate

PTP – **p**ermeability **t**ransition **p**ore

qPCR – **q**uantitative **PCR**

RE – **r**estriction **e**ndonuclease

RITOLS – **r**ibonucleotide **i**ncorporation **t**hrough**o**ut the **l**agging **s**trand

ROS – **r**eactive **o**xygen **s**pecies

RPM – **r**otations **p**er **m**inute

rRNA – **r**ibosomal **RNA**

RT – **r**oom **t**emperature

S – **S**vedberg **u**nit

SAM – **s**orting and **a**ssembly **m**achinery

SDM – **s**ite-**d**irected **m**utagenesis

SDS – **s**odium **d**odecyl **s**ulfate

sgRNA – **s**ingle **g**uide **RNA**

SIDS – **s**udden **i**nfant **d**eath **s**yndrome

siRNA – **s**mall **i**nterfering **RNA**

sncRNA – **s**mall **n**on**c**oding **RNA**

SOD2 – **s**uper**o**xide **d**ismutase **2** (MTS)

SSB – **s**ingle-**s**tranded **b**reak

SSC – **s**aline-**s**odium **c**itrate

ssDNA – single-stranded DNA

Su9 – ATPase **su**bunit **9**

TALE – **t**ranscription **a**ctivator-**l**ike **e**ffector

TALED – **TALE**-linked **d**eaminase

TALEN – **t**ranscription **a**ctivator-**l**ike **e**ffector **n**uclease

TAS – **t**ermination-**a**ssociated **s**equence (transcription)

TCA – **t**ri**c**arboxylic **a**cid (cycle)

TEFM – **t**ranscription **e**longation **f**actor (**m**itochondrial)

TFAM – **t**ranscription **f**actor **A** (**m**itochondrial)

TFB2M – **t**ranscription **f**actor **B2** (**m**itochondrial)

TIM – **t**ranslocase of the **i**nner **m**embrane

TOM – **t**ranslocase of the **o**uter **m**embrane

TOMM20 – **t**ranslocase of the **o**uter **m**itochondrial **m**embrane complex subunit **20**

T-REx – **t**etracycline **re**pressor

tRNA – **t**ransfer **RNA**

U – **u**nits

UTR – **u**n**t**ranslated **r**egion

UV – **u**ltra**v**iolet

VDAC – **v**oltage-**d**ependent **a**nion **c**hannel

WT – **w**ild **t**ype

ZFN – **z**inc-**f**inger **n**uclease

Δ – deletion

ΔΨm – mitochondrial membrane potential

LIST OF FIGURES AND TABLES

Figure I1. Structure of Human Mitochondria. 24
Figure I2. Mitochondrial Dynamics. 25
Figure I3. Glycolysis, β-oxydation and Krebs Cycle Fuel the Electron Transport Chain. 27
Figure I4. Human Mitochondrial DNA Organization. 30
Figure I5. Mitochondrial Nucleoid Organization. 32
Figure I6. The "static" and "dynamic" nucleoid models. 34
Figure I7. Models of Mammalian mtDNA Replication. 35
Figure I8. Mammalian Mitochondrial DNA Repair Pathways. 44
Figure I9. Mitochondrial Import of Proteins Bearing Various Targeting Signals. .. 48
Figure I10. mtDNA heteroplasmy and the threshold effect. 54
Figure I11. Dynamics of the mitochondrial DNA. 55
Figure I12. Mitochondrial copy number change during oogenesis. 57
Figure I13. The most common mutations in mtDNA associated with mitochondrial diseases. 59
Figure I14. Mitochondrial Replacement Therapy Techniques. 63
Figure I15. Two Therapeutic Strategies to Shift mtDNA Heteroplasmy Level. 67
Figure I16. Various Nucleases are Used for Mutant mtDNA Targeting. 69
Figure I17. Mitochondria-Targeted Base Editing Technologies. 80
Figure I18. Comparison of crRNA Delivery Methods and CRISPR Systems of Type II and Type V. 83
Figure M1. Gibson Assembly of pcDNA5-FRT-TO-MTS-AsCas12a. 98
Figure M2. Principle of a Stable Cell Line Generation using the Commercial Flp-In™ System 101
Figure M3. Primer design for the Site-Directed Mutagenesis. 104
Figure M4. Recombinant AsCas12a Proteins Purification using Immobilized Metal Affinity Chromatography. 112
Figure M5. Sample Preparation for mtDNA Linker-Ligated Sequencing. 117
Figure M6. Principle of mtDNA Free Ends Detection using Linker-Mediated PCR. 119
Figure R1. COX8A-AsCas12a Expression and Localization in human cells transfected with pMitoAsCas12a-COX8A. 126
Figure R2. COX8A-AsCas12a Expression and Localization in the Human Stable Cell Line. 128
Figure R3. Mitochondrial Localization of AsCas12a Bearing Various MTS. 132
Figure R4. Generation and Characterization of the Stable Cell Lines Expressing Su9-AsCas12a. 134

Figure R5. Analysis of the Su9-AsCas12a Expression, Localization and Activity in the Stable Cell Line. 137
Figure R6. The Effect of the Su9-AsCas12a Nuclease Expression on Mitochondrial Respiration, Protein Expression and Mitophagy. 141
Figure R7. Chemical Modifications of AsCas12a crRNA, their impact on the Function and Mitochondrial Import. 195
Figure R8. Effect of the Su9-AsCas12a Nuclease, both Active and DNase-dead, on mtDNA Copy Number in human cells. 197
Figure R9. Next Generation Sequencing of Linker-Ligated mtDNA after the mitoCRISPR system exposure. 204
Figure R10. AsCas12a is Capable to Cleave mtDNA Fragment in Complex with Two crRNAs. 207
Figure R11. Detection of Breaks in mtDNA by NGS of the LM-PCR products. ... 210
Figure R12. Detection of the Deletion in Human mtDNA Induced by the mitoCRISPR-Cas12a System. 214
Figure R13. Characterization of a new series of Samples for the Detection of the Deletion in Human mtDNA Induced by the mitoCRISPR-Cas12a System. 216
Figure R14. Detection of the Deletion in Human mtDNA Induced by the mitoCRISPR-Cas12a System by NGS. 220

Table 1. Recently developed mitochondrial CRISPR/Cas systems 82

1. INTRODUCTION

1.1. Mitochondria are essential organelles

1.1.1. Mitochondria structure and dynamics

Scientists identified the existence of cellular structures resembling modern mitochondria as far back as 1850 (**Lehninger A. L., 1964**). However, the term "mitochondria" was not officially introduced until 1898, when German microbiologist Carl Benda created it (**Ernster, L., & Schatz, G., 1981**). This term has its roots in ancient Greek, with "mitos" meaning "filament" and "chondros" meaning "granule," describing the common microscopic appearances of these organelles.

Mitochondria are organelles located in the cytoplasm of nearly all eukaryotic cells (**Karnkowska, A. *et al.*, 2016**). According to the current theories, mitochondria evolved from free-living bacteria, *α*-proteobacteria, and played a role in the emergence of eukaryotic cells through a process known as endosymbiosis (**Margulis L., 1970**; **Gray M. W., 2016**). The endosymbiotic hypothesis suggests that ancient eukaryotic cells "swallowed" primitive mitochondria, leading to a mutually beneficial relationship. This interaction, following significant genetic changes, enabled mitochondria to enhance energy production by generating adenosine triphosphate (ATP) through respiration, while the host cell provided a safe environment for the bacteria to sustain life (**Cavalier-Smith T., 2006**).

Mitochondria are enveloped by two phospholipid membranes: the outer mitochondrial membrane (OMM) and the inner mitochondrial membrane (IMM). These membranes split the organelle into two compartments: the matrix and the intermembrane space (IMS) (**Westermann B., 2010**) (**Figure I1A**).

Mitochondrial membranes exhibit significant differences in composition and characteristics, which stem from the organelle's endosymbiotic origin and the specific functions they fulfill. In particular, the OMM shares a closer lipid composition resemblance to eukaryotic cell membranes, representing an equal balance of 50% lipids and 50% proteins. It is notably characterized by its high cholesterol content, which can reach up to 10%. Conversely, the IMM is similar to bacterial membranes, enriched in cardiolipin, with a composition of 80% proteins and 20% lipids (**Krauss S., 2001**).

The IMM forms densely packed invaginations within the matrix, referred to as cristae (**Ernster, L., & Schatz, G., 1981**). Within these cristae, alongside numerous other proteins, the oxidative phosphorylation (OXPHOS) machinery is localized. The proposed rationale for the folding of the

IMM is to expand the available surface area for the energy production (**Joubert F. & Puff N., 2021**).

Furthermore, there are notable differences in permeability between the OMM and IMM. The OMM facilitates the transfer of ions and small molecules through voltage-dependent anion channels (VDACs), the IMM exclusively permits the free diffusion of water, oxygen (O_2), and carbon dioxide (CO_2) (**O'Rourke B., 2000**).

This selective permeability plays a crucial role in establishing an electrochemical gradient across the IMM, which serves as the foundation for ATP production and precise control of ion concentrations, including calcium, which is used for cellular signaling. Consequently, due to the limited permeability of the IMM, it contains a variety of transporters that facilitate the transfer of metabolites (**Palmieri F. & Pierri C. L., 2010**).

Next, the region situated between these two mitochondrial membranes, represents the intermembrane space (**Figure I1A**). Given the permeability of the outer membrane, its composition closely resembles that of the cytosol. However, due to its enrichment in H^+ protons, it has an approximate pH of 6.9 (**Porcelli, A. M. *et al.*, 2005**). This inequality in protons distribution between the compartments creates a proton gradient, and the resulting difference of charge forms the transmembrane potential of hydrogen ions (**Zorova L. D. *et al.*, 2018**) (**Figure I1B**).

Lastly, the mitochondrial matrix constitutes the mitochondrial compartment, enclosed by the inner mitochondrial membrane (**Figure I1A**). It possesses a higher viscosity compared to the cytosol and maintains a pH of around 7.8 (**Porcelli, A. M. *et al.*, 2005**). The mitochondrial matrix contains mitochondrial DNA (mtDNA) and all essential components for its biogenesis (**Figure I1A**), together with the variety of enzymes involved in different metabolic pathways within the mitochondria, which play a vital role within eukaryotic cells (**Shen K. *et al.*, 2022**).

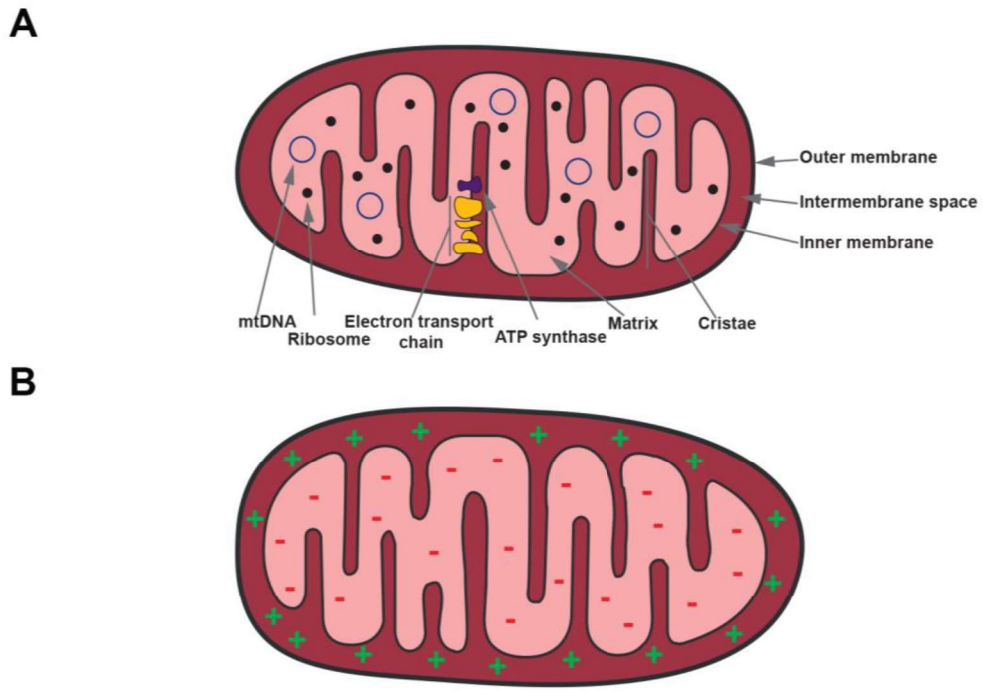


Figure I1. Structure of Human Mitochondria.

(A) The subcompartments of mitochondria. Adapted from Yusoff, A. A. M. *et al.*, 2015.
(B) The mitochondrial membrane potential (ΔΨm) generated by proton pumps.

Mitochondria are dynamic organelles that form a network of tube-like structures in cells (**Westermann B., 2010**) (**Figure I2**). They undergo fusion and fission processes to adapt to the cell's energy needs and metabolic state. Fusion allows mitochondria to share materials and enhance cell survival, while fragmentation is required for mitochondrial movement and removal of damaged parts through mitophagy (**Pickles S., Vigié P., Youle R. J., 2018**) (**Figure I2**). These processes are controlled by GTPase proteins, like dynamin-related protein 1 (Drp1) for fission and mitofusin 1, 2 (Mfn1, Mfn2) and optic atrophy protein 1 (OPA1) for fusion (**Hall, A. R. *et al.*, 2014**). OPA1 also maintains cristae structure (**Cogliati, S. *et al.*, 2013**) (**Figure I2**).

Mitochondrial shape and function are closely linked, with fragmented mitochondria often signaling on a dysfunction. Mutations in fission and fusion proteins can lead to OXPHOS failure and mitochondrial disease (**Civiletto, G. *et al.*, 2015**).

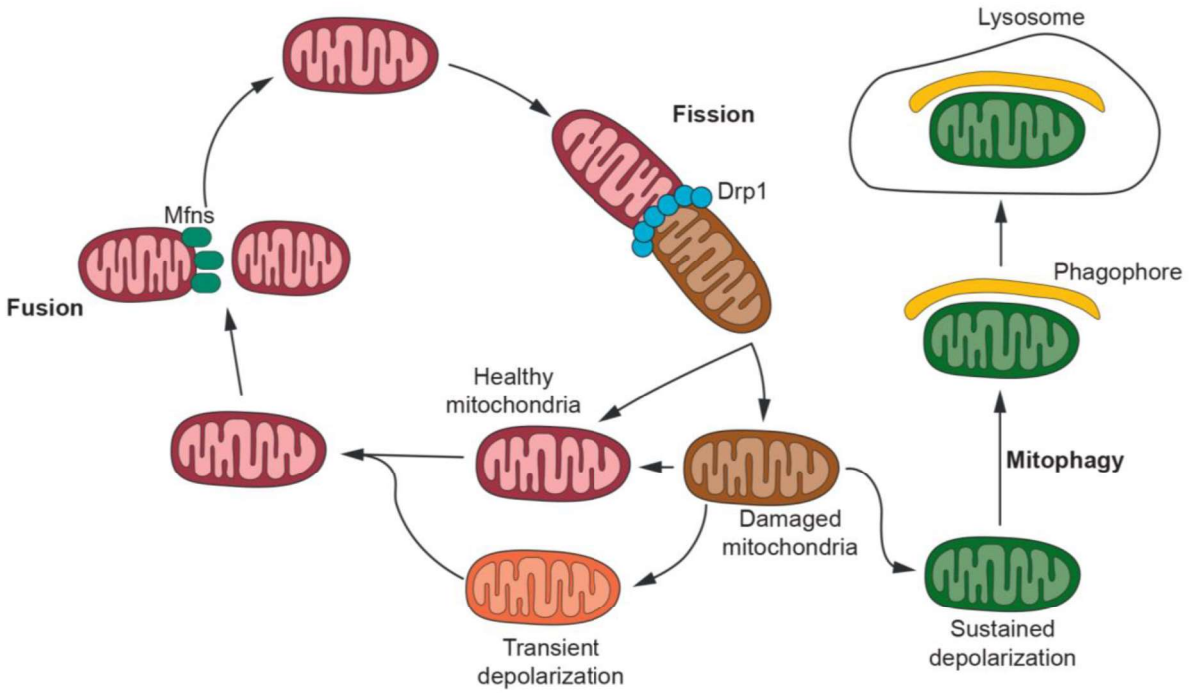


Figure I2. Mitochondria Dynamics.

Schematic representation of mitochondrial fusion, fission and mitophagy. Under normal conditions, mitochondria, typically tubular in shape, can be damaged by various stresses. Damaged mitochondria separate from the healthy network via fission. After repair, partially damaged ones can rejoin the network through fusion, while permanently damaged mitochondria are removed through autophagy. Adapted from Ren, Z. *et al.*, 1992.

1.1.2. Mitochondrial functions

Mitochondria are often referred to as the "powerhouse of the cell" because of their central role in energy production. However, over the past years, mitochondria have also been recognized as a signaling organelle involved in a wide array of physiological functions. These functions encompass calcium homeostasis, apoptosis, as well as the synthesis of heme and iron-sulfur clusters (**Protasoni M. & Zeviani M, 2021**).

Cells derive energy primarily from the conversion of ATP to ADP. To sustain this process, cells use nutrients to regenerate ATP. Glucose, for example, is gradually processed into carbon dioxide, and its hydrogen atoms combine with oxygen to form water. The initial stage of this process, called glycolysis, occurs in the cytosol and does not involve mitochondria, producing two ATP molecules and two pyruvate molecules from one glucose molecule (**Lehninger A. L., Nelson D. L., Cox M. M., 2005**).

To optimize ATP production, glycolysis is linked to the citric acid cycle (Krebs cycle) that takes place in mitochondria (**Lehninger A. L., Nelson D. L., Cox M. M., 2005**) (**Figure I3A**). Pyruvate from glycolysis enters the mitochondria and is converted to acetyl-CoA, which then participates in the Krebs cycle (**Figure I3A**). This cycle produces CO_2 and extracts electrons (hydrogen atoms) to yield a total of six NADH, two $FADH_2$, and two GTP from two glucose-derived acetyl-CoA molecules.

NADH and $FADH_2$ are crucial as they participate in oxidative phosphorylation (**Figure I3B**). In this process, electrons from NADH and $FADH_2$ are transferred through the electron transport chain (ETC) to oxygen, which is the final acceptor. This electron transfer is known as cellular respiration and is coupled with ATP production by ATP synthase (complex V). The complete oxidation of one glucose molecule results in the production of around 30 ATP molecules (**Alberts B., 2003**). Additionally, NADH and $FADH_2$ can be produced through fatty acid β-oxidation, where fatty acids are converted into acetyl-CoA, generating NADH and $FADH_2$ (**Adeva-Andany, M. M. *et al.*, 2019**).

The proton gradient created during respiration powers ATP synthase, which converts ADP and inorganic phosphate (Pi) into ATP (**Neupane, P. *et al.*, 2019**) (**Figure I3B**). In an average adult human, this process generates about 70 kg of ATP daily, providing the energy needed for all the body's energy-demanding processes.

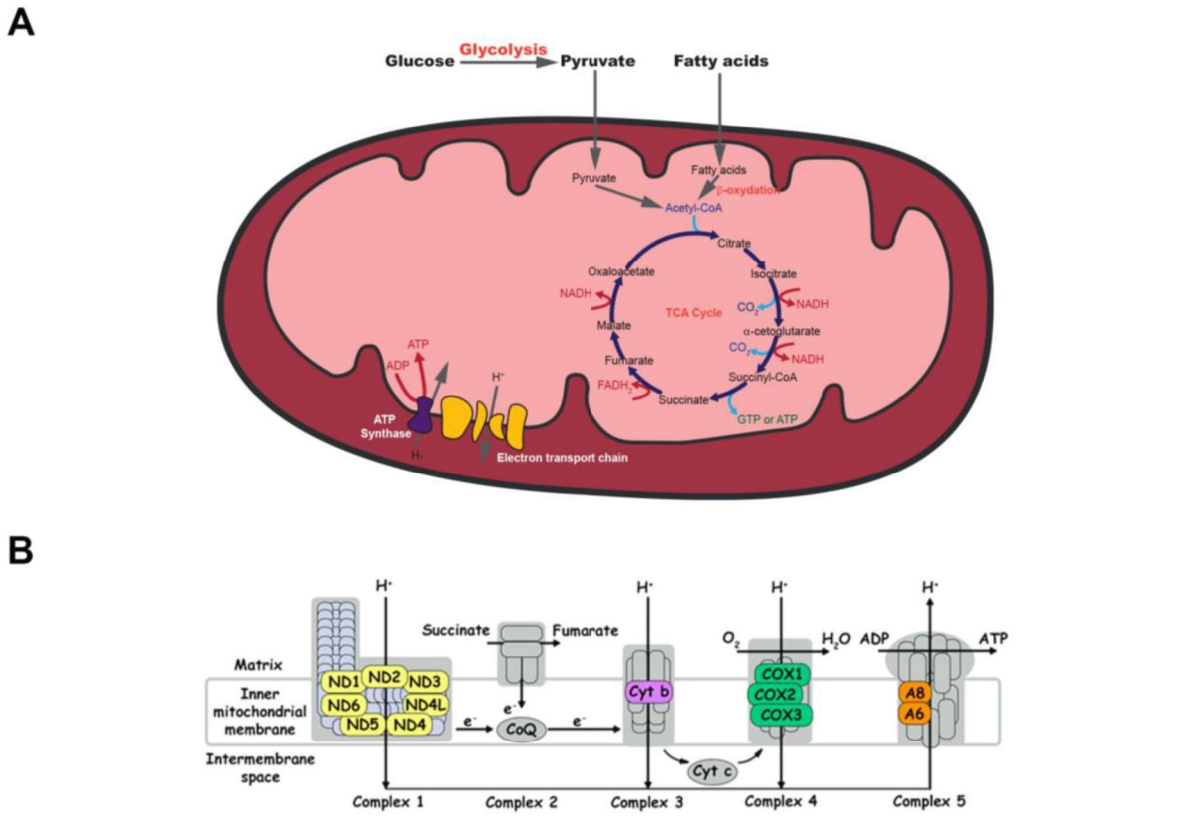


Figure I3. Glycolysis, β-oxydation and Krebs Cycle Fuel the Electron Transport Chain.

(A) The Krebs cycle (TCA cycle). The Krebs cycle summarizes a circular series of reactions in the mitochondria to metabolize AcCoA to two molecules of CO_2 with resultant generation of one molecule of GTP, three molecules of NADH, and one molecule of $FADH_2$.
(B) Respiratory chain complexes. Electrons are introduced into the respiratory chain through the oxidation process of two-electron carrier cofactors, NADH and FADH, occurring at complex I (NADH dehydrogenase) and complex II (succinate dehydrogenase). These electrons are subsequently conveyed to coenzyme Q (CoQ) by means of iron-sulfur clusters. Reduced CoQ can diffuse within the inner membrane, making contact with complex III (cytochrome c reductase), where it transfers the electrons to cytochrome c within the IMS. Finally, complex IV (cytochrome c oxidase) utilizes these electrons to reduce oxygen, ultimately forming water. During this electron transport, protons are transported across the membrane at complexes I, III, and IV. Complex V (ATP synthase) harnesses the free energy generated by this proton flux to synthesize ATP from ADP and inorganic phosphate within the matrix.
Adapted from Martínez-Reyes I. & Chandel N. S., 2020.

As previously mentioned, mitochondria play a vital role not only in energy production but also in various other cellular processes. For instant, calcium serves as a crucial element in cell signaling and is under the regulation of organelles like the endoplasmic reticulum (ER) and mitochondria. While calcium can easily penetrate the OMM via VDAC (**Colombini M., 1980**), its entry through the IMM is controlled by the mitochondrial calcium uniporter (MCU) and exchangers such as Na^+/Ca_2^+ or H^+/Ca_2^+ (**Giorgi, C. *et al.*, 2012**).

Mitochondrial play an important role in Ca_2^+ homeostasis, regulating its accumulation and efflux. These mitochondrial calcium waves play a pivotal role in determining cell destiny (**Rizzuto, R. *et al.*, 2012**). Elevated intracellular calcium levels can initiate cell death through mechanisms like necrosis or apoptosis by triggering the opening of a high-conductance channel in the IMM known as the permeability transition pore (PTP) (**Rasola A. & Bernardi P., 2011**). Moreover, calcium also has an impact on mitochondrial function. The accumulation of calcium within mitochondria stimulates ATP production by modulating the activity of enzymes in the TCA cycle (**Contreras, L. *et al.*, 2010**).

Mitochondria are key players in programmed cell death (apoptosis). Apoptosis can be triggered by diverse stressors or developmental processes. The mitochondrial (intrinsic) pathway starts with internal stress signals causing bioenergetic failure and a drop in mitochondrial membrane potential. This leads to mitochondrial outer membrane permeabilization (MOMP), followed by oligomerization of BAX and BAK proteins at the OMM and release of pro-apoptotic molecules, such as cytochrome c, into the cytosol. Cytochrome c will then interact with other proteins to form the apoptosome and induce the subsequent cleavage and activation of caspases leading to apoptosis (**Estaquier, J. *et al.*, 2012**).

There is a growing number of articles exploring the various functions of mitochondria in immune responses (**Angajala, A. *et al.*, 2018**). A recent study has shown that double-strand breaks in mtDNA (mtDSBs) can result in mitochondrial herniation, leading to the release of mitochondrial RNA into the cytoplasm and subsequently triggering an innate immune response (**Tigano M. *et al.*, 2021**).

In summary, the multifaceted functions of mitochondria underscore their importance in various cellular processes and health.

1.2. Features of mitochondrial DNA organization

1.2.1. Human mitochondrial DNA organization

It has been slightly a decade since the discovery of the DNA double helix, when in 1963, Magritt M.K. and Silvan Nass utilized electron microscopy to unveil DNAse-sensitive filament-like structures within mitochondria extracted from chicken embryonic cells (**Nass M. M. K., Nass S., 1963**). Shortly after, through biochemical analysis of highly purified mitochondrial fractions, it was confirmed that mitochondria possess their own double-stranded, circular DNA, distinct in structure from nuclear DNA (**Schatz G., Haslbrunner E., Tuppy H., 1964**).

Throughout the course of evolution, a majority of mitochondrial genes have either been lost or transferred to nuclear DNA (**Gustafsson C. M., Falkenberg M., Larsson N. G., 2016**). To date, it is established that mitochondrial DNA (mtDNA) comprises a 16.5 kb-long sequence encoding 13 subunits of four out of the five OXPHOS complexes, along with 22 tRNAs and 2 ribosomal RNAs (**Anderson, S. *et al.*, 1981**) (**Figure I4A**). In terms of its structure, mtDNA exhibits remarkable compactness, with minimal non-coding sequences (**Nicholls T. J., Minczuk M., 2014**).

The only exception is the mtDNA control region, which, although non-coding, possesses critical mtDNA regulatory elements: the heavy (HSP) and light (LSP) chain promoters, along with the heavy chain origin of replication (O_H) (**Figure I4B**). The distinction between the light (L) and heavy (H) strands lies in their composition, with the L strand being cytosine-rich and the H strand being guanine-rich (**Alexeyev M., 2020**). In addition to LSP and HSP, the existence of a second heavy chain promoter (HSP2) has been proposed, but its *in vivo* activity remains a subject of debate (**Litonin, D. *et al.*, 2010**; **Gustafsson C. M., Falkenberg M., Larsson N. G., 2016**) (**Figure I4A**). The recent discovery of a second light strand promoter, LSP2, located at the 3' end of the mitochondrial non-coding region (NCR), has significantly expanded our understanding of the coordination processes governing mitochondrial gene replication and transcription (**Tan, B. G. *et al.*, 2022**) (**Figure I4 A & B**).

The majority of mtDNA information is encoded by the H-strand and includes genes for two ribosomal RNAs (16S and 18S), fourteen transfer RNAs, and twelve proteins (**Figure I4A).** The light chain encodes eight tRNAs and only one protein (**Figure I4A**). All these proteins are the components of the OXPHOS complexes, including seven in complex I (MT-ND1-3, MT-ND4L, MT-ND4-6), one in complex III (cytochrome b), three in complex IV (MT-COI-III), and two in complex V (MT-ATP6 and 8) (**Figure I4A**) (**Wolstenholme DR., 1992**). Complex II and other subunits of the respiratory chain are encoded by the nuclear genome (**Lott, M. T. *et al.*, 2013**). Mitochondrial ribosomal and transfer RNAs, along with imported cytoplasmic proteins, create a distinct translational machinery in mitochondria, facilitating the expression of mtDNA using a genetic code distinct from nuclear genes (**Shokolenko I. N. & Alexeyev M. F., 2017**).

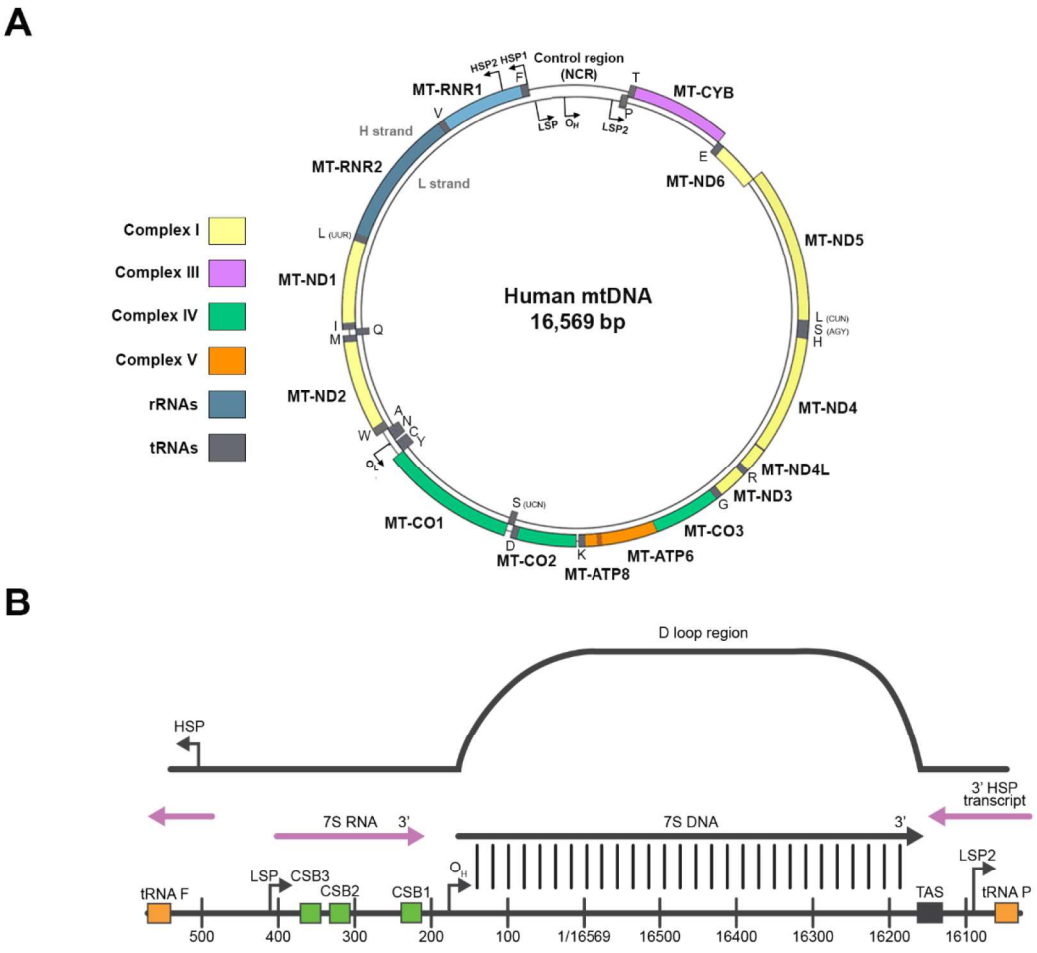


Figure I4. Human Mitochondrial DNA Organization.

(A) Map of human mtDNA. Genes are shown by different colors as indicated at the left : NADH dehydrogenase subunits (MT-ND1-ND6 and ND4L), cytochrome b (MT-CYB), cytochrome c oxidase subunits (MT-COI-III), ATP synthase 8 and 6 subunits (MT-ATP6, MT-ATP8), rRNA 12S (MT-RNR1) and 16S (MT-RNR2) and tRNAs (denoted by the one-letter code of the corresponding amino acids). HSP1, HSP2, LSP1 and LSP2 are heavy and light chain promoters; OH and OL are the origins of heavy and light chain replication. NCR, non-coding region (D-loop). Adapted from Tan, B. G. *et al.*, 2023.
(B) Schematic representation of the non-coding region (D-loop) of human mtDNA. Promoters for the H strand (HSP) and L strand (LSP1, LSP2) and the replication origin of the H strand (OH) are shown. CSB1, CSB2, and CSB3, conserved sequence blocks. Disruption of L strand transcription at CSB2 eventually leads to the formation of the RNA primer necessary for H-strand replication initiation. TAS, transcription termination-associated sequence. Adapted from Nicholls T. J. & Minczuk M., 2014.

The mitochondrial genome is encapsulated within a nucleoid, comprising both DNA and essential proteins required for maintaining its structural integrity and compactness. Extensive investigations into human mtDNA have revealed that the number of nucleoids within a cell can range from 1,000 to 10,000 copies depending on the specific tissue type (**Bogenhagen D. F., 2012**). Typically, calculations of nucleoid copy numbers are performed on a per-cell basis, rather than per individual

mitochondria. This is primarily due to the fact that mitochondria within cells often exist in a dynamic, interconnected state, forming a "mitochondrial network" that constantly changes shape through ongoing fusion and fission processes (**Hoitzing H., Johnston I. G., Jones N. S., 2015**). Consequently, quantifying the precise number of nucleoids per mitochondria proves to be a challenging process. As a rough estimate, it is believed that, on average, there are approximately 3.2 nucleoids per individual organelle (**Ekstrand, M. I. *et al.*, 2004**).

Similar to nuclear DNA, isolated mtDNA is notably larger in size than an individual mitochondrion. To be able to fit a nucleoid within a mitochondrion, its level of compaction must be condensed by a factor of 20. Clearly, proteins play a pivotal role in the packaging of mtDNA, with the TFAM (mitochondrial transcription factor A) proteins serving as the key player in mtDNA compactization (**Kukat, C. *et al.*, 2015**). It has been determined that, on average, there are 6 nucleotide bases per each TFAM protein.

In addition to TFAM, there are several other proteins associated with mtDNA. These proteins play an important role in regulating mtDNA transcription and replication, including mtSSB (an ortholog of the bacterial SSB protein that binds to single-stranded DNA during replication), POL*γ* (mitochondrial DNA polymerase gamma), POLRMT (mitochondrial RNA polymerase), and TWINKLE (mitochondrial DNA helicase) (**Shutt T. E. & Gray M. W., 2006**).

To date, the prevailing model for the organization of the mammalian mitochondrial genome is the "layered" model (**Bogenhagen D. F., Rousseau D., Burke S., 2008**) (**Figure I5**). According to this model, there is a central region where proteins responsible for critical processes such as mtDNA packaging, replication, and transcription are densely packed. In the layer above, proteins that are temporarily recruited to fulfill specific functions are localized. Translation and other essential processes take place at the periphery of the nucleoid. Additionally, this model suggests a connection between the nucleoid and the inner membrane protein of the mitochondrion (ATAD3), facilitated through its interaction with the D-loop of mtDNA (**Arguello, T. *et al.*, 2021**) (**Figure I5**).

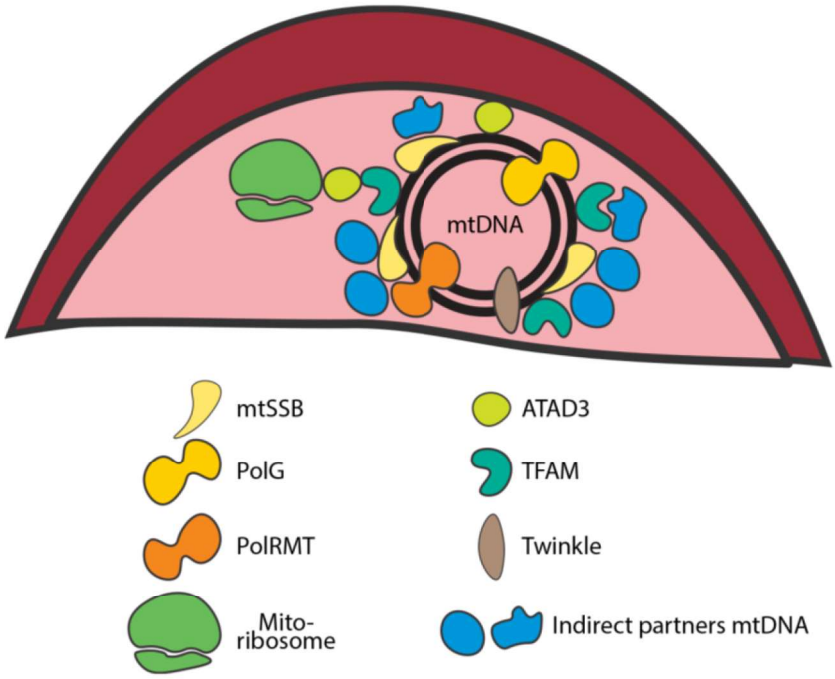


Figure I5. Mitochondrial Nucleoid Organization.

Spatial organization of nucleoid-associated proteins. Proteins that possess mtDNA-binding ability are located in the core region, whereas others indirect partners might interact with proteins in the core region or other mitochondrial proteins. ATAD3, ATPase family AAA-domain-containing protein; mtSSB, mitochondrial single-stranded DNA-binding protein; TFAM, mitochondrial transcription factor A; POLG, mitochondrial polymerase γ; POLRMT, mitochondrial RNA polymerase; mitochondrial helicase TWINKLE. Adapted from Lee, S. R. *et al.*, 2017.

For a while, there have been ongoing debates regarding the quantity of mtDNA enclosed within a single nucleoid. However, thanks to advancements in high-resolution microscopy techniques, this number has now been narrowed down to a range of 1-2 molecules per nucleoid (**Kukat, C. *et al.*, 2015**).

Yet, the mechanism governing the distribution of mtDNA within nucleoids remains a contentious issue. Currently, two models, namely the "static" and "dynamic" nucleoid, have been put forth to elucidate how mitochondrial nucleoids manage their genetic content and inheritance (**Figure I6**). The "static" nucleoid model states that individual nucleoids solely replicate the mtDNA they contain (**Jacobs H. T., Lehtinen S. K., Spelbrink J. N., 2000**). In contrast, the "dynamic" nucleoid model proposes the existence of intermolecular heterologous recombination of mtDNA, enabling nucleoids to freely exchange mtDNA molecules with one another (**D'Aurelio M. *et al.*, 2004**).

As of now, the question of which mitochondrial nucleoid model is accurate remains unresolved. Addressing this issue experimentally involves creating cell lines with identical nuclear

backgrounds but distinct mtDNA, as well as the ability to precisely distinguish mtDNA molecules at the nucleoid level.

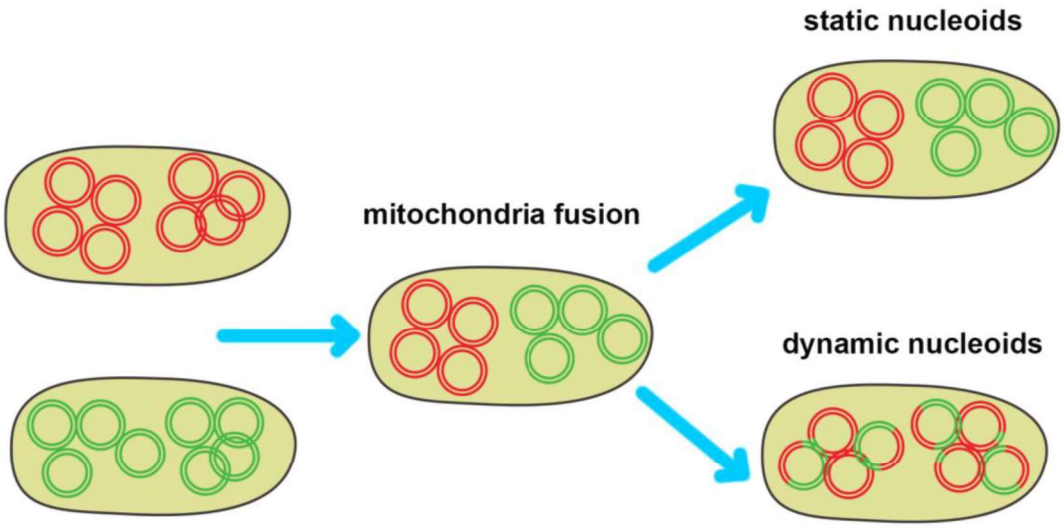


Figure I6. The "static" and "dynamic" nucleoid models.

Adapted from Gilkerson, R. W. *et al.*, 2008.

Additionally, there exists a theory based on purely bioinformatic analysis of the accumulation and distribution of mutations in mtDNA. This model suggests the existence of two classes of mtDNA molecules: a "stem subpopulation" responsible for actively replicating mtDNAs, which in turn renew the mtDNA pool, and a "worker subpopulation" residing in mitochondria with high respiratory activity (**Cote-L'Heureux A. *et al.*, 2023**). These "stem" mtDNAs inhabit mitochondria that have lower respiration rates, providing them with protection against reactive oxygen species. Consequently, mutations primarily occur in "worker" mtDNA molecules, which undergo rare replication events, preventing these mutations from clonally expanding and accumulating with age.

1.2.2. Human mitochondrial DNA replication

All proteins involved in the process of mtDNA replication are analogs of bacterial and phage enzymes (**Shutt T. E. & Gray M. W., 2006**).

One of the key participants in the initiation of replication is the TFAM protein. It has been shown that if this protein is present in the nucleoid at low concentrations, this stimulates exactly the

initiation of replication, and if the TFAM content is high, then transcription is initiated (**Lin C. S. *et al.*, 2012**).

Mitochondrial replication requires a DNA helicase, TWINKLE, which unwinds the double-stranded DNA template ahead of DNA polymerase γ (POLγ) (**Spelbrink J. N. *et al.*, 2001**). TWINKLE forms a hexamer and needs a specific fork structure to initiate unwinding.

POLγ is the main replicative polymerase in mitochondria, consisting of one catalytic subunit (POLγA) and two accessory subunits (POLγB) in human cells (**Yakubovskaya, E. *et al.*, 2006**). Knockout studies in mice have shown that both POLγA and POLγB are essential for embryonic development (**Hance N., Ekstrand M. I., Trifunovic A., 2005**). Pathological mutations in the structure of this enzyme lead to deletions (loss of sections of mtDNA) or depletions (reduction in mtDNA copy number up to its complete absence), which causes respiratory chain failure and the emergence of premature aging phenotypes (**Krasich R., Copeland W. C, 2017**).

Additionally, several other polymerases (PrimPol, DNA polymerase β, DNA polymerase θ, and DNA polymerase ζ) have been identified in mitochondria, primarily involved in mtDNA repair rather than replication (**Krasich R., Copeland W. C, 2017**).

POLγA possesses a 3′–5′ exonuclease domain for proofreading of the newly synthesized DNA. POLγ is highly accurate, with a low frequency of misincorporation (**Longley, M. J. *et al.*, 2001**). POLγB enhances interactions with the DNA template, increasing catalytic activity and processivity (**Carrodeguas J. A., Pinz K. G., Bogenhagen D. F., 2002**).

The mitochondrial single-stranded DNA-binding protein (mtSSB) binds to the single-stranded DNA, protecting it from nucleases and promoting mtDNA synthesis by stimulating TWINKLE activity and increasing POLγ processivity (**Mignotte B., Barat M., Mounolou J. C., 1985**).

Depending on the proposed replication model, the process of mtDNA duplication may slightly vary. The scientific community puts forward three hypotheses on this issue; the first two favour asynchronous mtDNA replication, and the third implies parallel, synchronous copying of mtDNA strands (**McKinney E. A., Oliveira M. T., 2013**) (**Figure I7**).

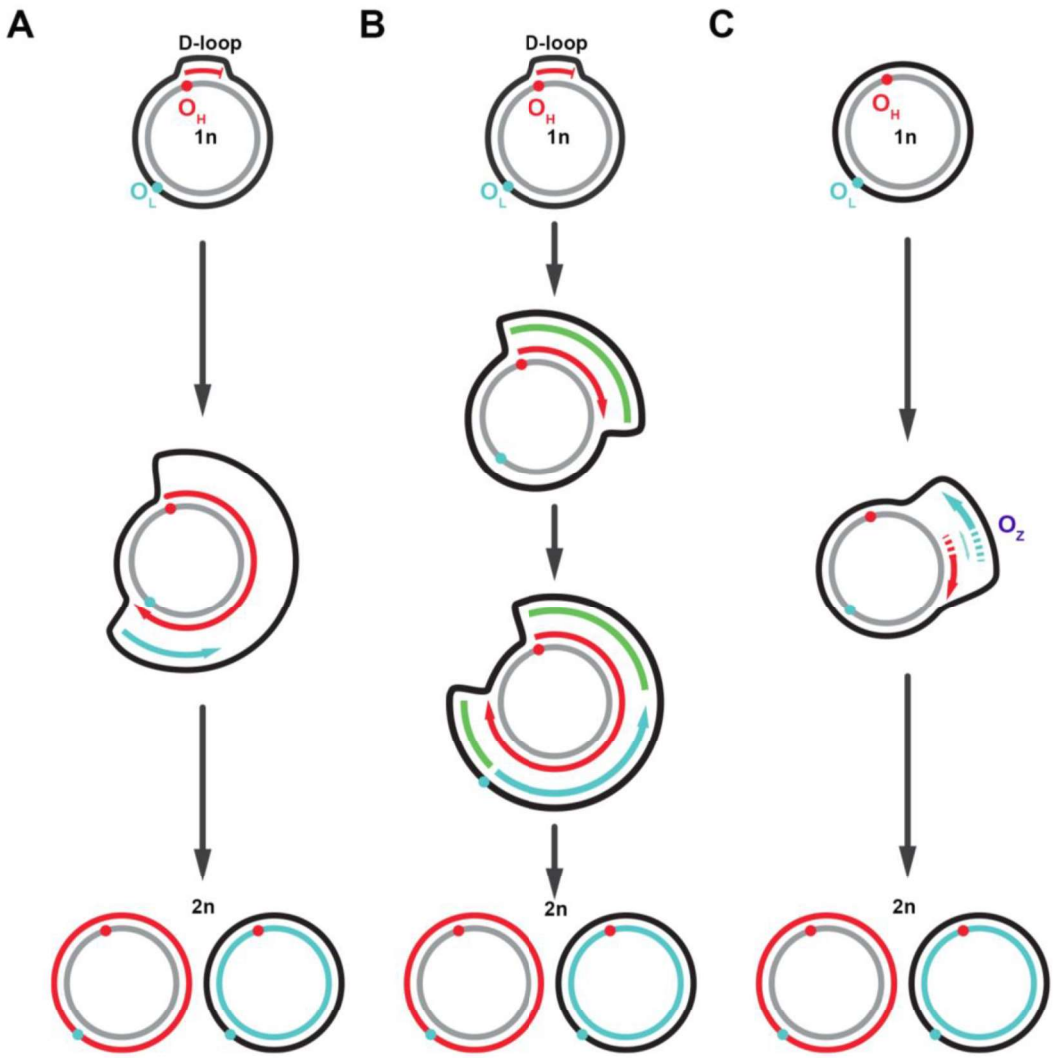


Figure I7. Models of Mammalian mtDNA Replication.

(A) The strand-displacement model.
(B) The RNA incorporated throughout the lagging strand (RITOLS) model.
(C) The synchronized (the leading and lagging strand-coupled) model.
OH, OL and OZ, origins of replication; nascent mtDNA strands are shown in red and blue, RNA – in green.
Adapted from McKinney E. A. & Oliveira M. T. , 2013.

The first mtDNA replication model, called the strand-displacement model, was proposed in 1972 (**Kasamatsu H., Robberson D. L., Vinograd J. A , 1972**) (**Figure I7A**). According to this model, replication starts at O_H in the non-coding region (**Figure I4B**), producing a new H-strand.

To begin H-strand replication, and POL*γ* requires an RNA primer, which is synthesized as a result of premature termination of L-strand transcription (**Chang D. D. & Clayton D. A., 1984**). During

the initial phase of replication, there's no simultaneous L-strand synthesis, and mtSSBs cover the displaced parental H-strand to prevent random RNA synthesis by POLRMT (**Wanrooij, S. *et al.*, 2008**). When the replication fork is about two-thirds through the genome, it passes O_L. The parental H-strand at O_L forms a stem-loop structure, preventing the binding of mtSSB proteins, and thus allowing POLRMT to initiate RNA synthesis by synthesizing a short primer (10-25 nucleotides long) (**Wong T. W. & Clayton D. A., 1985**). Then POL*γ* proceeds with L-strand DNA synthesis. H- and L-strands synthesis continues until both strands are fully replicated. Upon the completion of replication of each of the strands, to form a circular double-stranded molecule, they are ligated with DNA ligase III (**Shadel G. S. & Clayton D. A., 1997**). Thus, according to this model, mitochondrial replication is unidirectional, asymmetric and asynchronous.

Another model of mammalian mtDNA replication is the RITOLS model (ribonucleotide incorporation throughout the lagging strand) (**Yasukawa, T. *et al.*, 2006**) (**Figure I7B**). In this model, instead of mtSSB proteins, processed RNA molecules, such as rRNA, tRNA, and mRNA, are proposed to cover the displaced parental H-strand during mtDNA replication, forming a provisional lagging strand. However, skepticism exists regarding the RITOLS model because there's no identified molecular machinery explaining how processed transcripts can be threaded onto the displaced H-strand during mtDNA replication (**Reyes, A. *et al.*, 2013**).

Several factors challenge the RITOLS model: processed RNA molecules are typically folded, modified, and bound to proteins; RNase H1, present in mammalian mitochondria, actively degrades RNA molecules hybridized to single-stranded DNA (**Holmes, J. B. *et al.*, 2015**); and there are high levels of mtSSB in mammalian mitochondria, reducing the need for alternative modes of single-stranded DNA protection (**Miralles, F. J. *et al.*, 2014**). Thus, the RITOLS model remains unproven until solid biochemical evidence is provided for its individual reaction steps.

The third model resembles the "traditional" strand-coupled DNA synthesis where both the lagging and the leading strands are produced simultaneously from another origin of replication, Ori Z (O_Z), located between O_L and O_H (12,337 bp – 15,887 bp) (**Figure I7C**). According to this model, the replication forks move bidirectionally with the formation of Okazaki fragments on the lagging strand (**Bowmaker, M. *et al.*, 2003**). This model also has been experimentally confirmed (**Bowmaker, M. *et al.*, 2003**). Additionally, the presence in mitochondria of a protein apparatus that provides the function of Okazaki fragments also speaks in favour of the existence of this model.

It is believed that mitochondrial replication can follow any of the described mechanisms, with the choice depending on the cell's immediate needs. Asynchronous replication is generally faster than synchronous replication. Therefore, during periods requiring a substantial increase in mtDNA copies, such as active cell division, an asynchronous mechanism is likely employed, while in less critical situations, synchronous replication may occur (**Fish J, Raule N, Attardi G., 2004**; **Herbers, E. *et al.*, 2019**).

Anyway, after POL*γ* completes mitochondrial DNA replication, DNA ligase III joins the newly formed DNA strands (**Shadel G. S. & Clayton D. A., 1997**). Efficient ligation requires the removal of RNA primers used for DNA synthesis, which is likely done by RNase H1 (**Holmes, J. B. *et al.*, 2015**). POL*γ* then undergoes idling, involving cycles of polymerization and 3′–5′ exonuclease degradation at a nick in the DNA. This idling is crucial for proper ligation (**Macao, B. *et al.*, 2015**). When POL*γ* lacks exonuclease activity, it can't idle and continues DNA synthesis into the double-stranded DNA, creating a non-ligatable flap-like structure.

Coordination of replication and transcription of mitochondrial genome is crucial for mitochondrial biogenesis. In the absence of the transcription elongation factor TEFM, POLRMT initiates transcription at the LSP promoter but terminates at CSBII and produces a 120 nt replication primer at the O_H (**Figure I4B**) (**Agaronyan, K. *et al.*, 2015**). The primer is then used by the replisome to initiate replication of the H-strand. When TEFM is present, POLRMT does not terminate at CSBII and generates full-size transcripts. TEFM antitermination activity ensures that replication events do not interfere with the expression of mtDNA.

1.2.3. Human mitochondrial DNA transcription

In human mitochondria, transcription is facilitated by the DNA-dependent RNA polymerase known as POLRMT. This polymerase shares structural similarities with RNA polymerases found in T3 and T7 bacteriophages (**Ringel, R. *et al.*, 2011**). Unlike bacteriophage polymerases that can recognize promoters independently, POLRMT requires additional factors for transcription initiation (**Hillen, H. S. *et al.*, 2017**). It associates with mitochondrial transcription factor A (TFAM) and mitochondrial transcription factor B2 (TFB2M) to initiate transcription. TFAM participates in both mtDNA transcription and packaging, while TFB2M plays a key role in DNA melting during the transcription initiation. Recent findings reveal that TFAM, bound to DNA, recruits POLRMT to the promoter via its N-terminal extension, with TFB2M modifying POLRMT's structure to facilitate promoter opening (**Posse V. & Gustafsson C. M., 2017**).

Transcription of the mitochondrial genome initiates within the non-coding region, housing both the L-strand promoters (LSP) and H-strand promoters (HSP) (**Montoya, J. *et al.*, 1982**). Specifically, the light strand transcription originates from two promoters (LSP1, LSP2), governing the transcription of eight tRNAs and the MT-ND6 gene (**Figure I4A**) (**Tan, B. G. *et al.*, 2022**). The heavy strand comprises two promoters situated approximately 100 bp apart (**Figure I4A**).

There has been some debate considering the existence of a second heavy chain promoter. It was postulated that transcription from the H-strand promoters occurs unidirectionally, resulting in the generation of long polycistronic RNAs. The HSP1 promoter yields a transcript encompassing $tRNA^{Phe}$, $tRNA^{Val}$, and two rRNAs (12S and 16S), whereas transcription from HSP2 generates a transcript spanning nearly the entire genome (**Montoya, J. *et al.*, 1982**; **Montoya, J. *et al.*, 1983**). However, recent animal models (**Terzioglu, M. *et al.*, 2013**) and *in vitro* experiments (**Litonin, D. *et al.*, 2010**) indicate that heavy strand transcription is likely regulated by a sole promoter, and the variations in rRNA levels could be attributed to differences in turnover rates.

During the transcription elongation phase, POLRMT requires another factor called transcription elongation factor (TEFM) for processivity (**Minczuk, M. *et al.*, 2011**). TEFM promotes longer transcript formation by interacting with the C-terminal domain of POLRMT and newly synthesized mRNA and its depletion in cells reduces promoter-distal transcription elongation products (**Minczuk M. *et al.*, 2011**). TEFM also prevents G-quadruplex formation that hinders elongation at the CSB2, which is a site where LSP transcription is often prematurely terminated (**Pham, X. H. *et al.*, 2006**). This capability of TEFM to prevent premature termination serves as a switch from replication to transcription of the LSP-derived primary transcript.

The exact mechanism of mtDNA transcription termination remains unclear. Previously, it was thought that mitochondrial termination factor 1 (MTERF1) induced termination of the H-strand transcription by bending mtDNA (**Kruse B., Narasimhan N., Attardi G., 1989**). However, recent studies have challenged this notion, revealing that MTERF1 is involved in the termination of bidirectional transcription on both the heavy and light strands, notably, exhibiting a stronger affinity for the L-strand (**Yakubovskaya, E. *et al.*, 2010**). Termination-associated sequence, TAS, within the control region of mtDNA (**Figure I4B**), was found to serve as a terminator for both the replication and transcription initiated from the H-strand (**Jemt, E. *et al.*, 2015**). To conclude, further investigations are required to understand the precise mechanism of mitochondrial DNA transcription termination.

Mitochondrial transcription generates long polycistronic transcripts that subsequently undergo processing by mitochondrial RNases and further modification, if required (reviewed in **Jedynak-Slyvka M., Jabczynska A., Szczesny R. J., 2021**). Briefly, within the polycistronic transcript, each mRNA is surrounded by tRNA sequences on at least one side (**Ojala D., Montoya J., Attardi G., 1981**). The cleavage of these primary transcripts occurs at the 5'- and 3'-boundaries of these genes, a process facilitated by the distinctive secondary structure of tRNA, which is recognized by RNase P (**Anderson, S. *et al.*, 1981**). Additionally, with the exception of 12S and tRNAs, all RNA molecules undergo 3'-polyadenylation with the assistance of mitochondrial poly-A polymerase (mtPAP) (**Lapkouski M. & Hällberg B. M., 2015**). In the case of bacteria, polyadenylation serves as a marker for the targeted degradation of transcripts. However, in mitochondria, this process directly impacts the final levels of translation by affecting mRNA steady-state levels. For instance, deadenylation decreases the quantity of mt-mRNA of complex IV, while increasing the levels of mt-mRNA of complex I (**Nagaike, T. *et al.*, 2005**).

The mt-tRNAs undergo extensive post-transcriptional maturation including chemical nucleotide modifications and CCA addition at the 3′-end (**Yarham J. W. *et al.*, 20014**).

Ribosomal 16S and 12S rRNAs also require post-transcriptional modification of nucleosides, such as methylation and pseudouridynylation, required for the assembly of the mt-ribosomes (**Bohnsack M. T. & Sloan K. E., 2018**).

1.2.4. Human mitochondrial DNA translation

Mitochondrial translation of the 9 monocistronic mRNAs and the 2 dicistronic mRNAs (**Figure I4A**) can be divided into four stages, which closely resemble the steps that occur in the cytosol: initiation, elongation, termination, and recycling (**Koripella, R. K. *et al.*, 2021**). In addition to the previously discussed mitochondrial matrix processes, mitochondrial translation also exhibits several distinct features. One of these distinctive aspects is the alteration of the standard genetic code (**Osawa, S. *et al.*, 1992**). For instance, in vertebrate mitochondria, the UGA codon, typically a stop codon, encodes for tryptophan, while the AUA codon codes for methionine instead of isoleucine as it does in the standard genetic code. Furthermore, in mammals, mitochondria utilize a variety of non-standard start codons, including AUA, AUU, AUC, and GUG.

Regarding the stop codons, in mammals, mitochondria have two additional stop codons, AGA and AGG, alongside the standard ones (**Osawa, S. *et al.*, 1992**). However, for human mitochondria, it was demonstrated, that in translating mRNAs containing these non-standard stop codons, a one-nucleotide backward reading frame shift occurs just before termination. Consequently, the

actual termination takes place at the standard stop codons, UAA and UAG (**Temperley, R. *et al.*, 2010**).

The key player responsible for protein synthesis within mammalian mitochondria is the mitoribosome, which has a sedimentation rate of 55S and consists of two subunits: a large one called mt-LSU (39S) and a smaller one referred to as mt-SSU (28S). Recent advancements in electron cryo-microscopy have enabled the release of the structural details of human mitoribosome, allowing for an in-depth analysis of its composition and organization (**Amunts, A. *et al.*, 2015**).

In contrast to the bacterial ribosome, which primarily comprises a 2:1 RNA:protein ratio, the human mitoribosome has reversed this ratio. This shift is a result of both the deletion of specific rRNA domains and an overall increase in the mass of proteins associated with it. Notably, these proteins are predominantly situated at the periphery of the mitoribosome, leading to the hypothesis that their primary function is to safeguard the integrity of the rRNA. Like most ribosomes, the mitoribosome exhibits functional A-, P-, and E-sites, which play essential roles in the translation process (**Aibara, S. *et al.*, 2020**).

In humans, the mt-SSU consists of 12S rRNA and 30 proteins (**Amunts, A. *et al.*, 2015**). Unlike bacterial ribosomes, mitochondrial mRNAs lack a 5'- UTR (untranslated region), and correspondingly, the 12S rRNA does not carry an anti-Shine-Dalgarno sequence.

The mt-LSU consists of 16S rRNA and 53 proteins (**Amunts, A. *et al.*, 2015**). While in bacterial ribosomes, 5S rRNA serves as a scaffold in the small subunit, mitoribosomes employ mitochondrially encoded tRNAs, such as $tRNA^{Val}$ or $tRNA^{Phe}$, to fulfill this role (**Rorbach, J. *et al.*, 2016**). It's worth noting that these two tRNAs flank the rRNAs in the mitochondrial genome and are transcribed along with them into a long polycistronic RNA, which may partially explain their presence within the mitoribosome. And, surprisingly, if the quantity of one of these two tRNAs is compromised, the mitoribosome can incorporate the other tRNA in its place (**Rorbach, J. *et al.*, 2016**).

Many of the proteins involved in mitoribosome assembly are located in mitochondrial RNA granules (MRGs), which enhance the efficiency of gene expression (**Jourdain, A. A. *et al.*, 2015**). RMND1, an inner membrane protein, anchors the mitoribosome in close proximity to MRGs, where mRNA is synthesized and processed (**Janer, A. *et al.*, 2015**). Nevertheless, the exact role of this process is not fully understood. There is a hypothesis that this is done to ensure the accurate and efficient integration of hydrophobic proteins into the inner mitochondrial membrane

(**Watson K., 1972**). Additionally, biochemical fractionation experiments have shown that translation and the integration of mitochondrial proteins into the membrane occur in a coordinated manner (**Sevarino K. A. & Poyton R. O., 1980**).

1.2.5. Reparation of human mitochondrial DNA

Mitochondrial DNA can undergo damage in a manner similar to nuclear DNA. However, despite the presence of nearly all known repair systems in mitochondria (**Figure I8**), the effectiveness of mtDNA repair is considerably lower than that of nuclear DNA (**Alexeyev, M. *et al.*, 2013**). One contributing factor to this difference is the existence of a large number of mtDNA copies, which, to a certain extent, act as a safeguard against the stochastic effect of mutations. Thus, unlike nuclear DNA, where repair is the primary focus, damaged mtDNA molecules harboring abasic sites (**Xu, W. *et al.*, 2019**) or DNA double-stranded breaks (DSBs) (**Peeva, V. *et al.*, 2018**) are usually degraded than rather being repaired (**Figure I8**). Since mtDNA has strict copy-number control, selective removing of damaged mtDNA triggers the replication of undamaged copies, restoring the mtDNA pool (**Montier L. L. C., Deng J. J., Bai Y., 2009**).

Base excision repair (BER) (**Figure I8**, **left**) is a crucial process for repairing various types of DNA damage in both nuclear and mitochondrial genomes, including small adducts, oxidized bases, deaminated and hydrolyzed bases, and single-strand breaks (SSBs) (**Figure I8**, **far left**) resulting from transcription or replication issues (**Wallace S. S., 2014**; **Fontana G. A. & Gahlon H. L., 2020**). Recently, it was experimentally confirmed that SSBs undergo rapid repair, rather than a much slower process of mtDNA re-synthesis by replication (**Trombly, G. *et al.*, 2023**). Additionally, SSB may progress into DSB, then it will be predominantly subjected to degradation (**Peeva, V. *et al.*, 2018**). Less often, such DSB undergoes repair with the potential for the formation of deletions (**Nissanka, N. *et al.*, 2018**).

Most BER proteins are present in both the nucleus and mitochondria, but some are selectively localized to mitochondria, making mitochondrial BER highly efficient (**Boldinova, E. O. *et al.*, 2019**). This localization is often controlled by alternative promoters and splicing patterns, which encode signals for mitochondrial (MLS) or nuclear (NLS) localization.

BER is a highly conserved process found from bacteria to humans. The basic steps of BER include damaged DNA base recognition and removal, creating an abasic site, cleaving the abasic site, end processing, gap filling, and ligation to complete the repair (**Fortini, P. *et al.*, 2003**).

At the initiation of BER, DNA glycosylases are essential for recognizing and removing damaged DNA bases (**Jacobs A. L. & Schär P., 2012**). In mammalian mitochondria, seven out of eleven known DNA glycosylases have been identified (**Sharma N., Pasala M. S., Prakash A., 2019**). They can be categorized into mono-functional glycosylases (e.g., AAG, MUTYH, UNG) and bi-functional DNA glycosylases (e.g., OGG1, NEIL1, NEIL2, NTHL1) (**Mullins, E. A. *et al.*, 2019**). Mono-functional glycosylases generate abasic sites, which are further processed by apurinic/apyrimidinic endonuclease 1 (APE1). Bi-functional DNA glycosylases possess lyase activity and can cleave the abasic sites themselves.

During short-patch BER (SP-BER), APE1-generated 5'-deoxyribose phosphate is excised by Pol*γ*, followed by the insertion of a single nucleotide to fill the gap (**Longley, M. J. *et al.*, 1998**). In long-patch BER (LP-BER), Pol*γ* incorporates 2-6 nucleotides at the nick, and flap endonuclease 1 (FEN1) cleaves the 5' flap (**Akbari, M. *et al.*, 2008**). Additional enzymes like DNA replication helicase/nuclease 2 (DNA2) and 5'-exo/endonuclease (EXOG) help to remove 5' flaps during mitochondrial LP-BER (**Duxin J. P. *et al.*, 2009**). DNA ligase III (LAG3) seals the nick to complete the final ligation step in mitochondrial BER (**Simsek, D. *et al.*, 2011**).

Regarding SSB repair, this pathway is analogous to BER (**Hegde, M. L. *et al.*, 2012**) (**Figure I8**, **far left**). Initially, the presence of single-strand breaks is recognized, potentially facilitated by the poly-ADP-ribose polymerase 1 (PARP1), although its precise role in mitochondrial SSB repair remains uncertain (**Rossi, M. N. *et al.*, 2009**). Subsequently, APE1 and polynucleotide kinase/phosphatase (PNKP) process the DNA ends, ensuring proper preparation for repair (**Tahbaz N., Subedi S., Weinfeld M., 2012**). Tyrosyl DNA phosphodiesterase 1 (TDP1) plays a pivotal role by removing various adducts from the 3'-DNA ends, contributing to efficient repair (**Meagher M. & Lightowlers R. N., 2014**). Lastly, aprataxin (APTX) removes 5'-adenylate groups to enable correct DNA ligation.

Mitochondrial mismatch repair (MMR) remains incompletely characterized, and it's uncertain whether this repair pathway functions within mitochondria (**Figure I8**, **middle**). In the nucleus, MMR corrects base mismatches, crosslinks, and small insertions/deletions arising from DNA replication, recombination and repair, enhancing DNA maintenance fidelity (**Sancar, A. *et al.*, 2004**). Some evidence suggests MMR activity in mitochondria, including observations of microsatellite instability in colorectal cancer samples, indicating cancer-related MMR impairments, and *in vitro* repair assays of mtDNA mismatches in rat liver mitochondria lysates (**Habano W., Nakamura S., Sugai T., 1998**; **de Souza-Pinto, N. C. *et al.*, 2009**). Importantly, mitochondria lack key nuclear MMR proteins (e.g., MSH2, MSH3, and MSH6), and only the

multifunctional protein YB-1 has been directly implicated in mitochondrial MMR (**de Souza-Pinto, N. C. *et al.*, 2009**). YB-1 recognizes and binds mismatched DNA, initiating repair and interacting with glycosylase NEIL2 and nuclease APE1, suggesting crosstalk between MMR and BER for mtDNA maintenance.

Currently, robust evidence supporting *bona fide* mitochondrial MMR in mammalian cells is lacking. If it exists, mitochondrial MMR would differ significantly from nuclear MMR, particularly in lacking strand-bias (**Mason, P. A. *et al.*, 2003**). This means mitochondrial MMR cannot distinguish the strand with the misincorporated nucleotide from the one with the correct one. Mitochondrial MMR might be a trace of an ancestral mechanism that merged with BER throughout evolution. (reviewed in **Mason P.A. & Lightowlers R. N., 2003**).

DSBs mtDNA repair in mammals is still not fully understood. While nuclear genomes have well-established repair pathways like Homology-Directed Repair (HDR) and Non-Homologous End Joining (NHEJ) (**Figure I8**, **right**), mitochondrial DSBs in mammals undergo rapid degradation rather than conventional repair (**Sancar, A. *et al.*, 2004**; **Peeva, V. *et al.*, 2018**).

HDR involves searching for homologous templates to restore the integrity of broken DNA ends (**Sancar, A. *et al.*, 2004**). In contrast, NHEJ works by directly re-ligating the two sides of blunt-ended DSBs (**Sancar, A. *et al.*, 2004**). There's also an alternative NHEJ pathway known as Microhomology-Mediated End Joining (MMEJ) (**Sfeir A. & Symington L. S., 2015**). MMEJ relies on small regions of homology, typically ranging from 5 to 25 nucleotides, to guide the re-ligation of broken DNA. However, MMEJ results in the formation of short flaps that are degraded before end joining, making this pathway prone to mutational events, particularly small-scale deletions.

Nevertheless, despite conclusive evidence is lacking, HDR (**D'Aurelio M. *et al.*, 2004**), NHEJ (**Coffey G., Lakshmipathy U., Campbell C, 1999**), and MMEJ (**Tadi S. K. *et al.*, 2016**) pathways have been suggested to have a place in mitochondrial repair based on *in vitro* and *in vivo* experiments. Moreover, some DSB repair proteins have been found in mitochondria, including MRE11, RAD51, DNA2, Ku80, and XRCC4 (**Wisnovsky S. *et al.*, 2016**) (**Figure I8**, **right**). However, it's unclear how these individual proteins can reconstitute DSB repair complexes like those in the nucleus. The significance of mtDNA DSBs repair obviously requires more research for a clear understanding.

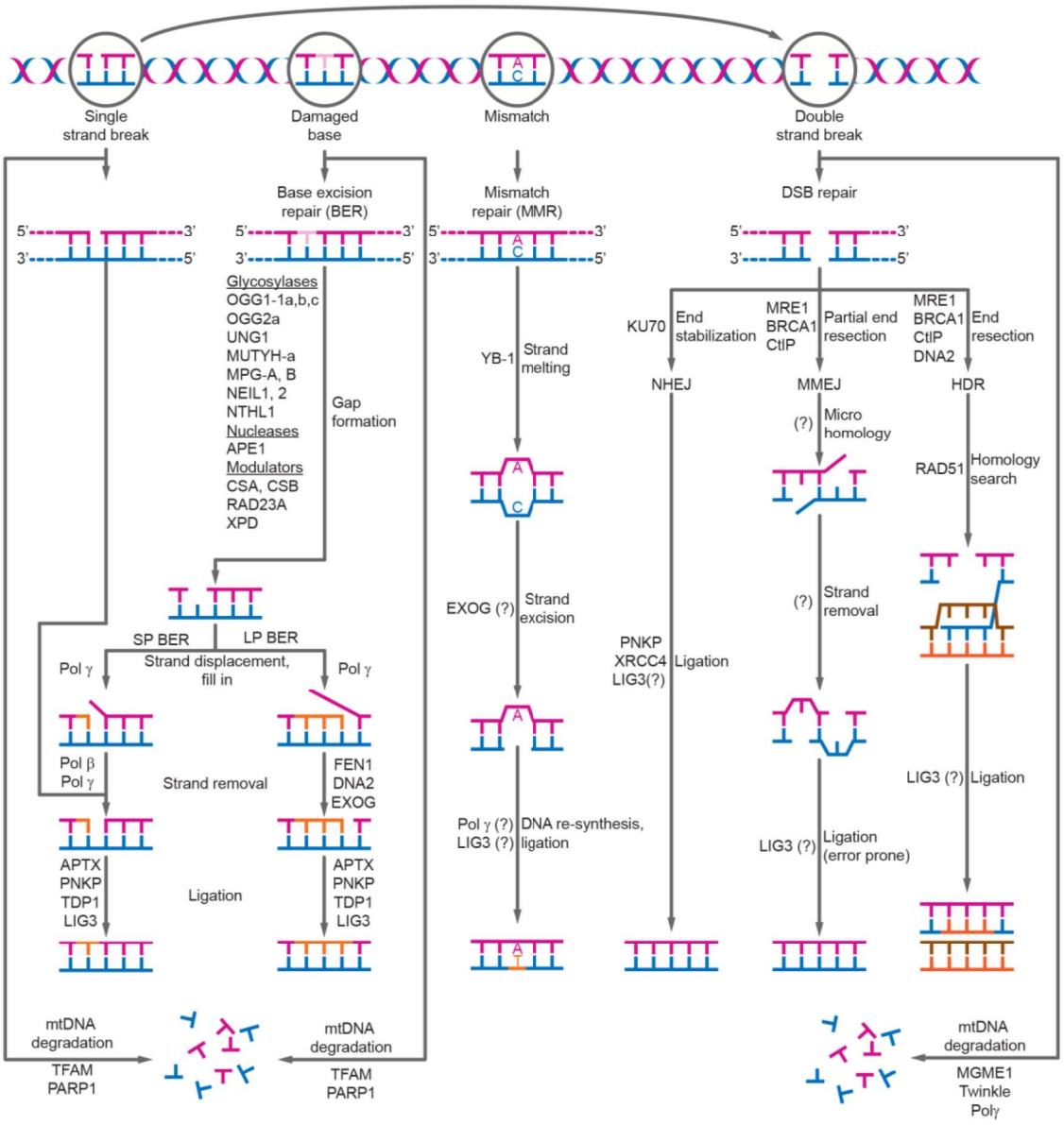


Figure I8. Mammalian Mitochondrial DNA Repair Pathways.

Repair proteins found in mitochondria are indicated. BER (left) repairs oxidized bases and abasic sites and comprises both short-patch (SP) and long-patch (LP) sub-pathways. SSB pathway (far left) is similar to BER. MMR (middle) still lacks convincing evidence regarding its activity in mitochondria; YB-1 is the only mitochondrial MMR protein identified. DSB (right) also lacks convincing evidence regarding efficient mitochondrial function. Proteins involved in mitochondrial non-homologous end-joining (NHEJ), microhomology-mediated repair (MMEJ) and homology-directed repair (HDR) were identified and appear as shared between the nucleus and the mitochondria. Cleaved mtDNA molecules can be also rapidly degraded.
Adapted from Fontana G. A. & Gahlon H. L., 2020.

1.3. Import of macromolecules into human mitochondria

As previously mentioned, according to the theory of symbiogenesis, mitochondria are believed to have originated from independent unicellular organisms that established a symbiotic relationship with ancestral eukaryotic cells. Over time, mitochondria evolved to coexist within these host cells. However, throughout evolution, a significant portion of mitochondrial genes migrated to the nucleus. Consequently, the products of these genes, essential for organelle function, are now imported from the cytosol (**Verechshagina, N. A. *et al.*, 2018**).

1.3.1. Protein import

According to the MitoCarta 2.0, 1158 proteins are required for the assembly and functioning of mitochondria in higher animals (**Calvo S. E., Clauser K. R., Mootha V. K., 2016**). The vast majority of these proteins are encoded in nuclear DNA. It follows from this that the functioning of mitochondria is determined by the coordinated work of two genomes.

Mitochondrial protein import is typically considered a post-translational process, where protein precursors are protected from cytosolic conditions by chaperones until they reach the mitochondria (**Young J. C., Hoogenraad N. J., Hartl F. U., 2003**). However, there is evidence that, for certain proteins, mitochondrial import can occur co-translationally (**Kaltimbacher, V. *et al.*, 2006**). In these cases, specific mRNAs for mitochondrial proteins are translated by cytosolic ribosomes located near the outer mitochondrial membrane. Signals present in the 3'-UTR and the coding region of these mRNAs play a role in directing them to the mitochondrial surface (**Michaud M., Maréchal-Drouard L., Duchêne A. M., 2014**). This co-translational import mechanism adds another layer of complexity to the regulation of mitochondrial protein import.

In most cases, mitochondrial proteins of nuclear origin are initially synthesized in the cytosol as precursor proteins (**Verechshagina, N. A. *et al.*, 2018**). These precursors are equipped with specific targeting signals, including N-terminal signal sequences (cleavable presequences) and internal import signals, to facilitate their import into mitochondria. These signals, known as mitochondrial targeting sequences (MTS), are short amino acid sequences that serve as recognition markers for mitochondrial import receptors. These receptors are responsible for delivering the precursor proteins to various subcompartments within the mitochondria.

The first step in the transport of these precursor proteins involves crossing the outer mitochondrial membrane, which is facilitated by a complex called the TOM complex (translocase of the outer mitochondrial membrane) (**Neupert W., Herrmann J. M., 2007**) (**Figure I9**). The yeast TOM

complex is composed of several proteins, including Tom70, Tom20, and Tom22, which act as receptors for the initial recognition of the targeting signals (**Guan, Z. *et al.*, 2021**). These receptors have both cytosolic and transmembrane domains, and in the case of Tom22, it also has a C-terminal domain that faces the intermembrane space. Tom20 primarily interacts with the N-terminal signal sequences of precursor proteins by binding to the hydrophobic region of an amphiphilic *α*-helix. On the other hand, precursor proteins with internal import signals are recognized by the Tom70 receptor (**Wu Y. & Sha B., 2006**).

All precursor proteins containing N-terminal signal sequences, coming from the TOM complex, are transported through the inner mitochondrial membrane thanks to the TIM23 (translocase of the inner mitochondrial membrane 23) complex (**Chacinska, A. *et al.*, 2003**) (**Figure I9**). During this translocation process, a transient supercomplex called the TOM-TIM23 supercomplex is formed. In this supercomplex, the N-terminus of the precursor protein already associates with the TIM23 complex, while the C-terminus remains associated with the TOM complex. This arrangement ensures the coordinated movement of the precursor protein through both mitochondrial membranes.

Upon reaching the inner mitochondrial membrane, the fate of the precursor protein is determined based on its specific signals. It can either be imported into the mitochondrial matrix or integrated into the lipid bilayer of the inner membrane, depending on the presence of specific hydrophobic import signals (**Hell K., Neupert W., Stuart R. A., 2001**). Translocating a protein across the inner membrane requires the presence of a membrane potential ($\Delta\psi$) and an ATP-dependent translocation motor (PAM), which facilitates the penetration of a protein into the matrix (**Geissler, A. *et al.*, 2000**). Once a precursor protein has entered the mitochondrial matrix, the N-terminal presequence can be cleaved by the mitochondrial processing peptidase (MPP) (**Gakh O., Cavadini P., Isaya G., 2002**) (**Figure I9**).

It's worth noting that the inner mitochondrial membrane contains another protein, Oxa1, which plays a role in integrating polypeptides that are synthesized in the mitochondrial matrix into this membrane (**Hell K., Neupert W., Stuart R. A., 2001**) (**Figure I9**). All these complicated steps ensure the precise processing and localization of proteins within the mitochondria, allowing them to perform their essential functions in this organelle.

Many mitochondrial outer membrane proteins have a specific shape called a *β*-barrel. Before integrating into the outer membrane, these proteins interact with chaperone complexes made up of small Tim-proteins like Tim9, Tim10, Tim8, and Tim13 in the intermembrane space

(**Wiedemann, N. *et al.*, 2004**) (**Figure I9**). The integration process starts with the β-signal being recognized by a group of proteins forming the SAM complex (sorting and assembly machinery), which consists of four subunits (**Figure I9**). The *β*-signal triggers the opening of a channel formed by the SAM complex (**Kutik, S. *et al.*, 2008**). Then, the precursor *β*-barrel protein penetrates the outer membrane through a local rearrangement of SAM complex components, initiated by the binding of the *β*-signal. The exact details of this process are still not fully understood.

Other mitochondrial outer membrane proteins such as Tom70 and Tom22 have N-terminal *α*-helical transmembrane segment allowing them to attach to the membrane. In this case, the OM protein Mim1 takes part in the membrane integration (**Becker, T. *et al.*, 2008**) (**Figure I9**). The accessory proteins Tom5, Tom6 and Tom7 are attached to the outer membrane by a transmembrane segment located at the C-terminus. In Tom22, the transmembrane segment is localized in the middle of the molecule.

Many intermembrane space proteins are small in size (7–16 kDa) and contain one or more cysteine motifs, consisting of two cysteine residues located three to nine amino acid residues apart. These cysteine residues are involved in the formation of disulfide bonds (Tim9 and Tim10) or in the binding of cofactors or metal ions (Cox17). The import of such proteins into the intermembrane space of mitochondria occurs with the participation of the Mia40 receptor and Erv1 sulfhydryl oxidase (**Chacinska, A. *et al.*, 2004**) (**Figure I9**). Mia40 forms temporary disulfide bonds with precursor proteins leaving the TOM complex into the intermembrane space. The function of Erv1 is to maintain Mia40 in an oxidized state for subsequent rounds of import (**Mesecke, N. *et al.*, 2005**).

The second translocation complex of the inner mitochondrial membrane is TIM22 (**Figure I9**). It integrates metabolite carriers with internal localization signals into the inner membrane. After the hydrophobic precursor protein enters the aqueous phase of the intermembrane space, it binds to the TIM22 (**Davis, A. J. *et al.*, 2007**). Using electron microscopy, it was possible to establish that the TIM22 complex has two pores (**Rehling, P. *et al.*, 2003**). In addition, TIM22, is a part of complex II of the respiratory chain in yeast (**Gebert, N. *et al.*, 2011**). As previously mentioned, the only necessary source of energy for the process of insertion of integral proteins into the IM is the membrane potential.

All this complicated recognition and transport processes ensure the precise delivery of mitochondrial proteins to their respective subcompartments within the mitochondria.

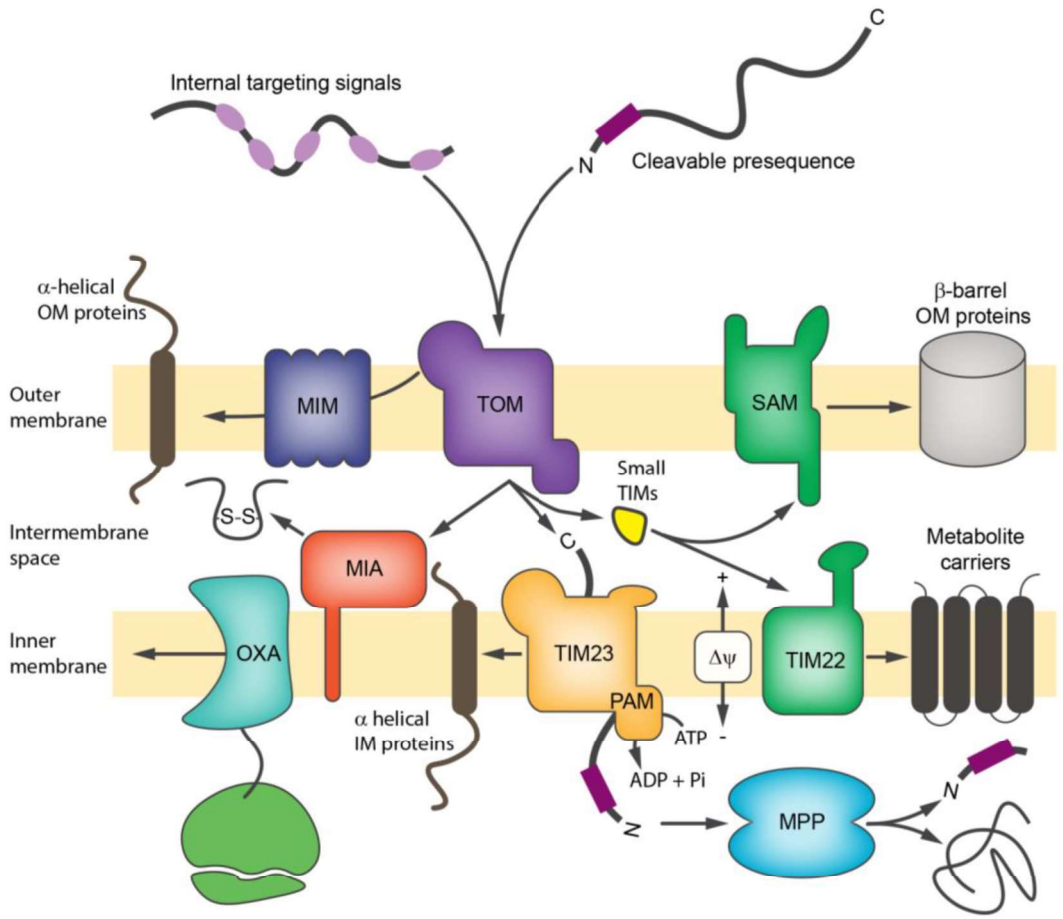


Figure I9. Mitochondrial Import of Proteins Bearing Various Targeting Signals.

Most proteins are initially made in the cytosol and then imported through the outer membrane translocase (TOM). They are sorted into different mitochondrial compartments like the outer membrane (OM), intermembrane space (IMS), inner membrane (IM), and matrix. The IMS import and assembly (MIA) machinery helps import and oxidize proteins with disulfide bonds. The TIM23 translocase sorts proteins to the inner membrane or matrix, often with PAM's assistance. The mitochondrial processing peptidase (MPP) removes amino-terminal presequences. Small TIM chaperones in the IMS transport β-barrel precursors to the SAM machinery of the outer membrane or to the TIM22 translocase in the inner membrane. Membrane potential (Δψ) facilitates protein translocation via TIM23 and TIM22. Some α-helical outer membrane proteins can insert directly into the outer membrane through the MIM complex. MtDNA-encoded proteins are exported to the inner membrane via the OXA translocase.
Adapted from Schmidt O., Pfanner N., Meisinger C. , 2010.

1.3.2. RNA import

Mitochondrial import is not limited to proteins, as it also includes nuclear-encoded noncoding RNAs (ncRNA). This phenomenon is observed in various organisms, although the specific RNAs involved and the mechanisms can vary (reviewed in **Jeandard, D. *et al.*, 2019** and **Chai P., Lebedenko C. G., Flynn R. A., 2023**).

For, example, in yeast *S. cerevisiae*, nuclear-encoded $tRNA^{Lys}$ binds to enolase (Eno2p) and undergoes structural changes, allowing recruitment to the mitochondrial surface by mitochondrial lysyl-tRNA synthetase (**Kazakova, H. A. *et al.*, 1999**). Subsequent RNA translocation into the mitochondrial matrix is facilitated by the TOM and TIM complexes (**Tarassov I., Entelis N., Martin R. P., 1995**). Plant cells, on the other hand, utilize a voltage-dependent anion channel-dependent pathway for RNA import into mitochondria (**Salinas, T. *et al.*, 2014**).

While the mechanisms of mitochondrial RNA import in plants and yeast are relatively well understood, this process in mammals is less characterized and requires further investigation (**Jeandard, D. *et al.*, 2019**). RNA translocation into mitochondria is known to be ATP-dependent, requires a membrane potential, and may involve TOM complex and/or VDAC channel for translocation across the OMM (**Campo M. L., Peixoto P. M., Martínez-Caballero S., 2017**). In contrast, the mechanism of RNA translocation through the IMS is better understood and involves polynucleotide phosphorylase (PNPase) (**Wang, G. *et al.*, 2010**).

PNPase is an exoribonuclease, with roles in RNA degradation and maintenance, found in both the mitochondrial matrix and IMS (**Chen, H. W. *et al.*, 2006**; **Golzarroshan, B. *et al.*, 2018**). PNPase's precise role in RNA import remains unclear, but structural studies suggest that it can recognize RNA structures, like stem-loop structures, and facilitate their import into the mitochondrial matrix (**Lin, C. L. *et al.*, 2012**). Research about PNPase's role in mitochondrial RNA import demonstrated that it selectively mediates the import of RNase P (**Doersen, C. J. *et al.*, 1985**), 5S rRNA (**Magalhaes P. J., Andreu A. L., Schon E. A., 1998**), and MRP RNAs (**Li, K. *et al.*, 1994**).

Experiments conducted in our laboratory and others have demonstrated that the inclusion of stem-loop motifs from human RNase MRP RNA, RNase P, and *S. cerevisiae* $tRNA^{Lys}_{CUU}$ (tRK1) D-hairpin and F-hairpin (**Kolesnikova, O. *et al.*, 2010**) serves as an effective determinant for mitochondrial import (**Wang, G. *et al.*, 2010**; **Tonin, Y. *et al.*, 2014**).

Additionally, in the previous studies of our and other groups, specific structural elements in 5S rRNA, which is thought to be a component of most of the mitoribosomes, were identified (**Greber B. J., Ban N., 2016**), that act as signals for its import into mitochondria (**Smirnov, A. *et al.*, 2008**). Incorporating these elements allowed cytosolic RNA to be transported into the organelle. However, a recent discovery of 5S RNA's resistance to RNases, which are typically used to assess mitochondrial import (**Jeandard, D. *et al.*, 2019**), may lead to false-positive results and overestimation of its mitochondrial import (**Jeandard, D. *et al.*, 2023**).

Little is known about mitochondrial import of long RNA molecules like mRNA and long noncoding RNA (lncRNA) (70 – 300 nucleotides) (**Jeandard, D. *et al.*, 2019**). SAMMSON is a lncRNA that's highly expressed in over 90% of melanoma samples (**Leucci, E. *et al.*, 2016**). It was found that SAMMSON directly interacts with the p32 protein, and its knockdown leads to a decrease in the p32 mitochondrial fraction (**Vendramin, R. *et al.*, 2018**). This, in turn, leads to a disruption in the synthesis of mitochondrial respiratory chain proteins, a drop in mitochondrial membrane potential, and, ultimately, cell apoptosis.

Given that SAMMSON is found to interact with p32, there's a hypothesis that it might also get imported into mitochondria (**Leucci, E. *et al.*, 2016**). However, this import process for SAMMSON has not yet been proven. Mitochondria are enclosed by a double membrane with a negative charge, which might explain why larger RNA molecules like lncRNAs and mRNAs are generally not imported into human mitochondria.

To date, several studies demonstrated that while lncRNAs can be imported into mitochondria only with the help of specific protein factors, which limits the amount of translocated molecules (**Leucci, E. *et al.*, 2016**; **Warren, J. M. *et al.*, 2021**), the shorter RNA molecules such as miRNA (microRNA) and siRNA (small interfering RNA) are targeted in a much more efficient and probably non-specific way and can be not only detectable, but also functional (**Zhang, X. *et al.*, 2014**).

Small ncRNAs (sncRNAs) are a category of non-coding RNAs shorter than 200 nucleotides, including miRNAs and siRNAs, which are approximately 22 nucleotides long (**Chen K. & Rajewsky N., 2007**). MiRNAs are initially synthesized as primary transcripts in the cell nucleus and then processed by the DROSHA/DGCR8 complex into single stem-loop precursor molecules called pre-miRNAs (**Treiber T., Treiber N., Meister G., 2019**). These pre-miRNAs are typically transported to the cytoplasm by Exportin5, where they undergo further cleavage by DICER1 to generate mature double-stranded miRNA duplexes. In mammalian cells, one RNA strand from the duplex, known as the guide strand, is incorporated into the RNA-binding protein argonaute 2 (AGO2), forming the miRNA-induced silencing complex (miRISC) (**Czech B., Hannon G. J., 2011**). MiRISC mainly recognizes the 3' untranslated region (3' UTR) of target mRNAs using the guide strand, leading to the downregulation of these mRNAs translation and stability.

In addition to their well-known role in negative post-transcriptional regulation, miRNAs are suggested to have non-canonical functions outside the cytoplasm. MiRNAs located in mitochondria are commonly referred to as "mitomiRs," which can originate from transcripts of either the mitochondrial or the nuclear genome (**Saint-Auret, G. *et al.*, 2011**). MitomiRs encoded

by the nuclear genome are more prevalent in mitochondria compared to those encoded by the mitochondrial genome, and they are often found in loci within or near mitochondrial genes to allow for coordinated regulation of their transcription (**Bandiera, S. *et al.*, 2013**). However, the precise mechanism of action of microRNAs within mitochondrial matrix is unclear, since mitochondrial mRNAs do not contain 3'UTRs and only one RISC component, AGO2, is presumably localized in the mitochondrial matrix (**Bandiera, S. *et al.*, 2011**).

Nevertheless, speaking of observed functions of mitomiRs, some of them were found to enhance the synthesis of selected mitochondrial proteins instead of inhibiting them. For example, miR-1 can stimulate mtND1 and mtCOXI mRNA translation in an AGO2-dependent manner, which is essential for muscle differentiation in mice (**Zhang, X. *et al.*, 2014**). On the contrary, miR-181c is expected to downregulate mtCOXI expression in rat heart (**Das, S. *et al.*, 2017**) and miR-378 downregulates mtATP6 expression in mouse HL-1 cells (**Jagannathan, R. *et al.*, 2015**). Other non-canonical functions of mitochondrial microRNAs can be expected, but a convincing demonstration of the relevant molecular mechanisms is difficult. Considering that miRNAs can affect the expression of nuclear genes involved in the biogenesis and functioning of mitochondria, it is not at all easy to exclude such indirect effects caused by their canonical action in the cytosol.

Additionally, in recent research, it was shown that not only miRNAs, but siRNAs can enter and function within human mitochondria, specifically targeting and silencing mitochondrial transcripts (**Gao, K. *et al.*, 2021**). This mitoRNAi effect was easily observed at the mRNA level, however, on the protein level, the effect was detectable in relatively unstable mitochondrial proteins such as the mtDNA-encoded complex IV subunits.

It's worth noting that despite the existing evidence, the topic of RNA import into human mitochondria remains a subject of debate. Some speculative arguments, such as concerns about the imported RNA's ability to carry out its usual functions, have been raised (**Gammage P. A., Moraes C. T., Minczuk M., 2018**). Nonetheless, continued research in this field may provide more insights into this process and potentially uncover new key players.

1.4. Human mtDNA mutations and their role in pathogenesis

1.4.1. Mitochondrial mutations. Heteroplasmy effect and its dynamic

It is widely acceptable that the close proximity of oxidative phosphorylation complexes and the lack of protective histones on mtDNA make the mitochondrial genome highly vulnerable to damage caused by reactive oxygen species (ROS), leading to a mutation rate of 10-100 times higher than that of the nuclear genome (**Floros, V. I. *et al.*, 2018**).

However, a study conducted by **Larsson *et al.* in 2018** revealed an interesting aspect of mitochondrial mutations. It was demonstrated that an increase in ROS levels within the mitochondria did not significantly impact the number of *de novo* mutations occurring in the mitochondrial genome. Additionally, the majority of mtDNA mutations observed in their study were of the transition type, which is typically associated with errors made by the Pol*γ* polymerase during replication. This suggests that the primary factor driving mtDNA mutations is likely the malfunction of the mitochondrial replication machinery. However, it's important to note that while these findings are compelling, they do not exclude the potential influence of ROS, minor intermolecular recombination, or the rudimentary mtDNA repair mechanism on mitochondrial genome mutations (**Floros, V. I. *et al.*, 2018**).

Considering that multiple copies of mtDNA can exist within a single cell, mutations, regardless of their origin, can impact either all of these molecules or only a subset of them (**Nissanka N. & Moraes C. T., 2020**). When all copies of mtDNA in a cell share the same mutation, this phenomenon is referred to as "homoplasmy." Conversely, when mutations are present in only some of the mtDNA molecules within a cell, it is described as a state of "heteroplasmy" (**Figure I10**).

The level of heteroplasmy can vary between cells in the same tissue or organ, between organs in the body of one person, and also between members of the same family (**Elson, J. L. *et al.*, 2001**). Heteroplasmic mutations cause a relatively mild biochemical effect, which usually affects only one organ or tissue (**McFarland, R. *et al.*, 2002**). Mutations that are in a state of homoplasmy affect several systems and organs at once, especially the brain, spinal cord, muscles, heart, and organs of the endocrine system. The level of heteroplasmy correlates with aerobic activity in tissues, and, consequently, with the severity of the manifestation of the clinical phenotype (**Rossignol, R. *et al.*, 2003**).

The clinical manifestation of mitochondrial diseases caused by mutations is primarily determined by the threshold effect of heteroplasmy (**Figure I10**). This threshold refers to the minimum number of mutant mtDNA copies required for clinical symptoms to appear (**Carelli V. & Morgia C., 2018**). The heteroplasmy threshold varies individually for each mtDNA mutation, typically falling within the range of 60 to 90% (**Rossignol, R. *et al.*, 2003**). Furthermore, heteroplasmy threshold may vary for different symptoms, and the rate of a disease progression within a specific individual can be influenced by environmental, genetic, and epigenetic factors. Predicting the rate of development and inheritance of mitochondrial diseases can be challenging, and disorders resulting from mtDNA mutations can be life-threatening. For example, both known m.8993T>G/C mutations have a heteroplasmy threshold above 70%. Heteroplasmy levels in the range of 70-90% are associated with NARP syndrome (Neuropathy, Ataxia, and Retinis Pigmentosa), while levels exceeding 90% lead to the predominance of clinical symptoms characteristic of Leigh syndrome (**Gorman G. S. *et al.*, 2016**) for which symptoms manifestation in childhood leads to the death of 10–50% of individuals within a year after the disease onset (**Naviaux R. K., 2004**).

In addition to the tissue-specific heteroplasmy threshold, evidence has been reported that the threshold for mtDNA point mutations (>80%) is significantly higher than the threshold effect for mtDNA deletions (>60%) ( ).

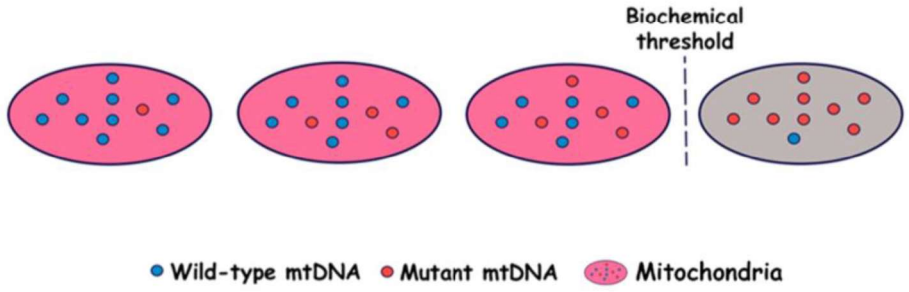


Figure I10. mtDNA Heteroplasmy and the Threshold Effect.

Mutant and wild-type mtDNA can coexist within the same cell. The clinical manifestation will be observed only when heteroplasmy ratio exceeds a certain threshold. Functional mitochondria are shown in pink, dysfunctional – in grey.
Adapted from Stewart J. B. & Chinnery P. F., 2015.

MtDNA mutations can occur within one molecule, one cell, or one tissue. However, there are mechanisms by which it can achieve high frequency in a population of cells.

The first mechanism is simple cell division. When a cell divides, mtDNA molecules are passed to daughter cells. In the case of homoplasmy, each daughter cell receives the same version of mtDNA, but if the cell initially had several variations of mitochondrial DNA, i.e., the phenomenon of heteroplasmy was observed, then daughter cells may receive an unequal number of mutant DNA molecules. This process is called vegetative (mitotic) segregation and explains the change in the level of heteroplasmy during horizontal gene transfer due to cell division (**Wallace D. C. and Chalkia D., 2013**) (**Figure I11**, **bottom right panel**).

Even in non-dividing (post-mitotic) cells, there are ongoing processes of mtDNA damage and replication. However, unlike nuclear DNA, there isn't a mechanism that guarantees the uniform replication of all mtDNA molecules. Additionally, in non-dividing cells, mtDNA can replicate through a process known as relaxed replication. This means that the replication of a random mtDNA molecule can happen more frequently than others, resulting in a change in the level of heteroplasmy within the cell (**Chinnery P. F. & Samuels D. C., 1999**) (**Figure I11**, **upper right panel**).

Another crucial phenomenon to consider is the mtDNA bottleneck (**Figure I11**, **left panel**). Early research in mammals demonstrated that a newly acquired heteroplasmic mtDNA mutation can become fixed and homoplasmic within three generations (**Olivo, P. D. *et al.*, 1983**). This suggests that only a small fraction of mitochondrial genes is randomly transmitted from mother to offspring.

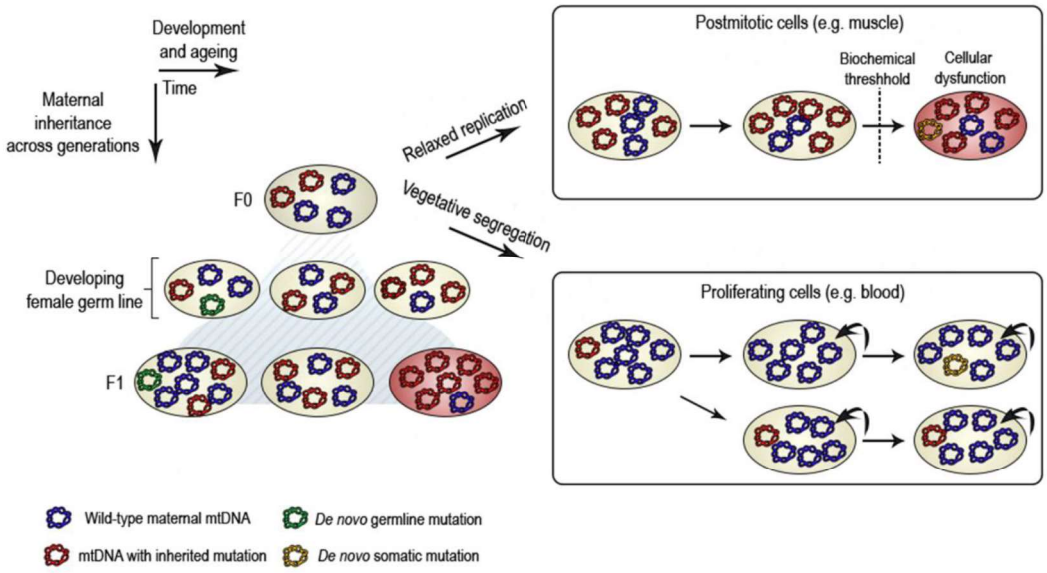


Figure I11. Dynamics of the Mitochondrial DNA.

Mitochondrial DNA heteroplasmy can change during a lifetime due to mitotic (vegetative) segregation in dividing cells and through relaxed replication in both non-dividing and dividing cells (right panels). Germline mtDNA mutations can become close to homoplasmic state due to the bottle neck effect (left panel). Adapted from Korchivaya ,E. *et al.*, 2022.

The 'bottleneck phenomenon' involves a significant reduction in mitochondrial content within cells during primary germ cell formation, followed by the restoration of their numbers during oogenesis (**Figure I11**, **left panel** and **Figure I12**). Approximately 0.01% of the mitochondria in the egg are estimated to contribute to the next generation (**Shoubridge E. A. & Wai T., 2007**). Variations in the transmission of mutant mitochondrial DNA determine the severity of clinical symptoms in families with heteroplasmic mtDNA mutations (**White S. L. *et al.*, 1999**). Therefore, the mtDNA bottleneck effect can rapidly segregate heteroplasmic variants into homoplasmy within a single generation or result in the ultimate fixation of a mutation over several generations, as mentioned earlier.

Interestingly, it was long believed that the human mitochondrial genome was exclusively inherited from the mother (**Birky Jr C., 2001**). However, subsequent research showed that paternal mtDNA can also enter the oocyte during fertilization, along with a small amount of sperm cytoplasm (**Sutovsky, P. *et al.*, 2000**; **Schwartz M. & Vissing J., 2002**; **Luo, C. *et al.*, 2018**). The reasons why paternal mtDNA can evade selection and gain a selective advantage for reproduction only in specific tissues upon entering the oocyte remain unknown. However, it's important to note that this phenomenon still lacks substantial evidence and is not widely accepted in the scientific community.

While it's challenging to pinpoint which of these mechanisms is the most significant, it is evident that these processes collectively can lead to changes in intracellular heteroplasmy levels during ontogenesis and possibly contribute to the development of mitochondrial diseases.

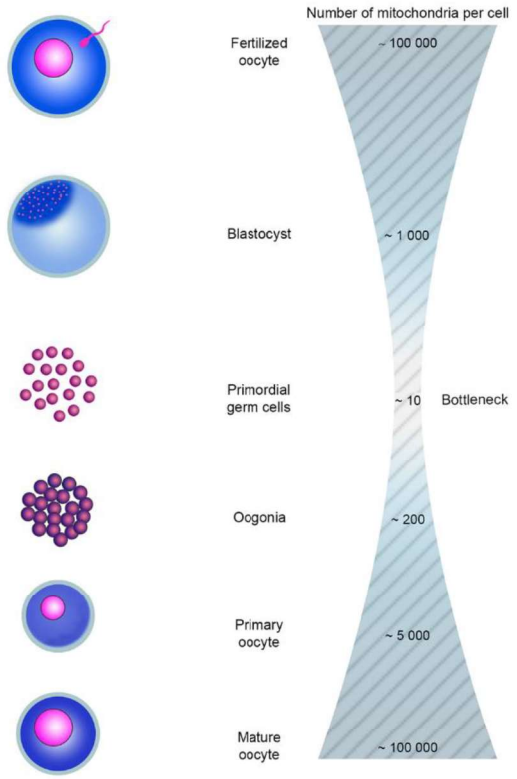


Figure I12. Mitochondrial Copy Number Change During Oogenesis.

Bottleneck effect happens during primodrial germ cells development. MtDNA copy number in various cell types (from primodrial germ cells to blastocyst) is shown. Adapted from Korchivaya, E. *et al.*, 2022.

1.4.2. mtDNA mutations and mitochondrial disorders

Mutations within the mitochondrial genome are responsible for a diverse range of neurodegenerative and neuromuscular disorders. These mutations can also be linked to various phenotypic expressions, including issues like infertility, reduced lifespan, coronary heart disease, early-onset Alzheimer's disease, and more (**Pipek, O. A. *et al.*, 2019**). The specific mitochondrial disease inheritance pattern is influenced by the origin of mitochondrial components. As a result, these diseases can be inherited through two primary mechanisms: autosomal inheritance,

characterized by mutations in nuclear DNA, and maternal inheritance, involving mutations in mtDNA.

To date, over 330 distinct mutations in human mtDNA have been discovered, each playing a role in the development of different diseases (**Nissanka N. & Moraes C. T., 2020**). It's important to note that this number continues to grow as more research is conducted in this field. Taken together, mtDNA pathogenic mutations affect 1 in 5000 individuals worldwide (**Gorman, G. S. *et al.*, 2015**). To date, these pathologies have not found adequate treatment (**Rahman J. & Rahman S., 2018**).

Mitochondrial diseases can arise not only from mutations in protein-coding genes but also from mutations in tRNA or ribosomal RNA genes, which can impact mitochondrial ATP production. **Figure I13** displays some of the most frequent and relatively well-studied mutations in human mtDNA (**DiMauro S. & Schon E. A., 2001**).

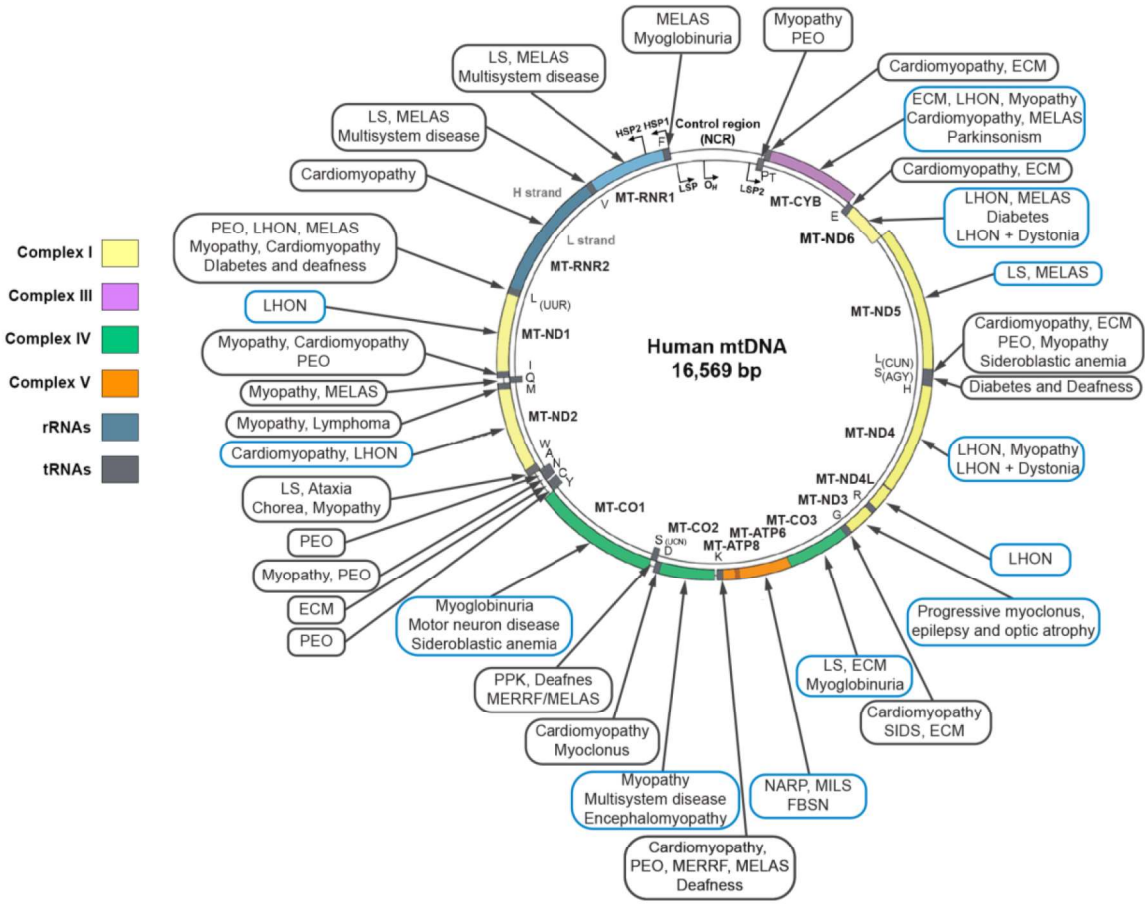


Figure I13. The Most Common Mutations in mtDNA Associated with Mitochondrial Diseases.

Diseases caused by mutations in mitochondrial ribosomal and tRNA genes are highlighted in black. Diseases associated with mutations in protein-coding mtDNA genes are shown in blue. Where, ECM - Encephalomyopathy; FBSN - Familial Bilateral Striatal Necrosis; LHON - Leber's Hereditary Optic Neuropathy; LS - Leigh Syndrome; MILS - Maternally Inherited Leigh Syndrome; MELAS - Mitochondrial Encephalomyopathy, Lactic Acidosis, Stroke-like Episodes; MERRF - Myoclonic Epilepsy with Ragged Red Fibers; NARP - Neuropathy, Ataxia, and Retinitis Pigmentosa; PEO - Progressive External Ophthalmoplegia; PPK - Palmoplantar Keratoderma; SIDS - Sudden Infant Death Syndrome. Adapted from DiMauro S. & Schon E. A., 2001.

With the development of sequencing techniques, identifying mtDNA polymorphisms became easier, yet linking these mutations to specific phenotypes remains challenging. Some clinical syndromes result from multiple point mutations at different mtDNA positions. For instance, Leber's hereditary optic neuropathy (LHON) is mainly caused by missense mutations at various positions in mtDNA, with varying levels of heteroplasmy (**Man P. Y. W., Turnbull D. M., Chinnery P. F., 2002**; **Kim J. Y., Hwang J. M., Park S. S., 2002**). LHON typically affects retinal ganglion layers and optic nerves and, surprisingly, exhibits gender predisposition, with more men experiencing visual acuity loss (50% against 10% for women) (**Man P. Y. W., Turnbull D. M., Chinnery P. F.,**

2002). This gender predisposition suggests additional genetic and environmental factors influencing LHON's expression.

Another example is the mt.8993T>G substitution in the ATP synthase gene. This mutation can lead to neuropathy, ataxia, and pigmentary retinopathy, known as NARP syndrome, or severe neurometabolic Leigh syndrome, depending on heteroplasmy levels, as mentioned previously (**Gorman, G. S. *et al.*, 2016**). Other mtDNA mutations like mt.4296G>A, mt.5523T>G, mt.5559A>G, mt.13513G>A, mt.13514A>G, mt.9191T>C, and mt.9478T>C are associated with Leigh syndrome but are rarer in the population compared to mt.8993T>G (**Moslemi, A. R. *et al.*, 2005**).

Mutations in genes involved in mitochondrial protein biosynthesis often cause myopathies and neurodegenerative disorders. The mt.8344A>G substitution in the lysine transfer RNA gene is the primary cause of myoclonic epilepsy with ragged muscle fibers (MERRF syndrome) (**Shoffner, J. M. *et al.*, 1990**), maternally inherited syndrome of diabetes mellitus and deafness (MIDD) (**Mancuso, M. *et al.*, 2014**), and progressive external ophthalmoplegia (PEO). The clinical manifestation depends on the predominance of mutant mtDNA copies, with more than 60% causing symptoms.

MELAS syndrome (mitochondrial encephalomyopathy, lactic acidosis, stroke-like episodes) is driven by point mutations in mtDNA, often affecting transfer RNAs (**Goto Y., Nonaka I., Horai S., 1990**). The mt.3243A>G mutation, for example, can result in various clinical phenotypes, including MELAS, MIDD, or combinations of these syndromes, depending on the level of heteroplasmy and other genetic, environmental, and epigenetic factors (**Nesbitt, V. *et al.*, 2013**).

The first identified mtDNA mutation was a large-scale "common" deletion, which has been linked to various diseases and accounts for approximately 12% of mitochondrial disorders in adults (**Nicolino, M. *et al.*, 1997**; **Gorman, G. S. *et al.*, 2016**). MtDNA deletions can vary in size from 1.8 to 8 kilobases and can occur anywhere in the mitochondrial genome, regardless of gene function and structure. To manifest pathological phenotype, the level of mutant mtDNA must reach at least 60%. Unlike point mutations, pathogenic mtDNA deletions often arise sporadically and are not inherited across generations (**Moraes, C. T. *et al.*, 1995**).

Furthermore, mtDNA deletions are typically flanked by short direct repeats, usually consisting of 3 to 13 nucleotides (**Samuels D. C., Schon E. A., Chinnery P. F., 2004**). However, recent research has shown that the presence of such repeats does not guarantee deletion formation.

Instead, the structure of mtDNA, specifically the contact zone within secondary structure, plays a critical role in deletion formation and facilitates it (**Shamanskiy, V. *et al.*, 2023**).

Additionally, the occurrence of mtDNA deletions was found to be associated with inherited mutations in nuclear genes whose products are involved in mtDNA maintenance and replication, such as Poly and Twinkle (**Tuppen, H. A. L. *et al.*, 2010**). Recent studies exploring mtDNA replication and repair mechanisms revealed that deletions can result from replication fork slippage, the joining of mtDNA double-strand breaks through microhomology, or a combination of these factors (**Phillips, A. F. *et al.*, 2017**).

The predominant theory regarding the propagation of mtDNA deletions suggests clonal expansion, driven by the faster replication of WT mtDNA molecules (**Diaz, F. *et al.*, 2002**; **Trifunov, S. *et al.*, 2018**). However, a study conducted by Gitschlang *et al.* investigated the potential replicative advantage of deleted mtDNA molecules, owing to their shorter length, but failed to find any evidence supporting this phenomenon in *C. elegans* (**Gitschlag, B. L. *et al.*, 2016**). Likewise, another study that examined the same issue in human skeletal muscle also reported no significant differences in the rate of clonal expansion among mtDNA deletions of different sizes (**Campbell, G. *et al.*, 2014**).

mtDNA deletions can cause syndromes like Kearns-Sayre syndrome (KSS), Pearson syndrome (PS), and progressive external ophthalmoplegia (CPEO) (**Holt I. J., Harding A. E., Morgan-Hughes J. A., 1988**). A common 4977 bp deletion can lead to all these syndromes (**Tuppen, H. A. L. *et al.*, 2010**). Pearson syndrome typically exhibits high mutant mtDNA levels in various tissues, often leading to early childhood death (**Lee, H. F. *et al.*, 2007**). When heteroplasmy levels exceed the threshold in adolescence, Kearns-Sayre syndrome may develop, characterized by muscle weakness and eye muscle paralysis (**Zeviani, M. *et al.*, 1988**). Chronic progressive external ophthalmoplegia has no specific onset age, making it challenging to distinguish it from other mitochondrial disorders (**Holt I. J., Harding A. E., Morgan-Hughes J. A., 1988**). Additionally, the accumulation of mtDNA deletions is a phenomenon observed in postmitotic tissues during the normal aging process (**Bender, A. *et al.*, 2006**). However, it becomes most pronounced in specific tissues such as the cerebral cortex and the basal ganglion of the brain, which are known to be affected by Alzheimer's disease and Parkinson's disease (**Bender, A. *et al.*, 2006**; **Wei Soong, N. *et al.*, 1992**).

1.5. Therapeutic strategies for mitochondrial disorders

Despite the substantial advancements in the field of mitochondrial biology and the continuous unravelling of molecular mechanisms underlying mitochondrial diseases, there is still a lack of effective treatments for patients affected by these conditions. Nonetheless, there is a vigorous pursuit of therapies for mitochondrial diseases, resulting in the development of various strategies aimed at preventing their transmission or reversing their effects.

1.5.1. Standard therapeutical treatment

The treatment of mitochondrial diseases remains largely anecdotal, primarily due to a limited evidence base and the absence of data from randomized trials (**Soldatov, V. O. *et al.*, 2022**). Among the prescribed treatments, many are categorized as medical foods (**Avula, S. *et al.*, 2014**). These interventions predominantly revolve around vitamin and cofactor-based mitochondrial therapies, aiming to enhance critical enzymatic reactions, mitigate oxidative stress, and eliminate toxic acyl-coenzyme A molecules that accumulate in mitochondrial diseases.

Additionally, patients are advised to make dietary and lifestyle adjustments (**Bough, K. J. *et al.*, 2006**). However, it's important to note that only small groups of patients respond positively to these treatments. This is because metabolic therapy methods are generally ineffective due to their lack of specificity, limited impact on mitochondria, and insufficient alignment with the underlying disease mechanisms.

1.5.2. Mitochondrial replacement therapy

Assisted reproductive techniques (ART) aimed at reducing or preventing the transmission of harmful mtDNA mutations (**Kirillova A., Mazunin I., 2022**). Initially, a method involving the microinjection of healthy mitochondria from a donor cytoplasm into recipient oocytes was introduced (**Cohen, J. *et al.*, 1997**). However, this technique was subsequently banned due to safety concerns. A modified version of this approach, known as mitochondrial replacement therapy (MRT) or cytoplasmic replacement therapy (CRT), has been developed to prevent the inheritance of mutant mtDNA (**Kang, E. *et al.*, 2016**). To date, MRT has received official approval only in the UK (2015) and in Australia (2022), strictly for the prevention of mitochondrial diseases (**Kirillova A., Mazunin I., 2022**).

MRT involves transferring the mother's genetic material into an enucleated oocyte obtained from a healthy donor. Currently, there are four main methods for performing MRT: maternal spindle transfer at metaphase II (**Zhang, J. *et al.*, 2017**), pronuclear transfer to an enucleated donor

zygote (**Hyslop, L. A. *et al.*, 2016**), 1st or 2nd polar body transfer, which involves transferring either the 1st polar body into the MII cytoplast before fertilization or the 2nd polar body into an enucleated zygote while removing one maternal pronucleus (**Wang, T. *et al.*, 2014**) (**Figure I14**). Extensive studies indicated that transferring an embryo with a low level of heteroplasmy is safe (**Zhang, J. *et al.*, 2017**). However, there remains a risk of heteroplasmy drift towards mutant mtDNA in subsequent generations or with age. It was observed that 15% of human embryonic stem cell lines derived from embryos following MRT exhibited a complete restoration of the mutant mtDNA pool (**Kang, E. *et al.*, 2016**). Such a phenomenon was named mtDNA carryover.

Recent research introduced a novel intriguing method for targeted elimination of maternal mtDNA through forced mitophagy in order to fight mtDNA carryover (**Fan, X. Y. *et al.*, 2022**). This technique involves labelling maternal mitochondria with an autophagy receptor in order to induce targeted mitophagy. As a result, a significant proportion of human blastocysts (77%) did not carry maternal mtDNA, and the average mtDNA heteroplasmy was greatly reduced (0,09%).

Despite the risks and limitations associated with MRT, it currently represents the only option for parents with high heteroplasmic or homoplasmic mtDNA mutations to give birth to a genetically related, healthy child. Future technologies that will solve mtDNA carryover problems will greatly improve the technique.

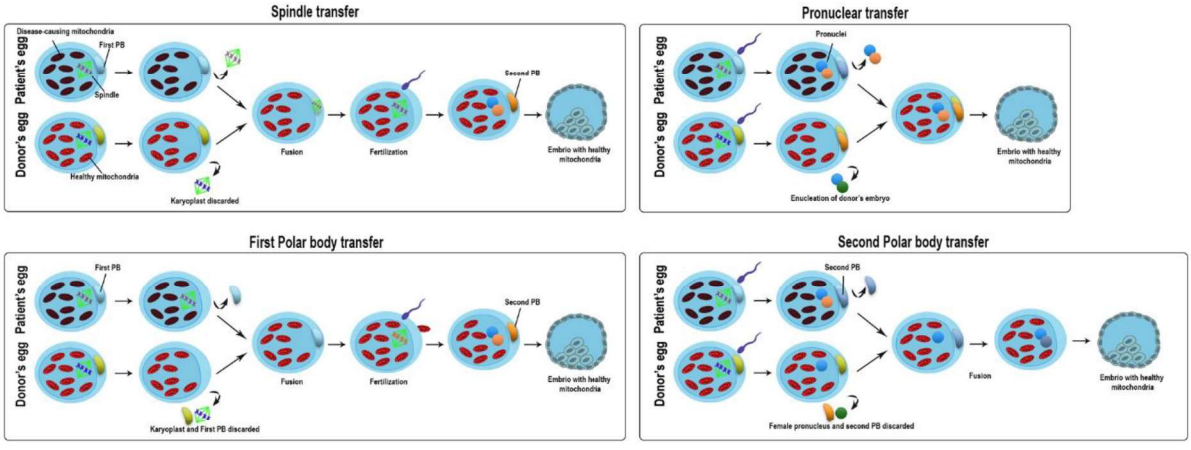


Figure I14. Mitochondrial Replacement Therapy Techniques.

Adapted from Korchivaya, E. *et al.*, 2022.

1.5.3. Allotopic strategy

The allotopic strategy involves inserting a healthy version of a defective mitochondrial gene into the nuclear genome and guiding the RNA or protein produced by that gene into the mitochondria using specific signals.

The strategy was first attempted in yeast in 1988, when the gene encoding the MT-ATP8 subunit coupled with the MTS of the ATPase subunit 9 from *Neurospora crassa* was inserted into the nuclear genome of this organism carrying a mutation in the mitochondrial MT-ATP8 gene (**Nagley P., Devenish R. J., 1989**). However, in humans, the system faced challenges since imported protein was not assembling into a functional ATPase complex (**Bokori-Brown M., Holt I. J, 2006**).

Only in 2016, stable allotopic expression of the MT-ATP8 and MT-ATP6 genes bearing MTS from the ATP5G1 subunit, allowed their integration into complex V, restoring ATP production (**Boominathan, A. *et al.*, 2016**).

Another strategy, based on the use of mitochondrially targeted adeno-associated viruses (AAV) was shown to be effective in the mitochondrial transfer of mutant human ND6 gene in murine mitochondria (**Yu, H. *et al.*, 2020**).

Many mtDNA mutations affect tRNA genes, disrupting mitochondrial protein synthesis and causing respiratory issues. In the team, an allotopic strategy using *S. cerevisiae* $tRNA^{Lys}$, which can be imported into mitochondria, was developed. This approach was successful in cells with the A8344G mutation linked to MERRF syndrome (**Kolesnikova, O. A. *et al.*, 2004**) and the A3243G mutation associated with MELAS syndrome (**Karicheva, O. Z. *et al.*, 2011**). Allotopic expression of modified $tRNA^{Lys}$ derivatives holds promise for addressing mutations in mitochondrial tRNA genes.

Another strategy of direct targeting of therapeutic molecules is "MITO-Porter". It is a technique employing liposomes for cargo delivery directly into mitochondria via membrane fusion. MITO-Porter consists of high-density specifically modified liposomes that efficiently escape macropinosomes to enter the cytosol while preserving cargo integrity. Following release from macropinosomes, MITO-Porter binds to the mitochondrial membrane through electrostatic interactions, promoting fusion with the mitochondrion. This approach showed promise in transferring of RNA and proteins into mitochondria (**Yamada Y., Harashima H., 2017**). The obvious limitation of this approach is a tremendously complicated process of synthesis of "MITO-Porter" carriers.

Overall, allotopic strategies offer potential solutions for mitochondrial diseases, but their success depends on various factors, including the nature of the targeted proteins and the specific mutations involved.

1.5.4. Anti-replicative strategy

One potential strategy to reduce mtDNA heteroplasmy level involves the targeted inhibition of mutant mtDNA replication. This approach was initially explored *in vitro* using peptide nucleic acids (PNAs) (**Taylor, R. W. *et al.*, 1997**). PNAs are synthetic analogs of oligonucleotides that replace the sugar-phosphate backbone with a pseudopeptide consisting of N-(2-aminoethyl)-glycine. This unique structure of PNAs demonstrates increased resistance to degradation by nucleases and proteases (**Demidov, V. V. *et al.*, 1994**) and allows for specific modifications enabling their targeted delivery into the mitochondrial matrix (**Chinnery, P. F. *et al.*, 1999**; **Muratovska, A. *et al.*, 2001**). PNAs also exhibit a higher affinity for binding to complementary single-stranded DNA compared to regular DNA (**Egholm, M. *et al.*, 1993**), and PNA:DNA duplexes with single-nucleotide mismatches are more stable than their DNA:DNA counterparts (**Orum, H. *et al.*, 1993**). In an *in vitro* replication experiment conducted under physiological conditions, it was demonstrated that PNAs can selectively hinder the replication of single-stranded mtDNA templates containing deletions or single-nucleotide mutations (**Taylor, R. W. *et al.*, 1997**). However, this promising outcome was not replicated in cell culture or isolated mitochondria. Despite successful import into the mitochondrial matrix, PNAs failed to inhibit the replication of mutant mtDNA (**Chinnery, P. F. *et al.*, 1999**; **Muratovska A. *et al.*, 2001**). This could be attributed to the ineffective binding of PNAs to mtDNA within the mitochondrial matrix or the displacement of PNAs bound to mtDNA during its transcription or replication. Currently, PNAs are non-suitable for reducing heteroplasmy level. Additional researches are required to identify modifications to PNA structure that enhance their binding efficiency to the target DNA sequence in living cells.

Another analogous approach to shift mutant mtDNA heteroplasmy level was implemented by several groups, including ours. A new anti-replicative strategy consisted of using short RNA molecules containing sequences complementary to target mtDNA in order to selectively inhibit its replication. To facilitate mitochondrial import, known import determinants such as F- and D-hairpin structures from yeast transfer RNA ($tRNA^{Lys}_{CUU}$) or α and γ domains of human 5S ribosomal RNA were incorporated into the structure of anti-replicative RNAs. Previous studies demonstrated that these structures were efficient in facilitating the import of RNA molecules into mitochondria (**Entelis, N. S. *et al.*, 2001**; **Smirnov, A. *et al.*, 2008**; **Kolesnikova, O. *et al.*, 2010**). The proposed

mechanism of action for anti-replicative RNAs is related to the inability of the helicase in the mitochondrial replisome to displace RNA in short RNA-DNA duplexes (**Bowmaker, M. *et al.*, 2003**). This approach was found to specifically reduce heteroplasmy levels in cybrid cell cultures affected by Kearns–Sayre syndrome with a large deletion (**Comte C. *et al.*, 2013**; **Loutre R. *et al.*, 2018**) and the pathogenic point mutation mt.13514A>G in the MT-ND5 gene (**Tonin, Y. *et al.*, 2014**; **Dovydenko, I. *et al.*, 2014**). This anti-replicative strategy based on RNAs definitely demonstrated more promise compared to PNAs.

1.5.5. Anti-genomic approaches

An alternative strategy for decreasing mutant mtDNA heteroplasmy levels involves the targeted removal of pathogenic mtDNA variants. Given the multiple copies of the mitochondrial genome, the existence of mechanisms for maintaining mtDNA copy numbers and the absence of efficient mechanisms for double-stranded breaks repair within mitochondria (**Moretton, A. *et al.*, 2017**), a promising approach to eliminate mutant mtDNA can consist in targeting of such molecules and introducing a double-stranded break. Following the introduction of such a break, linear mtDNA molecules will be rapidly degraded by components of the mitochondrial replication machinery, including mtDNA polymerase γ, DNA helicase Twinkle, and exonuclease MGME1 (**Peeva, V. *et al.*, 2018**). This degradation process will result in a shift of heteroplasmy (**Figure I15, upper panel**).

Various nucleases can be employed to create double-stranded breaks in DNA. Given that most proteins essential for mitochondrial function are encoded by nuclear DNA, evolution has established effective mechanisms for importing proteins into mitochondria through the TOM/TIM complexes (**Verechshagina, N. A. *et al.*, 2018**). Importantly, the fusion of a peptide corresponding to the mitochondrial targeting sequence (MTS) at the N-terminus of a protein was shown to facilitate its import into mitochondria (**Schmidt O., Pfanner N., Meisinger C., 2010**). Consequently, by incorporating an MTS into an enzyme with the ability to specifically recognize mutant mtDNA and induce a double-stranded break, it becomes feasible to reduce the mutant mtDNA heteroplasmy level. This principle underpins nearly all attempts aimed at developing tools for the targeted removal of pathogenic mtDNA, and, to date, such anti-genomic approaches hold great promise in treating diseases arising from mutations in mitochondrial DNA.

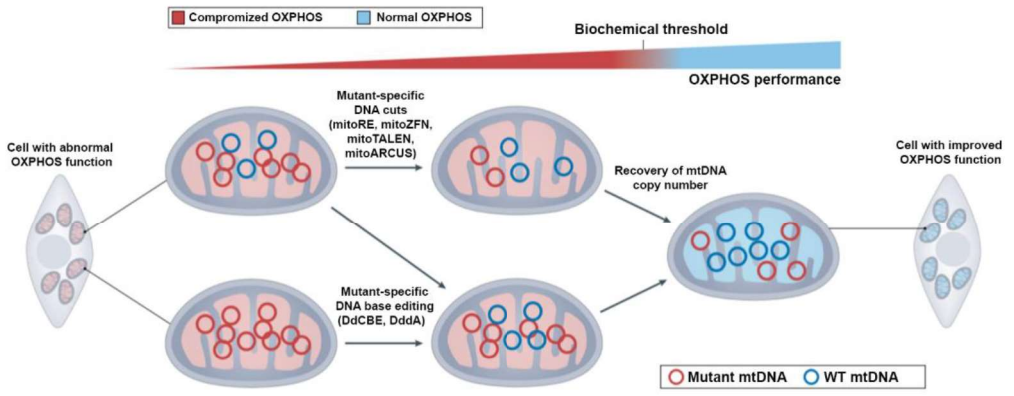


Figure I15. Two Therapeutic Strategies to Shift mtDNA Heteroplasmy Level.

The first strategy (upper panel) consists of introducing a double-stranded break in mutant mtDNA molecules to promote its degradation by using mitochondrial-targeted endonucleases such as restriction endonucleases(mitoREs), zinc-finger nucleases (mitoZFNs), transcription activator-like effector nucleases (mitoTALENs), ARCUS (mitoARCUS). The second strategy (lower panel) consists of reversing mtDNA mutations using base editors technics based on cytosine deaminase (DdCBE) and deoxyadenosine deaminase (DddA). Adapted from Silva-Pinheiro P. & Minczuk M., 2022. Adapted from Silva-Pinheiro P. & Minczuk M., 2022.

Various mitochondria-targeted nucleases have been developed to degrade mutant mtDNA and adjust heteroplasmy ratios (**Figure I15, upper panel** and **Figure I16**). Mitochondria-targeted restriction endonucleases (mitoREs) (**Figure I16A**), both native and artificial ones (mitoARCUS) (**Figure I16B**), have been successfully used to reduce mutant mtDNA levels in human cultured cells and mouse models (**Tanaka M. *et al.*, 2002**; **Srivastava S. & Moraes C. T., 2005**; **Alexeyev M. F. *et al.*, 2008**; **Zekonyte U. *et al.*, 2021**). However, such systems are highly limited by the occurrence of unique recognition sites, allowing targeting of specific pathogenic mutations in mtDNA. Additionally, the development of artificial nucleases demands significant time and resources.

The mitoREs limitations were addressed by creating nucleases that are able to target various sites in mtDNA by specific DNA recognition modules - zinc-finger proteins for mitoZFNs and TALE proteins for mitoTALENs (**Figure I16B & C**). These nucleases are typically composed of three essential components fused into a single protein: a mitochondrial localization signal, DNA-binding domains, and nuclease domains (**Bacman, S. R. *et al.*, 2013**; **Gammage, P. A. *et al.*, 2014**). For the mitochondrial localization signal, similar to modified restriction enzymes, targeting sequences derived from naturally imported mitochondrial proteins are employed (**Chin, R. M. *et al.*, 2018**). The nuclease domain corresponds to the FokI nuclease, which introduces a double-strand break into DNA without specific sequence requirements (**Hiroyuki S. & Susumu K., 1981**).

To achieve specific targeting of different regions in mtDNA, two distinct DNA-binding domains are used. MitoZFNs employ the DNA-binding domain of the zinc finger type (**Gammage, P. A. *et al.*, 2014**) (**Figure I16C**). It's worth noting that the DNA-binding domains of the zinc finger type are commonly found in transcription factors (**Ravasi, T. *et al.*, 2003**), usually bearing a nuclear localization signal (**Macara I. G., 2001**). To enable efficient import of mtZFNs into mitochondria and reduce the risk of non-specific cleavage of nuclear DNA, this nuclear localization signal must be exchanged for nuclear export signal (NES) (**Gammage, P. A. *et al.*, 2014**) (**Figure I16C**). For mitoTALENs, the DNA-binding domain is derived from the bacterial transcription activator-like effector (TALE) protein (**Bacman, S. R. *et al.*, 2013**) (**Figure I16D**).

To date, these tools have demonstrated success in shifting the level of heteroplasmy, involving point mutations and mtDNA deletions in cybrid cells and mouse models (**Minczuk M. *et al.*, 2008**; **Bacman, S. R. *et al.*, 2013**; **Gammage, P. A. *et al.*, 2014**; **Hashimoto M. *et al.*, 2015**; **Reddy P. *et al.*, 2015**; **Bacman, S. R. *et al.*, 2018**; **Gammage, P. A. *et al.*, 2018**; **Yang Y. *et al.*, 2018**; **Pereira C. V. *et al.*, 2018**).

Although strategies based on mitoZFNs and mitoTALENs show promise for mtDNA targeting, they still have limitations. Designing and engineering monomers for specific mtDNA recognition is a challenging and resource-consuming task. Additionally, for both mtZFNs and mitoTALENS, there's a need to experimentally validate each combination of modules to create a DNA-binding domain that can specifically and efficiently bind to the target DNA sequence. Moreover, the large size of protein-coding sequences exceeds the capacity of current virus-based delivery systems, such as AAV (**Mingozzi F. & High K. A., 2011**; **Moraes C. T., 2014**).

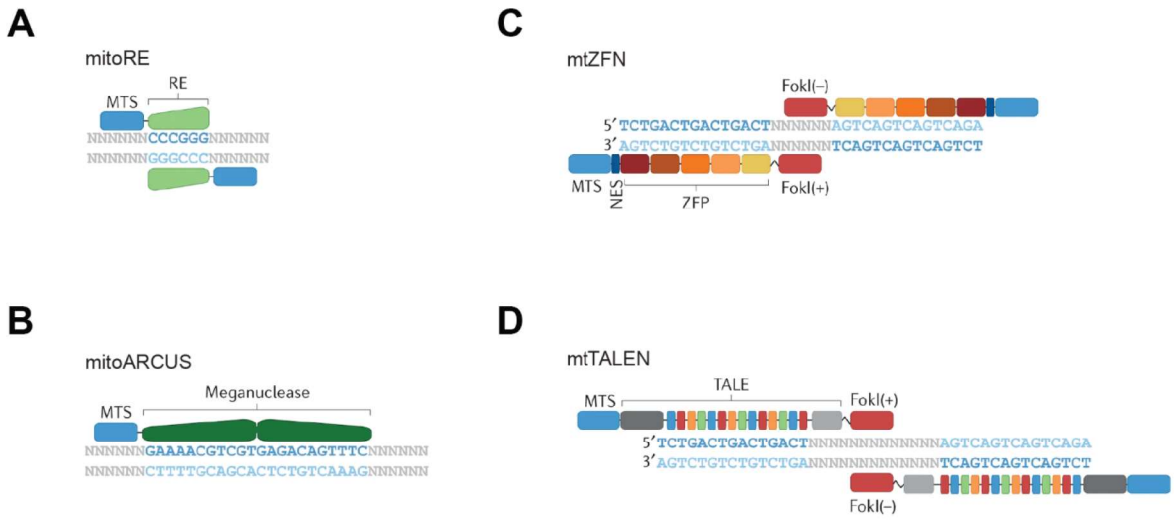


Figure I16. Various Nucleases are Used for Mutant mtDNA Targeting.

(A) mitoREs are enzymes that bind to and cleave mtDNA at a specific, but short recognition sequence.
(B) Mega nuclease, mitoARCUS, consists of two monomer domains and cleaves mtDNA at the specific recognition site, bigger than for REs.
(C) mitoZFNs consist of two monomers, each comprised of DNA recognition elements (one recognition domain for three nucleotides), and split FokI nuclease. When two FokI monomers are sufficiently close together they will dimerize and cleave the mtDNA.
(D) mitoTALENs consist of two monomers, each comprised of DNA recognition elements (one recognition domain for each nucleotide), and split FokI nuclease. When two FokI monomers are sufficiently close together they will dimerize and cleave the mtDNA. All the systems contain mitochondrial targeting signal (MTS); ZFNs additionally possess nuclear export signal (NES).
Adapted from Silva-Pinheiro P. & Minczuk M., 2022.

A more comprehensive exploration of the application of mitochondrially targeted REs, ZFNs and mitoTALENs in mitochondrial DNA manipulation, along with insights into future prospects, can be found in a review article, where I am a co-author (**Publication 1**).

Publication 1

Mitochondrial DNA Part A, 2019:

Future of human mitochondrial DNA editing technologies

Natalya Verechshagina[1], Natalia Nikitchina[1], Y. Yamada[2], H. Harashima[2], Masashi Tanaka[3,4], Konstantin Orishchenko[5], Ilya Mazunin[1,*]

[1] Laboratory of Molecular Genetics Technologies, Immanuel Kant Baltic Federal University, Kaliningrad, Russia
[2] Faculty of Pharmaceutical Sciences, Laboratory for Molecular Design of Pharmaceutics, Hokkaido University, Sapporo, Japan
[3] Department for Health and Longevity Research, National Institutes of Biomedical Innovation, Health and Nutrition, Ibaraki City, Osaka, Japan
[4] Department of Neurology, Juntendo University Graduate School of Medicine, Tokyo, Japan
[5] Laboratory of Cell Technologies, Institute of Cytology and Genetics SB RAS, Novosibirsk, Russia

MITOCHONDRIAL DNA PART A
https://doi.org/10.1080/24701394.2018.1472773

Taylor & Francis
Taylor & Francis Group

RESEARCH ARTICLE

Check for updates

Future of human mitochondrial DNA editing technologies

N. Verechshagina[a], N. Nikitchina[a], Y. Yamada[b], H. Harashima[b], M. Tanaka[c,d], K. Orishchenko[a,e] and I. Mazunin[a]

[a]Laboratory of Molecular Genetics Technologies, Immanuel Kant Baltic Federal University, Kaliningrad, Russia; [b]Faculty of Pharmaceutical Sciences, Laboratory for Molecular Design of Pharmaceutics, Hokkaido University, Sapporo, Japan; [c]Department for Health and Longevity Research, National Institutes of Biomedical Innovation, Health and Nutrition, Ibaraki City, Osaka, Japan; [d]Department of Neurology, Juntendo University Graduate School of Medicine, Tokyo, Japan; [e]Laboratory of Cell Technologies, Institute of Cytology and Genetics SB RAS, Novosibirsk, Russia

ABSTRACT

ATP and other metabolites, which are necessary for the development, maintenance, and functioning of bodily cells are all synthesized in the mitochondria. Multiple copies of the genome, present within the mitochondria, together with its maternal inheritance, determine the clinical manifestation and spreading of mutations in mitochondrial DNA (mtDNA). The main obstacle in the way of thorough understanding of mitochondrial biology and the development of gene therapy methods for mitochondrial diseases is the absence of systems that allow to directly change mtDNA sequence. Here, we discuss existing methods of manipulating the level of mtDNA heteroplasmy, as well as the latest systems, that could be used in the future as tools for human mitochondrial genome editing.

ARTICLE HISTORY
Received 4 April 2018
Accepted 28 April 2018

KEYWORDS
mitoRGEN; SpCas9; AsCpf1; mitoTALE; mitoRetron

Introduction

Human mitochondrial genome is a circular double-stranded string of DNA (mtDNA), which encodes two rRNAs, 22 tRNAs, and 11 protein-coding mRNAs, which are translated in the organelle matrix with the help of mitochondrial ribosomes into 13 functional subunits that constitute the oxidative phosphorylation system (Hällberg and Larsson 2014; Gustafsson et al. 2016). In addition to the generally described 37 genes mtDNA can code for two peptides: humanin (Hashimoto et al. 2001) and MOTS-c (Lee et al. 2016). Mutations in the mitochondrial genome are associated with both inherited disorders and aging (Khrapko and Turnbull 2014; Craven et al. 2017). The only hitherto described approaches for human mtDNA mutation elimination in cell lines use site-specific nucleases (Pereira and Moraes 2017). Recent ones include mitochondria-targeted restriction endonucleases (mitoREs), mitochondria-targeted zinc-fingers (mitoZFNs), and mitochondria-targeted TALENs (mitoTALENs). All these approaches are based on specific protein–nucleic acid interactions to cut out target mtDNA. Systems such as RNA-guided endonucleases (RGENs) (Jinek et al. 2012; Zetsche et al. 2015) or Retron (Lampson et al. 2005; Farzadfard and Lu 2014) seem to be more flexible and offer perspective due to their reliance on Watson–Crick interactions for specific mtDNA site recognition. State-of-the-art base editing systems, that do not cleave DNA (Komor et al. 2016; Gaudelli et al. 2017; Komor et al. 2017) also may be used to correct DNA mutations. The limitation on the ubiquitous use of these systems is their two-component nature: both RGENs and Retron systems include protein and RNA parts. Successful delivery of RNA moieties into mitochondria is very complicated, but there is experimental proof (Gammage et al. 2017; Kim et al. 2017). Moreover, homology-directed repair (HDR) relies on donor DNA as a homologous repair template.

The present article is the authors' opinion on the problems of human mtDNA editing technologies. The first part describes current techniques for manipulating mtDNA, which are limited to heteroplasmy level manipulation. Second part is about the newest approaches to augmenting mtDNA, that are being developed in several labs, including ours. Some ideas had already been presented in conference talks and are used in manuscript preparation. Others are hypothetical systems, that we are going to signify with an asterisk (*). But they had already been partially implemented by us, and will be finished and usable in the nearest future.

Molecular machines that use specific protein–nucleic acid interactions

This part describes the protein machinery, that recognizes and eliminates particular mtDNA haplotypes (Figure 1). Expanded field of molecular approaches to suppress mtDNA mutations includes the delivery of a correct gene product into mitochondria (protein or RNA) or blocking the mutant mtDNA replication process (Patrushev et al. 2014; Patananan et al. 2016). So again, here we are interested only in technologies that physically affect the constitution of the mitochondrial genetic code.

CONTACT I. Mazunin IMazunin@kantiana.ru Laboratory of Molecular Genetics Technologies, Immanuel Kant Baltic Federal University, Universitetskaya 2 St., Kaliningrad, Russian

© 2018 Informa UK Limited, trading as Taylor & Francis Group

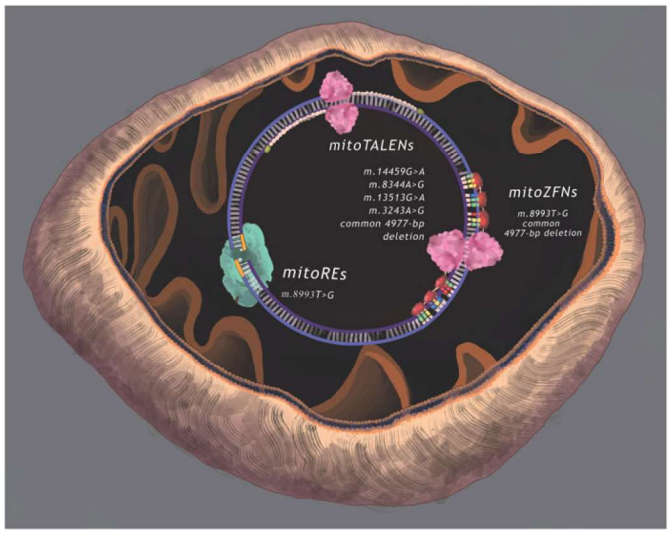


Figure 1. Currently used mitochondria-targeted nucleases. Mitochondria-targeted restriction endonucleases (mitoREs), mitochondria-targeted zinc-fingers (mitoZFNs), and mitochondria-targeted TALENs (mitoTALENs).

Mitochondria-targeted restriction endonucleases

For the first time, evidence of targeted manipulation of human mtDNA was published by Dr. Moraes from University of Miami (Srivastava and Moraes 2001). His team used a genetic construct, that encodes a codon-optimized version of the human restriction endonuclease *PstI*, fused with the mitochondrial target signal (MTS) from human *COX8A* gene. Human mtDNA has two sites for *PstI*, so Dr. Moraes was going to detect the deleted mtDNA and study the process of recombination inside the mitochondrion. However, the import of *PstI* was leading to mtDNA degradation – probably by internal mitochondrial exonucleases. Moreover, authors failed to register the ligation of compatible ends. The same result was published by another group, 15 years later, using the same modified restriction endonuclease (Moretton et al. 2017). It was concluded, that fast-dividing cells do not retain deleted mtDNA. Deleted mtDNA after *PstI* treatment was detected only in animal models, in the mitochondria of post mitotic cells (Srivastava and Moraes 2005; Fukui and Moraes 2008). Pathogenic mutation m.8993T > G creates a unique restriction site for *SmaI*. To level down mutant heteroplasmy in a cybrid cell line, Dr. Tanaka used mitochondrially modified *SmaI*. Interesting that up to five rounds of transfection are required to reliably shift down the mutant mtDNA haplotype (Tanaka et al. 2002). The last experiment in this field was done by Dr. Alexeyev using an isoschizomer – *XmaI* (Alexeyev et al. 2008). According to our knowledge, these are the only mitoREs. The absence of other examples is linked with the rarity of occurrence of unique recognition sites for mitoREs, that require a specific pathogenic mutation in mtDNA to occur.

Mitochondria-targeted zinc-fingers

The solution to the mitoREs problem is the creation of nucleases that would get imported into the mitochondria and specifically bind to a particular DNA haplotype. Pioneering work in the area was done in Dr. Minczuk's lab, when the mitoZFNs were imported into human cell mitochondria (Minczuk et al. 2006). It has been shown that a zinc-finger nuclease, fused to an MTS as well as a methyltransferase DNMT3a, is capable of selectively modifying the m.8993T > G site, halting the replication process of mutant mtDNA. The next generation of MitoZFNs specifically eliminated m.8993T > G mtDNA but was toxic to cells (Minczuk et al. 2008, 2010). Further modifications of the MitoZFNs system increased the specificity of recognition of mutant mtDNA and reduced toxicity (Gammage et al. 2016). In addition to m.8993T > G mtDNA haplotype elimination, the MitoZFNs system was used to shift down the common 4977-bp deletion heteroplasmy level (Gammage et al. 2014).

Mitochondria-targeted TALENs

Another example of a site-specific nuclease is the mitochondrially modified TAL-effector nuclease. For the first time, Dr. Moraes's group modified the TALEN system (Cermak et al. 2011) for effective import into the mitochondria to shift down the heteroplasmy level for m.14459G > A and common 4977-bp deletion (Bacman et al. 2013). In another research Dr. Moraes's group carried out successful experiments to shift down the heteroplasmy level for two other mtDNA mutations: m.8344A > G and m.13513G > A (Hashimoto et al. 2015). The developed approach was transferred to a mouse model, where it was also successful (Reddy et al. 2015). Using

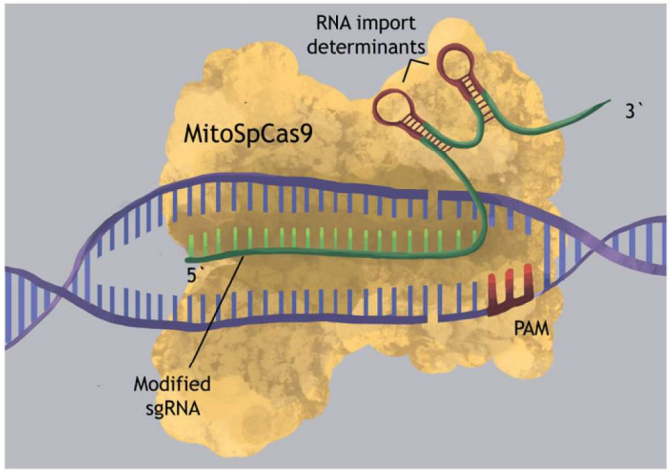


Figure 2. mitoRGEN/SpCas9. The nuclease is modified by mitochondrial target signal. Guid RNA is modified by RNA import determinant (at the moment there are four determinants for RNA import into human mitochondria: MRP, RP, HD and HF). The hairpins are inside of guide RNA scaffold structures: the tetraloop and stem loop 2, respectively.

the mitoTALEN system, it was shown by another group that double strand breaks in mtDNA result in a common 4977-bp deletion (Phillips et al. 2017). MitoTALENs system was used to shift down a high proportion of m.3243A > G mtDNA mutations in MELAS-iPSCs (Yang et al. 2018).

Molecular machines that use Watson–Crick interactions for specific mtDNA site recognition

As previously mentioned, two-component protein–RNA systems, such as RGENs and Retron, are more flexible for DNA recognition experiments than protein-only systems. On the one hand, they can be used as means of changing the recognition DNA site quicker, due to the big protein constituent remaining the same (for instance, Cas9 protein in RGEN/Cas9 system). On the other hand, the two-component system requires assembly into a functional machine inside the cell, and in our case – inside the mitochondria. It means that every time both the protein and the RNA-part of system should be delivered directly inside the mitochondria. Moreover, to edit the sequence of mtDNA we have to import a DNA fragment as a template for homologous recombination.

MitoRGEN/SpCas9

Everybody who works in genome engineering knows the RGEN/Cas9 system as the mainstream tool for editing the nuclear genomes of various organisms (Jinek et al. 2012; Jiang and Doudna 2017; Komor et al. 2017). To date, there is only one publication describing mitochondrial application of the RGEN/Cas9 system (Jo et al. 2015). It should be noted, that the results of some experiments, concerning SpCas9 delivery we failed to reproduce in our laboratories (Orishchenko et al. 2016). The absence of mitoRGEN systems is heated up by the periodic release of publications, speculating, why the system is still not available and whether it is possible to create it (Bacman et al. 2014; Hashimoto et al. 2015; Patananan et al. 2016; Craven et al. 2017; Chicherin et al. 2017; Gammage et al. 2017; Pereira and Moraes 2017).

Due to the two-component nature of RGEN/Cas9 system we think, both of them should be modified for effective import and assembly into a functional Cas9–gRNA complex inside of mitochondria (Figure 2). We have shown that, when modified with an MTS, SpCas9 (MitoCas9) can be effectively imported into the mitochondria of human cells (Orishchenko et al. 2016). Also, we have recently modified gRNA to import into mitochondria where in complex with MitoCas9 it had digested mtDNA (Verechshagina et al. 2017). Let us look at the structure of the modified gRNA more closely. It was previously observed, that the tetraloop and stem loop 2 of gRNA protrude outside of the Cas9–gRNA ribonucleoprotein complex, with the distal 4-bp of each stem is completely free of interactions with Cas9 amino acid side chains (Nishimasu et al. 2014). In Zhang's group, there was selected a minimal hairpin aptamer, which selectively binds dimerized MS2 bacteriophage coat proteins; it was appended to the sgRNA tetraloop and stem loop 2 to see if it could mediate transcriptional upregulation (Konermann et al. 2015). It is obvious that we could interchange the aptamer with any other hairpin structure. At the moment, there are four determinants for RNA import into human mitochondria: MRP and RP (Wang et al. 2010, 2015), HD and HF (Tonin et al. 2014; Dovydenko et al. 2015). As we have thought, the substitutions in the tetraloop and the stem loop 2 regions of the gRNA sequence do not affect Cas9 catalytic function *in vitro*. We found that only substitution of 4-bp in the tetraloop region of the gRNA by HF hairpin effectively imports the gRNA-HF into the mitochondria, where the complex mitoCas9–gRNA-HF cuts mtDNA. In

future experiments we are going to replace both the tetraloop and the stem loop 2 regions of the gRNA sequence simultaneously.

We have presented mitoRGEN/SpCas9 system as proof-of-concept solution. Further replacement of 20-bp of target-specific sequence in the gRNA-HF plasmid vector will allow the MitoCas9–gRNA-HF complex to eliminate other pathogenic mtDNA mutations. However, having changed target site for gRNA-HF let us not forget about the specificity of the system. In particular, m.3243A>**G** and m.8993T>**G** mutations create an N**G**G sequence in mtDNA that acts as a PAM site for SpCas9. It was found that a PAM sequence is critical for further DNA melting and the formation of a hybrid RNA–DNA duplex, as well as the conformational changes of the Cas9 nuclease (Anders et al. 2014; Palermo et al. 2017). Obviously, in that case, mitoRGEN/SpCas9 should eliminate only the mutant haplotype.

Previously described approaches all have the aim to shift down mtDNA copy number or shift mutant mtDNA heteroplasmy level – those are not really DNA editing technologies per se. But why are there still no human mtDNA editing technologies? One plausible reason for that is the peculiarity of the mitochondrial genome metabolism: to edit mtDNA we have to activate repair or/and recombination systems functionality – both still poorly understood (Kazak et al. 2012). There are experiments which demonstrate that double-strand breaks are not repaired, but rather broken mtDNA is eliminated, probably by mitochondrial nucleases (Moretton et al. 2017).

*MitoRGEN/AsCpf1**

Cpf1 is an alternative gene editing system for AT-rich sequences, that generates staggered ends in its PAM-distal target site (Zetsche et al. 2015; Yamano et al. 2016). As previously mentioned, in post-mitotic cell after *Pst*I treatment the resulting complementary sticky ends can be joined, forming a deletion in mtDNA (Srivastava and Moraes 2005; Fukui and Moraes 2008). It should be noted, that the existence of two restriction sites located between the origins of replication is an exception rather than a rule; deliberately creating mtDNA deletions, similar to the ones naturally present in the human population, seems unlikely with the use of known restriction endonucleases. Why are researchers so incredibly interested in an approach for deliberate mtDNA deletion creation? First, mtDNA deletions are the primary cause of mitochondrial disease and are likely to play a central role in the aging of post-mitotic tissues (Damas et al. 2014). Cells from patients with mtDNA deletions can be used to create cybrid lines to analyse mitochondrial physiology and to test novel gene therapy approaches. Second, it is hard to make several cybrid lines from one patient with different mtDNA deletions but similar nuclear background. However, it is important to understand the dynamics of mtDNA with different deletions: for instance the mtDNA deletions of different sizes, present in Substantia nigra samples of Parkinson's disease patients (Reeve et al. 2008; Nido et al. 2018). The MitoRGEN/AsCpf1 approach will make it possible to obtain cell lines with pre-planned deletions in mtDNA (Figure 3). For this, we would have to use two modified gRNAs which, after cutting will have compatible sticky ends. Due to the 'backwards' manner of DNA site recognition by the gRNA, an RNA import determinant should be added to 3′-end of the RNA-coding gene. In theory, the deleted mtDNA haplotype would be detected in a manner similar to *Pst*I treatment. Despite the limitation of having to take into account the PAM during gRNAs' production, there are several modification of AsCpf1 (Gao et al. 2017; Nishimasu et al. 2017) that would otherwise increase our

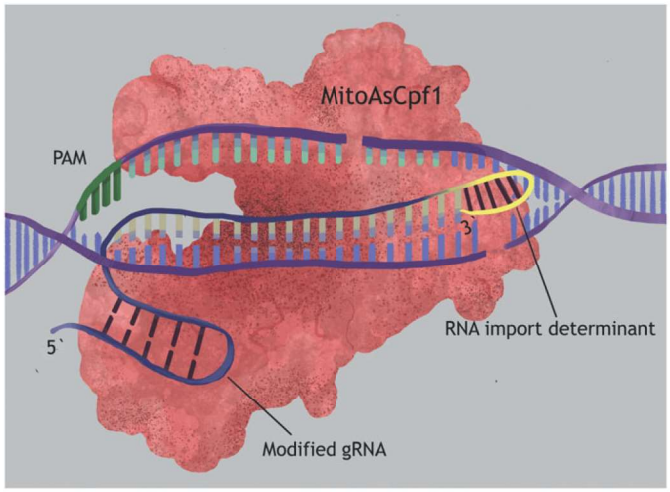


Figure 3. mitoRGEN/AsCpf1. Mitochondria-targeted RNA-guided endonuclease AsCpf1. The nuclease is modified by mitochondrial target signal. Guid RNA is modified by RNA import determinant (at the moment there are four determinants for RNA import into human mitochondria: MRP, RP, HD and HF). The RNA import determinants added to the 3′-end of the gRNA-coding gene.

success in pre-planed deleted mtDNA. In general terms, a pre-planned mtDNA deletion experiment might be described as follows. First of all, we should design the structure of modified gRNAs, which generate complementary sticky ends. Both the modified gRNA and mitoAsCpf1 genes should be cloned into the nuclear DNA of an iPS cell. We think that the expression activation of the integrated genes should be inducible and not start at the iPS cell stage. An alternative way is to use tissue-specific gene expression during iPS cell differentiation into nervous and muscular cells. As a result, we will have a mixture of wild-type mtDNA and deliberately deleted mtDNA in a state of heteroplasmy, that is characteristic in a person during a disease or natural aging. Creating animal models will open unprecedented prospects for studying the role of mtDNA deletions in the aging brain and body as a whole. The option of the MitoRGEN/AsCpf1 system with one modified gRNA can be used as an alternative to the mitoRGEN/SpCas9 system to modify the heteroplasmic mtDNA mutation.

MitoBE4-GAM и MitoABE 7.10**

The state-of-art base editing systems RGEN/BE4-GAM (Komor et al. 2017) and RGEN/ABE 7.10 (Gaudelli et al. 2017) may change nucleotides in a DNA sequence without the double-strand break phase. This approach seems very promising as a tool for real mtDNA editing in our opinion. The RGEN/BE4-GAM allows to correct the mutation C:G to T:A, whereas the RGEN/ABE 7.10 allows to correct more particular substitutions of A:T to G:C. The limitation in using these systems, in our opinion, is the lack of accuracy in the mutation correcting process: as a result off-target base-editing activity within several bases window can be detected (Komor et al. 2016). And again, as previously mentioned, to use the RNA-guided SpCas9 nuclease the PAM sequence should be taken into account during production of gRNA. However, there are other known nucleases that can be used in place of SpCas9 (Komor et al. 2017), as well as technologies for changing the way PAM is recognized (Kleinstiver et al. 2015a, 2015b).

Approaches for delivery of donor DNA as a homologous repair template

To repair DNA breaks by homologous recombination, a template DNA fragment should be imported. DNA import into the mitochondria has been described for both plant and animal cells, but such import is apparently nonspecific.

*MitoTALE**

We propose that dsDNA could be imported into human mitochondrion in link with DNA-binding protein using the TOM/TIM pathway (Figure 4). For instance, it could be a TAL-effector fused with an MTS in its N-tail. The system will include two parts: a modified recombinant DNA-binding protein (called MitoTALE) and a binding site at the 5′-end of the imported DNA molecule. We hope that the negative charge of DNA molecule will be enough to use the common cationic

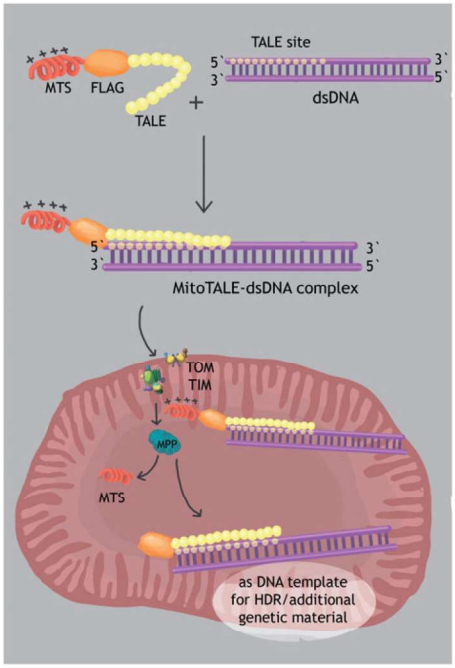


Figure 4. mitoTALE. The system includes protein part and particular target site on dsDNA. The mitoTALE–dsDNA complex is supposed to be imported into mitochondrion using the TOM/TIM protein pathway, where the dsDNA could be used as a template for homology-directed recombination or/and additional genetic material.

lipid nucleic acid transfection reagents. Another way to deliver the mitoTALE–dsDNA complex into the cells is fusing MitoTALE with an engineered super negatively charged GFP (Zuris et al. 2015) – if DNA charge is not sufficiently negative. Another modification of MitoTALE could contain the TAT domain, that allows the protein to penetrate into cells without the use of lipophilic transfection reagents (Del Gaizo et al. 2003). Imported dsDNAs are supposed to be expressed inside of the mitochondrion as functional genetic code, and could be used as a DNA template for homology-directed recombination or/and additional genetic material. Moreover, the mitoTALE system could increase RNA import efficiency if we encode RNA moieties into a DNA structure and import it into mitochondrion.

*RNA–DNA hybrids**

Oligonucleotides could be used as a DNA template for HDR. The structure of the oligonucleotide for homologous recombination could be a chimeric molecule, which would consist of a DNA fragment (template for HDR) and an RNA fragment (RNA import determinant), with the help of which the whole oligonucleotide would be delivered inside the mitochondria (Tonin et al. 2014a, 2014b). The DNA part of the chimeric nucleic acid will have a sequence, complementary to the

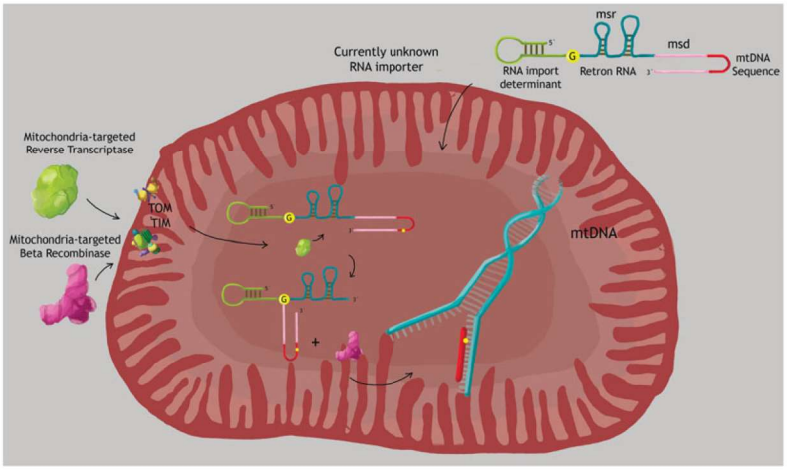


Figure 5. mitoRetron. Mitochondria-targeted reverse transcriptase and beta recombinase are supposed to be imported into mitochondrion using the TOM/TIM protein pathway. Modified retron RNA are supposed to be imported into mitochondrion using currently unknown RNA importer. Inside of mitochondrion the system will generate an ssDNA template for homology-directed recombination.

mtDNA fragment containing the pathogenic mutation with the exception of one nucleotide, the mutation, essentially making the imported DNA part a wild-type.

Bacterial retrons and MitoRetron*

Retrons are bacterial DNA sequences, that encode a reverse transcriptase as well as two RNA molecules, msr and msd, one of which (msd) is used as a template for the synthesis of single-stranded DNA. The RNA–DNA complex obtained by reverse transcription is called msDNA (Lampson et al. 2005). Some modifications of the bacterial retron system, including adding a recombinase from bacteriophage I and changing the msd sequence, allowed Lu's team to create a tool for successful editing of *E. coli* genome (Farzadfard and Lu 2014). Considering the evolutionary relationship of bacteria and mitochondria, it seems possible to adapt this system in a way that would work in the mitochondrial matrix. Moreover, there is evidence of functional activity of the bacterial retron system in the mammalian cell with subsequent discussion of using it as a vector for single-stranded DNA production (Mirochnitchenko et al. 1994). For this, it is necessary to conduct codon optimization of the RT Ec86 reverse transcriptase and Beta recombinase genes, modifying them with a MTS. The import of the RNA-part of the bacterial retron system could be done using previously described RNA import determinants (Dovydenko et al. 2015; Wang et al. 2015). It should be noted, that in such situation we exclude the stage of DNA template delivery process into the mitochondria, since msDNA already acts as a template for homologous recombination (Figure 5).

Additional delivery perspectives

Delivering editing systems to specific cells is a significant separate task, although some studies in this area have already begun (Ellis et al. 2013). After breakthrough research in the field of nucleic acid delivery into the mitochondria using modified AAV vector (Yu et al. 2012), new opportunities have opened up in this field. Despite the fact that AAV vectors have a small cloning capacity for packaging systems like RGEN or Retron, it is theoretically possible to use several such vectors to deliver fragments of the systems, that will then be assembled in the cytoplasm of the cell (Koo et al. 2013; Dyka et al. 2014), or even inside mitochondria. The problem with delivery of RNA moieties or DNA templates could be resolved by using MITO-Porter approach that seems to us very attractive for that (Yamada et al. 2008, 2017). MITO-Porter can be used to deliver a wide variety of carrier-encapsulated molecules, regardless of size or physicochemical properties, to the mitochondrion. Thus, MITO-Porter can directly achieve to deliver Cas9 protein/gRNA complex to mitochondria. Another promising direction is using the described editing systems during *in vitro* fertilization – analogous to replacing mitochondria in an egg with pathogenic mtDNA mutations (Tachibana et al. 2009; Craven et al. 2010; Kang et al. 2016). Thus, at present, the mitochondrial genome editing systems are only at the very beginning stage of their development, but there is no doubt that the appearance of such systems will lead to significant progress in the therapy of mitochondrial diseases and understanding of the fundamentals of mtDNA functioning.

Acknowledgements

We thank the members of the Laboratory of Molecular Genetics Technologies deeply for their help in editing the manuscript and Victoria Polomoshnova for the illustrations.

Disclosure statement

No potential conflict of interest was reported by the authors.

Funding

The research was supported by the Russian Science Foundation [No. 17-75-20015 to I.M.], by State Task Grant [No. 6.2116.2017/4.6 to I.M], by Grants-in-Aid for Scientific Research <KAKENHI> [16H01872 to M.T.] from the Ministry of Education, Culture, Sports, Science and Technology (MEXT), by Grants for Intractable/Rare Disorders [No. 16ek0109088h0002 to M.T.] from Japan Agency for Medical Research and Development (AMED), and by Grants-in-Aid of the Research on Intractable Diseases (Mitochondrial Disorder) from the Ministry of Health, Labour and Welfare of Japan (M.T.).

ORCID

K. Orishchenko http://orcid.org/0000-0001-9718-9038
I. Mazunin http://orcid.org/0000-0002-5448-9679

References

Alexeyev MF, Venediktova N, Pastukh V, Shokolenko I, Bonilla G, Wilson GL. 2008. Selective elimination of mutant mitochondrial genomes as therapeutic strategy for the treatment of NARP and MILS syndromes. Gene Ther. 15:516.

Anders C, Niewoehner O, Duerst A, Jinek M. 2014. Structural basis of PAM-dependent target DNA recognition by the Cas9 endonuclease. Nature. 513:569.

Bacman SR, Williams SL, Pinto M, Moraes CT. 2014. The use of mitochondria-targeted endonucleases to manipulate mtDNA. Methods Enzymol. 547:373–397.

Bacman SR, Williams SL, Pinto M, Peralta S, Moraes CT. 2013. Specific elimination of mutant mitochondrial genomes in patient-derived cells by mitoTALENs. Nat Med. 19:1111.

Cermak T, Doyle EL, Christian M, Wang L, Zhang Y, Baller JA, Somia NV, Bogdanove AJ, Voytas DF. 2011. Efficient design and assembly of custom TALEN and other TAL effector-based constructs for DNA targeting. Nucleic Acids Res. 39:e82 e82.

Chicherin IV, Levitsky SA, Krasheninnikov IA, Tarassov I, Kamenski PA. 2017. The prospects of gene therapy for mitochondrial diseases: can't we do without CRISPR/Cas9? VESTNIKRGMU. 3:46–51.

Craven L, Alston CL, Taylor RW, Turnbull DM. 2017. Recent advances in mitochondrial disease. Annu Rev Genom Hum Genet. 18:257–275.

Craven L, Tuppen HA, Greggains GD, Harbottle SJ, Murphy JL, Cree LM, Murdoch AP, Chinnery PF, Taylor RW, Lightowlers RN, et al. 2010. Pronuclear transfer in human embryos to prevent transmission of mitochondrial DNA disease. Nature. 465:82.

Damas J, Samuels DC, Carneiro J, Amorim A, Pereira F. 2014. Mitochondrial DNA rearrangements in health and disease-a comprehensive study. Hum Mutat. 35:1–14.

Del Gaizo V, MacKenzie JA, Payne RM. 2003. Targeting proteins to mitochondria using TAT. Mol Genet Metabol. 80:170–180.

Dovydenko I, Heckel AM, Tonin Y, Gowher A, Venyaminova A, Tarassov I, Entelis N. 2015. Mitochondrial targeting of recombinant RNA. Methods Mol Biol. 1265:209–225.

Dyka FM, Boye SL, Chiodo VA, Hauswirth WW, Boye SE. 2014. Dual adeno-associated virus vectors result in efficient in vitro and in vivo expression of an oversized gene, MYO7A. Hum Gene Ther Methods. 25:166–177.

Ellis BL, Hirsch ML, Porter SN, Samulski RJ, Porteus MH. 2013. Zinc-finger nuclease-mediated gene correction using single AAV vector transduction and enhancement by Food and Drug Administration-approved drugs. Gene Ther. 20:35.

Farzadfard F, Lu TK. 2014. Synthetic biology. Genomically encoded analog memory with precise in vivo DNA writing in living cell populations. Science. 346:1256272.

Fukui H, Moraes CT. 2008. Mechanisms of formation and accumulation of mitochondrial DNA deletions in aging neurons. Hum Mol Genet. 18:1028–1036.

Gammage PA, Gaude E, Van Haute L, Rebelo-Guiomar P, Jackson CB, Rorbach J, Pekalski ML, Robinson AJ, Charpentier M, Concordet JP, et al. 2016. Near-complete elimination of mutant mtDNA by iterative or dynamic dose-controlled treatment with mtZFNs. Nucleic Acids Res. 44:7804–7816.

Gammage PA, Moraes CT, Minczuk M. 2017. Mitochondrial genome engineering: the revolution may not be CRISPR-Ized. Trends Genet. 17:30191–30199.

Gammage PA, Rorbach J, Vincent AI, Rebar EJ, Minczuk M. 2014. Mitochondrially targeted ZFNs for selective degradation of pathogenic mitochondrial genomes bearing large-scale deletions or point mutations. EMBO Mol Med. 6:458–466.

Gao L, Cox DB, Yan WX, Manteiga JC, Schneider MW, Yamano T, Nishimasu H, Nureki O, Crosetto N, Zhang F. 2017. Engineered Cpf1 variants with altered PAM specificities. Nat Biotechnol. 35:789.

Gaudelli NM, Komor AC, Rees HA, Packer MS, Badran AH, Bryson DI, Liu DR. 2017. Programmable base editing of A•T to G•C in genomic DNA without DNA cleavage. Nature. 551:464.

Gustafsson CM, Falkenberg M, Larsson NG. 2016. Maintenance and expression of mammalian mitochondrial DNA. Annu Rev Biochem. 85:133–160.

Hällberg BM, Larsson NG. 2014. Making proteins in the powerhouse. Cell Metabol. 20:226–240.

Hashimoto M, Bacman SR, Peralta S, Falk MJ, Chomyn A, Chan DC, Williams SL, Moraes CT. 2015. MitoTALEN: a general approach to reduce mutant mtDNA loads and restore oxidative phosphorylation function in mitochondrial diseases. Mol Ther. 23:1592–1599.

Hashimoto Y, Ito Y, Niikura T, Shao Z, Hata M, Oyama F, Nishimoto I. 2001. Mechanisms of neuroprotection by a novel rescue factor humanin from Swedish mutant amyloid precursor protein. Biochem Biophys Res Commun. 283:460–468.

Jiang F, Doudna JA. 2017. CRISPR-Cas9 structures and mechanisms. Annu Rev Biophys. 46:505–529.

Jinek M, Chylinski K, Fonfara I, Hauer M, Doudna JA, Charpentier E. 2012. A programmable dual-RNA-guided DNA endonuclease in adaptive bacterial immunity. Science. 337:816–821.

Jo A, Ham S, Lee GH, Lee YI, Kim S, Lee YS, Shin JH, Lee Y. 2015. Efficient mitochondrial genome editing by CRISPR/Cas9. BioMed Res Int. 2015:305716.

Kang E, Wu J, Gutierrez NM, Koski A, Tippner-Hedges R, Agaronyan K, Platero-Luengo A, Martinez-Redondo P, Ma H, Lee Y, et al. 2016. Mitochondrial replacement in human oocytes carrying pathogenic mitochondrial DNA mutations. Nature. 540:270.

Kazak L, Reyes A, Holt IJ. 2012. Minimizing the damage: repair pathways keep mitochondrial DNA intact. Nat Rev Mol Cell Biol. 13:659.

Khrapko K, Turnbull D. 2014. Mitochondrial DNA mutations in aging. Prog Mol Biol Transl Sci. 127:29–62.

Kim KM, Noh JH, Abdelmohsen K, Gorospe M. 2017. Mitochondrial noncoding RNA transport. BMB Rep. 50:164.

Kleinstiver BP, Prew MS, Tsai SQ, Nguyen NT, Topkar VV, Zheng Z, Joung JK. 2015a. Broadening the targeting range of *Staphylococcus aureus* CRISPR-Cas9 by modifying PAM recognition. Nat Biotechnol. 33:1293.

Kleinstiver BP, Prew MS, Tsai SQ, Topkar VV, Nguyen NT, Zheng Z, Gonzales AP, Li Z, Peterson RT, Yeh JR, et al. 2015b. Engineered CRISPR-Cas9 nucleases with altered PAM specificities. Nature. 523:481.

Komor AC, Badran AH, Liu DR. 2017. CRISPR-based technologies for the manipulation of eukaryotic genomes. Cell. 168:20–36.

Komor AC, Kim YB, Packer MS, Zuris JA, Liu DR. 2016. Programmable editing of a target base in genomic DNA without double-stranded DNA cleavage. Nature. 533:420.

Komor AC, Zhao KT, Packer MS, Gaudelli NM, Waterbury AL, Koblan LW, Kim YB, Badran AH, Liu DR. 2017. Improved base excision repair inhibition and bacteriophage Mu Gam protein yields C:G-to-T:A base editors with higher efficiency and product purity. Sci Adv. 3:eaao4774.

Konermann S, Brigham MD, Trevino AE, Joung J, Abudayyeh OO, Barcena C, Hsu PD, Habib N, Gootenberg JS, Nishimasu H, et al. 2015. Genome-scale transcriptional activation by an engineered CRISPR-Cas9 complex. Nature. 517:583.

Koo T, Popplewell L, Athanasopoulos T, Dickson G. 2013. Triple trans-splicing adeno-associated virus vectors capable of transferring the

coding sequence for full-length dystrophin protein into dystrophic mice. Hum Gene Ther. 25:98–108.
Lampson BC, Inouye M, Inouye S. 2005. Retrons, msDNA, and the bacterial genome. Cytogenet Genome Res. 110:491–499.
Lee C, Kim KH, Cohen P. 2016. MOTS-c: a novel mitochondrial-derived peptide regulating muscle and fat metabolism. Free Radic Biol Med. 100:182–187.
Minczuk M, Kolasinska-Zwierz P, Murphy MP, Papworth MA. 2010. Construction and testing of engineered zinc-finger proteins for sequence-specific modification of mtDNA. Nat Protoc. 5:342.
Minczuk M, Papworth MA, Kolasinska P, Murphy MP, Klug A. 2006. Sequence-specific modification of mitochondrial DNA using a chimeric zinc finger methylase. Proc Natl Acad Sci. 103:19689–19694.
Minczuk M, Papworth MA, Miller JC, Murphy MP, Klug A. 2008. Development of a single-chain, quasi-dimeric zinc-finger nuclease for the selective degradation of mutated human mitochondrial DNA. Nucleic Acids Res. 36:3926–3938.
Mirochnitchenko O, Inouye S, Inouye M. 1994. Production of single-stranded DNA in mammalian cells by means of a bacterial retron. J Biol Chem. 269:2380–2383.
Moretton A, Morel F, Macao B, Lachaume P, Ishak L, Lefebvre M, Garreau-Balandier I, Vernet P, Falkenberg M, Farge G. 2017. Selective mitochondrial DNA degradation following double-strand breaks. PLoS One. 12:e0176795.
Nido GS, Dölle C, Flønes I, Tuppen HA, Alves G, Tysnes OB, Haugarvoll K, Tzoulis C. 2018. Ultradeep mapping of neuronal mitochondrial deletions in Parkinson's disease. Neurobiol Aging. 63:120–127.
Nishimasu H, Ran FA, Hsu PD, Konermann S, Shehata SI, Dohmae N, Ishitani R, Zhang F, Nureki O. 2014. Crystal structure of Cas9 in complex with guide RNA and target DNA. Cell. 156:935–949.
Nishimasu H, Yamano T, Gao L, Zhang F, Ishitani R, Nureki O. 2017. Structural basis for the altered PAM recognition by engineered CRISPR-Cpf1. Mol Cell. 67:139–147.
Orishchenko KE, Sofronova JK, Chupakhin EG, Lunev EA, Mazunin IO. 2016. Delivery Cas9 into mitochondria. Genes Cells. 11:100–105.
Palermo G, Ricci CG, Fernando A, Basak R, Jinek M, Rivalta I, Batista VS, McCammon JA. 2017. Protospacer adjacent motif-induced allostery activates CRISPR-Cas9. J Am Chem Soc. 139:16028–16031.
Patananan AN, Wu TH, Chiou PY, Teitell MA. 2016. Modifying the mitochondrial genome. Cell Metabol. 23:785–796.
Patrushev MV, Kamenski PA, Mazunin IO. 2014. Mutations in mitochondrial DNA and approaches for their correction. Biochemistry (Mosc). 79:1151–1160.
Pereira CV, Moraes CT. 2017. Current strategies towards therapeutic manipulation of mtDNA heteroplasmy. Front Biosci (Landmark Ed). 22:991–1010.
Phillips AF, Millet AR, Tigano M, Dubois SM, Crimmins H, Babin L, Charpentier M, Piganeau M, Brunet E, Sfeir A. 2017. Single-molecule analysis of mtDNA replication uncovers the basis of the common deletion. Mol Cell. 65:527–538.
Reddy P, Ocampo A, Suzuki K, Luo J, Bacman SR, Sugawara A, Okamura D, Tsunekawa Y, Wu J, Lam D, et al. 2015. Selective elimination of mitochondrial mutations in the germline by genome editing. Cell. 161:459–469.
Reeve AK, Krishnan KJ, Elson JL, Morris CM, Bender A, Lightowlers RN, Turnbull DM. 2008. Nature of mitochondrial DNA deletions in substantia nigra neurons. Am J Hum Genet. 82:228–235.
Srivastava S, Moraes CT. 2001. Manipulating mitochondrial DNA heteroplasmy by a mitochondrially targeted restriction endonuclease. Hum Mol Genet. 10:3093–3099.
Srivastava S, Moraes CT. 2005. Double-strand breaks of mouse muscle mtDNA promote large deletions similar to multiple mtDNA deletions in humans. Hum Mol Genet. 14:893–902.
Tachibana M, Sparman M, Sritanaudomchai H, Ma H, Clepper L, Woodward J, Li Y, Ramsey C, Kolotushkina O, Mitalipov S. 2009. Mitochondrial gene replacement in primate offspring and embryonic stem cells. Nature. 461:367.
Tanaka M, Borgeld HJ, Zhang J, Muramatsu SI, Gong JS, Yoneda M, Maruyama W, Naoi M, Ibi T, Sahashi K, et al. 2002. Gene therapy for mitochondrial disease by delivering restriction endonuclease SmaI into mitochondria. J Biomed Sci. 9:534–541.
Tonin Y, Heckel AM, Dovydenko I, Meschaninova M, Comte C, Venyaminova A, Pyshnyi D, Tarassov I, Entelis N. 2014a. Characterization of chemically modified oligonucleotides targeting a pathogenic mutation in human mitochondrial DNA. Biochimie. 100:192–199.
Tonin Y, Heckel AM, Vysokikh M, Dovydenko I, Meschaninova M, Rötig A, Munnich A, Venyaminova A, Tarassov I, Entelis N. 2014b. Modeling of antigenomic therapy of mitochondrial diseases by mitochondrially addressed RNA targeting a pathogenic point mutation in mitochondrial DNA. J Biol Chem. 289:13323–13334.
Verechshagina N, Orishchenko K, Shevtsova A, Nikitchina N, Mazunin I. Modified CRISPR/Cas9 system shifts down mtDNA copy number. EMBO/FEBS advanced lecture course 2017 – mitochondria in life, death and disease. Brindisi, Italy; [accessed 2017 Oct 9–13]. https://www.researchgate.net/publication/323384742_Modified_CRISPRCas9_system_shifts_down_mtDNA_copy_number.
Wang G, Chen HW, Oktay Y, Zhang J, Allen EL, Smith GM, Fan KC, Hong JS, French SW, McCaffery JM, et al. 2010. PNPASE regulates RNA import into mitochondria. Cell. 142:456–467.
Wang G, Shimada E, Nili M, Koehler CM, Teitell MA. 2015. Mitochondria-targeted RNA import. Methods Mol Biol. 1264:107–116.
Yamada Y, Akita H, Kamiya H, Kogure K, Yamamoto T, Shinohara Y, Yamashita K, Kobayashi H, Kikuchi H, Harashima H. 2008. MITO-Porter: a liposome-based carrier system for delivery of macromolecules into mitochondria via membrane fusion. Biochim Biophys Acta (BBA)-Biomembr. 1778:423–432.
Yamada Y, Ishikawa T, Harashima H. 2017. Validation of the use of an artificial mitochondrial reporter DNA vector containing a Cytomegalovirus promoter for mitochondrial transgene expression. Biomaterials. 136:56–66.
Yamano T, Nishimasu H, Zetsche B, Hirano H, Slaymaker IM, Li Y, Fedorova I, Nakane T, Makarova KS, Koonin EV, et al. 2016. Crystal structure of Cpf1 in complex with guide RNA and target DNA. Cell. 165:949–962.
Yang Y, Wu H, Kang X, Liang Y, Lan T, Li T, Tan T, Peng J, Zhang Q, An G, et al. 2018. Targeted elimination of mutant mitochondrial DNA in MELAS-iPSCs by mitoTALENs. Protein Cell. 9:283–297.
Yu H, Koilkonda RD, Chou TH, Porciatti V, Ozdemir SS, Chiodo V, Boye SL, Boye SE, Hauswirth WW, Lewin AS, et al. 2012. Gene delivery to mitochondria by targeting modified adenoassociated virus suppresses Leber's hereditary optic neuropathy in a mouse model. Proc Natl Acad Sci. 109:E1238–E1247.
Zetsche B, Gootenberg JS, Abudayyeh OO, Slaymaker IM, Makarova KS, Essletzbichler P, Volz SE, Joung J, van der Oost J, Regev A, et al. 2015. Cpf1 is a single RNA-guided endonuclease of a class 2 CRISPR-Cas system. Cell. 163:759–771.
Zuris JA, Thompson DB, Shu Y, Guilinger JP, Bessen JL, Hu JH, Maeder ML, Joung JK, Chen ZY, Liu DR. 2015. Cationic lipid-mediated delivery of proteins enables efficient protein-based genome editing in vitro and in vivo. Nat Biotechnol. 33:73.

View publication stats

1.5.6. mtDNA base editing technologies

Mutant mtDNA heteroplasmy shifting strategies utilizing programmable nucleases are not suitable for homoplasmic mtDNA mutations, where mutant mtDNA level represents 100%. Additionally, these approaches cannot introduce specific *de novo* nucleotide changes in mtDNA, which can be extremely useful in creating precise models of mitochondrial disorders. Another strategy, which can also be applicable to homoplasmic mutations, consists of the use of base editors in order to reverse mutations without introducing a break in mtDNA (**Figure I15**, **lower panel**).

The application of cytidine deaminases for genome editing was initially established for modifying the nuclear genome (**Komor, A. C. *et al.*, 2016**). This process involves the deamination of cytosine, which converts it into uracil. Polymerases then can recognize uracil as thymine, leading to the incorporation of adenine on the complementary strand during the first round of DNA replication. In a subsequent round of replication, polymerases use this incorporated adenine as a template to introduce thymine, effectively replacing the original cytosine (**Figure I17A**). This C-to-T (or G-to-A) and A-to-G (or T-to-C) (**Figure I17A & B**) editing of nuclear genes has been successfully accomplished using cytidine and adenine deaminases that act on single-stranded DNA (ssDNA) (**Koblan, L. W. *et al.*, 2018**). Sequence specificity and double-stranded DNA (dsDNA) unwinding in these processes was achieved by using a catalytically dead Cas9 (dCas9) guided by RNA. However, currently, dCas9-based DNA editors have not been adapted for the use in mitochondria, due to the inability to effectively import gRNA into mitochondria.

In 2020, a significant breakthrough was reported when researchers discovered a bacterial toxin called DddA capable of inducing specific C-to-T transitions in dsDNA (**Mok, B. Y. *et al.*, 2020**). This was a notable discovery because previously identified cytosine or adenine deaminases were being able to work only on a single-stranded DNA (**McDougall W. M., Okany C., Smith H. C., 2011**). To mitigate the toxic effects associated with this deaminase and eliminate non-specific deamination, it was divided into two halves, each of which was linked to a specific DNA-binding component. As a result, the full-length enzyme became active only when it was bound to the sequence surrounding the targeted base to be edited. This innovative architecture allowed for direct base editing of dsDNA, both in the nuclear genome and, once targeted to mitochondria, in the mitochondrial DNA (**Mok, B. Y. *et al.*, 2022**).

Various DNA-binding domains since then were employed to guide cytidine base editors (CBE) to specific locations within mtDNA, including TALE (**Mok, B. Y. *et al.*, 2022**) and zinc-finger domains (**Lim K., Cho S. I., Kim J. S., 2022**) (**Figure I17C**). Following the successful development of the

mitoDdCBE systems, the adenine base editor (ABE), TALED, was introduced (**Cho, S. I. *et al.*, 2022**). In this system, a split DddA was fused to a single-strand-specific adenine deaminase called TadA8e, allowing for precise A-to-G transitions. Additionally, a version that combined a full-length but catalytically inactive DddA with TadA8e in a single molecule was created (**Figure I17D**).

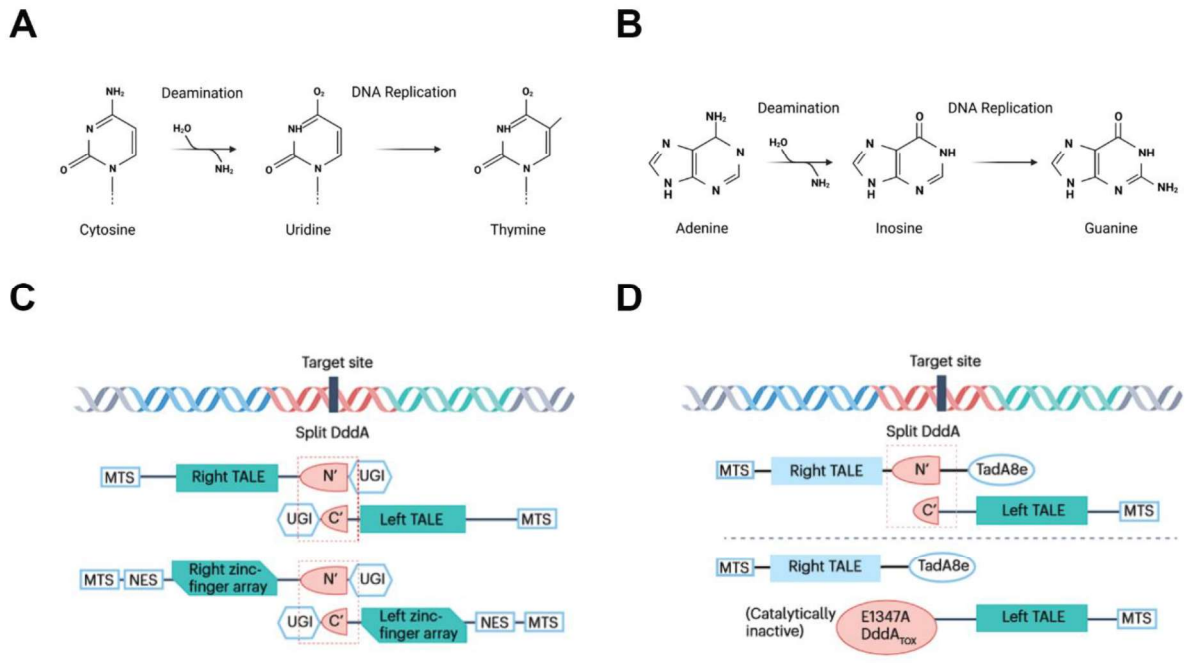


Figure I17. MMitochondria-Targeted Base Editing Technologies.

Simplified representation of cytosine **(A)** and adenin **(B)** deamination reactions used in base-editing.
(C) Mitochondria-targeted DdCBE (mitoDdCBE or mitoZF-DdCBE) catalyze C>T base transitions in dsDNA. DddAtox catalytic domain is split to reduce non-specific and cytotoxic activity. It is fused with a DNA binding domain and uracil glycosylase inhibitor (UGI) to block mitochondrial base excision repair, and sometimes includes a nuclear export signal (NES) to prevent nuclear localization.
(D) Mitochondria-targeted TALE-linked adenine deaminases (TALEDs) catalyze A>G base transitions in dsDNA. They employ the TadA8e enzyme and a DddAtox catalytic domain. The split version, similar to mitoDdCBE, splits DddAtox across two monomers, with only one containing TadA8 (ABE). The dimeric version uses two monomers to recognize and bind adjacent DNA sequences surrounding the mutation, with one monomer carrying the TadA8 enzyme and the other having a full-length catalytically inactive DddAtox domain. Adapted from Shoop W. K. *et al.*, 2023.

To date, mtDNA base editing techniques was utilised to introduce various disease-associated mutations into cultured human cell lines and animal models (**Mok, B. Y. *et al.*, 2020**; **Lee, H. *et al.*, 2021**; **Mok, B. Y. *et al.*, 2022**; **Cho, S. I. *et al.*, 2022**; **Silva-Pinheiro, P. *et al.*, 2023**). However, despite the considerable potential of base editors, they come with certain limitations.

Firstly, it's worth noting that ZFNs and TALENs are already limited by the packaging capacity of AAVs. Now, with the introduction of base editors, which contain even more additional components, this packaging challenge still remains the problem. Secondly, the efficiency of base editing is highly reliant on the specific targeting sequence, and this efficiency can vary significantly, ranging from 5% to 50% in cell cultures (**Mok, B. Y. *et al.*, 2020**). Moreover, base editors perform deamination within a relatively narrow editing window, typically consisting of 5 to 10 nucleotides. Consequently, all adenines or cytidines within this region may undergo deamination, leading to off-target effects. Generally, the off-target activity of base editors out of the editing window were reported to be around 1.0% (**Lim K., Cho S. I., Kim J. S., 2022**; **Cho, S. I. *et al.*, 2022**). However, it's essential to evaluate the specific off-target activity for each unique context. Furthermore, when mitochondria-targeted DdCBEs were employed, they were found to induce 5% off-target mutations in the nuclear genome of embryos, as revealed by whole-genome sequencing (**Wei Y. *et al.*, 2022**).

In conclusion, base editors show significant promise in shifting mtDNA heteroplasmy levels and in creating cell and animal models for mtDNA-associated diseases. However, substantial efforts are required to enhance their specificity and minimize off-target effects.

1.5.7. mitoCRISPR

CRISPR-Cas genome editing systems may solve the limitations of previously described editing approaches. CRISPR-Cas systems, while having shorter coding sequences, offer greater flexibility for DNA recognition experiments compared to protein-only systems due to their reliance on DNA–RNA interactions for specific mtDNA site recognition (**Jinek, M. *et al.*, 2012**). Furthermore, such systems were proven to be more efficient for genome editing, as well as more versatile and easier to target various DNA sequences by redesigning the RNA system's component, while keeping the protein constant. Consequently, it's not surprising that many laboratories worldwide, including ours, are actively exploring the adaptation of CRISPR technology to eliminate mutant mtDNA molecules and edit the mitochondrial genome.

However, the two-component system necessitates the assembly of a functional machine within the mitochondria, which requires direct delivery of both the protein and RNA components into the mitochondrial matrix (**Loutre, R. *et al.*, 2018**). As for the other described systems, the import of a Cas nuclease into mitochondria can be effectively achieved by fusing its N-terminus to an MTS (**Verechshagina, N. A. *et al.*, 2018**). Recent studies from our and other laboratories demonstrated mitochondrial targeting of Cas nucleases bearing various N-terminal MTS (listed in **Table 1**).

Table 1. Recently developed mitochondrial CRISPR/Cas systems (Publication 2)

Cas nuclease	sgRNA/crRNA	RNA delivery	Detection of sgRNA/crRNA localization	Effect on mtDNA	Reference
SpCas9	Unmodified sgRNA; sgRNA bearing yeast tRK1 F- and D-hairpins	RNA transfection	Northern blot hybridization of total and mitoplast RNA	decrease of mtDNA copy number; no shift in heteroplasmy level	Loutre *et al.*, 2018
SpCas9	Unmodified sgRNA	Transcribed from plasmid under control of U6 promoter	Not verified	decrease of mtDNA copy number;	Bian *et al.*, 2019
LbCas12a	Unmodified crRNA; crRNAs with the stem-loop motifs from RNase P RNA and from yeast tRK1	Transcribed from plasmid under control of U6 promoter	Northern blot hybridization of total and mitochondral RNA	Increase of mtDNA copy number	Antón *et al.*, 2020
SpCas9	Unmodified sgRNA; sgRNA with the stem-loop motif from RNase P RNA	Transcribed from plasmid under control of U6 promoter	Laser scanning microscopy of Alexa fluor 488-labeled RNA; RT-qPCR on total and mitochondrial RNA	Small reduction of mutant mtDNA	Hussain *et al.*, 2021
SpCas9	Unmodified sgRNA; sgRNA with the stem-loop motif from RNase P RNA	Transcribed from plasmid under control of U6 promoter	Not verified	Generation of InDels (<0.05%)	Wang *et al.*, 2021
SpCas9 SpCas9-BE3	Unmodified sgRNA; sgRNA with the stem-loop motif from RNase P RNA	Transcribed from plasmid under control of U6 promoter	Not verified	No change in mtDNA copy number; Unspecific C to T substitutions	Schmiderer *et al.*, 2022
SpCas9	Unmodified sgRNA	Transcribed from plasmid under control of U6 promoter	Laser scanning microscopy of FAM-labeled sgRNA	decrease of mtDNA copy number;	Bi *et al.*, 2022

In contrast, the import of gRNA component into mitochondria poses a significant challenge for applying CRISPR-Cas systems. In most of recent publications (**Table 1**), CRISPR/SpCas9 system have been applied, but the mitochondrial import of gRNA has never been convincingly demonstrated, thus raising uncertainty on the possible use of this system for mtDNA manipulations (**Gammage P. A., Moraes C. T., Minczuk M., 2018**).

We suggest two main reasons for this. First, the use of plasmids expressing gRNAs in the nucleus, being well established for the nuclear DNA applications, seems to be not convenient for gRNA mitochondrial targeting due to the need of efficient gRNA export from the nucleus (**Figure I18A**), which cannot be assured in the absence of the signals for RNA export (**Hamm J., Mattaj I. W., 1990**; **Good, P. D. *et al.*, 1997**; **Stewart M., 2019**). Second, sgRNAs of Cas9 system are rather long (about 100 bp) (**Nishimasu, H. *et al.*, 2014**) (**Figure I18B**), which can strongly decrease their mitochondrial targeting (**Jeandard, D. *et al.*, 2019**), as discussed also in section **1.3.2**.

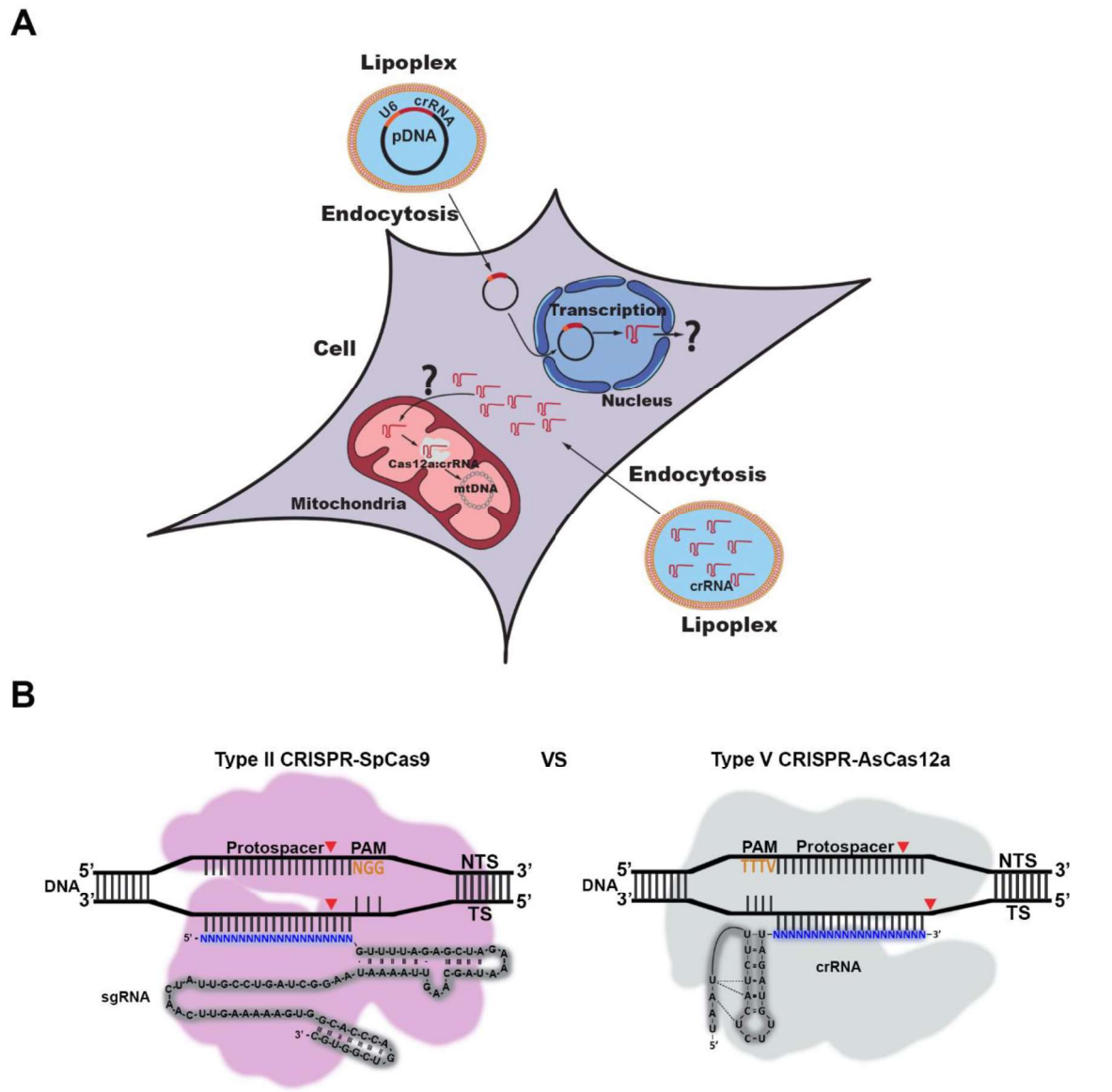


Figure I18. Comparison of crRNA Delivery Methods and CRISPR Systems of Type II and Type V.

(A) Cell delivery of crRNA by direct transfection with RNA (lower part), or by expressed from plasmid DNA in the nucleus (upper part).
(B) A comparison of CRISPR-Cas9 system versus CRISPR-Cas12a. Protospacer adjacentmotif (PAM) is shown in orange; generated double-stranded breaks are indicated by red triangles in both target (TS) and non-target DNA strands (NTS).

To address these problems, the main goal of the current PhD thesis study was to optimize the Type V CRISPR system, namely, AsCas12a, possessing better characteristics for mtDNA application.

AsCas12a, also known as AsCpf1, belongs to the class 2 Type V-A CRISPR-Cas system. It operates by catalyzing double-stranded DNA breaks using a single CRISPR RNA (crRNA) molecule (**Yamano, T. *et al.*, 2016**). Notably, AsCas12a employs a relatively short crRNA of 40-44 nucleotides, which could potentially make it a better candidate for mitochondrial import compared to the single guide RNA (sgRNA) used in the Type II CRISPR-Cas9 system (**Figure I18B**). The AsCas12a-crRNA ribonucleoprotein (RNP) complex initially identifies its dsDNA target by recognizing a T-rich protospacer-adjacent motif (PAM) (**Figure I18B**). Following target binding, the AsCas12a RNP unwinds the DNA, forming a crRNA-target strand (TS) heteroduplex while displacing the non-target strand (NTS) to create an R-loop structure (**Stella S., Alcón P., Montoya G., 2016**). Subsequently, Cas12a generates double-stranded DNA breaks with 5'-sticky ends using a single RuvC nuclease domain in a sequential manner. Given that AsCas12a recognizes a T-rich PAM sequence, in contrast to the G-rich PAM of SpCas9 (**Figure I18B**), it holds promise for targeting human mtDNA, which has a GC content of only 44%. This makes AsCas12a more advantageous for targeting sequences in human mtDNA. Additionally, AsCas12a has been reported to exhibit lower off-target activity compared to SpCas9 (**Zetsche, B. *et al.*, 2017**; **Kim D. *et al.*, 2016**).

As discussed in the **Publication 1**, it would be intriguing to investigate whether the mitochondrial-targeted AsCas12a can induce deletions in mtDNA due to its ability to generate 5'-overhang ends (**Figure I18B**). To achieve this, two crRNAs designed to leave cohesive ends should be developed. It would allow creation of cell and animal models bearing intended deletion to modulate and study mtDNA associated diseases and for fundamental study of mtDNA deletion propagation.

To date the only attempt to optimize AsCas12a for mtDNA targeting was initiated by Antón *et al.* in 2020, were they compared mitochondrial import of GFP-fused AsCas12a bearing various MTS, but neither the RNA import into mitochondria, nor the effect of the mitoAsCas12a on mtDNA was evaluated.

Therefore, in order to modify AsCas12 nuclease for its functioning inside human mitochondria, the following objectives were pursued:

OBJECTIVES:

- Optimization of the AsCas12a nuclease and its crRNA import into mitochondria of human cells;
- Proof-of-concept for the mitoCRISPR-Cas12a system specific activity on mtDNA in human cells;
- Developing a strategy for inducing a deletion in human mitochondrial DNA using the mitoCRISPR-Cas12a.

2. MATERIALS AND METHODS

2.1. Materials

2.1.1. Mammalian cell lines used in the study

HEK293 cell line:

The HEK293 cell line is immortalized cells derived from human embryonic kidneys. These cells were created through the transformation of human embryonic kidney cells using sheared adenovirus type 5 DNA (**Graham, F. L. *et al.*, 1977**). The nomenclature '293' signifies that it was Graham's 293rd experimental attempt.

Invitrogen™ Flp-In™ T-REx™ 293 cell line:

The commercially available cell line derived from HEK293 cells is specifically engineered for the efficient production of stable cell lines. It contains a single stably integrated FRT site at an active genomic locus, ensuring consistent gene expression levels in every cell. The Flp-In™ T-REx™-293 Cell Line contains stably integrated pFRTlacZeo and pcDNA™6TR (tetracycline repressor protein). This cell line is resistant to Zeocin (100 μg/mL) and blasticidin (15 μg/mL) antibiotics.

143B cell line:

The metastatic 143B subline was generated *in vitro* via a Ki-RAS oncogene transformation of the human osteosarcoma (HOS) TE85 cell line, isolated from the bone of a 13-year-old, White female with osteosarcoma.

2.1.2. Bacterial strains used in the study

E. coli XL1-blue cells:

XL1-Blue cells have improved miniprep DNA quality due to endonuclease (*endA*) deficiency and enhanced insert stability from recombination (*recA)* deficiency. The *hsdR* mutation prevents cloned DNA cleavage by the *Eco*K endonuclease system. The *lacIqZΔM15* gene on the F´ episome enables blue-white color screening, and these cells are tetracycline resistant.

E. coli Rosetta™(DE3) cells:

Rosetta™ host strains, derived from BL21, are designed to boost the expression of eukaryotic proteins containing rarely used *E. coli* codons. These strains carry tRNAs for AGG, AGA, AUA, CUA, CCC, GGA codons on a compatible chloramphenicol-resistant plasmid. This universal translation overcomes *E. coli*'s codon usage limitations, as the tRNA genes are driven by their native promoters.

2.1.3. Oligonucleotides used in the study

Name	Sequence: 5'- 3'	Ta, °C	Application
RNA5	AGAGTTTGATCCTGGCTCAGGA	61	Mycoplasma screening
RNA3	ACGAGCTGACGACAACCATGCAC	61	Mycoplasma screening
UNI –	TAATCCTGTTTGCTCCCCAC	61	Mycoplasma screening
F_ pY010	TGACGATGACAAGCTCATGACACAGTTCGAGGGC	60	GA
R_ pY010	CCTGTCAGCCCTGCTGTTGCGCAGCTCCTGGAT	60	GA
F_ pMito-Cas9	AGCAGGGCTGACAGGTCC	60	GA
R_ pMito-Cas9	GAGCTTGTCATCGTCATCCTTG	60	GA
F_(d5)CMV	TGTCGTAACAACTCCGCCCCATTG	60	SDM
R_(d5)CMV	CGGAACTCCATATATGGGCTATG	60	SDM
F_As_SOD2	CTGGCTCCGGTTTTGGGGTATCTGGGCTCCAGGCAG GACTACAAAGACCATGACGG	64	SDM
R_As_SOD2	CTGCCTGCTGGTGCCGCACACTGCCCGGCTCAACAT GCTAGCGGATCTGACGGT	64	SDM
F_As_ATG4D	AAGCCGGACCAGCTTTAGCAAGATCTCCAGCATCCA CCTCTGTGGCCGCCGCTACCGTTTCGACTACAAAGA CCATGACGG	64	SDM
R_As_ATG4D	TTAACCACCCAACCGTACTTGACGTTGTTCCAGGCTG TCAGGAACTTGGCCTTGAACTTCATGCTAGCGGATCT GACGGT	64	SDM
F_As_Su9	ATCCAGACTGGCTCCCCCCTCCAGACCCTCAAGCGC ACCCAGATGACCTCCATCGTCAACGCCACCACCCGC	64	SDM

	CAGGCTTTCCAGAAGCGCGCCTACTCTTCCGACTAC AAAGACCATGAC		
R_As_Su9	GGTGCGCTTGCTGACCTGAGCAACGCGGACAGCAG GGCGGGCAACCTTGGCGGAAGCAGCCATCCGGGAG GCCAGGCGAGAGGCGAGGACACGAGTGGAGGCCAT GCTAGCGGATCTGAC	64	SDM
F_FRT_As	GCGCAACTAACCCGCTGATCAGCCTCG	60	GA
R_FRT_As	GGAGGCCATACTAAACGAGCTCGTCGACGA	60	GA
F_SuAsCas12ato FRT	CGTTTAGTATGGCCTCCACTCGTGT	60	GA
R_SuAsCas12ato FRT	TCAGCGGGTTAGTTGCGCAGCTCCTGGA	60	GA
F_T7_AsCas12a	TAATACGACTCACTATAGGTAATTTCTACTCTTGTAGAT	60	*In vitro* transcription
R_T7_MRP	TCTTCGCATAGGGC	60	*In vitro* transcription
R_T7_HD	CGCGTTAGCCATC	60	*In vitro* transcription
R_T7_HF	CTCGGGGGATGTC	60	*In vitro* transcription
R_T7_NEG	AACTACCACCTACCTCC	60	*In vitro* transcription
L8080	TCTTGCACTCATGAGCTGTC	58	*In vitro* cleavage; Nested PCR
H11381	AAGTGGAGTCCGTAAAGAGG	58	*In vitro* cleavage; LM-PCR; Nested PCR

L3081	GTAATCCAGGTCGGTTTCT	58	*In vitro* cleavage
H8361	CTGTAAAGAGGTGTTGGTTC	58	*In vitro* cleavage
L7831	CATCCTTTACATAACAGACG	58	*In vitro* cleavage; LM-PCR; Nested PCR
H13555	AGGCGTTTGTGTATGATATGTTTGC	58	*In vitro* cleavage
F12981	CCTCCTCCTAGCAGCAGC	58	*In vitro* cleavage
H1813	GGTTATAATTTTTCATCTTTCCC	58	*In vitro* cleavage
L12640	TCGTTACATGGTCCATCATAG	58	*In vitro* cleavage
H15912	TCTCCGGTTTACAAGACTGG	58	*In vitro* cleavage
COX1 F	GGCTTCCTAGGGTTTATCGTGTGAGCAC	58	*In vitro* cleavage; LM-PCR; Nested PCR
F_AsCpf1-E993A	GTGGTGCTGGccAACCTGAATTTCG	65	SDM
R_AsCpf1-E993A	CACGGCCTGGTAGTGGAT	65	SDM
F_12S	GCACTTAAACACATCTCTGCC	58	qPCR
R_12S	TGAGATTAGTAGTATGGGAGTGG	58	qPCR
F_TST	GACTGGACTCGGGCCATATC	58	qPCR

R_TST	ACGTGGCAATGAGAGGCTG	58	qPCR
LMPCR1	GCGGTGACCCGGGAGATCTGTATTC	68	LM-PCR
LMPCR2	GAATACAGATC	68	LM-PCR

2.1.4. Antibodies used in the study

Name	Provider	Reference
Mouse monoclonal anti-GAPDH	Sigma-Aldrich	AB2302
Rabbit polyclonal anti-TFAM	Sigma-Aldrich	AB2547047
Goat polyclonal anti-Actin (C-11)	Santa Cruz Biotechnology	sc-1615
Mouse monoclonal anti-FLAG (clone M2)	Sigma-Aldrich	F1804
Rabbit polyclonal anti-TOMM20 (FL-145)	Santa Cruz Biotechnology	sc-11415
Rabbit polyclonal anti-MRPL4	Proteintech Group	27484-1-AP
Rabbit polyclonal anti-OPA1	Proteintech Group	27733-1-AP
Mouse monoclonal anti-AsCas12a	Sigma-Aldrich	MABE1823
Mouse monoclonal anti-COX1 (clone 1D6E1A8)	Abcam	ab14705
Mouse monoclonal anti-VDAC1 (clone B-6)	Santa Cruz Biotechnology	sc-390996RR
Mouse monoclonal anti-BECN1/Beclin-1 (E-8)	Santa Cruz Biotechnology	sc-48341

Mouse monoclonal anti-PINK1 (C-3)	Santa Cruz Biotechnology	sc-518052
Rabbit polyclonal anti-MGME1	Thermo Fisher Scientific	23178-1-AP
Rabbit polyclonal anti-Tubulin	Sigma-Aldrich	SAB4500087
Rabbit polyclonal anti-Goat IgG HRP	Sigma-Aldrich	A8919
Rabbit polyclonal anti-Mouse IgG HRP	Agilent	P0260
Donkey polyclonal anti-Rabbit IgG HRP	Sigma-Aldrich	NA934V
Goat polyclonal anti-Mouse IgG-Alexa Fluor 488	Thermo Fisher Scientific	A-11001
Goat polyclonal anti-Rabbit IgG-Alexa Fluor 647	Thermo Fisher Scientific	A-21246

2.1.5. Sequences of hybridization probes used in the study

Name	Sequence: 5'- 3'
Anti-crRNA-1	GTAGTATGGGAGTGGGAGGG
Anti-crRNA-6	TGTGATAAGGGTGGAGAGGT
Anti-crRNA-10	TTTGTTATGATGTCTGTGTG
Anti-crRNA-14	TTGGGTGCTAATGGTGGAGT
Anti-crRNA-30	ACTCCAAAGACCACATCATC
Anti-crRNA-31	AGCCTAGGGTGTTGTGAGTG

Anti-crRNA-34	GGAAAAGGTTGGGGAACAGC
Anti-crRNA-45 (crRNA-45-spacer)	GGTGGGGATCAATAGAGGGG
Anti-crRNA-52	CCTTCTTATTATTTGATCTA
Probe against cytosolic 5.8S rRNA	GGCCGCAAGTGCGTTCGAAG
Probe against the mitochondrial tRNAVal	GGTCAGAGCGGTCAAG

2.1.6. Sequences of crRNAs used in the study

Name	Sequence: 5'- 3'
crRNA-1 (D-loop)	UAAUUUCUACUCUUGUAGAUCCCUCCCACUCCCAUACUAC
crRNA-6 (D-loop)	UAAUUUCUACUCUUGUAGAUACCUCUCCACCCUUAUCACA
crRNA-10 (ND1)	UAAUUUCUACUCUUGUAGAUCACACAGACAUCAUAACAAA
crRNA-14 (tRNA proline)	UAAUUUCUACUCUUGUAGAUACUCCACCAUUAGCACCCAA
crRNA-30 (ND5)	UAAUUUCUACUCUUGUAGAUGAUGAUGGUCUUUGGAGU
crRNA-31 (ND4)	UAAUUUCUACUCUUGUAGAUCACUCACAACACCCUAGGCU
crRNA-34 (ND4)	UAAUUUCUACUCUUGUAGAUGCUGUUCCCCAACCUUUUCC
crRNA-34-NM (ND4)	UAAUUUCUACUCUUGUAGAUGCUGUUCCCCAACCUUUUCCUCC
crRNA-34-MRP (ND4)	UAAUUUCUACUCUUGUAGAUGCUGUUCCCCAACCUUUUCCUCCCGAGUCGCCCUAUGCGAAGA
crRNA-34-HD (ND4)	UAAUUUCUACUCUUGUAGAUGCUGUUCCCCAACCUUUUCCUCCCGCGAUGGCUAACGCG
crRNA-34HF (ND4)	UAAUUUCUACUCUUGUAGAUGCUGUUCCCCAACCUUUUCCUCCUCGGGACAUCCCCCGAG
crRNA-45 (ATP6)	UAAUUUCUACUCUUGUAGAUCCCCUCUAUUGAUCCCCACC

crRNA-45-spacer (ATP6)	CCCCUCUAUUGAUCCCCACC
crRNA-52 (ND3)	UAAUUUCUACUCUUGUAGAUUAGAUCAAAUAAUAAGAAGG
crRNA-1Up (COX1)	UAAUUUCUACUCUUGUAGAUUGUAUACGGGUUCUUCGAAU
crRNA-2Down (COX1)	UAAUUUCUACUCUUGUAGAUUGGAGGGUUCUUCUACUAUU

The scaffold and spacer sequences in crRNA molecules are colored in black and blue, respectively. Additional 3′-end RNA import motifs of tRK1 (HD and HF), RNase MRP RNA (MRP) are shown in red. The targeted region in human mitochondrial DNA for each crRNA is specified in parentheses in green.

2.2. Methods

2.2.1. Cell culture conditions and mycoplasma screening

HEK293 cell line and their derivatives were maintained at 37 °C, 5 % CO_2 in essential modified Eagle's medium (EMEM) (Sigma-Aldrich) containing 1 g/L D-glucose and supplemented with 1.5 g/L sodium bicarbonate (Sigma-Aldrich) and 0.11 g/L sodium pyruvate (Sigma-Aldrich), 10 % fetal bovine serum (Gibco, Fisher Scientific), 100 mg/L Penicillin-Streptomycin (Sigma-Aldrich) and 2.5 mg/L Amphotericin B (Sigma-Aldrich). The human osteosarcoma cell line 143B was cultivated under the same conditions, with the exception of the medium, which was based on Dulbecco's Modified Eagle Medium (DMEM) (Sigma-Aldrich) containing 4.5 g/L of D-glucose.

To divide cells when the confluency level exceeds 80% or to seed them into a new plate, the old cell medium is aspirated and the cells are washed with an appropriate amount of 1× phosphate-buffered saline (PBS) (Sigma-Aldrich). HEK293 cells and their derivatives have low adhesivity, allowing them to detach easily in PBS through active pipetting. Subsequently, the cells are transferred to a sterile 15 mL Falcon tube and pelleted by centrifugation at 600 g for 10 minutes at room temperature (RT). After centrifugation, the PBS is carefully aspirated without disturbing the cell pellet. The cells are then resuspended in preheated media at 37 °C, and the appropriate volume is seeded into a plate or flask.

For cell freezing, the cells are detached using the abovementioned method, but after centrifugation, the cell pellet is resuspended in a freezing media containing 90 % fetal bovine

serum (Gibco, Fisher Scientific) and 10 % dimethyl sulfoxide (DMSO) (Carl Roth GmbH). The cells are aliquoted into cryogenic storage vials, which are then placed in an insulated box and stored in a –80 °C freezer. After 16 hours, the cryogenic storage vials are transferred to a –150 °C freezer.

Before each experiment, cell cultures were tested for mycoplasma contamination by PCR with DreamTaq Green PCR Master Mix (Thermo Scientific), as described (**Dussurget, O., Roulland-Dussoix, D. *et al.*, 1994**) (see primers in section **2.1.3.**). Total DNA isolated with NucleoSpin® Tissue Mini Kit (Macherey-Nagel), according to the manufacturer's protocol, was used as a PCR template. Analysis of the PCR products was performed by electrophoresis in 1 % agarose gel (w/v) in 1× TAE buffer. EtBr-stained gels were visualized by Hero Lab Transilluminator UVT-28M (Herolab GmbH).

2.2.2. Gibson assembly

Primers with overhangs for Gibson assembly (GA) (**Figure M1**) were designed using SnapGene software V.2.8.3 (GSL Biotech) (see primers in section **2.1.3.**). PCR amplification was carried out using Phusion™ High-Fidelity DNA Polymerase (Thermo Scientific) in a total volume of 50 µL, with 5 ng of pDNA as the template. The resulting PCR products (50 µL) were visualized through electrophoresis in a 1 % agarose gel (w/v) in 1× TAE buffer. The EtBr-stained gels were examined using the Hero Lab Transilluminator UVT-28M (Herolab GmbH). The fragments of the insert and vector were cut out from the gel and purified using the NucleoSpin Gel and PCR Clean-up Mini kit (Macherey-Nagel) following the manufacturer's protocol. DNA concentrations were determined using the NanoDrop 1000 Spectrophotometer V3.5 (Thermo Scientific).

For the GA reaction, 50 ng of both the vector and the insert, along with 10 µL of 2× GA master mix (NEB), were mixed in a total reaction volume of 20 µL. The reaction was incubated at 50 °C for 1 hour. Subsequently, 10 µL of the reaction mixture were directly used for bacterial cell transformation.

Chemically competent *E. coli* XL1-Blue cells were transformed using a high-efficiency transformation protocol. The GA reaction was added to 100 µL of thawed competent cells and incubated on ice for 30 min. The cells were then heat-shocked at 42 °C for 90 seconds and placed back on ice for an additional 2 min. After that, 900 µL of prewarmed LB (Luria-Bertani broth) medium was added to the cells, and they were allowed to recover at 37 °C for 1 hour in a shaking incubator (250 RPM). Subsequently, 100 µL of the culture was plated on an LB agar Petri dish containing 100 µg/mL ampicillin. The dish was then incubated at 37 °C for 16-24 hours. Following

the incubation, colonies were inoculated into fresh LB media with the antibiotic, and after overnight incubation, the plasmids were isolated using the NucleoSpin Plasmid Mini kit (Macherey-Nagel) as per the provided protocol. The accuracy of the assembly was verified with Sanger sequencing at Eurofins Genomics.

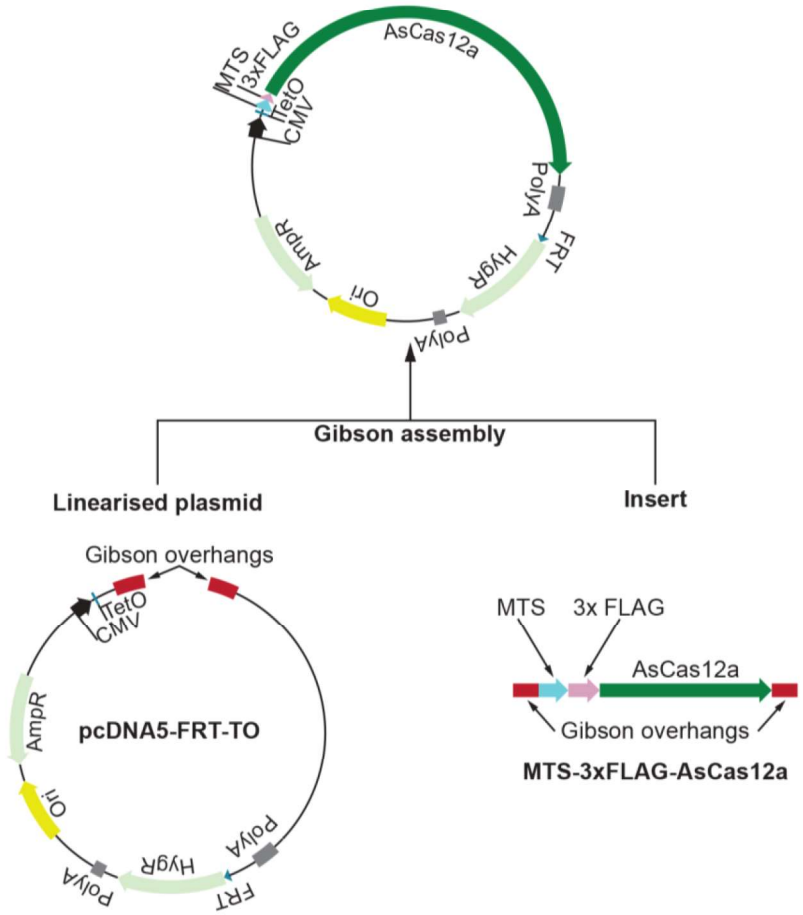


Figure M1. Gibson Assembly of pcDNA5-FRT-TO-MTS-AsCas12a.

Schematic representation of Gibson assembly design for the scarless recloning of the MTS-3×FLAG-AsCas12a coding region into pcDNA5-FRT-TO vector for subsequent stable cell line generation.

2.2.3. Subcellular fractionation to test the protein localization

HEK293 cells, cultured in 60 cm² dishes, were transfected with 14000 ng of plasmid DNA when they reached an 80 % confluency level using Lipofectamine® 3000 transfection reagent (ThermoFisher), following the manufacturer's protocol. After 24 hours of transfection, cells were detached as outlined in section 2.2.1.

For the generation of total cell extracts, cell pellets were lysed in a buffer consisting of 20 mM Tris-HCl (pH 7.4), 250 mM NaCl, and 0.25 % NP-40 detergent (Sigma-Aldrich), along with a cocktail of protease and phosphatase inhibitors (Sigma-Aldrich) at a 1:100 dilution. The lysates were then centrifuged at 14000 g for 15 minutes at 4 °C. The resulting supernatants were collected for subsequent experiments.

To acquire cytoplasmic protein extracts and purified mitochondria from the transfected cells, the Qproteome Mitochondria Isolation Kit (Qiagen) was employed following the manufacturer's recommended protocol. Subsequently, 6 volumes of mitochondrial lysis buffer (25 mM Tris-HCl, pH 7.4; 150 mM NaCl; 1 % Triton™ X-100; 1 mM EDTA; 5 % glycerol) were added to the mitochondrial pellet. Mitochondrial lysis was conducted at 4 °C over a 20-minute incubation period, with periodic vortexing every 5 minutes. Afterward, the mitochondrial lysate was centrifuged for 10 minutes at 10000 g and 4 °C. The resulting supernatant, enriched with mitochondrial proteins, was carefully collected into a clean tube.

Subsequently, the fractions were analyzed further by western blot hybridization, as described in section **2.2.4.** To verify the subcellular localization of the protein of interest, the membrane was hybridized with the control antibodies to TFAM, the mitochondrial matrix protein and GAPDH, as cytosolic marker. The list of antibodies can be found in section **2.1.4.**

2.2.4. Western blot hybridization

The cells ready for an analysis were detached and collected into a 1.5 mL tube following the procedure described in section **2.2.1.** The cell pellets were then resuspended in 1× PBS, ensuring a volume of no less than 50 μL, to facilitate sonication. Subsequently, all procedures were performed on ice unless otherwise specified.

To lyse the cells, the solutions were sonicated for 10 seconds using a Vibra-Cell™ VCX 750 Sonicator equipped with a 2 mm probe (Sonics & Materials, Inc.) at a frequency ranging from 20 to 50 kHz. The protein concentration in the cell lysates were determined using the Bradford assay at 595 nm. This measurement was carried out using ROTI®Nanoquant (Carl Roth GmbH) and the Bio-Rad SmartSpec Plus UV/Vis Spectrophotometer (Bio-Rad). The protein concentration was calculated using a calibration curve constructed from the optical density measurements of BSA samples with known concentrations.

20 μg of protein extracts, isolated as described above or in sections **2.2.3.**; **2.2.7.**, were mixed with Laemmle buffer (4 % SDS, 20 % glycerol, 10 % 2-mercaptoethanol, 0.004 % bromphenol

blue and 0.125 M Tris HCl, pH 6.8) and heated at 95 °C to denature the proteins. Denatured protein extracts were analyzed by 10% SDS-PAGE gel (although the percentage may vary depending on the desired resolution.) in TGS buffer (25 mM Tris base, 190 mM glycine, 0.1 % SDS, adjust pH to 8.3). Separation by electrophoresis was carried out at 150V for 1 hour 30 minutes. Following gel migration, the proteins were transferred on an Amersham Protran nitrocellulose membrane (GE Healthcare) by semi-dry transfer in 1× transfer buffer (48 mM Tris, 39 mM glycine, 20 % methanol, 0.04 % SDS) for 30 min using Trans-Blot® Turbo™ Transfer System (Bio-Rad).

The membrane was blocked using 1× TBST buffer (150 mM NaCl, 50 mM Tris-HCl, 0.1 % Tween-20, pH 7.6) supplemented with 5 % low-fat milk for either 1 hour and 30 minutes at room temperature (RT) or overnight at 4 °C. Subsequently, the membrane was rinsed with 1× TBST buffer and incubated with the appropriately diluted primary antibody in 1× TBST buffer for 1 hour at RT or overnight at 4°C with continuous agitation (refer to section **2.1.4.** for the list of antibodies). After the incubation, the primary antibodies were discarded, and the membrane was washed 3 times for 5 minutes each with 1× TBST buffer at RT. Next, the membrane was incubated with the appropriate dilution of HRP-conjugated secondary antibodies in 1× TBST buffer for 1 hour at RT with constant agitation, followed by another round of washes. The membrane was then subjected to revelation by incubating it for a few minutes in the revelation solution (100 mM Tris-HCl, pH 8.5, 30 % H_2O_2, 90 mM coumaric acid, 250 mM luminol). The visualization of the membrane was performed using the ChemiDoc Touch Imaging System (Bio-Rad), and the obtained images were analyzed with Image Lab software (v. 6.0.1) (Bio-Rad).

2.2.5. Flp-In T-REx monoclonal stable cell line generation

A monoclonal stable T-REx cell line was generated using the commercial Flp-In™ System (Thermo Fisher Scientific) (**Figure M2**), following the manufacturer's protocol.

In brief, to create the Flp-In™ expression cell line, the T-REx cell line was transfected at 70 % confluency in a 6-well plate with a 9:1 ratio of pOG44 Flp-Recombinase expression vector and pcDNA5-FRT-TO using 5 μL of Lipofectamine™ 2000 Transfection Reagent (Invitrogen) in 500 μL of Opti-MEM™ (Gibco, Fisher Scientific), according to the manufacturer's protocol. After 24 hours of transfection, the cells were washed with 1× PBS, and 2 mL of fresh EMEM media was added. Another 24 hours later, the cells were split in the plate for them to be at no more than 25 % confluency, and 75 μg/mL of hygromycin was added to the media to initiate the selection process.

The cells were allowed to propagate in the selective media, which was changed every 3 days, until cell foci could be identified. Subsequently, individual clones were isolated into a new 24-well plate using the clonal ring anchoring method (**Mathupala, S. P., & Sloan, A. E., 2009**) and maintained following standard procedures.

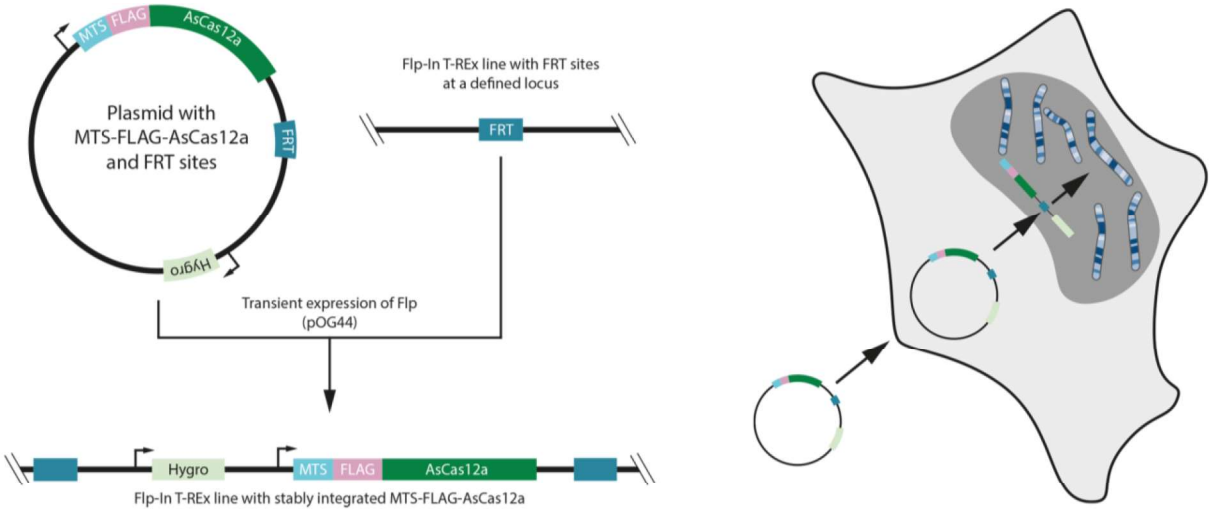


Figure M2. Principle of a Stable Cell Line Generation using the Commercial Flp-In™ System.

The pcDNA5-FRT-TO-MTS-AsCas12a plasmid is co-transfected with pOG44 (plasmid for transient expression of the Flp recombinase) into the Flp-In™ T-REx™ Host Cell Line. The Flp recombinase catalyzes a homologous recombination event between the FRT sites in the host cell's genome and the pcDNA5-FRT-TO-MTS-AsCas12a expression vector. Integration of the expression construct provides hygromycin resistance. The expression of the gene of interest is repressed by the Tet repressor and can be induced by tetracycline.

2.2.6. Isolation of crude mitochondria

Mitochondria were mainly isolated as described in (**Dovydenko, I. *et al.*, 2015**) with modifications. All procedures were carried out at 4 °C, unless specified differently. Briefly, 75 cm² of cells at 80-100 % confluency were washed once with 1× PBS and then detached and resuspended in 1 mL of prechilled Mito buffer (0.6 M sorbitol, 10 mM HEPES-KOH, pH 7.5, 1 mM EDTA). The cells were disrupted by 30 passages through 2 mL syringe with needle No26G (0,45x12 mm). Nuclei, cell debris and unbroken cells were pelleted by centrifugation for 10 min at 1000 g at 4 °C. The procedure was repeated 3 times with transferring the resulting supernatant each time to a new ice-cold tube. Mitochondria-rich pellet was obtained after high-speed centrifugation at 15,000 g at 4 °C for 30 min.

2.2.7. Submitochondrial fractionation to test the protein localization

Submitochondrial fractionation was performed as previously described (**Summer, S. *et al.*, 2020**, **Jeandard, D. *et al.*, 2023**) with modifications. In brief, the mitochondria-rich fraction corresponding to the pellet was obtained by differential centrifugation as described in the section **2.2.6.** For the proteinase K accessibility test, the mitochondrial pellet was carefully resuspended in 300 μL of Mito buffer (0.6 M sorbitol, 10 mM HEPES-KOH, pH 7.5, 1 mM EDTA) and split into three aliquots. The mitochondrial pellet was sedimented again with an excess of Mito buffer. After that, mitochondria were carefully resuspended in 100 μL of Mito buffer (for intact mitochondria), swelling buffer (10 mM HEPES-KOH, pH 7.5, 1 mM EDTA) (for mitoplasts) and lysis buffer (10 mM HEPES-KOH, pH 7.5, 1 mM EDTA, 0.5 % (w/v) n-dodecyl-β-maltoside) (to lyse mitochondria). Each tube was split into 2 aliquots, in which one was treated with 50 μg/mL proteinase K (Promega) for 20 min on ice. The reaction was stopped by adding PMSF to a final concentration of 1 mM in all the samples, including the non-treated ones. To precipitate the proteins, one-fourth of the total volume of 100% trichloroacetic acid was added, and the samples were incubated on ice for 10 minutes. Afterward, the samples were centrifuged at 14000 g for 10 minutes at 4 °C. The supernatant was discarded, and the pellet was washed twice with 500 μL of prechilled acetone through centrifugation at 14000 g for 10 minutes at 4 °C. The resulting supernatant was removed, and the protein pellet was dried overnight at room temperature.

Subsequently, the samples were analyzed further by western blot hybridization, as described in section **2.2.4.** To verify the submitochondrial localization of the protein of interest, the membrane was hybridized with the control antibodies, as, for instant, to TOMM20, the mitochondrial outer membrane protein facing the cytosol; OPA1, the mitochondrial inner membrane protein facing the inner membrane space; and MRPL4, the mitochondrial matrix protein. The list of antibodies can be found in section **2.1.4.**

2.2.8. Immunofluorescent staining and confocal laser scanning microscopy

Immunofluorescent staining was carried out as described (**Whelan D. R., & Bell T. D., 2015**) with modifications. Briefly, 0.15-0.20 cm² of cells were seeded into 8-well Nunc Lab-Tek slides (Thermo Fisher Scientific) that were pre-treated with 0.1 % gelatine for 1 hour at 37 °C. After 24 hours, if necessary, cells were either transfected or subjected to chemical treatment (for instant, the addition of tetracycline).

For transfection, the cell culture media was replaced with 200 µL of freshly preheated EMEM at 37 °C. To transfect the cells, 100 ng of a plasmid DNA were mixed with 0.5 µL of Lipofectamine™ 2000 Transfection Reagent (Invitrogen) in 100 µL of Opti-MEM™ (Gibco, Fisher Scientific), following the manufacturer's protocol, and added to the plate. Alternatively, to activate AsCas12a expression in the established Flp-In T-REx stable cell lines, the cell media was exchanged for 300 µL of fresh EMEM, and the nuclease expression was induced by adding 100 ng/mL of tetracycline. In both cases, the cells were left to propagate for an additional 24 hours.

To perform immunofluorescence staining, the cells were fixed in a pre-heated fixation buffer (4 % paraformaldehyde dissolved in PBS and adjusted to 3% using EMEM). The fixing process was carried out for 12 min at 37 °C. Subsequently, the fixation buffer was removed, and the cells were washed 5 times in a row with 1× PBS.

Next, the cells were permeabilized by adding the permeabilization buffer (0.5 % (v/v) Triton X-100 diluted with 1× PBS) and incubated for 15 min at RT. After another round of washing, the cells were blocked using the blocking buffer (5 % BSA diluted in 1× PBS). Once the incubation period was complete, the blocking solution was discarded, and primary antibodies, appropriately diluted in the blocking buffer (refer to the list of all antibodies in section **2.1.4.**), were added to the cells. The cells were then incubated with the primary antibodies for 3 h at RT.

Afterward, the cells were washed again, and secondary antibodies conjugated with a fluorescent marker, appropriately diluted in the blocking buffer, were added to the cells for 1 h at RT. Starting from this step, all incubations were performed in the dark. Once the incubation was over, the cells were washed, and the nuclei were stained by incubating the cells with 1 µg/ml of DAPI (Invitrogen) in 1× PBS for 10 min at RT, followed by washing.

The samples were imaged on LSM700 microscope (Carl Zeiss) under a 63×/1.4 oil objective in 1× PBS, with the help of Dr. Anna Smirnova. The images were visualized and analyzed using ImageJ 1.52a software (**Schneider, C. A. *et al.*, 2012**). To verify the mitochondrial localization of AsCas12a, the fluorescence profiles of signals attributed to both mitochondria and the protein of interest were assessed along a designated line using ImageJ 1.52a software.

2.2.9. Site-directed mutagenesis

To perform site-directed mutagenesis (SDM) (**Figure M3**), primers were generated using NEB Base Changer V_1.3.3 from the New England Bio Labs Inc. website (nebasechanger.neb.com) (refer to section **2.1.3.** for the list of primers). PCR amplification was performed using Phusion™

High-Fidelity DNA Polymerase (Thermo Scientific) in a total volume of 50 µL. As a template, 5 ng of pDNA was used. The resulting PCR products (10 µL) were visualized by electrophoresis in a 1 % agarose gel (w/v) in 1× TAE buffer. The EtBr-stained gels were viewed using the Hero Lab Transilluminator UVT-28M (Herolab GmbH).

To remove the remaining plasmid, 20 µL of the PCR reaction were digested with 2 µL of FastDigest DpnI (Thermo Scientific) for 1 hour at 37 °C. The reactions were then cleaned using the NucleoSpin Gel and PCR Clean-up Mini kit (Macherey-Nagel) following the manufacturer's recommendations. DNA concentrations were determined using the NanoDrop 1000 Spectrophotometer V3.5 (Thermo Scientific), and 200 ng of linear DNA was ligated with 5 U of T4 DNA Ligase (Thermo Scientific) for 2 hours at RT, following the manufacturer's protocol. Subsequently, 10 µL of the ligation reaction were directly used for bacterial cell transformation, as described in section **2.2.2.** Following colony inoculation and plasmid DNA isolation, 500 ng of isolated plasmids underwent a control digestion with FastDigest restriction endonucleases AanI and XmiI (Thermo Scientific). The correct assembly after SDM was further confirmed by Sanger sequencing at Eurofins Genomics.

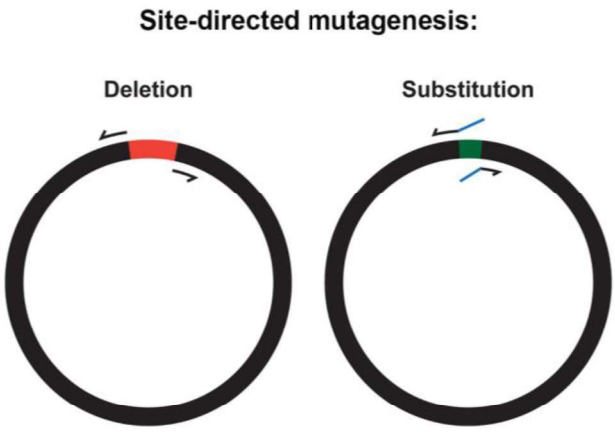


Figure M3. Primer Design for the Site-Directed Mutagenesis.

Schematic representation of primers design for site-directed mutagenesis, enabling either the creation of a deletion or a substitution in a plasmid. Deletions are engineered by designing non-mutagenic forward and reverse primers (shown in black) that flank the region to be deleted (shown in red). Substitutions (shown in green) are created by incorporating the desired sequence back-to-back at the 5'-ends of forward and reverse primers (shown in blue), whereas 3'-ends of both primers are complementary to the plasmid (shown in black).

2.2.10. Design of AsCas12a crRNAs

RNAfold (**Lorenz, R. *et al.*, 2011**) and Mfold web servers (**Zuker, M., 2003**) were used to predict secondary structures of AsCas12a crRNAs. To predict secondary structures of crRNAs upon dimer formation, RNAcofold web server was used (**Lorenz, R. *et al.*, 2011**). In order to search for the potential off-target sites of AsCas12a RNA-guided endonuclease, we used Cas-OFFinder algorithm (**Bae, S. *et al.*, 2014**).

In the reference human mtDNA sequence (GenBank NC_012920 gi:251831106), 530 sequences representing the canonical AsCas12a "TTTV" PAM were found (**Gao, L. *et al.*, 2017**). Following the PAM sites, subsequent 5' – 3' 20 bp sequences of spacers were supplemented at the 5' -end by the AsCas12a scaffold sequence – "UAAUUUCUACUCUUGUAGAU" (**Yamano, T. *et al.*, 2016**). crRNAs were analyzed for predicted probability of introducing unwanted changes (off-targets) into the nuclear genome by the AsCas12a-crRNA complex, as well as for predicted secondary structures. The list of crRNA can be found in section **2.1.6.**

2.2.11. *In vitro* transcription of AsCas12a crRNAs bearing import determinants

crRNAs were *in vitro* transcribed using HiScribe™ T7 High Yield RNA Synthesis Kit (NEB) according to the manufacturer's protocol. As a DNA template, we used PCR amplicons obtained from the plasmids encoding non-modified (NM) crRNAs and modified versions bearing RNA import determinants (MRP, HD, HF) using Phusion™ High-Fidelity DNA Polymerase (Thermo Scientific). The list of crRNA can be found in section **2.1.6.** T7 promoter was added to the sequence of forward primer (see section **2.1.3.**). *In vitro* transcribed crRNAs were purified using TRIzol™ Reagent (Invitrogen) according to the manufacturer's protocol. RNA concentrations were measured using NanoDrop 1000 Spectrophotometer V3.5 (Thermo Scientific). The quality of synthetic crRNAs was verified by electrophoresis in 8 M urea denaturing 10 % polyacrylamide gel. Following 1 hour migration at 20 mA, EtBr-stained gel was visualized by Hero Lab Transilluminator UVT-28M (Herolab GmbH).

2.2.12. Chemical synthesis of AsCas12a crRNAs

The oligoribonucleotides were synthesized by our collaborators (team of Dr. Vadim Shmanai, National Academy of Science of Belarus, Minsk, Belarus) using an automatic DNA/RNA synthesizer ASM 2000 (Biosset Ltd.) at 500 nmol scale on 1000 Å Universal support CPG

(Primetech ALC, 41 μmol/g) as described in our resent publication (**Shebanova, R. & Nikitchina, N. *et al.*, 2022**). Synthetic crRNAs were protected with terminal 2'-O-Methyl (2'-O-Me) and phosphorothioate (PS) modifications (**McMahon, M. A. *et al.*, 2018**). The list of crRNA can be found in section **2.1.6.**

Additional chemical modifications were introduced at the 3'-end of the AsCas12a crRNA. Cholesterol modification was directly incorporated during the solid-phase synthesis. Modifications involving azides of rhodamine (R6G) and berberine were accomplished through a click azide-alkyne cycloaddition reaction.

2.2.13. *In vitro* cleavage in cell lysate

mtDNA fragments were amplified with Phusion™ High-Fidelity DNA Polymerase (Thermo Scientific). As a PCR template, genomic DNA isolated from T-REx cell line (T-REx™-293 Cell Line, Invitrogen) by NucleoSpin® Tissue Mini Kit (Macherey-Nagel) according to the manufacturer's protocol was used. DNA oligonucleotides used for the template DNA amplification are listed in section **2.1.3.**

Cells with inducible expression of the Su9-AsCas12a nuclease were cultured in a 6-well plate. The expression of the nuclease was activated at 80 % confluency by the addition of tetracycline to a final concentration of 50 ng/mL. Alternatively, T-REx cell line was transfected at 80 % confluency in a 6-well plate with 1500 ng of pcDNA5-FRT-TO-Su9-AsCas12a/ddAsCas12a using 5 μL of Lipofectamine™ 2000 Transfection Reagent (Invitrogen) in 500 μL of Opti-MEM™ (Gibco, Fisher Scientific), according to the manufacturer's protocol. The media was supplemented with 50 ng/mL of tetracycline.

24 hours after the induction or transfection, cells were washed with 1× PBS and lysed by 50 μL/cm^2 lysis buffer (20 mM HEPES-KOH pH 7.5, 100 mM KCl, 5 mM $MgCl_2$, 1 mM DTT, 5 % glycerol, 0.1 % Triton X-100 and Protease Inhibitor cocktail (Roche Diognoctics)) and then rocked for 10 min at 4 °C. To remove cell debris, lysates were centrifuged for 10 min at 1000 g, 4 °C. The resulting supernatant was divided into aliquots and stored at –80 °C.

Cleavage reactions were carried out in a total volume of 20 μl and contained 18 μl of cell lysate, 150 ng of mtDNA fragment and 50 ng of crRNA (section **2.1.6.**) (if other not specified). Reactions were incubated for 30 min at 37 °C. After incubation, reactions were purified with NucleoSpin® PCR Clean-up Kit (Macherey-Nagel) according to the manufacturer's protocol. Analysis of the

cleavage products was performed by electrophoresis in 1 % agarose gel (w/v) in 1× TAE buffer. EtBr-stained gels were visualized by Hero Lab Transilluminator UVT-28M (Herolab GmbH).

Alternatively, to verify AsCas12a/crRNA functionality in cells, the HEK 293 T-REx cell lines, expressing AsCas12a nuclease upon the induction, were cultured in a 12-well plate and transfected at 80 % confluency with increasing amounts of AsCas12a crRNA (175, 250, 375 ng/cm^2) using Lipofectamine™ 2000 transfection reagent (Invitrogen) in 500 μL of Opti-MEM™ reduced serum medium (Gibco, Fisher Scientific). After 6 hours of transfection, the medium was changed to 2 mL of EMEM supplemented with 100 ng/mL of tetracycline to activate the nuclease expression. After 24 hours, the cell lysates were prepared as described above. The *in vitro* cleavage reactions contained the appropriate DNA template, but no additional crRNA was added, except for the control reaction.

2.2.14. Oxygen Consumption measurement

The T-REx and Flp-In T-REx-Su9-AsCas12a cell lines were cultured in 25 cm² flasks until they reached 80 % confluency. At this point, the cells were treated with 100 ng/mL of tetracycline 48 hours prior to the analysis. On the day of the experiment, the cells were detached and resuspended in 1 mL of preheated EMEM media. Cell counting was done using the Scepter™ 2.0 Handheld Automated Cell Counter with 60 μm sensors (Sigma-Aldrich) for further normalization.

Oxygen consumption measurement was performed using the Oxygraph+ System (Hansatech Instruments Ltd). Before the analysis, the oxygen sensor was calibrated following the manufacturer's protocol. The oxygraph chamber was equipped with a magnetic stirring bar for continuous mixing, and a water circulating pump maintained a constant temperature of 37 °C.

To initiate the measurement, 1 mL of cell suspension was loaded into the chamber, and basal respiration was recorded for 3 minutes until a stable oxygen consumption (flux) was achieved. Subsequently, 5 μl of 1 mg/mL oligomycin (Sigma-Aldrich) (5 µg/mL) was injected into the oxygraph chamber, and cellular respiration was recorded for 2 minutes until a stable oxygen flux signal was obtained. The oxygen consumption rate (OCR) upon oligomycin addition was repeated a second time, and the results were compared. Next, 10 μl of FCCP (Sigma-Aldrich) (0.5 μM) were injected into the chamber, and the signal was recorded for 2 minutes. When a stable signal was obtained, the addition of FCCP was repeated. The addition of FCCP was stopped when the OCR reached its maximal level and began to decline. Following the FCCP treatment, respiration

upon the addition of 5 µL of a mix of rotenone (Sigma-Aldrich) and antimycin A (Sigma-Aldrich) (0.2 µM and 5 µM, respectively) was recorded until a stable signal appeared (2 minutes).

The analysis of the OCR data was performed using Oxygraph Plus software (Hansatech) and the OCR was normalized by the number of cells.

2.2.15. RNA transfections for mitochondrial import evaluation

For AsCas12a crRNAs mitochondrial import analysis, cells were transfected at 80 % confluency in 75 cm^2 cell culture flask with 6 µg of chemically-synthesized or T7-transcribed crRNA using 20 µL of Lipofectamine™ 2000 transfection reagent (Invitrogen) in 9 mL Opti-MEM™ reduced serum medium (Gibco, Fisher Scientific). The list of crRNA can be found in section **2.1.6.** 6 h after transfection, the medium was changed to 12 mL of EMEM, and cells were left to propagate for another 48 h. After that, crude mitochondria were isolated from the transfected cells by differential centrifugation as described in section **2.2.6.**

2.2.16. RNA isolation from mitochondria

Mitochondria-rich fraction corresponding to the pellet was obtained by differential centrifugation from the cells transfected with AsCas12a crRNA (section **2.2.15.**) as described in section **2.2.6.** 50 µL of resuspended cells (1 mL) were taken for total RNA isolation prior to cell disruption for mitochondria isolation.

Mitochondria-rich pellet was carefully resuspended in 150 µL of Mito buffer (0.6 M sorbitol, 10 mM HEPES-KOH, pH 7.5, 1 mM EDTA). 30 µL of resuspended mitochondria were taken for lysate preparation (see below). To decrease possible cytosolic RNA contamination, 120 µL of 2× RNase A solution (20 µg/mL ribonuclease A from bovine pancreas, 4 mM $MgCl_2$, 200 mM NaCl) was added to the purified mitochondria. The reaction was incubated at room temperature for 7 min and then stopped by adding 500 µL of Mito buffer containing 4 mM EDTA. RNase A was washed out by centrifugation at 15,000 g at 4 °C for 15 min 3 times with 500 µL of Mito buffer, each time discarding the resulting supernatant. After the last centrifugation, mitochondria were resuspended in 300 µL of Mito buffer. In order to obtain mitoplasts, mitochondria were treated with 20 µg of digitonin (Sigma-Aldrich) for 7 min at room temperature. The resulting mitoplasts were centrifuged for 15 min at 15,000 g at 4 °C and washed ones with 500 µl of Mito buffer. To proceed with RNA isolation, the mitoplast pellet was resuspended in 500 µL of TRIzol™ Reagent (Invitrogen) and was either stored at −80 °C or treated immediately.

To prepare mitochondrial lysate, mitochondria were treated with n-dodecyl-β-D-maltoside (Sigma-Aldrich) (0.5 % final concentration (w/v)), 20 µg of digitonin (Sigma-Aldrich) and with an equal volume of 2× RNase A solution to degrade mitochondrial RNA and to demonstrate possible presence of RNase-resistant contaminant. After a brief pipetting, the mixture was left for incubation at room temperature for 10 min. To proceed with RNA isolation, the mitochondrial lysate was resuspended in 500 µL of TRIzol™ Reagent (Invitrogen).

2.2.17. Submitochondrial fractionation of RNA

Submitochondrial fractionation was performed as previously described (**Summer, S. *et al.*, 2020**, **Jeandard, D. *et al.*, 2023**) with modifications. In brief, the mitochondria-rich fraction corresponding to the pellet was obtained by differential centrifugation as described in section **2.2.6.**

For the RNase A/T_1 accessibility test, the mitochondrial pellet was carefully resuspended in 300 µL of Mito buffer (0.6 M sorbitol, 10 mM HEPES-KOH, pH 7.5, 1 mM EDTA) and split into three aliquots. The mitochondrial pellet was sedimented again with an excess of Mito buffer. After that, mitochondria were carefully resuspended in 100 µl of Mito buffer (for intact mitochondria), swelling buffer (10 mM HEPES-KOH, pH 7.5, 1 mM EDTA) (for mitoplasts) and lysis buffer (10 mM HEPES-KOH, pH 7.5, 1 mM EDTA, 0.5 % (w/v) n-dodecyl-β-maltoside) (to lyse mitochondria). Each tube was split into 2 aliquots, in which one was treated with 1.5 µL of RNase A/T_1 mix (2 mg/mL, 5.000 U/mL; Thermo Fisher Scientific) for 10 min at room temperature. For RNA extraction, 500 µL of TRIzol™ Reagent (Invitrogen) were added to the reaction.

2.2.18. Northern blot analysis

RNA was purified using TRIzol™ Reagent (Invitrogen) according to the manufacturer's protocol, followed by precipitation with isopropanol. RNA pellets were diluted in 15 µL of nuclease-free water. Northern blot analysis was performed as described (**Dovydenko, I. *et al.*, 2015**). Purified RNA samples were separated on a 10 % (w/v) denaturing polyacrylamide gel. After electrophoresis at 20 mA in 1× TBE until the bromophenol blue dye reached the middle of the gel, samples were electroblotted onto a nylon Amersham HybondN+ membrane (GE Healthcare) in a wet transfer camera in 0.5× TBE at 4 °C, 10 V, overnight. RNAs were fixed on the membrane by irradiation in a cross-linking UV chamber (Amersham Life Science), for 3 min at each side of the membrane at constant energy 1.500 × 100 µJ/cm^2. After that, membranes were pre-hybridized by rotating in a hybridization oven in 6× SSC, 0.1 % SDS, 10× Denhardt solution for 1 h at 65 °C.

The pre-hybridized membranes were incubated overnight with continuous rotation in 10 mL of prehybridization buffer supplemented with 5′-^{32}P-labeled antisense oligonucleotide probe at 56 °C. DNA oligonucleotide probes (10 pmol) (see section **2.1.5.**) were radiolabeled with γ-^{32}P-ATP using T4 polynucleotide Kinase (Thermo Scientific) and then purified by size exclusion chromatography with Micro Bio-Spin™ Chromatography Columns (Bio-Rad) according to the manufacturers' protocols. After hybridization, membranes were washed 3 times for 10 min in 5× SSC, 0.1 % SDS buffer, and sealed between two polyethylene sheets and exposed on the phosphoimager screen overnight. The hybridization signal was visualized on Typhoon Trio (GE Healthcare) and analyzed with ImageQuant TL (v. 7.0, GE Healthcare). Before proceeding with hybridization with other probes, membranes were stripped 3 times for 10 min in 0.02× SSC, 0.1 % SDS buffer at 80 °C.

2.2.19. Quantitative analysis of RNA import

After quantification using the Typhoon Trio scanner, the relative efficiency of RNA import into mitochondria was calculated as a ratio between the signal obtained with a probe specific for AsCas12a crRNA used for cell transfection and that obtained with the probe against the host mitochondrial tRNA (mt $tRNA^{Val}$) (**Dovydenko, I. *et al.*, 2015**). To detect possible AsCas12a crRNAs' protection against treatment with RNases not linked to the mitochondrial import, a control experiment consisting of the lysis of the portion of mitochondria was considered.

2.2.20. Expression and purification of recombinant AsCas12a nuclease

AsCas12a nuclease was expressed from the 6His-MBP-TEV-huAsCpf1plasmid vector (Addgene, Plasmid #90095) and purified from *E. coli* expression strain BL21-DE3 as described (**Zetsche, B. *et al.*, 2017**) with modifications. In brief, chemically competent BL21-DE3 cells were transformed, following the procedure outlined in section **2.2.2.** The plasmid-containing bacterial colony was picked and cultivated at 37 °C in 1 L of LB medium, supplemented with 100 μg/mL of ampicillin, until the optical density at 600 nm (OD600) reached 0.8. Subsequently, the temperature was lowered to 18 °C. Nuclease expression was induced by adding isopropyl-β-D-1-thiogalactopyranoside (IPTG) to a final concentration of 200 μM. The culture was then maintained at 18 °C for a duration of 12-16 hours. The cell pellet was collected by centrifugation at 8,000 g for 10 minutes at 4 °C and then resuspended in Buffer A (50 mM Tris-HCl, pH 8.0, 20 mM imidazole, 300 mM NaCl, and 5 mM 2-mercaptoethanol). Subsequently, the cells were lysed by

sonication for 30 minutes, with intervals of 1 minute, on ice. The resulting lysate was centrifuged at 12,000 g for 20 minutes at 4 °C. Following this, the supernatant was removed and filtered through a 0.2 μM filter (Millipore, Sigma), just before being applied to the cartridge.

For protein purification, ÄKTA start protein purification system (GE Healthcare) was used. The supernatant was loaded onto a HiTrap SP HP column (GE Healthcare), which had been equilibrated with Buffer A for 5 column volumes (CV). Then the column was washed with 10 CV of Buffer A. Subsequently, the elution of the protein was done in Buffer B (50 mM Tris-HCl, pH 8.0, 500 mM imidazole, 300 mM NaCl, and 5 mM 2-mercaptoethanol) (**Figure M4**). The expressed nuclease contains a cleavage site for the tobacco etch virus (TEV) protease. To eliminate the 6xHis6-tag, the protein was combined with TEV protease and subsequently dialyzed against Buffer C (20 mM Tris-HCl, pH 8.0, 40 mM imidazole, 300 mM NaCl, and 5 mM 2-mercaptoethanol) for 12 hours at 4 °C with continuous mixing. The purification of the AsCas12a nuclease was further conducted through gel filtration chromatography, with a HiLoad Superdex 200 16/60 column (GE Healthcare), which was pre-equilibrated with buffer D (10 mM Tris-HCl, pH 8.0, 150 mM NaCl, and 1 mM DTT) (**Figure M4**). Post-gel filtration, the nuclease was concentrated using an Amicon Ultra 10K filter (Millipore, Sigma). Subsequently, the purified AsCas12a was stored at –80 °C freezer.

For determining the protein concentration, the Qubit Protein Assay Kit (Thermo Fisher) was used, following the guidelines provided by the manufacturer. The assessment of protein quality was carried out through 8 % SDS-PAGE gel electrophoresis. The resulting image was visualized using the Gel Doc EZ Imager (BioRad).

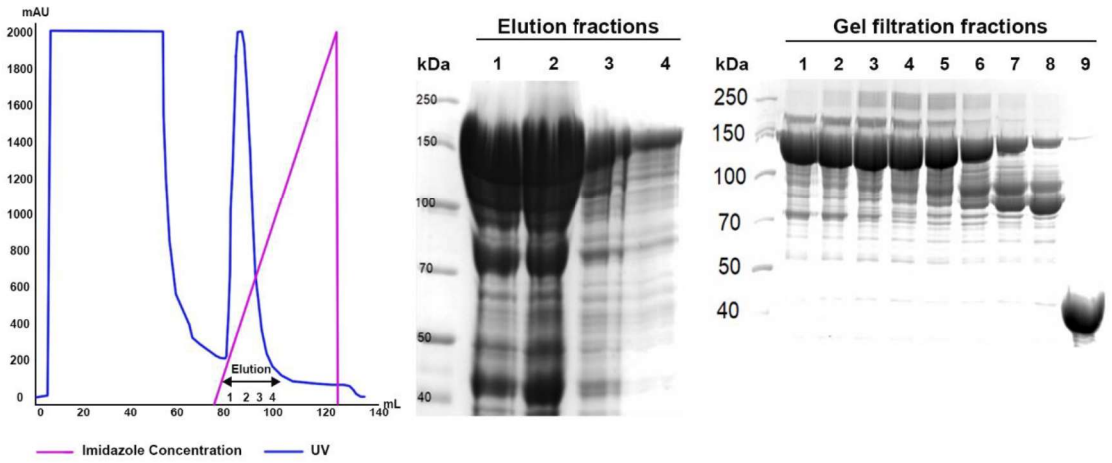


Figure M4. Recombinant AsCas12a Protein Purification using Immobilized Metal Affinity Chromatography.

On the left: chromatogram of AsCas12a purification using Ni-affinity column (ÄKTA start protein purification system). Elution fractions 1-4 were analyzed by SDS-PAGE (8%). The main band corresponds to the 6xHis-AsCas12a protein (middle panel). On the right: SDS-PAGE visualization of AsCas12a purification by gel filtration (HiLoad Superdex 200) after removing of the 6xHis-tag. AsCas12a nuclease (~150 kDa) (fractions 1-8), cleaved out 6xHis-tag (~45kDa) (fraction 9).

2.2.21. *In vitro* cleavage with the recombinant AsCas12a

In vitro cleavage assays with the recombinant AsCas12a nuclease (purified as described in section **2.2.20.**) were conducted in 30 μL volumes using 1× NEB2.1 buffer (NEB). The DNA substrates employed for these assays were fragments of human mtDNA amplified using Q5 High-Fidelity 2× Master Mix (NEB). Genomic DNA isolated from the T-REx cell line with GeneJET Genomic DNA Purification Kit (Thermo Scientific) was utilized as the template. Primers used for the amplification can be found in section **2.1.3.**

The standard reaction mixture contained 10 nM of DNA template, 30 nM of the nuclease, and 300 nM of the crRNA (section **2.1.6.**). The reactions were incubated for 30 minutes at 37 °C and then stopped by the addition of 40 μg of Proteinase K (Promega) and a further 15-minute incubation at 37 °C. Analysis of the cleavage products was performed by electrophoresis in 1 % agarose gel in 1× TBE buffer. EtBr staining gels were visualized by Gel Doc EZ Imager (Bio-Rad) and quantified with Image Lab™ Software 6.0.1 (Bio-Rad).

2.2.22. Total DNA isolation

Total DNA isolation from cells was performed using the phenol-chloroform extraction method. The cell pellet was obtained from cells cultured in 12-well plates, as described in section **2.2.1.** The process began by resuspending the cell pellet in 500 µL of lysis buffer (20 mM HEPES (pH 7.8), 75 mM NaCl, 50 mM EDTA) supplemented with 5 µL of Proteinase K (20 mg/mL), followed by incubation at 50 °C for 30 minutes. Subsequently, 25 µL of 20 % sarkosyl (Sigma-Aldrich) was added, and the lysis was continued for another 30 minutes at 50 °C. All subsequent procedures were conducted on ice.

After the incubation, an equal volume of phenol with pH 7-8 (Roth) was added, and the reactions were gently mixed for 10 minutes on a rotating wheel at 4 °C. To collect the aqueous phase containing DNA, the reactions were then centrifuged at 10 000 g for 15 minutes at 4 °C. The resulting supernatant was carefully transferred into a new pre-chilled tube, and 1 volume of chloroform:isoamyl alcohol (24:1) (Roth) was added. After another 10 minutes of mixing on the rotating wheel at 4 °C, the mixture was centrifuged for 15 minutes at 10 000 g, 4 °C. The obtained aqueous phase (supernatant) was transferred into another pre-chilled tube, and NaCl was added to a final concentration of 100 mM, followed by the addition of 1 volume of ice-cold isopropanol. The mixture was gently mixed, and DNA was precipitated at -20 °C for at least 30 minutes.

To complete the DNA precipitation, the tubes were centrifuged in a pre-chilled centrifuge at 13 000 g for 30 minutes at 4 °C. The resulting supernatant was discarded, and the DNA pellet was washed by adding 500 µL of ice-cold 80 % ethanol, followed by centrifugation for 15 minutes under the same parameters. The supernatant was then carefully removed without disturbing the DNA pellet, and the remaining ethanol was allowed to evaporate with the lid open for 10-15 minutes at RT. Finally, the DNA pellet was dissolved in molecular-grade water, and the DNA concentration was determined using the NanoDrop 1000 Spectrophotometer V3.5 (Thermo Scientific).

2.2.23. qPCR to determine mtDNA copy number

To quantify the mtDNA copy number within the cells, a real-time quantitative polymerase chain reaction (qPCR) was employed. Total DNA extraction from cells was conducted according to the process outlined in section **2.2.22.** The detection of DNA amplification was obtained using SsoAdvanced Universal SYBR Green Supermix (Bio-Rad) in the CFX96 Real-Time System / C1000 Touch Thermal Cycler system (Bio-Rad).

For each DNA sample, two separate reactions were prepared, each utilizing primers for either mitochondrial DNA (12S gene) or nuclear DNA (TST gene) amplification. The primer sequences can be found in section **2.1.3.** Each qPCR reaction was performed in a technical triplicate and the mean cycle threshold (Ct) value was calculated. The qPCR reaction volume of 20 µL consisted of 1× SYBR Green Supermix, 10 pmol of both forward and reverse primers for either mtDNA or nuclear DNA, and 20 ng of isolated total DNA. The reaction conditions were as follows: an initial denaturation at 95 °C for 3 minutes, followed by 40 cycles of denaturation at 95 °C for 15 seconds, and annealing/elongation at 58 °C for 30 seconds. Fluorescent levels were detected after each cycle. After completion of the amplification, a melt curve analysis was performed using the following protocol: starting at 4 °C, increasing to 95 °C in 0.5 °C increments with fluorescent detection at each step. The qPCR data were analyzed using Bio-Rad CFX Manager Software (version 3.1; Bio-Rad).

Relative mtDNA copy numbers were estimated using the 2−ΔΔCT method (**Livak, K. J. and Schmittgen, T. D., 2001**).

2.2.24. Knockdown of MGME1 with siRNA

Cells were transfected with DsiRNA against MGME1 (hs.Ri.MGME1.13.8, IDT) at a final concentration of 40 nM using Lipofectamine RNAiMAX transfection reagent (Invitrogen) according to the manufacturer's recommendations with slight modifications. Two hours prior to the transfection, the cell media was exchanged for Opti-MEM™ (Gibco, Fisher Scientific). The siRNA-Lipofectamine reaction mix was incubated for 20 minutes before being added to the cells. Six hours after transfection, the transfection media was replaced with a complete one (EMEM/DMEM). The initial siRNA transfection was conducted in suspension. Three days later, the transfection was repeated under standard adhesive cell conditions.

siRNA duplex sequences:

5'-rArGrCrCrUrUrGrGrArArArGrCrArUrArCrUrUrUrCrArCCC-3'
5'-rGrGrGrUrGrArArArGrUrArUrGrCrUrUrUrCrCrArArGrGrCrUrUrC-3'

2.2.25. mtDNA isolation for NGS

On the first day, cells cultivated in 75 cm² flasks were transfected with MGME1-targeting siRNAs at a final concentration of 40 nM (section **2.2.24.**). Following 24 hours after the transfection, cells were again transfected with a single crRNA at a dosage of 13 µg or with 6.75 µg for each crRNA

when two crRNAs were employed simultaneously (section **2.2.15.**). On the same day or the following day, the AsCas12a nuclease expression was induced by the addition of 50 ng/mL of tetracycline. All cells were detached on the fourth day.

The cell pellet was obtained as described in section **2.2.1.** A fraction of the cells, specifically 1.5 cm^2 (equivalent to 1/50 of the total), was taken for the preparation of 20 μL of cell lysate as detailed in section **2.2.13.** The remaining cells were suspended in 9 volumes of hypotonic buffer (20 mM HEPES (pH 7.5), 5 mM KCl, 1.5 mM $MgCl_2$, 2 mM DTT, 1 mM PMSF, 1 mg/mL BSA, and a 1/50 (v/v) proportion of Proteinase inhibitor cocktail (Roshe)). This suspension was kept on ice for a duration of 10 minutes. All the subsequent procedures were performed while maintaining the samples on ice.

Cell disruption was achieved using a Dounce homogenizer equipped with an ultra-thin piston 50-70 times. Directly following this step, a 2.5×Mito buffer (525 mM mannitol, 175 mM sucrose, 20 mM HEPES (pH 7.5), 5 mM EDTA, 2 mM DTT, 1 mM PMSF, 1 mg/mL BSA, and a 1/50 (v/v) proportion of Proteinase inhibitor cocktail (Roshe)) was added to the lysate to dilute it to 1x. The lysate underwent centrifugation at 1500 g for 10 minutes at 4 °C to pellet nuclei, cell debris, and unbroken cells. This centrifugation step was repeated twice with the resulting supernatant. Subsequently, high-speed centrifugation was conducted at 10 000 g for 30 minutes at 4 °C. The resulting mitochondrial pellet was resuspended in 1 mL of 1x DNase I buffer, consisting of 900 μL of 1× Mito buffer (210 mM mannitol, 70 mM sucrose, 20 mM HEPES pH 7.5, 2 mM EDTA, 2 mM DTT, 1 mM PMSF, 1 mg/mL BSA, 1/50 (v/v) of Proteinase inhibitor cocktail (Roshe)) and 100 μL of 10× DNase I buffer (100 mM Tris-HCl (7.5), 25 mM $MgCl_2$, 5 mM $CaCl_2$). From these resuspended mitochondria, a 20 μL aliquot (1/50) was taken for lysate preparation in a volume of 10 μl (section **2.2.13.**).

A DNAse I digestion was initiated by adding 20 U of DNAse I to the mixture, followed by incubation for 15 minutes with continuous rotation on a rotating wheel within a cold room (maintained at 4 °C). To stop the reaction, EDTA was introduced to a final concentration of 15 mM. Subsequently, the mixture was centrifuged for 15 minutes at 10 000 g and 4 °C. The mitochondrial pellet was subjected to two rounds of washing using an excess of 1x Mito buffer devoid of BSA.

The mitochondrial pellet was then resuspended in 200 μL of Lysis buffer (20 mM HEPES (pH 7.5), 75 mM NaCl, 50 mM EDTA) supplemented with 40 μg of Proteinase K. The tubes were incubated for 45 minutes on ice. Following this incubation, 10 μL of 20 % sarcosyl was added, and the

reactions were further incubated for 45 minutes at 50 °C. Post-incubation, an equal volume of phenol with a pH range of 7-8 (Roth) was added, and the reactions were gently mixed for 10 minutes on a rotating wheel at 4 °C. To collect the DNA-containing aqueous phase, the mixture was then centrifuged at 10 000 g for 15 minutes at 4 °C. The obtained supernatant was carefully transferred to a new pre-chilled tube, and 1 volume of chloroform:isoamyl alcohol (24:1) (Roth) was added. After an additional 10 minutes of mixing on the rotating wheel at 4 °C, the mixture underwent centrifugation for 15 minutes at 10 000 g and 4 °C. The resulting supernatant was transferred to another pre-chilled tube, and NaCl was added to achieve a final concentration of 100 mM. This was followed by the addition of an equal volume of ice-cold isopropanol.

The mixture was gently mixed, and DNA precipitation was done at -20 °C for at least 30 minutes. The isolated mtDNA was subsequently precipitated, following the procedure outlined in section **2.2.22.**

2.2.26. NGS of linker-ligated mtDNA

A quantity of 1 µg of isolated mtDNA (as described in section **2.2.26.**) underwent pre-treatment with Klenow Fragment (Thermo Fisher Scientific). For this, a reaction volume of 20 µL contained a mixture of 2 mM dNTPs, 2 U of Klenow Fragment, and 1× FastDigest reaction buffer from Thermo Fisher Scientific. The reaction was incubated at 37 °C for 15 minutes, followed by inactivation at 75 °C for 10 minutes. Subsequently, 200 ng of DNA from the previous reaction (equivalent to 4 µL) was ligated with an asymmetrical double-stranded linker, using 400,000 U of T4 DNA ligase (NEB). The total reaction volume was 60 µL. The ligation reaction was incubated at 16 °C for 16 hours, followed by inactivation at 65 °C for 10 minutes.

To prepare a unidirectional linker, 20 µM primers were mixed in 250 mM Tris-HCl (pH 8). After denaturation at 95 °C for 10 minutes, the temperature was gradually lowered until it reached RT. The primer list can be referred to in section **2.1.3.**

Next-Generation Sequencing (NGS) of 1 µg of linker-ligated mtDNA (**Figure M5**) was carried out at both the Skolkovo Institute of Science and Technology "Genomics Core Facility" (Moscow, Russia) and NOVOGENE (Baltimore, USA). DNA libraries were prepared on-site using Illumina TruSeq Nano DNA Sample Preparation Kit (Illumina). Sequencing was performed using an Illumina HiSeq4000 instrument (Illumina), and 75-bp paired-end reads were generated.

The obtained reads were graciously analyzed by Dr. Gábor Zsurka at the University of Bonn in Bonn, Germany.

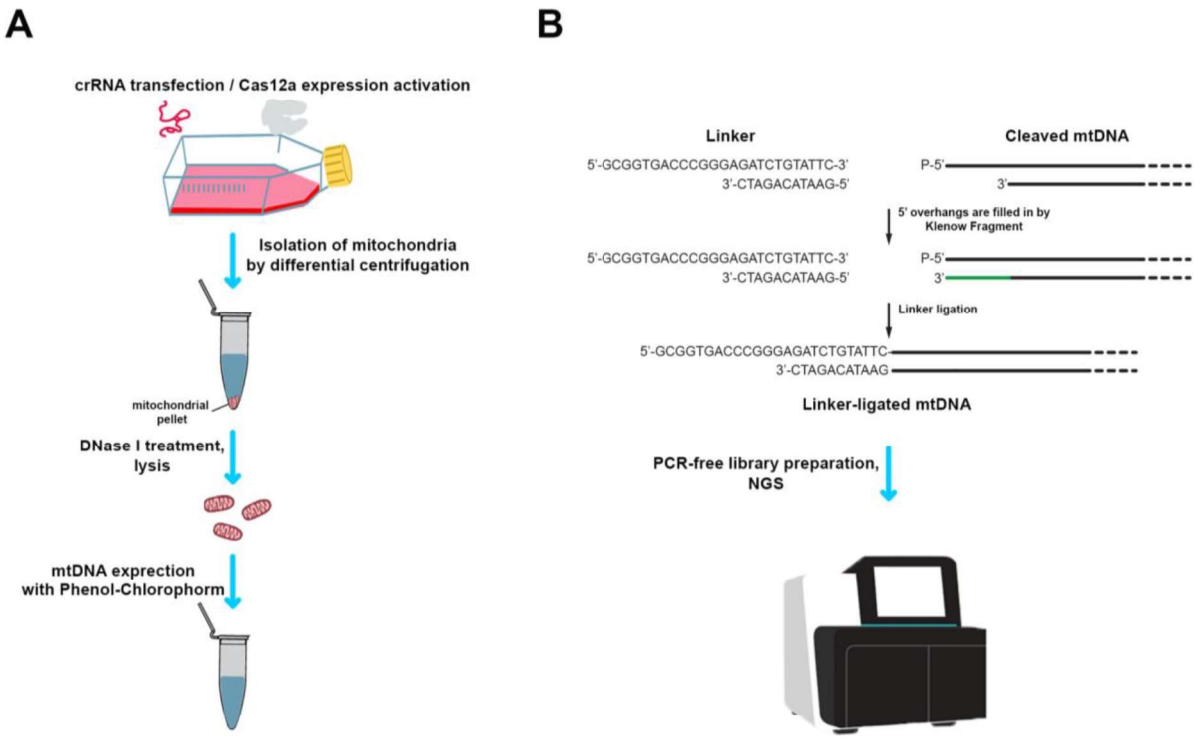


Figure M5. Sample Preparation for mtDNA Linker-Ligated Sequencing.

(A) Isolation of mitochondria and mtDNA from cultured human cells.
(B) Labelling of cleavage sites in mtDNA by ligation with an asymmetric double-stranded linker. Adapted from Peeva, V. *et al.*, 2018.

2.2.27. LM-PCR

Linker-mediated PCR (LM-PCR) (**Figure M6**) was carried out following the procedure described in **Peeva *et al.*, 2018**. The asymmetric double-stranded linker was annealed and subsequently ligated to mtDNA, as detailed in section **2.2.26.** The PCR amplification utilized the Phusion™ High-Fidelity DNA Polymerase (Thermo Scientific). Within a reaction volume of 12.5 μL, the components were as follows: 0.25 U of the polymerase, 2 mM dNTPs, 0.9 pmol of linker-specific primer, 7.5 pmol of mtDNA-specific primer, and 3 ng of linker-ligated mtDNA (section **2.2.26.**). The amplification protocol proceeded as follows: 98 °C for 30 seconds, followed by 42 cycles of 98 °C for 10 seconds and 68 °C for 1 minute, and a final elongation step at 72 °C for 5 minutes. The primer sequences can be found in section **2.1.3.**

To analyze the PCR products, electrophoresis was performed in 1 % agarose gel (w/v) in 1× TAE buffer. The resulting EtBr-stained gels were visualized using the Hero Lab Transilluminator UVT-28M (Herolab GmbH).

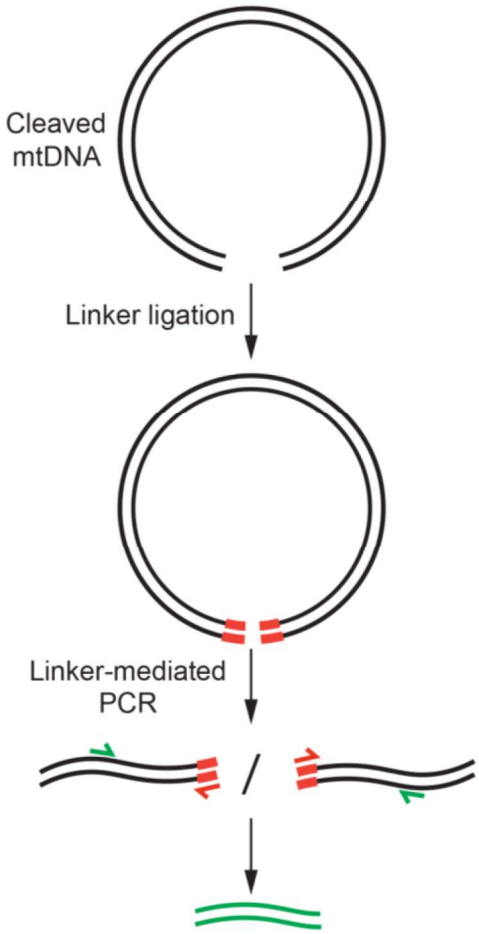


Figure M6. Principle of mtDNA Free Ends Detection using Linker-Mediated PCR.

mtDNA molecules are ligated with an asymmetric double-stranded linker (**Fig. M5**). To identify the sites of mtDNA cleavage, a PCR is conducted using primers that correspond to both the linker and specific regions of the mtDNA, either downstream or upstream of the break site. This method allows for the identification of cleavage events in the mtDNA.

2.2.28. Southern blot analysis

The obtained PCR fragments of mtDNA or the LM-PCR were subjected to electrophoresis on a 1 % agarose gel (w/v) in 1× TBE buffer. Following this, EtBr-stained gels were visualized using the Hero Lab Transilluminator UVT-28M from Herolab GmbH.

To further process the gel, it was placed within a glass cuvette and treated with a denaturing solution (1.5 M NaCl and 0.5 M NaOH), ensuring the gel was entirely covered. This step lasted for 5 minutes with constant shaking. Subsequently, the solution was exchanged, and the

denaturation process was repeated for another 15 minutes. After denaturation, the gel was rinsed with water and incubated three times in a neutralization solution (1.5 M NaCl and 0.5 M Tris-HCl at pH 8.0) for 10 minutes each time.

The transfer of DNA onto a Hybond-N+ nylon membrane (Amersham Biosciences) was achieved through passive transfer, conducted overnight. The transfer system was assembled in the following order from the bottom: a stack of filter paper, a piece of Whatman paper slightly larger than the gel, a membrane soaked in 10× SSC, the gel soaked in 10× SSC, another piece of Whatman paper, and a weight.

The next day, the nylon membrane was recovered, dried, and subjected to UV fixation at a power of 120,000 μJ/cm². The subsequent steps of probe labeling, hybridization, and detection were performed similar to the procedures outlined for Northern blot hybridization, as described in section **2.2.18.**

2.2.29. *In vitro* cleavage with the commercial AsCas12a protein

A total of 850 ng of AsCpf1 (AsCas12a) Nuclease NLS protein (abm) along with 50 ng of each crRNA were pre-incubated for 30 minutes at 37 °C in 1× Reaction Buffer. The list of crRNA can be found in section **2.1.6.** Subsequently, 170 ng of the template DNA (obtained as described in section **2.2.13.**) was introduced and incubated for another 30 minutes at 37 °C. After that, 20 μg of Proteinase K (Promega) were added to each sample and incubated for 10 minutes at 37 °C. The resulting DNA fragments were separated using a 1 % agarose gel, followed by staining with EtBr and visualization under UV light.

2.2.30. NGS of PCR/LM-PCR products

The products obtained from PCR/LM-PCR (section **2.2.27.**), utilizing either total or mtDNA as templates, were purified using NucleoSpin Gel and PCR Clean-up Mini kit (Macherey-Nagel) following the manufacturer's protocol. DNA concentrations was determined using Qubit dsDNA BR Assay Kit (Thermo Fisher). For library preparation, 100 ng of isolated DNA was employed, following the protocol of the NEBNext Ultra II FS DNA Library Prep Kit for Illumina (NEB). Adapters and indexes were sourced from the NEBNext Multiplex Oligos for Illumina (Dual Index Primers Set 1) (NEB). During the library preparation, DNA purification was conducted with NucleoMag kit for clean-up and size selection using NucleoMag SEP Mini separation plate (Macherey-Nagel).

Bioanalyser and Qubit quality controls of the libraries, as well as the sequencing, were performed at the Plateforme d'analyse de l'expression génique (IBMP, Strasbourg). 150-bp paired-end reads were generated using MiSeq (Illumina). The requested coverage was no less than 20 000 reads per sample.

The obtained reads were analyzed using the Galaxy server (version 23.1.rc1) (**Galaxy Community, 2022**). Quality reports were generated and analyzed using FastQC (**Andrews, S. *et al.*, 2010**). Adapter sequences were trimmed, and nucleotides with a quality score of less than 20 were filtered out using Trimmomatic (version 0.38) (**Bolger, A. M., Lohse, M., & Usadel, B., 2014**). Reads were then mapped to the reference mtDNA genome (GenBank NC_012920 gi:251831106) using BWA-MEM2 (version 2.2.1) (**Li. H, Ruan J, Durbin. R., 2008**). The resulting alignments were visualized using IGV (version 2.16.1) (PMC3346182). Sequencing data were processed using BAMtools (version 2.5.1) (**Robinson, J. T. *et al.*, 2001**) and SAMtools (version 1.13) (**Danecek, P. *et al.*, 2021**).

2.2.31. Nested PCR

Nested PCR with the first pair of primers was done using Phusion™ High-Fidelity DNA Polymerase (Thermo Scientific) in a total volume of 50 μL, utilizing 100 ng of total DNA as the template (refer to section **2.1.3.** for the primers list). The PCR program adhered to the manufacturer's instructions, with the exception of the annealing and elongation steps, which were both shortened to 20 seconds. The resulting PCR products were analyzed by electrophoresis in a 1 % agarose gel (w/v) in 1× TAE buffer. Visualization of the EtBr-stained gels was performed using the Hero Lab Transilluminator UVT-28M (Herolab GmbH).

After, the Nested PCR with the first pair of primers was purified using NucleoSpin Gel and PCR Clean-up Mini kit (Macherey-Nagel). The elution was performed in 30 μL. Half of the eluate was then utilized for the subsequent second PCR. The products of Nested PCR with the second pair of primers were analyzed with electrophoresis in a 2 % agarose gel.

Following this, the specific fragments of interest were cut from the gel and purified using the NucleoSpin Gel and PCR Clean-up Mini kit (Macherey-Nagel). These fragments were subsequently subjected to analysis by digestion with FastDigest XbaI restriction endonuclease (Thermo Fisher Scientific) and Sanger sequencing, which was conducted at Eurofins Genomics.

3. RESULTS

3.1. Import of AsCas12a nuclease into human mitochondria

To effectively target human mitochondrial DNA using CRISPR-Cas systems, both components of the system, namely the nuclease and its crRNA, need to be optimized for efficient import into mitochondria (**Loutre, R. *et al.*, 2018**).

3.1.1. Fusion of AsCas12a nuclease with COX8A MTS

During my Master's program, under the supervision of Ilya Mazunin, we developed a plasmid aimed at ensuring the mitochondrial import of the AsCas12a nuclease (**Figure R1A**). As a basis, we utilized a plasmid named "pMitoCas9" (**Orishchenko, K. E. *et al.*, 2016**). The transcribed mRNA originating from the plasmid comprised the COX8A MTS, a 3xFLAG epitope tag, the SpCas9 nuclease and the green fluorescent protein (GFP). During the mRNA translation, the pre-protein would be cleaved at the 2A site (**Liu, Z. *et al.*, 2017**), resulting in two distinct components: the COX8A-SpCas9 and GFP. While the latter should remain in the cytoplasm, the nuclease would be imported into the mitochondria through the TOM/TIM protein pathway. Using immunocytochemistry assays, the SpCas9 with COX8A MTS was demonstrated to be imported into human mitochondria (**Orishchenko, K. E. *et al.*, 2016**).

Therefore, in order to target AsCas12a to human mitochondria, we employed the Gibson assembly cloning technique (section **2.2.2.**) to substitute the SpCas9 sequence with the humanized AsCas12a sequence derived from pY010 (**Zetsche, B. *et. al.*, 2015**; Addgene, #69982). This led to the creation of the pMitoAsCas12a-COX8A construct (**Figure R1A**).

To confirm the localization of the AsCas12a nuclease bearing the COX8A MTS, we conducted subcellular fractionation of HEK293 cells 24 hours after transfection with pMitoAsCas12a-COX8A (**Figure R1A**) (section **2.2.3.**). The resulting protein fractions—total, cytosolic, and mitochondrial—were subjected to Western blot hybridization using TFAM and GAPDH as representatives of mitochondrial and cytosolic proteins, respectively (section **2.2.4.**). According to the obtained data, the modified AsCas12a nuclease was found in the mitochondrial protein fraction, indicating its localization within the mitochondria (**Figure R1B**).

The slight presence of GAPDH in the mitochondrial fraction could be attributed to potential contamination with the cytosolic fraction, or it could reflect the known association of GAPDH with mitochondria (**Hwang, S. *et al.*, 2015**). Additionally, the presence of AsCas12a nuclease was observed in the cytosolic fraction (**Figure R1B**). This cytosolic localization of the nuclease can be attributed to its initial translation within the cytosol before being imported into the mitochondria.

The limited amount of TFAM in the cytosolic fraction suggests that a portion of the mitochondria might have been disrupted during the isolation process (**Figure R1B**). Noteworthy, in this experiment, the mitochondria were not treated with Proteinase K, thus, we can conclude that the AsCas12a-COX8A protein is partially associated with mitochondria.

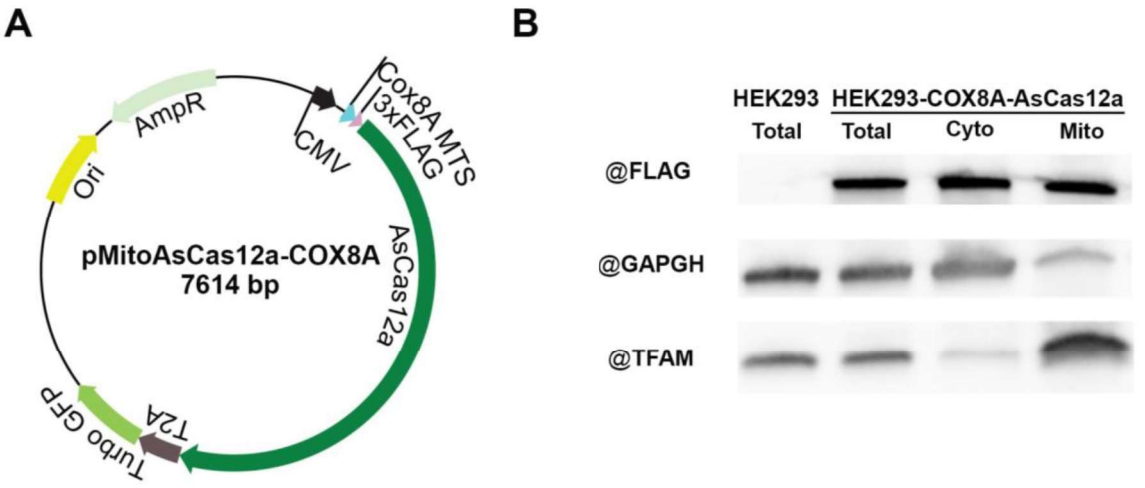


Figure R1. COX8A-AsCas12a Expression and Localization in Human Cells Transfected with pMitoAsCas12a-COX8A.

(A) Plasmid map of pMitoAsCas12a encoding AsCas12a nuclease (shown in green) bearing N-terminus COX8A MTS (shown in light-blue).
(B) Western blot analysis of total ("Total"), cytosolic ("Cyto") and mitochondrial ("Mito") fractions isolated from HEK293 cells transfected with pMitoAsCas12a-COX8A. Total fraction obtained from non-transfected HEK293 cells was used as a negative control. Antibodies are indicated at the left. GAPDH and TFAM served as cytosolic and mitochondrial markers, respectively.

After verifying the mitochondrial localization of AsCas12a, to achieve its controlled expression, we decided to introduce the mitoAsCas12a gene into the nuclear genome of the human Flp-In™ T-REx™ 293 cell line using the Invitrogen™ Flp-In™ System (**Figure M2**). For this, the AsCas12a nuclease, along with the N-terminal COX8A MTS, was reinserted from pMitoAsCas12a-COX8A (**Figure R1A**) into the pcDNA5-FRT-TO vector using the Gibson assembly method (section **2.2.2.**; **Figure M1**). The resulting plasmid (**Figure R2A**) was utilized to generate a stable cell line with the assistance of Nikita Shebanov (section **2.2.5.**; **Figure M2**). The successful integration of the nuclease gene was verified through antibiotic selection using hygromycin. Using Western blot hybridization performed on total cell lysates from the established stable cell line (section **2.2.4.**), we confirmed the expression of the AsCas12a nuclease upon the addition of tetracycline **Figure R2B**).

To confirm the localization of the COX8A-AsCas2a nuclease within the mitochondria of the newly created stable cell line, we performed submitochondrial fractionation (**Figure R2C**). Mitochondria, isolated by differential centrifugation from the stable cell line 24h after the mitoAsCas12a expression activation, were treated with hypotonic (swelling) buffer to obtain mitoplasts (mitochondria without the outer mitochondrial membrane) or were completely lysed as described in section **2.2.7.** All the fractions were treated or not with proteinase K. Notably, the mitoAsCas12a remained resistant to the treatment in intact and swollen mitochondria, disappearing only when the mitochondria were fully lysed, mirroring the behaviour of the matrix-localized mitoribosomal protein MRPL4 (**Figure R2C**). In contrast, the outer membrane protein TOMM20, facing the cytosol, was significantly reduced in the treated fractions. However, the inner membrane protein OPA1, which faces the inner membrane space, exhibited partial resistance to digestion following the rupture of the outer membrane (**Figure R2C**). This suggests that the swelling process was not fully complete due to the technical problem. Overall, the presence of the COX8A MTS-fused AsCas12a nuclease in the Proteinase K treated mitochondria and mitoplasts confirmed its localization within the mitochondrial matrix and/or the inter-membrane space.

To confirm the data obtained by the Western blot (**Figure R2C**), we performed immunofluorescent staining of the stable cell line 24h after the AsCas12a nuclease expression activation (section **2.2.8.**). The nuclease was stained with antibodies against FLAG-tag and mitochondria were stained with antibodies against TOMM20. Immunofluorescent microscopy performed with the help of Dr. Anna Smirnova showed a double localization of the mitoAsCas12a bearing COX8A MTS, namely, in mitochondria and the cytosol (**Figure R2D**). Notably, GFP, transcribed from the same plasmid, could not affect interpretation of the experimental results, since it does not sustain the fixation process (**Nybo K., 2012**).

Upon microscopy analysis, revealing the dual localization of the COX8A-AsCas12a within both the cytosol and mitochondria (**Figure R2D**), it became evident that the limitations of our prior experiment, which involved identifying localization through submitochondrial fractionation and Western blot (**Figure R2C**), stemmed from the absence of total and cytosolic fractions. This discrepancy between the two approaches could be attributed to this missing context. Furthermore, the co-localization of the nuclease in both compartments could provide an explanation for our observation of comparable nuclease quantities in both the cytosolic and mitochondrial fractions of cells transfected with pMitoAsCas12a-COX8A (**Figure R1**).

In conclusion, it became necessary for us to optimize the nuclease localization once again.

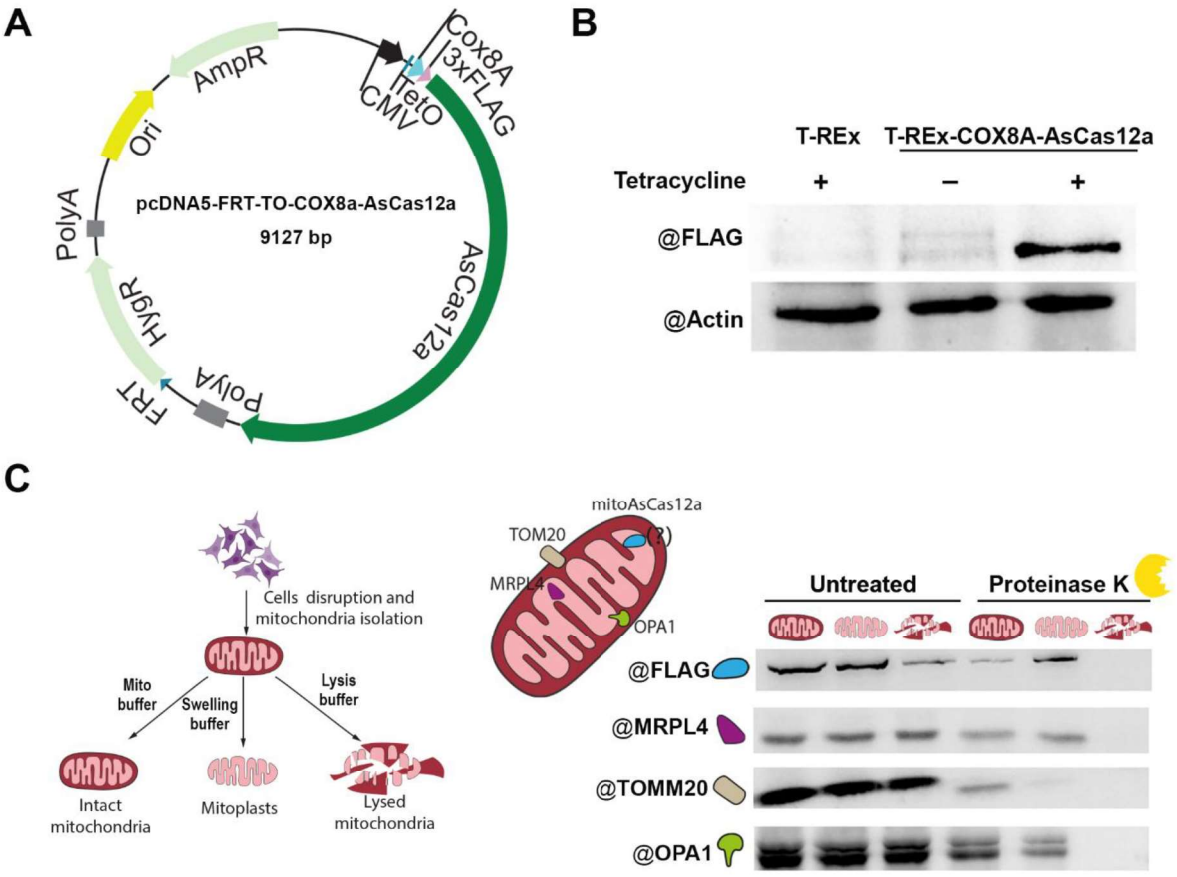

A
AmpR
Ori
TetO
CMV
Cox8A
3xFLAG
pcDNA5-FRT-TO-COX8a-AsCas12a
9127 bp
AsCas12a
PolyA
HygR
FRT
PolyA
B
T-REx
T-REx-COX8A-AsCas12a
Tetracycline
+
–
+
@FLAG
@Actin
C
Cells disruption and
mitochondria isolation
Mito
buffer
Swelling
buffer
Lysis
buffer
Intact
mitochondria
Mitoplasts
Lysed
mitochondria
mitoAsCas12a
TOM20
MRPL4
OPA1
Untreated
Proteinase K
@FLAG
@MRPL4
@TOMM20
@OPA1
D
Nuclei (DAPI)
@FLAG (Aexa Fluor 488)
@TOMM20 (Alexa Fluor 647)

Figure R2. COX8A-AsCas12a Expression and Localization in the Human Stable Cell Line.

(A) Plasmid map of pcDNA5-FRT-TO-COX8A-AsCas12a encoding AsCas12a (shown in green) bearing N-terminus MTS (shown in light-blue) used for generation of a stable cell line.
(B) Western blot analysis performed on a total cell lysate to examine the expression of COX8A-AsCas12a in the generated stable T-REx™ 293 cell line. Antibodies are indicated at the left. The transcription of the nuclease gene was induced by 100 ng/mL of tetracycline. Induced non-modified T-REx cells were used as a negative control.
(C) Schematic representation of submitochondrial fractionation (left panel). Intact mitochondria, swollen mitochondria (mitoplasts) and lysed mitochondria isolated from the cells expressing the COX8A-AsCas12a nuclease were treated or not with proteinase K, and the residual proteins were analyzed by Western blot hybridization (right panel). The hybridization probes are shown on the left: FLAG-tag - epitope tag fused to AsCas12a; MRPL4 - matrix-localized mitoribosomal protein; TOMM20 - mitochondrial outer-membrane protein facing the cytosol; OPA1 - inner membrane protein facing the inner membrane space. Mitochondria, mitoplasts and lysed mitochondria are schematically indicated above the panels.
(D) Immunofluorescent staining of the stable cell line expressing the COX8A-AsCas12a nuclease. The nuclease was stained with antibodies against FLAG-tag/Alexa Fluor 488 (shown in green), mitochondria were stained with antibodies against TOMM20/Alexa Fluor 647 (shown in red). DAPI was used to stain the nuclei (shown in blue).

3.1.2. Improvement of AsCas12a mitochondrial localization

In order to improve mitochondrial localization of the AsCas12a nuclease, we decided to try several strategies: **1)** to decrease protein expression level to prevent its aggregation in the cytosol and **2)** to use other mitochondrial targeting signals.

To reduce the expression level of AsCas12a, we decided to introduce a deletion in the human Cytomegalovirus (CMV) promoter region (**Figure R1A**), as previously described by Morita E. *et al.* in 2012. This deletion involved removing a significant portion of the enhancer region, which contains binding sites for various transcription factors. Specifically, the design of the deletion aimed to eliminate the Nuclear factor-kappa B (NF-κB) transcription factor binding site, while retaining the binding site for the Specificity protein 1 (Sp1), a zinc finger family transcription factor (**Morita, E. *et al.*, 2012**).

Regarding the MTS, in addition to the previously mentioned COX8A MTS, we aimed to compare MTS derived from various sources. These included the MTS from the *Neurospora crassa* ATPase subunit 9 (Su9), the MTS from the mammalian autophagy-related cysteine peptidase 4D (ATG4D), as outlined in the publication by **Antón, Z. *et al.* in 2020**. Furthermore, we were interested in testing the MTS from superoxide dismutase 2 (SOD2) (**Bacman, S. R. *et al.*, 2020**).

To assess the potential for AsCas12a mitochondrial import when fused with specific MTS, we analyzed MTS alone and MTS-AsCas12a amino acid compositions using ProtParam Expasy Server in order to predict theoretical pI, charge and grand average of hydropathy (GRAVY). The obtained data indicated that all the AsCas12a nuclease fusions with various MTS displayed

comparable negative GRAVY values (**Figure R3A**). This suggests that the resulting proteins possess hydrophilic properties, enhancing their solubility (**Chang, K. Y., and Yang, J. R., 2013**).

Considering the charges of the MTS and the complete proteins, it's essential to note that the mitochondrial matrix carries a negative charge. Thus, for efficient mitochondrial import, proteins should possess a positive charge. In this context, the SOD2 MTS appeared less favorable for fusion with the AsCas12a nuclease due to its relatively smaller positive charge, and even a negative charge in the full protein context (**Figure R3A**). Significantly, the COX8A MTS emerged as a promising candidate, with a predicted favorable performance. Moreover, the ATG4D and Su9 MTS were anticipated to be the most effective, owing to their notably high positive charge in the full protein context (**Figure R3A**). It's important to note that the predictions of protein parameters generated by the utilized server should be considered with caution, as they are based on analyzing the linear amino acid sequence. The accuracy of these predictions can vary when the protein is properly folded into its three-dimensional structure.

Nevertheless, to experimentally validate these predictions, using site-directed mutagenesis (SDM) (section **2.2.9.**; **Figure M3**), we introduced mutations into pMitoAsCas12a-COX8A (**Figure R1A**). We created 8 distinct plasmids, each carrying the AsCas12a nuclease fused with 4 different MTS (listed in **Figure R3A**) and designed to transcribe the AsCas12a nuclease under the regulation of either the full-sized or shortened CMV promoter region. The decrease of the nuclease expression under the control of the shortened promoter region was confirmed by Western blot hybridization of T-REx cell lysates 24h post-transfection (section **2.2.4.**; **Figure R3B**).

Next, cells transfected with these 8 plasmids were examined by immunofluorescent confocal laser scanning microscopy (section **2.2.8.**). The mitochondrial colocalization of the AsCas12a nuclease expressed from these plasmid versions was assayed by a semi-quantitative analysis of the images using fluorescence profiles along a line (**Figure R3C**).

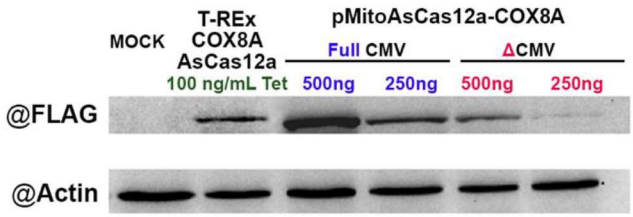
As predicted (**Figure R3A**), AsCas12a fused with the SOD2 MTS exhibited the poorest colocalization profile (**Figure R3C**). Notably, despite reducing the nuclease expression levels in mammalian cells, we were unable to completely eliminate the partial cytosolic localization of the COX8A-AsCas12a (**Figure R3C**). Regarding the AT4G MTS, we encountered challenges in observing a sufficient number of transfected cells under the microscope, which made it difficult to draw conclusive results. The AsCas12a nuclease fused with AT4G MTS, under the control of the shortened CMV promoter region, showed low expression levels (**Figure R3C**). We observed a

reduced fluorescence intensity using the same conditions. This could be attributed to either the low amount of plasmid entering the cells or the lower expression level of the AT4G-fused AsCas12a nuclease. Still, when expressed, the ATG4D-AsCas12a was localized with mitochondria (**Figure R3C**). Finally, the AsCas12a nuclease fused with the Su9 MTS demonstrated the best mitochondrial colocalization profile, with no detectable presence of the protein in the cytosol (**Figure R3C**), as expected (**Figure R3A**).

A

CONSTRUCT	MTS, aa	MTS charge	MTS pI	MTS GRAVY	Full charge	Full pI	Full GRAVY
pMitoAsCas12a-COX8A	29	+5	12.48	0.362	+1	7.65	-0.507
pMitoAsCas12a-SOD2	24	+3	10.76	0.163	-1	8.01	-0.492
pMitoAsCas12a-ATG4D	41	+10	11.17	-0.337	+6	8.31	-0.520
pMitoAsCas12a-Su9	69	+13	12.55	-0.272	+9	8.53	-0.513

B



C

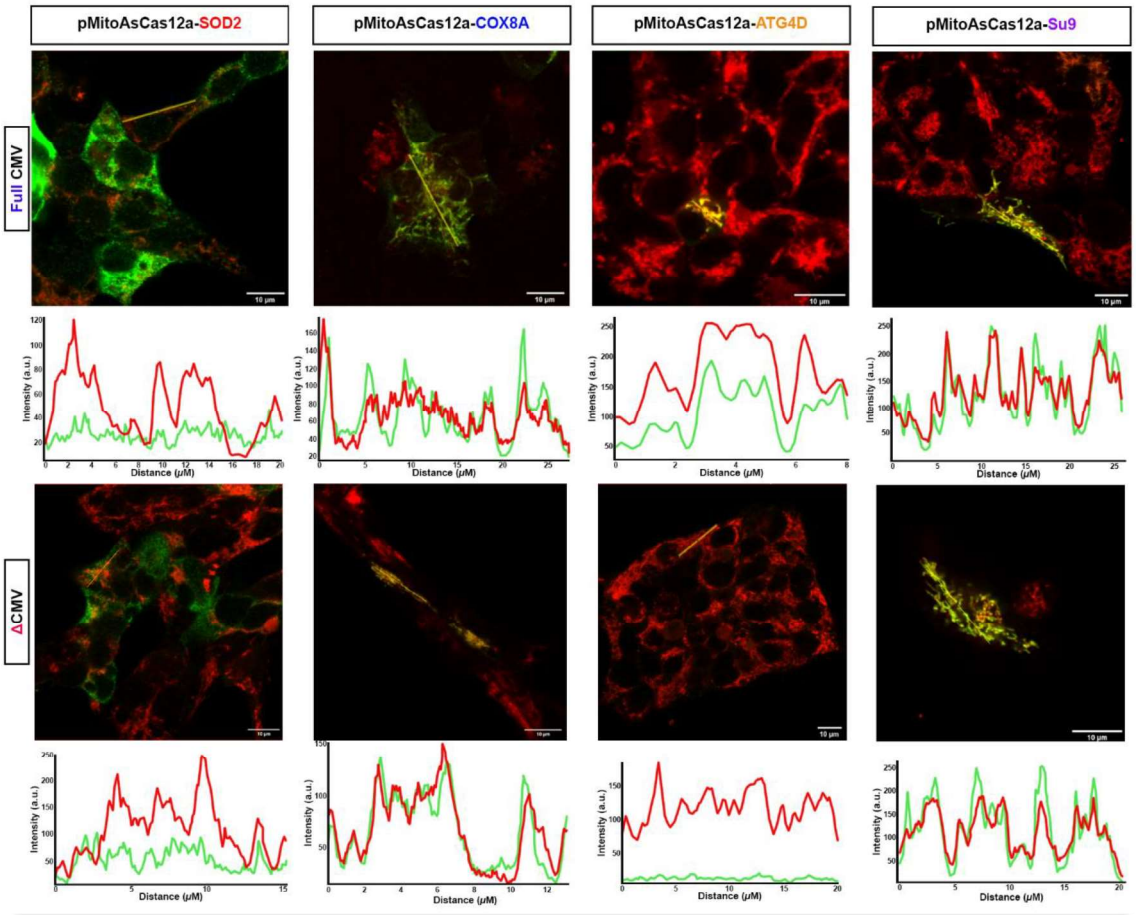


Figure R3. Mitochondrial Localization of AsCas12a Bearing Various MTS.

(A) Summary of the parameters used to predict the import efficiency of AsCas12a, which carries various MTS (COX8A, SOD2, ATG4D, and Su9, as indicated). Predicted pI values, charge, and grand average of hydropathy (GRAVY) were quantified for both the MTS alone and the entire MTS-3xFLAG-AsCas12a sequences using the ProtParam Expasy Server (https://web.expasy.org/protparam/).
(B) Western blot analysis of cells transfected with pMitoAsCas12a-COX8A plasmids bearing the full-sized or deleted CMV promoter region, as indicated above the panel. T-REx Cox8A AsCas12a, lysate from the Flp-In T-REx COX8A-AsCas12a stable cell line. MOCK, non-trasfected T-REx cells served as the negative control.
(C) Immunofluorescent staining of cells transiently transfected with pMitoAsCas12 plasmids indicated above the panels. the AsCas12a nuclease fused to various MTS was expressed under the control of the full-sized (upper panels) or shortened CMV promoter region (lower panels). The nuclease was stained with FLAG-tag/Alexa Fluor 488 antibodies (green signal), and mitochondria were stained with antibodies against TOMM20/Alexa Fluor 647 (red signal). To assess the mitochondrial colocalization of AsCas12a, a semi-quantitative analysis of the images was performed by measuring the fluorescence profiles of both signals along a line (shown under each panel). Scale bares: 10 μm; a.u. - arbitrary units.

3.1.3. Su9-AsCas12a stable cell line

After improving mitochondrial import of the AsCas12a nuclease, we decided to create a new stable cell line expressing the AsCas12a nuclease fused with the Su9 MTS. To achieve this, we utilized the Gibson assembly cloning technique (section **2.2.2.**; **Figure M1**) to reclone the AsCas12a nuclease bearing the Su9 MTS from pMitoAsCas12a plasmid into pcDNA5-FRT-TO vector (**Figure R4A**). Subsequently, using the Flp-In recombinant system (section **2.2.5.**; **Figure M2**), we created a new monoclonal HEK293 T-REx cell line expressing the Su9-AsCas12a in a tetracycline-inducible manner. Out of 6 individual clones, three were analyzed for the expression and localization of the Su9-AsCas12a nuclease.

Western blot hybridization of cell lysates with AsCas12a-specific antibodies revealed that all analyzed clones were capable of expressing the AsCas12a nuclease 24 hours upon tetracycline induction (section **2.2.4.**; **Figure R4B**). However, clones 2 and 3 exhibited lower levels of AsCas12a expression compared to clone 1, despite the equal loading of proteins on the gel.

To determine whether the Su9-AsCas12a colocalized with mitochondria in the isolated clones, we performed immunofluorescent staining 24 hours after the nuclease expression activation (section **2.2.8.**). The nuclease was stained with antibodies against the FLAG-tag, and mitochondria were stained with antibodies against TOMM20. Confocal laser scanning microscopy, assisted by Dr. Anna Smirnova, demonstrated that the Su9-AsCas12a nuclease was expressed in a tetracycline-inducible manner and colocalized with human mitochondria in clone 1 (**Figure R4C**). We also observed a small amount of the nuclease in non-induced cells of clone 1 which could be due to the promoter leakage caused by minimal amounts of tetracycline present in the culture media. Surprisingly, there was no expression of the nuclease upon induction in clones 2 and 3 (**Figure**

R4C). We suspect that these clones might have been heterogeneous, and we observed mostly a subpopulation of the cells not expressing AsCas12a. This could also explain the difference in expression levels shown by the western blot analysis (**Figure R4B**).

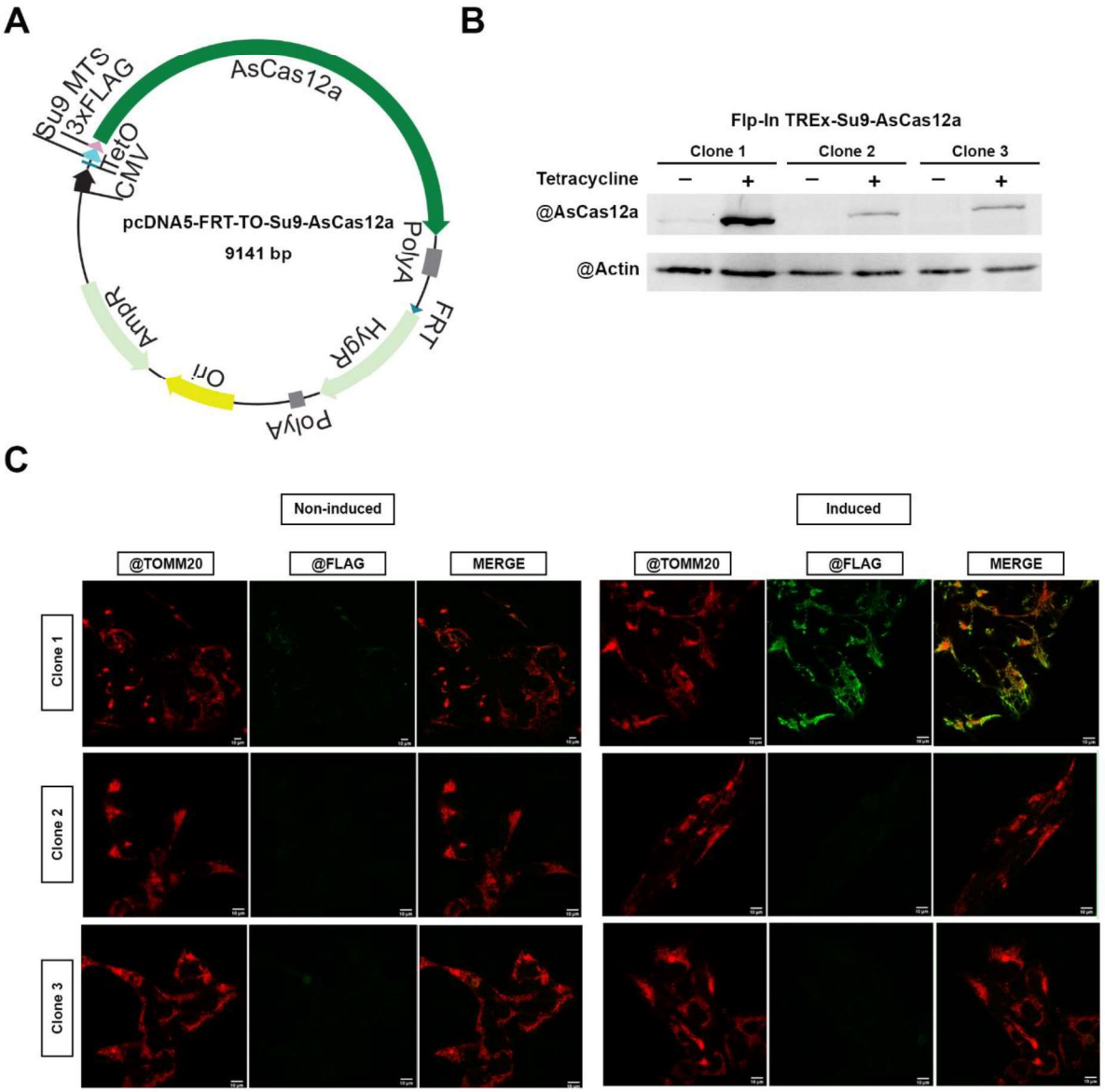


Figure R4. Generation and Characterization of the Stable Cell Lines Expressing the Su9-AsCas12a.

(A) Plasmid map of pcDNA5-FRT-TO-Su9-AsCas12a encoding AsCas12a (shown in green) bearing N-terminal Su9 MTS (shown in light-blue) used for generation of a stable cell lines.
(B) Western blot analysis performed on total cell lysates to assess the expression of the Su9-AsCas12a in the isolated monoclonal stable cell lines (Clone 1 – 3). The nuclease expression in the created stable cell lines was induced by 100 ng/mL of tetracycline.
(C) Immunofluorescent staining performed on the isolated monoclonal stable cell lines to analyze the expression and localization of the Su9-AsCas12a nuclease, both in the "Induced" state (expression induced with 100 ng/mL of tetracycline) and in the "Non-induced" state (without tetracycline induction), as indicated above the panels. The nuclease was specifically stained with antibodies against the FLAG-tag, shown in green, while mitochondria were stained with antibodies against TOMM20, shown in red. The appearance of a yellow signal indicated the colocalization of the nuclease with mitochondria. Scale bares: 10 μm.

Thus, we proceeded with isolated clone 1, which now will be referred to as the T-REx-Su9-AsCas12a stable cell line. To determine the optimal tetracycline concentration for activating the nuclease expression, we performed western blot hybridization on cell lysates from the newly generated stable cell line (section **2.2.4.**). The results indicated that the nuclease was expressed in a tetracycline-dependent way, and a concentration of 50 ng/mL of tetracycline was sufficient for activation of the AsCas12a nuclease expression (**Figure R5A**). We then assessed the stability of the Su9-AsCas12a in cells over time. Using the same technique (section **2.2.4.**), we analyzed total cell lysates at 1, 3, and 6 days after the nuclease expression activation (**Figure R5B**). The results revealed that the AsCas12a nuclease was still present in the cell lysate even on the 6th day after the induction, although the amount decreased over time (**Figure R5B**).

To validate mitochondrial localization of the Su9-AsCas12a in the new cell line, we performed the immunofluorescent staining 24 hours after the nuclease expression activation in the T-REx-Su9-AsCas12a cell line (section **2.2.8.**). The results confirmed our initial findings on the mitochondrial localization of the Su9-AsCas12a (**Figure R3C**, **Figure R4C**), validated using a semi-quantitative analysis of the images with fluorescence profiles taken along a line (**Figure R5C**). To complement the microscopy data, we conducted submitochondrial fractionation, as previously described (section **2.2.3.**). The results confirmed the presence of the Su9-AsCas12a nuclease in human mitoplasts treated with proteinase K (**Figure R5D**). All together, these findings indicate that the AsCas12a nuclease bearing the Su9 MTS is localized in the mitochondrial matrix.

Next, we evaluated the Su9-AsCas12a nuclease activity in the stable cell line through an *in vitro* experiment on site-specific cleavage of the DNA template corresponding to a fragment of mtDNA obtained by a PCR (section **2.2.13.**). The experiment was conducted in the cell lysate prepared from the T-REx-Su9-AsCas12a 24 hours after the induction, which was supplemented with crRNA (**Figure R5E**). The presence of observed cleavage products of the expected sizes on an agarose

gel indicated that the Su9-AsCas12a, expressed in the stable cell line, possessed specific DNA cleavage activity.

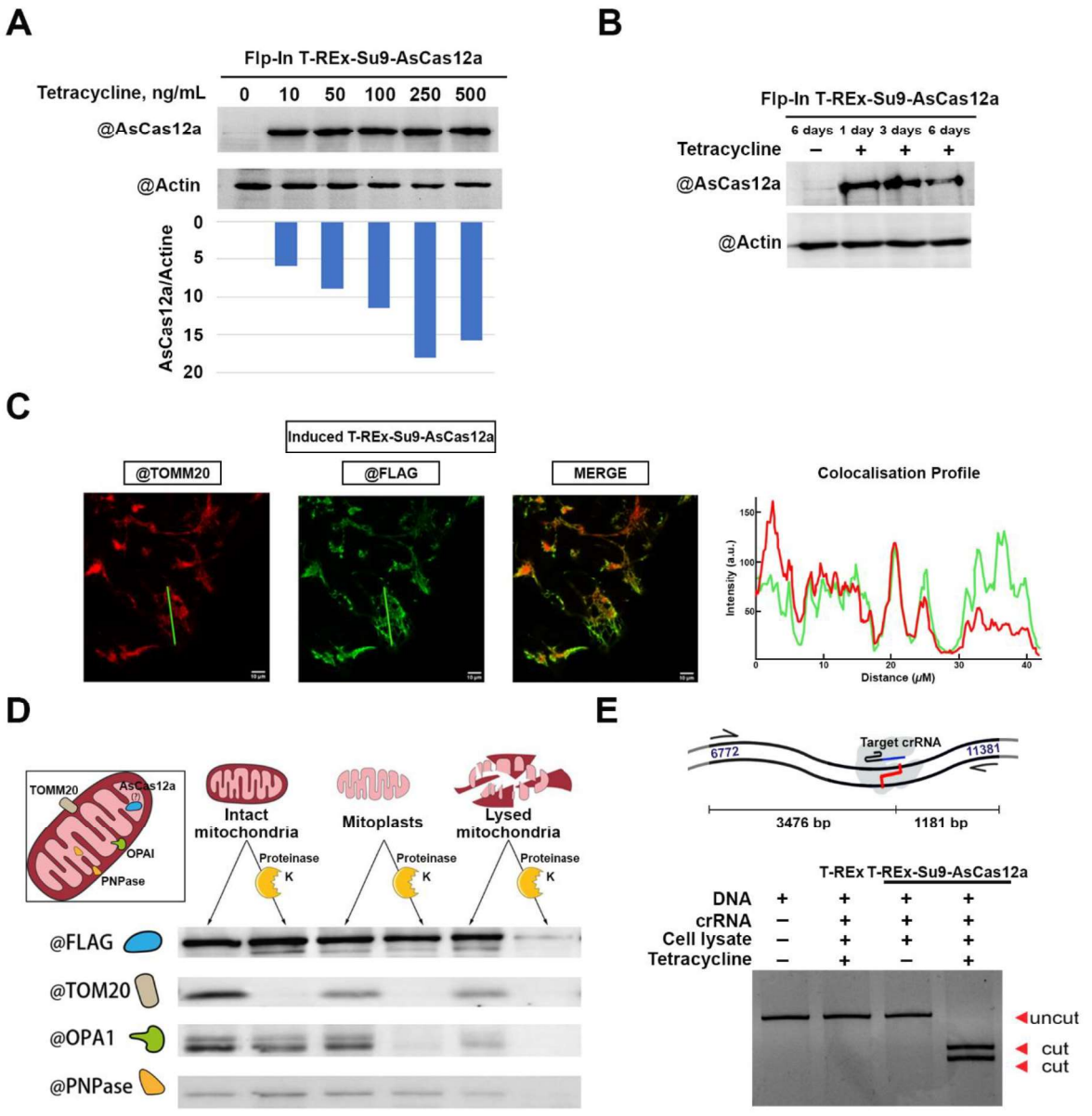


Figure R5. Analysis of the Su9-AsCas12a Expression, Localization and Activity in the Stable Cell Line.

(A) Western blot analysis performed on total cell lysates of the Su9-AsCas12a stable cell line, induced with various tetracycline concentrations (as indicated above the panel). Relative expression of AsCas12a normalized by actine is present on the panel below.
(B) Similar to **(A)**, but the cells were detached at different time points after activating the Su9-AsCas12a expression to assess its stability. The nuclease expression was induced by adding 50 ng/mL of tetracycline.
(C) Immunofluorescent staining was carried out on the Flp-In T-REx-Su9-AsCas2a stable cell line to verify the mitochondrial localization of the nuclease following expression activation with 50 ng/mL of tetracycline. The nuclease was labeled with antibodies against the FLAG-tag, shown in green, while mitochondria were labeled with antibodies against TOMM20, shown in red. To assess the mitochondrial colocalization of AsCas12a, a semi-quantitative analysis of the images was performed by measuring the fluorescence profiles of both signals along a line (Scale bares: 10 μm, a.u. - arbitrary units), shown at the right.
(D) Schematic representation of submitochondrial fractionation (as in **Fig. R2C**). Intact mitochondria, swollen mitochondria (mitoplasts) and lysed mitochondria isolated from the cells expressing the Su9-AsCas12a nuclease were treated or not with proteinase K, and the residual proteins were analyzed by Western blot hybridization. The antibodies are indicated on the left: FLAG-tag - epitope tag fused to AsCas12a; PNPase - inner membrane space and matrix-localized mitoribosomal protein; TOMM20 - mitochondrial outer-membrane protein facing the cytosol; OPA1- inner membrane protein facing the inner membrane space. Mitochondria, mitoplasts and lysed mitochondria are schematically indicated above the panels.
(E) Upper panel, schematic representation of target DNA (PCR fragment of human mtDNA, nucleotide numbers are indicated) containing AsCas12a PAM sequence; the cleavage site is marked with a red line. The sizes of the fragments corresponding to cleaved DNA template are given below the scheme. Lower panel, result of the cleavage of target DNA in cell lysates of T-REx-Su9-AsCas12a stable cell line induced with 50 ng/mL tetracycline. DNA template and crRNA were added into the reaction, as indicated above the gel. 1 % agarose gel electrophoresis revealed with ethidium bromide staining is shown. Lysate from the induced T-REx cell line served as a negative control.

3.1.4. Impact of the Su9-AsCas12a nuclease expression on mitochondrial respiration, protein synthesis and mitophagy in the stable cell line

In the study by **Antón, Z. *et al.* in 2020**, the authors investigated the effect of expressing the mitochondrial-targeted ortholog of AsCas12a, LbCas2a nuclease bearing the Su9 MTS, in a cell culture of retinal pigment epithelium hTERT RPE-1. Their findings revealed that this expression negatively impacted mitochondrial functionality, particularly mitochondrial respiration, while not significantly affecting mitochondrial morphology. However, the authors did not assess mtDNA copy numbers in both the control and nuclease-expressing cells.

Given this context, we aimed to investigate whether the expression of the Su9-AsCas12a nuclease in the HEK293-based cell line negatively impacts mitochondrial biogenesis. Thus, we performed measurements of the oxygen consumption rate in the intact T-REx and the T-REx-Su9-AsCas12a cells 48 hours after treating them with 50 ng/mL of tetracycline (section **2.2.14.**; **Figure R6A**). Initially, we measured the basal level of respiration before introducing any chemical reagents. Subsequently, we added oligomycin, an inhibitor of ATP synthase, to determine ATP-linked respiration. Next, we induced the uncoupling agent, FCCP, which led the electron transport

chain to function at its maximum rate by collapsing the inner membrane gradient. Finally, to halt the electron transport chain, we utilized rotenone and antimycin A, acting as complex I and complex III inhibitors, respectively (**Djafarzadeh S., Jakob S. M., 2017**).

The data obtained indicate that both cell lines exhibited normal mitochondrial respiration profiles (**Figure R6A**). However, there was a noticeable difference in spare respiratory capacity, which represents the gap between maximal and basal respiration; it was lower for the stable cell line expressing the nuclease. It is important to note that statistical analysis through repeat experiments would be necessary for a more robust conclusion. Nevertheless, based on this experiment, it appears that the expression of the nuclease after 48 hours had no significant impact on mitochondrial respiration.

Additionally, we aimed to investigate whether the expression of the Su9-AsCas12a and its import into mitochondria could lead to any alterations in mitochondrial translation and/or induce mitophagy. AsCas12a nuclease and its orthologs are known to possess *trans*-cleavage activity, which means they can degrade single-stranded DNA molecules in non-specific way upon binding to the target DNA:crRNA complex (**Chen, J. S. *et al.*, 2018**). Considering the presence of R-loops in human mtDNA (**Holt I. J., 2019**) and the import of small non-coding RNAs, such as miRNAs and siRNAs, into mitochondria (**Gao, K. *et al.*, 2021**), along with our recent discovery that AsCas12a crRNA can be divided into scaffold and spacer parts without affecting its cleavage activity, and even the spacer alone can effectively target cleavage (**Shebanova, R. & Nikitchina, N. *et al.*, 2022**) (see also section **3.2.2.**), one can hypothesize that targeting the AsCas12a nuclease to human mitochondria might induce non-specific hydrolysis of mtDNA, leading to mtDNA depletion and subsequently triggering mitophagy (**Van Houten, B., Hunter, S. E., & Meyer, J. N., 2016**) (**Figure R6B**).

Hence, we performed western blot analysis using total cell lysates from the Su9-AsCas12a stable cell line, which was induced with 50 ng/mL of tetracycline, to explore if the nuclease expression affects mitochondrial protein levels over a span of 24 to 96 hours (section **2.2.4.**; **Figure R6C**). To serve as a negative control, we treated HEK293 cells in the same manner. Our selected protein targets for investigation were COX1 (mitochondrially encoded and localized in the inner membrane complex), VDAC (nuclear encoded and localized in mitochondrial outer membrane), along with Beclin 1 and PINK1, which play important roles in autophagosome formation during mitophagy (**Figure R6B**).

The primary regulatory mechanism in mitophagy is the ROS/PTEN-induced kinase 1 (PINK1)/Parkin pathway (**Figure R6B**). Under normal conditions, PINK1 is imported into healthy mitochondria with intact membrane potential through the TOM/TIM import machinery. PINK1 is then cleaved by the mitochondrial intramembrane protease PARL, and the cleaved PINK1 is retrotranslocated to the cytosol, where it undergoes ubiquitination and degradation (**Jeyaraju, D. V. *et al.*, 2006**). Upon mitochondrial damage and loss of membrane potential, the import of PINK1 is disrupted, causing its accumulation on the outer mitochondrial membrane. PINK1-mediated phosphorylation of residual ubiquitins of the outer mitochondrial membrane proteins stimulates the recruitment of ubiquitin ligases (Parkin). Further ubiquitination serves as a recognition signal for autophagy adapters and facilitates the recruitment of LC3-decorated autophagosomes (**Niu, H. *et al.*, 2012**). Beclin 1, a protein involved in autophagosome nucleation and maturation, plays a direct role in PINK1/Parkin-mediated mitophagy (**Figure R6B**). It interacts with Parkin in the cytosol and facilitates its translocation to depolarized mitochondria during mitophagy activation. Additionally, Beclin 1 initiates the formation of autophagosomes at mitochondria by accumulating at mitochondria-associated membranes (MAM) upon mitochondrial depolarization and serving as an anchor protein (**Gelmetti, V. *et al.*, 2017**).

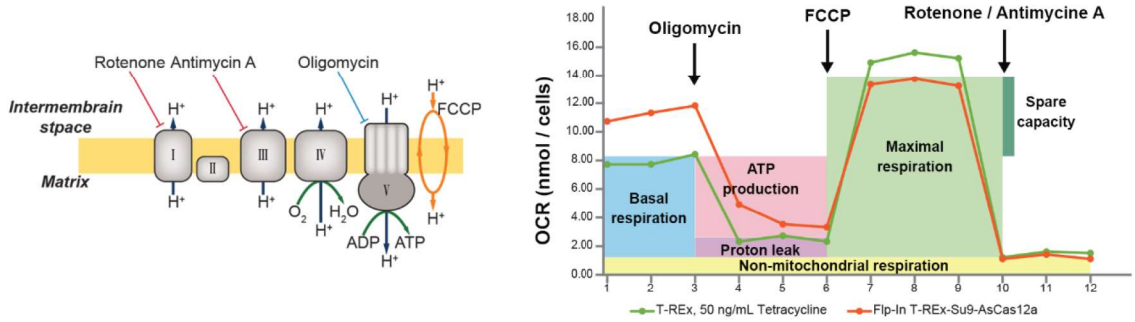
By western blots (section **2.2.4.**), we analyzed the expression levels of the mentioned proteins and found no changes upon the expression of the mitochondrial-targeted AsCas12a nuclease (**Figure R6C, Figure R6D**). According to the experimental results, we did not observe statistically significant differences in the expression levels of PINK1 and Beclin 1 within the Su9-AsCas12a stable cell line (**Figure R6D**). Notably, the PNK1/Parkin-mediated mitophagy pathway would typically lead to an increase in PINK1 upon activation, as it is degraded under normal conditions (**Figure R6B**). Regarding of Beclin 1, we did not expect an increase of its expression, since Beclin 1 becomes actively phosphorylated and translocated to the mitochondria upon mitophagy activation (**Figure R6B**). Thus, we may consider using antibodies targeting the phosphorylated form of Beclin 1 in future experiments.

Interestingly, we did observe a higher presence of VDAC in the stable cell line compared to HEK293 cells (**Figure R6D**). Although we lack a clear explanation for this observation, it underscores the need to repeat the experiment in triplicates, employing alternative antibodies for proteins encoded in the nuclear DNA but localized in mitochondria. For example, using antibodies against TOMM20 could provide additional insights.

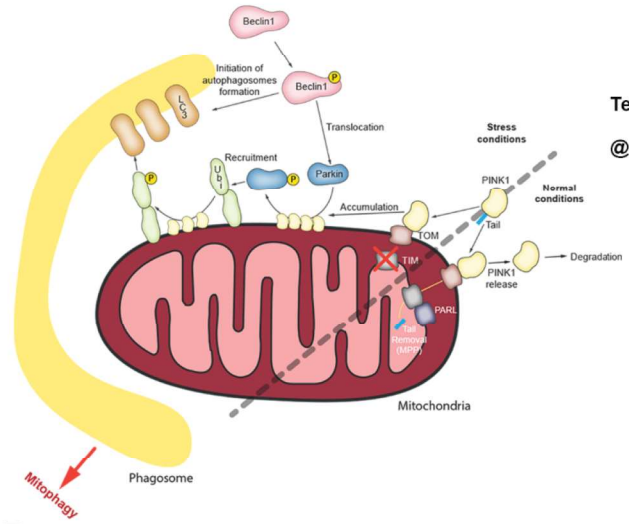
In conclusion, our findings suggest that, once expressed and targeted to mitochondria, the Su9-AsCas12a nuclease does not perform an impact on mtDNA expression, nor does it induce

mitophagy (**Figure R6C, Figure R6D**). However, it's important to highlight that this experiment lacks a positive control for mitophagy, which should be addressed in future studies.

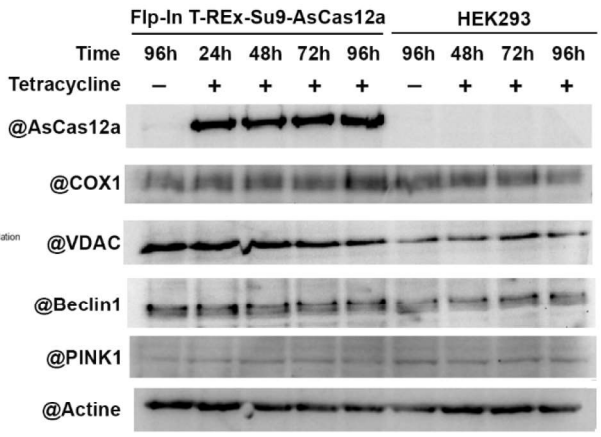
A



B



C



D

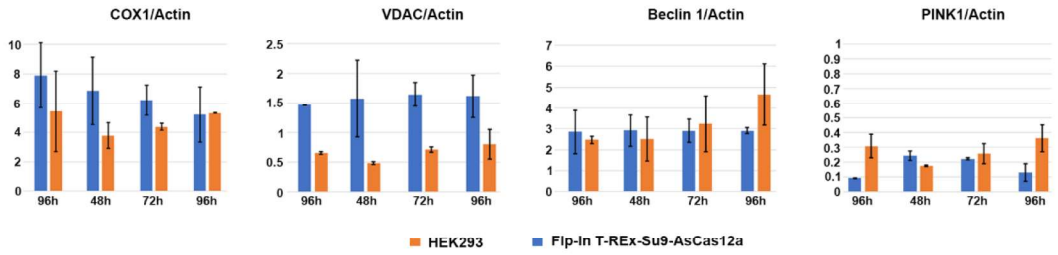


Figure R6. The Effect of the Su9-AsCas12a Nuclease Expression on Mitochondrial Respiration, Protein Expression and Mitophagy.

(A) On the left: Simplified scheme of the electron transport chain located within the inner mitochondrial membrane (Adapted from Underwood, E. *et al.*, 2020). Electron transfer is coupled to the transfer of protons (H+) across the inner mitochondrial membrane into the intermembrane space, creating a proton gradient. This gradient is utilized by complex V for ATP synthesis. The protons react with oxygen to generate water. Thus, the Oxygen Consumption Rate (OCR) can be monitored and used as a marker of mitochondrial respiration. The inhibitors of respiration complexes (oligomycin, antimycin A, and rotenone) and uncoupler (FCCP) are indicated. On the right: Mitochondrial respiration profiles generated from T-REx cells (indicated by the green line) and the Flp-In T-REx-Su9AsCas12a cells (indicated by the red line) 48 hours after treatment with 50 ng/mL of tetracycline. OCR measurements were performed in triplicates and normalized to the number of cells.
(B) Schematic representation of PINK1/Parkin-mediated mitophagy (Adapted from Huang, Y. F. *et al.*, 2020). See the text for details.
(C) Western blot analysis conducted on total cell lysates of the Su9-AsCas12a stable cell line, induced with 50 ng/mL of tetracycline, to investigate the impact of the nuclease expression on mitochondrial protein levels over a period of 24 to 96 hours. Specific antibodies (indicated on the left) were used to analyze the following proteins: COX1 (mitochondrially encoded and localized), VDAC (nuclear encoded and localized in mitochondria), as well as markers of mitophagy, Beclin 1 and PINK1. As a negative control, HEK293 cells were treated in the same manner.
(D) Quantifications of the mean steady-state levels of the mitochondrial proteins **(C)** normalized to actine; time points after the Su9-AsCas12a induction are indicated below graphs; n=2.

3.2. Import of AsCas12a crRNA into human mitochondria

After modifying the AsCas12a nuclease for import into human mitochondria, the subsequent step was to evaluate and, if feasible, enhance the mitochondrial import of AsCas12a crRNA.

For this, we applied all the experience of our team in studying the non-coding RNA mitochondrial import (**Jeandard, D. *et al.*, 2019; 2022**) and demonstrated that the crRNA of Type V CRISPR/AsCas12a system, characterized by a short size of 40-44 nucleotides (**Yamano, T. *et al.*, 2016**), can be detected in the matrix of human mitochondria, Then, we analysed mitochondrial import of crRNAs targeting different regions in mtDNA. We searched for the AsCas12a "TTTV" PAM sequences in human mitochondrial DNA and then, in collaboration with Prof. Vadim Shmanai (National Academy of Science of Belarus, Minsk, Belarus), we designed and chemically-synthesized a set of crRNAs targeting these sites (sections **2.2.10.** - **2.2.12.**) All the designed crRNAs were analyzed for their secondary structures, as well as for possible off-target activity in the nuclear genome.

It was revealed that several of crRNAs exhibited a higher enrichment in RNase-treated mitoplasts compared to other tested crRNAs. These crRNAs were characterized by longer hairpin stems and stable homodimer formation, suggesting that the presence of stable helix structures may facilitate their import into mitochondria (**Publication 2**).

Then, we applied different strategies aiming to improve the crRNA mitochondrial import.

Publication 2

Biochimie, 2023:

Targeting of CRISPR-Cas12a crRNAs into human mitochondria

Natalia Nikitchina[1], Egor Ulashchik[2], Vadim Shmanai[2], Anne-Marie Heckel[1], Ivan Tarassov[1], Ilya Mazunin[3] and Nina Entelis[1, *]

[1] UMR7156 – Molecular Genetics, Genomics, Microbiology, University of Strasbourg, Strasbourg, 67000, France
[2] Institute of Physical Organic Chemistry, National Academy of Science of Belarus, Minsk, 220072, Belarus
[3] Center for Molecular and Cellular Biology, Skolkovo Institute of Science and Technology, Moscow, 143026, Russia

ARTICLE IN PRESS

Biochimie xxx (xxxx) xxx

Contents lists available at ScienceDirect

Biochimie

journal homepage: www.elsevier.com/locate/biochi

Targeting of CRISPR-Cas12a crRNAs into human mitochondria

Natalia Nikitchina [a], Egor Ulashchik [b], Vadim Shmanai [b], Anne-Marie Heckel [a], Ivan Tarassov [a], Ilya Mazunin [c], Nina Entelis [a,*]

[a] UMR7156 – Molecular Genetics, Genomics, Microbiology, University of Strasbourg, Strasbourg, 67000, France
[b] Institute of Physical Organic Chemistry, National Academy of Science of Belarus, Minsk, 220072, Belarus
[c] Center for Molecular and Cellular Biology, Skolkovo Institute of Science and Technology, Moscow, 143026, Russia

ARTICLE INFO

Article history:
Received 15 May 2023
Received in revised form
10 August 2023
Accepted 4 September 2023
Available online xxx

Handling Editor: Dr B Friguet

Keywords:
RNA import
crRNA
Cas12a
MitoCRISPR
Targeting
Human mitochondria

ABSTRACT

Mitochondrial gene editing holds great promise as a therapeutic approach for mitochondrial diseases caused by mutations in the mitochondrial DNA (mtDNA). Current strategies focus on reducing mutant mtDNA heteroplasmy levels through targeted cleavage or base editing. However, the delivery of editing components into mitochondria remains a challenge. Here we investigate the import of CRISPR-Cas12a system guide RNAs (crRNAs) into human mitochondria and study the structural requirements for this process by northern blot analysis of RNA isolated from nucleases-treated mitoplasts. To investigate whether the fusion of crRNA with known RNA import determinants (MLS) improve its mitochondrial targeting, we added MLS hairpin structures at 3′-end of crRNA and demonstrated that this did not impact crRNA ability to program specific cleavage of DNA in lysate of human cells expressing AsCas12a nuclease. Surprisingly, mitochondrial localization of the fused crRNA molecules was not improved compared to non-modified version, indicating that structured scaffold domain of crRNA can probably function as MLS, assuring crRNA mitochondrial import. Then, we designed a series of crRNAs targeting different regions of mtDNA and demonstrated their ability to program specific cleavage of mtDNA fragments in cell lysate and their partial localization in mitochondrial matrix in human cells transfected with these RNA molecules. We hypothesize that mitochondrial import of crRNAs may depend on their secondary structure/sequence. We presume that imported crRNA allow reconstituting the active crRNA/Cas12a system in human mitochondria, which can contribute to the development of effective strategies for mitochondrial gene editing and potential future treatment of mitochondrial diseases.

© 2023 Elsevier B.V. and Société Française de Biochimie et Biologie Moléculaire (SFBBM). All rights reserved.

1. Introduction

Mitochondria play a vital role in eukaryotic cells, serving various functions, but their primary significance lies in the production of energy in the form of ATP through oxidative phosphorylation in the mitochondrial respiratory chain [1]. Although most of the organelle's macromolecules are encoded by the nuclear genome, mitochondria possess their own 16.5 kb DNA (mtDNA) which encodes 13 subunits of four out of the five OXPHOS complexes, 22 tRNAs and 2 ribosomal RNAs [2–4] (Fig. 1A). Mutations in these proteins, tRNAs or ribosomal RNAs can affect mitochondrial ATP production, resulting in a wide range of mitochondrial diseases, often associated with neuromuscular disorders [5,6]. The severity of mitochondrial diseases is highly associated with heteroplasmy level – a state when mutant and wild-type (WT) mtDNA molecules coexist in the same cell [7]. Taken together, mtDNA pathogenic mutations affect 1 in 5000 individuals worldwide [8]. To date, these pathologies have not found adequate treatment [9].

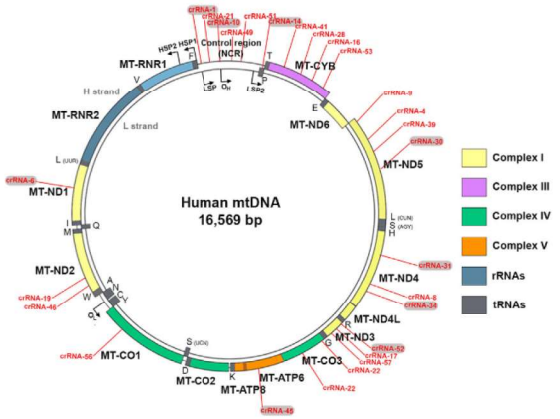
Mitochondrial gene editing offers a promising therapeutic approach to restore healthy mitochondrial function by reducing mutant mtDNA heteroplasmy level [10]. Currently, two main strategies have been proposed. The first strategy involves decreasing of mtDNA heteroplasmy level by inducing targeted cleavage of mutant mtDNA molecules. Due to the lack of repair mechanisms for double-strand breaks in human mitochondria, linearized mtDNA will be rapidly degraded, enabling the replication of WT mtDNA molecules to reconstitute the mtDNA pool [11]. Various mitochondria-targeted nucleases have been developed to degrade mutant mtDNA and adjust heteroplasmy ratios. Mitochondria-

* Corresponding author.
E-mail address: n.entelis@unistra.fr (N. Entelis).

https://doi.org/10.1016/j.biochi.2023.09.006
0300-9084/© 2023 Elsevier B.V. and Société Française de Biochimie et Biologie Moléculaire (SFBBM). All rights reserved.

Please cite this article as: N. Nikitchina, E. Ulashchik, V. Shmanai *et al.*, Targeting of CRISPR-Cas12a crRNAs into human mitochondria, Biochimie, https://doi.org/10.1016/j.biochi.2023.09.006

A



B

Name	Target	Sequence: 5'- 3'
crRNA-1	D-loop	UAAUUUCUACUCUUGUAGAUCCCUCCCACUCCCAUACUAC
crRNA-6	D-loop	UAAUUUCUACUCUUGUAGAUACCUCUCCACCCUUAUCACA
crRNA-10	MT-ND1	UAAUUUCUACUCUUGUAGAUCACACAGACAUCAUAACAAA
crRNA-14	mt tRNA^{Pro}	UAAUUUCUACUCUUGUAGAUACUCCACCAUUAGCACCCAA
crRNA-30	MT-ND5	UAAUUUCUACUCUUGUAGAUGAUGAUGUGGUCUUUGGAGU
crRNA-31	MT-ND4	UAAUUUCUACUCUUGUAGAUCACUCACAACACCCUAGGCU
crRNA-34	MT-ND4	UAAUUUCUACUCUUGUAGAUGCUGUUCCCCAACCUUUUCC
crRNA-45	MT-ATP6	UAAUUUCUACUCUUGUAGAUCCCCUCUAUUGAUCCCCACC
crRNA-52	MT-ND3	UAAUUUCUACUCUUGUAGAUUAGAUCAAAUAAUAAGAAGG

Fig. 1. Human mtDNA map with the representation of binding sites for 27 AsCas12a crRNAs bearing TTTV protospacer adjacent motif, designed for targeting different regions of mtDNA. (A) HSP, HSP2, LSP and LSP2 are heavy and light chain promoters; O_H and O_L are the origins of heavy and light chain replication; and the following genes are presented: NADH dehydrogenase subunits (*MT-ND1-ND6* and *ND4L*), cytochrome *b* (*MT-CYB*), cytochrome *c* oxidase subunits (*MT-COI-III*), ATP synthase 8 and 6 subunits (*MT-ATP6*, *MT-ATP8*), rRNA 12S (*MT-RNR1*) and 16S (*MT-RNR2*) and tRNAs (denoted by the one-letter code of the corresponding amino acids). The 9 crRNAs for which the possibility of mitochondrial import was evaluated are highlighted in grey. **(B)** Sequences of the 9 crRNAs used for mitochondrial import assays. The scaffold and spacer sequences in crRNA molecules are colored in black and blue, respectively. The targeted gene in human mitochondrial DNA is specified for each crRNA.

targeted restriction endonucleases (mitoREs), both native and artificial ones (mitoARCUS), have been successfully used to reduce mutated mtDNA levels in human cultured cells and mouse models [12–15]. However, such systems are highly limited by the occurrence of unique recognition sites, allowing targeting of specific pathogenic mutations in mtDNA. Additionally, the development of artificial nucleases demands significant time and resources. The mitoREs limitations were addressed by creating nucleases that are able to target specific sites in mtDNA by utilizing specific DNA recognition modules - zinc-finger proteins for mitoZFNs and TAL effector proteins for mitoTALENs. These approaches have demonstrated efficacy in modifying heteroplasmy ratios in cybrid cells and mouse models [16–24].

The second strategy, which can also be applicable for homoplasmic mutations, consists of the use of base editors in order to reverse mutations without introducing a break in mtDNA. Two types of base editors are currently employed for mtDNA editing: mitochondria-targeted TALE-linked or ZFN-linked double-stranded DNA deaminase (DddA)-derived cytosine base editors (DdCBEs) and mitochondria-targeted TALE-linked adenine deaminases (TALEDs) [25–29]. Although strategies based on mitoZFNs and mitoTALENs show promise for mtDNA targeting, they still have limitations. Designing and engineering monomers for specific mtDNA recognition is a challenging and resource consuming task. Moreover, the large size of protein coding sequences exceeds the capacity of current virus-based delivery systems, such as adeno-associated virus (AAV) [30,31].

In this regard, CRISPR-Cas systems, while having shorter coding sequences, offer greater flexibility for DNA recognition experiments compared to protein-only systems due to their reliance on DNA–RNA interactions for specific mtDNA site recognition [32]. Thus, they enable faster change of the DNA recognition site by use of different guide RNAs keeping the protein component constant. However, the two-component system necessitates the assembly of a functional machine within the mitochondria, which requires direct delivery of both the protein and RNA components into the mitochondrial matrix [33]. The import of proteins into mitochondria can be effectively achieved by fusing a mitochondrial targeting sequence (MTS) to the N-terminus of the protein of interest [34]. The MTS consists of an amphipathic α-helical peptide sequence that is recognized by receptors of the translocases of the outer membranes (TOM) that direct the protein to the mitochondrial matrix. Recent studies from our and other laboratories demonstrated mitochondrial targeting of Cas nucleases bearing various N-terminal MTS (listed in Table 1).

In contrast, the import of gRNA component into mitochondria

Table 1
Recently developed mitochondrial CRISPR/Cas systems.

Cas nuclease	sgRNA/crRNA	RNA delivery	Detection of sgRNA/crRNA localization	Effect on mtDNA	Reference
SpCas9	Unmodified sgRNA; sgRNA bearing yeast tRK1 F- and D-hairpins	RNA transfection	Northern blot hybridization of total and mitoplast RNA	decrease of mtDNA copy number; no shift in heteroplasmy level	[33]
SpCas9	Unmodified sgRNA	Transcribed from plasmid under control of U6 promoter	Not verified	decrease of mtDNA copy number;	[47]
LbCas12a	Unmodified crRNA; crRNAs with the stem-loop motifs from RNase P RNA and from yeast tRK1	Transcribed from plasmid under control of U6 promoter	Northern blot hybridization of total and mitochondral RNA	Increase of mtDNA copy number	[48]
SpCas9	Unmodified sgRNA; sgRNA with the stem-loop motif from RNase P RNA	Transcribed from plasmid under control of U6 promoter	Laser scanning microscopy of Alexa fluor 488-labeled RNA; RT-qPCR on total and mitochondrial RNA	Small reduction of mutant mtDNA	[49]
SpCas9	Unmodified sgRNA; sgRNA with the stem-loop motif from RNase P RNA	Transcribed from plasmid under control of U6 promoter	Not verified	Generation of InDels (<0.05%)	[50]
SpCas9 SpCas9-BE3	Unmodified sgRNA; sgRNA with the stem-loop motif from RNase P RNA	Transcribed from plasmid under control of U6 promoter	Not verified	No change in mtDNA copy number; Unspecific C to T substitutions	[51]
SpCas9	Unmodified sgRNA	Transcribed from plasmid under control of U6 promoter	Laser scanning microscopy of FAM-labeled sgRNA	decrease of mtDNA copy number;	[52]

poses a significant challenge for applying CRISPR-Cas systems. In most of recent publications (Table 1), CRISPR/SpCas9 system have been applied, but the mitochondrial import of gRNA has never been convincingly demonstrated, thus raising uncertainty on the possible use of this system for mtDNA manipulations [35]. We suggest two main reasons for this. First, the use of plasmids expressing gRNAs in the nucleus, being well established for the nuclear DNA applications, seems to be not convenient for gRNA mitochondrial targeting due to the need of efficient gRNA export from the nucleus (Fig. S1A), which cannot be assured in the absence of the signals for RNA export [36–38]. Second, sgRNAs of Cas9 system are rather long (about 100 bp) (Fig. S1B) [39], which can strongly decrease their mitochondrial targeting [40].

To address these problems, in this study, we deliver gRNAs into cells by direct Lipofectamine transfection (Fig. S1A), which had been used in our lab previously to provide mitochondrial import of various types of small non-coding RNAs [41,42], including SpCas9 sgRNA [33]. Then, we use an alternative CRISPR/Cas system, the Type V CRISPR/Cas12a, characterized by a shorter crRNA of 40–44 nucleotides (Fig. S1B) [43], which may represent a better substrate for mitochondrial import compared to sgRNA. Finally, we apply our long-term expertise and recent findings [44] to avoid possible false-positive data and provide evidence of AsCas12a crRNA targeting into mitochondria in transfected human cells.

Studies by our and other laboratories had shown that the motif required for the transport of RNA molecules into mitochondria is not a sequence, but a hairpin structure (Fig. S1C) [45,46]. These structures, referred to as MLS (mitochondrial localization signal), were initially discovered in our Selex experiments and further successfully tested for anti-replication strategy in a variety of human cell lines [33,41,42].

We aim to critically investigate whether various AsCas12 crRNAs can be successfully imported into human mitochondria and to study the structural requirements for this process. We show that fusion of crRNAs with MLS is not required for their targeting into mitochondria.

2. Materials and methods

2.1. Design of AsCas12a crRNAs

RNAfold [53] and Mfold web servers [54] were used to predict secondary structures of AsCas12a crRNAs. To predict secondary structures of crRNAs upon dimer formation, RNAcofold web server was used [53]. In order to search for the potential off-target sites of AsCas12a RNA-guided endonuclease, we used Cas-OFFinder algorithm [55].

In the reference human mtDNA sequence (GenBank NC_012920 gi:251831106), 530 sequences representing the canonical AsCas12a "TTTV" PAM (Fig. S1B) were found [56]. Following the PAM sites, subsequent 5′ – 3′ 20 bp sequences of spacers were supplemented at the 5′ -end by the AsCas12a scaffold sequence – "UAAUUUCUACUCUUGUAGAU" [43]. crRNAs were analyzed for predicted probability of introducing unwanted changes (off-targets) into the nuclear genome by the AsCas12a-crRNA complex, as well as for predicted secondary structures. crRNAs were rated according to these parameters and 27 of them were chosen for mitochondrial targeting assays (Table S3).

2.2. In vitro transcription of AsCas12a crRNAs bearing import determinants

crRNAs were *in vitro* transcribed using HiScribe™ T7 High Yield RNA Synthesis Kit (New England BioLabs) according to the manufacturer's protocol. As a DNA template, we used PCR amplicons obtained from the plasmids encoding non-modified (NM) crRNAs and modified versions bearing RNA import determinants (MRP, HD, HF) using Phusion™ High-Fidelity DNA Polymerase (Thermo Scientific) (Fig. S2). T7 promoter was added to the sequence of forward primer (Table S1). *In vitro* transcribed crRNAs were purified using TRIzol™ Reagent (Invitrogen) according to the manufacturer's protocol. RNA concentrations were measured using NanoDrop 1000 Spectrophotometer V3.5 (Thermo Scientific). The quality of

synthetic crRNAs was verified by electrophoresis in 8 M urea denaturing 10% polyacrylamide gel. Following 1 h migration at 20 mA, EtBr-stained gel was visualized by Hero Lab Trans-illuminator UVT-28 M (Herolab GmbH).

2.3. Chemical synthesis of AsCas12a crRNAs

The oligoribonucleotides were synthesized using an automatic DNA/RNA synthesizer ASM 2000 (Biosset Ltd.) at 500 nmol scale on 1000 Å Universal support CPG (Primetech ALC, 41 μmol/g) as described before [57]. Synthetic crRNAs were protected with terminal 2′-O-Methyl (2′-O-Me) and phosphorothioate (PS) modifications [58] (Fig. S3).

2.4. Cell culture conditions and RNA transfections

HEK 293 cells and the hAsCas12a HEK 293 T-REx stable cell line [57] were maintained at 37 °C, 5% CO_2 in essential modified Eagle's medium (EMEM) (Sigma-Aldrich) containing 1 g/L D-glucose and supplemented with 1.5 g/L sodium bicarbonate (Sigma-Aldrich) and 0.11 g/L sodium pyruvate (Sigma-Aldrich), 10% fetal bovine serum (Gibco, Fisher Scientific), 100 mg/L Penicillin-Streptomycin (Sigma-Aldrich) and 2.5 mg/L Amphotericin B (Sigma-Aldrich). The human osteosarcoma cell line 143B was cultivated under the same conditions, with the exception of the medium, which was based on Dulbecco's Modified Eagle Medium (DMEM) (Sigma-Aldrich) containing 4.5 g/L of D-glucose.

Before each experiment, cell cultures were tested for mycoplasma contamination by PCR with DreamTaq Green PCR Master Mix (Thermo Scientific), as described [59] (see primers in Table S1). Total DNA isolated with NucleoSpin® Tissue Mini Kit (Macherey-Nagel) according to the manufacturer's protocol was used as a PCR template.

For AsCas12a crRNAs mitochondrial import analysis, cells were transfected at 80% confluency in 75 cm^2 cell culture flask with 6 μg of chemically-synthesized or T7-transcribed crRNA using 20 μL of Lipofectamine™ 2000 transfection reagent (Invitrogen) in 9 mL Opti-MEM™ reduced serum medium (Gibco, Fisher Scientific). 6 h after transfection, the medium was changed to 12 mL of EMEM, and cells were left to propagate for another 48 h.

2.5. Test of AsCas12a/crRNAs activity in cell lysate

As DNA substrates for *in vitro* cleavage tests, we used mtDNA fragments amplified with Phusion™ High-Fidelity DNA Polymerase (Thermo Scientific) from genomic DNA isolated from T-REx cell line (T-REx™-293 Cell Line, Invitrogen, kat. #R71007) by NucleoSpin® Tissue Mini Kit (Macherey-Nagel) according to the manufacturer's protocol. DNA oligonucleotides used for the template DNA amplification are listed in Table S1.

For the *in vitro* cleavage assay, the hAsCas12a HEK 293 T-REx stable cell line was used [57]. Cells with inducible expression of the AsCas12a nuclease were cultured in 6-well plate. The expression of the nuclease was activated at 80% confluency by the addition of tetracycline to a final concentration of 100 ng/mL 24 h after induction, cells were washed with 1 × phosphate buffered saline (PBS) and lysed by 50 μL/cm^2 lysis buffer (20 mM HEPES-KOH pH 7.5, 100 mM KCl, 5 mM $MgCl_2$, 1 mM DTT, 5% glycerol, 0.1% Triton X-100 and Protease Inhibitor cocktail (Roche Diagnostics)) and then rocked for 10 min at 4 °C. To remove cell debris, lysates were centrifuged for 10 min at 1000 g, 4 °C. The resulting supernatant was divided into aliquots and stored at −80 °C.

Cleavage reactions were carried out in a total volume of 20 μL and contained 18 μL of cell lysate, 150 ng of PCR-obtained DNA substrate and 50 ng of crRNA. Reactions were incubated for 30 min at 37 °C. After incubation, reactions were purified with NucleoSpin® PCR Clean-up Kit (Macherey-Nagel) according to the manufacturer's protocol. Analysis of cleavage products was performed by electrophoresis in 1% agarose gel (w/v) in 1 × TAE buffer. EtBr-stained gels were visualized by Hero Lab Transilluminator UVT-28 M (Herolab GmbH).

Alternatively, to verify AsCas12a/crRNA functionality in cells, the hAsCas12a HEK 293 T-REx stable cell line was cultured in a 12-well plate and transfected at 80% confluency with increasing amounts of AsCas12a crRNA (175, 250, 375 ng/cm^2) using Lipofectamine™ 2000 transfection reagent (Invitrogen) in 500 μL of Opti-MEM™ reduced serum medium (Gibco, Fisher Scientific). After 6 h of transfection, the medium was changed to 2 mL of EMEM supplemented with 100 ng/mL of tetracycline to activate the nuclease expression. After 24 h, the cell lysates were prepared as described above. The *in vitro* cleavage reactions contained the appropriate DNA template, but no additional crRNA was added (except for the control reaction).

2.6. Mitochondria isolation and fractionation

Mitochondria were mainly isolated as described [42] with modifications. All procedures were carried out at 4 °C, unless specified differently. Briefly, transfected cells were washed once with 1 × phosphate buffered saline (PBS) and then detached and resuspended in 1 mL of prechilled Mito buffer (0.6 M sorbitol, 10 mM HEPES-KOH, pH 7.5, 1 mM EDTA). 50 μL of resuspended cells were taken for total RNA isolation. The rest of the cells were disrupted by 30 passages through 2 mL syringe with needle No26G (0,45 × 12 mm). Nuclei, cell debris and unbroken cells were pelleted by centrifugation for 10 min at 1000 g at 4 °C. The procedure was repeated 3 times with transferring the resulting supernatant each time to a new ice-cold tube. Mitochondria-rich pellet was obtained after high-speed centrifugation at 15,000 g at 4 °C for 30 min and then carefully resuspended in 150 μL of Mito buffer. 30 μL of resuspended mitochondria were taken for lysate preparation (see below). To decrease possible cytosolic RNA contamination, 120 μL of 2 × RNase A solution (20 μg/mL ribonuclease A from bovine pancreas, 4 mM $MgCl_2$, 200 mM NaCl) was added to the purified mitochondria. The reaction was incubated at room temperature for 7 min and then stopped by adding 500 μL of Mito buffer containing 4 mM EDTA. RNase A was washed out by centrifugation at 15,000 g at 4 °C for 15 min 3 times with 500 μL of Mito buffer, each time discarding the resulting supernatant. After the last centrifugation, mitochondria were resuspended in 300 μL of Mito buffer. In order to obtain mitoplasts, mitochondria were treated with 20 μg of digitonin (Sigma-Aldrich) for 7 min at room temperature. The resulting mitoplasts were centrifuged for 15 min at 15,000 g at 4 °C and washed ones with 500 μL of Mito buffer. To proceed with RNA isolation, the mitoplast pellet was resuspended in 500 μL of TRIzol™ Reagent (Invitrogen) and was either stored at −80 °C or treated immediately.

To prepare mitochondrial lysate, mitochondria were treated with n-dodecyl-β-D-maltoside (Sigma-Aldrich) (0.5% final concentration (w/v)), 20 μg of digitonin (Sigma-Aldrich) and with an equal volume of 2 × RNase A solution to degrade mitochondrial RNA and to demonstrate possible presence of RNase-resistant contaminant. After a brief pipetting, the mixture was left for incubation at room temperature for 10 min. To proceed with RNA isolation, the mitochondrial lysate was resuspended in 500 μL of TRIzol™ Reagent (Invitrogen).

Submitochondrial fractionation was performed as previously described [44,60] with modifications. In brief, the mitochondria-rich fraction corresponding to the pellet was obtained by differential centrifugation as described above. For the RNase A/T_1

accessibility test, the mitochondrial pellet was carefully resuspended in 300 μL of Mito buffer and split into three aliquots. The mitochondrial pellet was sedimented again with an excess of Mito buffer. After that, mitochondria were carefully resuspended in 100 μL of Mito buffer (for intact mitochondria), swelling buffer (10 mM HEPES-KOH, pH 7.5, 1 mM EDTA) (for mitoplasts) and lysis buffer (10 mM HEPES-KOH, pH 7.5, 1 mM EDTA, 0.5% (w/v) n-dodecyl-β-maltoside) (to lyse mitochondria). Each tube was split into 2 aliquots, in which one was treated with 1.5 μL of RNase A/T_1 mix (2 mg/mL, 5.000 U/mL; Thermo Fisher Scientific) for 10 min at room temperature. For RNA extraction, 500 μL of TRIzol™ Reagent (Invitrogen) were added to the reaction.

2.7. Northern blot analysis

RNA was purified from all the samples using TRIzol™ Reagent (Invitrogen) according to the manufacturer's protocol, followed by precipitation with isopropanol. RNA pellets were diluted in 15 μL of nuclease-free water. Northern blot analysis was performed as described [42]. Purified RNA samples were separated on a 10% (w/v) denaturing polyacrylamide gel. After electrophoresis at 20 mA in 1 × TBE until the bromophenol blue dye reached the middle of the gel, samples were electroblotted onto a nylon Amersham HybondN + membrane (GE Healthcare) in a wet transfer camera in 0.5 × TBE at 4 °C, 10 V, overnight. RNAs were fixed on the membrane by irradiation in a cross-linking UV chamber (Amersham Life Science), for 3 min at each side of the membrane at constant energy 1.500 × 100 μJ/cm^2. After that, membranes were pre-hybridized by rotating in a hybridization oven in 6 × SSC, 0.1% SDS, 10 × Denhardt solution for 1 h at 65 °C. The pre-hybridized membranes were incubated overnight with continuous rotation in the prehybridization buffer supplemented with 5′-^{32}P-labeled antisense oligonucleotide probe at 56 °C. DNA oligonucleotide probes (Table S2) were radiolabeled with γ-^{32}P-ATP using T4 polynucleotide Kinase (Thermo Scientific) and then purified by size exclusion chromatography with Micro Bio-Spin™ Chromatography Columns (Bio-Rad) according to the manufacturers' protocols. After hybridization, membranes were washed 3 times for 10 min in 5 × SSC, 0.1% SDS buffer, and sealed between two polyethylene sheets and exposed on the phosphoimager screen overnight. The hybridization signal was visualized on Typhoon Trio (GE Healthcare) and analyzed with ImageQuant TL (v. 7.0, GE Healthcare). Before proceeding with hybridization with other probes, membranes were stripped 3 times for 10 min in 0.02 × SSC, 0.1% SDS buffer at 80 °C.

2.8. Quantitative analysis of RNA import

After quantification using the Typhoon Trio scanner, the relative efficiency of RNA import into mitochondria was calculated as a ratio between the signal obtained with a probe specific for AsCas12a crRNA used for cell transfection and that obtained with the probe against the host mitochondrial tRNA (mt *tRNAVal*) [42]. To detect possible AsCas12a crRNAs' protection against treatment with RNases not linked to the mitochondrial import, a control experiment consisting of the lysis of the portion of mitochondria was considered.

3. Results

3.1. Design of AsCas12a crRNAs targeting various regions in human mitochondrial DNA

The selected 27 crRNAs are shown in Fig. 1A, Table S3. Capacity to be imported into mitochondria has been evaluated for nine crRNA from this list (Fig. 1A and B), characterised by different predicted secondary structures, probability of off-target cleavage in the nuclear genome and homodimer formation (Tables S4, S5 and S6).

3.2. AsCas12a crRNA can be imported into human mitochondria without additional import determinants

To ensure function of AsCas12a nuclease within human mitochondria, the presence of crRNA in the mitochondrial matrix is essential. To investigate whether the fusion of crRNA with known RNA import determinants [40] improve its mitochondrial targeting, we modified one of the designed crRNAs by adding stem-loop motifs of human RNase MRP RNA [45] and *S. cerevisiae* $tRNA^{Lys}_{CUU}$ (tRK1) D-hairpin and F-hairpin [46] (Fig. S1C).

Previously published crystal structure of the AsCas12a-RNA complex revealed that the crRNA 5′ handle adopts a pseudoknot structure, which is crucial for recognition and interaction between AsCas12a and crRNA [43]. It is worth noting that several nucleotides of the 5′ scaffold, including the terminal ones, are conserved among the CRISPR-Cas12a systems [61]. However, in the crystal structure, the absence of electron density for the terminal nucleotides of the 3′ guide segment and target DNA strand suggests that these regions are flexible and disordered [43]. Based on these published data, we hypothesized that this part of the crRNA could be modified without affecting the overall function of the complex. Therefore, we fused the MLS to the 3′-end of crRNA (Fig. 2A and B). Subsequently, we evaluated AsCas12a nuclease activity *in vitro*, using modified or unmodified crRNA, and observed complete cleavage of targeted DNA in all reactions (Fig. 2C and D).

We then tested whether these crRNAs could be delivered to mitochondria *in vivo*. For this, we transiently transfected HEK 293 cells with corresponding T7 transcripts and then analyzed total RNA and RNA isolated from mitoplasts using Northern blot hybridization (Fig. 3A). Control hybridization was carried out to verify that isolated mitoplasts were depleted of nuclear or cytosolic contamination (5.8S rRNA). A mitochondrial RNA ($tRNA^{Val}$) was used as a loading control. We observed strong enrichment of the crRNA hybridization signal in the mitoplast fraction only for non-modified and F-hairpin-modified crRNAs which indicates on the targeting of these molecules into mitochondria (Fig. 3B). In contrast, other MLS structures (MRP and HD) reduced the mitochondrial localization of the crRNA. Noteworthy, these data show that crRNA can be imported into mitochondria without additional hairpin structures, in agreement with our former observation for Cas9 gRNA [33] and with that of Antón et al., 2020 [48] for LbCas12a crRNA.

3.3. Mitochondrial import for AsCas12a crRNAs targeting various regions in human mtDNA

Once confirmed that AsCas12a crRNA does not require an additional MLS, the next question we addressed was: if crRNAs, designed to target various regions in human mitochondrial DNA and thus possessing different sequences, can be imported into mitochondria with comparable efficiency. For this, we selected 9 crRNAs (Fig. 1B), chosen based on variations in predicted secondary structures, with 2 of them possessing potential off-target sites in the nuclear genome (Tables S4 and S5). Prior to the evaluation of their mitochondrial import, we first confirmed the activity of all 9 crRNAs by *in vitro* cleavage assay in lysate of human cells expressing AsCas12a nuclease (Fig. 4).

To evaluate the import efficiency of the selected crRNAs, we included, as a control, an aliquot of purified mitochondria lysed with detergent and treated with RNase, which aimed to detect potential protection of RNA of interest unrelated to mitochondrial

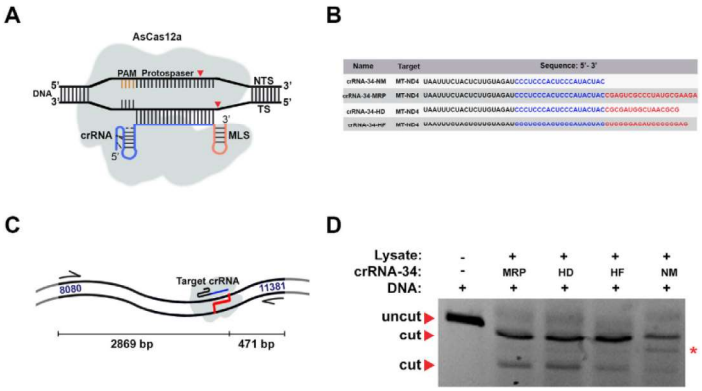


Fig. 2. Fusion of crRNA with MLS did not affect AsCas12a cleavage ability *in vitro*.
(A) Schematic representation of AsCas12a-crRNA-DNA complex. Mitochondrial localization signals (MLS) (see Fig. S1C) were added to the 3′-end of AsCas12a crRNA (shown in coral). **(B)** Sequences of the 4 crRNAs used in the import assays. The scaffold and spacer sequences in crRNA molecules are colored in black and blue, respectively. The targeted region in human mitochondrial DNA for each crRNA is specified. Additional 3′-end RNA import motifs of tRK1 (HD and HF), RNase MRP RNA (MRP) are shown in red. **(C)** Schematic representation of target DNA (PCR fragment of human mtDNA, nucleotide numbers are indicated) containing AsCas12a PAM sequence. The spacer moiety of target crRNA-34 is shown in blue, the scaffold part is shown in black, the cleavage site is marked with a red line. The sizes of the fragments corresponding to cleaved DNA template are given below scheme. **(D)** *In vitro* cleavage of target DNA by AsCas12a in complex with non-modified (NM) crRNA-34 or modified with the RNA import motifs (MLS) from tRK1 (HD and HF) or RNase MRP RNA (MRP). The addition of cell lysate containing AsCas12a nuclease, crRNA and DNA template is indicated above the gel. *In vitro* cleaved products were resolved by 1% (w/v) agarose gel electrophoresis and revealed with ethidium bromide staining. Additional DNA band marked with red asterisc originates from the cell lysate.

import (Fig. 5A). Surprisingly, the data demonstrated that crRNA-1 and 14 appeared to be protected from the nuclease treatment (Fig. 5B). This protection may be due to interaction with unknown proteins and/or to a stable secondary structure which was not predicted by the software used. In any case, we therefore cannot conclude about mitochondrial import of crRNA-1 and 14 in the used experimental conditions.

In contrast, we observed that crRNAs 31, 45, and 52 (Fig. 5B) as well as crRNAs 6, 10, and 34 (Fig. 5C) were efficiently degraded in mitochondrial lysate and still present in mitoplasts after RNase treatment indicating on their import into human mitochondria. The weak hybridization signals for crRNAs 45 and 34 in total RNA fraction may be due to the low transfection efficiency of the cells. We do not provide here the quantification of RNA import efficiency (as described in our previous papers [33,42], since the standard deviation obtained in 2–3 biological replicates exceeded 20%. The variability between biological replicates may be explained by the poor reproducibility of numerous experimental manipulations that can potentially affect the final outcome, such as cell transfection with RNA molecules, mitochondria isolation, and mitoplast preparation, but this does not affect the statement concerning the mitochondrial targeting.

Noteworthy, crRNAs 31 and 52 showed a higher enrichment in RNase-treated mitoplasts compared to the other tested crRNAs. To explain this observation, we analyzed the predicted alternative 2D structures for all crRNAs tested, as well as predicted secondary structures upon dimer formation (Tables S4 and S6). For crRNA-52 another possible secondary structure characterized by longer hairpin stem and a stable homodimer were predicted. Homodimer formation was also observed for crRNA-31. Based on our analysis, we can hypothesize that the import efficiency may be enhanced by the formation of stable helix structures that could act as import determinants [45].

To further confirm the data on the mitochondrial targeting of AsCas12a crRNAs' alternative predicted secondary structures and dimers, we compared the import of crRNA-45 and crRNA-30 in the hAsCas12a HEK 293 T-REx stable cell line and 143B osteosarcoma cells, respectively, using our recently developed CoLoc method [44]. We treated isolated mitochondria, mitoplasts, and mitochondrial lysate with a mix of RNase A and T_1 and compared the results to the untreated control samples (Fig. 6A). After RNase A/T_1 treatment of intact or swollen mitochondria, crRNA-45 remained resistant to digestion and only disappeared when the mitochondria were fully lysed, similar to the matrix-localized mitochondrial *tRNAVal* (Fig. 6B). Extensive nuclease treatment caused partial degradation of mitochondrial *tRNAVal*, however, the signal corresponding to crRNA persisted, thus providing further confirmation that AsCas12a crRNAs are indeed localized in the mitochondrial matrix.

We obtained comparable results for crRNA-30 import into mitochondria of cell line 143B (Fig. 6C), indicating that the crRNA import pathway is not cell line-specific. Interestingly, crRNA-30 characterised by a very compact predicted secondary structure and a stable homodimer, was not protected from the nucleases in the mitochondrial lysate, but is clearly enriched in the mitoplasts, supporting our hypothesis on the positive impact of the RNA secondary structure on its mitochondrial targeting.

We also confirmed the functionality of the AsCas12a/crRNA complex in the hAsCas12a HEK 293 T-REx stable cell line by performing an *in vitro* cleavage assay on the cell lysate obtained 48 h after transfecting the cells with increasing concentrations of crRNA-45 and activating the nuclease expression (Fig. 6D). The reactions contained the appropriate DNA template, but no additional crRNA (except for the control reaction). Specific crRNA-dependent DNA template cleavage was detected, demonstrating that crRNA designed to target mitochondrial DNA, introduced into human cells, can induce specific AsCas12a nuclease activity.

Recently, we demonstrated that AsCas12a crRNA can be split into two 20 bp parts, namely scaffold and spacer, without affecting its cleavage activity (Fig. S4A) [57]. We compared the mitochondrial import of crRNA-45 and its spacer part and found that the spacer part of crRNA can be targeted into human mitochondria of the hAsCas12a HEK 293 T-REx stable cell line (Fig. S4B). Thus, we

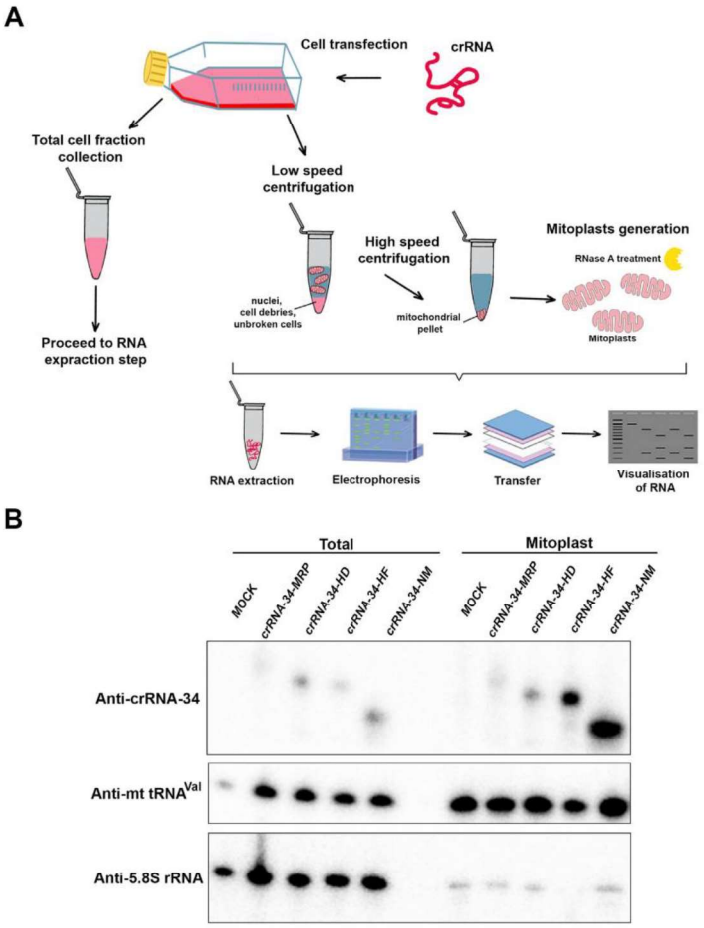


Fig. 3. Mitochondrial import of AsCas12a crRNAs bearing RNA import determinants.
(A) Schematic representation of the experiment pipeline. To evaluate the mitochondrial import of various AsCas12a crRNAs, we use Northern blot hybridization of total and mitochondrial RNA isolated from cultured human cells transfected with crRNAs. To improve the purity of isolated mitochondria and degrade RNA adhered to mitochondria from the cytosol, we treat them with RNase A with subsequent generation of mitoplasts. **(B)** Northern blot hybridization of the total or purified mitoplasts' RNAs isolated from the control HEK 293 cells (MOCK) or HEK 293 cells transfected with either non-modified crRNA-34 (NM) or crRNA-34 modified with 3′-MRP, 3′-HD, 3′-HF import determinants (Fig. 2B). The hybridization probes are shown on the left: crRNA-34 (top panel), mitochondrial *tRNAVal* (middle panel) and cytoplasmic 5.8S rRNA (lower panel).

suggest that the split AsCas12a crRNA variant could be used in further *in vivo* experiments for mtDNA targeting.

Therefore, we demonstrated that crRNA for AsCas12a system designed to target mitochondrial DNA, being introduced into human cells, can be imported into mitochondria and can induce specific DNA cleavage by AsCas12a nuclease. This finding opens the possibility to use CRISPR/Cas12 system for specific cleavage of mtDNA.

4. Discussion

Multiple alterations of human mitochondrial DNA were shown to be associated with severe impact on cellular respiration therefore leading to the onset of many diseases, mostly muscular or neurodegenerative, but also common diseases as cancer and diabetes (reviewed in Refs. [6,62]). Mitochondria are surrounded by a double membrane bearing a negative charge; therefore, there is no possibility to direct large DNA or mRNA molecules into the organelles with the aim to substitute the defective genes. Only some non-coding RNAs can be translocated into mitochondria from the cytosol (reviewed in Refs. [40,63–65]). Can this pathway be adapted for mitochondrial delivery of crRNAs, thus developing a mito-CRISPR/Cas system? This is currently a matter of controversy, since some speculative arguments (e.g., artefactual nature of the RNA import due to inability of imported RNA to perform their canonical functions) have been forwarded [35]. Nevertheless, several

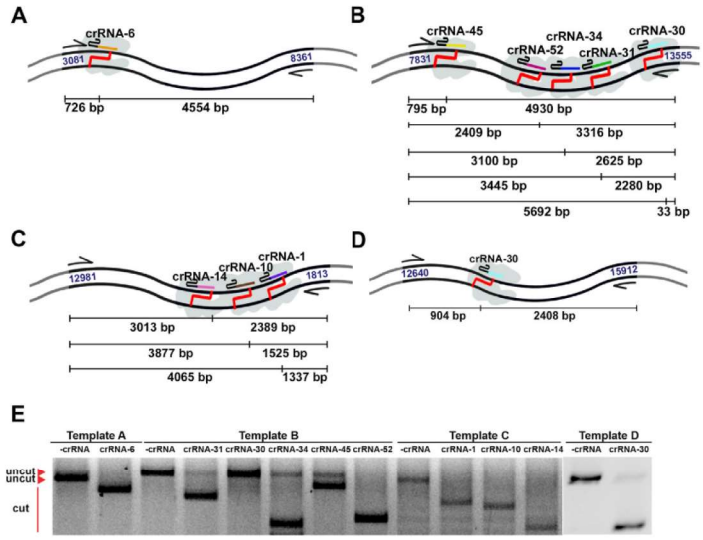


Fig. 4. AsCas12a can be programmed with crRNAs crRNAs targeting various regions in human mitochondrial DNA.
(A)–(D) Schematic representation of target DNA (PCR fragment of human mtDNA with corresponding numbers of nucleotides). The spacer moieties of target crRNAs are shown in color, the scaffold part is shown in black, and the cleavage site is marked with a red arrow. The size of the fragments corresponding to cleaved DNA template are given below the scheme. DNA "Template A" **(A)** contains protospacer sequence for crRNA-6; "Template B" **(B)** - for crRNAs 45, 52, 34, 31 and 30; "Template C" **(C)** - for crRNAs 14, 10, 1; and "Template D" **(D)** for crRNA-30. **(E)** *In vitro* cleavage of target DNA templates induced by crRNAs. DNA templates and crRNAs used in the reaction are indicated above the gel. "-crRNA" corresponds to a control reaction that does not contain any crRNAs. Since crRNA-30 generates short cleavage fragments **(B)**, which cannot be distinguished from a non-cleaved DNA template, the cleavage was made with the use of DNA template **(D)**. *In vitro* cleaved products were resolved by 1% (w/v) agarose gel electrophoresis and revealed with ethidium bromide staining.

laboratories still work in this direction [33,47–52]. We have previously demonstrated the possibility to address SpCas9 nuclease and a set of sgRNA molecules into mitochondria of cultured human cells and obtained a consequent decrease of mtDNA copy number [33], but could not detect specific mtDNA cleavage. We hypothesized that the main challenge consists in sub-efficient delivery of a rather long sgRNA (~100 bases) for CRISPR/Cas9 system into the mitochondria.

Several studies demonstrated that while long non-coding RNAs (75–300 nucleotides) can be imported into mitochondria only with the help of specific protein factors, which limits the amount of translocated molecules [66,67], the shorter RNA molecules such as miRNA and siRNA are targeted in a much more efficient and probably non-specific way and can be not only detectable, but also functional [68–70].

Here we demonstrate that 40 nucleotide-long crRNA of Type V CRISPR/Cas12 system, designed to target human mtDNA and introduced into human cells by lipophilic transfection, can be translocated into mitochondrial matrix. We show that crRNA can be imported into the mitochondria of HEK293 (Figs. 3B) and 143B osteosarcoma cells (Fig. 6C); therefore, this pathway does not depend on the expression of the hAsCas12a nuclease and is non cell line-specific. Given the functional activity of crRNA in the lysate of human cells expressing AsCas12a nuclease (see Fig. 6D), we hypothesize that these imported crRNA can make it possible to reconstitute an active Cas12a-crRNA system *in vivo*.

Molecular mechanisms of RNA translocation across mitochondrial membranes in humans remain poorly understood [40]. The TOM complex and/or VDAC channel may facilitate translocation through the OMM (reviewed in Ref. [71]), while polynucleotide phosphorylase (PNPase) involved in RNA import from the intermembrane space into the matrix [45,72,73]. The mechanism by which PNPase participates in RNA import is still unclear but could involve its conformational changes upon recognition of the stem-loop RNA structures (reviewed [40]). This model supports previous data of our and other labs on identified RNA hairpins (here referred for as MLS) which strongly improved the mitochondrial targeting of various RNA molecules [74–76] (Fig. S1C). Here we show that hairpin structures fused to the 3′-end of crRNA do not impact its ability to program specific cleavage of DNA *in vitro* (Fig. 2). Surprisingly, mitochondrial localization of the fused crRNA molecules was not improved by HF stem-loop and even decreased by hairpins MRP and HD compared to non-modified version (Fig. 3B). The finding that crRNAs are imported without addition of MLS can be explained by the secondary structure of crRNA for CRISPR-Cas12a system, which consists of two nearly equally sized moieties, a 5′-handle (scaffold) and a guide segment complementary to the target DNA sequences (referred to as the spacer) (Fig. S4A). Crystal structures of AsCas12a-crRNA complexes revealed that the crRNA scaffold adopts a pseudoknot structure [43]. One can hypothesize that this structure functions as MLS, assuring crRNA mitochondrial import by specific interaction with PNPase, while addition of supplementary MLS could make a longer RNA less efficient in mitochondrial translocation.

Analysis of mitochondrial import of crRNAs targeting different regions in mtDNA revealed that two crRNAs (31 and 52) exhibited a higher enrichment in RNase-treated mitoplasts compared to other tested crRNAs (Fig. 5). Further analysis revealed unique

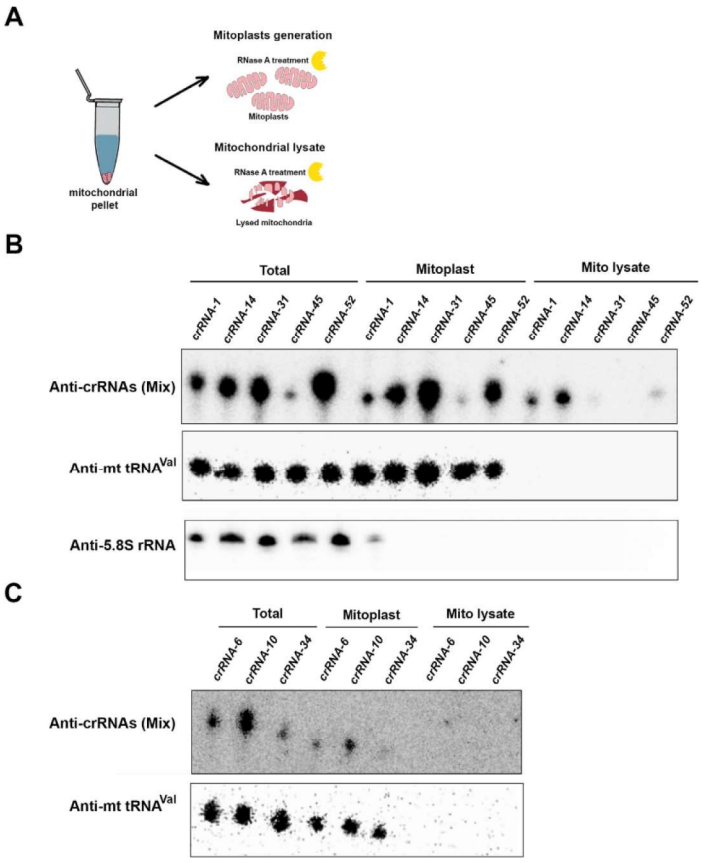


Fig. 5. Evaluation of mitochondrial import for AsCas12a crRNAs targeting various regions in human mtDNA.
(A) Schematic representation of a control experiment. **(B, C)** Northern blot hybridization of RNA isolated from the hAsCas12a HEK 293 T-REx stable cell line transfected with crRNAs 1, 14, 31, 45, 52 **(B)** and crRNAs 6, 10, and 34 **(C)**. RNA was isolated from cells ("Total"), RNase treated mitoplasts ("Mitoplast") and RNase treated mitochondrial lysates ("Mito lysate"). Hybridization probes used are indicated on the left: crRNAs (top panel), mitochondrial *tRNAVal* (middle panel) and cytoplasmic 5.8S rRNA (lower panel). Anti-crRNAs (Mix) probe represents the combination of probes to corresponding crRNAs (Table S2).

characteristics of these crRNAs, such as longer hairpin stems and stable homodimer formation (Tables S4 and S6), suggesting that the presence of stable helix structures may facilitate their import into mitochondria.

Recently, we demonstrated that AsCas12a crRNA can be split into two 20 bp parts, namely scaffold and spacer, without affecting its cleavage activity [57]. We, therefore, compared mitochondrial import of crRNA-45 and its spacer part and found that the spacer part of crRNA can be targeted into human mitochondria *per se* (Fig. S4B). This is in line with the reports on the import of small non-coding RNAs, miRNAs and siRNAs [70]. We are fully aware that the experimental estimation of RNA mitochondrial import can be biased and can give overestimated data [44]. For this reason, to remove possible RNA contaminants from the cytosol, we treated isolated mitochondria and mitoplasts with nucleases. To ensure accurate crRNA detection and mitigate false-positive results, we performed control experiments by lysing a portion of mitochondria before nuclease treatment. Detection of crRNA in both intact mitochondria and mitoplasts but not in the lysates, confirmed their localization in the mitochondrial matrix (Fig. 5A and 6A). Nevertheless, the final proof of concept should be obtained by a direct demonstration of specific mtDNA cleavage *in vivo*. We believe that our data provided here will be useful for further *in vivo* mtDNA targeting experiments.

Development of mitochondrial CRISPR/Cas12a system is challenging but very promising since it can be used as a therapeutic approach for specific cleavage of mutant mtDNA molecules, as well as a research tool to introduce InDel modifications in different parts of mtDNA for a better understanding of the molecular mechanisms of its replication, processing of the primary transcripts and the role of non-coding regulatory regions.

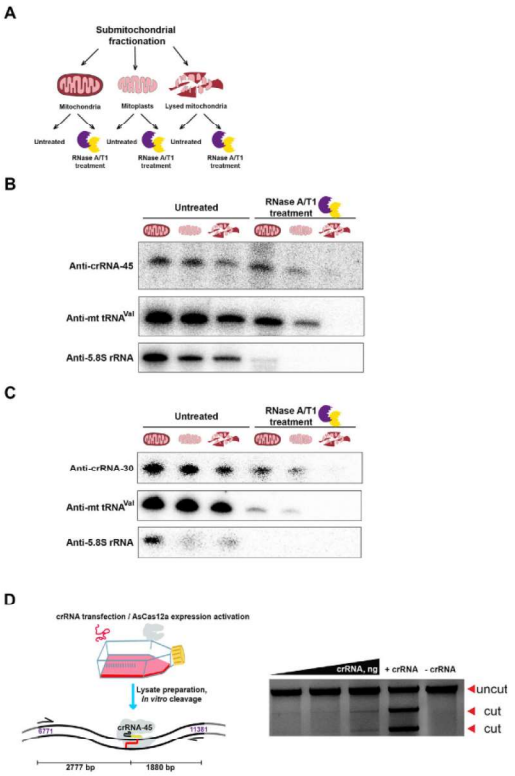


Fig. 6. Submitochondrial localization of AsCas12a crRNAs.
(A) Schematic representation of submitochondrial fractionation. (**B, C**) Intact mitochondria, mitoplasts and lysed mitochondria from the hAsCas12a HEK 293 T-REx stable cell line transfected with crRNA-45 (B) and from 143B cells transfected with crRNA-30 (C) were treated or not with the mix of RNase A/T_1, and the residual RNA molecules are analyzed by Northern blot hybridization. The hybridization probes are shown on the left: crRNA-45/30 (top panel), mitochondrial *tRNAVal* (middle panel) and cytoplasmic 5.8S rRNA (lower panel). Mitochondria, mitoplasts and lysed mitochondria are schematically indicated above the panels, as in **(A)**. **(D)** On the right, schematic representation of the *in vitro* cleavage of target DNA (PCR fragment of human mtDNA with corresponding numbers of nucleotides) in a cell lysate generated from the hAsCas12a HEK 293 T-REx stable cell line, transfected with crRNA-45 and induced with 100 ng/mL of tetracycline. The spacer moiety of crRNA-45 is shown in yellow, the scaffold part is shown in black, and the cleavage site is marked with a red arrow. The size of the fragments corresponding to cleaved DNA template are given below the scheme. On the left, *in vitro* cleavage of target DNA template induced by the increasing amounts of crRNA-45 used for the cells transfection (175–375 ng/cm^2). "-crRNA" corresponds to a control reaction that does not contain any crRNAs. "+crRNA" represents a positive control reaction for which 40 ng of chemically synthesized crRNA were added. *In vitro* cleaved products were resolved by 1% (w/v) agarose gel electrophoresis and revealed with ethidium bromide staining.

Data availability

All data presented in the manuscript is available upon request.

Funding

N.N., A.M., I.T. and N.E. were supported by IdEx Unistra [ANR-10-IDEX-0002], SFRI-STRAT'US project [ANR 20-SFRI-0012], EUR IMCBio [ANR17-EURE-0023] and the Région Grand Est (France). E.U. and V.S. were supported by grant from Belarusian Republican Foundation for Fundamental Research (BRFFR) X23RNF-041. I.M. was supported by grant from Russian Science Foundation No. 23-45-10010.

Declaration of competing interest

None declared.

Acknowledgments

The authors would like to express their gratitude to Pr. Joseph Schacherer (GMGM, Strasbourg) and Pr. Anne-Marie Duchêne (IBMP, Strasbourg) for insightful discussion. The authors also thank Dr. Alexandre Smirnov for providing an optimized protocol of RNA import test and all the members of the MITO team, UMR7156 GMGM for their help and support.

Appendix A. Supplementary data

Supplementary data to this article can be found online at https://doi.org/10.1016/j.biochi.2023.09.006.

References

[1] E.A. Schon, S. DiMauro, M. Hirano, Human mitochondrial DNA: roles of inherited and somatic mutations, Nat. Rev. Genet. 13 (2012) 878–890.
[2] S. Anderson, A.T. Bankier, B.G. Barrell, M.H. de Bruijn, A.R. Coulson, J. Drouin, I.C. Eperon, D.P. Nierlich, B.A. Roe, F. Sanger, P.H. Schreier, A.J. Smith, R. Staden, I.G. Young, Sequence and organization of the human mitochondrial genome, Nature 290 (1981) 457–465.
[3] R.M. Andrews, I. Kubacka, P.F. Chinnery, R.N. Lightowlers, D.M. Turnbull, N. Howell, Reanalysis and revision of the Cambridge reference sequence for human mitochondrial DNA, Nat. Genet. 23 (1999) 147.
[4] N. Pfanner, B. Warscheid, N. Wiedemann, Mitochondrial proteins: from biogenesis to functional networks, Nat. Rev. Mol. Cell Biol. 20 (2019) 267–284.
[5] S. DiMauro, E.A. Schon, Mitochondrial respiratory-chain diseases, N. Engl. J. Med. 348 (2003) 2656–2668.
[6] L. Craven, C.L. Alston, R.W. Taylor, D.M. Turnbull, Recent advances in mitochondrial disease, Annu. Rev. Genom. Hum. Genet. 18 (2017) 257–275.
[7] N. Nissanka, C.T. Moraes, Mitochondrial DNA heteroplasmy in disease and targeted nuclease-based therapeutic approaches, EMBO Rep. 21 (2020) e49612.
[8] G.S. Gorman, A.M. Schaefer, Y. Ng, N. Gomez, E.L. Blakely, C.L. Alston, C. Feeney, R. Horvath, P. Yu-Wai-Man, P.F. Chinnery, R.W. Taylor, D.M. Turnbull, R. McFarland, Prevalence of nuclear and mitochondrial DNA mutations related to adult mitochondrial disease, Ann. Neurol. 77 (2015) 753–759.
[9] J. Rahman, S. Rahman, Mitochondrial medicine in the omics era, Lancet 391 (2018) 2560–2574.
[10] Mitochondrial gene editing, Nature Reviews Methods Primers 3 (2023) 20.
[11] V. Peeva, D. Blei, G. Trombly, S. Corsi, M.J. Szukszto, P. Rebelo-Guiomar, P.A. Gammage, A.P. Kudin, C. Becker, J. Altmüller, M. Minczuk, G. Zsurka, W.S. Kunz, Linear mitochondrial DNA is rapidly degraded by components of the replication machinery, Nat. Commun. 9 (2018) 1727.
[12] M. Tanaka, H.J. Borgeld, J. Zhang, S. Muramatsu, J.S. Gong, M. Yoneda, W. Maruyama, M. Naoi, T. Ibi, K. Sahashi, M. Shamoto, N. Fuku, M. Kurata, Y. Yamada, K. Nishizawa, Y. Akao, N. Ohishi, S. Miyabayashi, H. Umemoto, T. Muramatsu, K. Furukawa, A. Kikuchi, I. Nakano, K. Ozawa, K. Yagi, Gene therapy for mitochondrial disease by delivering restriction endonuclease SmaI into mitochondria, J. Biomed. Sci. 9 (2002) 534–541.
[13] S. Srivastava, C.T. Moraes, Double-strand breaks of mouse muscle mtDNA promote large deletions similar to multiple mtDNA deletions in humans, Hum. Mol. Genet. 14 (2005) 893–902.
[14] M.F. Alexeyev, N. Venediktova, V. Pastukh, I. Shokolenko, G. Bonilla, G.L. Wilson, Selective elimination of mutant mitochondrial genomes as therapeutic strategy for the treatment of NARP and MILS syndromes, Gene Ther. 15 (2008) 516–523.
[15] U. Zekonyte, S.R. Bacman, J. Smith, W. Shoop, C.V. Pereira, G. Tomberlin, J. Stewart, D. Jantz, C.T. Moraes, Mitochondrial targeted meganuclease as a platform to eliminate mutant mtDNA in vivo, Nat. Commun. 12 (2021) 3210.
[16] M. Minczuk, M.A. Papworth, J.C. Miller, M.P. Murphy, A. Klug, Development of a single-chain, quasi-dimeric zinc-finger nuclease for the selective degradation of mutated human mitochondrial DNA, Nucleic Acids Res. 36 (2008) 3926–3938.
[17] S.R. Bacman, S.L. Williams, M. Pinto, S. Peralta, C.T. Moraes, Specific elimination of mutant mitochondrial genomes in patient-derived cells by

mitoTALENs, Nat Med 19 (2013) 1111–1113.
[18] P.A. Gammage, J. Rorbach, A.I. Vincent, E.J. Rebar, M. Minczuk, Mitochondrially targeted ZFNs for selective degradation of pathogenic mitochondrial genomes bearing large-scale deletions or point mutations, EMBO Mol. Med. 6 (2014) 458–466.
[19] M. Hashimoto, S.R. Bacman, S. Peralta, M.J. Falk, A. Chomyn, D.C. Chan, S.L. Williams, C.T. Moraes, MitoTALEN: a general approach to reduce mutant mtDNA loads and restore oxidative phosphorylation function in mitochondrial diseases, Mol. Ther. 23 (2015) 1592–1599.
[20] P. Reddy, A. Ocampo, K. Suzuki, J. Luo, S.R. Bacman, S.L. Williams, A. Sugawara, D. Okamura, Y. Tsunekawa, J. Wu, D. Lam, X. Xiong, N. Montserrat, C.R. Esteban, G.H. Liu, I. Sancho-Martinez, D. Manau, S. Civico, F. Cardellach, M. Del Mar O'Callaghan, J. Campistol, H. Zhao, J.M. Campistol, C.T. Moraes, J.C. Izpisua Belmonte, Selective elimination of mitochondrial mutations in the germline by genome editing, Cell 161 (2015) 459–469.
[21] S.R. Bacman, J.H.K. Kauppila, C.V. Pereira, N. Nissanka, M. Miranda, M. Pinto, S.L. Williams, N.G. Larsson, J.B. Stewart, C.T. Moraes, MitoTALEN reduces mutant mtDNA load and restores tRNA(Ala) levels in a mouse model of heteroplasmic mtDNA mutation, Nat Med 24 (2018) 1696–1700.
[22] P.A. Gammage, C. Viscomi, M.L. Simard, A.S.H. Costa, E. Gaude, C.A. Powell, L. Van Haute, B.J. McCann, P. Rebelo-Guiomar, R. Cerutti, L. Zhang, E.J. Rebar, M. Zeviani, C. Frezza, J.B. Stewart, M. Minczuk, Genome editing in mitochondria corrects a pathogenic mtDNA mutation in vivo, Nat Med 24 (2018) 1691–1695.
[23] Y. Yang, H. Wu, X. Kang, Y. Liang, T. Lan, T. Li, T. Tan, J. Peng, Q. Zhang, G. An, Y. Liu, Q. Yu, Z. Ma, Y. Lian, B.S. Soh, Q. Chen, P. Liu, Y. Chen, X. Sun, R. Li, X. Zhen, P. Liu, Y. Yu, X. Li, Y. Fan, Targeted elimination of mutant mitochondrial DNA in MELAS-iPSCs by mitoTALENs, Protein Cell 9 (2018) 283–297.
[24] C.V. Pereira, S.R. Bacman, T. Arguello, U. Zekonyte, S.L. Williams, D.R. Edgell, C.T. Moraes, mitoTev-TALE: a monomeric DNA editing enzyme to reduce mutant mitochondrial DNA levels, EMBO Mol. Med. 10 (2018).
[25] B.Y. Mok, M.H. de Moraes, J. Zeng, D.E. Bosch, A.V. Kotrys, A. Raguram, F. Hsu, M.C. Radey, S.B. Peterson, V.K. Mootha, J.D. Mougous, D.R. Liu, A bacterial cytidine deaminase toxin enables CRISPR-free mitochondrial base editing, Nature 583 (2020) 631–637.
[26] H. Lee, S. Lee, G. Baek, A. Kim, B.C. Kang, H. Seo, J.S. Kim, Mitochondrial DNA editing in mice with DddA-TALE fusion deaminases, Nat. Commun. 12 (2021) 1190.
[27] P. Silva-Pinheiro, P.A. Nash, L. Van Haute, C.D. Mutti, K. Turner, M. Minczuk, In vivo mitochondrial base editing via adeno-associated viral delivery to mouse post-mitotic tissue, Nat. Commun. 13 (2022) 750.
[28] S.I. Cho, S. Lee, Y.G. Mok, K. Lim, J. Lee, J.M. Lee, E. Chung, J.S. Kim, Targeted A-to-G base editing in human mitochondrial DNA with programmable deaminases, Cell 185 (2022) 1764–1776.e1712.
[29] A library of base editors for the precise ablation of all protein-coding genes in the mouse mitochondrial genome, in: P. Silva-Pinheiro, C.D. Mutti, L. Van Haute, C.A. Powell, P.A. Nash, K. Turner, M. Minczuk (Eds.), Nat. Biomed. Eng. 7 (5) (2023) 692–703.
[30] F. Mingozzi, K.A. High, Therapeutic in vivo gene transfer for genetic disease using AAV: progress and challenges, Nat. Rev. Genet. 12 (2011) 341–355.
[31] C.T. Moraes, A magic bullet to specifically eliminate mutated mitochondrial genomes from patients' cells, EMBO Mol. Med. 6 (2014) 434–435.
[32] M. Jinek, K. Chylinski, I. Fonfara, M. Hauer, J.A. Doudna, E. Charpentier, A programmable dual-RNA-guided DNA endonuclease in adaptive bacterial immunity, Science 337 (2012) 816–821.
[33] R. Loutre, A.M. Heckel, A. Smirnova, N. Entelis, I. Tarassov, Can mitochondrial DNA be CRISPRized: pro and contra, IUBMB Life 70 (2018) 1233–1239.
[34] N.A. Verechshagina, Y.M. Konstantinov, P.A. Kamenski, I.O. Mazunin, Import of proteins and nucleic acids into mitochondria, Biochemistry (Mosc.) 83 (2018) 643–661.
[35] P.A. Gammage, C.T. Moraes, M. Minczuk, Mitochondrial genome engineering: the revolution may not Be CRISPR-ized, Trends Genet. 34 (2018) 101–110.
[36] J. Hamm, I.W. Mattaj, Monomethylated cap structures facilitate RNA export from the nucleus, Cell 63 (1990) 109–118.
[37] P.D. Good, A.J. Krikos, S.X. Li, E. Bertrand, N.S. Lee, L. Giver, A. Ellington, J.A. Zaia, J.J. Rossi, D.R. Engelke, Expression of small, therapeutic RNAs in human cell nuclei, Gene Ther. 4 (1997) 45–54.
[38] M. Stewart, Polyadenylation and nuclear export of mRNAs, J. Biol. Chem. 294 (2019) 2977–2987.
[39] H. Nishimasu, F.A. Ran, P.D. Hsu, S. Konermann, S.I. Shehata, N. Dohmae, R. Ishitani, F. Zhang, O. Nureki, Crystal structure of Cas9 in complex with guide RNA and target DNA, Cell 156 (2014) 935–949.
[40] D. Jeandard, A. Smirnova, I. Tarassov, E. Barrey, A. Smirnov, N. Entelis, Import of non-coding RNAs into human mitochondria: a critical review and emerging approaches, Cells (2019) 8.
[41] Y. Tonin, A.M. Heckel, I. Dovydenko, M. Meschaninova, C. Comte, A. Venyaminova, D. Pyshnyi, I. Tarassov, N. Entelis, Characterization of chemically modified oligonucleotides targeting a pathogenic mutation in human mitochondrial DNA, Biochimie 100 (2014) 192–199.
[42] I. Dovydenko, A.M. Heckel, Y. Tonin, A. Gowher, A. Venyaminova, I. Tarassov, N. Entelis, Mitochondrial targeting of recombinant RNA, Methods Mol. Biol. 1265 (2015) 209–225.
[43] T. Yamano, H. Nishimasu, B. Zetsche, H. Hirano, I.M. Slaymaker, Y. Li, I. Fedorova, T. Nakane, K.S. Makarova, E.V. Koonin, R. Ishitani, F. Zhang, O. Nureki, Crystal structure of Cpf1 in complex with guide RNA and target DNA, Cell 165 (2016) 949–962.
[44] D. Jeandard, A. Smirnova, A.M. Fasemore, L. Coudray, N. Entelis, K.U. Förstner, I. Tarassov, A. Smirnov, CoLoC-seq probes the global topology of organelle transcriptomes, Nucleic Acids Res. 51 (2023) e16.
[45] G. Wang, H.W. Chen, Y. Oktay, J. Zhang, E.L. Allen, G.M. Smith, K.C. Fan, J.S. Hong, S.W. French, J.M. McCaffery, R.N. Lightowlers, H.C. Morse 3rd, C.M. Koehler, M.A. Teitell, PNPASE regulates RNA import into mitochondria, Cell 142 (2010) 456–467.
[46] O. Kolesnikova, H. Kazakova, C. Comte, S. Steinberg, P. Kamenski, R.P. Martin, I. Tarassov, N. Entelis, Selection of RNA aptamers imported into yeast and human mitochondria, RNA 16 (2010) 926–941.
[47] W.P. Bian, Y.L. Chen, J.J. Luo, C. Wang, S.L. Xie, D.S. Pei, Knock-in strategy for editing human and zebrafish mitochondrial DNA using mito-CRISPR/cas9 system, ACS Synth. Biol. 8 (2019) 621–632.
[48] Z. Antón, G. Mullally, H.C. Ford, M.W. van der Kamp, M.D. Szczelkun, J.D. Lane, Mitochondrial import, health and mtDNA copy number variability seen when using type II and type V CRISPR effectors, J. Cell Sci. 133 (2020).
[49] S.A. Hussain, M.E. Yalvac, B. Khoo, S. Eckardt, K.J. McLaughlin, Adapting CRISPR/Cas9 system for targeting mitochondrial genome, Front. Genet. 12 (2021) 627050.
[50] B. Wang, X. Lv, Y. Wang, Z. Wang, Q. Liu, B. Lu, Y. Liu, F. Gu, CRISPR/Cas9-mediated mutagenesis at microhomologous regions of human mitochondrial genome, Sci. China Life Sci. 64 (2021) 1463–1472.
[51] L. Schmiderer, D. Yudovich, L. Oburoglu, M. Hjort, J. Larsson, Site-specific CRISPR-based mitochondrial DNA manipulation is limited by gRNA import, Sci. Rep. 12 (2022) 18687.
[52] R. Bi, Y. Li, M. Xu, Q. Zheng, D.F. Zhang, X. Li, G. Ma, B. Xiang, X. Zhu, H. Zhao, X. Huang, P. Zheng, Y.G. Yao, Direct evidence of CRISPR-Cas9-mediated mitochondrial genome editing, Innovation 3 (2022) 100329.
[53] R. Lorenz, S.H. Bernhart, C. Höner Zu Siederdissen, H. Tafer, C. Flamm, P.F. Stadler, I.L. Hofacker, ViennaRNA package 2.0, Algorithm Mol. Biol. 6 (2011) 26.
[54] M. Zuker, Mfold web server for nucleic acid folding and hybridization prediction, Nucleic Acids Res. 31 (2003) 3406–3415.
[55] S. Bae, J. Park, J.S. Kim, Cas-OFFinder: a fast and versatile algorithm that searches for potential off-target sites of Cas9 RNA-guided endonucleases, Bioinformatics 30 (2014) 1473–1475.
[56] L. Gao, D.B.T. Cox, W.X. Yan, J.C. Manteiga, M.W. Schneider, T. Yamano, H. Nishimasu, O. Nureki, N. Crosetto, F. Zhang, Engineered Cpf1 variants with altered PAM specificities, Nat. Biotechnol. 35 (2017) 789–792.
[57] R. Shebanova, N. Nikitchina, N. Shebanov, V. Mekler, K. Kuznedelov, E. Ulashchik, R. Vasilev, O. Sharko, V. Shmanai, I. Tarassov, K. Severinov, N. Entelis, I. Mazunin, Efficient target cleavage by Type V Cas12a effectors programmed with split CRISPR RNA, Nucleic Acids Res. 50 (2022) 1162–1173.
[58] M.A. McMahon, T.P. Prakash, D.W. Cleveland, C.F. Bennett, M. Rahdar, Chemically modified cpf1-CRISPR RNAs mediate efficient genome editing in mammalian cells, Mol. Ther. 26 (2018) 1228–1240.
[59] O. Dussurget, D. Roulland-Dussoix, Rapid, sensitive PCR-based detection of mycoplasmas in simulated samples of animal sera, Appl. Environ. Microbiol. 60 (1994) 953–959.
[60] S. Summer, A. Smirnova, A. Gabriele, U. Toth, A.M. Fasemore, K.U. Förstner, L. Kuhn, J. Chicher, P. Hammann, G. Mitulović, N. Entelis, I. Tarassov, W. Rossmanith, A. Smirnov, YBEV is an essential biogenesis factor for mitochondrial ribosomes, Nucleic Acids Res. 48 (2020) 9762–9786.
[61] B. Zetsche, J.S. Gootenberg, O.O. Abudayyeh, I.M. Slaymaker, K.S. Makarova, P. Essletzbichler, S.E. Volz, J. Joung, J. van der Oost, A. Regev, E.V. Koonin, F. Zhang, Cpf1 is a single RNA-guided endonuclease of a class 2 CRISPR-Cas system, Cell 163 (2015) 759–771.
[62] N. Gueguen, G. Lenaers, P. Reynier, V. Weissig, M. Edeas, Mitochondrial dysfunction in mitochondrial medicine: current limitations, pitfalls, and tomorrow, Methods Mol. Biol. 2276 (2021) 1–29.
[63] M. Gusic, H. Prokisch, ncRNAs: new players in mitochondrial health and disease? Front. Genet. 11 (2020) 95.
[64] L. Sang, H.Q. Ju, Z. Yang, Q. Ge, Z. Zhang, F. Liu, L. Yang, H. Gong, C. Shi, L. Qu, H. Chen, M. Wu, H. Chen, R. Li, Q. Zhuang, H. Piao, Q. Yan, W. Yu, L. Wang, J. Shao, J. Liu, W. Wang, T. Zhou, A. Lin, Mitochondrial long non coding RNA GAS5 tunes TCA metabolism in response to nutrient stress, Nat. Metab. 3 (2021) 90–106.
[65] J. Huang, S. Wu, P. Wang, G. Wang, Non-coding RNA regulated cross-talk between mitochondria and other cellular compartments, Front. Cell Dev. Biol. 9 (2021) 688523.
[66] C.R. Goding, Targeting the lncRNA SAMMSON reveals metabolic vulnerability in melanoma, Cancer Cell 29 (2016) 619–621.
[67] J.M. Warren, T. Salinas-Giegé, D.A. Triant, D.R. Taylor, L. Drouard, D.B. Sloan, Rapid shifts in mitochondrial tRNA import in a plant lineage with extensive mitochondrial tRNA gene loss, Mol. Biol. Evol. 38 (2021) 5735–5751.
[68] X. Zhang, X. Zuo, B. Yang, Z. Li, Y. Xue, Y. Zhou, J. Huang, X. Zhao, J. Zhou, Y. Yan, H. Zhang, P. Guo, H. Sun, L. Guo, Y. Zhang, X.D. Fu, MicroRNA directly enhances mitochondrial translation during muscle differentiation, Cell 158 (2014) 607–619.
[69] E. Barrey, G. Saint-Auret, B. Bonnamy, D. Damas, O. Boyer, X. Gidrol, Pre-microRNA and mature microRNA in human mitochondria, PLoS One 6 (2011) e20220.
[70] K. Gao, M. Cheng, X. Zuo, J. Lin, K. Hoogewijs, M.P. Murphy, X.D. Fu, X. Zhang,

Active RNA interference in mitochondria, Cell Res. 31 (2021) 219–228.
[71] M.L. Campo, P.M. Peixoto, S. Martínez-Caballero, Revisiting trends on mitochondrial mega-channels for the import of proteins and nucleic acids, J. Bioenerg. Biomembr. 49 (2017) 75–99.
[72] B. Golzarroshan, C.L. Lin, C.L. Li, W.Z. Yang, L.Y. Chu, S. Agrawal, H.S. Yuan, Crystal structure of dimeric human PNPase reveals why disease-linked mutants suffer from low RNA import and degradation activities, Nucleic Acids Res. 46 (2018) 8630–8640.
[73] V. Vedrenne, A. Gowher, P. De Lonlay, P. Nitschke, V. Serre, N. Boddaert, C. Altuzarra, A.M. Mager-Heckel, F. Chretien, N. Entelis, A. Munnich, I. Tarassov, A. Rötig, Mutation in PNPT1, which encodes a polyribonucleotide nucleotidyltransferase, impairs RNA import into mitochondria and causes respiratory-chain deficiency, Am. J. Hum. Genet. 91 (2012) 912–918.
[74] O.Z. Karicheva, O.A. Kolesnikova, T. Schirtz, M.Y. Vysokikh, A.M. Mager-Heckel, A. Lombès, A. Boucheham, I.A. Krasheninnikov, R.P. Martin, N. Entelis, I. Tarassov, Correction of the consequences of mitochondrial 3243A>G mutation in the MT-TL1 gene causing the MELAS syndrome by tRNA import into mitochondria, Nucleic Acids Res. 39 (2011) 8173–8186.
[75] C. Comte, Y. Tonin, A.M. Heckel-Mager, A. Boucheham, A. Smirnov, K. Auré, A. Lombès, R.P. Martin, N. Entelis, I. Tarassov, Mitochondrial targeting of recombinant RNAs modulates the level of a heteroplasmic mutation in human mitochondrial DNA associated with Kearns Sayre Syndrome, Nucleic Acids Res. 41 (2013) 418–433.
[76] G. Wang, E. Shimada, J. Zhang, J.S. Hong, G.M. Smith, M.A. Teitell, C.M. Koehler, Correcting human mitochondrial mutations with targeted RNA import, Proc. Natl. Acad. Sci. U. S. A. 109 (2012) 4840–4845.

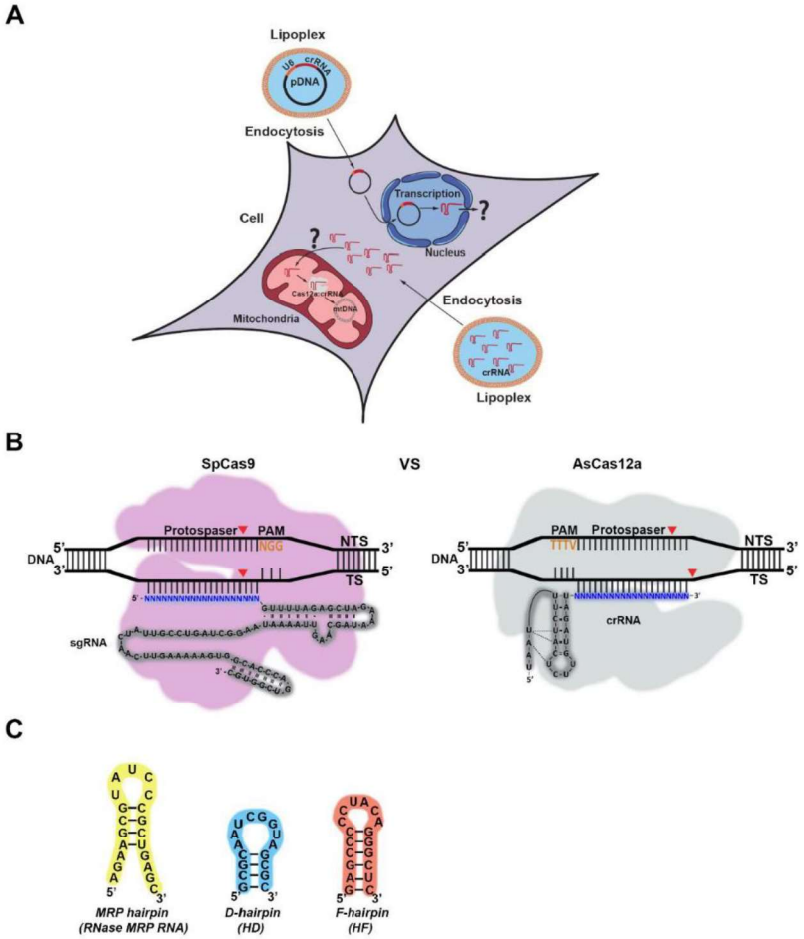


Fig. S1. Comparative analysis of delivery methods, CRISPR systems and RNA import motifs.

(A) Cell delivery of crRNA by direct transfection with RNA (lower part), or by expressed from plasmid DNA in the nucleus (upper part).

(B) A comparison of CRISPR-Cas9 system versus CRISPR-Cas12a. Protospacer adjacent motif (PAM) is shown in orange; generated double-stranded breaks are indicated by red triangles in both target (TS) and non-target DNA strands (NTS).

(C) RNA import motifs identified in human RNase MRP RNA (shown in yellow) and *S. cerevisiae* $tRNA^{Lys}_{CUU}$ (tRK1) D-hairpin (HD) (shown in blue) and F-hairpin (HF) (shown in coral).

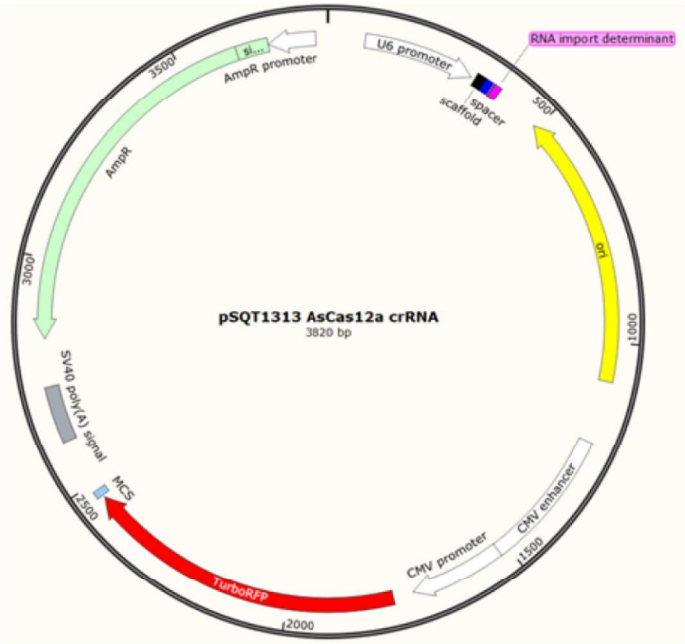
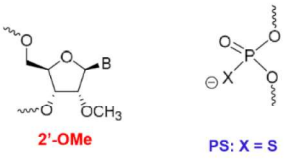


Fig. S2. Plasmid map of pSQT1313 AsCas12a crRNA encoding AsCas12a crRNA which bears RNA import determinants under the control of U6 promoter. This plasmid was used as a template for *in vitro* transcription (Generated using SnapGene software, GSL Biotech). The positions of the AsCas12a crRNA-34 scaffold and spacer coding parts on the plasmid map are shown in black and blue rectangles, respectively. Additional 3′-end RNA import motifs of tRK1 (HD and HF), RNase MRP RNA (MRP) are shown in crimson. Accordingly, the AsCas12a crRNA without an additional RNA import motif (crRNA-34-NM) does not possess this part.

A



B

5'-UA$_s$AUUUCUACUCUUGUAGAUCCCCUCUAUUGAUCCCCAC$_s$C-3'

Fig. S3. AsCas12a synthetic crRNAs protected with terminal modifications.

(A) Structures of chemically modified nucleotides substituted in AsCas12a crRNAs bearing 2'-O-Methyl (2'-O-Me) and phosphorothioate (PS) substitutions (adapted from McMahon, Moira A., et all., 2018 (DOI:10.1016/j.ymthe.2018.02.031).

(B) Representative full sequence of AsCas12a crRNA-45 with terminal 2'-O-Me and PS modifications. 2'-O-Me-substituted nucleotides are indicated in red, PS-substituted nucleotides are indicated in blue.

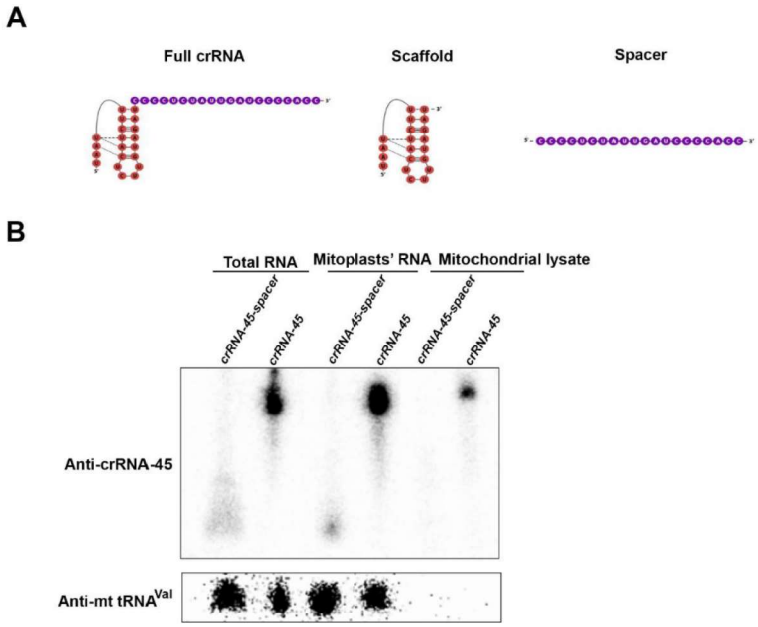


Fig. S4. Spacer part of split AsCas12a crRNA was found to be imported into human mitochondria.

(A) AsCas12a crRNA consists of two parts, namely the 5' scaffold or direct repeat (depicted in red circles) and the guide segment or spacer (depicted in purple circles). The direct repeat is responsible for forming a pseudoknot structure, which serves as a recognition region for Cas12a, while the spacer enables the nuclease to locate and perform cleavage activity on the intended target site. In the split crRNA version, the scaffold and spacer components are separated. The nucleotide sequence corresponds to crRNA-45.

(B) Northern blot hybridization of total RNA, mitoplast RNA, and mitochondrial lysate RNA isolated from the hAsCas12a HEK 293 T-REx stable cell line transfected with either the full crRNA-45 or the spacer part only. The hybridization probes used are displayed on the left: crRNA-45-spacer (top panel) and mitochondrial $tRNA^{Val}$ (lower panel).

Supplementary Table S1. Sequences of oligonucleotides used in the study

Name	Sequence: 5'- 3'
F_T7_AsCas12a	TAATACGACTCACTATAGGTAATTTCTACTCTTGTAGAT
R_T7_MRP	TCTTCGCATAGGGC
R_T7_HD	CGCGTTAGCCATC
R_T7_HF	CTCGGGGGATGTC
R_T7_NEG	AACTACCACCTACCTCC
RNA5	AGAGTTTGATCCTGGCTCAGGA
RNA3	ACGAGCTGACGACAACCATGCAC
UNI –	TAATCCTGTTTGCTCCCCAC
L8080	TCTTGCACTCATGAGCTGTC
H11381	AAGTGGAGTCCGTAAAGAGG
L3081	GTAATCCAGGTCGGTTTCT
H8361	CTGTAAAGAGGTGTTGGTTC
L7831	CATCCTTTACATAACAGACG
H13555	AGGCGTTTGTGTATGATATGTTTGC
F12981	CCTCCTCCTAGCAGCAGC
H1813	GGTTATAATTTTTCATCTTTCCC
L12640	TCGTTACATGGTCCATCATAG
H15912	TCTCCGGTTTACAAGACTGG

Supplementary Table S2. Sequences of hybridization probes used in the study

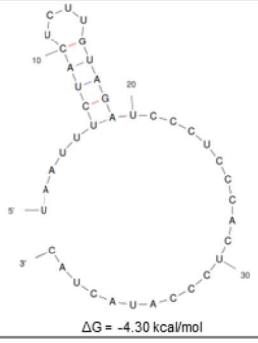
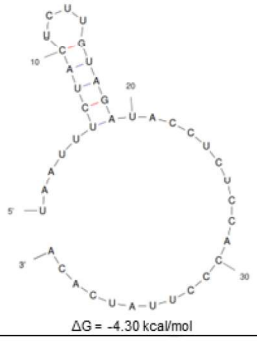
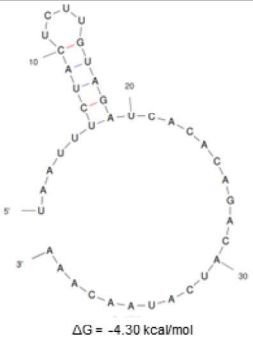
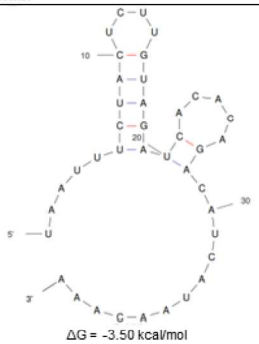
Name	Sequence: 5'- 3'
Anti-crRNA-1	GTAGTATGGGAGTGGGAGGG
Anti-crRNA-6	TGTGATAAGGGTGGAGAGGT
Anti-crRNA-10	TTTGTTATGATGTCTGTGTG
Anti-crRNA-14	TTGGGTGCTAATGGTGGAGT
Anti-crRNA-30	ACTCCAAAGACCACATCATC
Anti-crRNA-31	AGCCTAGGGTGTTGTGAGTG
Anti-crRNA-34	GGAAAAGGTTGGGGAACAGC
Anti-crRNA-45 (crRNA-45-spacer)	GGTGGGGATCAATAGAGGGG
Anti-crRNA-52	CCTTCTTATTATTTGATCTA
Probe against cytosolic 5.8S rRNA	GGCCGCAAGTGCGTTCGAAG
Probe against the mitochondrial tRNAVal	GGTCAGAGCGGTCAAG

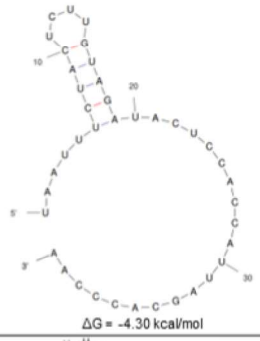
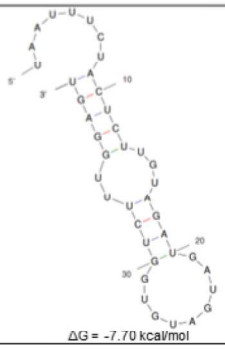
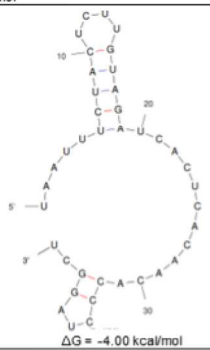
Supplementary Table S3. Resulting list of AsCas12a crRNAs

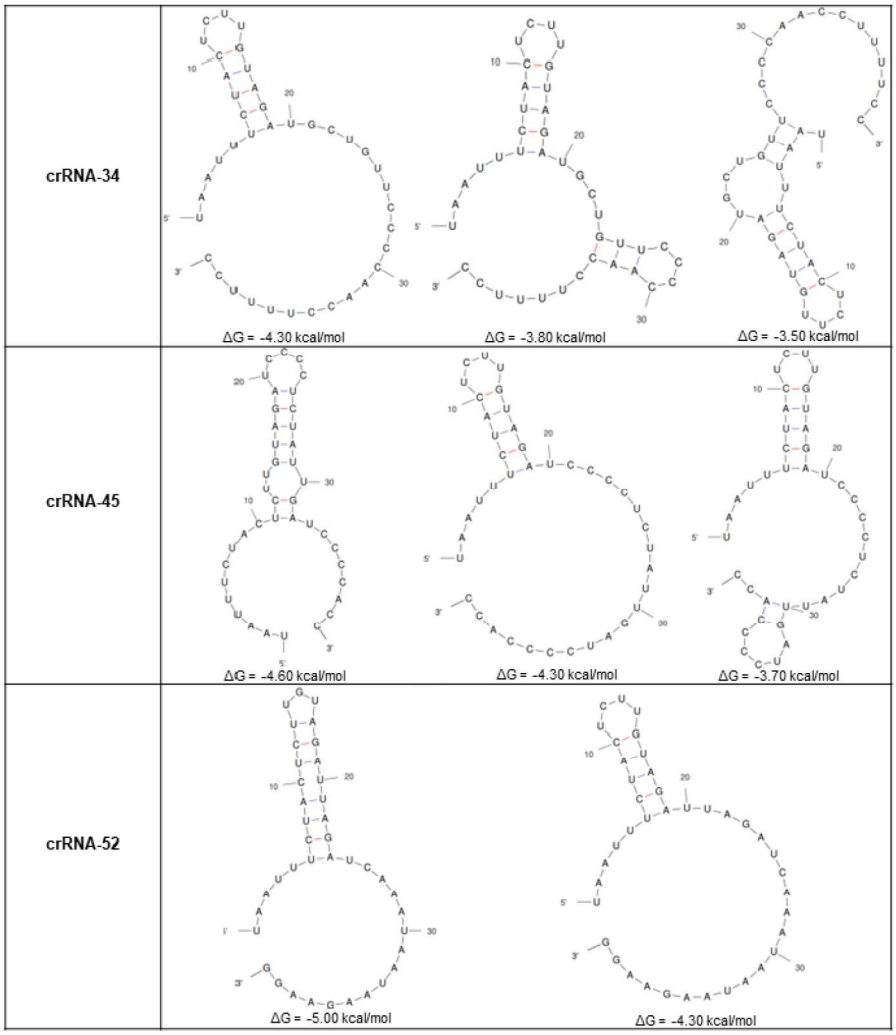
Name	Sequence: 5'- 3'
crRNA-1	UAAUUUCUACUCUUGUAGAUCCCUCCCACUCCCAUACUAC
crRNA-4	UAAUUUCUACUCUUGUAGAUCCCCGCAUCCCCCUUCCAAA
crRNA-6	UAAUUUCUACUCUUGUAGAUACCUCUCCACCCUUAUCACA
crRNA-8	UAAUUUCUACUCUUGUAGAUCUCCGACCCCCUAACAACCC
crRNA-9	UAAUUUCUACUCUUGUAGAUACAGCACCAAAUCUCCACCU

crRNA-10	UAAUUUCUACUCUUGUAGAUCACACAGACAUCAUAACAAA
crRNA-11	UAAUUUCUACUCUUGUAGAUACUUCCACUCCAUAACGCUC
crRNA-14	UAAUUUCUACUCUUGUAGAUACUCCACCAUUAGCACCCAA
crRNA-16	UAAUUUCUACUCUUGUAGAUACUUCAUCUUGCCCUUCAUU
crRNA-17	UAAUUUCUACUCUUGUAGAUUCCAUAAAAUUCUUCUUAGU
crRNA-19	UAAUUUCUACUCUUGUAGAUAACAUACAAAACCCACCCCA
crRNA-21	UAAUUUCUACUCUUGUAGAUACAGUCACCCCCCAACUAAC
crRNA -22	UAAUUUCUACUCUUGUAGAUACUUUACAUCCAAACAUCAC
crRNA-28	UAAUUUCUACUCUUGUAGAUCUAUUCGCCUACACAAUUCU
crRNA-31	UAAUUUCUACUCUUGUAGAUCACUCACAACACCCUAGGCU
crRNA-34	UAAUUUCUACUCUUGUAGAUGCUGUUCCCCAACCUUUUCC
crRNA-39	UAAUUUCUACUCUUGUAGAUUCAUUACUAACAACAUUUCC
crRNA-41	UAAUUUCUACUCUUGUAGAUGCCCACUAAGCCAAUCACUU
crRNA-46	UAAUUUCUACUCUUGUAGAUUAUGUUCAAACUGUCAUUUU
crRNA-49	UAAUUUCUACUCUUGUAGAUUCGCACCUACGUUCAAUAUU
crRNA-51	UAAUUUCUACUCUUGUAGAUCCGUACAUAGCACAUUACAG
crRNA-52	UAAUUUCUACUCUUGUAGAUUAGAUCAAAUAAUAAGAAGG
crRNA-53	UAAUUUCUACUCUUGUAGAUAUCAAUCGCCCACAUCACUC
crRNA-56	UAAUUUCUACUCUUGUAGAUAUCACAACAAUUAUCAAUAU
crRNA-57	UAAUUUCUACUCUUGUAGAUACUACCACAACUCAACGGCU
crRNA-45	UAAUUUCUACUCUUGUAGAUCCCCUCUAUUGAUCCCCACC
crRNA-30	UAAUUUCUACUCUUGUAGAUGAUGAUGUGGUCUUUGGAGU

Supplementary Table S4. Predicted secondary structures of crRNAs used in the study

Name	Predicted secondary structures
crRNA-1	 ΔG = -4.30 kcal/mol
crRNA-6	 ΔG = -4.30 kcal/mol
crRNA-10	 ΔG = -4.30 kcal/mol  ΔG = -3.50 kcal/mol

crRNA-14	 ΔG = -4.30 kcal/mol
crRNA-30	 ΔG = -7.70 kcal/mol
crRNA-31	 ΔG = -4.30 kcal/mol  ΔG = -4.00 kcal/mol



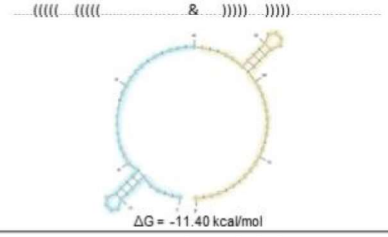
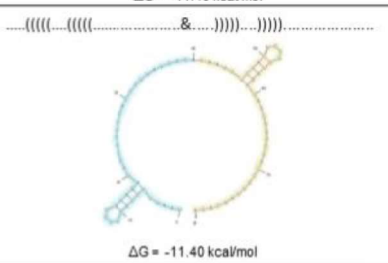
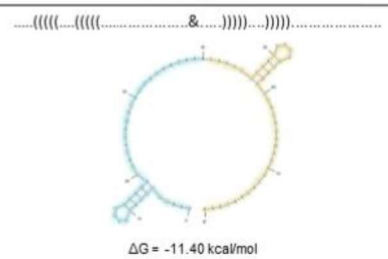
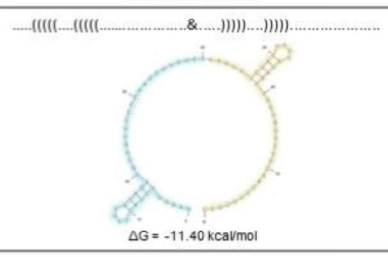
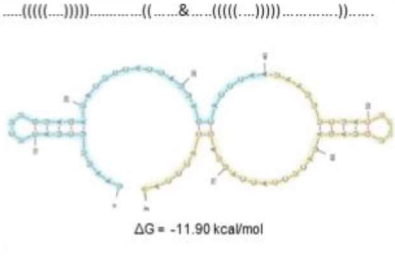
The most probable crRNAs secondary structures with the minimum free energy at 37° C were predicted using Mfold web server. If the number of predicted structures was more then 3 (the case for crRNA 34 and 45), only 3 first structures were taken for the demonstration.

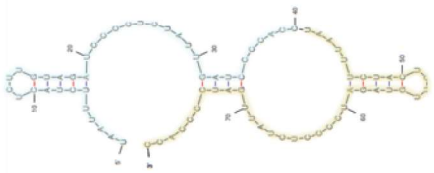
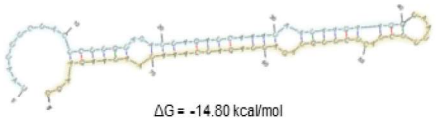
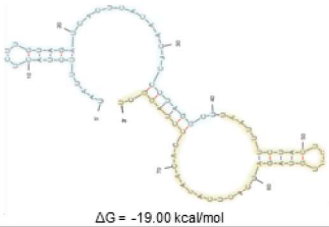
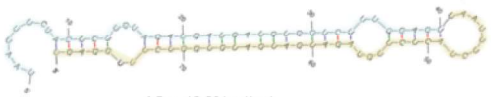
Supplementary Table S5. List of potential off-target sites of AsCas12a endonuclease guided with crRNAs used in the study

Name	Target	Chromosome	Position	Direction
crRNA-1	crRNA: TTTVCCCTCCCACTCCCATACTAC DNA: TTTCCCCTCCCACTCCCATACTAC	chrM	452	+
crRNA-6	crRNA: TTTVACCTCTCCACCCTTATCACA DNA: TTTAACCTCTCCACCCTTATCACA	chrM	3783	+
crRNA-10	crRNA: TTTVCACACAGACATCATAACAAA DNA: TTTCCACACAGACATCATAACAAA	chrM	264	+
crRNA-14	crRNA: TTTVACTCCACCATTAGCACCCAA DNA: TTTAACTCCACCATTAGCACCCAA	chrM	15969	+
crRNA-30	crRNA: TTTVGATGATGTGGTCTTTGGAGT DNA: TTTCGATGATGTGGTCTTTGGAGT	chrM	13504	-
	crRNA: TTTVGATGATGTGGTCTTTGGAGT DNA: TTTCGATGATGTGGTCTTTGGAGT	chr5	134925267	+
crRNA-31	crRNA: TTTVCACTCACAACACCCTAGGCT DNA: TTTACACTCACAACACCCTAGGCT	chrM	11252	+
crRNA-34	crRNA: TTTVGCTGTTCCCCAACCTTTTCC DNA: TTTAGCTGTTCCCCAACCTTTTCC	chrM	10906	+
crRNA-45	crRNA: TTTVCCCCTCTATTGATCCCCACC DNA: TTTCCCCCTCTATTGATCCCCACC	chrM	8601	+
	crRNA: TTTVCCCCTCTATTGATCCCCACC DNA: TTTCCCCCTCTATTGATCCCCACC	chr1	633770	+
	crRNA: TTTVCCCCTCTATTGATCCCCACC DNA: TTTCCCCCTCTATTGATCCCCACC	chr2	87825177	+
crRNA-52	crRNA: TTTVTAGATCAAATAATAAGAAGG DNA: TTTCTAGATCAAATAATAAGAAGG	chrM	10239	-

Potential target sites were searched for PAM type of AsCpf1 (AsCas12a) from *Acidaminococcus* sp.: 5'-TTTV-3' (V = G or C or A). Homo sapiens (GRCh38/hg38) genome was used as a target genome. No mismatches (MM) were allowed in DNA:crRNA complex (MM number = 0). The resulting table contains the following information: chromosome (chr) number (Chromosome), nucleotide position (Position), direction ("+" for 5'-3', "-" for 3'-5' DNA strand) (Direction) and potential off-target DNA sequences (Target). As can be seen in the table, crRNAs 30 and 45 have 1 and 2 off-target sites, respectively.

Supplementary Table S6. Predicted secondary structures of crRNAs upon dimer formation.

Name	Homodimer prediction
crRNA-1	
crRNA-6	
crRNA-10	
crRNA-34	
crRNA-14	

crRNA-45	.....(((((....))))).....((((.....&.....(((((....))))).....)))).....  ΔG = -13.00 kcal/mol
crRNA-52	.....(((((..(((.(((((.(((.((((((...&.....))))))..))).)))).)))).)))))...  ΔG = -14.80 kcal/mol
crRNA-31	.....(((((....))))).....((((((..&.....(((((....))))).....))))))..  ΔG = -19.00 kcal/mol
crRNA-30	.....(((((...((((.(((.((((..(((((&.....))))).)))).))).))).)))))..)))))  ΔG = -19.60 kcal/mol

The optimal secondary structures of the crRNAs' homodimers in dot-bracket notation with a minimum free energy were predicted using RNAcofold web server. The free energy value of -11.40 is derived from the energy of the bonds formed within the hairpin regions of each individual crRNA. "&" separates the two structures. The dot-bracket notations were visualsed using Mfold web server.

3.2.1. Fusion of AsCas12a crRNA with hairpin import determinants

We decided to check whether the fusion of AsCas12a crRNA with known RNA import determinants (MLS) (**Jeandard, D. *et al.*, 2019**) improve its mitochondrial targeting. For this, we modified one of the designed crRNAs (crRNA-34, targeting MT-ND4, section **2.1.6.**) by adding stem-loop motifs of human RNase MRP RNA (**Wang, G. *et al.*, 2010**) and *S. cerevisiae* $tRNA^{Lys}_{CUU}$ (tRK1) D-hairpin and F-hairpin (**Wang, G. *et al.*, 2010**; **Tonin, Y. *et al.*, 2014**). We added MLS hairpin structures at the 3'-end of crRNA and demonstrated that this did not impact crRNA ability to program specific cleavage of DNA in lysate of human cells expressing AsCas12a nuclease. Surprisingly, mitochondrial localization of the fused crRNA molecules in HEK293 cell line, analysed by Northern blot hybridization, was not improved compared to the non-modified version. The finding that crRNAs are imported without addition of MLS can be explained by the secondary structure of AsCas12a crRNA, which consists of two nearly equally sized moieties, a 5'-handle (scaffold) and a guide segment complementary to the target DNA sequences (spacer). Crystal structures of AsCas12a-crRNA complex revealed that crRNA scaffold adopts a pseudoknot structure (**Yamano, T. *et al.*, 2016**). One can hypothesize that this structure functions as MLS, assuring AsCas12a crRNA mitochondrial import by specific interaction with PNPase, while addition of supplementary MLS could make a longer RNA less efficient in mitochondrial translocation (**Publication 2**).

3.2.2. Possibility to shorten or split AsCas12a crRNA

AsCas12a crRNA consists of a 5'-handle (scaffold) part and a guide (spacer) segment complementary to the target DNA sequences. As mentioned in **Introduction section**, the import of small non-coding RNAs like miRNAs and siRNAs into mitochondria had been demonstrated (**Gao, K. *et al.*, 2021**), suggesting that short RNA molecules might possess a higher ability to be imported into human mitochondria.

We started by *in vitro* cleavage experiments using the recombinant AsCas12a nuclease (section **2.2.20.**, **Figure M4**) and it was shown that the removal of a significant portion of the hairpin scaffold had a negligible impact on the cleavage of target DNA by the AsCas12a nuclease. Subsequently, we proceeded to demonstrate that when AsCas12a crRNA was split into two separate moieties, scaffold and spacer, it exhibited the remarkable ability to catalyze highly specific and efficient cleavage of the target DNA. This new construct, which we termed "split" crRNA was chemically synthetized by our collaborators.

What surprised us was the discovery that when the AsCas12a was charged with a high dosage of the spacer crRNA segment only, it retained the capacity to specifically cleave DNA substrates. These intriguing observations were further confirmed in lysates derived from human cells that expressed AsCas12a.

As previously highlighted, Cas12a enzymes exhibit the ability to catalyze specific cleavage of double-stranded DNA (dsDNA) targets, as well as the specific cleavage of single-stranded DNA (ssDNA) targets. Additionally, these enzymes are known for their collateral degradation activity, which involves the nonspecific cleavage of ssDNA induced by the cleavage of the target. Given these characteristics, we conducted investigations to determine whether the collateral cleavage activity of AsCas12a could be promoted by split crRNA. The obtained results confirmed that AsCas12a in complex with split crRNA possessed all known DNA cleavage activities. In collaboration with the laboratory of Prof. Severinov, Rutgers University (USA), these findings were validated across various AsCas12a orthologs, namely FnCas12a and LbCas12a, in *in vitro* settings (**Publication 3**).

Moreover, this phenomenon was extended to the newly identified Type V CRISPR-RbCas12a system, which exhibited the same capabilities when employing split crRNA. It's worth noting that I was actively involved in the isolation of recombinant AsCas12a and conducting *in vitro* cleavage reactions, which contributed to the publication detailing the discovery of the RbCas12a nuclease (see **Publication 4** in **Annex section**).

Based on these findings, we recently compared the mitochondrial import of full and split versions of AsCas12a crRNA and found that its spacer part can be targeted into human mitochondria of the T-REx-Su9-AsCas12a stable cell line (**Publication 2**). However, it's important to note that our attempts to detect the scaffold part of the crRNA by northern hybridization proved challenging. This difficulty could potentially be linked to the secondary structure of the scaffold. Our efforts involving multiple hybridization probes and conditions aimed to prevent hairpin formation did not yield successful outcomes.

Overall, we demonstrated that crRNA for the AsCas12a system designed to target mitochondrial DNA, being introduced into human cells, can be imported into mitochondria and can induce specific DNA cleavage by AsCas12a nuclease. This finding opens the possibility to use CRISPR/Cas12 system for specific cleavage of mtDNA.

Publication 3

Nucleic acids research, 2022:

Efficient target cleavage by Type V Cas12a effectors programmed with split CRISPR RNA

Regina Shebanova[1,†], Natalia Nikitchina[1,2,†], Nikita Shebanov[1], Vladimir Mekler[3], Konstantin Kuznedelov[3], Egor Ulashchik[4], Ruslan Vasilev[5,6], Olga Sharko[4], Vadim Shmanai[4], Ivan Tarassov[2], Konstantin Severinov[1,3,7,*], Nina Entelis[2] and Ilya Mazunin[1,*]

[1] Center of Life Sciences, Skolkovo Institute of Science and Technology, Moscow, 143026, Russia
[2] UMR7156 – Molecular Genetics, Genomics, Microbiology, University of Strasbourg, Strasbourg, 67000, France
[3] Waksman Institute of Microbiology, Rutgers The State University of New Jersey, Piscataway, 08854, USA
[4] Institute of Physical Organic Chemistry, National Academy of Science of Belarus, Minsk, 220072, Belarus
[5] National Research Center "Kurchatov Institute", Moscow, 123098, Russia
[6] Lomonosov Moscow State University, Moscow, 119991, Russia
[7] Center for Precision Genome Editing and Genetic Technologies for Biomedicine, Institute of Gene Biology, Russian Academy of Sciences, Moscow, 119334, Russia

[†]The authors wish it to be known that, in their opinion, the first two authors should be regarded as joint First Authors.

1162–1173 *Nucleic Acids Research, 2022, Vol. 50, No. 2* *Published online 24 December 2021*
https://doi.org/10.1093/nar/gkab1227

Efficient target cleavage by Type V Cas12a effectors programmed with split CRISPR RNA

Regina Shebanova[1,†], Natalia Nikitchina[1,2,†], Nikita Shebanov[1], Vladimir Mekler[3], Konstantin Kuznedelov[3], Egor Ulashchik[4], Ruslan Vasilev[5,6], Olga Sharko[4], Vadim Shmanai[4], Ivan Tarassov[2], Konstantin Severinov[1,3,7,*], Nina Entelis[2] and Ilya Mazunin[1,*]

[1]Center of Life Sciences, Skolkovo Institute of Science and Technology, Moscow 143026, Russia, [2]UMR7156 – Molecular Genetics, Genomics, Microbiology, University of Strasbourg and Centre National de la Recherche Scientifique (C.N.R.S.), Strasbourg 67000, France, [3]Waksman Institute of Microbiology, Rutgers The State University of New Jersey, Piscataway 08854, USA, [4]Laboratory of Bioconjugate Chemistry, Institute of Physical Organic Chemistry, National Academy of Science of Belarus, Minsk 220072, Belarus, [5]Kurchatov Genomics Center, National Research Center "Kurchatov Institute", Moscow 123098, Russia, [6]Faculty of Biology, Lomonosov Moscow State University, Moscow 119991, Russia and [7]Center for Precision Genome Editing and Genetic Technologies for Biomedicine, Institute of Gene Biology, Russian Academy of Sciences, Moscow 119334, Russia

Received October 26, 2021; Revised November 24, 2021; Editorial Decision November 26, 2021; Accepted December 01, 2021

ABSTRACT

CRISPR RNAs (crRNAs) that direct target DNA cleavage by Type V Cas12a nucleases consist of constant repeat-derived 5′-scaffold moiety and variable 3′-spacer moieties. Here, we demonstrate that removal of most of the 20-nucleotide scaffold has only a slight effect on *in vitro* target DNA cleavage by a Cas12a ortholog from *Acidaminococcus* sp. (AsCas12a). In fact, residual cleavage was observed even in the presence of a 20-nucleotide crRNA spacer moiety only. crRNAs split into separate scaffold and spacer RNAs catalyzed highly specific and efficient cleavage of target DNA by AsCas12a *in vitro* and in lysates of human cells. In addition to dsDNA target cleavage, AsCas12a programmed with split crRNAs also catalyzed specific ssDNA target cleavage and non-specific ssDNA degradation (collateral activity). V-A effector nucleases from *Francisella novicida* (FnCas12a) and *Lachnospiraceae bacterium* (LbCas12a) were also functional with split crRNAs. Thus, the ability of V-A effectors to use split crRNAs appears to be a general property. Though higher concentrations of split crRNA components are needed to achieve efficient target cleavage, split crRNAs open new lines of inquiry into the mechanisms of target recognition and cleavage and may stimulate further development of single-tube multiplex and/or parallel diagnostic tests based on Cas12a nucleases.

INTRODUCTION

The CRISPR-Cas systems provide adaptive immunity to bacteria and archaea (1–3). They consist of CRISPR (clustered regularly interspaced short palindromic repeats) arrays and CRISPR-associated (Cas) proteins (Figure 1A). CRISPR arrays are composed of identical repeats separated by variable spacer sequences acquired from mobile genetic elements through the function of site-specific integrases composed of Cas1, Cas2, and, in some cases, Cas4 proteins. CRISPR arrays are transcribed into pre-CRISPR RNAs, which are processed at the repeat sequences generating short CRISPR RNAs (crRNAs). Individual crRNAs program Cas effector nucleases to recognize and cleave nucleic acids containing protospacers—sequences complementary to spacers. To prevent self immunity that could arise through recognition of CRISPR array spacers from which crRNAs are derived, many effectors require, in addition to crRNA spacer-target protospacer complementarity, the presence of a short Protospacer Adjacent Motif (PAM) that is specifically recognized by the effector protein. Since there is no PAM sequence in the repeat, targeting of the array is prevented.

At present, two classes, six types and numerous subtypes of CRISPR-Cas systems have been described and some have been harnessed for genomic editing (4–6). AsCas12a,

*To whom correspondence should be addressed. Tel: +7 952 799 92 79; Email: I.Mazunin@skoltech.ru
Correspondence may also be addressed to Konstantin Severinov. Email: severik@waksman.rutgers.edu
†The authors wish it to be known that, in their opinion, the first two authors should be regarded as joint First Authors.

© The Author(s) 2021. Published by Oxford University Press on behalf of Nucleic Acids Research.
This is an Open Access article distributed under the terms of the Creative Commons Attribution License (http://creativecommons.org/licenses/by/4.0/), which permits unrestricted reuse, distribution, and reproduction in any medium, provided the original work is properly cited.

Downloaded from https://academic.oup.com/nar/article/50/2/1162/6482588 by guest on 15 September 2023

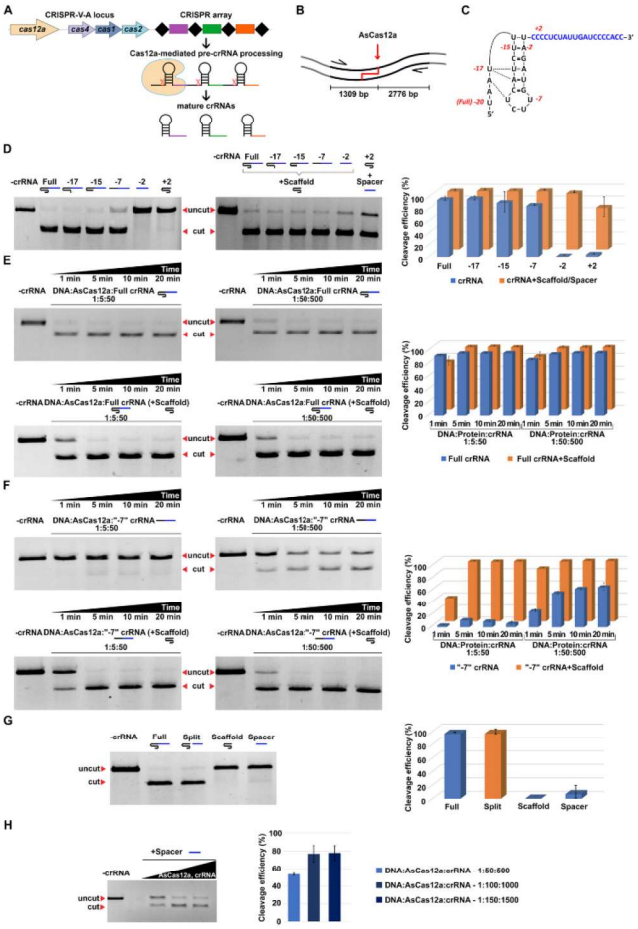


Figure 1. Addition of scaffold RNA stimulates target DNA cleavage by AsCas12a programmed with 5′ truncated crRNAs. (**A**) Schematic representation of Cas12a-mediated pre-crRNA processing. A subtype V-A CRISPR-Cas locus organization is shown (22). Genes coding for proteins responsible for interference (Cas12a) and adaptation (Cas4, Cas1, Cas2) are labeled and shown by colored arrows. The CRISPR array consists of spacers (colored rectangles) separated by repeats (black rhombi). Processing of the CRISPR array transcript (pre-crRNA) is carried out at the repeats by the Cas12a nuclease. (**B**) Schematics of the *in vitro* target DNA cleavage assay. A fragment of DNA containing the target site complementary to the crRNA spacer is amplified with PCR primers (indicated by arrows). Cleavage by AsCas12a programmed with crRNA recognizing the target is indicated by a red arrow and results in the appearance of cleavage products of indicated lengths. (**C**) The crRNA used for target recognition and cleavage. The scaffold moiety (black font) adopts a pseudoknot structure (12); the spacer sequence is highlighted in blue-coloured font. The numbers in red indicate the 5′-terminal nucleotides of truncated variants of crRNA tested. In the +2 variant, 18 nucleotides from the 3′-end of the spacer were eliminated. (**D**) Results of *in vitro* target cleavage assay with AsCas12a programmed with truncated crRNAs (indicated above the gel). The reactions contained 10 nM of the target, 500 nM of recombinant AsCas12a, and 5 μM of indicated crRNAs (a 1:50:500 ratio). Reactions were incubated 30 min at 37°C and products were resolved by agarose gel electrophoresis. Only the uncut target and one of the cleavage products (2776 bp) are shown. In the rightmost gel reactions were supplemented with 5 μM of scaffold or spacer RNA, as indicated. The results were quantified using ImageLab software. Mean cleavage efficiencies from four independent experiments and standard deviations are shown. (**E**, **F**) Kinetics and concentration dependence of target cleavage by AsCas12a programmed with full-sized (**E**) or –7 (**F**) crRNAs. Reactions proceeded for 1, 5, 10 and 20 minutes and were carried out at the indicated target:AsCas12a:crRNA ratios. Gels at the bottom of each panel show the results of cleavage assays conducted in the presence of equimolar amounts of scaffold crRNA moiety. Mean cleavage efficiencies and standard deviations from three independent experiments are shown on the right. (**G**) Target DNA cleavage by AsCas12a programmed with 3 μM full-sized, split, or separate scaffold and spacer crRNA moieties at a 1:30:300 target:AsCas12a:RNA ratio. 'Split' reactions contained both the scaffold and spacer RNAs. Mean cleavage efficiencies and standard deviations from three independent experiments are shown on the right. (**H**) Cleavage by AsCas12a programmed with increasing concentrations (5, 10 and 15 μM) of spacer RNA, corresponding to 1:50:500, 1:50:1000 and 1:50:1500 DNA:AsCas12a:crRNA ratios. Mean cleavage efficiencies and standard deviations calculated from three independent experiments are shown.

Downloaded from https://academic.oup.com/nar/article/50/2/1162/6482588 by guest on 15 September 2023

a class 2 Type V-A effector nuclease from *Acidaminococcus* sp., has been used to edit genomes in a number of organisms, including human cells (7–10). The crRNAs used by the AsCas12a effector consist of two nearly equally sized moieties, a repeat-derived scaffold (also referred to as the 5′-handle), which is identical for different crRNAs, and a variable spacer or guide segment complementary to target DNA sequences (Figure 1A). Like other V-A effectors, AsCas12a alone is able to process pre-crRNA transcripts into mature crRNAs (11).

To date, structures of three type V-A Cas effector proteins, AsCas12a (12), LbCas12a from a *Lachnospiraceae bacterium* (13), and FnCas12a from *Francisella novicida* (14) charged with cognate crRNAs and bound to target DNA have been determined. These structures revealed that the crRNA scaffold adopts a pseudoknot structure, rather than a simple stem–loop predicted from its nucleotide sequence (12). The Cas12a proteins interact with this pseudoknot (13). Cas12a/crRNA complexes recognize T-rich PAMs located at the 3′ ends of their targets and induce a staggered double-stranded break within the region complementary to crRNA spacer (12,15). Unlike other effectors, the Cas12a enzymes can also catalyse specific cleavage of single-stranded targets complementary to crRNA spacer (a single cut is introduced in this case) and nonspecific (collateral) ssDNA degradation stimulated by the recognition of either single- or double-stranded targets (16,17).

Previous studies analyzed crRNA structure requirements for DNA cleavage by Cas12a nucleases (13,14,18). It was demonstrated that extending the length of crRNA at the 5′ (i.e. scaffold) end enhances mammalian gene editing efficiency by AsCas12a (19). This approach was used to extend AsCas12a crRNAs with switchable domains activated by trigger RNAs via strand displacement, which can be adapted for transcriptional control of gene expression in *Escherichia coli* (20). On the other hand, shortening of the scaffold and/or spacer crRNA moiety decreased the FnCas12a and AsCas12a cleavage activities (15,18). It was also shown that the FnCas12a nuclease activity depends on the secondary structure of crRNA scaffold and is sensitive to nucleotide changes in this region (15). In this work, we studied the effect of truncation and splitting of crRNAs on *in vitro* target DNA cleavage by Cas12a nucleases. We demonstrate that the cleavage activity persists after substantial reduction of the crRNA scaffold length and can even be detected upon complete removal of the scaffold, i.e. in the presence of a 20-nucleotide RNA matching the spacer moiety only. Further, we show that the residual AsCas12a nuclease activity charged with spacer RNA can be brought to levels typical for effectors charged with full-sized crRNA by the *in trans* addition of a 20-base scaffold RNA. This is observed both in a pure *in vitro* system and in human cell lysates. When programmed with cognate split crRNAs AsCas12a, and two other V-A effectors tested—FnCas12a, and LbCas12a—demonstrated specific dsDNA target cleavage, specific ssDNA target cleavage, and non-specific collateral degradation of ssDNA stimulated by target recognition. We conclude that the ability to use split crRNAs is a general property of V-A effectors. Though split crRNAs are functional at higher concentrations than full-sized crRNAs, we propose that the use of split crRNAs for specific recognition and cleavage of DNA templates opens ways for future mechanistic research and practical applications of Cas12a effectors that require multiplexing and/or simultaneous interrogation of multiple targets.

MATERIALS AND METHODS

Cas nucleases

AsCas12a and SpCas9 nucleases were expressed from plasmid vectors (Addgene, Plasmids #90095, #62374) and purified from *E. coli* expression strain BL21-DE3 as described (8) with modifications. Briefly, the lysate of cells was loaded onto a HiTrap Chelating HP column (GE Healthcare) equilibrated with a buffer containing 20 mM imidazole. The recombinant protein was eluted with a buffer containing 500 mM imidazole, mixed with TEV protease (for AsCas12a), and dialyzed at 4°C for 12 h. Then the proteins were concentrated using Amicon Ultra 10K filter (Millipore) and applied to HiLoad Superdex 200 16/60 column (GE Healthcare). Fractions containing either AsCas12a or SpCas9 were collected, concentrated and then snap-frozen in liquid nitrogen in small aliquots that were stored at –80°C until use. The protein concentration was measured using Qubit Protein Assay Kit (Thermo Fisher) according to the manufacturer's instructions. The protein quality was tested by SDS-PAGE gel electrophoresis and visualized after Coomassie blue staining. LbCas12a and FnCas12a were purchased from OriGene Technologies and Biocat GmbH, respectively.

In vitro DNA cleavage assay

All RNAs and DNA oligonucleotides used in this study are listed in Supplementary Table S1 provided by PRIMETECH ALC and IDT. The chemical synthesis of modified crRNA molecules is described in Supplementary Data.

In vitro cleavage assays were carried out in 30 μl in 1× NEB2.1 buffer (NEB). DNA substrates for *in vitro* cleavage represent fragments of DNA amplified by PCR in Q5® High-Fidelity 2X Master Mix (M0492L, NEB). As a template, genomic DNA isolated from T-REx cell line (T-REx™-293 Cell Line, Invitrogen, kat. # R71007) by GeneJET Genomic DNA Purification Kit (K0722, Thermo Scientific™) was used. DNA concentration was measured by Qubit 3.0 fluorometer using Qubit DNA BR Assay Kit (Q32853, Thermo Scientific™). The standard reaction containing 10 nM of DNA template, 500 nM of the nuclease, and various amounts of crRNA. Reactions were incubated for 30 min at 37°C and stopped by the addition of 40 μg of Proteinase K (Promega) and additional incubation at 37°C for 15 min. Analysis of cleavage products was performed by electrophoresis in 1% agarose gel in 1× TBE buffer. EtBr staining gels were visualized by Gel Doc EZ Imager (Bio-Rad) and quantified with Image Lab™ Software 6.0.1 (Bio-Rad).

To assess specific and non-specific DNase activity of AsCas12a, LbCas12a and FnCas12a both ssDNA and dsDNA templates were used. Bacteriophage φX174 virion ssDNA and RF IdsDNA were purchased from NEB. DNA oligonucleotide duplexes were formed by mixing labelled strand and unlabeled complementary strand at a molar

Downloaded from https://academic.oup.com/nar/article/50/2/1162/6482588 by guest on 15 September 2023

ratio of 1:1.5 in Nuclease-Free Duplex Buffer (IDT), heating for 2 min at 95°C and slow cooling to 20°C. The complexes were reconstituted in reaction buffer by mixing one of the Cas12a nucleases and corresponding full-sized crRNA or split crRNA at a 1:2 molar ratio followed by 20-min incubation at RT. Complexes were kept on ice before use. All cleavage reactions were carried out in 10 μL buffer containing 40 mM Tris–HCl, pH 7.5, 50 mM NaCl, 5 mM $MgCl_2$, 0.5 mM TCEP, 0.1 mg/mL BSA, at 37°C for 30 min. Nonspecific digestion of 10 nM φX174 DNA was performed by 25 nM Cas12a–crRNA complex in the presence of 60 nM target ssDNA or dsDNA (activators). Reactions were quenched with Gel Loading Dye Purple (NEB) containing 0.4 mg/mL heparin and cleavage products were resolved by 1% agarose gel electrophoresis pre-stained with EtBr.

Fluorescein labelled ss/dsDNA substrates were used at 40 nM concentration to demonstrate specific cleavage activity of complexes at 150 nM concentration and nonspecific activity at 50 nM concentration. 60 nM ssDNA DNA was used as an activator. The reactions were terminated by the addition of formamide-containing loading buffer with 0.4 mg/ml heparin and heated in a boiling water bath for 1 min. Products were resolved by urea-denaturing 10% PAGE. Gels were imaged by Amersham Typhoon scanner.

Fluorescence assay of beacon DNA binding

Fluorescence measurements were performed using a QuantaMaster QM4 spectrofluorometer (PTI) in binding buffer (20 mM Tris–HCl (pH 7.5), 50 mM NaCl, 0.1 mM DTT and 5 mM $MgCl_2$) at 25ºC. Double-stranded beacon DNA was formed by mixing equimolar amounts of synthetic complementary strands (final concentrations were within low μM range) in a buffer containing 20 mM Tris, pH 7.5, 100 mM NaCl by heating for 2 min at 90ºC and slowly cooling the reactions down to 20ºC. The beacon DNA construct shown in Figure 3A was previously described in (21). The protospacer adjacent motif (PAM)-distal ends of the beacon target and non-target strands were labelled with fluorescein and Iowa BlackFQ, respectively. Final assay mixtures (800 μl) contained 40 nM of one of the Cas12a nucleases, 1 nM Cas12a beacon and 60 nM of corresponding full-sized crRNA or its fragments (scaffold and spacer). In control experiment, 100 nM spacer was added in the absence of AsCas12a. Time-dependent fluorescence changes were monitored after the addition of a negligible volume of Cas12a beacon to a cuvette followed by manual mixing; the mixing dead-time was 15 s.

DNA cleavage assay in hAsCas12a expressing cell lysate

The hAsCas12a gene was introduced into human HEK 293 T-REx cell line nuclear genome using the Flp-In™ System (Flp-In™ T-REx™-293 Cell Line, Invitrogen) allowing controlled expression by the tet-on system. Successful integration was monitored by antibiotic selection with hygromycin B (100 μg/mL, Invivogen) and blasticidin (5 μg/ml, Invivogen). Expression of AsCas12a nuclease in the stable HEK 293 T-REx cell line was induced by 100 ng/ml tetracycline for 24 h and assayed by Western blotting using FLAG-tag specific antibodies (Sigma-Aldrich, F1804).

Cells with inducible expression of the AsCas12a nuclease were cultured in 6-well plate at 37°C, 5% CO_2 in standard essential modified Eagle's medium (EMEM) containing 4.5 g/l D-glucose, and 5 mg/ml uridine supplemented with 10% fetal bovine serum. The expression of the nuclease was activated at 60–80% confluency by the addition of tetracycline to a final concentration 100 ng/ml. Twenty four hours post-induction, cells were washed with 1× PBS, resuspended in 500 μl lysis buffer (20 mM HEPES–KOH pH 7.5, 100 mM KCl, 5 mM $MgCl_2$, 1 mM DTT, 5% glycerol, 0.1% Triton X-100 and Protease Inhibitor cocktail) and rotated for 10 min at 4°C. To remove cell debris, lysates were centrifuged for 10 min at 10 000g, 4°C and the supernatant was snap-frozen in small aliquots and stored at –80°C until use.

The cleavage reactions were carried out in the cleavage buffer (20 mM HEPES–KOH pH 7.5, 100 mM KCl, 5 mM $MgCl_2$, 1 mM DTT, 5% glycerol) containing 4 nM of PCR-obtained DNA template (oligonucleotide primers are listed in Supplementary Table S1) and various amounts of crRNA 30 min at 37°C and stopped by the addition of 40 μg of Proteinase K (Promega). After 15-min incubation at 37°C products were purified with NucleoSpin PCR Clean-up kit (Macherey-Nagel). Analysis of cleavage products was performed by electrophoresis in 1% agarose gel in 1× TAE buffer. EtBr-stained gels were visualized by Hero Lab Transilluminator UVT-28M (Herolab GmbH) and quantified with Image Lab™ Software 6.0.1 (Bio-Rad).

T7E1 assays

HEK 293 T-REx hAsCas12a cells were cultured in 100 mm dishes and transfected with 4 μg of full-sized crRNA or 2 μg of each moiety of split RNA (scaffold and spacer) targeting *DNMT1* gene (RNAs sequences can be found in Supplementary Table S1). Expression of AsCas12a nuclease was induced by 100 ng/mL tetracycline. Cells were collected 24 h after transfection, and genomic DNA was isolated using GeneJET Genomic DNA Purification Kit (K0722, Thermo Scientific™) according to the manufacture's protocol. Genomic fragments were amplified with Phusion High Fidelity polymerase (New England Biolabs) (oligonucleotide primers are listed in Supplementary Table S1). PCR reactions were cleaned up with Qiagen Gel purification Kit (Qiagen). Hybridization of PCR products was carried out in 19 μl reaction mix containing 1000 ng DNA, 2 μl Nebuffer 2 (NEB) and 1 μl of T7 Endonuclease (NEB) with following conditions: denaturation at 95°C for 5 min, annealing at 95–85°C –2°C/s, at 85–25°C –0.1°C/s. Reactions were incubated for 1 h at 37°C. Products were seprated on a 2% agarose gel and visualised with Ethidium Bromide.

RESULTS

5′ truncated and split crRNAs, as well as spacer-only RNAs support specific target cleavage by AsCas12a *in vitro*

Recombinant AsCas12a was tested with a set of chemically synthesized crRNAs truncated from the 5′-end, i.e., harbouring a scaffold moiety of different lengths and a constant 20-nt spacer moiety (versions –17, –15, –7 and –2, Figure 1C) in an *in vitro* DNA cleavage assay. As a cleavage substrate, a PCR-amplified fragment containing an asymmet-

Downloaded from https://academic.oup.com/nar/article/50/2/1162/6482588 by guest on 15 September 2023

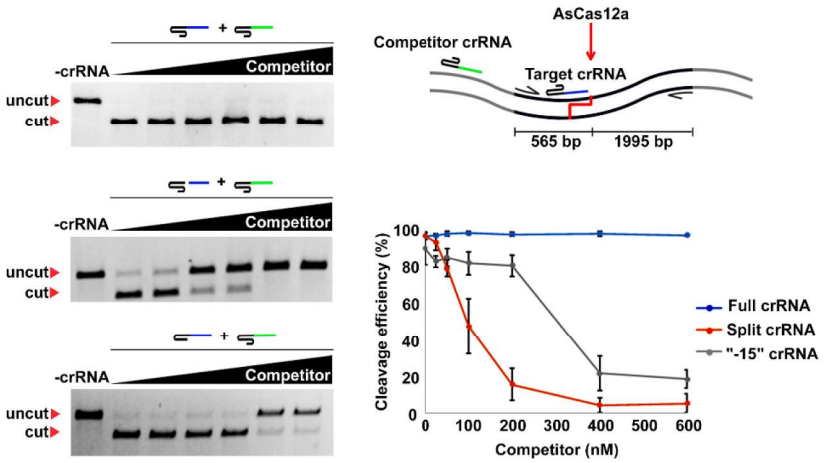


Figure 2. Effect of split crRNA on AsCas12a cleavage activity in presence of competitor crRNA. At top right, schematics of the target cleavage assay in the presence of competitor crRNA is shown. The assay is conducted as in Figure 1B but in the presence of a competitor crRNA that recognizes a target located outside of the amplified cleavage substrate. The spacer moieties of target and competitor crRNAs are shown in blue and green, correspondingly. Below, the results of cleavage assays with AsCas12a programmed with 500 nM of full-sized, split, or -15 crRNAs (a 1:5:50 target:AsCas12a:crRNA ratio) in the presence of increasing concentrations (0, 25, 50, 100, 200, 400, 600 nM) of competitor crRNA are presented; mean cleavage efficiencies and standard deviations calculated from three independent experiments are shown on the right.

rically located target sequence complementary to crRNA spacer with upstream consensus PAM was used (Figure 1B). The truncated crRNA versions used here match those studied by Zetsche *et al.* (15). Full-sized crRNA with a 20-nt scaffold was used as a positive control. An RNA that consisted of a full-sized scaffold extended by just two extra nucleotides of the spacer (version +2) was also tested. The reaction products were separated by gel electrophoresis, visualized by ethidium bromide staining and the extent of DNA substrate cleavage was quantified as described in the Materials and Methods. As can be seen from the leftmost gel in Figure 1D, the AsCas12a nuclease was surprisingly tolerant to 5′-truncations of the scaffold. At the conditions of the experiment, more than 80% target cleavage was observed in reactions containing full-sized, –17 and –15 crRNAs, and >60% of the DNA substrate was cleaved when the crRNA scaffold moiety was reduced to just seven nucleotides (version –7). Effectors charged with –2 and +2 crRNAs were inactive.

We were interested to determine whether the lack of activity of the –2 crRNA version could be complemented by the addition of scaffold RNA. Effectors charged with other crRNA versions were also tested in the presence of the scaffold. As can be seen from the rightmost gel in Figure 1D, the *in trans* addition of scaffold RNA stimulated target cleavage in the presence of –7 and –2 crRNA versions, which reached almost the same level as that seen with full-sized crRNA. Reciprocally, the addition of the 20-nt RNA spacer stimulated cleavage by the inactive effector charged with the +2 version (essentially, a scaffold RNA), which reached 80%.

We next investigated the kinetics and concentration dependence of target DNA cleavage by AsCas12a charged by either full-sized or truncated (version –7) crRNAs. As can be seen from Figure 1E, upper panels, in reactions containing full-sized crRNA, target DNA was cleaved ∼90% just after 1-min incubation at either 1:5:50 or 1:50:500 target DNA:AsCas12a:crRNA molar ratios and the addition of equimolar amounts of scaffold RNA did not affect target DNA cleavage in the presence of full-sized crRNA (Figure 1E, lower panels). In reactions containing the –7 crRNA in a 1:5:50 target DNA:AsCas12a:crRNA ratio target cleavage was undetectable. At a higher 1:50:500 ratio, partial target cleavage was observed (from 25 to 60% over the course of the reaction). Both the velocity and the extent of target cleavage were dramatically increased when reactions containing the –7 crRNA were supplemented with equimolar amounts of scaffold added *in trans*: the cleavage reaction was 40% complete after 1-minute incubation at low 1:5:50 target DNA:AsCas12a:crRNA ratio (98% after 5-min incubation) and 87% complete after 1-min incubation at the high 1:50:500 ratio (Figure 1F).

The results obtained with the +2 crRNA version supplemented with spacer RNA suggested that AsCas12a is able to locate and cleave its targets when supplemented with split crRNA containing separate scaffold and spacer moieties. Indeed, as can be seen from Figure 1G, the simultaneous addition of two crRNA moieties (a condition further referred to as 'split crRNA') induced specific cleavage of the target, which was as efficient as that induced by full-sized crRNA (∼95%) at the conditions of the experiment. Neither the spacer nor the scaffold RNAs taken separately caused

Downloaded from https://academic.oup.com/nar/article/50/2/1162/6482588 by guest on 15 September 2023

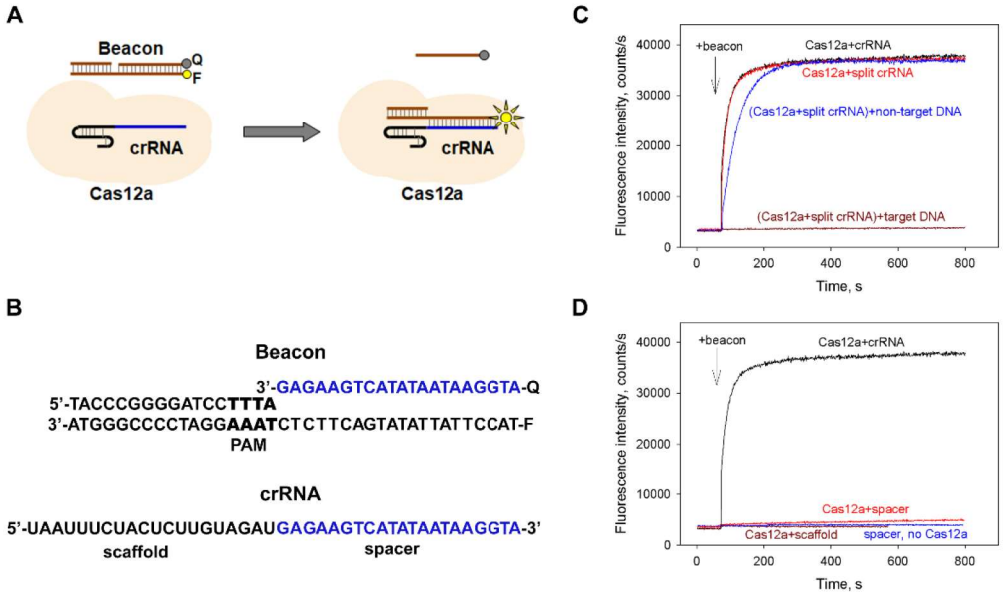


Figure 3. Analysis of the DNA target binding by the Cas12a loaded with split crRNA by the Cas beacon assay. (**A**) Principle of the Cas12a beacon assay. The circles labeled F and Q indicate the fluorophore and quencher. (**B**) Structures of the Cas12a beacon and of the crRNA used to program AsCas12a. The crRNA spacer and corresponding sequences of the beacon are highlighted in blue font, the PAM sequence is highlighted in bold font. (**C**) Time dependence of the increase in fluorescence upon the addition of 1 nM beacon to 40 nM AsCas12a loaded with 60 nM full-sized crRNA (black curve) or split crRNA (red curve) and effects of target (in brown) and non-target (in blue) DNA competitors on beacon binding to split crRNA-AsCas12a. (**D**) Time dependence of the increase in fluorescence upon the addition of 1 nM beacon to 40 nM AsCas12a loaded with 60 nM full-sized crRNA (in black), scaffold (in brown) or spacer (in red) crRNA fragments and to a control sample containing 100 nM spacer crRNA in the absence of AsCas12a (in blue).

substrate cleavage at these conditions. Efficient cleavage of cognate targets was also observed when split crRNAs with unrelated spacer sequences were tested (Supplementary Materials, Figure S1). Thus, split crRNA activity is not dependent on the sequence of the crRNA spacer moiety.

Because split crRNA/AsCas12a can cleave the DNA template quite efficiently, we wondered whether the spacer RNA moiety alone could also induce cleavage. We surmised that though no cleavage was obtained in the presence of spacer RNA in the experiment shown in Figure 1G, increasing the concentration of spacer RNA may allow the binding to the effector and target cleavage. An alternative scenario would be that the binding of the scaffold RNA is required for productive interaction with the spacer RNA by, for example, inducing a conformational change in the effector, and thus no target cleavage in the presence of spacer RNA shall be observed even at high concentrations. As can be seen from Figure 1H, increasing the concentration of spacer RNA from 5 to 15 μM led to dose-dependent DNA substrate cleavage by AsCas12a. These data demonstrate that AsCas12a charged with a 20-nt spacer RNA is capable of sequence-specific PAM-dependent cleavage of DNA substrates. This is possible only at high concentrations of RNA and a protein:RNA ratio of at least 1:20.

Functional biochemical and biophysical analyses of split crRNA and spacer RNA interaction with the AsCas12a effector

To compare the binding of full-sized and split crRNA to AsCas12a, we performed *in vitro* DNA cleavage assay in the presence of increasing amounts of another crRNA (hereafter referred to as 'crRNA competitor') that targeted a sequence that was absent from the DNA cleavage substrate (Figure 2). The competitor was added to 30 nM AsCas12a together with full-sized, truncated, or split crRNA, followed by the addition of the target. As can be seen from Figure 2, the addition of up to 600 nM competitor had no effect on the cleavage of 10 nM target DNA by the effector charged with full-sized cognate crRNA present at 500 nM concentration. In contrast, cleavage by the effector charged with the truncated -15 crRNA was inhibited 50% in the presence of ∼300 nM competitor RNA, suggesting ∼2-fold reduction of affinity for AsCas12a compared to full-sized crRNA. Target cleavage by the effector charged with split crRNA was inhibited 50% in the presence of 100 nM competitor, indicating that split RNA affinity for the effector is reduced ∼5-fold compared to full-sized crRNA.

To obtain further information on the split crRNA–AsCas12a complexes and their interactions with target DNA, a fluorescence Cas beacon method was implemented, following a strategy that was earlier used to monitor the in-

Downloaded from https://academic.oup.com/nar/article/50/2/1162/6482588 by guest on 15 September 2023

teractions of various effector complexes with crRNAs and target DNAs (21,23,24). A schematic representation of the Cas12a beacon assay is shown in Figure 3A. The beacon is a fluorescently labeled derivative of target DNA. It is prepared by annealing three oligonucleotides to generate a 38 bp fragment of DNA comprising a 13 bp DNA upstream of PAM, a consensus AsCas12a PAM TTTA, and a 21-bp downstream segment recognized by the crRNA spacer. The PAM-distal ends of the beacon target and non-target strands are labeled with a fluorophore and a quencher, respectively. The baseline fluorescence intensity of a beacon is low due to quenching of the fluorescence label by a nearby quencher via the FRET mechanism. Binding of Cas12a–crRNA complex to the beacon should separate DNA strands bearing the fluorophore and the quencher, leading to a readily detectable increase in fluorescence intensity (Figure 3A). Indeed, upon the addition of the beacon shown in Figure 3B to AsCas12a pre-incubated with full-sized crRNA, the fluorescence intensity rapidly increased, reaching peak intensity in about a minute (Figure 3C). The kinetics of beacon binding to AsCas12a preincubated with split crRNA was identical to that observed with full-sized crRNA (Figure 3C), implying that the AsCas12a complexes with full-sized and split crRNAs have comparable DNA binding activities.

We also performed competition assays in which beacon binding to split crRNA–AsCas12a was monitored in the presence of either target DNA or non-target DNA that bore no complementarity with the crRNA sequence. Preincubation of split crRNA–Cas12a complex with target DNA for 15 min led to severe inhibition of beacon binding, while non-target DNA exerted only a modest effect (Figure 3C). This result indicated that split crRNA–AsCas12a formed a stable and specific complex with target DNA, thus corroborating data obtained in the DNA cleavage assay (Figure 1G). The fluorescence signal increased very slowly upon the beacon addition to a sample containing 40 nM AsCas12a and 60 nM spacer RNA (Figure 3D). The rate of signal increase in this experiment was about 500-fold lower than that observed when AsCas12a was programmed with full-sized or split crRNAs. This observation suggests that spacer RNA alone endows AsCas12a with a low affinity for target DNA. This fully corresponds with our finding that a spacer moiety is able to induce cleavage of the DNA substrate only at high concentrations (Figure 1H) that can not be reached in the beacon assay. No increase in beacon fluorescence intensity was observed in the presence of AsCas12a preincubated with the scaffold RNA or in the presence of spacer RNA without AsCas12a (Figure 3D). The latter control experiment shows that spacer RNA alone cannot anneal to the beacon and induce an increase in fluorescence under the conditions used.

Data presented in Figure 1D shows that AsCas12a charged with spacer RNA and the +2 scaffold extended by two first nucleotides of the spacer moiety can recognize and cleave DNA targets. The result implies that split crRNA can accommodate extra nucleotides at the split site without compromising its function. To further investigate the importance of 5′- and 3′-extremities of the scaffold and spacer RNA moieties for split crRNA function we synthetized split versions bearing 5′- or 3′-terminal biotin modifications on the spacer and scaffold RNAs and tested them in the *in vitro* cleavage assay. Among all possible combinations tested, only the 3′-end biotin modification of the scaffold strongly decreased the DNA substrate cleavage efficiency (Figure 4A). This effect is surprising, given that the elongation of the scaffold 3′-end by two nucleotides had no strong effect (Figs. 1D and 4B), indicating that a non-nucleotide compound can disturb the scaffold-effector interaction. Biotin modification at the 5′-end of the spacer RNA did not influence the DNA substrate cleavage; however, a 2-nt extension of the spacer towards the junction site caused an additional decrease of cleavage in combination with the +2 version of the scaffold (Figure 4B).

Cas12a enzymes catalyze not only specific dsDNA target cleavage but also specific cleavage of ssDNA targets and nonspecific (collateral) degradation of single-stranded DNA (ssDNA) induced by target cleavage (16,17). To check whether collateral cleavage activity of AsCas12a can be promoted by split crRNA, we pre-assembled AsCas12a with split crRNA and incubated with ssDNA or dsDNA targets in the presence of φX174 ssDNA that had no sequences matching crRNA. As can be seen from Figure 5A, cleavage of φX174 ssDNA was induced by recognition of either double-stranded and single-stranded targets by AsCas12a charged with control full-sized crRNA (lanes 4 and 6, correspondingly) or with split crRNA (lanes 8 and 10). No φX174 cleavage was observed in reactions without target DNA (lanes 3 and 7), or in the presence of non-target DNA (lanes 5 and 9).

To check for specific ssDNA cleavage activity of AsCas12a charged with split crRNA, 3′ terminally fluorescein-labeled target DNA substrates (see Supplementary Table S1) were used (17). Corresponding dsDNA substrates were used as controls. As can be seen from Figure 5B, AsCas12a charged with either full-sized or split crRNA cleaved double-stranded and single-stranded targets at the same positions (compare lanes 2 and 4, and lanes 9 and 11, respectively). Besides bands resulting from site-specific ssDNA cleavage, fast-mobility degradation products resulting from non-specific ssDNA cleavage activity described before (17) were seen both with full-sized and split crRNA charged effectors. We also showed that upon activation by a non-labeled target-strand substrate (activator), AsCas12a charged with either full-sized or split crRNA completely degraded labeled ss DNA (lanes 8 and 15), while leaving dsDNA intact (lanes 7 and 14), as was first reported in (16).

Split crRNA is active in lysates of human cells expressing AsCas12a

We next tested whether split crRNA can promote specific target cleavage in eukaryotic cell lysates. For this, a human cell line expressing hAsCas12a in a Tet-inducible manner was constructed (Figure 6A). Cleavage of target DNA was assayed in the lysate of induced cells supplemented with increasing concentrations of full-sized, split, or spacer crRNAs. The results revealed that cleavage activities of the hAsCas12a programmed with full-sized and split crRNAs are comparable at crRNA concentrations >800 nM but at lower concentrations the AsCas12a nuclease programmed by full-sized crRNA outperformed the one charged with the

Downloaded from https://academic.oup.com/nar/article/50/2/1162/6482588 by guest on 15 September 2023

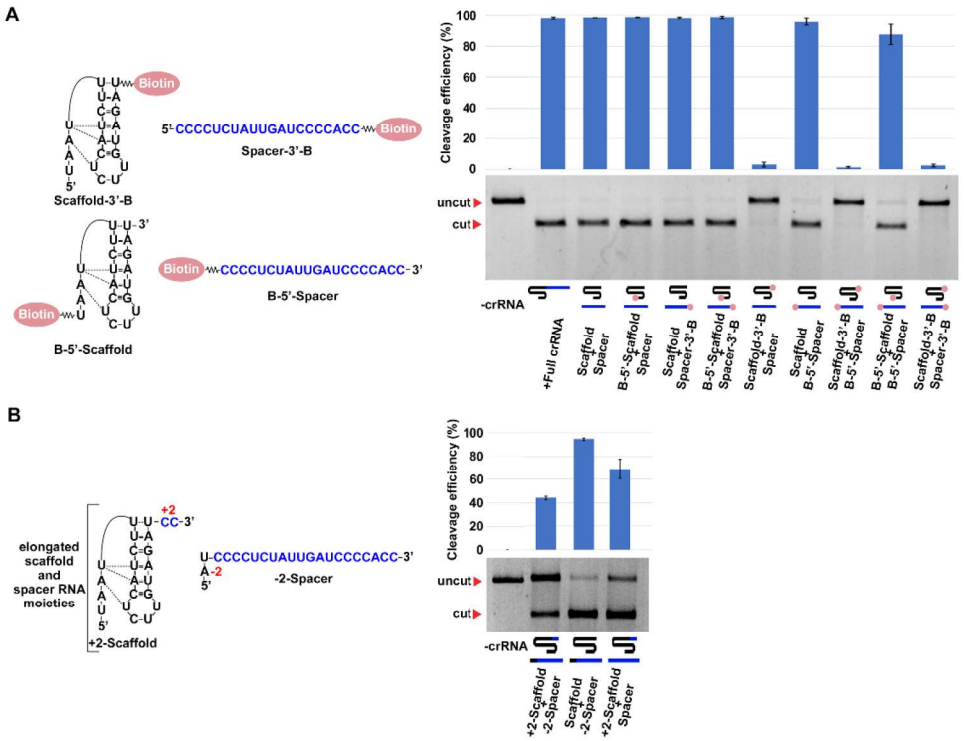


Figure 4. Effect of terminal modifications of spacer and scaffold RNAs on the activity of AsCs12a. (**A**) Scaffold and spacer crRNA moieties bearing either 5′- or 3′-terminal biotin modifications (shown as red ovals) were analyzed in the *in vitro* cleavage assay in all possible combinations. Mean cleavage efficiencies and standard deviations calculated from three independent experiments are shown. (**B**) As in (A), but using scaffold and spacer versions elongated by two non-complementary nucleotides ('+2-Scaffold' and ' 2-Spacer', correspondingly).

split version (Figure 6B). This corroborates data obtained with competitor crRNA (Figure 2) indicating lower affinity of split crRNA for AsCas12a. Nevertheless, the results demonstrate that split crRNA can induce specific cleavage of target DNA by AsCas12a nuclease expressed in human cells in the presence of all of the components of the cell lysate, most notably a large excess of cellular RNA. Target cleavage was only observed when >25 μM of spacer RNA was added to the lysate (Figure 6C), a concentration that is much higher than that needed for target cleavage in the pure system (Figure 1H). The result indicates that spacer RNA is poorly competing with cellular RNA present in the lysate. Scaffold RNA alone did not induce any DNA cleavage even at high concentrations, as expected.

We attempted to show specific cleavage induced by split RNA in human cells expressing hAsCas12a. However, at the conditions used, we did not detect target cleavage in cells transfected with split crRNA though ~13% target cleavage was detected in cells transfected with corresponding full-sized crRNA (Supplementary Figure S2).

Cas12a nucleases other than AsCas12a can use split crRNA

We next determined whether Cas12a enzymes from *Lachnospiraceae bacterium* (LbCas12a) and *Francisella novicida* (FnCas12a) can be programmed for target recognition and cleavage with cognate split crRNAs. The DNA binding properties of FnCas12a and LbCas12a complexed with intact and split crRNAs were followed by measuring the kinetics of beacon binding to FnCas12a and LbCas12a preincubated with corresponding crRNAs (Figure 7A, B). We found that kinetics of beacon binding to FnCas12a preincubated with split crRNA was almost identical to that obtained with full-sized crRNA (Figure 7B), similarly to what was observed with AsCas12a (Figure 3C). In contrast, LbCas12a preincubated with split crRNA bound beacon significantly slower than LbCas12a preincubated with intact crRNA (Figure 7B). These data imply that the LbCas12a complex with split crRNA binds its targets less efficiently than the complex with full-sized crRNA. No change in beacon fluorescence was observed in experiments with FnCas12a and LbCas12a preincubated with the spacer or scaf-

Downloaded from https://academic.oup.com/nar/article/50/2/1162/6482588 by guest on 15 September 2023

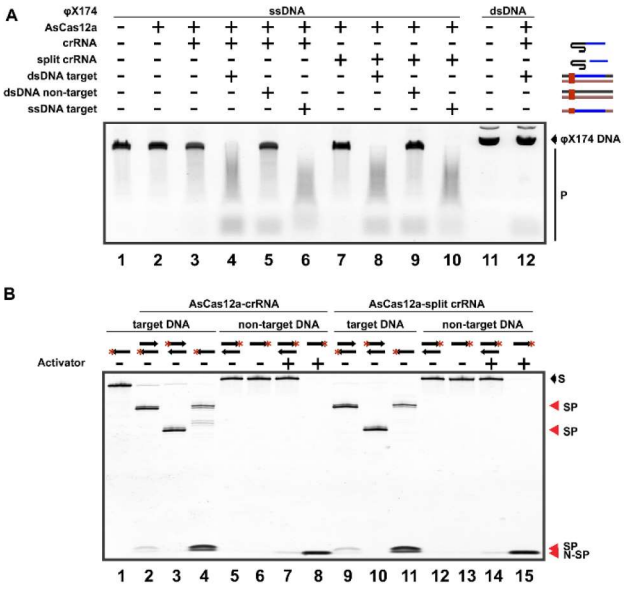


Figure 5. All known AsCas12a DNA cleavage activities are supported by split crRNA. (**A**) Non-specific ssDNA cleavage activity of AsCas12a against the φX174 ssDNA bearing no sequences matching crRNA was tested in the presence of full-sized and split crRNAs. Reactions were conducted in the presence of double-stranded DNA cleavage substrate matching the crRNA spacer, a single-stranded cleavage substrate with a sequence complementary to crRNA spacer and a functional PAM, or in the presence of double-stranded DNA bearing no sequences matching crRNA. Reaction products were resolved by agarose gel electrophoresis and revealed by ethidium bromide staining. Intact φX174 DNA and products of collateral cleavage activity are indicated. (**B**) Fluorescein-labeled (red asterisk) target and non-target DNA substrates, in the single-stranded or double-stranded form (shown schematically at the top of the gel and listed in Supplementary Table S1) were combined with AsCas12a programmed with the full-sized or split crRNA. 'Activator' is a non-labeled single-stranded oligonucleotide containing complementary to crRNA spacer and bearing a functional PAM. Reaction products were resolved by denaturing 10% PAGE. Substrate ('S') and specific ('SP') and non-specific ('N-SP') cleavage products are indicated on the right.

fold RNAs alone (Figure 7B), suggesting that spacer moieties interact with the effectors weakly or, alternatively, effectors complexes with spacer RNAs have low affinity for the targets.

The ability of split crRNAs to support target-activated nonspecific cleavage of ssDNA by LbCas12a and FnCas12a was also tested (Figure 7C and Supplementary Table S1). LbCas12a and FnCas12a in complex with split crRNA introduced site-specific cuts in dsDNA and ssDNA targets (Figure 7C). Both enzymes charged with split crRNAs were capable of target-activated degradation of non-specific ssDNA (Figure 7C) but not of dsDNA. We conclude that at least three distinct members of type V Cas12a nucleases, when programmed with split crRNA, can efficiently bind and cleave their targets and catalyze target-induced collateral degradation of ssDNA.

To determine whether the ability to use split RNAs might be a common property of Class 2 effectors, we performed *in vitro* target DNA cleavage assay using the most actively studied and widely used type II-A SpCas9 nuclease (1). The effector was charged with a single-guide RNA or its split version consisting of a 20-nt long spacer RNA complementary to the target and a longer RNA corresponding to the rest of sgRNA (referred to as 'scaffold' in Supplementary Figure S3). Only a very low level of DNA cleavage by SpCas9 was detected even at the highest concentrations of split RNA components (Supplementary Figure S3). It thus appears that, unlike Cas12a enzymes, SpCas9 and, by extension, other Cas9 nucleases, are unable to efficiently use split crRNA for target recognition and cleavage.

DISCUSSION

The principal finding of this paper is the demonstration that different Type V Cas12a effectors can recognize and cleave their targets and perform target-activated collateral damage degradation of single-stranded DNA when charged with two short RNAs—one consisting of repeat-derived scaffold moiety of full-sized crRNA and another consisting of a spacer recognizing the target through complementary interactions. Crystal structures of AsCas12a/crRNA complexes revealed that the crRNA scaffold adopts a pseudoknot structure and is tightly bound in a groove between two AsCas12a monomers in a sequence-specific manner (12). The AsCas12a crRNA scaffold nucleotides U-10 and A-18 form a reverse Hoogsteen A:U base pair and participate in pseudoknot formation, which is additionally stabilized by non-canonical hydrogen bonding between U-10

Downloaded from https://academic.oup.com/nar/article/50/2/1162/6482588 by guest on 15 September 2023

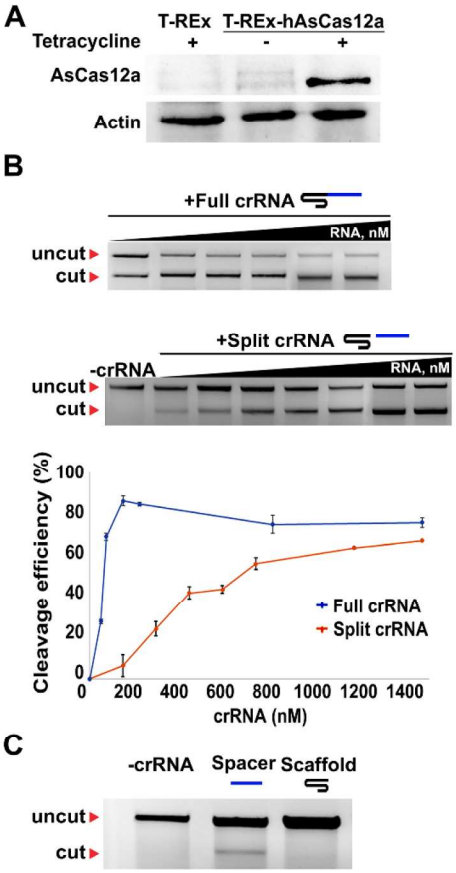


Figure 6. Split crRNA is active in lysates of human cells expressing AsCas12a. (**A**) Western blot analysis of hAsCas12a production in the stable HEK 293 T-REx-hAsCas12a cell line. FLAG-tag specific antibodies were used for hAsCas12a protein detection; actin specific antibodies were used for loading control. hAsCas12a gene transcription was induced by 100 ng/mL tetracycline. (**B**) Cleavage of the same DNA target is in Figure 1B was conducted in whole-cell lysates of induced cells in the presence of increasing concentrations of the full-sized or split crRNAs. Mean cleavage efficiencies and standard deviations calculated from three independent experiments are shown. (**C**) DNA template *in lysate* cleavage by spacer moiety of crRNA. DNA cleavage reaction in the presence of 27 μM spacer of scaffold crRNAs, incubated for 120 min at 37°C.

and A-19 and between A-12, U-13 and U-17 (Figure 1C). The scaffold pseudoknot structure is ordered in both binary (Cas12a/crRNA) and ternary (Cas12a/crRNA/dsDNA) complexes; in contrast, the entire spacer moiety is disordered in the binary complex (13). It has been suggested that the initial binding of Cas12a to a PAM sequence in template DNA can induce conformational changes resulting in preordering of the seed sequence comprising the first 8 scaffold-proximal nucleotides of the spacer (14). In the ternary complex, the heteroduplex between the target DNA strand and the spacer moiety of crRNA is accommodated in a positively charged central channel between the two lobes of the protein in a sequence-independent manner (9,14).

Previous studies analyzed the crRNA structure requirements for DNA cleavage by LbCas12a and FnCas12a nucleases (13,14). In the case of FnCas12a, deletion of 5′-terminal scaffold nucleotides A-19, A-18 and U-17 had little effect on DNA template cleavage efficiency (15). When a 5′-terminal deletion also removed U-16, the DNA cleavage was seriously affected, and further shortening of the scaffold completely abolished cleavage. Since A-19, A-18 and U-17 participate in the pseudoknot formation, deletion of these bases should turn the pseudoknot structure into a hairpin. Since in the hairpin U-16 forms a non-canonical pair with U-1, it appears that the hairpin structure rather than the pseudoknot is required for efficient target recognition and cleavage. Indeed, mutations that disrupt the helical part of the hairpin abolish target cleavage by FnCas12a. Our analysis shows that high concentrations of truncated –7 version of AsCas12a crRNA that is unable to form a hairpin are required for DNA cleavage. This is in agreement with previously published data on FnCas12a nuclease, where a similar truncation was tested (15). For crRNA version –15, which contains the hairpin forming part of the scaffold but cannot form the pseudo-knot structure, we detect efficient target DNA cleavage but the binding of this version to the effector is decreased compared to the full-sized crRNA.

Our data show that a 20-nt spacer RNA, when present at sufficiently high concentrations, induces target cleavage by AsCas12a. The result implies that the scaffold does not play an essential role during the target recognition/cleavage reactions. By strong binding to the effector, the scaffold moiety may either simply increase the affinity of the spacer part of crRNA to the effector or it may induce a conformational change that stabilises the interaction of the spacer part with the binary complex or of the RNA/DNA heteroduplex in the ternary complex. Strong binding of the scaffold to LbCas12a was previously demonstrated and excess of scaffold RNA inhibited DNA cleavage by LbCas12a effector charged with full-sized crRNA (13). Our data show that crRNA scaffold, when present separately, strongly increases the ability of spacer RNA to induce target cleavage by AsCas12a effector. Since in split crRNA the scaffold is physically separated from the spacer, it follows that the binding of the scaffold can not stimulate target recognition/cleavage by simple increase of the local concentration of the spacer. We, therefore, predict that crystallographic analysis of a Cas12a effector bound with a crRNA scaffold shall reveal conformational changes that affect the site that interacts with the spacer.

Despite substantial differences in their amino acid sequences, the Cas12a orthologs tested here have very similar structures of the crRNA scaffold which differ only in the loop region (nucleotides –8–9, Figure 7A) (25). While FnCas12a and AsCas12a scaffolds differ only by a single nucleotide in the –9 position, the LbCas12a scaffold has a distinct loop sequence UAAGU (UCUU and UGUU in AsCas12a and FnCas12a, correspondingly). This loop

Downloaded from https://academic.oup.com/nar/article/50/2/1162/6482588 by guest on 15 September 2023

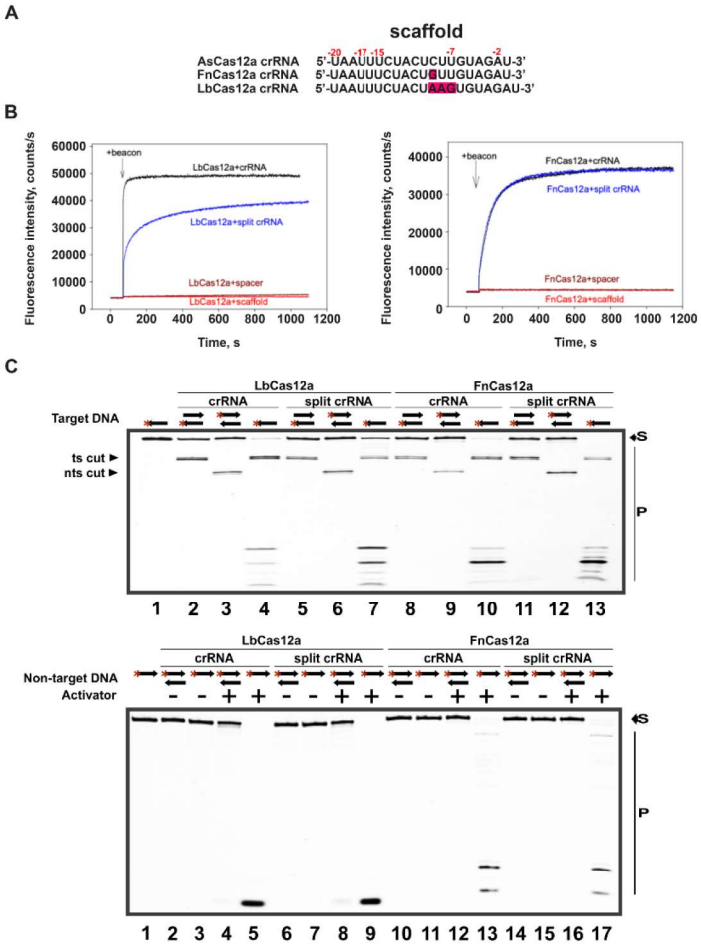


Figure 7. FnCas12a and LbCas12a effector nucleases programmed with cognate split crRNAs recognize and cleave their targets. (**A**) Sequences of the crRNA scaffold moiety for three V-A effector nucleases, As/Lb/FnCas12a (26). The nucleotide differences are highlighted in crimson. (**B**) Time dependence of beacon fluorescence increase upon the addition of the beacon to FnCas12a and LbCas12a loaded with full-sized crRNA (in black), split crRNA (in blue), scaffold (in red) or spacer (in brown) RNAs. The structures of the beacons and crRNAs are shown in Supplementary Table S1. (**C**) To demonstrate specific cleavage activity, fluorescein-labeled (red asterisk) target ssDNA (one arrow pictogram) and target dsDNA (two arrows pictogram) were digested by LbCas12a or FnCas12a in complex with full-sized (crRNA) or split crRNA. Activator-induced non-specific ssDNA cleavage activity was demonstrated using fluorescein-labeled non-specific ssDNA/dsDNA in the presence or absence of ssDNA activator. 'Ts cut' - target strand cut, and 'nts cut' - non-target strand cut, products of site-specific target DNA cleavage. Substrate ('S') and cleavage products ('P') were resolved by denaturing 10% PAGE.

may contribute to the less efficient binding of LbCas12a charged with split crRNA in the beacon experiments (Figure 7B).

Our data on the split crRNA/Cas12a system may not just help to understand the molecular mechanism of Cas12a better but can be useful for *in vitro* applications of Cas12a in DETECTR-based diagnostics (16). By combining short, 20-nt RNA mixes containing a single scaffold and multiple spacer parts, multiplex recognition of different targets can be achieved at significant cost saving compared to a situation when the same targets have to be probed with individual 40-nt full-sized crRNAs. Further down the road, split crRNAs may be useful in genome editing, however, the problem of delivery and/or stability of very short RNAs would have to be addressed first. The *in vitro* work presented here shows that both sides of the split site in crRNA can be

Downloaded from https://academic.oup.com/nar/article/50/2/1162/6482588 by guest on 15 September 2023

modified without compromising activity, which may be a promising opening to address the stability issue.

DATA AVAILABILITY

All data presented in the manuscript is available upon request.

SUPPLEMENTARY DATA

Supplementary Data are available at NAR Online.

FUNDING

Russian Foundation of Basic Research [19-29-04101 to R.S., N.S., N.N., E.U., I.M.]; IdEx Unistra [ANR-10-IDEX-0002]; SFRI-STRATUS project [ANR 20-SFRI-0012]; EUR IMCBio [ANR17-EURE-0023] to I.T., N.E., N.N.; N.N. was awarded a Grand Est PhD fellowship (France) and Skoltech (Russia); R.V. was supported by a grant from Ministry of Science and Higher Education of the Russian Federation allocated to the Kurchatov Center for Genome Research [075-15-2019-1659]; work in K.S. labs was supported by grant NIH R01 [GM10407] and Ministry of Science and Higher Education of the Russian Federation contract [075-15-2019-1661]. Funding for open access charge: Skolkovo Institute of Science and Technology.

Conflict of interest statement. None declared.

REFERENCES

1. Barrangou,R., Fremaux,C., Deveau,H., Richards,M., Boyaval,P., Moineau,S., Romero,D.A. and Horvath,P. (2007) CRISPR provides acquired resistance against viruses in prokaryotes. *Science*, **315**, 1709–1712.
2. Brouns,S.J., Jore,M.M., Lundgren,M., Westra,E.R., Slijkhuis,R.J., Snijders,A.P., Dickman,M.J., Makarova,K.S., Koonin,E.V. and van der Oost,J. (2008) Small CRISPR RNAs guide antiviral defense in prokaryotes. *Science*, **321**, 960–964.
3. Jackson,S.A., McKenzie,R.E., Fagerlund,R.D., Kieper,S.N., Fineran,P.C. and Brouns,S.J. (2017) CRISPR-Cas: adapting to change. *Science*, **356**, eaal5056.
4. Jinek,M., Chylinski,K., Fonfara,I., Hauer,M., Doudna,J. and Charpentier,E. (2012) A programmable dual-RNA-guided DNA endonuclease in adaptive bacterial immunity. *Science*, **337**, 816–821.
5. Makarova,K.S., Wolf,Y.I., Iranzo,J., Shmakov,S.A., Alkhnbashi,O.S., Brouns,S.J.J., Charpentier,E., Cheng,D., Haft,D.H., Horvath,P. *et al.* (2020) Evolutionary classification of CRISPR-Cas systems: a burst of class 2 and derived variants. *Nat. Rev. Microbiol.*, **18**, 67–83.
6. Shivram,H., Cress,B.F., Knott,G.J. and Doudna,J.A. (2021) Controlling and enhancing CRISPR systems. *Nat. Chem. Biol.*, **17**, 10–19.
7. Kleinstiver,B., Tsai,S., Prew,M., Nguyen,N., Welch,M., Lopez,J., McCaw,Z., Aryee,M. and Joung,J. (2016) Genome-wide specificities of CRISPR-Cas Cpf1 nucleases in human cells. *Nat Biotechnol.*, **34**, 869–874.
8. Zetsche,B., Heidenreich,M., Mohanraju,P., Fedorova,I., Kneppers,J., DeGennaro,E., Winblad,N., Choudhury,S., Abudayyeh,O., Gootenberg,J. *et al.* (2017) Multiplex gene editing by CRISPR-Cpf1 using a single crRNA array. *Nat Biotechnol.*, **35**, 31–34.
9. Gao,L., Cox,D., Yan,W., Manteiga,J., Schneider,M., Yamano,T., Nishimasu,H., Nureki,O., Crosetto,N. and Zhang,F. (2017) Engineered Cpf1 variants with altered PAM specificities. *Nat Biotechnol.*, **35**, 789–792.
10. Zhang,L., Zuris,J.A., Viswanathan,R., Edelstein,J.N., Turk,R., Thommandru,B., Rube,H.T., Glenn,S.E., Collingwood,M.A., Bode,N.M. *et al.* (2021) AsCas12a ultra nuclease facilitates the rapid generation of therapeutic cell medicines. *Nat. Commun.*, **12**, 3908.
11. Fonfara,I., Richter,H., Bratovič,M., Le Rhun,A. and Charpentier,E. (2016) The CRISPR-associated DNA-cleaving enzyme Cpf1 also processes precursor CRISPR RNA. *Nature*, **532**, 517–521.
12. Yamano,T., Nishimasu,H., Zetsche,B., Hirano,H., Slaymaker,I., Li,Y., Fedorova,I., Nakane,T., Makarova,K., Koonin,E. *et al.* (2016) Crystal structure of Cpf1 in complex with guide RNA and target DNA. *Cell*, **165**, 949–962.
13. Dong,D., Ren,K., Qiu,X., Zheng,J., Guo,M., Guan,X., Liu,H., Li,N., Zhang,B., Yang,D. *et al.* (2016) The crystal structure of Cpf1 in complex with CRISPR RNA. *Nature*, **532**, 522–526.
14. Swarts,D., van der Oost,J. and Jinek,M. (2017) Structural basis for guide RNA processing and seed-dependent DNA targeting by CRISPR-Cas12a. *Mol. Cell*, **66**, 221–233.
15. Zetsche,B., Gootenberg,J., Abudayyeh,O., Slaymaker,I., Makarova,K., Essletzbichler,P., Volz,S., Joung,J., van der Oost,J., Regev,A. *et al.* (2015) Cpf1 is a single RNA-guided endonuclease of a class 2 CRISPR-Cas system. *Cell*, **163**, 759–771.
16. Chen,J.S., Ma,E., Harrington,L.B., Da Costa,M., Tian,X., Palefsky,J.M. and Doudna,J.A. (2018) CRISPR-Cas12a target binding unleashes indiscriminate single-stranded DNase activity. *Science*, **360**, 436–439.
17. Li,S.Y., Cheng,Q.X., Liu,J.K., Nie,X.Q., Zhao,G.P. and Wang,J. (2018) CRISPR-Cas12a has both cis- and trans-cleavage activities on single-stranded DNA. *Cell Res.*, **28**, 491–493.
18. McMahon,M., Prakash,T., Cleveland,D., Bennett,C. and Rahdar,M. (2018) Chemically modified Cpf1-CRISPR RNAs mediate efficient genome editing in mammalian cells. *Mol Ther.*, **26**, 1228–1240.
19. Park,H., Liu,H., Wu,J., Chong,A., Mackley,V., Fellmann,C., Rao,A., Jiang,F., Chu,H., Murthy,N. *et al.* (2018) Extension of the crRNA enhances Cpf1 gene editing in vitro and in vivo. *Nat Commun.*, **9**, 3313.
20. Oesinghaus,L. and Simmel,F. (2019) Switching the activity of Cas12a using guide RNA strand displacement circuits. *Nat Commun.*, **10**, 2092.
21. Mekler,V., Kuznedelov,K., Minakhin,L., Murugan,K., Sashital,D. and Severinov,K. (2019) CRISPR-Cas molecular beacons as tool for studies of assembly of CRISPR-Cas effector complexes and their interactions with DNA. *Methods Enzymol.*, **616**, 337–363.
22. Gao,P., Yang,H., Rajashankar,K.R., Huang,Z. and Patel,D.J. (2016) Type V CRISPR-Cas Cpf1 endonuclease employs a unique mechanism for crRNA-mediated target DNA recognition. *Cell Res.*, **26**, 901–913.
23. Swarts,D.C., Mosterd,C., van Passel,M.W. and Brouns,S.J. (2012) CRISPR interference directs strand specific spacer acquisition. *PLoS One*, **7**, e35888.
24. Mekler,V., Minakhin,L., Semenova,E., Kuznedelov,K. and Severinov,K. (2016) Kinetics of the CRISPR-Cas9 effector complex assembly and the role of 3′-terminal segment of guide RNA. *Nucleic. Acids. Res.*, **44**, 2837–2845.
25. Mekler,V., Minakhin,L. and Severinov,K. (2017) Mechanism of duplex DNA destabilization by RNA-guided Cas9 nuclease during target interrogation. *Proc. Natl. Acad. Sci. U.S.A.*, **114**, 5443–5448.
26. Tu,M., Lin,L., Cheng,Y., He,X., Sun,H., Xie,H., Fu,J., Liu,C., Li,J., Chen,D. *et al.* (2017) A 'new lease of life': FnCpf1 possesses DNA cleavage activity for genome editing in human cells. *Nucleic Acids Res.*, **45**, 11295–11304.

Downloaded from https://academic.oup.com/nar/article/50/2/1162/6482588 by guest on 15 September 2023

SUPPLEMENTARY MATERIALS

Chemical synthesis of RNA

The oligoribonucleotides were synthesized using an automatic DNA/RNA synthesizer ASM-2000 (Biosset Ltd.) at 0.5 μmol scale on 1000 Å Universal support CPG (Primetech ALC, 41 μmol/g). Dichloroacetic acid (3% (v/v) in dichloromethane) was used as the detritylation agent. Coupling step was performed with 5-benzylthio-1H-tetrazole (0.3 M in acetonitrile) and standard 2'-O-TBDMS protected phosphoramidites (0.1 M in acetonitrile) (ChemGenes Corp.). Biotin modification was introduced with commercially available phosphoramidite (Primetech ALC). On oxidation step 0.02 M iodine in a mixture of THF, water, and pyridine was used. Capping was done with CAP A (15 % (v/v) acetic anhydride in THF) and CAP B (16 % (v/v) N-methylimidazole in THF). Oligonucleotides were cleaved and deprotected with ammonium hydroxide/40% aqueous methylamine (1:1 v/v) at 65 °C for 1.5 h. The TBDMS groups were cleaved with NEt_3 3HF (55 % (v/v) in DMSO) solution at 65 °C for 2.5 h.

Oligonucleotides were purified by preparative ion-exchange HPLC or by PAGE. IE HPLC was done with a linear gradient from 10 to 60% buffer B for 40 min at a flow rate of 1 mL/min (Agilent 1260 infinity). Buffer A was 50 mM Tris–HCl pH 7.6 in sterile water/acetonitrile (9 : 1 v/v), buffer B - 600 mM $NaClO_4$ and 50 mM Tris–HCl pH 7.6 in sterile water/acetonitrile (9 : 1 v/v). The column was Tosoh Bioscience LLC TSKGEL SUPERQ-5PW 7.5X75 (thermostated at 55 °C). Fractions containing pure oligonucleotides were evaporated and desalted using acetone precipitation. Preparative PAGE was done in 17 % denaturing (6,5 M urea) gells (19:1 acrylamide to bisacrylamide ratio). Oligonucleotides were extracted from gel with 0.5 M NH_4OAc, 1 mM EDTA, pH 8.0, and precipitated with EtOH. Purified oligonucleotides were characterized by UV-photometry, analytical HPLC, and PAGE.

Supplementary Table 1. Sequences of oligonucleotides used in the study

name	sequence
RNA	
crRNA	UAAUUUCUACUCUUGUAGAUCCCCUCUAUUGAUCCCCACC
crRNA 2	UAAUUUCUACUCUUGUAGAUGAGAAGUCAUAUAAUAAGGUA
crRNA competitor / PAM2 crRNA	UAAUUUCUACUCUUGUAGAUGCUGUUCCCCAACCUUUUCC
crRNA-scaffold	UAAUUUCUACUCUUGUAGAU
crRNA-spacer	CCCCUCUAUUGAUCCCCACC
crRNA 2 spacer	GAGAAGUCAUAUAAUAAGGUA
crRNA-scaffold-5bio	biotin-UAAUUUCUACUCUUGUAGAU
crRNA-scaffold-3bio	UAAUUUCUACUCUUGUAGAU-biotin
crRNA-spacer-5bio	biotin-CCCCUCUAUUGAUCCCCACC
crRNA-spacer-3bio	CCCCUCUAUUGAUCCCCACC-biotin
"-15" crRNA	UCUACUCUUGUAGAUCCCCUCUAUUGAUCCCCACC
"-17" crRNA	UUUCUACUCUUGUAGAUCCCCUCUAUUGAUCCCCACC

"-7" crRNA	UGUAGAUCCCCUCUAUUGAUCCCCACC
"-2" crRNA / "-2-Spacer"	AUCCCCUCUAUUGAUCCCCACC
"+2" crRNA	UAAUUUCUACUCUUGUAGAUCC
PAM2 spacer	GCUGUUCCCCAACCUUUUCC
Lb crRNA	UAAUUUCUACUAAGUGUAGAUGAGAAGUCAUAUAAUAAGGUA
Lb crRNA scaffold	UAAUUUCUACUAAGUGUAGAU
Fn crRNA	UAAUUUCUACUGUUGUAGAUGAGAAGUCAUAUAAUAAGGUA
Fn crRNA scaffold	UAAUUUCUACUGUUGUAGAU
Fn crRNA spacer	GAGAAGUCAUAUAAUAAGGUA
sgRNA	GAGUUUUAUGGCGUCAGCGAGUUUUAGAGCUAGAAAUAGCAAG UUAAAAUAAGGCUAGUCCGUUAUCAACUUGAAAAAGUGGCACC GAGUCGGUGCU
sgRNA-spacer	GAGUUUUAUGGCGUCAGCGA
sgRNA-scaffold	GUUUUAGAGCUAGAAAUAGCAAGUUAAAAUAAGGCUAGUCCGU UAUCAACUUGAAAAAGUGGCACCGAGUCGGUGCU
DNMT1 crRNA	UAAUUUCUACUCUUGUAGAUCUGAUGGUCCAUGUCUGUUA

DNMT1 crRNA-spacer	CUGAUGGUCCAUGUCUGUUA
DNA primers	
L7336	GATTTGAGAAGCCTTCGCTTC
H11381	AAGTGGAGTCCGTAAAGAGG
L2797	GTCCTAAACTACCAAACCTGC
H4501	TGTGCCTGCAAAGATGGTAG
7831F	CATCCTTTACATAACAGACG
13555R	AGGCGTTTGTGTATGATATGTTTGC
F DNMT1	CCACACATGTGAACGGACAGATTGAC
R DNMT1	AGCCCGAGAGAGTGCCTCAGGT
DNA	
Target DNA	5'TACCCGGAGATCGTTTAGAGAAGTCATATAATAAGGTAACTGTT AGAAGCTTGG3' NTS 3'ATGGGCCTCTAGCAAATCTCTTCAGTATATTATTCCATTGACAAT CTTCGAACC5' TS
Non-target DNA	5'TACCCGGAGATCGTTTACTCTTCAGTATATTATTCCATACTGTTA GAAGCTTGG3' NTS 3'ATGGGCCTCTAGCAAATGAGAAGTCATATAATAAGGTATGACAA TCTTCGAACC5' TS

Target DNA labeled	5'TACCCGGAGATCGTTTAGAGAAGTCATATAATAAGGTAACTGTT AGAAGCTTGG3' NTS 3'/36FAM/ATGGGCCTCTAGCAAATCTCTTCAGTATATTATTCCATT GACAATCTTCGAACC-5' TS 5'/36FAM/TACCCGGAGATCGTTTAGAGAAGTCATATAATAAGGTA ACTGTTAGAAGCTTGG3' NTS 3'ATGGGCCTCTAGCAAATCTCTTCAGTATATTATTCCATTGACAAT CTTCGAACC5' TS
Non-target DNA labeled	5'AGCTTGTCTGCCATGGACATGCAGACTATACTGTTATTGTTGTAC AGACCGAATTCCC/36FAM/3' 3'TCGAACAGACGGTACCTGTACGTCTGATATGACAATAACAACAT GTCTGGCTTAAGGG5' 5'/56FAM/AGCTTGTCTGCCATGGACATGCAGACTATACTGTTATTG TTGTACAGACCGAATTCCC-' 3'TCGAACAGACGGTACCTGTACGTCTGATATGACAATAACAACAT GTCTGGCTTAAGGG5'

The PAM and protospacer/target sequences in DNA oligos are colored in red and blue, respectively. The spacer moieties of RNA oligos are colored in.

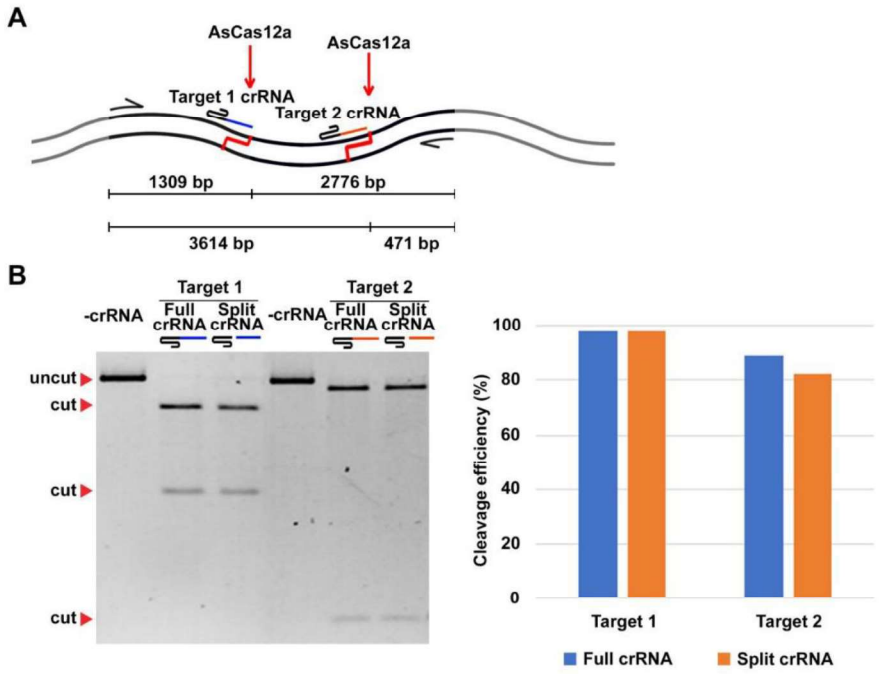


Figure S1. Split crRNA activity is not dependent on the sequence of the crRNA spacer moiety.

(A) Schematic representation of target DNA containing two AsCas12a PAM sequences. Spacer moieties of target crRNAs are shown in blue and orange, the cleavage sites are marked with red arrows. The sizes of the fragments corresponding to cleaved DNA template are given below the scheme for each cleavage site.

(B) *In vitro* cleavage of target DNA by AsCas12a loaded with 500 nM of full-sized or split crRNAs targeting different sites ("Target 1" or "Target 2", as indicated above the panel). Cleavage efficiencies calculated from the gel presented are shown.

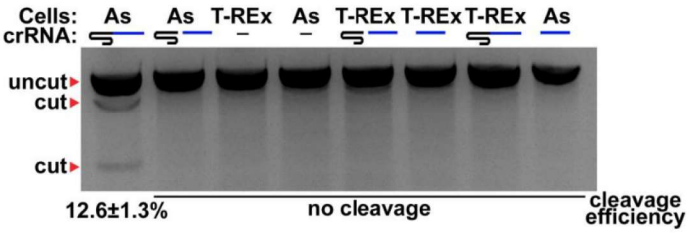


Figure S2. CRISPR/AsCas12a genome editing in HEK293 cells encoding hAsCas12a.

A mismatch-specific T7E1 endonuclease assay was used to analyze DNA flanking AsCas12a target site - DNMT1. HEK293 T-REx hAsCas12a ("As") was transfected with either full-sized or split crRNA (as indicated above the panel) followed by activation of nuclease gene expression. As a control, we used HEK293 T-REx cell line ("T-REx"). Mock transfection was performed to evaluate the effect of the transfection reagent on cells.

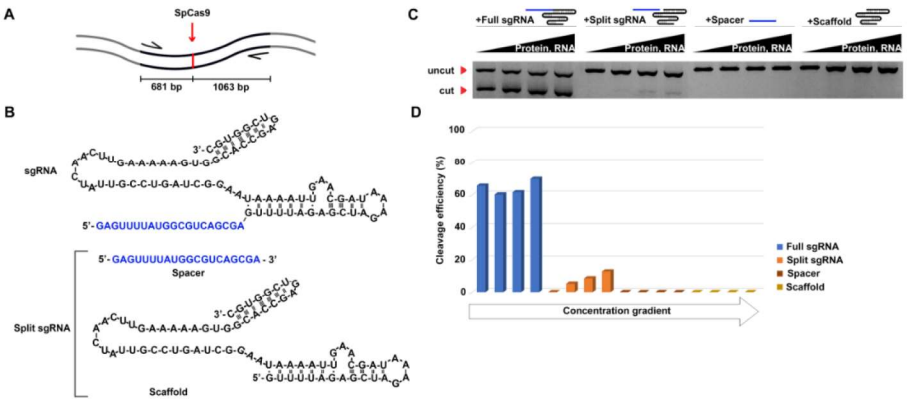


Figure S3. Effect of full-length and split sgRNA versions on SpCas9 cleavage activity.

(A) Schematic representation of the target DNA construct used as a template in the *in vitro* cleavage assay. The black arrows correspond to DNA oligonucleotides used for PCR

amplification of cleavage substrate. The SpCas9 cleavage site is represented with the red arrow. The expected sizes of cleavage products are indicated below the scheme.

(B) Sequence of sgRNAs used. The spacer moiety of the SpCas9 sgRNA is highlighted in blue font and the scaffold moiety is highlighted in black font.

(C) The products of *in vitro* cleavage of the DNA template by purified SpCas9 in the presence of increasing amounts (1, 3, 6, and 8 μM) of indicated sgRNA forms.

(D) Quantification of target DNA cleavage efficiency.

3.2.3. AsCas12a crRNA conjugation with chemical residues

An alternative strategy we aimed to employ for improving the import of AsCas12a crRNA into mitochondria involved conjugating them with ligands known for their affinity to mitochondria and their ability to penetrate the mitochondrial membrane. Initially, we selected cholesterol, rhodamine dye R6G, and berberine as the ligands to explore this approach (**Figure R7A**). This strategy was initiated but not finalized in the frame of my thesis work.

The use of cholesterol as a modifier of small RNA molecules at the terminal position is based on the fact that it is an important bioregulator as well as a structural component of cell membranes. Mitochondrial membrane functionality and the synthesis of steroids rely on the presence of cholesterol, despite its limited abundance. Cholesterol is crucial for maintaining membrane integrity and facilitating steroidogenesis. Unlike various other cellular membranes, mitochondrial membranes, especially the IMM, exhibit relatively lower cholesterol content. This distinct feature highlights the significance of targeted cholesterol transportation to the IMM, where it undergoes conversion into pregnenolone, thereby regulating steroidogenesis (**Elustondo, P. *et al.*, 2017**). Cholesterol is imported into mitochondria through lipid transfer proteins and multiprotein complexes located at the interfaces between mitochondrial membranes and other cellular membranes (**Elustondo, P. *et al.*, 2017**).

Rhodamine 6G, a fluorescent dye, possesses the ability to penetrate living cells. Its positive charge and lipophilic nature make it a suitable choice as a mitochondria-specific dye. Studies have indicated its strong binding affinity to the inner mitochondrial membrane, and at elevated concentrations (micrograms per milliliter), it can act as an inhibitor of oxidative phosphorylation (**Gear, A.R., 1974**). Although there is no reported evidence of Rhodamine 6G being detected within the mitochondrial matrix, we decided to explore its conjugation with crRNA, understanding that it might become localized at the inner mitochondrial membrane.

Berberine is a natural alkaloid present in plants of the *Berberidaceae* family. This positively charged molecule exhibits the capability to permeate cell membranes (**Caliceti, C. *et al.*, 2016**). Berberine holds a prominent place in traditional Chinese medicine and boasts pharmacological effects, including anti-inflammatory and antioxidative properties, and even a therapeutic impact against obesity (**Jin, Y., Khadka, D. B., & Cho, W. J., 2016**). Notably, berberine has been reported to accumulate within mitochondria, with this accumulation dependent on the mitochondrial transmembrane potential (**Pereira, G. C. *et al.*, 2007**). The working hypothesis regarding berberine's entry into mitochondria centers on its interaction with the adenine nucleotide

translocator (ANT). A recent publication has convincingly demonstrated berberine's affinity for specific non-Watson-Crick G-quadruplex (GQ) structures, enhancing their formation and stability. When berberine hydrochloride was administered to patient fibroblasts carrying the pathogenic mtDNA m.10191C variant associated with Leigh syndrome, it prompted the formation of GQ structures. This intervention led to a reduction in mutant mtDNA heteroplasmy levels due to the role of mitochondrial Pol *γ*, which favored the replication of the normal allele due to its inability to replicate GQ regions (**Naeem, M. M. *et al.*, 2019**).

Thus, a set of AsCas12a crRNAs (based on crRNA-45, targeting MT-ATP6, section **2.1.6**) bearing 3'-end chemical modifications, which might impact mitochondrial import efficiency, were synthesized by our collaborator Vadim Shmanai (National Academy of Science of Belarus, Minsk, Belarus) (**Figure R7A,** section **2.2.12.**). In an *in vitro* cleavage assay with the purified recombinant AsCas12a nuclease (section **2.2.20.**, **Figure M4**), all the complexes with the modified crRNAs were capable of cutting the DNA template (**Figure R7B**). Notably, the complex containing the crRNA modified with cholesterol demonstrated the lowest activity. Consequently, we excluded this crRNA variant from further experiments. Evaluation of the mitochondrial import of conjugated crRNAs using our standard test (section **2.2.16.**) demonstrated that all modified crRNAs appeared to be protected from the nuclease treatment in the lysate of mitochondria (**Figure R7C**). As a result, we were unable to draw definitive conclusions about the mitochondrial import of these chemically-modified crRNAs under the conditions of our experiment. We believe that concrete evidence regarding the mitochondrial import of these crRNAs can only be obtained through a direct demonstration of specific mtDNA cleavage *in vivo*.

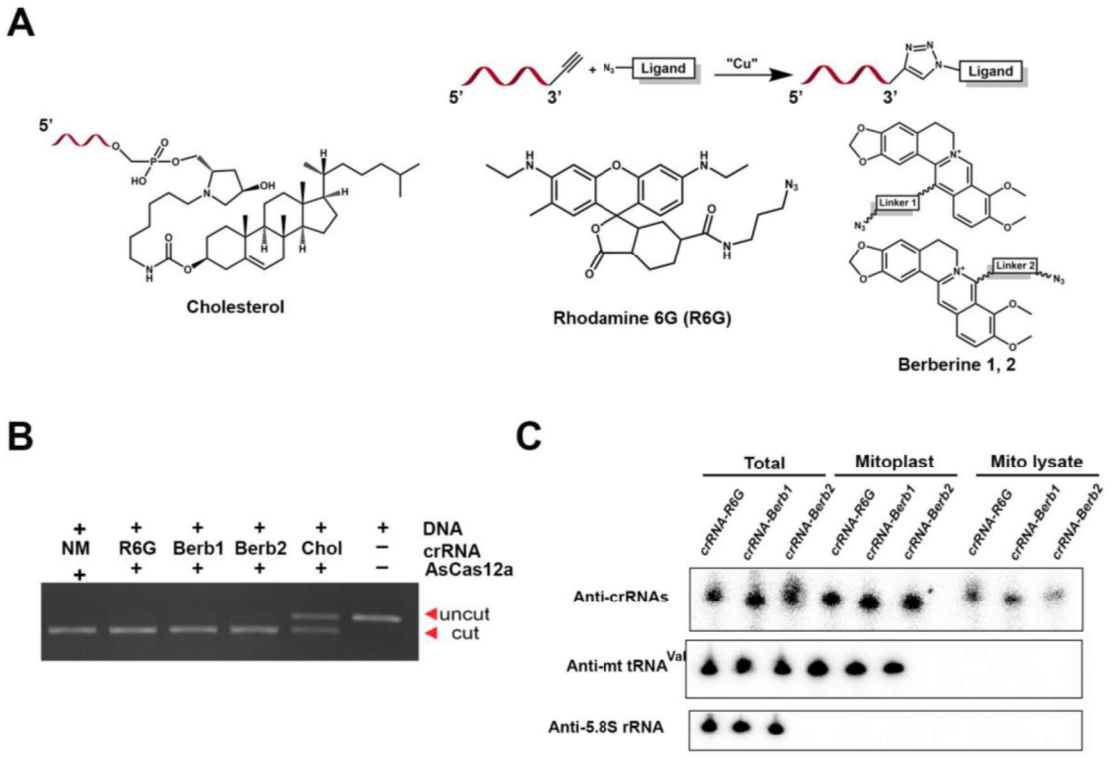


Figure R7. Chemical Modifications of AsCas12a crRNA, their impact on the Function and Mitochondrial Import.

(A) The chemical modifications introduced at the 3'-end of AsCas12a crRNA (crRNA-45). Cholesterol modification was directly incorporated during the solid-phase synthesis. Modifications involving azides of rhodamine (R6G) and berberine were accomplished through the copper-catalyzed azide-alkyne cycloaddition.
(B) *In vitro* cleavage assay with purified AsCas12a nuclease and chemically-modified crRNAs. The cleavage was visualized in an agarose gel with EtBr staining. DNA:Protein:RNA – 1:3:30. Where "NM" - non-modified crRNA, "R6G", "Berb1" and "Berb2" - crRNAs modified with functional derivatives of rhodamine 6G, berberine 1 and 2, respectively.
(C) Northern blot hybridization of RNA isolated from the Su9-AsCas12a stable cell line transfected with chemically-modified crRNAs, as indicated above the panel. RNA was isolated from cells ("Total"), RNase treated mitoplasts ("Mitoplast") and RNase treated mitochondrial lysates ("Mito lysate"). Hybridization probes used are indicated on the left: crRNA (top panel), mitochondrial $tRNA^{Val}$ (middle panel) and cytoplasmic 5.8S rRNA (lower panel).

3.3. Functional assessment of the mitoAsCas12a system functionality *in vivo*

The most important part of the project, representing the proof-of-concept should consist in the detection of specific cleavage in mtDNA induced by the mitoCRISPR system.

3.3.1. Analysis of the Su9-AsCas12a cleavage activity and mtDNA levels in cultured human cells

To start with, we investigated the potential reduction in mtDNA copy number in the newly acquired stable cell line. We expected to see a decrease in mtDNA copy number after the mitoCRISPR system exposure since it was demonstrated that linear mtDNA molecules are rapidly degraded by the components of mitochondrial replication machinery (**Peeva, V. *et al.*, 2018**).

To serve as a negative control for the AsCas12a nuclease cleavage activity, we introduced a mutation (E993A) into the RuvC endonuclease domain (**Figure R8A**). This mutation results in the generation of a DNase-dead version of AsCas12a (referred to as ddAsCas12a), which no longer possesses DNase activity against both strands of target DNA (**Yamano, T. *et al.*, 2016**). The mutation was introduced using site-directed mutagenesis (section **2.2.9**; **Figure M3**) in pcDNA5-FRT-TO-Su9-AsCas12 plasmid vector (**Figure R4A**). Verification of the ddAsCas12a expression was performed using Western blot analysis of total cell lysates from the cells transfected with the modified plasmid (section **2.2.4.**; **Figure R8B**).

In an *in vitro* cleavage assay in a cell lysate obtained from the transfected cells (section **2.2.13.**), we observed no target DNA cleavage by the ddAsCas12a-crRNA complex, thus confirming the loss of its DNA cleavage capability (**Figure R8C**). As expected, the active AsCas12a-crRNA complex exhibited the ability to cleave the target DNA; however, the cleavage was not complete (**Figure R8C**). This partial cleavage is likely attributed to the lower abundance of the nuclease in the cells due to the lower transfection efficiency with plasmids, often observed during the microscopy (data not shown). In comparison, within the Su9-AsCas12a stable cell line, where each cell expresses the nuclease, the cleavage was observed to be complete in the same conditions (**Figure R5E**). Finally, the mitochondrial localization of the ddAsCas12a nuclease fused with the Su9 MTS was determined by immunofluorescent staining of the transfected cells (section **2.2.8.**; **Figure R8D**).

Then, we performed qPCR analysis of total DNA extracted from the cells, transfected with either the Su9-AsCas12a or its inactive DNase-dead version, both with and without crRNA-34 targeting MT-ND4 (section **2.2.23.**). We examined the cells at various time points, but no reduction in relative mtDNA copy number was observed in any of these conditions (**Figure R8E**). This implies that if a specific cleavage event did take place, it wasn't efficient enough to bring about any changes in the mtDNA copy number.

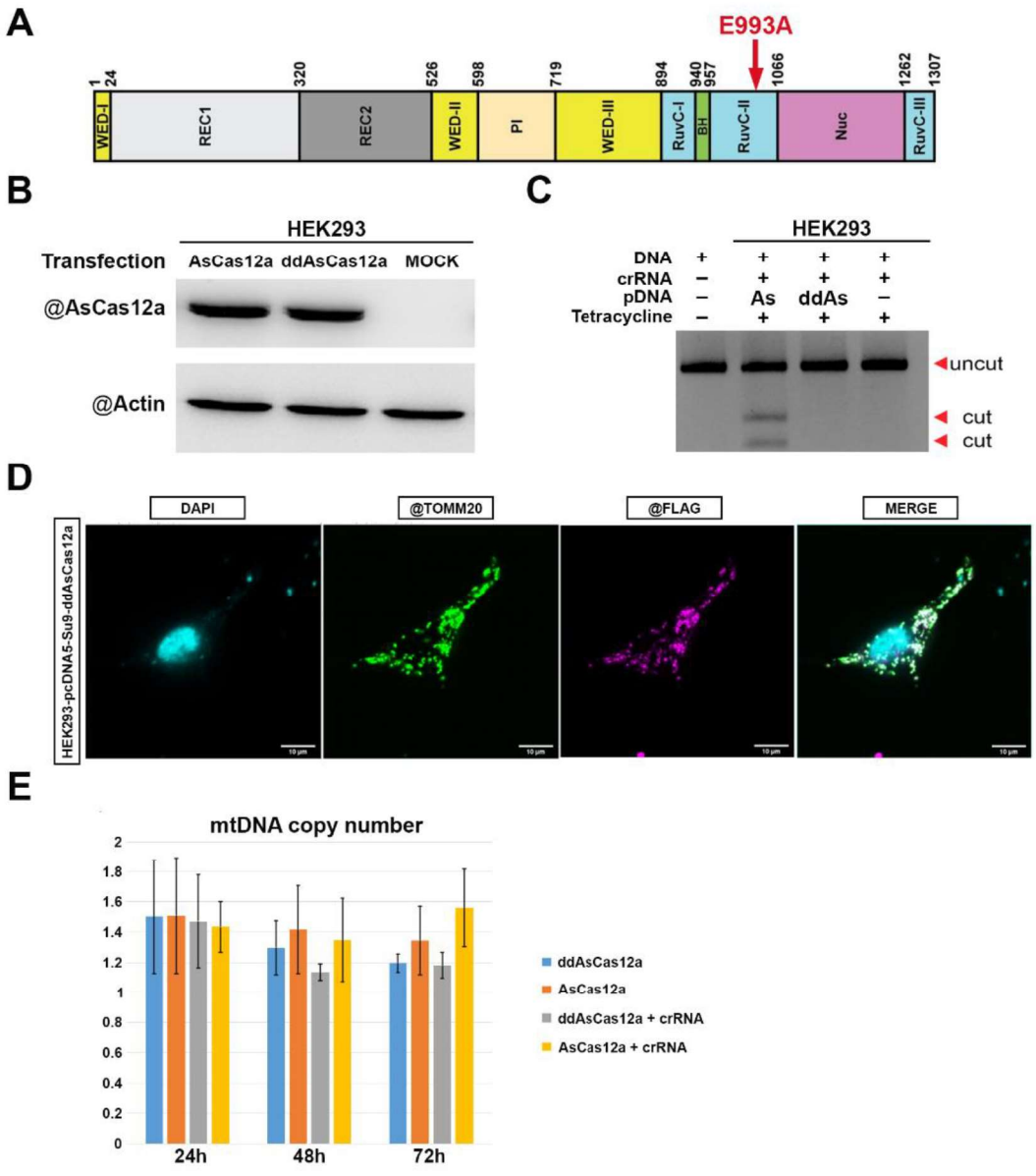

A
E993A
1
24
320
526
598
719
894
940
957
1066
1262
1307
WED-I
REC1
REC2
WED-II
PI
WED-III
RuvC-I
BH
RuvC-II
Nuc
RuvC-III
B
HEK293
Transfection
AsCas12a
ddAsCas12a
MOCK
@AsCas12a
@Actin
C
HEK293
DNA
crRNA
pDNA
Tetracycline
As
ddAs
uncut
cut
cut
D
DAPI
@TOMM20
@FLAG
MERGE
HEK293-pcDNA5-Su9-ddAsCas12a
E
mtDNA copy number
2
1.8
1.6
1.4
1.2
1
0.8
0.6
0.4
0.2
0
24h
48h
72h
ddAsCas12a
AsCas12a
ddAsCas12a + crRNA
AsCas12a + crRNA

Figure R8. Effect of the Su9-AsCas12a Nuclease, both Active and DNase-dead, on mtDNA Copy Number in Human Cells.

(A) Domain organization of AsCas12a (Adapted from Yamano, T. *et al.*, 2016). WED - wedge lobe, consisting of three domains; REC - α-helical recognition lobe, consisting of two domains; PI - PAM-interacting domain; RuvC domain - endonuclease active center, containing three motifs; BH - bridge helix; NUC - nuclease domain. The E993A mutation (highlighted by the red arrow) within the RuvC domain results in the generation of a ddAsCas12a variant,lacking the DNase activities targeting both strands of DNA. The amino acid positions numbers are indicated above the scheme.
(B) Western blot of total lysates obtained from HEK293 cells, transfected with either pcDNA5-FRT-TO-Su9-AsCas12a or ddAsCas12a plasmids or empty vector (MOCK), cultivated in cell media supplemented with 50 ng/mL of tetracycline.
(C) *In vitro* cleavage of target DNA in cell lysates of HEK293 cell line, transfected with either pcDNA5-FRT-TO-Su9-AsCas12a ("As") or ddAsCas12a ("ddAs") plasmid vectors. Cultur media was supplemented with 50 ng/mL of tetracycline when indicated. The addition of the plasmids ("pDNA"), crRNA, DNA template and tetracycline is indicated above the gel. *In vitro* cleaved products after incubation for 30 min at 37 °C were resolved by 1 % agarose gel electrophoresis.
(D) Immunofluorescent staining of HEK293 cells transfected with pcDNA5-FRT-TO-Su9-ddAsCas12a. The nuclease was stained with antibodies against the FLAG-tag, shown in green, while mitochondria were stained with antibodies against TOMM20, shown in magenta. Nuclei were stained with DAPI, shown in blue. The colocalization of the nuclease with mitochondria is indicated by the white signal. Scale bares: 10 μm.
(E) qPCR analysis of mtDNA copy number in HEK293 cells at several time points after transfection with either pcDNA5-FRT-TO-Su9-AsCas12a ("AsCas12a") or ddAsCas12a ("ddAsCas12a") plasmids with or without co-transfection with crRNA-34. mtDNA copy number was quantified using the 2−ΔΔCT method (section **2.2.23**). Non-transfected HEK293 cells served for normalization (mtDNA copy number taken as 1). Mean values with standard deviations are present; n = 3.

The cleavage of mtDNA by a CRISPR system, most probably, faces limitations due to the inefficient delivery of crRNA into the mitochondria (**Gammage P. A., Moraes C. T., Minczuk M., 2018**). It's important to note that our experiment utilized a single crRNA targeting mtDNA. In a previously published study from our lab by **Loutre, R. *et al.* in 2018**, it was demonstrated that reduction in mtDNA copy number *ex vivo* was achieved only when two sgRNAs targeting mtDNA were employed together with the mitochondria-targeted SpCas9 nuclease. In another recent article by **Bi, R. *et al.* in 2022**, a decrease in mtDNA levels was observed in HEK293 cells transfected with plasmids encoding the mitoSpCas9 and its corresponding sgRNA, however, this decrease was noticeable only after sorting the cells by fluorescence for both systems components 48 hours post-transfection.

Noteworthy, based on the results of our experiment, it's evident that mtDNA content did not decrease when treated with the nuclease alone. This suggests that AsCas12a doesn't induce a significant level of nonspecific cleavage when its crRNA is absent (**Figure R8E**).

Clearly, the conditions of this experiment need to be adjusted and optimized. It would be interesting to assess mtDNA copy number after several transfection rounds using crRNAs that target different sites within mtDNA, possibly bearing chemical modifications as well (as described in section **3.2.3**).

3.3.2. mtDNA free ends detection after the mitoCRISPR system exposure

Although we did not observe a decrease in mtDNA levels, we aimed to detect specific cleavage events in human mtDNA introduced due to the crRNA-programmed nuclease activity of the Su9-AsCas12a *ex vivo*, using more sensitive approaches.

For this, we applied a strategy, developed in the lab of Prof. Kunz, for free mtDNA ends detection consisting of next-generation sequencing of linker-ligated mtDNA (**Peeva, V. *et al.*, 2018**; **Figure M5**).

However, due to the rapid degradation of linearized mtDNA by the components of mitochondrial replication machinery, we needed to protect free ends of mtDNA formed as a result of the mitoCRISPR system cleavage. MGME1, a mitochondrial 5'-3' exonuclease, together with the 3'-5' exonuclease activity of mitochondrial DNA Pol γ, were shown to be the key players of linearized mtDNA degradation (**Peeva, V. *et al.*, 2018**).

To minimize the degradation of linear mtDNA, we applied siRNA targeting MGME1 to perform its knockdown (section **2.2.24.**). By analyzing MGME1 levels in cells, transfected with 40 nM of MGME1 siRNA, using Western blot, we observed a reduction in MGME1 expression three days post-transfection (**Figure R9A**). Furthermore, even six days after a single transfection, MGME1 expression level was not fully recovered. Such a decrease in MGME1 expression was not observed upon the control transfection with scrambled siRNA.

We subsequently designed an experimental workflow enabling the further detection of mtDNA breaks (**Figure R9B**). Initially, the Su9-AsCas12a stable cell line was subjected to MGME1-targeting siRNA treatment, as described in section **2.2.24.**. After a 24-hour interval, the cells were transfected with crRNA-45, designed to target human mtDNA (MT-ATP6) (section **2.2.25.**). We chose to activate the AsCas12a nuclease expression on the same day and the next day as the crRNA (**Figure R9B**). Therefore, cells were exposed to nuclease for 24 (**Figure R9B**, **"Day 3"**) or 48 hours (**Figure R9B**, **"Day 2"**), which is also 48 hours after the crRNA transfection and 3 days after anti-MGME1 siRNA transfection.

Thereafter, we proceeded with mitochondria and mtDNA isolation as outlined in section **2.2.25**, and a portion of cells and mitochondria was set aside for an *in vitro* cleavage test within total and mitochondrial lysates (section **2.2.25.**).

The obtained results provided an indication of the system's activity within the cells already 24 hours after exposure to the mitoCRISPR (**"Day 3, Total"** in **Figure R9C**). 48 hours post-induction, we observed even more noticeable cleavage in the cell lysate (**"Day 2, Total"** in **Figure R9C**). Importantly, bends corresponding to the target DNA-specific cleavage emerged in the mitochondrial lysate as well (**"Day 2, Mito"** in **Figure R9C**). This finding suggests that the system requires a 48-hour timeframe to effectively direct its components to mitochondria and manifest activity. It is important to note that the mitochondria used for the cleavage reaction were not subjected to RNase treatment (section **2.2.25.**). This additional step may help to prevent possible contamination of the reaction with crRNA molecules that could potentially adhere to mitochondria from the cytosol.

Then, isolated mtDNA was ligated to an asymmetric double-stranded linker with a known sequence, serving to label mtDNA breaks for the linker-ligated whole genome sequencing (section **2.2.26.**, **Figure M5**). Library preparation and next-generation sequencing (NGS) of the linker-ligated mtDNA was carried out at the "Genomics Core Facility" at Skolkovo Institute of Science and Technology (Moscow, Russia). The obtained reads were aligned to the reference mitochondrial sequence, and subsequently, they were checked for the presence of the linker sequence. This process identified a set of break events in both the forward and reverse strands of mtDNA (**"Free ends Forward"** and **"Free ends Reverse"** in **Figure R9E**). Following this, all the identified breaks, represented by the number of reads containing the linker, were summarized for each strand of each sample and normalized to the sample-specific average coverage (**"Breaks/Coverage Forward"** and **"Breaks/Coverage Reverse"** in **Figure R9E**). This analysis, generously conducted by Dr. Gábor Zsurka from the University of Bonn (Germany) revealed a 2-3-fold increase in mtDNA fragmentation in samples treated with the nuclease and crRNA, compared to the control samples (in samples treated only with the nuclease, mtDNA fragmentation levels were comparable to the untreated control), indicating on the system's activity (**Figure R9E**, **upper part of the table in light-blue**). Unfortunately, we obtained an extremely low mtDNA enrichment (only 2-3% of the reads were aligned to mtDNA) due to the nuclear DNA contamination. Thus, the mtDNA coverage was not enough to precisely identify specific cleavage events at the expected positions in mtDNA (nucleotide position 8622-8628 in human mtDNA for crRNA-45). Due to this issue, all the break events were evenly distributed across the entire mtDNA sequence, with each nucleotide position having a comparable frequency of normalized break sums when plotted into a line graph (**Figure R9F**). In turn, we expected to observe a notable rise in the normalized sum of the breaks at the specific nucleotide positions where the cleavage was expected to occur by the AsCas12a-crRNA-45 complex.

Another series of cell transfection experiments was performed as previously, but crRNA-1Up, 2Down, or both, targeting MT-COX1 mtDNA region (**Figure R9D**, **upper panel**) were used for transfection simultaneously with the Su9-AsCas12a induction (**"Day 2"** in **Figure R9B**). First, we aimed to detect free ends of mtDNA using the linker-mediated PCR technique (**Peeva, V. *et al.*, 2018**; **Figure M5**). For this, isolated mtDNA was ligated to an asymmetric double-stranded linker to label mtDNA breaks. Subsequently, to detect the mtDNA cleavage events, we employed linker-mediated PCR, where one primer was complementary to the linker, while the other primer targeted mtDNA in close proximity to the predicted cleavage site (~600 bp) (section **2.2.27.**, **Figure M5**, **Figure R9D**, **upper panel**).

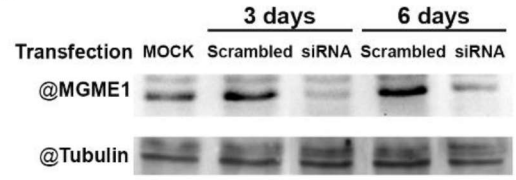
We examined the results of LM-PCR on the agarose gel, but mainly a DNA smear was observed, except for the positive control representing mtDNA cleaved *in vitro* with the recombinant AsCas12a and the same crRNAs (**"PC"** in **Figure R9D**, **lower panel**). To detect the PCR fragments of interest (**Figure R9D**, **upper panel**), we conducted Southern blot hybridization using an oligonucleotide probe targeting mtDNA, which had also been used as a primer for LM-PCR (section **2.2.28.**, **Figure R9D**, **upper panel**). When the hybridization signal was revealed, fragments of the expected size, resulting from the predicted mitoAsCas12a cleavage in complex with crRNA-1Up, 2Down or with both crRNAs, were detected in samples where cells were treated with either one of two crRNAs or with both simultaneously (**Figure R9D**, **lower panel**). In a negative control, consisting of the cells treated only with the nuclease without the addition of any crRNA, a faint signal of smaller size was observed (**"NTC"** in **Figure R9D**, **lower panel**) probably due to a non-specific binding of the probe. These data clearly indicate on the specific mtDNA cleavage by mitoAsCas12a/crRNA system.

To validate this, the library preparation and linker-ligated whole genome sequencing were performed by NOVOGENE (Baltimore, USA) in collaboration with Prof. Samarjit Das from Johns Hopkins University (USA) and kindly analysed by Dr. Gábor Zsurka from the University of Bonn (Germany). Unfortunately, in this experiment, amount of reads aligned to mtDNA was only slightly improved (to 2-8%, **Figure R9E**, **lower part of the table in purple**), and we were not able to detect specific cleavage events. Nevertheless, as in the previous experiment, mtDNA fragmentation (estimated as Breaks/Average coverage) was 2-4 fold increased in samples from the cells transfected with crRNAs compared with the MOCK-transfected and the AsCas12a nuclease treated control. The best difference was detected for mtDNA from the cells transfected with two crRNAs simultaneously.

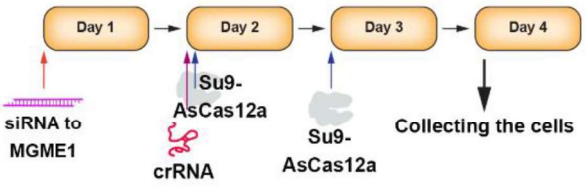
Consequently, further improvement of mitochondria and mtDNA purification techniques is necessary to achieve an enhanced purity of isolated mitochondria and to minimize both nuclear DNA contamination and mtDNA disruption during the isolation process, which can affect the analysis.

Overall, the findings presented in this chapter indicate the activity of the mitochondrial-targeted CRISPR/AsCas12a system, although its efficiency looks to be rather low.

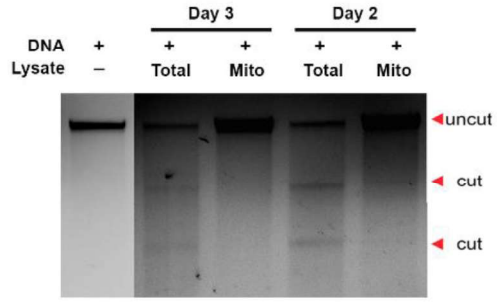
A



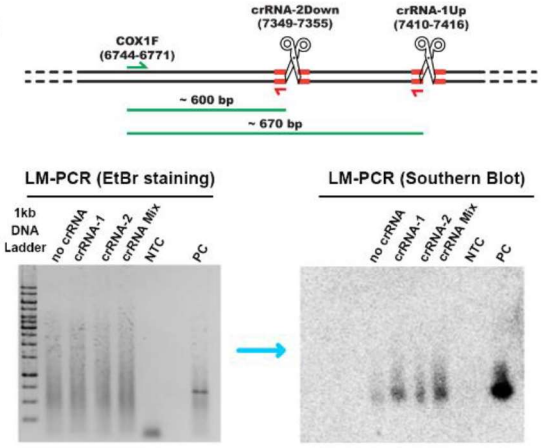
B



C



D



E

Sample	Reads paired-end	Mito Aligned	Average Coverage	Free ends Forward	Free ends Reverse	Breaks/Cover Forward	Breaks/Cover Reverse
MOCK	6826496	3%	361	1805	1591	5.00	4.41
AsCas12a (D2)	6957108	3%	415	1809	1641	4.36	3.95
crRNA-45/AsCas12a (D2)	7618834	1.78%	602	7704	7432	12.80	12.35
crRNA-45/AsCas12a (D3)	50855006	2.12%	268	2519	2374	9.40	8.86
AsCas12a (D2)	5981765	4,08%	5004	3485	4560	0.69	0.90
crRNA-1Up/AsCas12a(D2)	4652939	5.59%	2823	5470	5319	1.93	1.88
crRNA-3DR/AsCas12a (D2	4201846	2.05%	862	3373	3045	3.91	3.53
crRNA-MIX/AsCas12a (D2	4963680	7.65%	1992	11425	8699	5.74	4.37

F

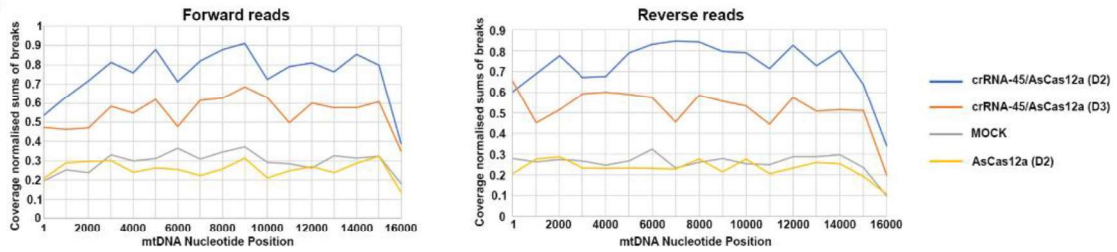


Figure R9. Next Generation Sequencing of Linker-Ligated mtDNA after the mitoCRISPR system exposure.

(A) Western blot hybridization of total lysates from the Su9-AsCas12a stable cell line, prepared 3 and 6 days after transfection with 40 nM siRNA against MGME1. MOCK and scrambled siRNA transfections served as a negative control. Tubulin-specific antibodies were used as a loading control.
(B) Experimental pipeline for cells treatment with the mitoCRISPR system in order to detect free ends of mtDNA by NGS of the linker-ligated mtDNA. On the first day, the Su9-AsCas12a stable cell line was transfected with siRNA to MGME1. 24 hours after, the cells were transfected with one or two crRNAs targeting human mtDNA. On the same day or the next day (Day 2 or Day 3), the AsCas12a nuclease expression was induced by the addition of tetracycline. All the cells were detached on the fourth day.
(C) *In vitro* cleavage of mtDNA fragment in total cell ("Total") and mitochondrial ("Mito") lysates obtained from experiment detailed in **(B)** with crRNA 45. "Day 2" and "Day 3" indicate that the AsCas12a nuclease was expressed for either 48 or 24 hours before the cells detachment. The agarose gel was visualized using EtBr staining, and overexposed to enhance the visualization of the cleaved fragments.
(D) LM-PCR on mtDNA extracted from the Su9-AsCas12a stable cell line, transfected as in (**B**, **Day 2**) with crRNAs targeting the MT-COX1 gene ("crRNA 1" - crRNA-1Up, "crRNA 2" - crRNA-2Down, and "Mix" - both crRNAs). Scheme of LM-PCR is given on the above panel. NTS is a negative no-template control, PC is a positive control obtained on mtDNA cleaved *in vitro* with the recombinant AsCas12a nuclease. Left panel, agarose gel stained with EtBr; Right panel, Southern blot hybridization with probe COX1F, as indicated on the scheme.
(E) Characteristics of fmtDNA samples from the cells treated with the mitoCRISPR system **(B)** derived from the NGS analysis, including paired-read count, mtDNA alignment percentage, average coverage, number of breaks (linker-positions) in forward and reverse reads, and coverage normalized sum of these breaks. The samples from two independent NGS runs are highlited in light-blue and purple.
(F) Graphs depicting the sum of breaks for forward and reverse paired-reads across nucleotide positions in mtDNA, normalized to average coverage, for the four samples from (**E**, **upper part in light-blue.**).

3.4. Use of the Type V CRISPR-Cas system to induce a deletion in human mitochondrial DNA

After confirming the activity of the developed mitoAsCas12a system, even though the current efficiency still needs improvement, our next objective was to determine whether it is possible to manipulate mtDNA rather than solely degrading it.

As discussed in **Introduction section**, many neuromuscular diseases in humans are caused by mutations in mtDNA. The severity of these diseases depends on the level of heteroplasmy, where both mutant and wild-type mtDNA coexist in the same cell (**Nissanka, N., Moraes, C. T., 2020**). Deletions in mtDNA stand as the primary cause of mitochondrial diseases, and such mutations also contribute to tissue aging (**Kraysberg, Y. *et al.*, 2006**). However, the precise mechanisms behind deletion formation and dynamics remain unknown (**Nissanka N., Minczuk M., Moraes C.T., 2019**).

Developing novel methods to model mtDNA dysfunction in cell cultures and living organisms holds crucial importance for experimental therapy and the long-term treatment of mitochondrial diseases. Until now, only a limited number of mouse models for mtDNA diseases have been developed and characterized (**Stewart J. B., 2021**), including the ΔmtDNA4696 “mito-mice,” which represent the first and only heteroplasmic mouse model with a pathogenic mtDNA deletion (**Inoue, K. *et al.*, 2000**).

The Type V CRISPR-AsCas12a system, which recognizes AT-rich PAM sequences and cleaves DNA at nucleotide positions 17th–19th downstream of the PAM on the non-target DNA strand, as well as at the 21st – 23rd positions of the target strand, generating 3–5 nucleotide-long 5'-overhangs (**Selkova, P. *et al.*, 2020**), holds potential for creating cell lines and animal models with specific mtDNA deletions using 2 crRNAs to generate cohesive ends that can be ligated (**Verechshagina, N. *et al.*, 2019**; **Figure R10A**).

To initiate our investigation on a possibility to induce a deletion in mtDNA using the mitoAsCas12a system, we selected two crRNAs, namely crRNA-45 and crRNA-34, targeting MT-ATP6 and MT-ND4 (**Publication 2**; section **2.1.6.**), that were predicted to induce cleavage in mtDNA, yielding complementary 5'-overhangs (**Figure R10A**).

3.4.1. *In vitro* cleavage programmed by two crRNAs

To check the activity of these crRNAs, we conducted *in vitro* cleavage tests using each individual crRNA in complex with a commercial AsCas12a nuclease (section **2.2.29.**). The obtained results demonstrated the efficient cleavage ability of both crRNAs on the template DNA (**Figure R10B**).

Subsequently, we aimed to verify whether these two crRNAs could program the DNA template cleavage when employed simultaneously. The results obtained from the *in vitro* cleavage tests revealed a complete cleavage of the initial DNA template, resulting in the appearance of a band corresponding to the cut induced by both crRNAs (**shown by red arrow** in **Figure R10C**). However, a DNA fragment of 3099 bp indicative of the cleavage by only one of the two crRNAs (crRNA-34) was still observed on the gel (**shown by green arrow** in **Figure R10C**), meaning that crRNA-45 failed to induce the complete DNA-template cleavage when both crRNAs were applied together. One possible explanation can be connected to the experimental protocol – prior to introducing the DNA template into the cleavage reaction, both crRNAs are initially pre-incubated with the nuclease within the same tube (section **2.2.29.**). This could potentially induce a competition between the crRNAs for binding to the protein, especially considering the crRNAs concentration was 1.3 times greater than that of the protein. In future experiments, we are considering changing the protein quantity and/or performing a pre-incubation of only one crRNA with AsCas12a before introducing the second, to see if we can observe different patterns in the cleavage results.

Another hypothesis stems from the fact that AsCas12a rapidly releases the cleavage product distal to the PAM sequence, but not the product proximal to the PAM (**Singh, D. *et al.*, 2018**). In this context, it is possible that if AsCas12a initiates the first cleavage at the crRNA-34 targeting

site, it may remain bound to the DNA fragment preventing the second cleavage in complex with crRNA-45 (**Figure R10C**). In any case, our data demonstrate a possibility to introduce a double cleavage into mtDNA.

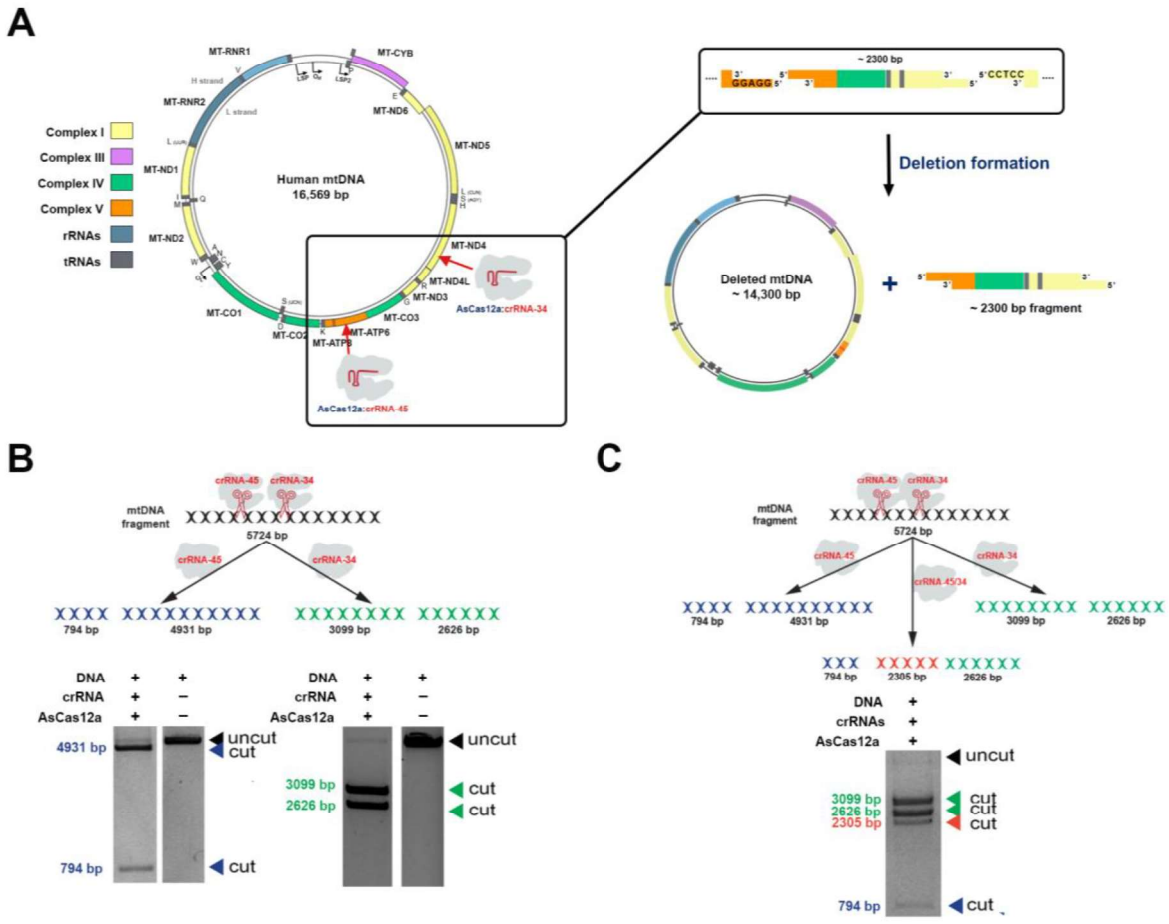


Figure R10. AsCas12a is Capable to Cleave mtDNA Fragment in Complex with Two crRNAs.

(A) Strategy for inducing deletions in human mtDNA using Type V CRISPR-Cas12a system.
(B) *In vitro* cleavage of mtDNA fragment using commercial AsCas12a nuclease in complex with crRNA-45 (left panel) and crRNA-34 (right panel). The components added are indicated above the gel. The products of *in vitro* cleavage were separated using 1 % agarose gel electrophoresis and visualized with EtBr staining. The upper panel displays a schematic representation of the target DNA (a PCR fragment of human mtDNA). The sizes of fragments corresponding to the cleaved DNA template are shown below the scheme. Here, the blue and green DNA fragments correspond to cleavages by the nuclease in complex with crRNA-45 or crRNA-34, respectively.
(C) Similar to **(B),** the target DNA was cleaved by the AsCas12a nuclease programmed with both crRNAs 45 and 34. A red DNA fragment emerges only when both cleavages occur.

3.4.2. Detection of AsCas12a-crRNAs mtDNA specific cleavage by linker-mediated PCR and NGS

After performing *in vitro* tests, we moved to experiments with mammalian cells. As our previous approach using the whole genome sequencing of linker-ligated mtDNA didn't allow the precise identification of the cleavage position (**Figure R9F**), we aimed to change our strategy to detect specific cleavages by performing NGS of the products of linker-mediated PCR (**Figure M6**).

Also, to address concerns about the potential impact of residual MGME1 exonuclease activity (**Figure R9A**) interfering with accurate cleavage detection, we modified our experimental pipeline. Particularly, we treated the Su9-AsCas12a stable cell line with siRNA against MGME1 twice within three-day interval (section **2.2.24.**), as was described in **Peeva V. *et al.*, 2018** (**Figure R11A**). Following this treatment, we transfected the cells with two crRNAs designed to introduce a deletion in mtDNA (**Figure R10A**) and subsequently activated the nuclease expression (**Figure R11A**).

After the cells were treated with siRNA and all the system components (**Figure R11A**), they were detached, and total DNA was isolated. In order to identify the free ends of mtDNA, generated as a result of the Su9-AsCas12a cleavage in complex with crRNAs 34 and 45, LM-PCR was performed using the linker-specific primer, along with the mtDNA-specific primers positioned either downstream of the crRNA-45 cleavage site to detect this specific cleavage or upstream of the crRNA-34 cleavage site to identify that particular cut (section **2.2.27.**, **Figure M6**, **Figure R11B**, **upper panel**).

Upon analysis of the LM-PCR products obtained with the downstream primer (**Figure R11B**, **upper panel**), we observed a band of 800 bp of the anticipated size, potentially indicating the AsCas12a/crRNA-45 cleavage in the sample transfected with crRNAs (**Figure R11B**, **left panel**). In contrast, such a band was absent in a control sample treated only with the nuclease.

To detect the cleavage introduced by the nuclease programmed with crRNA-34, we performed LM-PCR using a primer targeting mtDNA upstream of the anticipated cleavage site (**Figure R11B**, **upper panel**). However, we did not observe the expected 500 bp PCR product, which could indicate the free ends of mtDNA formed after the AsCas12a/crRNA-34 cleavage (**Figure R11B**, **right panel**). Furthermore, there appeared to be no visible difference in the amplified fragments between the control sample and the transfected cells (**Figure R11B**, **right panel**). To validate

these observations, we proceeded with the next step: performing NGS of the obtained LM-PCR products in order to gain insights into the sequences and origins of the observed bands.

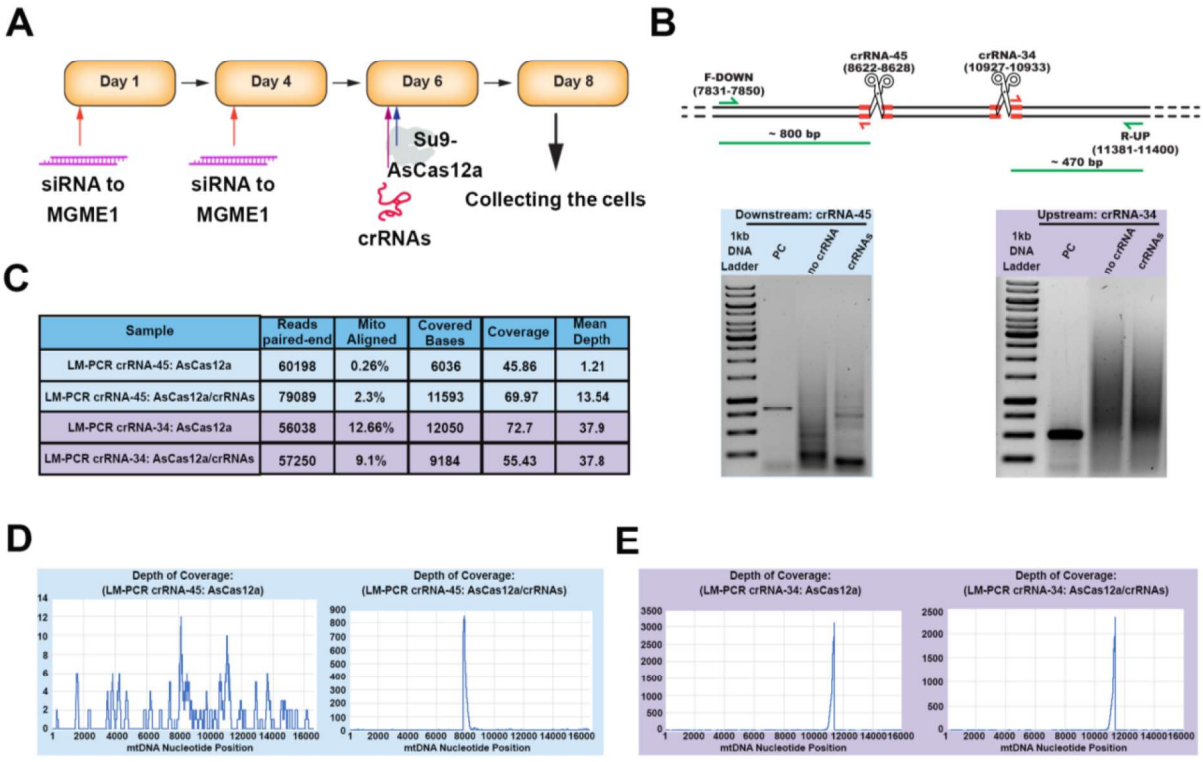
We performed NGS of the LM-PCR products, following the procedures outlined in section **2.2.30.**. The analysis of the data revealed that approximately 0.3% to 13% of linker-containing reads were aligned to the reference mtDNA sequence (**Figure R11C**). The remaining reads aligned to the nuclear genome (data not shown). This outcome is expected, considering that the linker ligation could have occurred at the breaks within the nuclear DNA, likely due to its degradation during total DNA isolation, and these breaks were then amplified during the LM-PCR.

To validate breaks within mtDNA, we examined the obtained alignments (**Figs. R11D** and **R11E**). Notably, in the sample treated with both crRNAs and the AsCas12a nuclease, specifically analyzed for the crRNA-45-induced cleavage, the main peak of reads aligned between the precise primer binding site on one end and ~ 300 bp before the predicted crRNA-45 cleavage site (MT-ATP6 gene, 8622-8628 bp (**Figure R11B**, **upper panel**)) on the other (**Figure R11D**). This gap can be explained by possible degradation of the linearized mtDNA, for instance, due to the 3'-5' exonuclease activity of mitochondrial POLG. In contrast, the control sample treated just with the AsCas12a nuclease displayed a limited number of non-specific breaks dispersed throughout the entire mtDNA sequence (**Figure R11D**). Accounting for the amount of the aligned reads in the negative control, it's reasonable to suggest that the efficiency of the mitoCRISPR system activity may represent about 2% (**Figure R11C**). Of course, for a more robust confirmation, the experiment should be repeated under optimized conditions, preferably employing PCR-free whole mtDNA sequencing to minimize potential PCR-related biases.

Regarding the cleavage, induced by the nuclease programmed with crRNA-34, we observed a main peak in the expected position of the primer binding site (11400 bp) and ~ 50 bp after crRNA-34 cleavage site (MT-ND4 gene, 10927-10933 bp) (**Figure R11B**, **upper panel**, **Figure R11E**). However, the same peak was also present in the nuclease-treated sample with no crRNAs, even with a slightly lower depth of coverage (**Figure R11E**). This implies that the nuclease might introduce this nonspecific cleavage even without its corresponding crRNA, or such a break could have occurred by an accident during DNA isolation followed by the linker ligation and LM-PCR amplification. Such an outcome can explain the previous observations of the similarity between the two samples on the agarose gel (**Figure R11B**).

In summary, our results confirm the capability of the modified AsCas12a system to introduce specific breaks in mtDNA, at least for one of the two crRNAs intended for deletion creation. This

serves as additional indirect evidence of AsCas12a crRNA's potential to be imported into the mitochondrial matrix. As for crRNA-34, further experiments involving both crRNAs are required to validate these observations and establish statistically significant findings.



Sample	Reads paired-end	Mito Aligned	Covered Bases	Coverage	Mean Depth
LM-PCR crRNA-45: AsCas12a	60198	0.26%	6036	45.86	1.21
LM-PCR crRNA-45: AsCas12a/crRNAs	79089	2.3%	11593	69.97	13.54
LM-PCR crRNA-34: AsCas12a	56038	12.66%	12050	72.7	37.9
LM-PCR crRNA-34: AsCas12a/crRNAs	57250	9.1%	9184	55.43	37.8

Figure R11. Detection of Breaks in mtDNA by NGS of the LM-PCR products.

(A) Experimental pipeline for cells treatment with the mitoCRISPR system. On the Day 1 and Day 4, the Su9-AsCas12a stable cell line was transfected with siRNA to MGME1. Day 6, the cells were transfected with two crRNAs targeting human mtDNA. On the same day, the AsCas12a nuclease expression was induced by the addition of tetracycline. All the cells were detached on the Day 8, and total DNA was isolated.

(B) On the panel above, schematic design of LM-PCR with primers downstream of the crRNA-45 binding site and upstream of crRNA-34 binding site. On the left panel (highlighted in blue), LM-PCR with a primer downstream of the crRNA-45 targeting site, allowing the identification of free ends in mtDNA produced due to the impact of the mitoAsCas12a complexed with this crRNA. On the right panel (highlighted in purple), a similar approach was employed for crRNA-34, using a primer upstream of the cleavage site. As a positive control ("PC"), total DNA treated in vitro with the nuclease programmed with both crRNAs was used. As a negative control, total DNA isolated from cells subjected to siRNA and the nuclease treatment with no crRNAs transfection was utilized. LM-PCR products were visualized on a 1 % agarose gel stained with EtBr.

(C) General statistics derived from NGS analysis of the LM-PCR reactions shown in **(B)**. Total paired-read count, mtDNA alignment percentage, covered bases (number of covered bases with deph ≥ 1), coverage (percentage of covered bases), mean depth (mean depth of coverage) are shown.

(D) The depth of coverage across the reference mtDNA genome for aligned reads of the LM-PCR with a primer situated downstream of the crRNA-45 targeting site.

(E) Analogous to **(D)**, the depth of coverage analysis for NGS data obtained from the LM-PCR with a primer upstream of the crRNA-34 cleavage site.

3.4.3. PCR amplification of mtDNA molecules bearing the induced deletion

To further assess the activity of the mitoAsCas12a within mitochondria and to confirm the formation of the intended deletion, we again transfected the Su9-AsCas12a stable cell line with the two crRNAs designed to create compatible sticky ends (**Figure R11A**). This time, a broader range of control samples was incorporated, including MOCK control, samples with or without the nuclease or crRNAs, and samples with or without MGME1 knockdown.

To detect the deletion in mtDNA, we performed PCR on isolated total DNA (section **2.2.22.**) using primers flanking the deletion (**Figure R12A**, **upper panel**). We minimized the elongation step during the PCR to identify the time which allow selective amplification of shorter mtDNA molecules containing the deletion while suppressing the amplification of WT molecules (**Figure R12B**). To increase sensitivity and specificity of the detection we used Southern blot hybridization (section **2.2.28.**).

We acknowledge the possibility of the amplification of nuclear mitochondrial DNA segments (NUMTS), which could influence result interpretation. To address this concern, the primers were checked using Primer-BLAST software (NIH) before the PCR. A potential off-target sequence in the nuclear genome was identified, yielding a fragment approximately the same size as the deletion-bearing fragment (**Figure R12A**, **upper and lower panels**). This can be due to annealing of the forward primer to NUMTS region in Chromosome 6 (**Figure R12A**, **lower panel**). Hence, for the Southern blot, we utilized the reverse primer (**R1** (7831-7850) in **Figure R12A**, **upper panel**) for hybridization specific to mtDNA only.

We analysed the isolated DNA samples using this approach, and a band, corresponding to mtDNA molecules bearing the deletion in the samples treated with both components of the mitoCRISPR system, i.e., the AsCas12a nuclease and crRNAs, was revealed. Notably, the signal intensity was higher in the sample where MGME1 activity was inhibited (**Figure R12C**). Thus, we have obtained promising data regarding the creation of the intended deletion in human mtDNA using the mitoCRISPR-Cas12a system (**Figure R12C**). However, to definitively confirm the sequence of the DNA fragment, the yield of the current PCR wasn't sufficient. Aiming to amplify mtDNA fragment carrying the deletion while minimizing the amplification of the nuclear DNA, we decided to apply a Nested PCR strategy (**Green M. R., Sambrook J., 2019**; **Figure R12D**).

Following the first round of the Nested PCR with the first pair of primers (section **2.2.31.**), that were predicted to have no off-targets in the nuclear genome, we were able to detect DNA fragments of the expected size (2.3 kb, **Figure R12D**) upon agarose gel visualization only in the samples treated with both crRNAs and the nuclease, transfected or not with siRNA to MGME1 (**Figure R12E**). It is worth mentioning that numerous additional bands were also present in all the samples (**Figure R12E**). These bands could potentially arise from the degradation of mtDNA in cells or during DNA isolation and/or amplification of the nuclear DNA, even though this was not predicted bioinformatically.

Before the second round of the Nested PCR (**Figure R12D**), we purified the reactions that contained the band of interest (**samples 5, 6** in **Figure R12E**) using a commercial PCR clean-up kit, aiming to eliminate additional bands up to 1 kb (section **2.2.31.**). We also included the MOCK sample (**sample 1** in **Figure R12E**) in our further analysis as a control.

We then continued with the Nested PCR with the second pair of primers (section **2.2.31.**; **Figure R12D**). The expected band of 0.9 kb (**Figure R12D**), corresponding to the deleted mtDNA molecule, was observed in the samples treated with both the nuclease and crRNAs, as previously (**Figure R12F**). Remarkably, in the MOCK control sample, a DNA fragment of much smaller size than expected was amplified.

After extracting bands from the gel, we subjected them to digestion with XbaI restriction endonuclease (section **2.2.31.**). This step was performed to confirm the mitochondrial origin of the amplified DNA since there are two XbaI binding sites within the amplified region of mtDNA, and one of these sites should disappear upon the deletion formation (**Figure R12D**), but no XbaI sites were detected in corresponding regions of NUMTS. As expected, upon XbaI digestion, amplicon from the sample 6, treated with the AsCas12a nuclease, crRNAs, and where MGME1 activity was inhibited, was completely cleaved, confirming the amplification of mtDNA bearing the deletion (**Figure R12D**and **Figure R12F**). In the sample 5, treated with the nuclease and crRNAs, where MGME1 activity remained, DNA was also cleaved as expected, however, the cleavage was partial (**Figure R12F**). This incomplete cleavage suggests that this DNA amplicon can be heterogeneous and possibly contains contamination, originating from the nuclear DNA. In contrast, amplicon of the MOCK control sample remained uncut, further suggesting that this result is due to nonspecific amplification (**Figure R12F**).

Further, the amplicons obtained (**Figure R12F**) were analysed by Sanger sequencing. The results confirmed the presence of the mtDNA deletion induced by the mitoCRISPR-Cas12a system in

the sample 6, where MGME1 activity was inhibited (**Figure R12G**). In contrast, the amplicon obtained from the sample 5, treated with the system's components, where MGME1 remained active, exhibited an aborted termination near the crRNAs' binding sites (**Figure R12G**). We speculate that this phenomenon may come from the DNA heterogeneity within the sample, which is supported by the results of the XbaI cleavage (**Figure R12F**). DNA heterogeneity is not tolerated by Sanger sequencing and leads to sequencing abortion. Alternatively, this could be explained by mtDNA free ends degradation by MGME1.

Notably, both the forward and reverse reads, obtained from sequencing the MOCK control sample, were aligned to a short region of the mtDNA reference sequence (**Figure R12G**). No mismatches were detected, minimizing the possibility of the band originating from nuclear DNA.

Therefore, for the first time, we demonstrated the presence of a deletion in human mtDNA induced by a CRISPR-system.

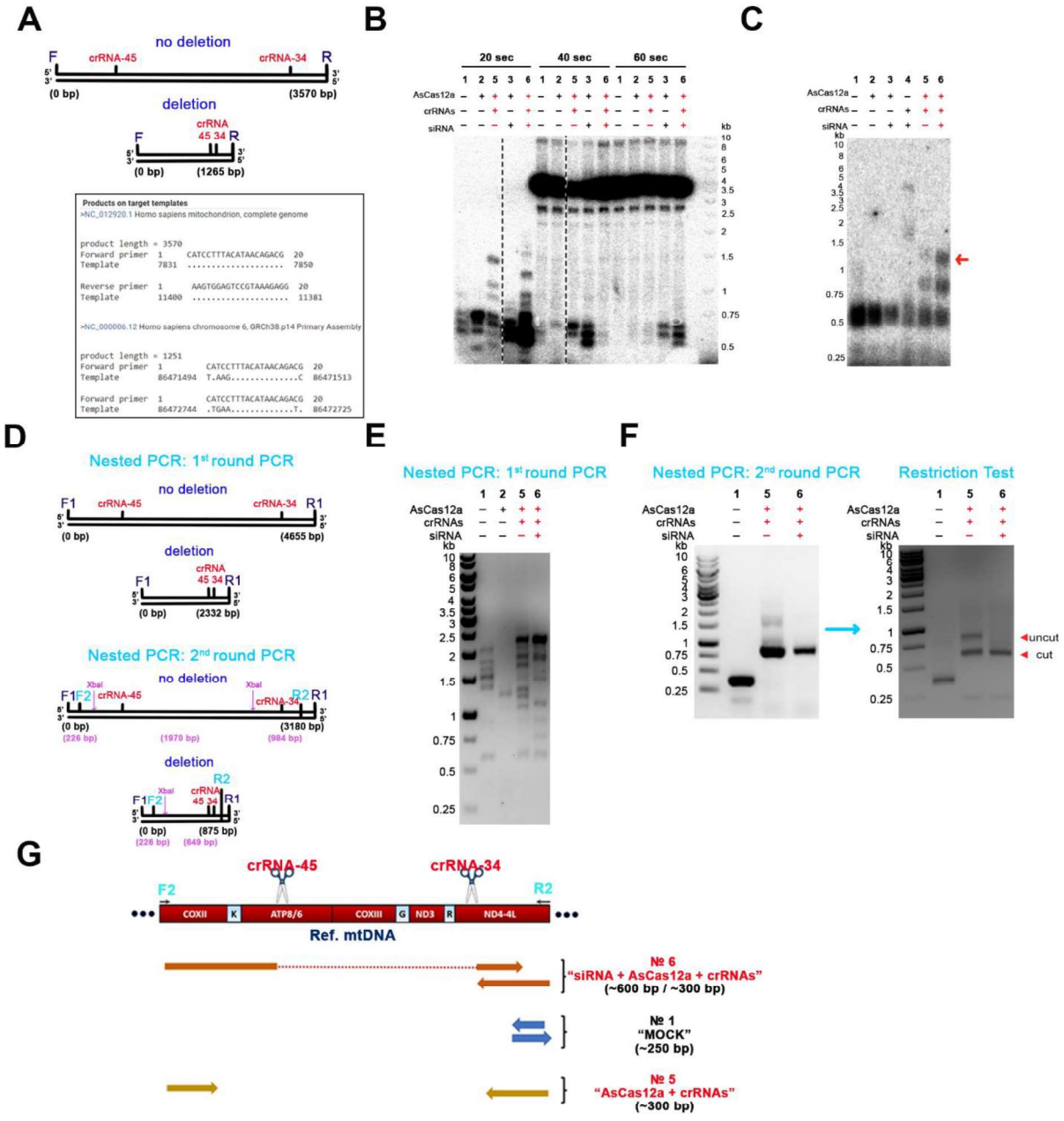

A
no deletion
F
crRNA-45
crRNA-34
R
(0 bp)
(3570 bp)
deletion
crRNA 45 34
(0 bp)
(1265 bp)
Products on target templates
>NC_012920.1 Homo sapiens mitochondrion, complete genome
product length = 3570
Forward primer 1 CATCCTTTACATAACAGACG 20
Template 7831 7850
Reverse primer 1 AAGTGGAGTCCGTAAAGAGG 20
Template 11400 11381
>NC_000006.12 Homo sapiens chromosome 6, GRCh38.p14 Primary Assembly
product length = 1251
Forward primer 1 CATCCTTTACATAACAGACG 20
Template 86471494 T.AAG.....C 86471513
Forward primer 1 CATCCTTTACATAACAGACG 20
Template 86472744 .TGAA.....T. 86472725
B
20 sec
40 sec
60 sec
AsCas12a
crRNAs
siRNA
kb
C
D
Nested PCR: 1st round PCR
no deletion
F1
crRNA-45
crRNA-34
R1
(0 bp)
(4655 bp)
deletion
(2332 bp)
Nested PCR: 2nd round PCR
XbaI
F2
R2
(226 bp)
(1970 bp)
(984 bp)
(3180 bp)
(875 bp)
(649 bp)
E
Nested PCR: 1st round PCR
F
Nested PCR: 2nd round PCR
Restriction Test
uncut
cut
G
crRNA-45
crRNA-34
F2
R2
COXII
K
ATP8/6
COXIII
G
ND3
R
ND4-4L
Ref. mtDNA
№ 6
"siRNA + AsCas12a + crRNAs"
(~600 bp / ~300 bp)
№ 1
"MOCK"
(~250 bp)
№ 5
"AsCas12a + crRNAs"
(~300 bp)

Figure R12. Detection of the Deletion in Human mtDNA Induced by the mitoCRISPR-Cas12a System.

(A) Upper panel, scheme of a PCR with primers (F and R) flanking the mtDNA deletion. The sizes of expected PCR products are indicated in brackets. Binding sites for crRNAs 34 and 45 are shown. Lower panel, F and R primers analysis for the non-specific amplification using Primer-BLAST software (NIH).
(B) Extracted DNA from the cells as indicated above the gel was used for the PCR optimization for the shorter fragments detection with primers F and R **(A)** followed by Southern blot hybridization. Elongation time used in the PCR is indicated above. The numbers of the samples (1-6) are consistent throughout the figure.
(C) Extracted DNA from the cells as indicated above the gel was used for the PCR with primers F and R **(A)** and the products were visualized by Southern blot hybridization. Fragment of mtDNA bearing the deletion is marked with the red arrow.
(D) Design of Nested PCR amplification for mtDNA. The sizes of expected PCR products in the case of the deletion or not are indicated in black brackets. Binding sites for crRNAs 34 and 45 and XbaI endonuclease recognition sites, are shown in red. The size of the fragments after digestion with XbaI are indicated in brackets colored in purple.
(E) First round of Nested PCR with primers F1 and R1, specifically designed to prevent the amplification of nuclear DNA.
(F) Second round of Nested PCR with t primers F2 and R2 (left panel). The amplicons were subsequently treated with XbaI endonuclease (right panel).
(G) Results of Sanger sequencing of the mtDNA amplicons obtained after the second round of Nested PCR **(F)**. The sequences are shown by arrows, their orientation indicating whether they are obtained from forward (from F2) or reverse (R2) primer. The approximate size of reads obtained for each sample is indicated within brackets. The absence of the nucleotides correspondAng to expected deletion are shown by dotted line.

3.4.4. NGS validation of the deletion boundaries

Our next objective was to perform NGS to confirm the data obtained from Sanger sequencing regarding the deletion formation. For this, we repeated the procedure of the Su9-AsCas12a stable cell line transfection with crRNA-34 and crRNA-45, as previously detailed (**Figure R11A**). For this experiment, we included a set of control samples as before: MOCK control, samples treated with or without the nuclease or crRNAs, and samples with or without inhibited MGME1 exonuclease activity. But this time, each sample had three biological replicates to ensure statistical validity for further analysis.

Before mtDNA analysis, we checked the Su9-AsCas12a nuclease expression and the knockdown of MGME1 expression using Western blot hybridization (section **2.2.4.**). The results show that, as expected, the samples treated with tetracycline demonstrated the Su9-AsCas12a nuclease expression, while the MGME1 expression level was noticeably reduced in all the samples following siRNA treatment (**Figure R13A**).

We also performed total DNA isolation (section **2.2.22.**) and examined whether the treatment of the cells with the nuclease and both crRNAs influenced the mtDNA copy number (section **2.2.23.**). However, 48 hours post-exposure to the mitoCRISPR-Cas12a system, there were no significant changes in mtDNA copy number (**Figure R13B**). This outcome was consistent with the previous observation when cells were treated with the nuclease and a single crRNA targeting mtDNA (**Figure R8E**).

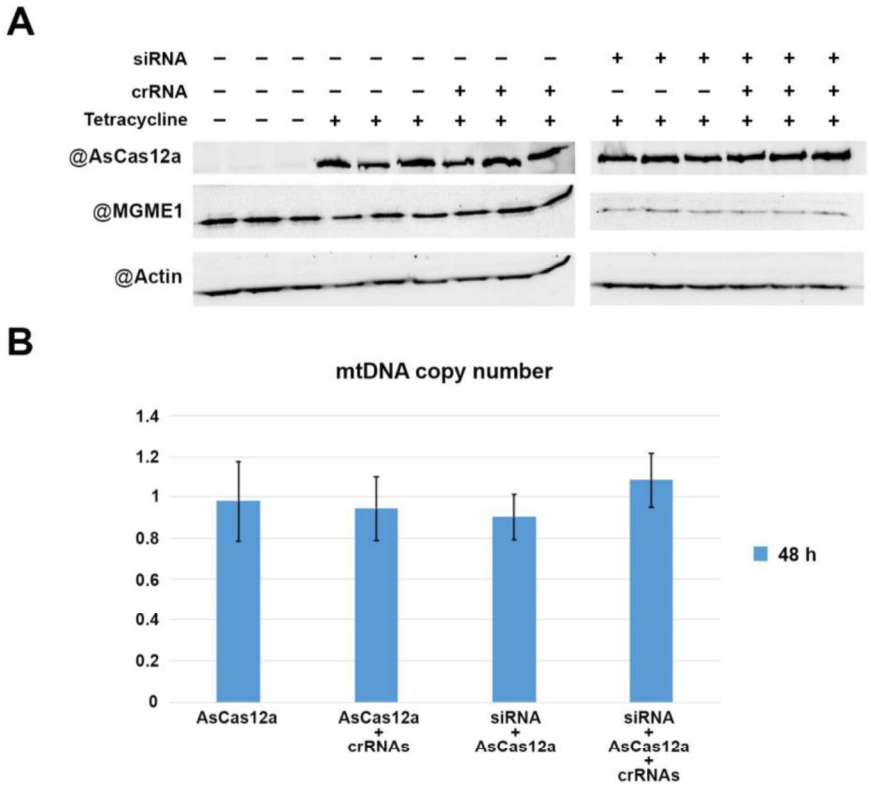


Figure R13. Characterization of a New Series of Samples for the Detection of the Deletion in Human mtDNA Induced by the mitoCRISPR-Cas12a System.

(A) Analysis of the AsCas12a expression and the knockdown of MGME1 by Western blot of total lysates from the Su9-AsCas12a stable cell line, prepared 48 hours after Su9-AsCas12a induction and transfection with crRNAs as indicated above the gel.
(B) qRT-PCR analysis of mtDNA copy number in the Su9-AsCas12a stable cell line 48 hours after treating the cells with siRNA to MGME1, the Su9-AsCas12a and crRNA-34 and 45. Relative mtDNA copy number was quantified using the 2−ΔΔCT method. MOCK transfection of the stable cell line was used for normalization (mtDNA copy number = 1). Mean values with standard deviations are present; n = 3.

Although we did not observe changes in mtDNA copy numbers, we had previously obtained evidence of the modified CRISPR system's activity within human mitochondria. So, to detect the deletion induced by AsCas12a in complex with two crRNAs, we proceeded with further analysis of isolated total DNA.

We applied the previously mentioned strategy of Nested PCR (section **2.2.31.**) to obtain material for subsequent NGS analysis. Prior to the library preparation, the samples were purified with

magnetic beads to perform size-selection and eliminate contaminant bands less than 500 bp. The successful removal of the short fragments was validated with BioAnalyzer.

The obtained reads were analyzed and aligned to the reference human mtDNA genome (section **2.2.30.**). Here we show the data obtained on a single replicate of each experiment. In all the samples nearly 100% of all reads were aligned to mtDNA (**Figure R14A**). Notably, the number of covered bases was lower in the samples treated with the nuclease and both crRNAs, with or without the knockdown of MGME1 (**Figure R14A**).

Next, we visualized the obtained alignments using Integrative Genomics Viewer (IGV). Upon initial inspection of the coverage profiles across the samples, we noticed a significant increase in the depth of coverage near the primer binding sites used for amplification in all the NGS samples (**F2** and **R2** in **Figure R12D**; **Figure R14C-G**), as it was observed previously with Sanger sequencing (**Figure R12G**for the samples “MOCK” and "ACs12a + crRNAs"). Consequently, the coverage profiles exhibited a drop in the middle of the aligned region, even when reads covering this region were present (from 200 to 3000 reads) (**Figure R14C-G**). The enrichment of coverage at the primer binding sites may be attributed to possible contamination of the samples with the primers or short primer-containing fragments, despite conducting the size-selection prior to NGS. Alternatively, this phenomenon could be a result of non-specific primers annealing to either mtDNA or nuclear DNA, resulting in the formation of short amplicons. In any case, these reads significantly complicated the accurate interpretation of the obtained data.

Nevertheless, we can see a clear difference between control samples and mtDNA from cells expressing the mitoAsCas12a nuclease and transfected with crRNAs.

The Type V CRISPR-AsCas12a system is expected to cleave DNA at nucleotide positions 17th–19th downstream of the PAM on the non-target DNA strand, as well as at the 21st – 23rd positions of the target strand, generating 3–5 nucleotide-long 5'-overhangs. (**Figure R14B**).

In the sample from the cells treated with the Su9-AsCas12a nuclease, crRNAs and siRNA against MGME1, the cleavage ends were mapped precisely at the expected nucleotide positions for crRNA-45 and crRNA-34 (**Figure R14B**, **Figure R14C, upper panel**).

Closer analysis of the cleavage sites revealed that upon the expected deletion formation, two types of nucleotide rearrangements occurred (**Figure R14C, lower panel**). In 80% of the reads the cleavage happened after nucleotides 8622/10927 giving the sequence “TCCTCC’ at the

deletion boundaries. Nevertheless, we observed that two nucleotides (8621(C), 8622(C)) were missing. This can be explained by the 3'-5' exonuclease activity of PolG. Another possibility of such a minor deletion formation can be due to DSB reparation by MMEJ mechanism (see **Figure I8**). In any case, more convincing data should be provided from the analysis of several biological replicates.

In another 20% of the reads, we detected duplication of the overhangs created by the AsCas12a nuclease cleavage, resulting in "CCT/ACCTCCTCC" (**Figure R14C, lower panel**). Interestingly, we observed T/A heterogeneity of nucleotide corresponding to mtDNA nucleotide position 8623/10928, which can be explained by the natural variations of the AsCas12a nuclease cleavage site (**Figure R14B**).

In the sample containing AsCas12a and both crRNAs, but no siRNA against MGME1, the coordinates of the main drop in the depth of coverage also matched the expected sites (**Figure R14D**). For crRNA-45, the cleavage occurred after 8622 bp, and for crRNA-34, after 10927 bp, each cutting 17 nucleotides after the PAM for the non-target DNA strand (**Figure R14D, lower panel**). Despite the rapid degradation of linearized mtDNA molecules in the presence of active MGME1, a surprisingly high amount of mtDNA molecules were able to ligate to form the intended deletion (**Figure R14D**).

In the control sample containing AsCas12a nuclease alone (**Figure R14E**), the main drop in coverage was seen at positions 9348 bp and 10838 bp of the reference mtDNA genome. This raises the question of whether another naturally occurring mtDNA variant with a deletion was preferentially amplified due to the reduced PCR elongation time, or if this deletion resulted from the non-specific cleavage by AsCas12a nuclease without its crRNA (**Figure R14E**). It is worth noting that the coordinates of the deletion in this sample also did not correspond to the cleavage sites of crRNA-34 and crRNA-45 (**Figure R14B**). Considering the fact that MGME1 exonuclease was not inhibited in the sample, it means that if a break in mtDNA occurred, its extremities should be degraded by MGME1. Noteworthy, similar deletion was observed in the sample containing both AsCas12a and crRNAs (**Figure R14D**), however, in the presence of crRNAs, the cleavage occurred mostly at the crRNA-targeted sites rather than at non-specific ones (compare **Figure R14D** and **E**).

Regarding the other control treated with the AsCas12a nuclease and siRNA to inhibit the expression of MGME1 exonuclease, the coordinates of the main drop in coverage did not correspond to the crRNAs binding sites (**Figure R14F**).

In the MOCK control sample (**Figure R14G**), the drop in the depth of coverage also occurred at coordinates different from the expected cleavage positions of crRNA-45 and crRNA-34 (**Figure R14B**). The left peak appeared at 8355 bp, which is before the AsCas12a cleavage site in complex with crRNA-45. The right peak at 9938 bp was considerably ahead of the expected cleavage site of the nuclease with crRNA-34. This suggests the possibility of a naturally occurred deletion in mtDNA in the Su9-AsCas12a stable cell line, which was also amplified during Nested PCR. Interestingly, the observed "empty" deleted region between 9 and 9.3 kb showed a similar pattern as in the control treated with the AsCas12a nuclease and siRNA (**Figure R14F**), suggesting the existence of an mtDNA variant carrying a small deletion.

We have to admit that our approach of Nested PCR resulted in detection of mtDNA deletions of different size even in control cells. Further analysis of other replicates is necessary to obtain statistically significant data and to better understand the source of the additional breaks in mtDNA. Nevertheless, only in cells transfected with two crRNAs we clearly observed deletion in mtDNA which boundaries corresponded to expected cleavage by Su9-AsCas12a/crRNA complex.

In summary, for the first time, using both Sanger and next-generation sequencing, we have demonstrated that a deletion in human mtDNA can be induced by a CRISPR/Cas system targeted to mitochondria.

A

Sample	Reads paired-end	Mito Aligned	Covered Bases	Coverage	Mean Depth
MOCK	60176	98.76%	4403	26.57	402.37
AsCas12a	69741	98.85%	4156	25.083	467.15
siRNA + AsCas12a	112499	97.57%	4411	26.62	698.41
AsCas12a/crRNAs	102378	97.84%	3470	20.94	628.27
siRNA + AsCas12a/crRNAs	64351	98.45%	2461	14.85	404.89

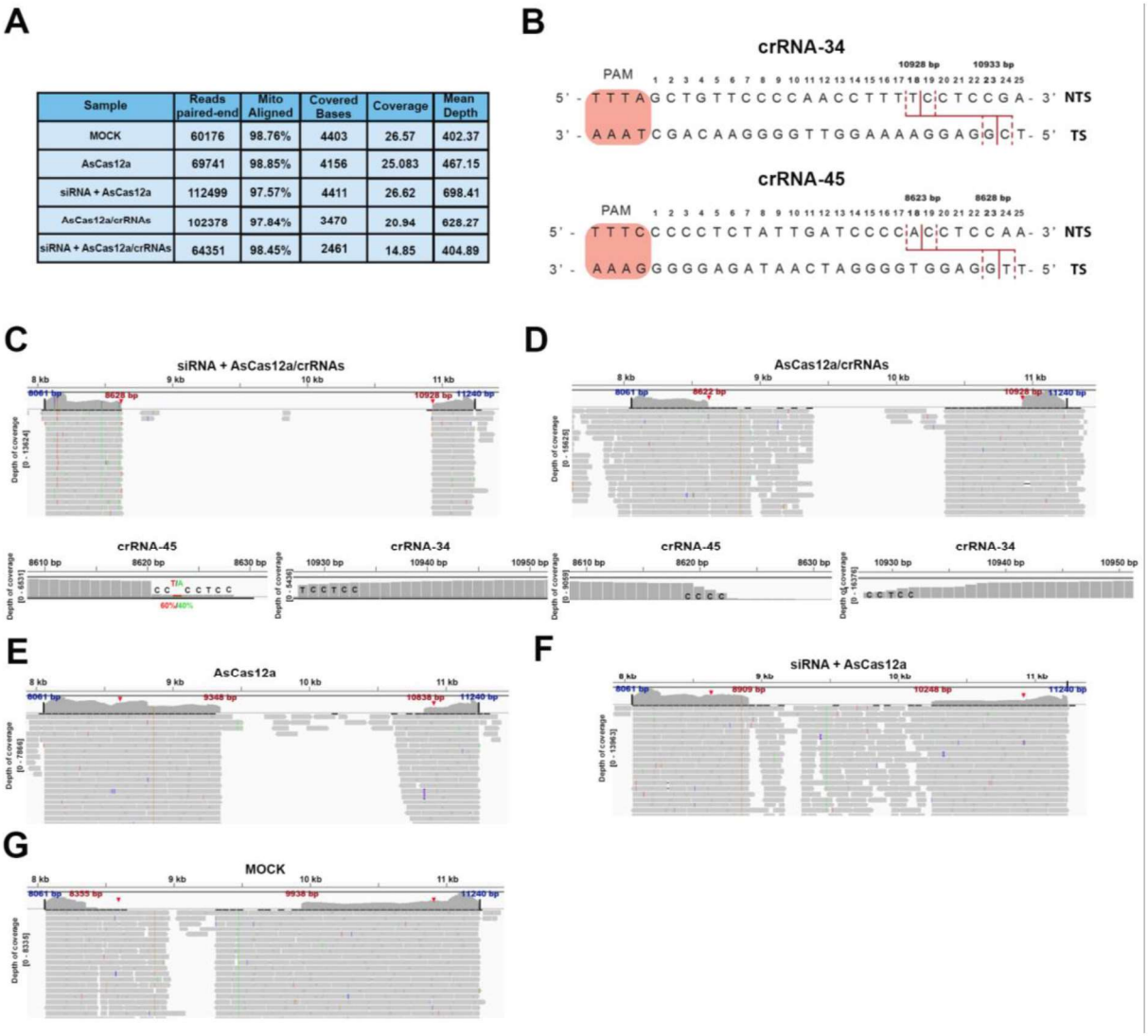


Figure R14. Detection of the Deletion in Human mtDNA Induced by the mitoCRISPR-Cas12a System by NGS.

(A) General statistics derived from NGS analysis of the Nested PCR reactions (**Fig. R12D**) on total DNA obtained from the samples shown in **Fig. R13**. These includes, total paired-read count, mtDNA alignment percentage, covered bases (number of covered bases with deph ≥ 1), coverage (percentage of covered bases), mean depth (mean depth of coverage).
(B) Representation of cleavage sites in mtDNA induced by AsCas12a in complex with crRNA-34 (upper panel), and crRNA-45 (lower panel), designed to leave compatible sticky ends. The Type V CRISPR/AsCas12a system recognizes AT-rich PAM sequences (shown in red) and cleaves DNA at nucleotide positions 17–19 downstream of the PAM on the non-target DNA strand ("NTS"), as well as at the 21st – 23rd positions of the target strand ("TS"), generating 3–5 nucleotide-long 5'-overhangs. Red lines represent the possible DNA cleavage events, the less frequent cuts are shown with dotted lines. The corresponding nucleotide positions in human mtDNA are shown above.
(C – G) Coverage profiles of mtDNA visualized with IGV: for **(C)** the nuclease with crRNAs and with inhibited MGME1 activity. Coverage depth for each sample is displayed alongside the panels. mtDNA coordinates are above the panels, with primer start points in blue and potential deletion sites in red. The red arrowes indicate the expected cleavage sites for the AsCas12a nuclease in complex with crRNAs, were present. On lower panel, zoomed view of mtDNA ends generated by the mitoCRISPR system **(C)**, including sequences of nucleotides at the boundaries and percentage of base frequency in case of mismatches; **(D)** the nuclease with crRNA-45 and 34, including zoomed view of mtDNA ends on the deletion boundaries on the lower panel, as for **(C)**; **(E)** the Su9-AsCas12a nuclease-treated; (F) the nuclease and MGME1 siRNA-treated; (G) "MOCK" control.

4. CONCLUSIONS AND PERSPECTIVES

Mitochondria are essential organelles of eukaryotic cells. Among their many functions, the production of energy in the form of ATP, which takes place in the mitochondrial respiratory chain through the process of oxidative phosphorylation, is of primary importance. Although most of the macromolecules found in the organelle are encoded by the nuclear genome, mitochondria also contain their own genome, mtDNA. Pathogenic mutations in mtDNA cause a broad spectrum of mitochondrial diseases, often associated with neuromuscular disorders. These pathologies have not found adequate treatment yet (**Rahman J. & Rahman S., 2018**).

Each cell harbors just one nuclear genome and hundreds of mitochondrial ones. Most mtDNA mutations are "heteroplasmic", which means that mutant and wild-type mtDNA molecules coexist within the same cell. Thus, the phenotypic expression of these mutations is very closely correlated with heteroplasmy level, and the appearance of the defects will be observed only when this level exceeds a certain threshold (**Nissanka N. & Moraes C. T., 2020**).

The only described approaches for mutant mtDNA elimination in human cell lines use site-specific nucleases, namely, mitochondria-targeted restriction endonucleases, mitoZinc-fingers, and mitoTALENs (**Publication 1**). The last two systems were recently employed for mtDNA editing in order to reverse mutations without introducing a break in mtDNA. Yet, all these approaches are based on specific protein–nucleic acid interactions. An interesting therapeutic strategy to shift mutant mtDNA heteroplasmy level could consist in modifying CRISPR-Cas systems for their import and functioning in human mitochondria. Such systems may be more flexible due to their reliance on RNA-DNA interaction for the specific mtDNA site recognition. However, not only the Cas nuclease but also the guide RNA molecules must be efficiently targeted to the organelle. Recently, my host team has developed such a mitochondrial CRISPR/Cas9 system, but a shift of the heteroplasmy level has not been achieved.

During this thesis project, we concentrated our efforts on the Type V CRISPR-Cas12a system, namely, AsCas12a, characterized by shorter crRNAs, which may represent a better substrate for mitochondrial import compared to longer sgRNA of the Type II CRISPR-Cas9 system.

4.1. Import of AsCas12a nuclease into human mitochondria

To evaluate mitochondrial import of the AsCas12a nuclease and obtain the controlled expression, we developed a monoclonal cell line with tetracycline-inducible expression of the mitoAsCas12a bearing COX8a MTS. We analyzed different subcellular fractions using Western blot and confirmed the presence of the modified AsCas12a nuclease in human mitochondria. However,

immunofluorescent microscopy also showed a double localization of the mitoAsCas12a bearing COX8a MTS, namely, in mitochondria and the cytosol.

In order to improve mitochondrial localization of the nuclease, we tried two strategies: 1) to decrease protein expression level to prevent its aggregation in cytosol and 2) use other mitochondrial targeting signals. Using site-directed mutagenesis, a deletion of CMV promoter region was introduced in a plasmid vector encoding AsCas12a nuclease fused with the COX8a MTS. The decrease in the nuclease expression level was confirmed by Western blot approach. Regarding the MTS, together with COX8a MTS, we compared MTS from *Neurospora crassa* ATPase subunit 9 (Su9), MTS from mammalian autophagy-related cysteine peptidase 4D (ATG4D) and from superoxide dismutase 2 (SOD2). By implementing the site-directed mutagenesis technique, we obtained plasmid constructs encoding AsCas12a bearing various MTS. Mitochondrial import of the 4 versions of mitoAsCas12a protein under the control of full-size or shortened promoter region was tested using immunofluorescent laser scanning microscopy.

Decreasing the nuclease expression level in mammalian cells did not eliminate the protein's partial cytosolic localization. On the other hand, the AsCas12a nuclease fused with Su9 MTS provided the best mitochondrial colocalization profile with the absence of the protein in the cytosol.

Thus, we created a new stable cell line that expresses AsCas12a with an improved mitochondrial localization. The expressed nuclease in the created stable cell line was confirmed to be perfectly colocalized with mitochondria by submitochondrial fractionation and Western Blot and by immunofluorescent microscopy. The Su9-AsCas12a nuclease activity in the stable cell line was evaluated using *in vitro* cleavage tests. The influence of the mitoAsCas12a expression on mitochondria was addressed, and no detectable effects on mitochondrial respiration or translation were observed following the activation of the nuclease expression. However, it will be important to repeat the respiration test to obtain statistically significant data.

Following the expression of the Su9-AsCas12a nuclease, no evidence of mitophagy induction was found. To further confirm this observation, future studies should address this point by including a positive control for mitophagy, such as treating cells with a chemical uncoupler like FCCP. Another approach to assess mitophagy could involve analyzing the colocalization of mitochondria with lysosomes and autophagosomes through live-cell fluorescence microscopy, which should be increased in the case of mitophagy.

Although we have not observed the mitoAsCas12a in the nucleus thus far, as a precautionary measure to prevent any potential nuclear localization and possible off-target editing within the

nucleus, we can consider incorporating a nuclear export signal (NES) at the carboxy terminus of the protein (**Gammage, P. A. *et al.*, 2014**).

4.2. Import of AsCas12a crRNA into human mitochondria

Next, we investigated the import of CRISPR-Cas12a system crRNAs into human mitochondria and studied the structural requirements for this process by northern blot hybridization of RNA isolated from nucleases-treated mitoplasts. Studies by our and other laboratories had shown that the motif required for the transport of RNA molecules into mitochondria is not a sequence, but a hairpin structure (**Kolesnikova, O. *et al.*, 2010**; **Wang, G. *et al.*, 2010**). To investigate whether the fusion of crRNA with known RNA import determinants (MLS) improve its mitochondrial targeting, we added MLS hairpin structures at 3'-end of crRNA and demonstrated that this did not impact crRNA ability to program specific cleavage of DNA in lysate of human cells expressing the AsCas12a nuclease. Surprisingly, mitochondrial localization of the fused crRNA molecules was not improved compared to non-modified version, indicating that structured scaffold domain of crRNA can probably function as MLS, assuring crRNA mitochondrial import.

We designed a series of crRNAs targeting different regions of mtDNA and demonstrated their ability to program specific cleavage of mtDNA fragments in cell lysate and their partial localization in mitochondrial matrix in human cells transfected with these RNA molecules. According to the obtained data, we hypothesized that mitochondrial import of these crRNAs may depend on their secondary structure/sequence.

To further confirm the data on the mitochondrial targeting of AsCas12a crRNAs' secondary structure, we performed additional import tests using a recently developed in our laboratory method for submitochondrial fractionation of RNA (**Jeandard, D. *et al.*, 2022**). We demonstrated mitochondrial import of AsCas12a crRNAs using HEK293 cells, the Su9-AsCas12a stable cell line and 143B osteosarcoma cells, indicating that this pathway does not depend on the expression of the hAsCas12a nuclease and is not cell line-specific (**Publication 2**).

We currently have a collection of 27 crRNAs targeting various regions of mtDNA. In perspective, we should continue evaluating their mitochondrial import to corroborate the observed findings regarding structural requirements for AsCas12a crRNAs import.

Aiming to improve crRNAs import efficiency, AsCas12a crRNA was split into two individual 20 bp moieties (scaffold and spacer RNAs). We demonstrated that split crRNA catalyzed highly specific and efficient cleavage of target DNA (**Publication 3**). These observations were also confirmed in lysates of human cells expressing AsCas12a. The newly discovered Type V CRISPR-RbCas12a

system was also found to possess the same abilities in utilizing split crRNA. We compared the mitochondrial import of crRNA-45 and its spacer part and found that the spacer part of crRNA can be targeted into human mitochondria. We therefore believe that the split AsCas12a crRNA variant could be used in further *in vivo* experiments for mtDNA targeting.

As an alternative strategy to enhance the mitochondrial import of AsCas12a crRNAs, crRNAs with chemical modifications at the 3' end (cholesterol, rhodamine R6G, and berberine) were synthesized and tested. In an *in vitro* cleavage assay with the purified recombinant AsCas12a nuclease, all complexes of the modified crRNAs with the recombinant protein were capable of cutting the DNA template. However, evaluation of their mitochondrial import demonstrated that all modified crRNAs appeared to be protected from the nuclease treatment per se. We therefore were not able to conclude about mitochondrial import of the chemically-modified crRNAs in the used experimental conditions.

It's worth noting that this strategy was initiated during my thesis work but was not finalized. We believe that obtaining concrete evidence regarding the mitochondrial import of different crRNAs can only be achieved through a direct demonstration of specific mtDNA cleavage *in vivo*.

4.3. Functional assessment of the mitoAsCas12a system functionality *in vivo*

The most important part of the project, representing the proof-of-concept consisted in the detection of specific cleavage in mtDNA induced by the mitoCRISPR system.

To start with, we investigated the mtDNA copy number in the newly developed stable cell line. Using qPCR analysis of total DNA isolated from cells treated with the Su9-AsCas12a and its crRNA targeting a specific mtDNA site at various time points, we did not observe any decrease in mtDNA copy number. This result remained the same when the cells were treated with the nuclease in complex with two crRNAs targeting mtDNA, contrary to what was previously reported for the SpCas9 nuclease with two gRNAs (**Loutre, R. *et al.*,2018**).

We hypothesize that the efficiency of the system is limited by the import of RNA system component into mitochondria. If cleavage did occur, it was not sufficient enough to cause a measurable shift in mtDNA copy number. Definitely, the conditions of this experiment need further adjustment and optimization. For example, we can assess mtDNA copy numbers after several rounds of treating the cells with the mitoCRISPR system, using crRNAs that target different sites within mtDNA, potentially incorporating the chemical modifications. Testing several concentrations of crRNA during transfection may also enhance the effect, together with the use

of more efficient AsCas12a variants that also possess less off-target activity (**Kleinstiver, B. P. *et al.*, 2019**; **Zhang, L. *et al.*, 2021**).

While we previously did not detect a reduction in mtDNA levels following the application of the newly developed mitoCRISPR system, our objective was to establish a proof-of-concept by confirming specific cleavage events in human mtDNA induced by the crRNA-programmed nuclease activity of the Su9-AsCas12a *ex vivo*. We tried to achieve this using more sensitive approaches.

In order to confirm specific crRNA-programmed nuclease activity of mitoAsCas12a *ex vivo*, we applied a published strategy for free mtDNA ends detection consisting in next-generation sequencing of linker-ligated mtDNA (**Peeva, V. *et al.*, 2018**). To inhibit the rapid degradation of linearized mtDNA, the mitochondrial exonuclease (MGME1) was inactivated with siRNA (**Peeva, V. *et al.*, 2018**) prior transfecting the stable cell line, expressing the mitoAsCas12a, with crRNA-45.

Before proceeding to NGS, we conducted an *in vitro* cleavage test in lysed mitochondria, isolated from the treated cells. This test revealed specific cleavage of an mtDNA fragment, confirming the presence of the nuclease and its crRNA inside the mitochondria. This experiment should be repeated, with the additional step of treating isolated mitochondria with RNases to eliminate the possibility of contamination by crRNA molecules adhering to mitochondria from the cytosol.

For NGS analysis, isolated mtDNA was ligated to an asymmetric double-stranded linker with a known sequence to label mtDNA breaks. Following library preparation and NGS, the obtained reads were aligned to sample-specific reference mitochondrial sequences and screened for the linker sequence. The analysis revealed a 2-4 fold increase in mtDNA fragmentation in samples treated with the nuclease and crRNA compared to control samples. Unfortunately, due to the low mtDNA enrichment (1-3%) in the samples, the mtDNA coverage was insufficient to identify the specific cleavage at the expected position in mtDNA.

We then repeated NGS of linker-ligated mtDNA under the same conditions, but this time, the cells were treated with crRNAs targeting a different region in mtDNA, specifically MT-COX1. To detect free ends in mtDNA, we performed linker-mediated PCR on total DNA isolated from the cells before NGS. Following the LM-PCR, we conducted Southern blot hybridization with an mtDNA probe, revealing PCR fragments of the expected size in the samples treated with the nuclease and crRNAs, thus confirming the cleavage.

Upon analyzing the NGS data, we once again observed a significant increase in mtDNA breaks compared to the controls. Unfortunately, despite the slightly higher percentage of mtDNA in the samples (2-8%), we were not able to visualize the cleavage sites at the expected positions within mtDNA. Therefore, further optimization of mitochondrial and mtDNA purification techniques is required. One potential approach is to use magnetic beads coated with antibodies against TOMM20 for mitochondria isolation, which can enhance mitochondria and mtDNA purity while minimizing nuclear DNA contamination.

To further evaluate the activity of the mitoAsCas12a in mitochondria, the stable cell line was transfected with two crRNAs designed to leave compatible sticky ends to detect a deletion induced by the mitoCRISPR-AsCas12a system. We believed that this experimental design would facilitate the detection of the system's impact on mtDNA.

Through NGS after LM-PCR, we successfully detected cleavage induced by one of the crRNAs (crRNA-45). Unfortunately, for the second crRNA (crRNA-34), we observed the same break in the control sample, suggesting that it might have occurred during the mtDNA isolation procedure or due to the non-specific activity of the AsCas12a nuclease. To address this issue, we plan to repeat the experiment including cells treated with the DNase-dead AsCas12a, serving as a negative control.

PCR of isolated DNA with primers flanking the deletion were analyzed using Southern blot hybridization, revealing the expected band corresponding to the mtDNA molecule bearing the deletion in the samples containing the mitoCRISPR system. To increase the PCR sensitivity, we designed and performed a Nested PCR. The obtained DNA was enough to perform Sanger sequencing which confirmed the presence of mtDNA deletion induced by the system. Subsequent NGS confirmed the Sanger sequencing data obtained regarding the deletion. We could see a clear difference between control samples and mtDNA from cells expressing the mitoAsCas12a nuclease and transfected with crRNAs. Moreover, through the analysis of the crRNAs' cleavage sites, we were able to precisely identify the cleavage positions induced by the system.

In the sample from the cells treated with the Su9-AsCas12a nuclease, crRNAs and siRNA to MGME1, the cleavage ends were mapped precisely at the expected nucleotide positions for crRNA-45 and crRNA-34, confirming the intended deletion. However, closer analysis of the deletion borders revealed duplication of the sticky overhangs formed by AsCas12a in 20% of the cases. In the majority of the reads (80%), we observed that two nucleotides were missing.

This is unclear which molecular mechanisms can be implicated in these rearrangements. One can hypothesize, the role of the 3'-5' exonuclease activity of PolG or double-stranded break reparation by micro-homology mediated end joining mechanism, which usually causes nucleotides deletions (**Fontana G. A., Gahlon H. L., 2020**). Regarding the observed duplication, it could possibly occur due to the sticky ends being filled-in by DNA polymerase following blunt-end ligation. Further analysis of biological replicates of this experiment will allow us to understand the fate of mtDNA after CRISPR/Cas12a cleavage. Certainly, essential control including the use of the DNase-dead AsCas12a as a negative control, should be included to ensure the reliability of our findings.

We also suppose that the PCR approach we initially selected to detect mtDNA deletions, which involved the minimized elongation time, may not have been optimal since it resulted in amplification of pre-existing deletions in mtDNA that had naturally occurred. To address this issue, we plan to perform PCR-free NGS of the whole mtDNA. This approach will not only eliminate the problem of amplifying natural deletions but also allow us to accurately quantify the mtDNA molecules bearing deletions induced by the mito-AsCas12a. Additionally, we are considering using qPCR with primers specific to mtDNA outside of the deletion region and either within the deletion region or flanking it, as another approach to estimate the efficiency of deletion formation.

In our analysis of human mtDNA, we have identified 30 pairs of crRNAs able to generate compatible sticky ends, four located on the heavy mtDNA strand and 26 on the light strand. These crRNAs will be used to induce various deletions in mtDNA. Furthermore, it would be particularly intriguing to investigate whether an mtDNA deletion can be induced by AsCas12a in complex with crRNAs that do not produce cohesive ends or by the SpCas9 nuclease that introduces double-stranded blunt DNA ends.

The Type V CRISPR-Cas12a system has shown potential as a tool for creating deletions in mtDNA. This capability opens opportunities for generating cybrid cell lines or even animal models bearing induced deletions in mtDNA, which can allow studying their dynamics and physiological effect.

CONCLUSIONS:

- The Su9 MTS was proven to provide the best mitochondrial localization for AsCas12a nuclease;
- Using Flp-In recombinant system, we created a stable HEK cell line expressing the Su9-AsCas12a in a tetracycline-inducible way, which was shown to be enzymatically active and perfectly localized within mitochondria;
- We demonstrated that mitochondrial import of crRNAs does not require an additional MLS, while the import of crRNAs targeting different regions in human mtDNA varies depending on their secondary structure;
- Split crRNA demonstrated highly specific and efficient cleavage of target DNA, and at least spacer part of split crRNA was found to be imported into mitochondria;
- Next generation sequencing of linker-ligated mtDNA demonstrated increase of breaks in mtDNA in cells, expressing the mitoAsCas12a-crRNA system;
- In cells, expressing the ascas12a and transfected with crRNAs, we detected specific mtDNA cleavage by LM-PCR coupled with Southern blot and NGS;
- For the first time, we demonstrated the presence of a deletion in human mtDNA induced by a CRISPR-system using Sanger sequencing and NGS of mtDNA amplicons.

PERSPECTIVES:

- Evaluate the efficiency of mtDNA deletion formation induced by the mitoCRISPR system by using qPCR and NGS;
- Analyze the mitoCRISPR-AsCas12a off-target effects on mitochondrial and nuclear DNA using whole mtDNA sequencing;
- Improve the mitoCRISPR system mtDNA cleavage efficiency by: 1) Optimization of crRNA mitochondrial import by introducing chemical modifications and by the use of split crRNA molecules; 2) Use of engineered Cas12a nucleases with enhanced cleavage activity and specificity;
- Apply developed strategy of induction of mtDNA deletions to generate cellular and animal models for studies of deletions propagation and their pathogenic effects and possible therapeutic approaches;
- Apply the mitoCRISPR-AsCas12a system to shift the heteroplasmy level in human cells bearing pathogenic mutations in mtDNA.

LIST OF ARTICLES:

1) "Future of human mitochondrial DNA editing technologies", Verechshagina, N., **Nikitchina, N.**, Yamada, Y., Harashima, H., Tanaka, M., Orishchenko, K., & Mazunin, I. (2019). Mitochondrial DNA Part A, 30(2), 214-221. **DOI:** 10.1080/24701394.2018.1472773 **(Published)**

2) "Efficient target cleavage by Type V Cas12a effectors programmed with split CRISPR RNA", Shebanova, R. & **Nikitchina, N.**, Shebanov, N., Mekler, V., Kuznedelov, K., Ulashchik, E., Vasilev, R., Sharko, O., Shmanai, V., Tarassov, I., Severinov, K., Entelis, N., Mazunin, I. (2022). Nucleic acids research, 50(2), 1162-1173. **DOI:** 10.1093/nar/gkab1227 **(Published)**

3) "Targeted Modification of Mammalian DNA by a Novel Type V Cas12a Endonuclease from *Ruminococcus bromii*", Vasilev, R., Gunitseva, N., Shebanova, R., Korzhenkov, A., Vlaskina, A., Evteeva, M., Polushkina, I., **Nikitchina, N.**, Toschakov, S., Kamenski, P., Patrushev, M., Mazunin, I. (2022). International Journal of Molecular Sciences, 23(16), 9289. **DOI:** 10.3390/ijms23169289 **(Published)**

4) "Targeting of CRISPR-Cas12a crRNAs into human mitochondria", **Nikitchina, N.**, Ulashchik, E., Shmanai, V., Heckel, A. M., Tarassov, I., Mazunin, I., Entelis, N. (2023). Biochimie **(Accepted)**

5) "Use of the type V CRISPR-Cas system to induce a deletion in human mitochondrial DNA", **Nikitchina, N.**, Heckel, A. M., Smirnova, A., Shebanov, N., Ulashchik, E., Shmanai, V., Tarassov, I., Mazunin, I., Entelis, N. **(In preparation)**

LIST OF CONFERENCES:

1) *The 11th World Congress on Targeting Mitochondria 2020*, 28 – 30 October 2020, online conference: «Use Of The Type 2 Crispr-Cas System For Human Mitochondrial Genome Editing», **Natalia Nikitchina**, Ilya Mazunin, Nina Entelis, Ivan Tarassov **(Oral)**

2) *"The Doctoral School Days 2021" (ED Days 2021)*, organized by the University of Strasbourg, 1 – 2 April 2021, Strasbourg, France: «Efficient target cleavage by Type V Cas12a effector

programmed with split CRISPR RNA», **Natalia Nikitchina**, Nina Entelis, Konstantin Severinov, Ilya Mazunin **(Poster)**

3) *CRISPR and Translational Medicine Congress*, organized by the University of Bordeaux, March 31 – 1 April 1 2022, Bordeaux, France: «Efficient target cleavage by Type V Cas12a effector programmed with split CRISPR RNA», **Natalia Nikitchina**, Regina Shebanova, Nikita Shebanov, Ivan Tarassov, Konstantin Severinov, Nina Entelis, Ilya Mazunin **(Oral)**

4) *CRISPR CONFERENCE 2023*, June 27 – July 1 2023, Würzburg, Germany: «Use of the type V CRISPR-Cas system to induce a deletion in human mitochondrial DNA», **Natalia Nikitchina**, Anne-Marie Heckel, Ilya Mazunin, Ivan Tarassov, Nina Entelis **(Poster)**

5. BIBLIOGRAPHY

Adeva-Andany MM, Carneiro-Freire N, Seco-Filgueira M, Fernández-Fernández C, Mouriño-Bayolo D. Mitochondrial β-oxidation of saturated fatty acids in humans. Mitochondrion. 2019;46:73-90.

Agaronyan K, Morozov YI, Anikin M, Temiakov D. Mitochondrial biology. Replication-transcription switch in human mitochondria. Science. 2015;347(6221):548-51.

Aibara S, Singh V, Modelska A, Amunts A. Structural basis of mitochondrial translation. Elife. 2020;9.

Akbari M, Visnes T, Krokan HE, Otterlei M. Mitochondrial base excision repair of uracil and AP sites takes place by single-nucleotide insertion and long-patch DNA synthesis. DNA Repair (Amst). 2008;7(4):605-16.

Alberts, B.; Johnson, A.; Lewis, J.; Raff, M.; Roberts, K.; Walter, P. Molecular Biology of the Cell, 4th ed.; Garland Science: New York, NY, USA, 2002.

Alexeyev M, Shokolenko I, Wilson G, LeDoux S. The maintenance of mitochondrial DNA integrity--critical analysis and update. Cold Spring Harb Perspect Biol. 2013;5(5):a012641.

Alexeyev M. Mitochondrial DNA: the common confusions. Mitochondrial DNA A DNA Mapp Seq Anal. 2020;31(2):45-7.

Alexeyev, N. Venediktova, V. Pastukh, I. Shokolenko, G. Bonilla, G.L. Wilson, Selective elimination of mutant mitochondrial genomes as therapeutic strategy for the treatment of NARP and MILS syndromes, Gene Ther, 15 (2008) 516-523.

Amunts A, Brown A, Toots J, Scheres SHW, Ramakrishnan V. Ribosome. The structure of the human mitochondrial ribosome. Science. 2015;348(6230):95-8.

Anderson S, Bankier AT, Barrell BG, de Bruijn MH, Coulson AR, Drouin J, et al. Sequence and organization of the human mitochondrial genome. Nature. 1981;290(5806):457-65.

Andrews S. et al. FastQC: a quality control tool for high throughput sequence data. – 2010.

Angajala A, Lim S, Phillips JB, Kim JH, Yates C, You Z, et al. Diverse Roles of Mitochondria in Immune Responses: Novel Insights Into Immuno-Metabolism. Front Immunol. 2018;9:1605.

Antón, Z., Mullally, G., Ford, H.C., van der Kamp, M.W., Szczelkun, M.D. and Lane, J.D. (2020) Mitochondrial import, health and mtDNA copy number variability seen when using type II and type V CRISPR effectors. J Cell Sci, 133.

Arguello T, Peralta S, Antonicka H, Gaidosh G, Diaz F, Tu YT, et al. ATAD3A has a scaffolding role regulating mitochondria inner membrane structure and protein assembly. Cell Rep. 2021;37(12):110139.

Avula S, Parikh S, Demarest S, Kurz J, Gropman A. Treatment of mitochondrial disorders. Curr Treat Options Neurol. 2014;16(6):292.

B. Wang, X. Lv, Y. Wang, Z. Wang, Q. Liu, B. Lu, Y. Liu, F. Gu, CRISPR/Cas9-mediated mutagenesis at microhomologous regions of human mitochondrial genome, Sci China Life Sci, 64 (2021) 1463-1472.

Bacman SR, Gammage PA, Minczuk M, Moraes CT. Manipulation of mitochondrial genes and mtDNA heteroplasmy. Methods Cell Biol. 2020;155:441-87.

Bacman SR, Williams SL, Moraes CT. Intra- and inter-molecular recombination of mitochondrial DNA after in vivo induction of multiple double-strand breaks. Nucleic Acids Res. 2009;37(13):4218-26.

Bacman SR, Williams SL, Pinto M, Peralta S, Moraes CT. Specific elimination of mutant mitochondrial genomes in patient-derived cells by mitoTALENs. Nat Med. 2013;19(9):1111-3.

Bacman, J.H.K. Kauppila, C.V. Pereira, N. Nissanka, M. Miranda, M. Pinto, S.L. Williams, N.G. Larsson, J.B. Stewart, C.T. Moraes, MitoTALEN reduces mutant mtDNA load and restores tRNA(Ala) levels in a mouse model of heteroplasmic mtDNA mutation, Nat Med, 24 (2018) 1696-1700.

Bae, S., Park, J. and Kim, J.S. (2014) Cas-OFFinder: a fast and versatile algorithm that searches for potential off-target sites of Cas9 RNA-guided endonucleases. Bioinformatics, 30, 1473-1475.

Bandiera S, Matégot R, Girard M, Demongeot J, Henrion-Caude A. MitomiRs delineating the intracellular localization of microRNAs at mitochondria. Free Radic Biol Med. 2013;64:12-9.

Bandiera S, Rüberg S, Girard M, Cagnard N, Hanein S, Chrétien D, et al. Nuclear outsourcing of RNA interference components to human mitochondria. PLoS One. 2011;6(6):e20746.

Barrey, E., Saint-Auret, G., Bonnamy, B., Damas, D., Boyer, O. and Gidrol, X. (2011) Pre-microRNA and mature microRNA in human mitochondria. PLoS One, 6, e20220.

Becker T, Pfannschmidt S, Guiard B, Stojanovski D, Milenkovic D, Kutik S, et al. Biogenesis of the mitochondrial TOM complex: Mim1 promotes insertion and assembly of signal-anchored receptors. J Biol Chem. 2008;283(1):120-7.

Bender A, Krishnan KJ, Morris CM, Taylor GA, Reeve AK, Perry RH, et al. High levels of mitochondrial DNA deletions in substantia nigra neurons in aging and Parkinson disease. Nat Genet. 2006;38(5):515-7.

Bi R, Li Y, Xu M, Zheng Q, Zhang DF, Li X, et al. Direct evidence of CRISPR-Cas9-mediated mitochondrial genome editing. Innovation (Camb). 2022;3(6):100329.

Bian, Y.L. Chen, J.J. Luo, C. Wang, S.L. Xie, D.S. Pei, Knock-In Strategy for Editing Human and Zebrafish Mitochondrial DNA Using Mito-CRISPR/Cas9 System, ACS Synth Biol, 8 (2019) 621-632.

Birky CW, Jr. The inheritance of genes in mitochondria and chloroplasts: laws, mechanisms, and models. Annu Rev Genet. 2001;35:125-48.

Bogenhagen DF, Rousseau D, Burke S. The layered structure of human mitochondrial DNA nucleoids. J Biol Chem. 2008;283(6):3665-75.

Bogenhagen DF. Mitochondrial DNA nucleoid structure. Biochim Biophys Acta. 2012;1819(9-10):914-20.

Bohnsack MT, Sloan KE. The mitochondrial epitranscriptome: the roles of RNA modifications in mitochondrial translation and human disease. Cell Mol Life Sci. 2018;75(2):241-60.

Bokori-Brown M, Holt IJ. Expression of algal nuclear ATP synthase subunit 6 in human cells results in protein targeting to mitochondria but no assembly into ATP synthase. Rejuvenation Res. 2006;9(4):455-69.

Boldinova EO, Khairullin RF, Makarova AV, Zharkov DO. Isoforms of Base Excision Repair Enzymes Produced by Alternative Splicing. Int J Mol Sci. 2019;20(13).

Bolger AM, Lohse M, Usadel B. Trimmomatic: a flexible trimmer for Illumina sequence data. Bioinformatics. 2014;30(15):2114-20.

Boominathan A, Vanhoozer S, Basisty N, Powers K, Crampton AL, Wang X, et al. Stable nuclear expression of ATP8 and ATP6 genes rescues a mtDNA Complex V null mutant. Nucleic Acids Res. 2016;44(19):9342-57.

Bough KJ, Wetherington J, Hassel B, Pare JF, Gawryluk JW, Greene JG, et al. Mitochondrial biogenesis in the anticonvulsant mechanism of the ketogenic diet. Ann Neurol. 2006;60(2):223-35.

Bowmaker M, Yang MY, Yasukawa T, Reyes A, Jacobs HT, Huberman JA, et al. Mammalian mitochondrial DNA replicates bidirectionally from an initiation zone. J Biol Chem. 2003;278(51):50961-9.

C.T. Moraes, A magic bullet to specifically eliminate mutated mitochondrial genomes from patients' cells, EMBO Mol Med, 6 (2014) 434-435.

C.V. Pereira, S.R. Bacman, T. Arguello, U. Zekonyte, S.L. Williams, D.R. Edgell, C.T. Moraes, mitoTev-TALE: a monomeric DNA editing enzyme to reduce mutant mitochondrial DNA levels, EMBO Mol Med, 10 (2018).

Caliceti, C., Franco, P., Spinozzi, S., Roda, A. and Cicero, A.F. (2016) Berberine: New Insights from Pharmacological Aspects to Clinical Evidences in the Management of Metabolic Disorders. Curr Med Chem, 23, 1460-1476.

Calvo SE, Clauser KR, Mootha VK. MitoCarta2.0: an updated inventory of mammalian mitochondrial proteins. Nucleic Acids Res. 2016;44(D1):D1251-7.

Campbell G, Krishnan KJ, Deschauer M, Taylor RW, Turnbull DM. Dissecting the mechanisms underlying the accumulation of mitochondrial DNA deletions in human skeletal muscle. Hum Mol Genet. 2014;23(17):4612-20.v.

Campo ML, Peixoto PM, Martínez-Caballero S. Revisiting trends on mitochondrial mega-channels for the import of proteins and nucleic acids. J Bioenerg Biomembr. 2017;49(1):75-99.

Carelli V, La Morgia C. Clinical syndromes associated with mtDNA mutations: where we stand after 30 years. Essays Biochem. 2018;62(3):235-54.

Carrodeguas JA, Pinz KG, Bogenhagen DF. DNA binding properties of human pol gammaB. J Biol Chem. 2002;277(51):50008-14.

Cavalier-Smith T. Origin of mitochondria by intracellular enslavement of a photosynthetic purple bacterium. Proc Biol Sci. 2006;273(1596):1943-52.

Chacinska A, Pfannschmidt S, Wiedemann N, Kozjak V, Sanjuán Szklarz LK, Schulze-Specking A, et al. Essential role of Mia40 in import and assembly of mitochondrial intermembrane space proteins. Embo j. 2004;23(19):3735-46.

Chacinska A, Rehling P, Guiard B, Frazier AE, Schulze-Specking A, Pfanner N, et al. Mitochondrial translocation contact sites: separation of dynamic and stabilizing elements in formation of a TOM-TIM-preprotein supercomplex. Embo j. 2003;22(20):5370-81.

Chai P, Lebedenko CG, Flynn RA. RNA Crossing Membranes: Systems and Mechanisms Contextualizing Extracellular RNA and Cell Surface GlycoRNAs. Annu Rev Genomics Hum Genet. 2023;24:85-107.

Chang DD, Clayton DA. Precise identification of individual promoters for transcription of each strand of human mitochondrial DNA. Cell. 1984;36(3):635-43.

Chang KY, Yang JR. Analysis and prediction of highly effective antiviral peptides based on random forests. PLoS One. 2013;8(8):e70166.

Chen HW, Rainey RN, Balatoni CE, Dawson DW, Troke JJ, Wasiak S, et al. Mammalian polynucleotide phosphorylase is an intermembrane space RNase that maintains mitochondrial homeostasis. Mol Cell Biol. 2006;26(22):8475-87.

Chen K, Rajewsky N. The evolution of gene regulation by transcription factors and microRNAs. Nat Rev Genet. 2007;8(2):93-103.

Chen, J.S., Ma, E., Harrington, L.B., Da Costa, M., Tian, X., Palefsky, J.M. and Doudna, J.A. (2018) CRISPR-Cas12a target binding unleashes indiscriminate single-stranded DNase activity. Science, 360, 436-439.

Chin RM, Panavas T, Brown JM, Johnson KK. Optimized Mitochondrial Targeting of Proteins Encoded by Modified mRNAs Rescues Cells Harboring Mutations in mtATP6. Cell Rep. 2018;22(11):2818-26.

Chinnery PF, Samuels DC. Relaxed replication of mtDNA: A model with implications for the expression of disease. Am J Hum Genet. 1999;64(4):1158-65.

Chinnery PF, Taylor RW, Diekert K, Lill R, Turnbull DM, Lightowlers RN. Peptide nucleic acid delivery to human mitochondria. Gene Ther. 1999;6(12):1919-28.

Cho SI, Lee S, Mok YG, Lim K, Lee J, Lee JM, et al. Targeted A-to-G base editing in human mitochondrial DNA with programmable deaminases. Cell. 2022;185(10):1764-76.e12.

Civiletto G, Varanita T, Cerutti R, Gorletta T, Barbaro S, Marchet S, et al. Opa1 overexpression ameliorates the phenotype of two mitochondrial disease mouse models. Cell Metab. 2015;21(6):845-54.

Clay Montier LL, Deng JJ, Bai Y. Number matters: control of mammalian mitochondrial DNA copy number. J Genet Genomics. 2009;36(3):125-31.

Coffey G, Lakshmipathy U, Campbell C. Mammalian mitochondrial extracts possess DNA end-binding activity. Nucleic Acids Res. 1999;27(16):3348-54.

Cogliati S, Frezza C, Soriano ME, Varanita T, Quintana-Cabrera R, Corrado M, et al. Mitochondrial cristae shape determines respiratory chain supercomplexes assembly and respiratory efficiency. Cell. 2013;155(1):160-71.

Cohen J, Scott R, Schimmel T, Levron J, Willadsen S. Birth of infant after transfer of anucleate donor oocyte cytoplasm into recipient eggs. Lancet. 1997;350(9072):186-7.

Colombini M. Structure and mode of action of a voltage dependent anion-selective channel (VDAC) located in the outer mitochondrial membrane. Ann N Y Acad Sci. 1980;341:552-63.

Comte C, Tonin Y, Heckel-Mager AM, Boucheham A, Smirnov A, Auré K, et al. Mitochondrial targeting of recombinant RNAs modulates the level of a heteroplasmic mutation in human mitochondrial DNA associated with Kearns Sayre Syndrome. Nucleic Acids Res. 2013;41(1):418-33.

Contreras L, Drago I, Zampese E, Pozzan T. Mitochondria: the calcium connection. Biochim Biophys Acta. 2010;1797(6-7):607-18.

Cote-L'Heureux A, Maithania YNK, Franco M, Khrapko K. Are some mutations more equal than others? Elife. 2023;12.

Czech B, Hannon GJ. Small RNA sorting: matchmaking for Argonautes. Nat Rev Genet. 2011;12(1):19-31.

Danecek P, Bonfield JK, Liddle J, Marshall J, Ohan V, Pollard MO, et al. Twelve years of SAMtools and BCFtools. Gigascience. 2021;10(2).

Das S, Kohr M, Dunkerly-Eyring B, Lee DI, Bedja D, Kent OA, et al. Divergent Effects of miR-181 Family Members on Myocardial Function Through Protective Cytosolic and Detrimental Mitochondrial microRNA Targets. J Am Heart Assoc. 2017;6(3).

D'Aurelio M, Gajewski CD, Lin MT, Mauck WM, Shao LZ, Lenaz G, et al. Heterologous mitochondrial DNA recombination in human cells. Hum Mol Genet. 2004;13(24):3171-9.

Davis AJ, Alder NN, Jensen RE, Johnson AE. The Tim9p/10p and Tim8p/13p complexes bind to specific sites on Tim23p during mitochondrial protein import. Mol Biol Cell. 2007;18(2):475-86.

Demidov VV, Potaman VN, Frank-Kamenetskii MD, Egholm M, Buchard O, Sönnichsen SH, et al. Stability of peptide nucleic acids in human serum and cellular extracts. Biochem Pharmacol. 1994;48(6):1310-3.

Diaz F, Bayona-Bafaluy MP, Rana M, Mora M, Hao H, Moraes CT. Human mitochondrial DNA with large deletions repopulates organelles faster than full-length genomes under relaxed copy number control. Nucleic Acids Res. 2002;30(21):4626-33.

DiMauro S, Schon EA. Mitochondrial DNA mutations in human disease. Am J Med Genet. 2001;106(1):18-26.

Djafarzadeh S, Jakob SM. High-resolution Respirometry to Assess Mitochondrial Function in Permeabilized and Intact Cells. J Vis Exp. 2017(120).

Doersen CJ, Guerrier-Takada C, Altman S, Attardi G. Characterization of an RNase P activity from HeLa cell mitochondria. Comparison with the cytosol RNase P activity. J Biol Chem. 1985;260(10):5942-9.

Dovydenko, I., Heckel, A.M., Tonin, Y., Gowher, A., Venyaminova, A., Tarassov, I. and Entelis, N. (2015) Mitochondrial targeting of recombinant RNA. *Methods Mol Biol*, **1265**, 209-225.

Dovydenko, I., Tarassov, I., Venyaminova, A. and Entelis, N. (2016) Method of carrier-free delivery of therapeutic RNA importable into human mitochondria: Lipophilic conjugates with cleavable bonds. Biomaterials, 76, 408-417.

Dussurget, O. and Roulland-Dussoix, D. (1994) Rapid, sensitive PCR-based detection of mycoplasmas in simulated samples of animal sera. *Appl Environ Microbiol*, **60**, 953-959.

Duxin JP, Dao B, Martinsson P, Rajala N, Guittat L, Campbell JL, et al. Human Dna2 is a nuclear and mitochondrial DNA maintenance protein. Mol Cell Biol. 2009;29(15):4274-82.

Egholm M, Buchardt O, Christensen L, Behrens C, Freier SM, Driver DA, et al. PNA hybridizes to complementary oligonucleotides obeying the Watson-Crick hydrogen-bonding rules. Nature. 1993;365(6446):566-8.

Ekstrand MI, Falkenberg M, Rantanen A, Park CB, Gaspari M, Hultenby K, et al. Mitochondrial transcription factor A regulates mtDNA copy number in mammals. Hum Mol Genet. 2004;13(9):935-44.

Elson JL, Andrews RM, Chinnery PF, Lightowlers RN, Turnbull DM, Howell N. Analysis of European mtDNAs for recombination. Am J Hum Genet. 2001;68(1):145-53.

Elustondo, P., Martin, L.A. and Karten, B. (2017) Mitochondrial cholesterol import. Biochim Biophys Acta Mol Cell Biol Lipids, 1862, 90-101.

Ernster L, Schatz G. Mitochondria: a historical review. J Cell Biol. 1981;91(3 Pt 2):227s-55s.

Estaquier J, Vallette F, Vayssiere JL, Mignotte B. The mitochondrial pathways of apoptosis. Adv Exp Med Biol. 2012;942:157-83.

Fan XY, Guo L, Chen LN, Yin S, Wen J, Li S, et al. Reduction of mtDNA heteroplasmy in mitochondrial replacement therapy by inducing forced mitophagy. Nat Biomed Eng. 2022;6(4):339-50.

Fish J, Raule N, Attardi G. Discovery of a major D-loop replication origin reveals two modes of human mtDNA synthesis. Science. 2004;306(5704):2098-101.

Floros VI, Pyle A, Dietmann S, Wei W, Tang WCW, Irie N, et al. Segregation of mitochondrial DNA heteroplasmy through a developmental genetic bottleneck in human embryos. Nat Cell Biol. 2018;20(2):144-51.

Fontana GA, Gahlon HL. Mechanisms of replication and repair in mitochondrial DNA deletion formation. Nucleic Acids Res. 2020;48(20):11244-58.

Fortini P, Pascucci B, Parlanti E, D'Errico M, Simonelli V, Dogliotti E. The base excision repair: mechanisms and its relevance for cancer susceptibility. Biochimie. 2003;85(11):1053-71.

Gakh O, Cavadini P, Isaya G. Mitochondrial processing peptidases. Biochim Biophys Acta. 2002;1592(1):63-77.

Gammage PA, Moraes CT, Minczuk M. Mitochondrial Genome Engineering: The Revolution May Not Be CRISPR-Ized. Trends Genet. 2018;34(2):101-10.

Gammage PA, Rorbach J, Vincent AI, Rebar EJ, Minczuk M. Mitochondrially targeted ZFNs for selective degradation of pathogenic mitochondrial genomes bearing large-scale deletions or point mutations. EMBO Mol Med. 2014;6(4):458-66.

Gammage, C. Viscomi, M.L. Simard, A.S.H. Costa, E. Gaude, C.A. Powell, L. Van Haute, B.J. McCann, P. Rebelo-Guiomar, R. Cerutti, L. Zhang, E.J. Rebar, M. Zeviani, C. Frezza, J.B. Stewart, M. Minczuk, Genome editing in mitochondria corrects a pathogenic mtDNA mutation in vivo, Nat Med, 24 (2018) 1691-1695.

Gammage, P.A., Moraes, C.T. and Minczuk, M. (2018) Mitochondrial Genome Engineering: The Revolution May Not Be CRISPR-Ized. Trends Genet, 34, 101-110.

Gao, K., Cheng, M., Zuo, X., Lin, J., Hoogewijs, K., Murphy, M.P., Fu, X.D. and Zhang, X. (2021) Active RNA interference in mitochondria. Cell Res, 31, 219-228.

Gao, L., Cox, D.B.T., Yan, W.X., Manteiga, J.C., Schneider, M.W., Yamano, T., Nishimasu, H., Nureki, O., Crosetto, N. and Zhang, F. (2017) Engineered Cpf1 variants with altered PAM specificities. Nat Biotechnol, 35, 789-792.

Gear, A.R. (1974) Rhodamine 6G. A potent inhibitor of mitochondrial oxidative phosphorylation. J Biol Chem, 249, 3628-3637.

Gebert N, Gebert M, Oeljeklaus S, von der Malsburg K, Stroud DA, Kulawiak B, et al. Dual function of Sdh3 in the respiratory chain and TIM22 protein translocase of the mitochondrial inner membrane. Mol Cell. 2011;44(5):811-8.

Geissler A, Krimmer T, Bömer U, Guiard B, Rassow J, Pfanner N. Membrane potential-driven protein import into mitochondria. The sorting sequence of cytochrome b(2) modulates the deltapsi-dependence of translocation of the matrix-targeting sequence. Mol Biol Cell. 2000;11(11):3977-91.

Gelmetti, V., De Rosa, P., Torosantucci, L., Marini, E.S., Romagnoli, A., Di Rienzo, M., Arena, G., Vignone, D., Fimia, G.M. and Valente, E.M. (2017) PINK1 and BECN1 relocalize at mitochondria-associated membranes during mitophagy and promote ER-mitochondria tethering and autophagosome formation. Autophagy, 13, 654-669.

Gilkerson, R.W., Schon, E.A., Hernandez, E. and Davidson, M.M. (2008) Mitochondrial nucleoids maintain genetic autonomy but allow for functional complementation. J Cell Biol, 181, 1117-1128.

Giorgi C, Agnoletto C, Bononi A, Bonora M, De Marchi E, Marchi S, et al. Mitochondrial calcium homeostasis as potential target for mitochondrial medicine. Mitochondrion. 2012;12(1):77-85.

Gitschlag BL, Kirby CS, Samuels DC, Gangula RD, Mallal SA, Patel MR. Homeostatic Responses Regulate Selfish Mitochondrial Genome Dynamics in C. elegans. Cell Metab. 2016;24(1):91-103.

Goding, C.R. (2016) Targeting the lncRNA SAMMSON Reveals Metabolic Vulnerability in Melanoma. Cancer Cell, 29, 619-621.

Golzarroshan B, Lin CL, Li CL, Yang WZ, Chu LY, Agrawal S, et al. Crystal structure of dimeric human PNPase reveals why disease-linked mutants suffer from low RNA import and degradation activities. Nucleic Acids Res. 2018;46(16):8630-40.

Good, A.J. Krikos, S.X. Li, E. Bertrand, N.S. Lee, L. Giver, A. Ellington, J.A. Zaia, J.J. Rossi, D.R. Engelke, Expression of small, therapeutic RNAs in human cell nuclei, Gene Ther, 4 (1997) 45-54.

Gorman GS, Chinnery PF, DiMauro S, Hirano M, Koga Y, McFarland R, et al. Mitochondrial diseases. Nat Rev Dis Primers. 2016;2:16080.

Gorman GS, Schaefer AM, Ng Y, Gomez N, Blakely EL, Alston CL, et al. Prevalence of nuclear and mitochondrial DNA mutations related to adult mitochondrial disease. Ann Neurol. 2015;77(5):753-9.

Goto Y, Nonaka I, Horai S. A mutation in the tRNA(Leu)(UUR) gene associated with the MELAS subgroup of mitochondrial encephalomyopathies. Nature. 1990;348(6302):651-3.

Graham, F.L., Smiley, J., Russell, W.C. and Nairn, R. (1977) Characteristics of a human cell line transformed by DNA from human adenovirus type 5. J Gen Virol, 36, 59-74.

Gray MW. Mitochondrial evolution. Cold Spring Harb Perspect Biol. 2012;4(9):a011403.

Greber BJ, Ban N. Structure and Function of the Mitochondrial Ribosome. Annu Rev Biochem. 2016;85:103-32.

Green MR, Sambrook J. Nested Polymerase Chain Reaction (PCR). Cold Spring Harb Protoc. 2019;2019(2).

Guan Z, Yan L, Wang Q, Qi L, Hong S, Gong Z, et al. Structural insights into assembly of human mitochondrial translocase TOM complex. Cell Discov. 2021;7(1):22.

Gustafsson CM, Falkenberg M, Larsson NG. Maintenance and Expression of Mammalian Mitochondrial DNA. Annu Rev Biochem. 2016;85:133-60.

Habano W, Nakamura S, Sugai T. Microsatellite instability in the mitochondrial DNA of colorectal carcinomas: evidence for mismatch repair systems in mitochondrial genome. Oncogene. 1998;17(15):1931-7.

Hall AR, Burke N, Dongworth RK, Hausenloy DJ. Mitochondrial fusion and fission proteins: novel therapeutic targets for combating cardiovascular disease. Br J Pharmacol. 2014;171(8):1890-906.

Hamm, I.W. Mattaj, Monomethylated cap structures facilitate RNA export from the nucleus, Cell, 63 (1990) 109-118.

Hance N, Ekstrand MI, Trifunovic A. Mitochondrial DNA polymerase gamma is essential for mammalian embryogenesis. Hum Mol Genet. 2005;14(13):1775-83.

Hashimoto, S.R. Bacman, S. Peralta, M.J. Falk, A. Chomyn, D.C. Chan, S.L. Williams, C.T. Moraes, MitoTALEN: A General Approach to Reduce Mutant mtDNA Loads and Restore Oxidative Phosphorylation Function in Mitochondrial Diseases, Mol Ther, 23 (2015) 1592-1599.

Hegde ML, Mantha AK, Hazra TK, Bhakat KK, Mitra S, Szczesny B. Oxidative genome damage and its repair: implications in aging and neurodegenerative diseases. Mech Ageing Dev. 2012;133(4):157-68.

Hell K, Neupert W, Stuart RA. Oxa1p acts as a general membrane insertion machinery for proteins encoded by mitochondrial DNA. Embo j. 2001;20(6):1281-8.

Herbers, E., Kekäläinen, N.J., Hangas, A., Pohjoismäki, J.L. and Goffart, S. (2019) Tissue specific differences in mitochondrial DNA maintenance and expression. Mitochondrion, 44, 85-92.

Hillen HS, Morozov YI, Sarfallah A, Temiakov D, Cramer P. Structural Basis of Mitochondrial Transcription Initiation. Cell. 2017;171(5):1072-81.e10.

Hoitzing H, Johnston IG, Jones NS. What is the function of mitochondrial networks? A theoretical assessment of hypotheses and proposal for future research. Bioessays. 2015;37(6):687-700.

Holmes JB, Akman G, Wood SR, Sakhuja K, Cerritelli SM, Moss C, et al. Primer retention owing to the absence of RNase H1 is catastrophic for mitochondrial DNA replication. Proc Natl Acad Sci U S A. 2015;112(30):9334-9.

Holt IJ, Harding AE, Morgan-Hughes JA. Deletions of muscle mitochondrial DNA in patients with mitochondrial myopathies. Nature. 1988;331(6158):717-9.

Holt, I.J. (2019) The mitochondrial R-loop. Nucleic Acids Res, 47, 5480-5489.

Huang YF, Gu CJ, Wang Q, Xu L, Chen J, Zhou W, et al. The protective effort of GPCR kinase 2-interacting protein-1 in neurons via promoting Beclin1-Parkin induced mitophagy at the early stage of spinal cord ischemia-reperfusion injury. Faseb j. 2020;34(2):2055-74.

Hussain, M.E. Yalvac, B. Khoo, S. Eckardt, K.J. McLaughlin, Adapting CRISPR/Cas9 System for Targeting Mitochondrial Genome, Front Genet, 12 (2021) 627050.

Hwang S, Disatnik MH, Mochly-Rosen D. Impaired GAPDH-induced mitophagy contributes to the pathology of Huntington's disease. EMBO Mol Med. 2015;7(10):1307-26.

Hyslop LA, Blakeley P, Craven L, Richardson J, Fogarty NM, Fragouli E, et al. Towards clinical application of pronuclear transfer to prevent mitochondrial DNA disease. Nature. 2016;534(7607):383-6.

Inoue K, Nakada K, Ogura A, Isobe K, Goto Y, Nonaka I, et al. Generation of mice with mitochondrial dysfunction by introducing mouse mtDNA carrying a deletion into zygotes. Nat Genet. 2000;26(2):176-81.

Jacobs AL, Schär P. DNA glycosylases: in DNA repair and beyond. Chromosoma. 2012;121(1):1-20.

Jacobs HT, Lehtinen SK, Spelbrink JN. No sex please, we're mitochondria: a hypothesis on the somatic unit of inheritance of mammalian mtDNA. Bioessays. 2000;22(6):564-72.

Jagannathan R, Thapa D, Nichols CE, Shepherd DL, Stricker JC, Croston TL, et al. Translational Regulation of the Mitochondrial Genome Following Redistribution of Mitochondrial MicroRNA in the Diabetic Heart. Circ Cardiovasc Genet. 2015;8(6):785-802.

Janer A, van Karnebeek CD, Sasarman F, Antonicka H, Al Ghamdi M, Shyr C, et al. RMND1 deficiency associated with neonatal lactic acidosis, infantile onset renal failure, deafness, and multiorgan involvement. Eur J Hum Genet. 2015;23(10):1301-7.

Jeandard, D., Smirnova, A., Fasemore, A.M., Coudray, L., Entelis, N., Förstner, K.U., Tarassov, I. and Smirnov, A. (2023) CoLoC-seq probes the global topology of organelle transcriptomes. Nucleic Acids Res, 51, e16.

Jeandard, D., Smirnova, A., Tarassov, I., Barrey, E., Smirnov, A. and Entelis, N. (2019) Import of Non-Coding RNAs into Human Mitochondria: A Critical Review and Emerging Approaches. Cells, 8.

Jedynak-Slyvka M, Jabczynska A, Szczesny RJ. Human Mitochondrial RNA Processing and Modifications: Overview. Int J Mol Sci. 2021;22(15).

Jemt E, Persson Ö, Shi Y, Mehmedovic M, Uhler JP, Dávila López M, et al. Regulation of DNA replication at the end of the mitochondrial D-loop involves the helicase TWINKLE and a conserved sequence element. Nucleic Acids Res. 2015;43(19):9262-75.

Jesus C, Hesse C, Rocha C, Osório N, Valado A, Caseiro A, et al. Prevalence of antibodies to a new histo-blood system: the FORS system. Blood Transfus. 2018;16(2):178-83.

Jeyaraju, D.V., Xu, L., Letellier, M.C., Bandaru, S., Zunino, R., Berg, E.A., McBride, H.M. and Pellegrini, L. (2006) Phosphorylation and cleavage of presenilin-associated rhomboid-like protein (PARL) promotes changes in mitochondrial morphology. Proc Natl Acad Sci U S A, 103, 18562-18567.

Jin, Y., Khadka, D.B. and Cho, W.J. (2016) Pharmacological effects of berberine and its derivatives: a patent update. Expert Opin Ther Pat, 26, 229-243.

Jinek M, Chylinski K, Fonfara I, Hauer M, Doudna JA, Charpentier E. A programmable dual-RNA-guided DNA endonuclease in adaptive bacterial immunity. Science. 2012;337(6096):816-21.

Joubert F, Puff N. Mitochondrial Cristae Architecture and Functions: Lessons from Minimal Model Systems. Membranes (Basel). 2021;11(7).

Jourdain AA, Koppen M, Rodley CD, Maundrell K, Gueguen N, Reynier P, et al. A mitochondria-specific isoform of FASTK is present in mitochondrial RNA granules and regulates gene expression and function. Cell Rep. 2015;10(7):1110-21.

Kaltimbacher V, Bonnet C, Lecoeuvre G, Forster V, Sahel JA, Corral-Debrinski M. mRNA localization to the mitochondrial surface allows the efficient translocation inside the organelle of a nuclear recoded ATP6 protein. Rna. 2006;12(7):1408-17.

Kang E, Wu J, Gutierrez NM, Koski A, Tippner-Hedges R, Agaronyan K, et al. Mitochondrial replacement in human oocytes carrying pathogenic mitochondrial DNA mutations. Nature. 2016;540(7632):270-5.

Karicheva OZ, Kolesnikova OA, Schirtz T, Vysokikh MY, Mager-Heckel A-M, Lombès A, et al. Correction of the consequences of mitochondrial 3243A>G mutation in the MT-TL1 gene causing the MELAS syndrome by tRNA import into mitochondria. Nucleic Acids Research. 2011;39(18):8173-86.

Karnkowska A, Vacek V, Zubáčová Z, Treitli SC, Petrželková R, Eme L, et al. A Eukaryote without a Mitochondrial Organelle. Curr Biol. 2016;26(10):1274-84.

Kasamatsu H, Robberson DL, Vinograd J. A novel closed-circular mitochondrial DNA with properties of a replicating intermediate. Proc Natl Acad Sci U S A. 1971;68(9):2252-7.

Kauppila JHK, Bonekamp NA, Mourier A, Isokallio MA, Just A, Kauppila TES, et al. Base-excision repair deficiency alone or combined with increased oxidative stress does not increase mtDNA point mutations in mice. Nucleic Acids Res. 2018;46(13):6642-69.

Kazakova HA, Entelis NS, Martin RP, Tarassov IA. The aminoacceptor stem of the yeast tRNA(Lys) contains determinants of mitochondrial import selectivity. FEBS Lett. 1999;442(2-3):193-7.

Kim D, Kim J, Hur JK, Been KW, Yoon SH, Kim JS. Genome-wide analysis reveals specificities of Cpf1 endonucleases in human cells. Nat Biotechnol. 2016;34(8):863-8.

Kim JY, Hwang JM, Park SS. Mitochondrial DNA C4171A/ND1 is a novel primary causative mutation of Leber's hereditary optic neuropathy with a good prognosis. Ann Neurol. 2002;51(5):630-4.

Kirillova A, Mazunin I. Operation "mitochondrial wipeout" - clearing recipient mitochondria DNA during the cytoplasmic replacement therapy. J Assist Reprod Genet. 2022;39(10):2205-7.

Kleinstiver BP, Sousa AA, Walton RT, Tak YE, Hsu JY, Clement K, et al. Engineered CRISPR-Cas12a variants with increased activities and improved targeting ranges for gene, epigenetic and base editing. Nat Biotechnol. 2019;37(3):276-82.

Kobayashi, A., Takeiwa, T., Ikeda, K. and Inoue, S. (2023) Roles of Noncoding RNAs in Regulation of Mitochondrial Electron Transport Chain and Oxidative Phosphorylation. Int J Mol Sci, 24.

Koblan LW, Doman JL, Wilson C, Levy JM, Tay T, Newby GA, et al. Improving cytidine and adenine base editors by expression optimization and ancestral reconstruction. Nat Biotechnol. 2018;36(9):843-6.

Kolesnikova OA, Entelis NS, Jacquin-Becker C, Goltzene F, Chrzanowska-Lightowlers ZM, Lightowlers RN, et al. Nuclear DNA-encoded tRNAs targeted into mitochondria can rescue a mitochondrial DNA mutation associated with the MERRF syndrome in cultured human cells. Hum Mol Genet. 2004;13(20):2519-34.

Kolesnikova, O., Kazakova, H., Comte, C., Steinberg, S., Kamenski, P., Martin, R.P., Tarassov, I. and Entelis, N. (2010) Selection of RNA aptamers imported into yeast and human mitochondria. Rna, 16, 926-941.

Komor AC, Kim YB, Packer MS, Zuris JA, Liu DR. Programmable editing of a target base in genomic DNA without double-stranded DNA cleavage. Nature. 2016;533(7603):420-4.

Koripella RK, Deep A, Agrawal EK, Keshavan P, Banavali NK, Agrawal RK. Distinct mechanisms of the human mitoribosome recycling and antibiotic resistance. Nat Commun. 2021;12(1):3607.

Krasich R, Copeland WC. DNA polymerases in the mitochondria: A critical review of the evidence. Front Biosci (Landmark Ed). 2017;22(4):692-709.

Krauss, Stefan. "Mitochondria: Structure and role in respiration." e LS (2001).

Kraytsberg Y, Kudryavtseva E, McKee AC, Geula C, Kowall NW, Khrapko K. Mitochondrial DNA deletions are abundant and cause functional impairment in aged human substantia nigra neurons. Nat Genet. 2006;38(5):518-20.

Kruse B, Narasimhan N, Attardi G. Termination of transcription in human mitochondria: identification and purification of a DNA binding protein factor that promotes termination. Cell. 1989;58(2):391-7.

Kukat C, Davies KM, Wurm CA, Spåhr H, Bonekamp NA, Kühl I, et al. Cross-strand binding of TFAM to a single mtDNA molecule forms the mitochondrial nucleoid. Proc Natl Acad Sci U S A. 2015;112(36):11288-93.

Kutik S, Stojanovski D, Becker L, Becker T, Meinecke M, Krüger V, et al. Dissecting membrane insertion of mitochondrial beta-barrel proteins. Cell. 2008;132(6):1011-24.

L. Schmiderer, D. Yudovich, L. Oburoglu, M. Hjort, J. Larsson, Site-specific CRISPR-based mitochondrial DNA manipulation is limited by gRNA import, Sci Rep, 12 (2022) 18687.

Lapkouski M, Hällberg BM. Structure of mitochondrial poly(A) RNA polymerase reveals the structural basis for dimerization, ATP selectivity and the SPAX4 disease phenotype. Nucleic Acids Res. 2015;43(18):9065-75.

Lee H, Lee S, Baek G, Kim A, Kang BC, Seo H, et al. Mitochondrial DNA editing in mice with DddA-TALE fusion deaminases. Nat Commun. 2021;12(1):1190

Lee HF, Lee HJ, Chi CS, Tsai CR, Chang TK, Wang CJ. The neurological evolution of Pearson syndrome: case report and literature review. Eur J Paediatr Neurol. 2007;11(4):208-14.

Lee, S.R. and Han, J. (2017) Mitochondrial Nucleoid: Shield and Switch of the Mitochondrial Genome. Oxid Med Cell Longev, 2017, 8060949.

Legati A, Zanetti N, Nasca A, Peron C, Lamperti C, Lamantea E, et al. Current and New Next-Generation Sequencing Approaches to Study Mitochondrial DNA. J Mol Diagn. 2021;23(6):732-41.

Lehninger A. L. et al. The mitochondrion. Molecular basis of structure and function //The mitochondrion. Molecular basis of structure and function. – 1964.

Lehninger, A. L., Nelson, D. L., & Cox, M. M. (2005). Lehninger principles of biochemistry. Macmillan.

Leucci E, Vendramin R, Spinazzi M, Laurette P, Fiers M, Wouters J, et al. Melanoma addiction to the long non-coding RNA SAMMSON. Nature. 2016;531(7595):518-22.

Li H, Ruan J, Durbin R. Mapping short DNA sequencing reads and calling variants using mapping quality scores. Genome Res. 2008;18(11):1851-8.

Li K, Smagula CS, Parsons WJ, Richardson JA, Gonzalez M, Hagler HK, et al. Subcellular partitioning of MRP RNA assessed by ultrastructural and biochemical analysis. J Cell Biol. 1994;124(6):871-82.

Lim K, Cho SI, Kim JS. Nuclear and mitochondrial DNA editing in human cells with zinc finger deaminases. Nat Commun. 2022;13(1):366.

Lin CL, Wang YT, Yang WZ, Hsiao YY, Yuan HS. Crystal structure of human polynucleotide phosphorylase: insights into its domain function in RNA binding and degradation. Nucleic Acids Res. 2012;40(9):4146-57.

Lin CS, Lee HT, Lee SY, Shen YA, Wang LS, Chen YJ, et al. High mitochondrial DNA copy number and bioenergetic function are associated with tumor invasion of esophageal squamous cell carcinoma cell lines. Int J Mol Sci. 2012;13(9):11228-46.

Litonin D, Sologub M, Shi Y, Savkina M, Anikin M, Falkenberg M, et al. Human mitochondrial transcription revisited: only TFAM and TFB2M are required for transcription of the mitochondrial genes in vitro. J Biol Chem. 2010;285(24):18129-33.

Liu Z, Chen O, Wall JBJ, Zheng M, Zhou Y, Wang L, et al. Systematic comparison of 2A peptides for cloning multi-genes in a polycistronic vector. Scientific Reports. 2017;7(1):2193.

Livak KJ, Schmittgen TD. Analysis of Relative Gene Expression Data Using Real-Time Quantitative PCR and the 2−ΔΔCT Method. Methods. 2001;25(4):402-8.

Longley MJ, Nguyen D, Kunkel TA, Copeland WC. The fidelity of human DNA polymerase gamma with and without exonucleolytic proofreading and the p55 accessory subunit. J Biol Chem. 2001;276(42):38555-62.

Longley MJ, Prasad R, Srivastava DK, Wilson SH, Copeland WC. Identification of 5'-deoxyribose phosphate lyase activity in human DNA polymerase gamma and its role in mitochondrial base excision repair in vitro. Proc Natl Acad Sci U S A. 1998;95(21):12244-8.

Lorenz, R., Bernhart, S.H., Höner Zu Siederdissen, C., Tafer, H., Flamm, C., Stadler, P.F. and Hofacker, I.L. (2011) ViennaRNA Package 2.0. Algorithms Mol Biol, 6, 26.

Lott MT, Leipzig JN, Derbeneva O, Xie HM, Chalkia D, Sarmady M, et al. mtDNA Variation and Analysis Using Mitomap and Mitomaster. Curr Protoc Bioinformatics. 2013;44(123):1.23.1-6.

Loutre R, Heckel AM, Jeandard D, Tarassov I, Entelis N. Anti-replicative recombinant 5S rRNA molecules can modulate the mtDNA heteroplasmy in a glucose-dependent manner. PLoS One. 2018;13(6):e0199258.

Loutre, R., Heckel, A.M., Smirnova, A., Entelis, N. and Tarassov, I. (2018) Can Mitochondrial DNA be CRISPRized: Pro and Contra. IUBMB Life, 70, 1233-1239.

Luo S, Valencia CA, Zhang J, Lee NC, Slone J, Gui B, et al. Biparental Inheritance of Mitochondrial DNA in Humans. Proc Natl Acad Sci U S A. 2018;115(51):13039-44.

Macao B, Uhler JP, Siibak T, Zhu X, Shi Y, Sheng W, et al. The exonuclease activity of DNA polymerase γ is required for ligation during mitochondrial DNA replication. Nat Commun. 2015;6:7303.

Macara IG. Transport into and out of the nucleus. Microbiol Mol Biol Rev. 2001;65(4):570-94, table of contents.

Magalhães PJ, Andreu AL, Schon EA. Evidence for the presence of 5S rRNA in mammalian mitochondria. Mol Biol Cell. 1998;9(9):2375-82.

Mancuso M, Orsucci D, Angelini C, Bertini E, Carelli V, Comi GP, et al. The m.3243A>G mitochondrial DNA mutation and related phenotypes. A matter of gender? J Neurol. 2014;261(3):504-10.

Margulis, L. Origin of Eukaryotic Cells: Evidence and Research Implications for a Theory of the Origin and Evolution of Microbial, Plant, and Animal Cells on the Precambrian Earth; Yale University Press: London, UK, 1970.

Martínez-Reyes, I. and Chandel, N.S. (2020) Mitochondrial TCA cycle metabolites control physiology and disease. Nat Commun, 11, 102.

Mason PA, Lightowlers RN. Why do mammalian mitochondria possess a mismatch repair activity? FEBS Lett. 2003;554(1-2):6-9.

Mason PA, Matheson EC, Hall AG, Lightowlers RN. Mismatch repair activity in mammalian mitochondria. Nucleic Acids Res. 2003;31(3):1052-8.

Mathupala, S. and Sloan, A.A. (2009) An agarose-based cloning-ring anchoring method for isolation of viable cell clones. Biotechniques, 46, 305-307.

McDougall WM, Okany C, Smith HC. Deaminase activity on single-stranded DNA (ssDNA) occurs in vitro when APOBEC3G cytidine deaminase forms homotetramers and higher-order complexes. J Biol Chem. 2011;286(35):30655-61.

McFarland R, Clark KM, Morris AA, Taylor RW, Macphail S, Lightowlers RN, et al. Multiple neonatal deaths due to a homoplasmic mitochondrial DNA mutation. Nat Genet. 2002;30(2):145-6.

McKinney EA, Oliveira MT. Replicating animal mitochondrial DNA. Genet Mol Biol. 2013;36(3):308-15.

McMahon, M.A., Prakash, T.P., Cleveland, D.W., Bennett, C.F. and Rahdar, M. (2018) Chemically Modified Cpf1-CRISPR RNAs Mediate Efficient Genome Editing in Mammalian Cells. Mol Ther, 26, 1228-1240.

Meagher M, Lightowlers RN. The role of TDP1 and APTX in mitochondrial DNA repair. Biochimie. 2014;100:121-4.

Michaud M, Maréchal-Drouard L, Duchêne AM. Targeting of cytosolic mRNA to mitochondria: naked RNA can bind to the mitochondrial surface. Biochimie. 2014;100:159-66.

Mignotte B, Barat M, Mounolou JC. Characterization of a mitochondrial protein binding to single-stranded DNA. Nucleic Acids Res. 1985;13(5):1703-16.

Minczuk M, He J, Duch AM, Ettema TJ, Chlebowski A, Dzionek K, et al. TEFM (c17orf42) is necessary for transcription of human mtDNA. Nucleic Acids Res. 2011;39(10):4284-99.

Minczuk, M.A. Papworth, J.C. Miller, M.P. Murphy, A. Klug, Development of a single-chain, quasi-dimeric zinc-finger nuclease for the selective degradation of mutated human mitochondrial DNA, Nucleic Acids Res, 36 (2008) 3926-3938.

Mingozzi, K.A. High, Therapeutic in vivo gene transfer for genetic disease using AAV: progress and challenges, Nat Rev Genet, 12 (2011) 341-355.

Miralles Fusté J, Shi Y, Wanrooij S, Zhu X, Jemt E, Persson Ö, et al. In vivo occupancy of mitochondrial single-stranded DNA binding protein supports the strand displacement mode of DNA replication. PLoS Genet. 2014;10(12):e1004832.

Mok BY, de Moraes MH, Zeng J, Bosch DE, Kotrys AV, Raguram A, et al. A bacterial cytidine deaminase toxin enables CRISPR-free mitochondrial base editing. Nature. 2020;583(7817):631-7.

Mok BY, Kotrys AV, Raguram A, Huang TP, Mootha VK, Liu DR. CRISPR-free base editors with enhanced activity and expanded targeting scope in mitochondrial and nuclear DNA. Nat Biotechnol. 2022;40(9):1378-87.

Montoya J, Christianson T, Levens D, Rabinowitz M, Attardi G. Identification of initiation sites for heavy-strand and light-strand transcription in human mitochondrial DNA. Proc Natl Acad Sci U S A. 1982;79(23):7195-9.

Montoya J, Gaines GL, Attardi G. The pattern of transcription of the human mitochondrial rRNA genes reveals two overlapping transcription units. Cell. 1983;34(1):151-9.

Moraes CT, Sciacco M, Ricci E, Tengan CH, Hao H, Bonilla E, et al. Phenotype-genotype correlations in skeletal muscle of patients with mtDNA deletions. Muscle Nerve Suppl. 1995;3:S150-3.

Moretton A, Morel F, Macao B, Lachaume P, Ishak L, Lefebvre M, et al. Selective mitochondrial DNA degradation following double-strand breaks. PLoS One. 2017;12(4):e0176795.

Morita, E., Arii, J., Christensen, D., Votteler, J. and Sundquist, W.I. (2012) Attenuated protein expression vectors for use in siRNA rescue experiments. *Biotechniques*, **0**, 1-5.

Mullins EA, Rodriguez AA, Bradley NP, Eichman BF. Emerging Roles of DNA Glycosylases and the Base Excision Repair Pathway. Trends Biochem Sci. 2019;44(9):765-81.

Muratovska A, Lightowlers RN, Taylor RW, Turnbull DM, Smith RA, Wilce JA, et al. Targeting peptide nucleic acid (PNA) oligomers to mitochondria within cells by conjugation to lipophilic cations: implications for mitochondrial DNA replication, expression and disease. Nucleic Acids Res. 2001;29(9):1852-63.

Naeem, M.M., Maheshan, R., Costford, S.R., Wahedi, A., Trajkovski, M., Plavec, J., Yatsunyk, L.A., Ciesielski, G.L., Kaufman, B.A. and Sondheimer, N. (2019) G-quadruplex-mediated reduction of a pathogenic mitochondrial heteroplasmy. Hum Mol Genet, 28, 3163-3174.

Nagaike T, Suzuki T, Katoh T, Ueda T. Human mitochondrial mRNAs are stabilized with polyadenylation regulated by mitochondria-specific poly(A) polymerase and polynucleotide phosphorylase. J Biol Chem. 2005;280(20):19721-7.

Nagley P, Devenish RJ. Leading organellar proteins along new pathways: the relocation of mitochondrial and chloroplast genes to the nucleus. Trends in Biochemical Sciences. 1989;14(1):31-5.

Nass MM, Nass S. INTRAMITOCHONDRIAL FIBERS WITH DNA CHARACTERISTICS. I. FIXATION AND ELECTRON STAINING REACTIONS. J Cell Biol. 1963;19(3):593-611.

Naviaux RK. Developing a systematic approach to the diagnosis and classification of mitochondrial disease. Mitochondrion. 2004;4(5-6):351-61.

Nesbitt V, Pitceathly RD, Turnbull DM, Taylor RW, Sweeney MG, Mudanohwo EE, et al. The UK MRC Mitochondrial Disease Patient Cohort Study: clinical phenotypes associated with the m.3243A>G mutation--implications for diagnosis and management. J Neurol Neurosurg Psychiatry. 2013;84(8):936-8.

Neupane P, Bhuju S, Thapa N, Bhattarai HK. ATP Synthase: Structure, Function and Inhibition. Biomol Concepts. 2019;10(1):1-10.

Neupert W, Herrmann JM. Translocation of proteins into mitochondria. Annu Rev Biochem. 2007;76:723-49.

Nicholls TJ, Minczuk M. In D-loop: 40 years of mitochondrial 7S DNA. Exp Gerontol. 2014;56:175-81.

Nicolino M, Ferlin T, Forest M, Godinot C, Carrier H, David M, et al. Identification of a large-scale mitochondrial deoxyribonucleic acid deletion in endocrinopathies and deafness: report of two unrelated cases with diabetes mellitus and adrenal insufficiency, respectively. J Clin Endocrinol Metab. 1997;82(9):3063-7.

Nishimasu, F.A. Ran, P.D. Hsu, S. Konermann, S.I. Shehata, N. Dohmae, R. Ishitani, F. Zhang, Nureki, Crystal structure of Cas9 in complex with guide RNA and target DNA, Cell, 156 (2014) 935-949.

Nissanka N, Bacman SR, Plastini MJ, Moraes CT. The mitochondrial DNA polymerase gamma degrades linear DNA fragments precluding the formation of deletions. Nat Commun. 2018;9(1):2491.

Nissanka N, Minczuk M, Moraes CT. Mechanisms of Mitochondrial DNA Deletion Formation. Trends Genet. 2019;35(3):235-44.

Nissanka N, Moraes CT. Mitochondrial DNA heteroplasmy in disease and targeted nuclease-based therapeutic approaches. EMBO Rep. 2020;21(3):e49612.

Niu H, Xiong Q, Yamamoto A, Hayashi-Nishino M, Rikihisa Y. Autophagosomes induced by a bacterial Beclin 1 binding protein facilitate obligatory intracellular infection. Proc Natl Acad Sci U S A. 2012;109(51):20800-7.

Nybo K. GFP imaging in fixed cells. Biotechniques. 2012;52(6):359-60.

Ojala D, Montoya J, Attardi G. tRNA punctuation model of RNA processing in human mitochondria. Nature. 1981;290(5806):470-4.

Olivo PD, Van de Walle MJ, Laipis PJ, Hauswirth WW. Nucleotide sequence evidence for rapid genotypic shifts in the bovine mitochondrial DNA D-loop. Nature. 1983;306(5941):400-2.

Orishchenko, K.E., Sofronova, J.K., Chupakhin, E.G., Lunev, E.A., & Mazunin, I. O. (2016) Delivery Cas9 into mitochondria. Genes & Cells, 11(2), 100-105.

O'Rourke B. Pathophysiological and protective roles of mitochondrial ion channels. J Physiol. 2000;529 Pt 1(Pt 1):23-36.

Orum H, Nielsen PE, Egholm M, Berg RH, Buchardt O, Stanley C. Single base pair mutation analysis by PNA directed PCR clamping. Nucleic Acids Res. 1993;21(23):5332-6.

Osawa S, Jukes TH, Watanabe K, Muto A. Recent evidence for evolution of the genetic code. Microbiol Rev. 1992;56(1):229-64.

Ott M, Amunts A, Brown A. Organization and Regulation of Mitochondrial Protein Synthesis. Annu Rev Biochem. 2016;85:77-101.

Palmieri F, Pierri CL. Mitochondrial metabolite transport. Essays Biochem. 2010;47:37-52.

Peeva V, Blei D, Trombly G, Corsi S, Szukszto MJ, Rebelo-Guiomar P, et al. Linear mitochondrial DNA is rapidly degraded by components of the replication machinery. Nature Communications. 2018;9(1):1727.

Pereira, G.C., Branco, A.F., Matos, J.A., Pereira, S.L., Parke, D., Perkins, E.L., Serafim, T.L., Sardão, V.A., Santos, M.S., Moreno, A.J. et al. (2007) Mitochondrially targeted effects of berberine [Natural Yellow 18, 5,6-dihydro-9,10-dimethoxybenzo(g)-1,3-benzodioxolo(5,6-a) quinolizinium] on K1735-M2 mouse melanoma cells: comparison with direct effects on isolated mitochondrial fractions. J Pharmacol Exp Ther, 323, 636-649.

Pham XH, Farge G, Shi Y, Gaspari M, Gustafsson CM, Falkenberg M. Conserved sequence box II directs transcription termination and primer formation in mitochondria. J Biol Chem. 2006;281(34):24647-52.

Phillips AF, Millet AR, Tigano M, Dubois SM, Crimmins H, Babin L, et al. Single-Molecule Analysis of mtDNA Replication Uncovers the Basis of the Common Deletion. Mol Cell. 2017;65(3):527-38.e6.

Pickles S, Vigié P, Youle RJ. Mitophagy and Quality Control Mechanisms in Mitochondrial Maintenance. Curr Biol. 2018;28(4):R170-r85.

Pipek OA, Medgyes-Horváth A, Dobos L, Stéger J, Szalai-Gindl J, Visontai D, et al. Worldwide human mitochondrial haplogroup distribution from urban sewage. Sci Rep. 2019;9(1):11624.

Porcelli AM, Ghelli A, Zanna C, Pinton P, Rizzuto R, Rugolo M. pH difference across the outer mitochondrial membrane measured with a green fluorescent protein mutant. Biochem Biophys Res Commun. 2005;326(4):799-804.

Posse V, Gustafsson CM. Human Mitochondrial Transcription Factor B2 Is Required for Promoter Melting during Initiation of Transcription. J Biol Chem. 2017;292(7):2637-45.

Protasoni M, Zeviani M. Mitochondrial Structure and Bioenergetics in Normal and Disease Conditions. Int J Mol Sci. 2021;22(2).

Rahman J, Rahman S. Mitochondrial medicine in the omics era. Lancet. 2018;391(10139):2560-74.

Rai PK, Craven L, Hoogewijs K, Russell OM, Lightowlers RN. Advances in methods for reducing mitochondrial DNA disease by replacing or manipulating the mitochondrial genome. Essays Biochem. 2018;62(3):455-65.

Rasola A, Bernardi P. Mitochondrial permeability transition in Ca(2+)-dependent apoptosis and necrosis. Cell Calcium. 2011;50(3):222-33.

Ravasi T, Huber T, Zavolan M, Forrest A, Gaasterland T, Grimmond S, et al. Systematic characterization of the zinc-finger-containing proteins in the mouse transcriptome. Genome Res. 2003;13(6b):1430-42.

Reddy, A. Ocampo, K. Suzuki, J. Luo, S.R. Bacman, S.L. Williams, A. Sugawara, D. Okamura, Y. Tsunekawa, J. Wu, D. Lam, X. Xiong, N. Montserrat, C.R. Esteban, G.H. Liu, I. Sancho-Martinez, D. Manau, S. Civico, F. Cardellach, M. Del Mar O'Callaghan, J. Campistol, H. Zhao, J.M. Campistol, C.T. Moraes, J.C. Izpisua Belmonte, Selective elimination of mitochondrial mutations in the germline by genome editing, Cell, 161 (2015) 459-469.

Rehling P, Model K, Brandner K, Kovermann P, Sickmann A, Meyer HE, et al. Protein insertion into the mitochondrial inner membrane by a twin-pore translocase. Science. 2003;299(5613):1747-51.

Ren, Z., Zhang, X., Ding, T., Zhong, Z., Hu, H., Xu, Z. and Deng, J. (2020) Mitochondrial Dynamics Imbalance: A Strategy for Promoting Viral Infection. Front Microbiol, 11, 1992.

Reyes A, Kazak L, Wood SR, Yasukawa T, Jacobs HT, Holt IJ. Mitochondrial DNA replication proceeds via a 'bootlace' mechanism involving the incorporation of processed transcripts. Nucleic Acids Res. 2013;41(11):5837-50.

Ringel R, Sologub M, Morozov YI, Litonin D, Cramer P, Temiakov D. Structure of human mitochondrial RNA polymerase. Nature. 2011;478(7368):269-73.

Rizzuto R, De Stefani D, Raffaello A, Mammucari C. Mitochondria as sensors and regulators of calcium signalling. Nat Rev Mol Cell Biol. 2012;13(9):566-78.

Robinson JT, Thorvaldsdóttir H, Winckler W, Guttman M, Lander ES, Getz G, et al. Integrative genomics viewer. Nat Biotechnol. 2011;29(1):24-6.

Rorbach J, Gao F, Powell CA, D'Souza A, Lightowlers RN, Minczuk M, et al. Human mitochondrial ribosomes can switch their structural RNA composition. Proc Natl Acad Sci U S A. 2016;113(43):12198-201.

Rossi MN, Carbone M, Mostocotto C, Mancone C, Tripodi M, Maione R, et al. Mitochondrial localization of PARP-1 requires interaction with mitofilin and is involved in the maintenance of mitochondrial DNA integrity. J Biol Chem. 2009;284(46):31616-24.

Rossignol R, Faustin B, Rocher C, Malgat M, Mazat JP, Letellier T. Mitochondrial threshold effects. Biochem J. 2003;370(Pt 3):751-62.

Salinas T, El Farouk-Ameqrane S, Ubrig E, Sauter C, Duchêne AM, Maréchal-Drouard L. Molecular basis for the differential interaction of plant mitochondrial VDAC proteins with tRNAs. Nucleic Acids Res. 2014;42(15):9937-48.

Samuels DC, Schon EA, Chinnery PF. Two direct repeats cause most human mtDNA deletions. Trends Genet. 2004;20(9):393-8.

Sancar A, Lindsey-Boltz LA, Unsal-Kaçmaz K, Linn S. Molecular mechanisms of mammalian DNA repair and the DNA damage checkpoints. Annu Rev Biochem. 2004;73:39-85.

Schatz G, Haslbrunner E, Tuppy H. DEOXYRIBONUCLEIC ACID ASSOCIATED WITH YEAST MITOCHONDRIA. Biochem Biophys Res Commun. 1964;15(2):127-32.

Schmidt O, Pfanner N, Meisinger C. Mitochondrial protein import: from proteomics to functional mechanisms. Nat Rev Mol Cell Biol. 2010;11(9):655-67.

Schneider C.A., Rasband W.S., Eliceiri K.W. NIH Image to ImageJ: 25 years of image analysis. Nat. Methods. 2012; 9:671–675.

Schwartz M, Vissing J. Paternal inheritance of mitochondrial DNA. N Engl J Med. 2002;347(8):576-80.

Selkova P, Vasileva A, Pobegalov G, Musharova O, Arseniev A, Kazalov M, et al. Position of Deltaproteobacteria Cas12e nuclease cleavage sites depends on spacer length of guide RNA. RNA Biol. 2020;17(10):1472-9.

Sevarino KA, Poyton RO. Mitochondrial membrane biogenesis: identification of a precursor to yeast cytochrome c oxidase subunit II, an integral polypeptide. Proc Natl Acad Sci U S A. 1980;77(1):142-6.

Sfeir A, Symington LS. Microhomology-Mediated End Joining: A Back-up Survival Mechanism or Dedicated Pathway? Trends Biochem Sci. 2015;40(11):701-14.

Shadel GS, Clayton DA. Mitochondrial DNA maintenance in vertebrates. Annu Rev Biochem. 1997;66:409-35.

Shamanskiy V, Mikhailova AA, Tretiakov EO, Ushakova K, Mikhailova AG, Oreshkov S, et al. Secondary structure of the human mitochondrial genome affects formation of deletions. BMC Biol. 2023;21(1):103.

Sharma N, Pasala MS, Prakash A. Mitochondrial DNA: Epigenetics and environment. Environ Mol Mutagen. 2019;60(8):668-82.

Shebanova, R., Nikitchina, N., Shebanov, N., Mekler, V., Kuznedelov, K., Ulashchik, E., Vasilev, R., Sharko, O., Shmanai, V., Tarassov, I. et al. (2021) Efficient target cleavage by Type V Cas12a effectors programmed with split CRISPR RNA. Nucleic Acids Research, 50, 1162-1173.

Shen K, Pender CL, Bar-Ziv R, Zhang H, Wickham K, Willey E, et al. Mitochondria as Cellular and Organismal Signaling Hubs. Annu Rev Cell Dev Biol. 2022;38:179-218.

Shoffner JM, Lott MT, Lezza AM, Seibel P, Ballinger SW, Wallace DC. Myoclonic epilepsy and ragged-red fiber disease (MERRF) is associated with a mitochondrial DNA tRNA(Lys) mutation. Cell. 1990;61(6):931-7.

Shokolenko IN, Alexeyev MF. Mitochondrial transcription in mammalian cells. Front Biosci (Landmark Ed). 2017;22(5):835-53.

Shoop WK, Bacman SR, Barrera-Paez JD, Moraes CT. Mitochondrial gene editing. Nature Reviews Methods Primers. 2023;3(1):19.

Shoubridge EA, Wai T. Mitochondrial DNA and the mammalian oocyte. Curr Top Dev Biol. 2007;77:87-111.

Shutt TE, Gray MW. Bacteriophage origins of mitochondrial replication and transcription proteins. Trends Genet. 2006;22(2):90-5.

Silva-Pinheiro P, Minczuk M. The potential of mitochondrial genome engineering. Nat Rev Genet. 2022;23(4):199-214.

Silva-Pinheiro P, Nash PA, Van Haute L, Mutti CD, Turner K, Minczuk M. In vivo mitochondrial base editing via adeno-associated viral delivery to mouse post-mitotic tissue. Nat Commun. 2022;13(1):750.

Silva-Pinheiro, C.D. Mutti, L. Van Haute, C.A. Powell, P.A. Nash, K. Turner, M. Minczuk, A library of base editors for the precise ablation of all protein-coding genes in the mouse mitochondrial genome, Nat Biomed Eng, (2022).

Simsek D, Furda A, Gao Y, Artus J, Brunet E, Hadjantonakis AK, et al. Crucial role for DNA ligase III in mitochondria but not in Xrcc1-dependent repair. Nature. 2011;471(7337):245-8.

Singh D, Mallon J, Poddar A, Wang Y, Tippana R, Yang O, et al. Real-time observation of DNA target interrogation and product release by the RNA-guided endonuclease CRISPR Cpf1 (Cas12a). Proc Natl Acad Sci U S A. 2018;115(21):5444-9.

Smirnov A, Tarassov I, Mager-Heckel AM, Letzelter M, Martin RP, Krasheninnikov IA, et al. Two distinct structural elements of 5S rRNA are needed for its import into human mitochondria. Rna. 2008;14(4):749-59.

Soldatov VO, Kubekina MV, Skorkina MY, Belykh AE, Egorova TV, Korokin MV, et al. Current advances in gene therapy of mitochondrial diseases. J Transl Med. 2022;20(1):562.

Soong NW, Hinton DR, Cortopassi G, Arnheim N. Mosaicism for a specific somatic mitochondrial DNA mutation in adult human brain. Nat Genet. 1992;2(4):318-23.

Spelbrink JN, Li FY, Tiranti V, Nikali K, Yuan QP, Tariq M, et al. Human mitochondrial DNA deletions associated with mutations in the gene encoding Twinkle, a phage T7 gene 4-like protein localized in mitochondria. Nat Genet. 2001;28(3):223-31.

Srivastava, C.T. Moraes, Double-strand breaks of mouse muscle mtDNA promote large deletions similar to multiple mtDNA deletions in humans, Hum Mol Genet, 14 (2005) 893-902.

Stella S, Alcón P, Montoya G. Structure of the Cpf1 endonuclease R-loop complex after target DNA cleavage. Nature. 2017;546(7659):559-63.

Stewart JB. Current progress with mammalian models of mitochondrial DNA disease. J Inherit Metab Dis. 2021;44(2):325-42.

Stewart, J.B. and Chinnery, P.F. (2015) The dynamics of mitochondrial DNA heteroplasmy: implications for human health and disease. Nat Rev Genet, 16, 530-542.

Stewart, Polyadenylation and nuclear export of mRNAs, J Biol Chem, 294 (2019) 2977-2987.

Strauβ A, Lahaye T. Zinc fingers, TAL effectors, or Cas9-based DNA binding proteins: what's best for targeting desired genome loci? Mol Plant. 2013;6(5):1384-7.

Sugisaki H, Kanazawa S. New restriction endonucleases from Flavobacterium okeanokoites (FokI) and Micrococcus luteus (MluI). Gene. 1981;16(1-3):73-8.

Summer, S., Smirnova, A., Gabriele, A., Toth, U., Fasemore, A.M., Förstner, K.U., Kuhn, L., Chicher, J., Hammann, P., Mitulović, G. et al. (2020) YBEY is an essential biogenesis factor for mitochondrial ribosomes. Nucleic Acids Res, 48, 9762-9786.

Sutovsky P, Moreno RD, Ramalho-Santos J, Dominko T, Simerly C, Schatten G. Ubiquitinated sperm mitochondria, selective proteolysis, and the regulation of mitochondrial inheritance in mammalian embryos. Biol Reprod. 2000;63(2):582-90.

Tadi SK, Sebastian R, Dahal S, Babu RK, Choudhary B, Raghavan SC. Microhomology-mediated end joining is the principal mediator of double-strand break repair during mitochondrial DNA lesions. Mol Biol Cell. 2016;27(2):223-35.

Tahbaz N, Subedi S, Weinfeld M. Role of polynucleotide kinase/phosphatase in mitochondrial DNA repair. Nucleic Acids Res. 2012;40(8):3484-95.

Tan BG, Mutti CD, Shi Y, Xie X, Zhu X, Silva-Pinheiro P, et al. The human mitochondrial genome contains a second light strand promoter. Mol Cell. 2022;82(19):3646-60.e9.

Tanaka, H.J. Borgeld, J. Zhang, S. Muramatsu, J.S. Gong, M. Yoneda, W. Maruyama, M. Naoi, T. Ibi, K. Sahashi, M. Shamoto, N. Fuku, M. Kurata, Y. Yamada, K. Nishizawa, Y. Akao, N. Ohishi, S. Miyabayashi, H. Umemoto, T. Muramatsu, K. Furukawa, A. Kikuchi, I. Nakano, K. Ozawa, K. Yagi, Gene therapy for mitochondrial disease by delivering restriction endonuclease SmaI into mitochondria, J Biomed Sci, 9 (2002) 534-541.

Tarassov I, Entelis N, Martin RP. An intact protein translocating machinery is required for mitochondrial import of a yeast cytoplasmic tRNA. J Mol Biol. 1995;245(4):315-23.

Taylor RW, Chinnery PF, Turnbull DM, Lightowlers RN. Selective inhibition of mutant human mitochondrial DNA replication in vitro by peptide nucleic acids. Nat Genet. 1997;15(2):212-5.

Temperley R, Richter R, Dennerlein S, Lightowlers RN, Chrzanowska-Lightowlers ZM. Hungry codons promote frameshifting in human mitochondrial ribosomes. Science. 2010;327(5963):301.

Terzioglu M, Ruzzenente B, Harmel J, Mourier A, Jemt E, López MD, et al. MTERF1 binds mtDNA to prevent transcriptional interference at the light-strand promoter but is dispensable for rRNA gene transcription regulation. Cell Metab. 2013;17(4):618-26.

The Galaxy platform for accessible, reproducible and collaborative biomedical analyses: 2022 update. Nucleic Acids Res. 2022;50(W1):W345-w51.

Tigano M, Vargas DC, Tremblay-Belzile S, Fu Y, Sfeir A. Nuclear sensing of breaks in mitochondrial DNA enhances immune surveillance. Nature. 2021;591(7850):477-81.

Tonin Y, Heckel AM, Vysokikh M, Dovydenko I, Meschaninova M, Rötig A, et al. Modeling of antigenomic therapy of mitochondrial diseases by mitochondrially addressed RNA targeting a pathogenic point mutation in mitochondrial DNA. J Biol Chem. 2014;289(19):13323-34.

Treiber T, Treiber N, Meister G. Regulation of microRNA biogenesis and its crosstalk with other cellular pathways. Nat Rev Mol Cell Biol. 2019;20(1):5-20.

Trifunov S, Pyle A, Valentino ML, Liguori R, Yu-Wai-Man P, Burté F, et al. Clonal expansion of mtDNA deletions: different disease models assessed by digital droplet PCR in single muscle cells. Sci Rep. 2018;8(1):11682.

Trombly G, Said AM, Kudin AP, Peeva V, Altmüller J, Becker K, et al. The Fate of Oxidative Strand Breaks in Mitochondrial DNA. Antioxidants (Basel). 2023;12(5).

Tuppen HA, Blakely EL, Turnbull DM, Taylor RW. Mitochondrial DNA mutations and human disease. Biochim Biophys Acta. 2010;1797(2):113-28.

Underwood E, Redell JB, Zhao J, Moore AN, Dash PK. A method for assessing tissue respiration in anatomically defined brain regions. Sci Rep. 2020;10(1):13179.

Van Houten B, Hunter SE, Meyer JN. Mitochondrial DNA damage induced autophagy, cell death, and disease. Front Biosci (Landmark Ed). 2016;21(1):42-54.

Vendramin R, Verheyden Y, Ishikawa H, Goedert L, Nicolas E, Saraf K, et al. SAMMSON fosters cancer cell fitness by concertedly enhancing mitochondrial and cytosolic translation. Nat Struct Mol Biol. 2018;25(11):1035-46.

Verechshagina N, Nikitchina N, Yamada Y, Harashima H, Tanaka M, Orishchenko K, et al. Future of human mitochondrial DNA editing technologies. Mitochondrial DNA A DNA Mapp Seq Anal. 2019;30(2):214-21.

Verechshagina NA, Konstantinov YM, Kamenski PA, Mazunin IO. Import of Proteins and Nucleic Acids into Mitochondria. Biochemistry (Mosc). 2018;83(6):643-61.

Wallace DC, Chalkia D. Mitochondrial DNA genetics and the heteroplasmy conundrum in evolution and disease. Cold Spring Harb Perspect Biol. 2013;5(11):a021220.

Wallace SS. Base excision repair: a critical player in many games. DNA Repair (Amst). 2014;19:14-26.

Wang G, Chen HW, Oktay Y, Zhang J, Allen EL, Smith GM, et al. PNPASE regulates RNA import into mitochondria. Cell. 2010;142(3):456-67.

Wang T, Sha H, Ji D, Zhang HL, Chen D, Cao Y, et al. Polar body genome transfer for preventing the transmission of inherited mitochondrial diseases. Cell. 2014;157(7):1591-604.

Wang, G., Chen, H.W., Oktay, Y., Zhang, J., Allen, E.L., Smith, G.M., Fan, K.C., Hong, J.S., French, S.W., McCaffery, J.M. et al. (2010) PNPASE regulates RNA import into mitochondria. Cell, 142, 456-467.

Wanrooij S, Fusté JM, Farge G, Shi Y, Gustafsson CM, Falkenberg M. Human mitochondrial RNA polymerase primes lagging-strand DNA synthesis in vitro. Proc Natl Acad Sci U S A. 2008;105(32):11122-7.

Warren JM, Salinas-Giegé T, Triant DA, Taylor DR, Drouard L, Sloan DB. Rapid Shifts in Mitochondrial tRNA Import in a Plant Lineage with Extensive Mitochondrial tRNA Gene Loss. Mol Biol Evol. 2021;38(12):5735-51.

Watson K. The organization of ribosomal granules within mitochondrial structures of aerobic and anaerobic cells of Saccharomyces cerevisae. J Cell Biol. 1972;55(3):721-6.

Wei Y, Li Z, Xu K, Feng H, Xie L, Li D, et al. Mitochondrial base editor DdCBE causes substantial DNA off-target editing in nuclear genome of embryos. Cell Discov. 2022;8(1):27.

Westermann B. Mitochondrial fusion and fission in cell life and death. Nat Rev Mol Cell Biol. 2010;11(12):872-84.

Whelan, D.R. and Bell, T.D. (2015) Image artifacts in single molecule localization microscopy: why optimization of sample preparation protocols matters. Sci Rep, 5, 7924.

White SL, Collins VR, Wolfe R, Cleary MA, Shanske S, DiMauro S, et al. Genetic counseling and prenatal diagnosis for the mitochondrial DNA mutations at nucleotide 8993. Am J Hum Genet. 1999;65(2):474-82.

Wiedemann N, Truscott KN, Pfannschmidt S, Guiard B, Meisinger C, Pfanner N. Biogenesis of the protein import channel Tom40 of the mitochondrial outer membrane: intermembrane space components are involved in an early stage of the assembly pathway. J Biol Chem. 2004;279(18):18188-94.

Wisnovsky S, Jean SR, Kelley SO. Mitochondrial DNA repair and replication proteins revealed by targeted chemical probes. Nat Chem Biol. 2016;12(7):567-73.

Wolstenholme DR. Animal mitochondrial DNA: structure and evolution. Int Rev Cytol. 1992;141:173-216.

Wong TW, Clayton DA. In vitro replication of human mitochondrial DNA: accurate initiation at the origin of light-strand synthesis. Cell. 1985;42(3):951-8.

Wu Y, Sha B. Crystal structure of yeast mitochondrial outer membrane translocon member Tom70p. Nat Struct Mol Biol. 2006;13(7):589-93.

Xu W, Boyd RM, Tree MO, Samkari F, Zhao L. Mitochondrial transcription factor A promotes DNA strand cleavage at abasic sites. Proc Natl Acad Sci U S A. 2019;116(36):17792-9.

Yakubovskaya E, Chen Z, Carrodeguas JA, Kisker C, Bogenhagen DF. Functional human mitochondrial DNA polymerase gamma forms a heterotrimer. J Biol Chem. 2006;281(1):374-82.

Yakubovskaya E, Mejia E, Byrnes J, Hambardjieva E, Garcia-Diaz M. Helix unwinding and base flipping enable human MTERF1 to terminate mitochondrial transcription. Cell. 2010;141(6):982-93.

Yamada Y, Harashima H. MITO-Porter for Mitochondrial Delivery and Mitochondrial Functional Analysis. Handb Exp Pharmacol. 2017;240:457-72.

Yamano, T., Nishimasu, H., Zetsche, B., Hirano, H., Slaymaker, I.M., Li, Y., Fedorova, I., Nakane, T., Makarova, K.S., Koonin, E.V. et al. (2016) Crystal Structure of Cpf1 in Complex with Guide RNA and Target DNA. Cell, 165, 949-962.

Yang, H. Wu, X. Kang, Y. Liang, T. Lan, T. Li, T. Tan, J. Peng, Q. Zhang, G. An, Y. Liu, Q. Yu, Z. Ma, Y. Lian, B.S. Soh, Q. Chen, P. Liu, Y. Chen, X. Sun, R. Li, X. Zhen, P. Liu, Y. Yu, X. Li, Y. Fan, Targeted elimination of mutant mitochondrial DNA in MELAS-iPSCs by mitoTALENs, Protein Cell, 9 (2018) 283-297.

Yarham JW, Lamichhane TN, Pyle A, Mattijssen S, Baruffini E, Bruni F, et al. Defective i6A37 modification of mitochondrial and cytosolic tRNAs results from pathogenic mutations in TRIT1 and its substrate tRNA. PLoS Genet. 2014;10(6):e1004424.

Yasukawa T, Reyes A, Cluett TJ, Yang MY, Bowmaker M, Jacobs HT, et al. Replication of vertebrate mitochondrial DNA entails transient ribonucleotide incorporation throughout the lagging strand. Embo j. 2006;25(22):5358-71.

Young JC, Hoogenraad NJ, Hartl FU. Molecular chaperones Hsp90 and Hsp70 deliver preproteins to the mitochondrial import receptor Tom70. Cell. 2003;112(1):41-50.

Yu H, Sant DW, Wang G, Guy J. Mitochondrial Transfer of the Mutant Human ND6T14484C Gene Causes Visual Loss and Optic Neuropathy. Transl Vis Sci Technol. 2020;9(11):1.

Yusoff, Abdul Aziz Mohamed, et al. "Understanding mitochondrial DNA in brain tumorigenesis." Molecular considerations and evolving surgical management issues in the treatment of patients with a brain tumor (2015): 3-28.\

Yu-Wai-Man P, Turnbull DM, Chinnery PF. Leber hereditary optic neuropathy. J Med Genet. 2002;39(3):162-9.

Zekonyte, S.R. Bacman, J. Smith, W. Shoop, C.V. Pereira, G. Tomberlin, J. Stewart, D. Jantz, C.T. Moraes, Mitochondrial targeted meganuclease as a platform to eliminate mutant mtDNA in vivo, Nat Commun, 12 (2021) 3210.

Zetsche, B., Gootenberg, J.S., Abudayyeh, O.O., Slaymaker, I.M., Makarova, K.S., Essletzbichler, P., Volz, S.E., Joung, J., van der Oost, J., Regev, A. et al. (2015) Cpf1 is a single RNA-guided endonuclease of a class 2 CRISPR-Cas system. Cell, 163, 759-771.

Zetsche, B., Heidenreich, M., Mohanraju, P., Fedorova, I., Kneppers, J., DeGennaro, E.M., Winblad, N., Choudhury, S.R., Abudayyeh, O.O., Gootenberg, J.S. et al. (2017) Multiplex gene editing by CRISPR-Cpf1 using a single crRNA array. Nat Biotechnol, 35, 31-34.

Zeviani M, Moraes CT, DiMauro S, Nakase H, Bonilla E, Schon EA, et al. Deletions of mitochondrial DNA in Kearns-Sayre syndrome. Neurology. 1988;38(9):1339-46.

Zhang J, Liu H, Luo S, Lu Z, Chávez-Badiola A, Liu Z, et al. Live birth derived from oocyte spindle transfer to prevent mitochondrial disease. Reprod Biomed Online. 2017;34(4):361-8.

Zhang L, Zuris JA, Viswanathan R, Edelstein JN, Turk R, Thommandru B, et al. AsCas12a ultra nuclease facilitates the rapid generation of therapeutic cell medicines. Nat Commun. 2021;12(1):3908.

Zhang X, Zuo X, Yang B, Li Z, Xue Y, Zhou Y, et al. MicroRNA directly enhances mitochondrial translation during muscle differentiation. Cell. 2014;158(3):607-19.

Zorova LD, Popkov VA, Plotnikov EY, Silachev DN, Pevzner IB, Jankauskas SS, et al. Mitochondrial membrane potential. Anal Biochem. 2018;552:50-9.

Zuker, M. (2003) Mfold web server for nucleic acid folding and hybridization prediction. Nucleic Acids Res, 31, 3406-3415.

6. ANNEXES

Publication 4

International Journal of Molecular Sciences, 2022:

Efficient introducing large gene deletions in human cell line by a novel Type V-A effector from *Ruminococcus bromii*

Ruslan Vasilev[1,2*], Natalia Gunitseva[1], Regina Shebanova[3], Aleksei Korzhenkov[1], Anna Vlaskina[1], Marta Evteeva[1], Irina Polushkina[1], Natalia Nikitchina[3,4], Stepan Toshchakov[1], Piotr Kamenski[2], Maksim Patrushev[1] and Ilya Mazunin[3*]

[1] Kurchatov Genomics Center, National Research Center "Kurchatov Institute", Moscow, 123098, Russia

[2] Faculty of Biology, Lomonosov Moscow State University, Moscow, 119991, Russia

[3] Center of Life Sciences, Skolkovo Institute of Science and Technology, Moscow, 143026, Russia

[4] UMR7156 – Molecular Genetics, Genomics, Microbiology, University of Strasbourg, Strasbourg, 67000, France

International Journal of
Molecular Sciences

MDPI

Article

Targeted Modification of Mammalian DNA by a Novel Type V Cas12a Endonuclease from *Ruminococcus bromii*

Ruslan Vasilev [1,2,*], Natalia Gunitseva [1], Regina Shebanova [3], Aleksei Korzhenkov [1], Anna Vlaskina [1], Marta Evteeva [1], Irina Polushkina [1], Natalia Nikitchina [3,4], Stepan Toshchakov [1], Piotr Kamenski [2], Maxim Patrushev [1] and Ilya Mazunin [3,5,*]

[1] Kurchatov Genomics Center, National Research Center "Kurchatov Institute", 123098 Moscow, Russia
[2] Faculty of Biology, Lomonosov Moscow State University, 119991 Moscow, Russia
[3] Center of Life Sciences, Skolkovo Institute of Science and Technology, 143026 Moscow, Russia
[4] UMR7156–Molecular Genetics, Genomics, Microbiology, University of Strasbourg and Centre National de la Recherche Scientifique (CNRS), 67000 Strasbourg, France
[5] Medical Genomics LLC, 119192 Moscow, Russia
* Correspondence: ruavasilev@gmail.com (R.V.); i.mazunin@skoltech.ru (I.M.)

Abstract: Type V Cas12a nucleases are DNA editors working in a wide temperature range and using expanded protospacer-adjacent motifs (PAMs). Though they are widely used, there is still a demand for discovering new ones. Here, we demonstrate a novel ortholog from *Ruminococcus bromii* sp. entitled RbCas12a, which is able to efficiently cleave target DNA templates, using the particularly high accessibility of PAM 5′-YYN and a relatively wide temperature range from 20 °C to 42 °C. In comparison to *Acidaminococcus* sp. (AsCas12a) nuclease, RbCas12a is capable of processing DNA more efficiently, and can be active upon being charged by spacer-only RNA at lower concentrations in vitro. We show that the human-optimized RbCas12a nuclease is also active in mammalian cells, and can be applied for efficient deletion incorporation into the human genome. Given the advantageous properties of RbCas12a, this enzyme shows potential for clinical and biotechnological applications within the field of genome editing.

Keywords: Cas endonuclease; CRISPR; genome editing; mammalian cells; site-directed mutagenesis

check for updates

Citation: Vasilev, R.; Gunitseva, N.; Shebanova, R.; Korzhenkov, A.; Vlaskina, A.; Evteeva, M.; Polushkina, I.; Nikitchina, N.; Toshchakov, S.; Kamenski, P.; et al. Targeted Modification of Mammalian DNA by a Novel Type V Cas12a Endonuclease from *Ruminococcus bromii*. *Int. J. Mol. Sci.* **2022**, *23*, 9289. https://doi.org/10.3390/ijms23169289

Academic Editor: Qunxin She

Received: 18 July 2022
Accepted: 16 August 2022
Published: 18 August 2022

Publisher's Note: MDPI stays neutral with regard to jurisdictional claims in published maps and institutional affiliations.

Copyright: © 2022 by the authors. Licensee MDPI, Basel, Switzerland. This article is an open access article distributed under the terms and conditions of the Creative Commons Attribution (CC BY) license (https://creativecommons.org/licenses/by/4.0/).

1. Introduction

CRISPR/Cas systems are hosted in archaeal and bacterial genomes, at times within their mobile elements, and are generally accepted as a type of "immune system" for protection against nucleic acid invaders. These systems contain short fragments of invader DNA, that is, spacers surrounded by repetitive nucleotide sequences called direct repeats. Depending on the CRISPR subtype variant, *cas* genes can be located downstream or upstream from the repeats at the same locus and encode spacer integration elements, including the genes encoding the effector complex, *cas1*, *cas2*, and occasionally *cas4*. The effector module involved in target DNA cleavage consists of several independent proteins, in the case of the Class 1 system, or a single multidomain protein, in the case of the Class 2 system. Effectors are typically programed using one or two RNA molecules for successful target recognition. Most CRISPR/Cas systems require the presence of a protospacer-adjacent motif (PAM), which allows the complex to distinguish spacers already located at CRISPR modules from the DNA of novel invaders [1–3]. The first effector, Cas9 of *Streptococcus pyogenes*, was discovered in 2012, and is currently the most widely used RNA-guided DNA endonuclease in many areas of life sciences [4]. SpCas9 requires a G-rich PAM and two RNA molecules, crRNA and tracrRNA, which can be artificially combined in the format of a single-guide RNA (sgRNA). The assembled nucleoprotein complex in the presence of a dsDNA matrix generates RNA-guided, blunt-ended, double-strand breaks 3 nts upstream of the PAM site. During the last decade, a number of Cas9 orthologs have been discovered, characterized,

and modified, providing more sensitive, efficient, and/or PAM-independent enzymes in the arsenal of researchers and commercial companies [5]. Another recently discovered ortholog, Cas12a [6], can be considered as an alternative to Cas9 due to its distinct features. Firstly, its ability to address T-rich PAMs allows for the editing of additional target motifs. Secondly, it needs to be charged with a short single RNA, which is easier to synthesize or encode for cell delivery agents. Thirdly, Cas12a induces 5′-staggered double-stranded DNA breaks in contrast to Cas9. Fourth, one of the important differences between Cas9 and Cas12a is the ability of Cas12a to process crRNA. Finally, there is an unpredictable activity of Cas12a proteins required to exert collateral activity in relation to any ssDNA molecules after dsDNA target cleavage. This property has been successfully adapted for a number of possible Cas12a-based diagnostic tools [7–9].

To the best of our knowledge, there have been 19 Cas12a orthologs applied for genome editing in human cells thus far [10–16] (Table S1). Due to the heat sensitivity of plant cells above room temperature, the search for temperature-tolerant Cas12a orthologs, as well as the development of temperature-insensitive Cas12a mutants, is of particular interest for plant genome editing. In this study, we addressed some biochemical features and the fundamental possibility of using the novel Cas12a ortholog from *Ruminococcus bromii* sp., called RbCas12a. We demonstrate that RbCas12a is an active RNA-guided DNA endonuclease that can efficiently introduce double-stranded breaks in DNA fragments with a three-nucleotide 5′-YYN PAM, where Y represents C or T. The logo 5′-YYN was proved by testing all possible combinations with an in vitro cleavage experiment. The RbCas12a was found to function well in a temperature range of 25–42 °C. We also demonstrate that RbCas12a can be used to edit genomic DNA contained in human HEK293T cells. Based on our findings, we believe that RbCas12a has the potential to become a molecular tool, providing an expanded range of target motifs in genome engineering applications.

2. Results

2.1. Characterization of CRISPR–Cas12 Subtype VA Endonuclease from Ruminococcus bromii sp.

Comparative sequence and protein architecture analysis showed that the novel nuclease from *Ruminococcus bromii* was most closely related to the CRISPR–Cas12a Type V family of enzymes, which contain a single RuvC nuclease domain that is responsible for RNA-guided DNA cleavage (Figure 1). Catalytic Asp1194 and Glu1290 amino acid residues (numeration for multiple alignment), which are conserved in all known Cas12a orthologs, were also present in RbCas12a.

Because of the sequence and protein architecture similarity between RbCas12a and other Cas12a orthologs, and LbCas12a in particular (Figure 1B), we chose to use 5′-TTTG PAM for initial experiments. In order to study the RbCas12a system requirements, we performed an in vitro DNA cleavage assay using the purified RbCas12a nuclease, chemically synthesized crRNAs, and PCR-derived DNA substrate. According to published data, a number of different noncustom cleavage buffers, as well as NEBuffers, for Cas12a-family nucleases, have been used. We were interested in determining which of the buffers was the most suitable for in vitro DNA cleavage by the RbCas12a nuclease. We found no differences in the tested buffers, and chose to use NEBuffer 2 in the experiments referred to below (Figure S1). The reaction products were separated by gel electrophoresis and visualized by ethidium bromide staining, and the extent of DNA substrate cleavage was quantified as described in the Materials and Methods. To further examine RbCas12a properties, we were interested in determining whether divalent cations could affect RbCas12a cleavage ability. Seven ions, including Ca^{2+}, Ni^{2+}, Mn^{2+}, Mg^{2+}, Zn^{2+}, Cu^{2+}, and Co^{2+} were investigated as potential cofactors of the enzyme. As shown in Figure 2, Mn^{2+} and Mg^{2+} had a comparable effect on the RbCas12a cleavage activity, with only slightly higher efficiency observed for Mg^{2+}, whereas Ni^{2+} and Zn^{2+} showed low activity of the nuclease. Although RbCas12a retained the ability to cleave the target in the presence of Co^{2+} ions, only half of the DNA was found to be cleaved in three series of experiments. Ca^{2+} and Cu^{2+} drastically affected

the reactions without any traces of cleavage found on the gel. As expected, the control reaction with no divalent cation addition showed the absence of endonucleolytic activity.

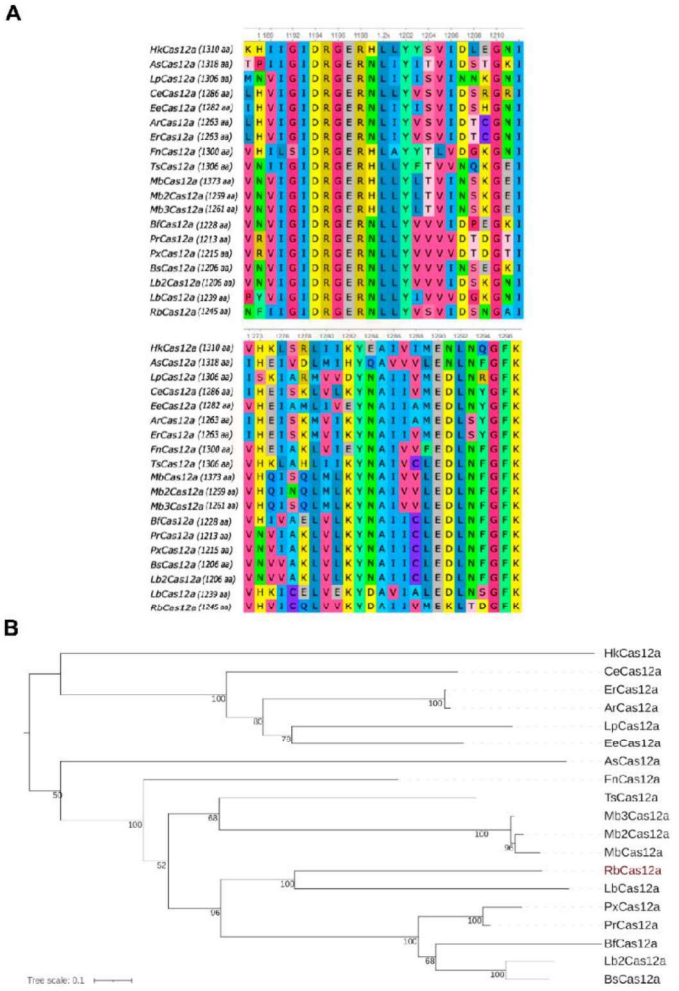


Figure 1. Relationship of RbCas12a to other Cas12a orthologs. (**A**) Multiple sequence alignments of RbCpf1 with common orthologs of 18 Cas12a proteins that function in human cells. Catalytic Asp1194 and Glu1290 residues (numeration shown here for total alignment) are conserved (HkCas12a, *Helcococcus kunzii* ATCC 51366; CeCas12a, *Coprococcus eutactus* sp.; ErCas12a, *Eubacterium rectale* sp.; ArCas12a, *Agathobacter rectalis* strain 2789STDY5834884; LpCas12a, *Lachnospira pectinoschiza* strain 2789STDY5834886; EeCas12a, *Lachnospira eligens* ATCC 27750; AsCas12a, *Acidaminococcus* sp. BV36L; FnCas12a, *Francisella novicida* U112; TsCas12a, *Thiomicrospira* sp. XS5; Mb3Cas12a, *Moraxella bovoculi* sp.; Mb2Cas12a, *Moraxella bovoculi* AAX08_00205; MbCas12a, *Moraxella bovoculi* 237; RbCas12a, *Ruminococcus bromii* sp.; LbCas12a, *Lachnospiraceae bacterium* ND2006; PxCas12a, *Pseudobutyrivibrio xylanivorans* strain DSM 10317; PrCas12a, *Pseudobutyrivibrio ruminis* CF1b; BfCas12a, *Butyrivibrio fibrisolvens* MD2001; Lb2Cas12a, *Lachnospiraceae bacterium* MA2020; BsCas12a, *Butyrivibrio* sp. NC3005). (**B**) Neighbor-joining tree without distance corrections.

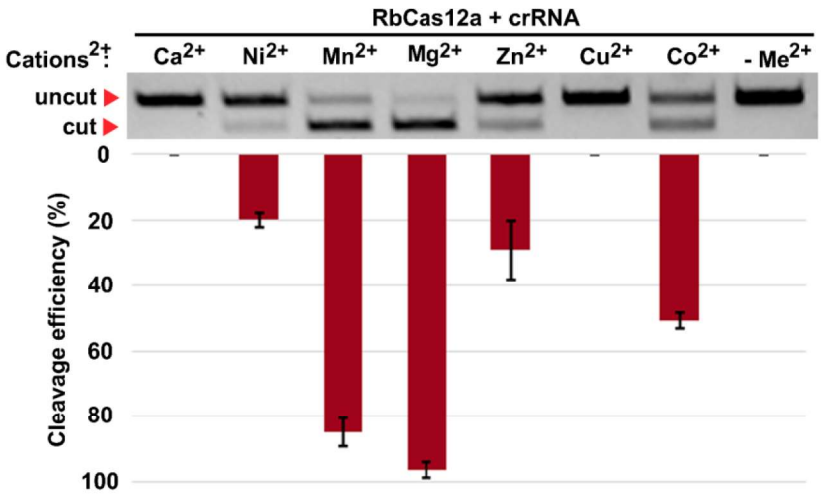


Figure 2. Effect of divalent cations on RbCas12a cleavage activity. Mean cleavage efficiencies and standard deviations calculated from three independent experiments of Me^{2+}-dependent in vitro cleavage reactions are shown. Reactions in the same buffer but without any Me^{2+} addition served as controls.

2.2. *PAM Requirement of RbCas12a*

Although 5′-TTTG PAM was found to be suitable for efficient DNA template cleavage, next, we investigated the PAM preferences of RbCas12a. We tested its ability to cleave linear DNA PAM libraries containing a target site flanked by eight randomized nucleotides at the 5′-end (Figure 3A). RbCas12a in a complex with crRNA was incubated with the PAM library at 37 °C for 1 h, and cleaved and uncleaved molecules were purified after agarose gel electrophoresis, and sequenced using the Illumina platform (Figure 3B). The bioinformatic analysis allowed us to determine the RbCas12a PAM logo. The data presented in Figure 3C shows that RbCas12a is capable of cleaving targets flanked by a 5′-YYN PAM.

To further investigate RbCas12a PAM preferences, we created several corresponding PAM sites to cleave target DNA templates. We varied the four nucleotides, one at a time, at each of the three positions of the 5′-YYN PAM sequences. As shown in Figure 4 (upper panel), there was no preference for nucleotides in the N position of PAM. These experiments reveal that PAM position-1 was unrestricted for RbCas12a, while thymidine was disfavored by, for example, AsCas12a and LbCas12a nucleases. To investigate the effects of the first two nucleotides on cleavage efficiency, we tested the activity of the RbCas12a/crRNA complex with all possible 5′-YYN combinations but for 5′-TTD (where D represents T, A, or G). The results show that the efficiency of RbCas12a-mediated DNA cleavage of 5′-TCB and 5′-CTS was ~80% (where B represents C, T, or G; and S represents G or C), which is similar to 5′-TT(N) PAM variants (Figure 4, bottom panel). Much less efficient cleavages were detectable for the 5′-CCT and 5′- TCA PAMs (which were ~27%), whereas the 5′-CCA-, 5′-CCG-, and 5′-CTT-PAM-flanked protospacer was cleaved with just ~10%. Taken together, these results clearly demonstrate that RbCas12a requires a PAM defined as 5′-YYN for cleavage, at least in a pure in vitro system. It should be noted that 5′-CCV and 5′-CTW (where V represents C, A, or G; and W represents A or T) were not able to cleave DNA templates with efficiencies of more than 25% under the conditions of the experiment.

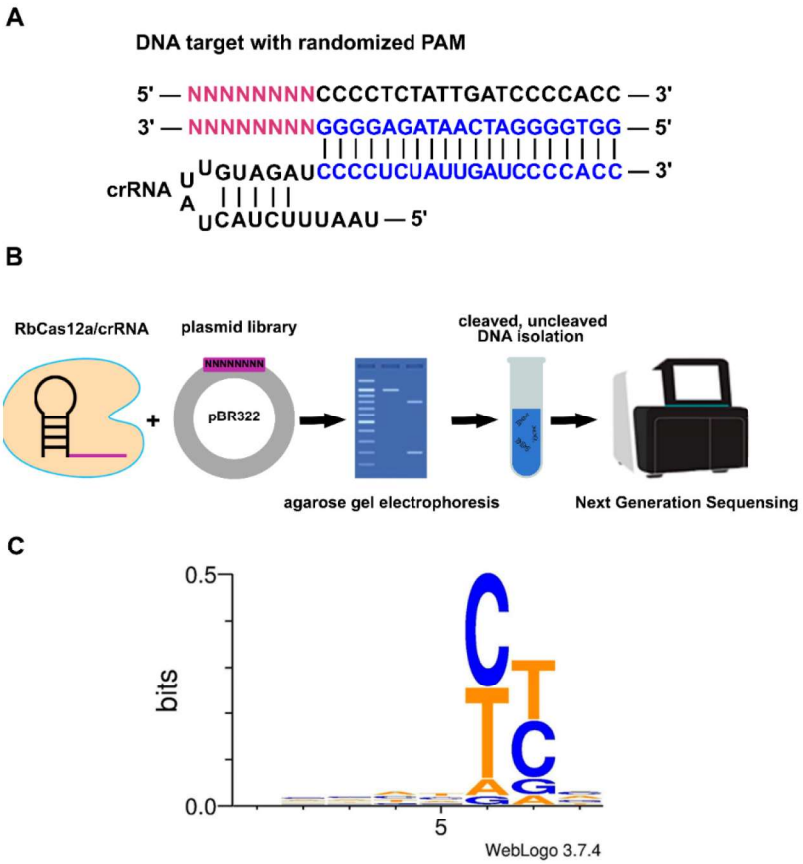


Figure 3. *Ruminococcus bromii* CRISPR–Cas Type V system PAM sequence logo determined by linear DNA PAM library sequencing. (**A**) Schematic of the RbCas12a crRNA–DNA-targeting complex. The target DNA contains eight random nucleotides at the 5′-end PAM region. (**B**) Schematic illustration of the experimental assay used to discover the RbCas12a PAM position and identity. (**C**) Sequence logo for the determined RbCas12a PAM.

2.3. *In Vitro Cleavage of DNA by RbCas12a*

Next, we investigated the kinetics of target DNA cleavage by RbCas12a or AsCas12a programed by appropriate crRNAs. As shown in Figure 5, in reactions containing the RbCas12a/crRNA complex, the target DNA was cleaved by ~27% after incubation for just 1 s. In the reaction containing the AsCas12a/crRNA complex, the target DNA was cleaved by ~15% only after 15 s of incubation. The cleavage reactions were ~50% complete after 15-s incubation with target DNA:RbCas12a:crRNA, and after 30-s incubation with target DNA:AsCas12a:crRNA. After 20-min incubation, both RbCas12a and AsCas12a cleaved ~95% of the target DNA under the experimental conditions. All subsequent experiments were performed using a 20-min incubation time interval. In the experiment, we used a DNA template with TTC PAM sequence.

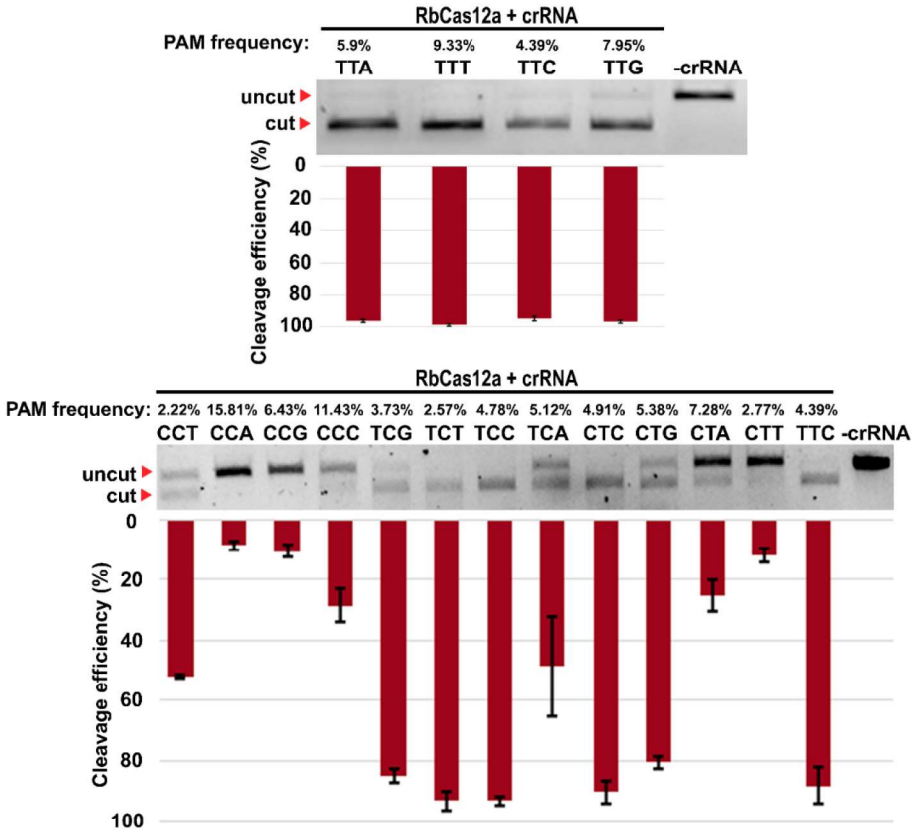


Figure 4. Investigation of RbCas12a PAM sequence by in vitro cleavage assay. The reactions contained 1.4 nM target DNA bearing the same protospacer but varying in the 5′-PAM sequence (as indicated above the panel), 346 nM recombinant RbCas12a, and 550 nM crRNA (a 0.1:35:55 nM ratio). Reactions were incubated for 30 min at 37 °C, and products were resolved by agarose gel electrophoresis. PAM frequency refers to the frequency of exact PAM in the cleaved PAM library. Mean cleavage efficiencies and standard deviations from three independent experiments are shown below the gel.

Recently, we demonstrated that the cleavage activity of at least three V-A nucleases (AsCas12, LbCas12a, and FnCas12a) persists after a substantial reduction in the crRNA scaffold length, up to its complete removal, at high concentrations of crRNA. Furthermore, we showed that the trans-addition of a 20-base scaffold RNA rescued the cleavage activity of these enzymes. Thus, we proposed the concept of split crRNA, which, in a complex with V-A nucleases, was comparable to cleavage activity observed with full-sized crRNA [17]. Here, we expand our observations and investigate the ability of RbCas12 to be programed with split crRNAs. As shown in Figure 6A, in reactions containing both full-sized and split crRNAs, the target DNA was cleaved by ~90% under the conditions of the experiment. We previously showed that increasing the spacer-only crRNA concentration could increase the cleavage efficacy of AsCas12a [17]. The data presented in Figure 6B demonstrate that increasing the concentration of spacer RNA from 0.5 to 5 μM causes dose-dependent DNA substrate cleavage by RbCas12a. It is possible to cleave the DNA template reasonably efficiently (~50% after a 20-min incubation) at a protein:RNA ratio of more than 1:500.

Efficient cleavage of cognate targets was also observed when split crRNAs with unrelated spacer sequences were tested (Figure S2).

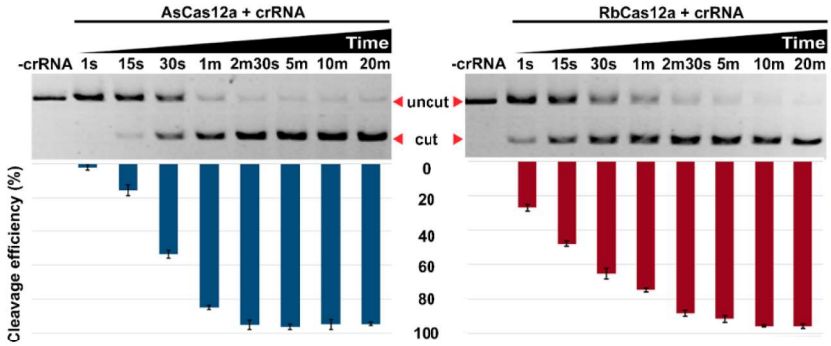


Figure 5. Effect of time on RbCas12a/crRNA and AsCas12a/crRNA cleavage activity. Target DNA cleavage by AsCas12a or RbCas12a programed with 500 nM crRNA at 1:3:30 target:Cas12a:RNA ratio. Mean cleavage efficiencies and standard deviations calculated from three independent experiments are shown.

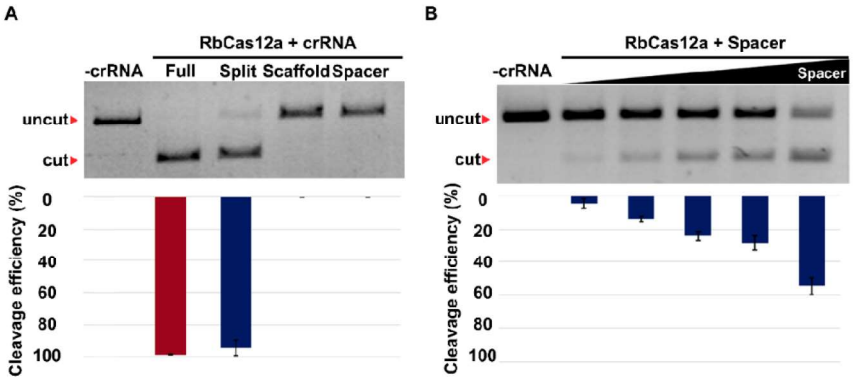


Figure 6. Effect of split crRNA and spacer-only RNA on RbCas12a cleavage activity. (**A**) Target DNA cleavage by RbCas12a programed with 0.3 µM full-sized split or separate scaffold and spacer crRNA moieties at a 1:3:30 target:RbCas12a:RNA ratio. "Split" reactions contained both the scaffold and spacer RNAs. Mean cleavage efficiencies and standard deviations calculated from three independent experiments are shown. (**B**) Cleavage by RbCas12a programed with increasing concentrations (0.5, 1, 2, 2.5, and 5 µM of spacer RNA, corresponding to 1:5:50, 1:5:100, 1:5:200, 1:5:250, and 1:5:500 DNA:RbCas12a:crRNA ratios). Mean cleavage efficiencies and standard deviations calculated from three independent experiments are shown.

2.4. Activity of RbCas12a at Different Temperatures

In order to clarify the temperature range of RbCas12a activity, the stability of the enzyme in the NEBuffer 2 was measured by thermofluor assay. This fluorescent-dye-based method allowed us to examine the melting point of a protein under particular conditions. As shown in Figure 7, the Tm of RbCas12a was calculated as 45.5 °C. Next, in vitro cleavage reactions at different temperatures were performed, showing the inability of the ribonucleoprotein (RNP) complex to assemble and cleave dsDNA at temperatures higher than 45.5 °C, because of the process of unfolding RbCas12a and crRNA (Figure 8).

In the experiment, we used a DNA template with a TTC PAM sequence. Surprisingly, nuclease efficiency was not affected at 42 °C compared to 37 °C. This might be explained by the environmental conditions of *Ruminococcus bromii*, as human gut temperature is slightly higher compared with other parts of the body. The RbCas12a RNP complex was able to cleave template DNA successfully even at 30 °C, although with reduced efficiency in some replicates, showing 61.3% cleavage efficiency (s.d. 29.2). RbCas12a was still able to cleave target DNA at lower temperatures, down to 20 °C, although with significantly less efficiency. It is important to note that, according to our data, RbCas12a RNP complex formation is unstable at 20 °C, showing 5.4% to 35.5% cleavage efficiency, which means that the particular temperature point is close to the lowest temperature limit of the protein activity in vitro. As expected, we did not observe any DNA cleavage at 15 °C, confirming that RbCas12a cannot efficiently bind to crRNA. Nevertheless, successful RNP complex formation and subsequent efficient cutting events depend not only upon temperature conditions, but also the particular spacer and PAM sequences.

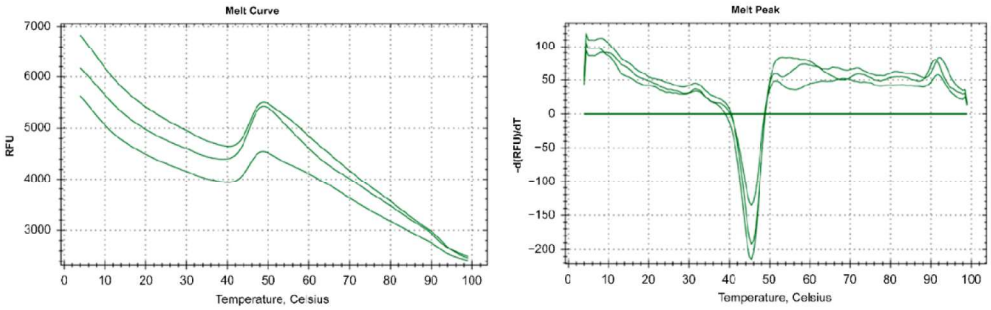


Figure 7. Thermofluor assay of RbCas12a. The left panel shows the melt curves, and the right panel shows the first derivative of the melt curves. The assay was performed with three independent replicas. The melt point of RbCas12a is 45.5 °C.

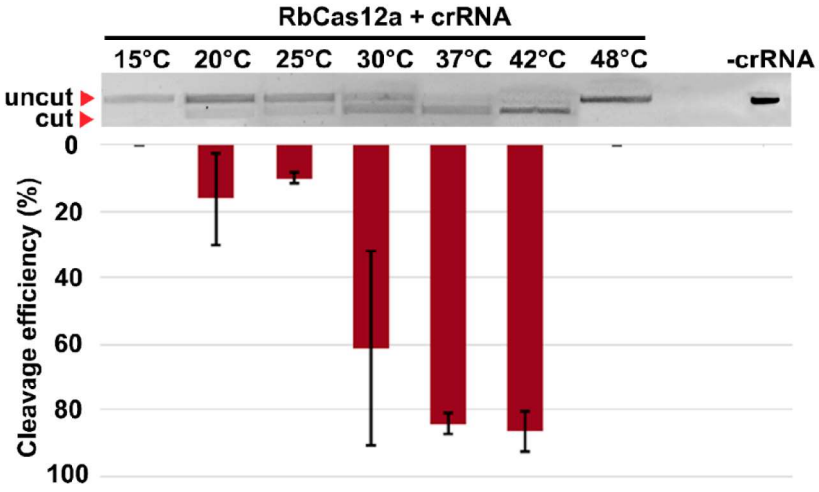


Figure 8. Effect of temperature on RbCas12a cleavage activity. Target DNA cleavage by RbCas12a programed with 500 nM crRNA at 1:3:30 target:Cas12a:RNA ratio. Mean cleavage efficiencies and standard deviations calculated from three independent experiments are shown.

2.5. *RbCas12a Nuclease Is Active in Human Cells*

We tested RbCas12a activity in human cells. A codon-optimized RbCas12a gene was cloned into plasmid vectors under the regulation of the CMV promoter. Three nuclear localization sequences (NLS) were added to the N-end of the protein, and one to the C-end, to enhance its import to the nucleus after translation. Appropriate crRNA coding sequences were cloned into independent plasmid vectors under the control of the U6 promoter. RbCas12a was targeted to the human *DNMT1*, *EMX1*, and *VEGFA* genes. We also checked the presence of nucleases via RT-PCR (Figure S3). Across the three genes assessed, there were no statistical differences ($p > 0.05$) with control samples (without crRNA/RbCas12a transfection) under the conditions of the experiment.

We theorize that, in the absence of detectable target cleavages in cells transfected with separate crRNA, using two different crRNAs simultaneously could produce results. To test this assumption, two different crRNAs simultaneously targeting the human *DNMT1* gene were used. As shown in Figure 9, we detected a band corresponding to the deleted DNA fragment after PCR. The efficiencies of the repeats were ~15–25%, except in one case, where ~77% was obtained. We performed Sanger sequencing on several colonies that hosted cloned PCR fragments, and detected breaks approximately −16–19 nts upstream of the PAM for both crRNAs under the experimental conditions (Figure 9, bottom panel). Encouraged by these high efficiencies, we decided to achieve a more detailed picture of break site flanking deletions by performing NGS on deleted PCR products for both test days.

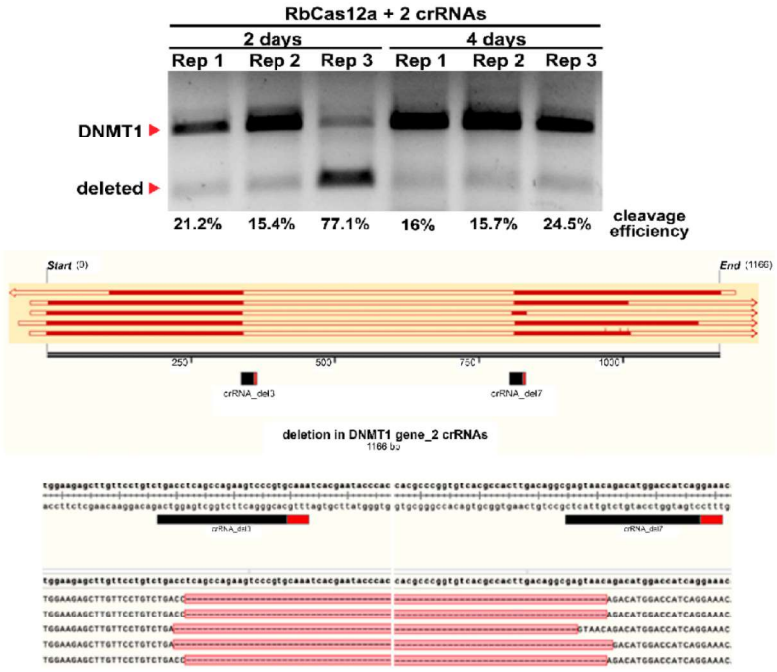


Figure 9. Targeting the human *DNMT1* gene with two crRNAs led to deletions. Top: Agarose gel visualization of PCR products after cell culture transfection with plasmids encoding RbCas12a and two crRNAs. Three independent experiments are shown as Rep1–3 on the second and fourth days of the experiment. Middle: A schematic representation of the PCR product with two guide RNAs highlighted. Bottom: Detailed maps with nucleotide sequences, created with SnapGene software.

We must clarify what we mean by "break sites". As each NGS read consists of both deleted protospacer DNA regions linked to each other, we call the link sites "break sites". That is, the place of transition from one protospacer to another. As can be seen from Figure 10, the most common break sites were between 19 and 20 nts within the protospacer region of the left arm of deletions, and between 17 and 18 nts within the protospacer region of the right arm of deletions. The results show that the efficiency of the aforementioned break sites was ~35% for both left and right crRNAs at the conditions of the experiment. It is interesting to note that the distribution of the break sites inside the sequence protospacer for the right crRNA appears unimodal, while it appears bimodal for the left one. This might be a consequence of cleavage efficiency of the DNA template by the crRNA/RbCas12a complex. Another peak value for left crRNA break sites was ~23%, and localized between 18 and 19 bps. The cleavage reactions were ~10% complete for both left and right crRNAs, but at different sites: after 21, 22, and 23 bps inside the sequence protospacer for the left crRNA, and after 14 and 15 bps for the right one. There was no significant difference (chi-squared test p-value > 0.05) in the break efficiencies between the second and fourth days of the experiment. There was also no statistical relationship between the first and second break sites in the experiment. These results indicate that RbCas12a is active in human cells.

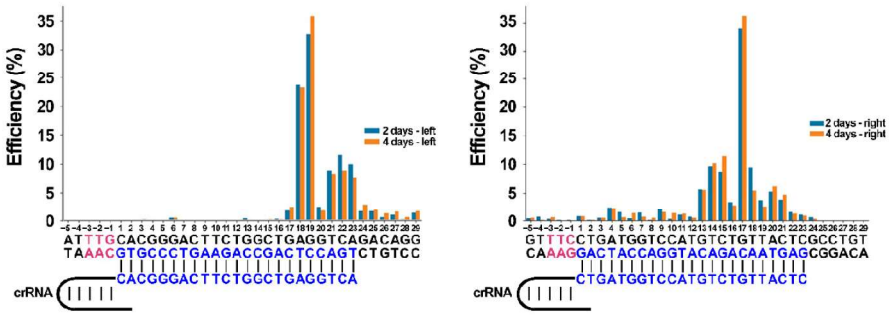


Figure 10. Frequencies of break site flanking deletion. On the left side of the figure, a crRNA is indicated, which, complexed with RbCas12a, forms break sites flanking the left arm of the deletion. On the right side of the figure, the right crRNA is indicated. PAM sequences on both target and nontarget strands are highlighted in red font. The protospacer position on the target DNA strand and spacer moiety of crRNA is highlighted in blue font. Relative coverage depth in the edited region was calculated as depth coverage in certain positions divided by mean coverage depth outside of the edited region. DNA break efficiency after a certain position was assessed as the difference between relative depth in two neighboring positions.

3. Discussion

The CRISPR–Cas12 subtype V-A system (Cas12a), also known as Cpf1, is a genome editing tool that is considered as an alternative to Cas9 nucleases. Although SpCas9 is still more commonly used than nucleases of the Cas12a family, the latter have gained momentum in medical practice and breeding biotechnologies, mainly due of their smaller size in terms of both nucleases and crRNA. Here, we present a novel RNA-guided DNA endonuclease from *Ruminococcus bromii*, which belongs to the Cas12a subtype. It was assigned to the Cas12a family according to four independent lines of evidence: (i) RbCas12a is clustered with other Cas12a enzymes in the phylogenetic tree; (ii) the scaffold of the crRNA is similar to those of previously published Cas12a orthologs; (iii) the PAM is similar to those of other Cas12a orthologs, and consists of 'YYN' nucleotides; (iv) the amino acid sequence of RbCas12a shares the same conservative catalytic sites with other Cas12a orthologs.

As previously mentioned, Cas12a orthologs have been characterized, among others, as having very similar structures among the crRNA scaffolds, which differ only in the loop region (Table S1). Among the 19 Cas12a orthologs known to us that can cleave chromatin in human cells, there are ones that possess three, four, or five nucleotides in the loop region of the crRNA. For instance, AsCas12a and ErCas12a crRNA loops consist of UCUU nucleotides. FnCas12a, ArCas12a, BfCas12a, and TsCas12a possess UGUU nucleotides, and MbCas12a possesses UUUU nucleotides. CeCas12a is the only known Cas12a ortholog capable of editing the human genome, whose four-nucleotide crRNA loop region does not contain two terminal uridines, but a CG-dinucleotide instead. The loop region of crRNA for BsCas12a, HkCas12a, PxCas12a, Lb2Cas12a, and RbCas12a, reported here, consists of UAUU nucleotides. The only crRNA, to our knowledge, consisting of three UUU nucleotides in the loop, forms an RNP complex with the EeCas12a nuclease. The longest loop regions that are composed of five nucleotides, UGUGU, UGUGU, and UAAGU, are inherent in LpCas12a, PrCas12a, and LbCas12a, respectively. A similar UGUUU loop region is typical for Mb2Cas12a and Mb3Cas12a crRNAs, of which both were found in different strains of *Moraxella bovoculi* sp. It is worth noting that the similarity of the loop region of crRNA is not correlated with the phylogenetic affinity (grouped on the nearest branches) of amino acid sequences of Cas12a nucleases (Figure 1B). RbCas12a programmed with crRNA matched to As/ErCas12a is still able to cleave target DNA template (data not shown). This means that point mutations in the loop do not affect the protein binding activity of crRNA, as this region does not participate in ribonucleoprotein interactions. Thus, the diversity of loop sequence variants can be explained by an accumulation of random mutations that are not subject to targeted evolutionary selection.

To comprehensively characterize the in vitro conditions of the target DNA cleavage by RbCas12a, we harnessed a set of divalent cation-contained salts supplemented into the reaction buffer. Recently, it was reported that the presence of manganese ions, AsCas12a, in contrast to LbCas12a, almost completely degrades dsDNA in the absence of crRNA [18]. Our data show that the RbCas12a RNP complex is able to utilize magnesium as well as manganese ions for efficient crRNA-guided dsDNA cleavage without nonspecific degradation of the matrix. Moreover, zinc and nickel can act as cofactors for RbCas12a, although with reduced efficiency. Interestingly, calcium did not support the RbCas12a binding and cleavage activity, in contrast to previously reported data on FnCas12a [19]. In summary, these results confirm the thesis stated in [18], that diverse Cas12a orthologs possess different preferences for metal ions.

We further characterized the RbCas12a RNP complex formation possibility and its targeting efficiency over a relatively wide range of temperatures, from 20 °C to 42 °C. In contrast to previously reported approaches [20], we incubated separate contents of reactions at appropriate temperatures in different tubes, thus allowing crRNA, protein, and target DNA structure formation corresponding to the particular temperature point. After that, crRNAs were mixed with RbCas12a at the same temperature in a preincubation step, which could help determine whether the RNP complex is to be, or not to be, assembled. In the end, a potentially contained RNP solution was supplemented with DNA exhibiting EDTA inactivation after incubation. Since every step in these experiments was performed at appropriate temperatures, the results might be considered as more closely reflecting native properties of nucleases. It should be noted that, in the experiments conducted at routine room temperatures, mixing of reaction contents followed by incubation at appropriate temperatures resulted in dsDNA cleavage in a wide range of conditions, from 4 °C to 100 °C, most likely due to the rapid rate of cleavage (data not shown). Nevertheless, one has to take into account that this data should not be considered as results reflecting the in vivo activity of the nucleases, but can be applied to a number of in vitro applications of CRISPR/Cas12a-based methods. Moreover, the cleavage rates presented here and in similar studies indicate the results of particular experiment conditions (cleavage buffer; RNA:protein:DNA ratio; spacer and PAM sequences, i.e., specificity of particular crRNA), and should not be translated to other investigations. Despite these limitations, the

aforementioned experiments may help us to understand the nature of the enzyme and its activity in vitro more clearly. In addition, as biotechnological and agricultural demand for enzymes that are active at lower temperatures constantly grows, we suppose that relatively efficient cleavage at up to 20 °C can present an opportunity for further studies focusing on plant genome editing, as such experiments are still very sensitive to temperature conditions.

In numerous reports, it was shown that similar, but different in detail, 5′T-rich PAM sequences are required for distinct Cas12a nucleases. In spite of this fact, and the published efforts on broadening PAM accessibility [21–23], it still remains a challenge to target not just desirable, but any T-rich locus of a genome. Results of the experiments from PAM studies show that AsCas12a and LbCas12a have sequences of 5′-TTTV, while those for FnCas12a and MbCas12a are both 5′-TTN [10]. In addition to the canonical PAM sequences, Cas12a also exhibits relaxed PAM recognition for suboptimal C-containing PAMs by forming altered interactions with the targeted DNA duplex. The presented novel nuclease RbCas12a recognizes almost all 5′-YYN PAMs, which, to the best of our knowledge, is the least stringent PAM reported to date. The reader may find the logarithmic-scale visualization of this finding in Figures 4 and S4.

Despite the advantages of RbCas12a among known orthologs, there are still several reasons why Cas12a cannot completely replace Cas9 in most genome editing techniques. First of all, engineered state-of-the-art Cas9 nucleases are almost PAM-independent, whereas Cas12a is yet to be modified to target all Cas9-accessible loci. Second, Cas12a proteins show reduced activity in relation to nucleosome-occluded genome regions, and require nucleosome unwrapping agents, such as dCas9, to access the targeted locus [24]. Finally, Cas9 nickases are used for precise genome modifications, bypassing DSBs and HDR through prime editing. No Cas12a nickase with proven activity in eukaryotic cells has been engineered to date. It was recently published that a Cas12a_M3 variant nicks the target strand of DNA in vitro without DSB generation, although in a sluggish manner [25]. Further studies will show the effectiveness of Cas12a_M3 or its derivatives in vivo, and will possibly pave the way for the engineering of nickase-based Cas12a prime and base editors. Overcoming the highlighted challenges will put Cas12a on a par with Cas9 in genome editing applications.

According to previously published data, Cas12a/crRNA complexes can differ in cleavage efficiency in both in vitro and in vivo experiments. Chromatin accessibility seems to be one of the reasons for these differences, although this requires additional investigation. In this work, we show that in spite of the absence of genome editing traces when using one crRNA, it is still possible to utilize the CRISPR/Cas12a nuclease for targeted genome deletion incorporation. Using two crRNAs simultaneously increases the cleavage efficiency by incorporating at least a 471 bp deletion, in our case. A number of publications examining whether one Cas12a ortholog or the other can be applied for mammalian genome editing report the absence of discovered mutations after cell culture transfections using the T7E1 assay. Here we provide evidence that these observations in some cases can be false-negative. To the best of our knowledge, there is only one protocol for Cas12a utilization, reported by the Jinek group [26], describing ~500 bp deletion incorporation in mouse ES cells, transfected by RNP charged with two different crRNAs. In the present study, we demonstrate the ability to use another Cas12a ortholog. With great efficiency in creating the deletion, we co-transfected the HEK293T human cell line with three plasmid vectors, one of which encoded the nuclease and two encoded other crRNAs.

Our data on the crRNA/RbCas12a help to extend the opportunities of genome editing. The principal finding of this paper is the demonstration that the RbCas12a effector can be used for human genome deletion formation with high efficiency. It is interesting to note that the absence of detectable cleavage when using only one crRNA does not mean the absence of the functional activity of the effector. Carefully and effectively created deletions could be used for cell model creation for human diseases caused by fragment deletions. The main limitation of the present article is that proof of suitable PAM patterns and expanded range of temperature in a pure was demonstrated only in an in vitro system. The effectiveness of

deletion creation should also be checked using different PAMs and temperatures. Future research on the current topic needs to uncover the off-target effects of the new RbCas12a ortholog, and compare the results with other widely used Cas12a effectors.

4. Materials and Methods

4.1. Database Mining for Nuclease Identification

Mining of the NCBI nr/nt database resulted in the identification of RbCas, possessing the typical Cas12a domain structure, however, showing only 46.26% identity to the closest experimentally characterized LbCas12a from *Lachnospiraceae bacterium* ND2006.

4.2. Phylogenetic Tree Reconstruction

In total, 18 Cas12a proteins functioning in mammalian cells and their close orthologs (HkCas12a, *Helcococcus kunzii* ATCC 51366; AsCas12a, *Acidaminococcus* sp. BV36L; Lp-Cas12a, *Lachnospira pectinoschiza* strain 2789STDY5834886; CeCas12a, *Coprococcus eutactus sp.*; EeCas12a, *Lachnospira eligens* ATCC 27750; ArCas12a, *Agathobacter rectalis* strain 2789STDY5834884; ErCas12a, *Eubacterium rectale* sp.; FnCas12a, *Francisella novicida* U112; TsCas12a, *Thiomicrospira* sp. XS5; MbCas12a, *Moraxella bovoculi 237*; Mb2Cas12a, *Moraxella bovoculi* AAX08_00205; Mb3Cas12a, *Moraxella bovoculi* sp.; BfCas12a, *Butyrivibrio fibrisolvens* MD2001; PrCas12a, *Pseudobutyrivibrio ruminis* CF1b; PxCas12a, *Pseudobutyrivibrio xylanivorans* DSM 10317; BsCas12a, *Butyrivibrio* sp. NC3005; Lb2Cas12a, *Lachnospiraceae bacterium* MA2020; LbCas12a, *Lachnospiraceae bacterium* ND2006; RbCas12a, *Ruminococcus bromii* sp.) [13] were selected for multiple sequence alignment with RbCpf1. The sequences were aligned using MAFFT v.7.475 [27] with L-INS-i algorithm and BLOSUM62 evolutionary model. The maximum-likelihood phylogenetic tree was reconstructed using IQ-TREE2 v.2.1.2 [28]. Evolutionary model LG + F + I + G4 was automatically selected using ModelFinder and Bayesian Information Criterion; 1000 bootstraps were performed.

4.3. Plasmid Cloning

To confirm the presence of the *cas12a* gene in the samples, PCR was performed with the primers Fwd_test and Rev_test (sequences are listed in Table S2). Fifty microliters of the reaction mixture were mixed using Q5® High-Fidelity 2X Master Mix (New England Biolabs, Ipswich, MA, USA), according to the manufacturer's instructions. Three of the seven samples that contained target fragments (~590 bp) were further utilized in PCR reactions to amplify the whole gene with the 5′-phosphorylated primers RbCpf_Fwd_Nde and RbCpf_Rev_Xho. Target fragments were excised from agarose gel, and DNA was extracted using the QIAGEN Gel Extraction Kit (Qiagen, Hilden, Germany) according to the manufacturer's instructions. Next, *cas12a*-containing fragments were cloned into the linearized pUC118 vector (HincII endonuclease, QuickCIP, and T4 DNA ligase, New England Biolabs, Ipswich, MA, USA). Plasmids were transformed into *E. coli* TOP10 strain and screened by PCR the next day. Any positive colonies were inoculated into Luria–Bertani media for overnight growth at 37 °C. Plasmids were extracted with a Monarch® Plasmid Miniprep Kit (New England Biolabs, Ipswich, MA, USA) and sequenced on Illumina MiSeq (Illumina, San Diego, CA, USA). Next, *cas12a* genes from three samples were cloned into the pET30a+ vector using NdeI and XhoI sites and further transformed, as previously described. To confirm successful assembly, the extracted plasmid DNA was restricted and analyzed on agarose gel. Human and plant codon optimization was performed by DAPCEL, Inc. (Cleveland, OH, USA) by the selection of synonymous codons to ensure the correct co-translational folding of the proteins in a target host. The plasmid vector containing hRbCas12a in the pcDNA3.1(+) backbone was created by GenScript LCC (Piscataway, NJ, USA). To confirm the successful import of the nuclease into the nucleus, three additional nuclear localization signals (NLSs) were introduced into the N-terminus of human-optimized proteins by sequential restriction–ligation steps using HindIII restriction endonuclease (New England Biolabs, Ipswich, MA, USA). Briefly, two SV40-NLS-containing complementary oligonucleotides with scattered phosphorylated ends

were annealed and subsequently ligated into HindIII-linearized and dephosphorylated hRbCas12a-pcDNA3.1(+). All crRNA-coding plasmid vectors for human cell culture were constructed as follows: first, the RFP gene under the control of the CMV promoter was cloned into pSQT1313 obtained from Addgene (#53370). Next, the RbCas12a crRNA scaffold with two BsmBI sites was cloned using site-directed mutagenesis. All spacers were then cloned at the BsmBI sites by annealing two complementary oligonucleotides with staggered ends.

4.4. Recombinant Protein Purification

For recombinant products, the *E. coli* Rosetta strain was transformed with the plasmid DNA, and clones were grown in Luria–Bertani (LB) medium at 37 °C overnight. The next morning, bacterial suspensions were inoculated into fresh LB medium and cultivated for 3 h at 37 °C, followed by cooling to room temperature. Then, IPTG was added, and the cells were incubated at 18 °C overnight. The cell lysate was loaded onto a Ni-NTA Superflow 5-mL column (Qiagen, Hilden, Germany) and equilibrated with a buffer containing 5 mM imidazole. The recombinant protein was eluted with a buffer containing 300 mM imidazole and the buffer was exchanged with 50 mM phosphate buffer (pH 7.4). Then, the protein was applied to MonoS 10/100 (GE Life Science, Carlsbad, CA, USA) and eluted with a linear gradient of NaCl in the same buffer. Fractions containing RbCas12a were collected, concentrated to ~12 mg/mL, and snap-frozen with liquid nitrogen in small aliquots that were stored at −80 °C until use. The protein concentration was measured using the Qubit Protein Assay Kit (Thermo Fisher, Carlsbad, CA, USA), according to the manufacturer's instructions. Protein quality was assessed by SDS-PAGE and visualized by Coomassie blue staining.

4.5. PAM Identification

Two M13-flanked, reverse-complemented 100-bp oligos with 8-bp degenerate fragments (Sintol, Moscow, Russia) adjacent to the protospacer were utilized as templates in the independent PCR reactions (Q5 DNA Polymerase; New England Biolabs, Ipswich, MA, USA). Amplicons were analyzed by agarose gel electrophoresis followed by gel extraction using a Qiagen Gel Extraction Kit (Qiagen, Hilden, Germany). The resulting fragments were restricted by EaeI (New England Biolabs, Ipswich, MA, USA) and cloned into the pBR322 vector linearized by EagI and PvuII (New England Biolabs, Ipswich, MA, USA), followed by transformation into the *E. coli* TOP10 strain. Since EaeI and EagI form compatible sticky ends, the fragment's insertion orientation was determined. Sixteen hours after transformation, more than 180,000 colonies were washed off the plates, and the plasmid library was extracted using the GenElute™ HP Plasmid Maxiprep Kit (Sigma, Merck KGaA, Darmstadt, Germany). Next, the obtained pDNA was cut using RbCas12a and gel-analyzed. Reactions were incubated for 30 min at 37 °C, and products were resolved by agarose gel electrophoresis. Cut and uncut fragments were eluted from the gel and used as an input for fragment library preparation with the Ultra II Library Prep kit (New England Biolabs, Ipswitch, MA, USA). The resulting libraries were checked using the Bioanalyzer 2100 instrument (Agilent, Santa Clara, CA, USA) and sequenced with the MiSeq™ instrument (Illumina, San Diego, CA, USA) using 250-bp paired-end reads. A total of 517 thousand raw read pairs were obtained and subjected to stringent quality trimming with CLC Genomics Workbench v.20.0 (Qiagen, Hilden, Germany). The trimming parameters were as follows: the quality score limit of error probability was 0.01, and of allowed ambiguities was 0. Trimmed overlapping reads were merged with SeqPrep tool (https://github.com/jstjohn/SeqPrep (accessed on 15 July 2021)) using default parameters, resulting in approximately 480 thousand merged reads. For the alignment, only the reads containing an exact 20-nt match to PAM-flanking sequences were used (flanking motif search was performed with the seqkit grep command of the SeqKit package). The final alignment contained 180 thousand reads. The flanking sequences of the PAMs were trimmed from the alignment using CLC Genomics Workbench

(Qiagen, Hilden, Germany), and the trimmed alignment was used as an input for the WebLogo server.

4.6. Checking Different PAM Sequences to Run the Protospacer Cleavages

To create DNA templates with different PAMs but the same protospacer, we used a site-directed mutagenesis (SDM) approach. The initially constructed PAM TTG was mutated in three ways, resulting in all four possible TTN variants for the same protospacer. SDM was performed using the Q5® Site-Directed Mutagenesis Kit (New England Biolabs, Ipswich, MA, USA), according to the manufacturer's instructions, with the primers listed in Table S2. Successful amplification was verified by performing electrophoresis on a 1% 1× TAE agarose gel. Plasmid DNA was extracted using the Monarch® Plasmid Miniprep Kit (New England Biolabs, Ipswich, MA, USA). To confirm the authenticity of the PAMs identified by NGS sequencing and WebLogo representation (see Results), pUC119 plasmid vector was cleaved using 13 different crRNAs targeting protospacers with YYN PAMs: 12 crRNAs targeting CTN and TCN PAMs, and TTC-targeting crRNA as the control. The oligonucleotides used in this study are listed in Table S2. All crRNAs were obtained by in vitro transcription using the HiScribe™ T7 High Yield RNA Synthesis Kit (New England Biolabs, Ipswich, MA, USA). Briefly, 53 pmol complementary oligonucleotides were equimolar mixed, heated at 95 °C for 5 min, incubated at room temperature for 30 min, and subsequently used as a matrix. Overnight RNA synthesis was performed with 10 mM final concentration of each NTP in 30 µL reactions, followed by DNAse I treatment. Obtained crRNAs were then extracted using Trizol (Thermo Scientific, Carlsbad, CA, USA) according to the manufacturer's instructions. RNA concentration was measured on Qubit 3.0 using a Qubit RNA HS Assay Kit (Thermo Scientific, Carlsbad, CA, USA).

4.7. In Vitro DNA Cleavage Assays

In vitro cleavage assays with the purified RbCas12a nuclease were carried out in a volume of 30 µL in 1× NEBuffer 2 (New England Biolabs, Ipswich, MA, USA). Next, 10 nM PCR-obtained DNA template, 500 nM of the nuclease, and 5000 nM crRNA were incubated for 30 min at 37 °C, and the reaction was stopped by the addition of Proteinase K (New England Biolabs, Ipswich, MA, USA) at a final concentration of 1 µg/µL, followed by incubation at room temperature for 15 min. Reaction analysis was performed by electrophoresis on a 1% agarose gel in TBE buffer. EtBr prestaining gels were visualized using a Gel Doc EZ Imager (Bio-Rad) and quantified with Image Lab™ Software v.6.0.1 (Bio-Rad, Hercules, CA, USA). DNA substrates for in vitro cleavage assays represent fragments of DNA amplified by PCR in Q5® High-Fidelity 2X Master Mix (New England Biolabs, Ipswich, MA, USA). Genomic DNA was isolated from the T-REx cell line (T-REx™-293 Cell Line, #R71007; Invitrogen, Carlsbad, CA, USA) using the GeneJET Genomic DNA Purification Kit (Thermo Scientific, Carlsbad, CA, USA). DNA concentration was measured on a Qubit 3.0 fluorometer using a Qubit DNA BR Assay Kit (Thermo Scientific, Carlsbad, CA, USA). Oligonucleotide primers and RNA moieties provided by Lumiprobe RUS Ltd. (Moscow, Russia) are listed in Supplementary Table S2. For the study of divalent cation impact on RbCas12a activity, 900 pM of linear dsDNA bearing 5′TTC PAM, 550 nM crRNA, and 350 nM protein were mixed in the cleavage buffer (containing 10 mM Tris-HCl (pH 7.9) and 50 mM NaCl), and supplemented with 10 mM of either CaCl2, MgSO4, MnCl2, ZnSO4, Ni(NO3)2, CuSO4, or CoCl2 (Sigma-Aldrich, Merck KGaA, Darmstadt, Germany), followed by incubation for 30 min at 37 °C. Reactions were stopped by the addition of 100 mM EDTA, and run in 1xTAE agarose gel electrophoresis with ethidium bromide prestaining.

4.8. Thermostability Assay and Activity at Different Temperatures

To investigate RbCas12a thermostability, a fluorescent-based assay was performed using ProteOrange Protein Gel Stain 5000× (Lumiprobe RUS Ltd., Moscow, Russia) under the following conditions: we used 9 µg purified RbCas12a, 12.5 µL NEBuffer 2 (New England Biolabs, Ipswich, MA, USA), and 2.5 µL ProteOrange Protein Gel Stain (diluted

to 50×) in 25-µL reactions. A thermal curve was constructed for both the negative control (without protein) and reactions containing RbCas12a (each in triplicate) from 4 °C to 95 °C, with increments of 0.5 °C and signal registration every 10 s. To determine the temperature dependence of RbCas12a\crRNA complex formation, and consequently, RbCas12a activity, in vitro cleavage reactions were carried out to completion at the point temperatures. First, 225 nM RbCas12a, 375 nM crRNA, and 500 pM DNA bearing 5′-TTC PAM in 1x NEBuffer 2 were first incubated in separate tubes at corresponding temperatures for 5 min. Next, ribonucleoprotein (RNP) complexes were obtained by mixing RNA and RbCas12a, followed by incubation at the same temperature for 15 min. RNP complexes were further supplemented with DNA, followed by an additional 20-min incubation step. Last, 83 mM EDTA was added to the reactions for complete inactivation of the enzyme. Cleavage efficiency was analyzed by agarose gel electrophoresis in TAE.

4.9. Human Cell Culture and Transfection

T-REx™-293 cells were cultivated in Dulbecco's modified Eagle medium (Thermo Fisher, Carlsbad, CA, USA) with 10% fetal bovine serum (Thermo Fisher Scientific, Carlsbad, CA, USA) and 1% penicillin–streptomycin (Thermo Fisher, Carlsbad, CA, USA) at 37 °C with 5% CO2 until 85% confluence. The transfection, which was 1 day following cell plating, was performed in 6-well plates using Lipofectamine 3000 Reagent (Thermo Fisher, Carlsbad, CA, USA), according to the manufacturer's protocol. A total of 2000 ng hRbCas12a plasmid and 2000 ng crRNA plasmid were used to target the *DNMT1*, *VEGFA*, or *EMX1* genes. *DNMT1* was targeted using either one crRNA plasmid or two plasmids (each crRNA encoded in separate plasmids), with the latter aimed at obtaining a respective deletion. At 48 h after transfection, cells were washed three times with PBS and lysed with NP40 Cell Lysis Buffer (Invitrogen, Carlsbad, CA, USA) containing 0.2 mg/mL Proteinase K. Cells transfected with both plasmids were processed either 2 days or 4 days after transfection.

4.10. RbCas12a mRNA Detection by RT-PCR

Two days after transfection, the cells were harvested, washed with PBS, and total RNA was extracted with TRIzol (Thermo Fisher, Carlsbad, CA, USA). cDNA was obtained using the ProtoScript® II First Strand cDNA Synthesis Kit (New England Biolabs, Ipswich, MA, USA). Real-time PCR amplification of cDNA was carried out in a 20-µL reaction mixture containing 10 µL EvaGreen Supermix (Bio-Rad, Hercules, CA, USA), 500 nM of each primer, 100 ng cDNA, and RNase-free water. The thermal cycling conditions for cDNA used in the CFX96 thermocycler (Bio-Rad, Hercules, CA, USA) were as follows: 95 °C for 3 min, 39 cycles at 95 °C for 10 s, 56 °C for 5 s, and 68 °C for 10 s.

4.11. Indel and Mismatch Frequency Analysis

The reads were mapped to the reference sequences using minimap2 v.2.19-r1057 [29] in short-read mapping mode. Coverage depth at certain positions was measured using samtools v.1.12 [30]. Relative coverage depth in the edited region was calculated as depth coverage in certain positions divided by mean coverage depth outside of the edited region. DNA break efficiency after a certain position was assessed as the difference between relative depth in two neighboring positions. The chi-squared test was used to determine the significance of the discrepancy between 48- and 96-h experiments. Mismatch and deletion frequencies in experiments with a single crRNA was assessed using bam-readcount v.1.0 (https://github.com/genome/bam-readcount (accessed on 13 September 2021)) with default settings.

4.12. Statistics

All statistical analyses were performed in R language (v.4.1.2). The exact replication numbers are indicated in the figure legends. The findings in all the figures of the gel images were successfully reproduced under similar experimental conditions at least three times independently. Differences were considered significant at the level of $p < 0.05$.

Supplementary Materials: The following supporting information can be downloaded at: https://www.mdpi.com/article/10.3390/ijms23169289/s1.

Author Contributions: R.V. and I.M. designed research; R.V., N.G., R.S., A.V., M.E., I.P. and N.N. performed research; A.K. and S.T. analyzed data; M.P., P.K. and I.M. supervised; and R.V. and I.M. wrote the manuscript with input from all authors. All authors read and approved the final manuscript.

Funding: R.V.: N.G., A.V., A.K., and M.P. were supported by grants from the Ministry of Science and Higher Education of the Russian Federation allocated to the Kurchatov Center for Genome Research (agreement number 075-15-2019-1659). RS, NN, and IM were supported by the Russian Foundation for Basic Research (19-29-04101). S.T. was supported by the Russian Foundation for Basic Research (20-04-60190). R.V. and P.K. are members of the Moscow University Science and Education School "Molecular Technologies of the Living Systems and Synthetic Biology". The work was partly done on the equipment purchased in the frame of the Moscow University Program of Development.

Institutional Review Board Statement: Not applicable.

Informed Consent Statement: Not applicable.

Data Availability Statement: All data presented in the manuscript is available upon request.

Acknowledgments: The authors thank Anastasia Kirillova for the language editing.

Conflicts of Interest: The authors declare no conflict of interest.

References

1. Barrangou, R.; Fremaux, C.; Deveau, H.; Richards, M.; Boyaval, P.; Moineau, S.; Romero, D.A.; Horvath, P. CRISPR provides acquired resistance against viruses in prokaryotes. *Science* **2007**, *315*, 1709–1712. [CrossRef] [PubMed]
2. Brouns, S.J.; Jore, M.M.; Lundgren, M.; Westra, E.R.; Slijkhuis, R.J.; Snijders, A.P.; Dickman, M.J.; Makarova, K.S.; Koonin, E.V.; van der Oost, J. Small CRISPR RNAs guide antiviral defense in prokaryotes. *Science* **2008**, *321*, 960–964. [CrossRef] [PubMed]
3. Jackson, S.A.; McKenzie, R.E.; Fagerlund, R.D.; Kieper, S.N.; Fineran, P.C.; Brouns, S.J. CRISPR-Cas: Adapting to change. *Science* **2017**, *356*, eaal5056. [CrossRef] [PubMed]
4. Jinek, M.; Chylinski, K.; Fonfara, I.; Hauer, M.; Doudna, J.A.; Charpentier, E. A programmable dual-RNA-guided DNA endonuclease in adaptive bacterial immunity. *Science* **2012**, *337*, 816–821. [CrossRef]
5. Gasiunas, G.; Young, J.K.; Karvelis, T.; Kazlauskas, D.; Urbaitis, T.; Jasnauskaite, M.; Grusyte, M.M.; Paulraj, S.; Wang, P.H.; Hou, Z.; et al. A catalogue of biochemically diverse CRISPR-Cas9 orthologs. *Nat. Commun.* **2020**, *11*, 5512. [CrossRef] [PubMed]
6. Zetsche, B.; Gootenberg, J.S.; Abudayyeh, O.O.; Slaymaker, I.M.; Makarova, K.S.; Essletzbichler, P.; Volz, S.E.; Joung, J.; van der Oost, J.; Regev, A.; et al. Cpf1 is a single RNA-guided endonuclease of a class 2 CRISPR-Cas system. *Cell* **2015**, *163*, 759–771. [CrossRef]
7. Gootenberg, J.S.; Abudayyeh, O.O.; Kellner, M.J.; Joung, J.; Collins, J.J.; Zhang, F. Multiplexed and portable nucleic acid detection platform with Cas13, Cas12a, and Csm6. *Science* **2018**, *360*, 439–444. [CrossRef]
8. Li, S.Y.; Cheng, Q.X.; Wang, J.M.; Li, X.Y.; Zhang, Z.L.; Gao, S.; Cao, R.B.; Zhao, G.P.; Wang, J. CRISPR-Cas12a-assisted nucleic acid detection. *Cell Discov.* **2018**, *4*, 20. [CrossRef]
9. Kaminski, M.M.; Abudayyeh, O.O.; Gootenberg, J.S.; Zhang, F.; Collins, J.J. CRISPR-based diagnostics. *Nat. Biomed. Eng.* **2021**, *5*, 643–656. [CrossRef]
10. Tóth, E.; Czene, B.C.; Kulcsár, P.I.; Krausz, S.L.; Tálas, A.; Nyeste, A.; Varga, É.; Huszár, K.; Weinhardt, N.; Ligeti, Z.; et al. Mb- and FnCpf1 nucleases are active in mammalian cells: Activities and PAM preferences of four wild-type Cpf1 nucleases and of their altered PAM specificity variants. *Nucleic Acids Res.* **2018**, *46*, 10272–10285. [CrossRef]
11. Teng, F.; Li, J.; Cui, T.; Xu, K.; Guo, L.; Gao, Q.; Feng, G.; Chen, C.; Han, D.; Zhou, Q.; et al. Enhanced mammalian genome editing by new Cas12a orthologs with optimized crRNA scaffolds. *Genome Biol.* **2019**, *20*, 15. [CrossRef] [PubMed]
12. Zetsche, B.; Abudayyeh, O.O.; Gootenberg, J.S.; Scott, D.A.; Zhang, F. A Survey of Genome Editing Activity for 16 Cas12a Orthologs. *Keio J. Med.* **2020**, *69*, 59–65. [CrossRef] [PubMed]
13. Ahn, W.C.; Park, K.H.; Bak, I.S.; Song, H.N.; An, Y.; Lee, S.J.; Jung, M.; Yoo, K.W.; Yu, D.Y.; Kim, Y.S.; et al. In vivo genome editing using the Cpf1 ortholog derived from Eubacterium eligens. *Sci. Rep.* **2019**, *9*, 13911. [CrossRef] [PubMed]
14. Tran, M.H.; Park, H.; Nobles, C.L.; Karunadharma, P.; Pan, L.; Zhong, G.; Wang, H.; He, W.; Ou, T.; Crynen, G.; et al. A more efficient CRISPR-Cas12a variant derived from Lachnospiraceae bacterium MA2020. *Mol. Ther. Nucleic Acids* **2021**, *24*, 40–53. [CrossRef] [PubMed]
15. Wierson, W.A.; Simone, B.W.; WareJoncas, Z.; Mann, C.; Welker, J.M.; Kar, B.; Emch, M.J.; Friedberg, I.; Gendron, W.A.C.; Barry, M.A.; et al. Expanding the CRISPR Toolbox with ErCas12a in Zebrafish and Human Cells. *CRISPR J.* **2019**, *2*, 417–433. [CrossRef]
16. Chen, P.; Zhou, J.; Wan, Y.; Liu, H.; Li, Y.; Liu, Z.; Wang, H.; Lei, J.; Zhao, K.; Zhang, Y.; et al. A Cas12a ortholog with stringent PAM recognition followed by low off-target editing rates for genome editing. *Genome Biol.* **2020**, *21*, 78. [CrossRef]

17. Shebanova, R.; Nikitchina, N.; Shebanov, N.; Mekler, V.; Kuznedelov, K.; Ulashchik, E.; Vasilev, R.; Sharko, O.; Shmanai, V.; Tarassov, I.; et al. Efficient target cleavage by Type V Cas12a effectors programmed with split CRISPR RNA. *Nucleic Acids Res.* **2022**, *50*, 1162–1173. [CrossRef]
18. Li, B.; Yan, J.; Zhang, Y.; Li, W.; Zeng, C.; Zhao, W.; Hou, X.; Zhang, C.; Dong, Y. CRISPR-Cas12a Possesses Unconventional DNase Activity that Can Be Inactivated by Synthetic Oligonucleotides. *Mol. Ther. Nucleic Acids* **2020**, *19*, 1043–1052. [CrossRef]
19. Singh, D.; Mallon, J.; Poddar, A.; Wang, Y.; Tippana, R.; Yang, O.; Bailey, S.; Ha, T. Real-time observation of DNA target interrogation and product release by the RNA-guided endonuclease CRISPR Cpf1 (Cas12a). *Proc. Natl. Acad. Sci. USA* **2018**, *115*, 5444–5449. [CrossRef]
20. Teng, F.; Cui, T.; Feng, G.; Guo, L.; Xu, K.; Gao, Q.; Li, T.; Li, J.; Zhou, Q.; Li, W. Repurposing CRISPR-Cas12b for mammalian genome engineering. *Cell Discov.* **2018**, *4*, 63. [CrossRef]
21. Gao, L.; Cox, D.B.T.; Yan, W.X.; Manteiga, J.C.; Schneider, M.W.; Yamano, T.; Nishimasu, H.; Nureki, O.; Crosetto, N.; Zhang, F. Engineered Cpf1 variants with altered PAM specificities. *Nat. Biotechnol.* **2017**, *35*, 789–792. [CrossRef] [PubMed]
22. Kleinstiver, B.P.; Sousa, A.A.; Walton, R.T.; Tak, Y.E.; Hsu, J.Y.; Clement, K.; Welch, M.M.; Horng, J.E.; Malagon-Lopez, J.; Scarfò, I.; et al. Engineered CRISPR-Cas12a variants with increased activities and improved targeting ranges for gene, epigenetic and base editing. *Nat. Biotechnol.* **2019**, *37*, 276–282. [CrossRef] [PubMed]
23. Zhang, L.; Zuris, J.A.; Viswanathan, R.; Edelstein, J.N.; Turk, R.; Thommandru, B.; Rube, H.T.; Glenn, S.E.; Collingwood, M.A.; Bode, N.M.; et al. AsCas12a ultra nuclease facilitates the rapid generation of therapeutic cell medicines. *Nat. Commun.* **2021**, *12*, 3908. [CrossRef] [PubMed]
24. Strohkendl, I.; Saifuddin, F.A.; Gibson, B.A.; Rosen, M.K.; Russell, R.; Finkelstein, I.J. Inhibition of CRISPR-Cas12a DNA targeting by nucleosomes and chromatin. *Sci. Adv.* **2021**, *7*, eabd6030. [CrossRef] [PubMed]
25. Paul, B.; Chaubet, L.; Verver, D.E.; Montoya, G. Mechanics of CRISPR-Cas12a and engineered variants on λ-DNA. *Nucleic Acids Res.* **2022**, *50*, 5208–5225. [CrossRef] [PubMed]
26. Kissling, L.; Monfort, A.; Swarts, D.C.; Wutz, A.; Jinek, M. Preparation and electroporation of Cas12a/Cpf1-guide RNA complexes for introducing large gene deletions in mouse embryonic stem cells. *Methods Enzym.* **2019**, *616*, 241–263. [CrossRef]
27. Nakamura, T.; Yamada, K.D.; Tomii, K.; Katoh, K. Parallelization of MAFFT for large-scale multiple sequence alignments. *Bioinformatics* **2018**, *34*, 2490–2492. [CrossRef]
28. Minh, B.Q.; Schmidt, H.A.; Chernomor, O.; Schrempf, D.; Woodhams, M.D.; von Haeseler, A.; Lanfear, R. IQ-TREE 2: New Models and Efficient Methods for Phylogenetic Inference in the Genomic Era. *Mol. Biol. Evol.* **2020**, *37*, 1530–1534. [CrossRef]
29. Li, H. Minimap2: Pairwise alignment for nucleotide sequences. *Bioinformatics* **2018**, *34*, 3094–3100. [CrossRef]
30. Li, H.; Handsaker, B.; Wysoker, A.; Fennell, T.; Ruan, J.; Homer, N.; Marth, G.; Abecasis, G.; Durbin, R. The Sequence Alignment/Map format and SAMtools. *Bioinformatics* **2009**, *25*, 2078–2079. [CrossRef]

SUPPLEMENTARY MATERIALS

Supplementary Table S1. Cas12a orthologs and their ability to edit the genomes of human cells

Cas12a orthologs	Short title	Scaffold nucleotide sequence, 5'-3'	Paper where was showed human cell gene editing, doi
Lachnospira eligens ATCC 27750	EeCas12a	UAAUUUCUACU UUGUAGAU	10.1038/ s41598-019-50423-6
Moraxella bovoculi 237	MbCas12a	UAAUUUCUACU UUUGUAGAU	10.1093/nar/gky815
Eubacterium rectale	ErCas12a	UAAUUUCUACU CUUGUAGAU	10.1089/crispr.2019.0026
Acidaminococcus sp	AsCas12a	UAAUUUCUACU CUUGUAGAU	10.1093/nar/gky815
Ruminococcus bromii sp.	**RbCas12a**	UAAUUUCUACU AUUGUAGAU	**current study**
Butyrivibrio sp. NC3005	BsCas12a	UAAUUUCUACU AUUGUAGAU	10.1186/ s13059-019-1620-8
Lachnospiraceae bacterium MA2020	Lb2Cas12a	UAAUUUCUACU AUUGUAGAU	10.1096/fj.202001013RR
Helcococcus kunzii ATCC 51366	HkCas12a	UAAUUUCUACU AUUGUAGAU	10.1186/ s13059-019-1620-8
Pseudobutyrivibrio xylanivorans strain DSM 10317	PxCas12a	UAAUUUCUACU AUUGUAGAU	10.1186/ s13059-019-1620-8
Francisella novicida	FnCas12a	UAAUUUCUACU GUUGUAGAU	10.1093/nar/gky815
Thiomicrospira sp. XS5	TsCas12a	UAAUUUCUACU GUUGUAGAU	10.2302/kjm.2019-0009-OA
Agathobacter rectalis strain 2789STDY5834884	ArCas12a	UAAUUUCUACU GUUGUAGAU	10.1186/ s13059-019-1620-8
Butyrivibrio fibrisolvens MD2001	BfCas12a	UAAUUUCUACU GUUGUAGAU	10.1186/ s13059-020-01989-2
Lachnospiraceae bacterium ND2006	LbCas12a	UAAUUUCUACUAAGUGUAGAU	10.1093/nar/gky815
Moraxella bovoculi AAX08_00205	Mb2Cas12a	UAAUUUCUACUGUUUGUAGAU	10.2302/kjm.2019-0009-OA
Moraxella bovoculi sp.	Mb3Cas12a	UAAUUUCUACUGUUUGUAGAU	10.1126/science.aau5174
Coprococcus eutactus sp.	CeCas12a	UAAUUUCUACU UCGGUAGAU	10.1186/ s13059-020-01989-2
Lachnospira pectinoschiza strain 2789STDY5834886	LpCas12a	UAAUUUCUACUGUGUGUAGAU	10.1186/ s13059-019-1620-8
Pseudobutyrivibrio ruminis CF1b	PrCas12a	UAAUUUCUACUGUGUGUAGAU	10.1186/ s13059-019-1620-8

Supplementary Table S 2. Sequence of oligonucleotides used in the study (T7 promoter complementary region of oligonucleotides is highlighted green, protospacer complementary region is highlighted red, scaffold is black)

DNA oligonucleotides 5'->3'	
Fwd_test	GGATGCAACTGAATCCTGTAG
Rev_test	TACCGCATAAGCCGGAATAAG
Fwd_RbCpf_Nde	TGAACATATGATGCAAGAGCGTAAAAAAATATCGCATC
Rev_RbCpf_Xho	ATCTACTCGAGATTATTCGCCATATCATTCTCCTGAACA
Fwd_NLS_Nhe_Hind	CTAGATGCCGAAGAAAAAGCGCAAGGTCA
Rev_NLS_Nhe_Hind	AGCTTGACCTTGCGCTTTTTCTTCGGCAT
Fwd_NLS_Hind	AGCTCCCGAAGAAAAAGCGCAAGGTCA
Rev_NLS_Hind	AGCTTGACCTTGCGCTTTTTCTTCGGG
Fwd_dnmt1_spacer1	TAGAAAGGAAGTCTTGGCTGGCCTTCC
Rev_dnmt1_spacer1	AAAAGGAAGGCCAGCCAAGACTTCCTT
Fwd_dnmt1_spacer2	TAGATCACGGGACTTCTGGCTGAGGTCA
Rev_dnmt1_spacer2	AAAATGACCTCAGCCAGAAGTCCCGTGA
Fwd_dnmt1_spacer3	TAGATCTGATGGTCCATGTCTGTTACTC
Rev_dnmt1_spacer3	AAAAGAGTAACAGACATGGACCATCAGA
Fwd_vegfa_spacer	TAGATCTAGGAATATTGAAGGGGGCAGG
Rev_vegfa_spacer	AAAACCTGCCCCCTTCAATATTCCTAGA
Fwd_emx1_spacer	TAGATTCCTCCGGTTCTGGAACCACACC
Rev_emx1_spacer	AAAAGGTGTGGTTCCAGAACCGGAGGAA

Fwd_dnmt1_del_ngs	GACAGACACACGGAGTGTCTAGCT
Rev_dnmt1_del_ngs	AATTTGGCTCAGCAGGCACC
Fwd_dnmt1_sp1_ngs	CAAGGGCAGCTCAGTGGTGACTT
Rev_dnmt1_sp1_ngs	CTGAGTCACGTGAGTTGATCCCCAT
Fwd_dnmt1_sp2_ngs	GACAGACACACGGAGTGTCTAGCT
Rev_dnmt1_sp2_ngs	GAAGCTGTTGTGTGAGGTTCGCTTATC
Fwd_dnmt1_sp3_ngs	CAGAACTAGTCCTTAGCAGCT
Rev_dnmt1_sp3_ngs	CTCTGGGGACCGTTTGAG
Fwd_vegfa_ngs	GGGTCACTCCAGGATTCC
Rev_vegfa_ngs	CCAAGGTTCACAGCCTGAAA
Fwd_emx1_ngs	GCCTCCTGAGTTTCTCATCTG
Rev_emx1_ngs	CTAGTCATTGGAGGTGACATCG
Fwd_SDM_T	TTTGGAATTTTGTGCCACTTCTG
Fwd_SDM_A	TTTGGAATTTAGTGCCACTTCTG
Fwd_SDM_C	TTTGGAATTTCGTGCCACTTCTG
Rev_SDM	GGTTTACCTTGACCCCTATAG
Fwd_PAM_library	GTAAAACGACGGCCAGTGCCGCAGTACTGATCATNNNNNNNNCCCCTCTATTGATCCCCACCTCCAAATATCTCATCAACAACGTCATAGCTGTTTCCTG

Rev_PAM_library	CAGGAAACAGCTATGACGTTGTTGATGAGATATTTGGAGGTGGGGA TCAATAGAGGGGNNNNNNNNATGATCAGTACTGCGGCACTGGCCG TCGTTTTAC
Fwd_RbCpf_RT	AGTGACGACTTGAAGGCTGA
Rev_RbCpf_RT	CGTCACATGGCAGCTTAGAC
Fwd_T7_guide	TAATACGACTCACTATAGG
Rev_TCA_guide	CTAAGAAACCATTATTATCAATCTACAAGAGTAGAAATTACCCTATA GTGAGTCGTATTA
Rev_TCG_guide	GGGTTCCGCGCACATTTCCCATCTACAAGAGTAGAAATTACCCTATA GTGAGTCGTATTA
Rev_TCC_guide	CGTCAGGTGGCACTTTTCGGATCTACAAGAGTAGAAATTACCCTAT AGTGAGTCGTATTA
Rev_TCT_guide	AAAGTGCCACCTGACGTCTAATCTACAAGAGTAGAAATTACCCTAT AGTGAGTCGTATTA
Rev_CTA_guide	TATTTAGAAAAATAAACAAAATCTACAAGAGTAGAAATTACCCTATA GTGAGTCGTATTA
Rev_CTG_guide	AATAATGGTTTCTTAGACGTATCTACAAGAGTAGAAATTACCCTATA GTGAGTCGTATTA
Rev_CTC_guide	CCGTCATCACCGAAACGCGCATCTACAAGAGTAGAAATTACCCTAT AGTGAGTCGTATTA
Rev_CTT_guide	AAAAGTGCCACCTGACGTCTATCTACAAGAGTAGAAATTACCCTAT AGTGAGTCGTATTA
Rev_CCA_guide	ACATTTCCCCGAAAAGTGCCATCTACAAGAGTAGAAATTACCCTAT AGTGAGTCGTATTA
Rev_CCG_guide	AGACGTCAGGTGGCACTTTTATCTACAAGAGTAGAAATTACCCTATA GTGAGTCGTATTA
Rev_CCC_guide	GACGTCAGGTGGCACTTTTCATCTACAAGAGTAGAAATTACCCTAT AGTGAGTCGTATTA
Rev_CCT_guide	ATAATGGTTTCTTAGACGTCATCTACAAGAGTAGAAATTACCCTATA GTGAGTCGTATTA
Rev_TTC_guide	GTCAGGTGGCACTTTTCGGGATCTACAAGAGTAGAAATTACCCTAT AGTGAGTCGTATTA
crRNA_site1	rUrArArUrUrUrCrUrArCrUrArUrUrGrUrArGrArUrCrCrCrCrUrCrUrArUr UrGrArUrCrCrCrCrArCrC
Fwd_gDNA_site1	TCTTGCACTCATGAGCTGTC
Rev_gDNA_site1	GTTGAGGGTTATGAGAGTAGC

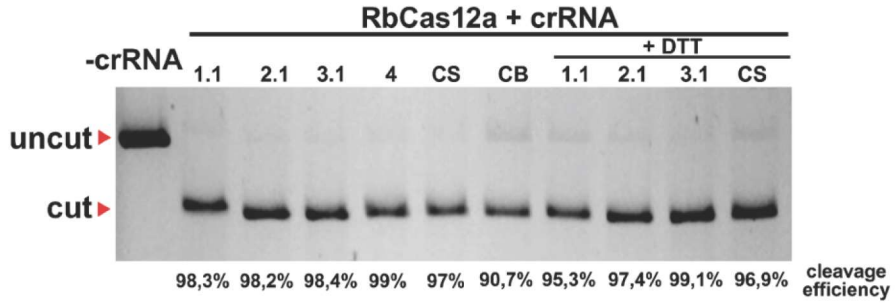


Figure S1. Effect of buffers on RbCas12a crRNA cleavage activity. Target DNA cleavage by RbCas12a programmed with 500 nM crRNA at a 1:3:30 target:RbCas12a:RNA ratio in various conditions. The effect of NEBuffer 1.1 (1.1), NEBuffer 2.1 (2.1), NEBuffer 3.1 (3.1), NEBuffer 4 (4), CutSmart (CS) and cleavage buffer (CB) either supplemented or not with DTT were tested. Mean cleavage efficiencies from three independent experiments are shown below the gel.

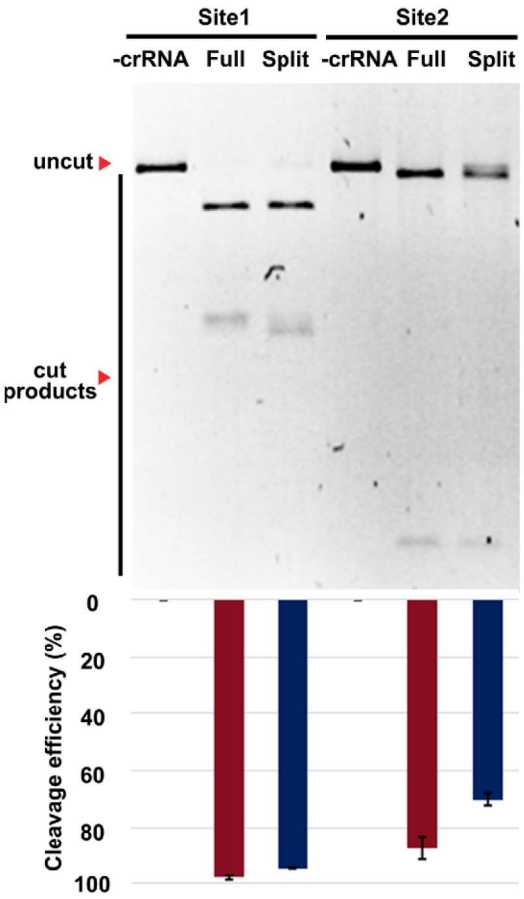


Figure S2. Split crRNA activity is not dependent on the sequence of the crRNA spacer moiety. Target DNA *in vitro* cleavage by RbCas12a loaded with full-sized or split crRNAs (500 nM) bearing different guide sequences ('Site1' and 'Site2' as indicated above the panel). The cleavage efficiencies calculated from one experiment are shown on the bottom. Mean cleavage efficiencies and standard deviations calculated from three independent experiments are shown.

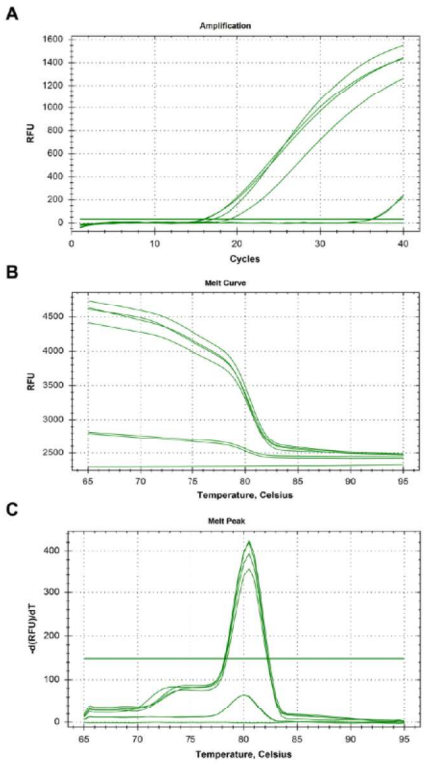


Figure S3. Real-time RT-PCR of RbCas12a mRNA extracted from HEK293T in 24 and 48 hours after transfection (500 ng and 2500 ng of hRbCas12a plasmid vector). **(A)** The signal grows exponentially from cycle 15 in four samples with hRbCas12a plasmid vector. In two mock samples where the plasmid vector was not added the signal is observed from cycle 35. **(B), (C)** Melt curves and peaks indicate specificity of the primer pair.

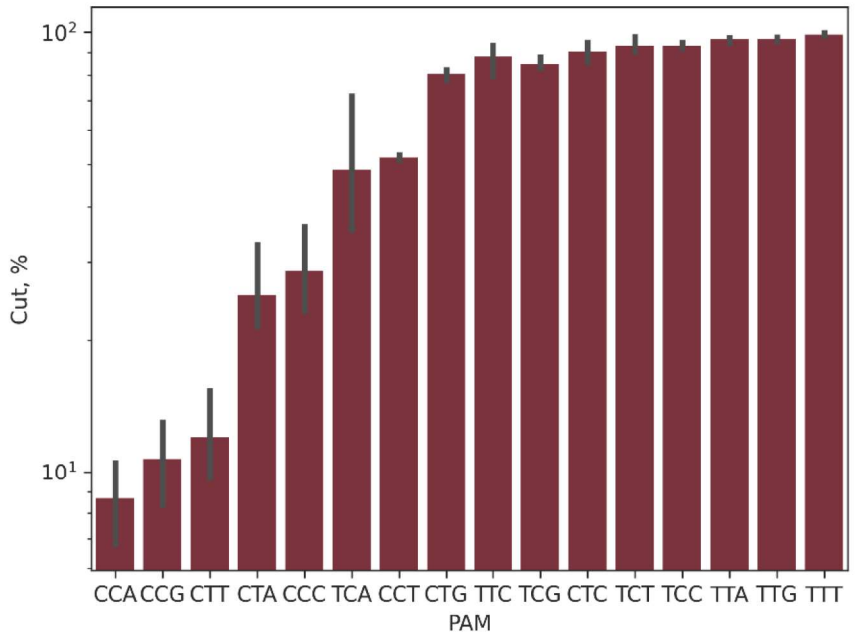


Figure S4. Investigation of RbCas12a 5'-YYN PAM sequence by *in vitro* cleavage assay. Bar plots display the LFC depletion of PAM containing DNA sequences following treatment with RbCas12a.

Nucleotide sequence of RbCas12a

ATGCAAGAGCGTAAAAAAATATCGCATCTTACACACAGAAATTCAGTTAAAAAAACAATTAGGATGCAACTGAATCCTGTAGGT
AAAACAATGGATTATTTTCAAGCAAAGCAAATTCTTGAAAATGATGAAAAGCTTAAAGAGAACTATCAGAAAATCAAGGAAAT
AGCAGACAGGTTTTACAGAAATTTAAATGAGGATGTACTTTCAAAAACCGGGTTAGATAAATTAAAAGATTATGCTGAAATTTA
CTATCACTGTAATACGGATGCAGACCGAAAAAGACTTGATGAATGTGCATCGGAATTAAGGAAAGAAATCGTCAAAAATTTTA
AGAATAGAGATGAGTATAACAAACTATTCGATAAAAGGATGATTGAGATAGTTCTTCCCCAGCATCTTAAAAACGAGGACGAAA
AGGAAGTTGTAGCCTCATTTAAAAATTTCACAACATACTTTACAGGTTTCTTCACTAACAGAAAAAATATGTATTCGGACGGAG
AAGAATCCACGGCAATCGCATATAGATGCATTAACGAAAATTTGCCTAAACATCTTGACAATGTCAAGGCCTTTGAAAAAGCAA
TTTCTAAACTATCCAAAAACGCAATTGATGATTTAGATGCCACTTATTCCGGCTTATGCGGTACAAATTTGTATGATGTTTTTACA
GTTGATTATTTTAACTTTTTGCTTCCACAATCCGGAATTACCGAATATAACAAAATCATCGGCGGTTACACAACAAGCGACGGTA
CAAAAGTTAAGGGTATTAACGAATATATAAATTTGTACAATCAACAAGTATCCAAACGGGATAAAATTCCTAATCTTCAAATTTT
GTATAAACAAATTTTAAGTGAGAGTGAAAAGGTATCATTCATACCGCCAAAGTTTGAAGATGACAACGAACTTTTATCGGCTGT
TTCAGAGTTTTACGCAAACGACGAAACCTTTGACGGGATGCCATTAAAAAAAGCAATTGATGAAACAAAGCTATTATTCGGCA
ATTTAGATAATTCCTCTCTTAATGGAATTTACATTCAAAATGACCGATCCGTGACAAATCTGTCAAACAGTATGTTCGGTTCTTGG
TCGGTAATAGAAGATTTATGGAACAAAAATTATGACTCCGTTAATTCAAACAGCAGAATCAAAGATATTCAAAAGCGTGAAGAC
AAAAGAAAAAAAGCATACAAAGCAGAAAAGAAACTTTCACTTTCATTTTTACAGGTTTTGATTTCCAATTCCGAAAATGATGA
AATCAGAAAAAAGTCTATCGTAGATTACTACAAGACTTCTTTAATGCAACTTACCAACAATTTATCAGACAAATACAACGAAGC
AGCACCTCTGTTCAGTGAAAATTACGATAATGAAAAAGGTTTGAAAAATGACGATAAATCTATTTCATTAATTAAAAATTTTCTT
GATGCCATAAAAGAAATTGAAAAATTCATAAAGCCTTTGTCCGAAACTAATATTACAGGTGAGAAAAATGATTTGTTTTACAGT
CAGTTCACACCATTACTTGATAATATCAGCAGAATAGACATATTATATGATAAGGTCAGAAACTATGTTACACAAAAACCGTTTT
CAACCGATAAAATCAAGCTTAACTTTGACAATTACCAGCTATTAAACGGCTGGGATAAAGACAAAGAAAGAGAGTACGGAGCC
GTTTTGCTTTGTAAAGATGAAAAGTATTATCTTGCAATCATAGATAAAAGCAATAATCGTATTTTGGAAAATATTGATTTTCAAGA
CTGCGATGAAAGCGATTGTTACGAAAAGATAATTTACAAGCTTCTCCCCACTCCAAATAAAATGCTTCCAAAAGTTTTCTTTGC
AAAAAAGCACAAAAAACTTTTGTCACCGTCAGACGAAATACTTAAAATTTATAAAAGCGGCACTTTCAAAAAAGGTGATAAGT
TCAGCCTTGATGATTGCCATAAGTTAATTGATTTCTACAAAGAATCATTCAAAAAGTACCCAAAATGGTTAATTTATAACTTTAAA
TTCAAAAAAACAAACGAATATAACGATATCCGCGAATTTTATAATGATGTTGCTTTACAGGGATATAATATTTCAAAAATGAAAA
TCCCGACATCATTTATTGACAAACTTGTAGATGAAGGAAAAATCTATCTTTTCCAACTCTACAACAAAGACTTTTCACCGCATAG
CAAGGGTACTCCTAATCTGCATACACTTTATTTTAAAATGTTATTTGATGAAAGAAATCTTGAAGATGTGGTGTATAGGCTTAAC
GGTGAGGCAGAAATGTTTTATCGTCCTGCAAGTATAAAATATGACAAACCCACTCATCCCAAAAACACACCGATAAAAAATAA
AAATACACTCAATGATAAAAAAGCAAGCACTTTTCCTTATGACTTAATTAAAGATAAACGCTACACTAAATGGCAGTTTTCACTT
CACTTCCCTATTACCATGAATTTTAAAGCTCCGGATAGGGCAATGATCAATGATGATGTCAGAAATCTGCTGAAATCCTGCAACA
ACAATTTCATCATAGGAATTGACAGAGGCGAAAGAAACTTGCTTTATGTCAGCGTAATTGACAGCAACGGTGCTATAATATATC
AGCACTCACTCAATATTATCGGAAACAAGTTTAAAGGAAAAACATACGAAACTAACTACCAGGAAAAACTTGCAACAAGAGA
AAAAGAGCGTACGGAACAGCGCCGTAACTGGAAAGCAATTGAGAGTATAAAAGAACTCAAAGAGGGCTATATCAGTCAGGCT
GTGCATGTTATATGTCAGCTTGTTGTCAAGTACGATGCAATCATCGTTATGGAAAAGCTGACTGACGGATTCAAACGAGGCAGA
ACAAAGTTTGAAAAACAGGTTTATCAGAAATTTGAAAAAATGCTGATTGACAAACTTAATTACTATGTTGACAAAAAGCTTGAT
CCCGATGAAGAAGGCGGTTTACTTCATGCCTACCAGCTTACGAACAAGCTTGAGAGCTTTGATAAGCTTGGTACGCAAAGCGG
TTTTATTTTCTATGTTCGTCCTGATTTTACAAGCAAAATTGATCCCGTTACCGGCTTTGTAAATTTGTTGTACCCTCGATATGAAA
ACATTGACAAAGCCAAAGATATGATTTCAAGATTTGACGATATAAGATACAATGCCGGCGAGGACTTTTTTGAATTTGACATTGA
TTACGATAAGTTTCCAAAGACTGCGTCTGACTATCGCAAAAAGTGGACAATCTGTACTAACGGCGAAAGGATTGAAGCTTTCA
GAAATCCCGCAAACAATAACGAATGGAGTTATCGTACAATAATTCTTGCAGAAAAATTCAAAGAATTATTTGATAACAATTCTAT
AAATTATCGTGATTCTGACGATTTGAAAGCTGAAATTCTTTCACAGACAAAGGGCAAATTTTTTGAGGATTTCTTCAAATTATTA
AGACTTACCCTACAGATGCGAAACAGTAACCCTGAAACAGGCGAGGACCGTATTCTTTCTCCCGTCAAGGACAAAAACGGCA
ATTTTTACGACAGTTCAAAATATGATGAAAAGAGCAAGCTTCCGTGTGACGCCGATGCAAACGGTGCGTACAACATTGCCCGC
AAAGGTTTGTGGATTGTTGAACAATTCAAAAAATCCGATAATGTTTCAACTGTCGAACCGGTAATTCACAATGACAAATGGCTG
AAATTTGTTCAGGAGAATGATATGGCGAATAATCTCGAG

Amino-acid sequence of RbCas12a

MQERKKISHLTHRNSVKKTIRMQLNPVGKTMDYFQAKQILENDEKLKENYQKIKEIADRFYRNLNEDVLSKTGLDKLKDYAEIYY
HCNTDADRKRLDECASELRKEIVKNFKNRDEYNKLFDKRMIEIVLPQHLKNEDEKEVVASFKNFTTYFTGFFTNRKNMYSDGEEST
AIAYRCINENLPKHLDNVKAFEKAISKLSKNAIDDLDATYSGLCGTNLYDVFTVDYFNFLLPQSGITEYNKIIGGYTTSDGTKVKGIN
EYINLYNQQVSKRDKIPNLQILYKQILSESEKVSFIPPKFEDDNELLSAVSEFYANDETFDGMPLKKAIDETKLLFGNLDNSSLNGIYI
QNDRSVTNLSNSMFGSWSVIEDLWNKNYDSVNSNSRIKDIQKREDKRKKAYKAEKKLSLSFLQVLISNSENDEIRKKSIVDYYKTS
LMQLTNNLSDKYNEAAPLFSENYDNEKGLKNDDKSISLIKNFLDAIKEIEKFIKPLSETNITGEKNDLFYSQFTPLLDNISRIDILYDKV
RNYVTQKPFSTDKIKLNFDNYQLLNGWDKDKEREYGAVLLCKDEKYYLAIIDKSNNRILENIDFQDCDESDCYEKIIYKLLPTPNK
MLPKVFFAKKHKKLLSPSDEILKIYKSGTFKKGDKFSLDDCHKLIDFYKESFKKYPKWLIYNFKFKKTNEYNDIREFYNDVALQGY
NISKMKIPTSFIDKLVDEGKIYLFQLYNKDFSPHSKGTPNLHTLYFKMLFDERNLEDVVYRLNGEAEMFYRPASIKYDKPTHPKNTPI
KNKNTLNDKKASTFPYDLIKDKRYTKWQFSLHFPITMNFKAPDRAMINDDVRNLLKSCNNNFIIGIDRGERNLLYVSVIDSNGAIIY
QHSLNIIGNKFKGKTYETNYQEKLATREKERTEQRRNWKAIESIKELKEGYISQAVHVICQLVVKYDAIIVMEKLTDGFKRGRTKFE
KQVYQKFEKMLIDKLNYYVDKKLDPDEEGGLLHAYQLTNKLESFDKLGTQSGFIFYVRPDFTSKIDPVTGFVNLLYPRYENIDKAK
DMISRFDDIRYNAGEDFFEFDIDYDKFPKTASDYRKKWTICTNGERIEAFRNPANNNEWSYRTIILAEKFKELFDNNSINYRDSDDLK
AEILSQTKGKFFEDFFKLLRLTLQMRNSNPETGEDRILSPVKDKNGNFYDSSKYDEKSKLPCDADANGAYNIARKGLWIVEQFKKS
DNVSTVEPVIHNDKWLKFVQENDMANNLE

Human optimized nucleotide sequence of RbCas12a with nuclear localization signals

(SV40 NLS is highlighted red, nucleoplasmin NLS is blue)

ATGCCGAAGAAAAAGCGCAAGGTCAAGCTCCCGAAGAAAAAGCGCAAGGTCAAGCTCCCGAAGAAAAAGCGCAAGGTCAA
GCTTATGCAAGAACGCAAGAAGATTAGTCATCTGACCCATAGAAACTCCGTGAAGAAGACCATCCGTATGCAATTAAACCCGG
TCGGCAAGACCATGGACTACTTCCAAGCCAAGCAAATCCTGGAGAACGACGAGAAGCTGAAGGAAAACTACCAAAAGATCA
AGGAGATTGCCGACCGTTTCTATAGAAACTTAAACGAAGACGTCCTGAGCAAGACTGGTTTGGACAAGTTAAAGGACTACGCT
GAGATCTATTACCATTGTAACACGGACGCCGACCGTAAGAGACTGGACGAGTGTGCCAGTGAGTTACGTAAGGAGATCGTAAA
GAACTTCAAGAACAGAGACGAATACAACAAGCTATTTGACAAGCGTATGATCGAAATTGTGCTGCCGCAACATCTGAAGAACG
AAGACGAGAAGGAGGTGGTCGCGTCTTTCAAGAACTTTACCACCTACTTCACCGGCTTTTTTACTAACAGAAAGAACATGTAC
AGTGACGGAGAGGAGTCGACGGCCATCGCCTACAGATGTATCAACGAGAACTTACCGAAGCATCTGGACAACGTAAAGGCAT
TCGAGAAGGCTATCAGTAAGCTATCGAAGAACGCCATCGACGACTTAGACGCAACTTACTCGGGCTTATGTGGAACCAACTTG
TACGACGTGTTCACCGTGGACTACTTCAACTTCTTGCTGCCGCAATCGGGAATCACTGAGTACAACAAGATCATCGGCGGCTAC
ACCACCTCTGACGGCACCAAGGTGAAAGGTATCAACGAGTACATTAACTTGTACAACCAACAAGTCTCGAAGCGTGACAAGA
TCCCGAACCTGCAAATCTTGTACAAGCAAATCTTAAGTGAAAGTGAGAAGGTCAGCTTTATTCCACCGAAGTTCGAGGACGAC
AACGAGCTGTTAAGTGCTGTGAGCGAATTTTACGCCAACGACGAGACTTTCGACGGTATGCCGTTAAAGAAGGCCATCGACGA
GACCAAGCTATTATTTGGCAACTTAGACAACTCGAGTCTGAACGGAATCTACATCCAAAACGACCGTTCGGTTACCAACTTAAG
CAACAGTATGTTTGGCAGTTGGAGTGTGATTGAGGACTTATGGAACAAGAACTACGACTCGGTGAACTCTAACTCTAGAATCA
AGGACATCCAAAAGCGCGAGGACAAGAGAAAGAAGGCCTACAAGGCCGAGAAGAAGCTGAGCCTGAGCTTCTTACAAGTGT
TGATCTCGAACTCGGAGAACGACGAGATCAGAAAGAAGAGTATCGTCGACTACTACAAGACTAGTTTAATGCAACTGACTAAC
AACTTAAGCGACAAGTACAACGAGGCCGCCCCGTTATTTAGTGAGAACTACGACAACGAGAAGGGCTTGAAGAACGACGACA
AGAGTATCAGCTTAATCAAGAACTTCCTGGACGCAATTAAGGAGATCGAGAAGTTTATTAAGCCGTTGTCGGAGACTAACATCA
CCGGCGAAAAGAACGACTTGTTCTACAGTCAATTTACCCCGTTACTGGACAACATCTCTAGAATTGACATTTTATACGACAAGG
TAAGAAACTACGTGACCCAAAAGCCATTCAGCACTGACAAGATCAAGCTGAACTTCGACAACTACCAACTATTAAACGGCTGG
GACAAGGACAAGGAGAGAGAATACGGAGCGGTGTTGCTGTGTAAGGACGAGAAGTACTACCTGGCCATCATTGACAAGTCTA
ACAACCGCATCTTGGAGAACATCGACTTCCAAGACTGTGACGAGTCTGACTGTTACGAGAAGATTATCTACAAGCTGCTTCCG
ACTCCGAACAAGATGCTGCCGAAGGTGTTTTTCGCCAAGAAGCATAAGAAGCTGTTGAGCCCAAGCGACGAGATTCTGAAGA
TCTACAAGTCTGGCACTTTTAAGAAGGGCGACAAGTTTTCTCTGGACGACTGTCATAAGTTAATCGACTTTTACAAGGAGAGCT
TTAAGAAGTACCCGAAGTGGTTAATCTACAACTTCAAGTTTAAGAAGACCAACGAGTACAACGACATCCGTGAGTTCTACAAC
GACGTGGCTTTACAAGGTTACAACATCAGCAAGATGAAGATCCCGACCTCTTTCATCGACAAGCTGGTCGACGAGGGAAAGAT
CTACCTGTTTCAACTTTACAACAAGGACTTCAGCCCACATTCTAAGGGCACTCCGAACTTACATACCCTGTACTTCAAGATGTTA
TTCGACGAGAGAAACCTGGAGGACGTTGTTTACCGTCTGAACGGCGAAGCCGAGATGTTCTACCGCCCGGCCAGTATTAAGTA
CGACAAGCCGACTCATCCGAAGAACACCCCAATTAAGAACAAGAACACCCTTAACGACAAGAAGGCCTCTACTTTCCCGTAC
GACTTAATCAAGGACAAGCGTTACACTAAGTGGCAATTCAGCCTGCATTTTCCGATCACTATGAACTTCAAGGCTCCAGACCGT
GCCATGATTAACGACGACGTAAGAAACTTATTAAAGTCGTGTAACAACAACTTTATCATTGGAATCGACAGAGGCGAGAGAAA
CTTGCTGTACGTATCTGTCATCGACTCTAACGGCGCTATTATTTACCAACATAGCCTTAACATCATCGGAAACAAGTTCAAGGGA
AAGACCTACGAGACTAACTACCAAGAGAAGCTGGCCACCAGAGAGAAGGAACGCACGGAGCAACGTCGCAACTGGAAGGCC
ATCGAAAGTATTAAGGAGCTTAAGGAAGGCTACATCAGTCAAGCTGTTCATGTGATTTGTCAACTGGTGGTAAAGTACGACGC
CATCATCGTGATGGAGAAGTTAACTGACGGATTTAAGCGTGGCAGAACCAAGTTCGAGAAGCAAGTGTACCAAAAGTTCGAG
AAGATGTTAATCGACAAGCTGAACTACTACGTGGACAAGAAGCTGGACCCGGACGAGGAGGGCGGCTTACTGCATGCATACC
AACTGACGAACAAGCTGGAATCTTTCGACAAGCTGGGCACGCAATCTGGCTTCATCTTTTACGTGCGCCCGGACTTCACCTCT
AAGATCGACCCGGTGACTGGCTTCGTCAACTTGTTGTACCCGCGTTACGAGAACATCGACAAGGCAAAGGACATGATCAGCA
GATTCGACGACATTAGATACAACGCAGGCGAAGACTTCTTCGAGTTCGACATCGACTACGACAAGTTCCCGAAGACTGCGAGT
GACTACCGTAAGAAGTGGACCATCTGTACTAACGGCGAGCGTATCGAGGCTTTTAGAAACCCGGCCAACAACAACGAGTGGA
GTTACCGCACCATTATCCTGGCCGAGAAGTTTAAGGAGTTATTCGACAACAACAGTATTAACTACCGCGACAGTGACGACTTGA
AGGCTGAGATCCTGAGCCAAACCAAGGGCAAGTTCTTCGAAGACTTTTTTAAGTTATTAAGACTGACTCTACAAATGCGTAAC
AGTAACCCGGAGACCGGCGAAGACCGCATCCTGAGTCCGGTAAAGGACAAGAACGGAAACTTCTACGACAGTAGCAAGTAC
GACGAGAAGTCTAAGCTGCCATGTGACGCAGACGCCAACGGCGCGTACAACATCGCACGTAAGGGCTTGTGGATCGTGGAGC
AATTTAAGAAGTCGGACAACGTGAGCACTGTAGAGCCAGTCATCCATAACGACAAGTGGTTAAAGTTCGTGCAAGAAAACGA
CATGGCGAACAACAAGCGGCCTGCGGCTACTAAGAAGGCTGGGCAGGCTAAGAAGAAGAAG

RESUME LONG EN FRANCAIS

1. INTRODUCTION

Les mitochondries sont des organites essentiels des cellules eucaryotes. Parmi leurs nombreuses fonctions, la production d'énergie sous forme d'ATP, qui a lieu dans la chaîne respiratoire mitochondriale grâce au processus de phosphorylation oxidative (OXPHOS), est primordiale. Bien que la plupart des macromolécules trouvées dans l'organite soient codées par le génome nucléaire, les mitochondries contiennent également leur propre génome, l'ADNmt. Cet ADN de 16,5 kb code pour 13 sous-unités de quatre des cinq complexes OXPHOS, 22 ARNt et 2 ARN ribosomiques (**Anderson, S. *et al.*, 1981**). Les mutations de ces protéines, d'ARNt ou d'ARN ribosomiques, peuvent affecter la production d'ATP mitochondriale, entraînant un large éventail de maladies mitochondriales, souvent associées à des troubles neuromusculaires (**Nissanka N. & Moraes C. T., 2020**). La gravité des maladies mitochondriales est dépendante du niveau d'hétéroplasmie - un état dans lequel des molécules d'ADNmt mutantes et de type sauvage (WT) coexistent dans la même cellule (**Rossignol, R. *et al.*, 2003**). Ainsi, l'expression phénotypique de ces mutations est très étroitement corrélée au niveau d'hétéroplasmie, et l'apparition des défauts ne sera observée que lorsque ce niveau dépassera un certain seuil (**Nissanka N. & Moraes C. T., 2020**). Prises ensemble, les mutations pathogèniques de l'ADNmt affectent 1 individu sur 5 000 (**Gorman, G. S. *et al.*, 2015**). À ce jour, ces pathologies n'ont pas trouvé de traitement adéquat (**Rahman J. & Rahman S., 2018**).

Diverses nucléases ciblées sur les mitochondries ont été développées pour dégrader l'ADNmt mutant et, de ce fait, changer le niveau d'hétéroplasmie. Les endonucléases de restriction ciblées sur les mitochondries (mitoRE), natives et artificielles (mitoARCUS), ont été utilisées avec succès pour réduire les niveaux d'ADNmt mutant dans des cellules humaines cultivées et des modèles de souris (**Verechshagina, N. A. *et al.*, 2019**). Cependant, ces systèmes sont fortement limités par la rareté dapparition de sites de reconnaissance uniques, permettant le ciblage de mutations pathogènes spécifiques dans l'ADNmt. De plus, le développement de nucléases artificielles nécessite beaucoup de temps et de ressources.

Les limitations des mitoRE ont été résolues en créant des nucléases capables de cibler divers sites de l'ADNmt par des modules de reconnaissance d'ADN spécifiques - des protéines à doigts de zinc pour les mitoZFN et des protéines TALE pour les mitoTALEN. Ces nucléases sont généralement composées de trois composants essentiels fusionnés en une seule protéine: un signal de localisation mitochondriale, des domaines de liaison à l'ADN et des domaines nucléases (**Bacman, S. R. *et al.*, 2013**; **Gammage, P. A. *et al.*, 2014**). Pour le signal

de localisation mitochondriale, similaire aux enzymes de restriction modifiées, des séquences de ciblage dérivées de protéines mitochondriales naturellement importées sont utilisées (**Chin, R. M. *et al.*, 2018**). Le domaine nucléase correspond à la nucléase FokI, qui introduit une cassure double brin dans l'ADN sans exigences de séquence spécifiques (**Hiroyuki S. & Susumu K., 1981**).

Pour obtenir un ciblage spécifique de différentes régions d'ADNmt, deux domaines distincts de liaison à l'ADN sont utilisés. Les MitoZFN utilisent le domaine de liaison à l'ADN du type doigts de zinc (**Gammage, P. A. *et al.*, 2014**). Il convient de noter que les domaines de liaison à l'ADN du type doigt de zinc se trouvent couramment dans les facteurs de transcription (**Ravasi, T. *et al.*, 2003**), portant généralement un signal de localisation nucléaire (**Macara I. G., 2001**). Pour permettre une importation efficace des mtZFN dans les mitochondries et réduire le risque de clivage non spécifique de l'ADN nucléaire, ce signal de localisation nucléaire doit être échangé contre un signal d'exportation nucléaire (NES) (**Gammage, P. A. *et al.*, 2014**). Pour les mitoTALEN, le domaine de liaison à l'ADN est dérivé de la protéine effectrice de type activateur de transcription bactérienne (TALE) (**Bacman, S. R. *et al.*, 2013**). À ce jour, ces outils ont réussi à modifier le niveau d'hétéroplasmie des mutations ponctuelles et des délétions d'ADNmt dans des cellules cybrides et des modèles de souris (**Verechshagina, N. A. *et al.*, 2019**). De plus, les deux derniers systèmes ont récemment été utilisés pour l'édition de l'ADNmt afin d'inverser les mutations sans introduire de rupture dans l'ADNmt (**Silva-Pinheiro, P. *et al.*, 2023**).

Bien que les stratégies basées sur les mitoZFN et les mitoTALEN soient prometteuses pour le ciblage de l'ADNmt, elles ont des limites. Toutes ces approches sont basées sur des interactions spécifiques protéine-acide nucléique. Concevoir et fabriquer des monomères pour la reconnaissance spécifique de l'ADNmt est une tâche difficile et coûteuse. Pour les mitoZFN et les mitoTALENS, il est nécessaire de valider expérimentalement chaque combinaison de modules afin de créer un domaine de liaison à l'ADN capable de se lier spécifiquement et efficacement à la séquence d'ADN cible. De plus, la grande taille des séquences codant pour les protéines dépasse la capacité des systèmes d'administration actuels basés sur des virus, tels que l'AAV (**Mingozzi F. & High K. A., 2011**; **Moraes C. T., 2014**).

Les systèmes CRISPR-Cas peuvent résoudre les limites des approches d'édition décrites précédemment. Ces systèmes, tout en ayant des séquences codantes plus courtes, offrent une plus grande flexibilité par rapport aux systèmes uniquement protéiques en raison de leur dépendance aux interactions ADN-ARN pour la reconnaissance spécifique de sites d'ADNmt (**Jinek, M. *et al.*, 2012**). En outre, de tels systèmes se sont révélés plus efficaces pour l'édition du génome nucléaire, ainsi que plus polyvalents et plus faciles à cibler diverses séquences

d'ADN en modifiant le composant du système ARN, tout en maintenant la protéine constante. Il n'est donc pas surprenant que de nombreux laboratoires à travers le monde, y compris le nôtre, explorent activement l'adaptation de la technologie CRISPR pour éliminer les molécules d'ADNmt mutantes et modifier le génome mitochondrial.

AsCas12a, également connu sous le nom d'AsCpf1, appartient au système CRISPR-Cas de classe 2 de type VA. Il fonctionne en catalysant les clivages d'ADN double brin à l'aide d'une seule molécule d'ARN-guide CRISPR (ARNcr) (**Yamano, T. *et al.*, 2016**).En plus, AsCas12a utilise un ARNcr relativement court de 40 à 44 nucléotides, ce qui pourrait potentiellement en faire un meilleur candidat pour l'importation mitochondriale par rapport à l'ARN guide de plus grade taille (sgRNA) utilisé dans le système CRISPR-Cas9 de type II. Le complexe ribonucléoprotéine (RNP) AsCas12a-crRNA identifie initialement sa cible ADNdb en reconnaissant un motif adjacent au "protoespacer" (PAM) riche en T. Après la liaison à la cible, le RNP AsCas12a déroule l'ADN, formant un hétéroduplex de brin cible (TS) avec l'ARNcr, tout en déplaçant le brin non cible (NTS) pour créer une structure en boucle R (**Stella S., Alcón P., Montoya G., 2016**). Par la suite, Cas12a génère des clivages d'ADN double brin avec des extrémités adhésives en 5' en utilisant un seul domaine nucléase RuvC de manière séquentielle. Étant donné qu'AsCas12a reconnaît une séquence PAM riche en T, contrairement à la PAM riche en G de SpCas9, il est prometteur pour cibler l'ADNmt humain, qui a une teneur en GC de seulement 44 %. Cela rend AsCas12a plus avantageux pour cibler des séquences dans l'ADNmt humain. De plus, AsCas12a présenterait une activité hors cible inférieure à celle de SpCas9 (**Zetsche, B. *et al.*, 2017; Kim D. *et al.*, 2016**).

En ce qui concerne les caractéristiques d'AsCas12a, il serait intéressant d'étudier si le système ciblé sur les mitochondries peut non seulement dégrader l'ADNmt, mais également y introduire des réarrangements, par exemple en induisant des délétions dans l'ADNmt grâce à sa capacité à générer des extrémités en 5' en surplomb. Pour y parvenir, deux crRNA conçus pour laisser des extrémités cohésives devraient être développés. Cela permettrait la création de modèles cellulaires et animaux portant une délétion prévue pour moduler et étudier les maladies associées à l'ADNmt et pour une étude fondamentale de la propagation de la délétion de l'ADNmt.

À ce jour, la seule tentative d'optimisation d'AsCas12a pour le ciblage de l'ADNmt a été effectuée par **Antón *et al.*** en 2020, où l'importation mitochondriale d'AsCas12a fusionné avec GFP portant divers MTS a été comparée, mais ni l'importation d'ARN dans les mitochondries, ni l'effet du mitoAsCas12a sur l'ADNmt n'ont été évalués.

Ainsi, afin de modifier la nucléase AsCas12 et l'ARNcr pour son fonctionnement au sein des mitochondries humaines, les objectifs suivants ont été poursuivis au cours de ce travail de thèse :

OBJECTIFS:

- Optimisation de l'importation de la nucléase AsCas12a et de son ARNcr dans les mitochondries des cellules humaines;
- Analyse de l'activité spécifique du système mitoCRISPR-Cas12a sur l'ADNmt et de ses possibles cibles non spécifiques;
- Développement d'une stratégie pour induire une délétion dans l'ADN mitochondrial humain en utilisant mitoCRISPR-Cas12a.

2. RÉSULTATS

2.1. Importation de la nucléase AsCas12a dans les mitochondries humaines

Pour évaluer l'importation mitochondriale de la nucléase AsCas12a et obtenir l'expression contrôlée, nous avons développé une lignée cellulaire monoclonale avec l'expression de la mitoAsCas12a portant COX8a MTS inductible par la tétracycline. Nous avons analysé différentes fractions subcellulaires par Western blot et confirmé la présence de la nucléase AsCas12a modifiée dans les mitochondries humaines. Cependant, la microscopie immunofluorescente a démontré une double localisation de la mitoAsCas12a portant le COX8a MTS, à savoir dans les mitochondries et le cytosol.

Afin d'améliorer la localisation mitochondriale de la nucléase AsCas12a, nous avons essayé deux stratégies : 1) diminuer le niveau d'expression de la protéine pour empêcher son agrégation dans le cytosol et 2) utiliser d'autres signaux de ciblage mitochondrial. Par mutagenèse dirigée, une délétion de la région promotrice du CMV a été introduite dans un vecteur plasmidique codant pour la nucléase AsCas12a fusionnée avec le MTS COX8a. La diminution du niveau d'expression de la nucléase a été confirmée par l'approche Western blot. En ce qui concerne le MTS, nous avons comparé le MTS de la sous-unité ATPase 9 (Su9) de *Neurospora crassa*, le MTS de la cystéine peptidase 4D liée à l'autophagie des mammifères (ATG4D) et de la superoxyde dismutase 2 (SOD2) avec le MTS de COX8a. En mettant en œuvre la technique de mutagenèse dirigée, nous avons obtenu des constructions plasmidiques codant pour AsCas12a portant divers MTS. L'importation mitochondriale des 8 versions de la protéine mitoAsCas12a sous le contrôle d'une région promotrice de taille réelle ou raccourcie a été testée par microscopie à balayage laser immunofluorescente.

La diminution du niveau d'expression de la nucléase dans les cellules de mammifères n'a pas éliminé la localisation cytosolique partielle de la protéine. D'autre part, la nucléase AsCas12a fusionnée avec Su9 MTS a fourni le meilleur profil de colocalisation mitochondriale avec l'absence de la protéine dans le cytosol.

Ainsi, nous avons créé une nouvelle lignée cellulaire stable exprimant AsCas12a avec une localisation mitochondriale améliorée. Il a été confirmé que la nucléase exprimée dans la lignée cellulaire stable créée était parfaitement colocalisée avec les mitochondries par fractionnement sous-mitochondrial et Western Blot et par microscopie immunofluorescente. L'activité nucléase Su9-AsCas12a dans la lignée cellulaire stable a été évaluée à l'aide de tests de clivage *in vitro*. L'influence de l'expression de mitoAsCas12a sur les mitochondries a été abordée et aucun effet détectable sur la respiration ou la traduction des mitochondries n'a été observé suite à l'activation de l'expression de la nucléase. Cependant, il sera important de répéter le test respiratoire pour obtenir des données statistiquement significatives.

Suite à l'expression de la nucléase Su9-AsCas12a, aucune preuve d'induction de mitophagie n'a été trouvée. Pour confirmer davantage cette observation, de futures études devraient aborder ce point en incluant un contrôle positif de la mitophagie, tel que le traitement des cellules avec un découpleur chimique comme le FCCP. Une autre approche pourrait consister à analyser la colocalisation des mitochondries avec des lysosomes et des autophagosomes par microscopie à fluorescence de cellules vivantes, qui devrait être augmentée dans le cas de la mitophagie.

Bien que nous n'ayons pas observé le mitoAsCas12a dans le noyau jusqu'à présent, par mesure de précaution pour éviter toute localisation nucléaire potentielle et une éventuelle édition hors cible dans le noyau, nous pouvons envisager d'incorporer un signal d'exportation nucléaire (NES) à l'extrémité carboxy du protéine (**Gammage, P. A. *et al.*, 2014**).

2.2. Importation d'ARNcr AsCas12a dans les mitochondries humaines

Ensuite, nous avons étudié l'importation des ARNcr du système CRISPR-Cas12a dans les mitochondries humaines et les exigences structurelles de ce processus par hybridation type Northern d'ARN isolés des mitoplastes traités par des nucléases. Des études menées par notre laboratoire et d'autres ont montré que le motif requis pour le transport des molécules d'ARN dans les mitochondries n'est pas une séquence, mais une structure en épingle à cheveux (**Kolesnikova, O. *et al.*, 2010**; **Wang, G. *et al.*, 2010**). Pour déterminer si la fusion de l'ARNcr avec des déterminants d'importation d'ARN (MLS) connus améliore son ciblage mitochondrial, nous avons ajouté des structures en épingle à cheveux MLS à l'extrémité 3' de

l'ARNcr et avons démontré que cela n'avait pas d'impact sur la capacité de l'ARNcr à programmer le clivage spécifique de l'ADN dans le lysat de cellules humaines exprimant la nucléase AsCas12a. Étonnamment, la localisation mitochondriale des molécules d'ARNcr recombinantes n'a pas été améliorée par rapport à la version non modifiée, ce qui indique que le domaine d'échafaudage structuré de l'ARNcr peut probablement fonctionner comme MLS, assurant l'importation mitochondriale de l'ARNcr.

Nous avons conçu une série d'ARNcr ciblant différentes régions de l'ADNmt et démontré leur capacité à programmer le clivage spécifique de fragments d'ADNmt dans le lysat cellulaire et leur localisation partielle dans la matrice mitochondriale de cellules humaines transfectées avec ces molécules d'ARN. D'après les données obtenues, nous avons émis l'hypothèse que l'importation mitochondriale de ces ARNcr pourrait dépendre de leur structure secondaire.

Pour confirmer davantage les données sur le ciblage mitochondrial de la structure secondaire des ARNcr AsCas12a, nous avons effectué des tests d'importation supplémentaires en utilisant une méthode récemment développée dans notre laboratoire pour le fractionnement sous-mitochondrial de l'ARN (**Jeandard, D. *et al.*, 2022**). Nous avons démontré l'importation mitochondriale d'ARNcr AsCas12a en utilisant des cellules HEK293, la lignée cellulaire stable Su9-AsCas12a et des cellules d'ostéosarcome 143B, indiquant que cette voie ne dépend pas de l'expression de la nucléase hAsCas12a et n'est pas spécifique à la lignée cellulaire (**Nikitchina, N. *et al.*, 2023**).

Nous disposons actuellement d'une collection de 27 crRNA ciblant diverses régions de l'ADNmt. En perspective, nous devrions continuer à évaluer leur importation mitochondriale pour corroborer les résultats observés concernant les exigences structurelles pour l'importation des ARNcr AsCas12a.

Dans le but d'améliorer l'efficacité de l'importation des ARNcr, l'ARNcr AsCas12a a été partitionné en deux fragments individuels de 20 b (ARN dit d'échafaudage et d'espacement). Nous avons démontré que l'ARNcr divisé catalysait un clivage hautement spécifique et efficace de l'ADN cible (**Shebanova, R. & Nikitchina, N. *et al.*, 2022**). Ces observations ont également été confirmées dans des lysats de cellules humaines exprimant AsCas12a. Le système CRISPR-RbCas12a de type V récemment découvert s'est également avéré posséder les mêmes capacités de l'utilisation de l'ARNc divisé. Nous avons comparé l'importation mitochondriale du crRNA complète et de sa partie espaceur et avons découvert que la partie espaceur du crRNA peut être ciblée dans les mitochondries humaines. Nous pensons donc que la version partitionnée (*split*) de l'ARNcr AsCas12a pourrait ensuite être utilisé dans des expériences *in vivo* pour cibler l'ADNmt.

Comme stratégie alternative pour améliorer l'importation mitochondriale des ARNcr AsCas12a, des ARNcr présentant des modifications chimiques à l'extrémité 3' (cholestérol, rhodamine R6G et berbérine) ont été synthétisés et testés. Dans un test de clivage *in vitro* avec la nucléase AsCas12a recombinante purifiée, tous les ARNcr modifiés étaient capables de couper la matrice d'ADNmt. Cependant, l'évaluation de leur importation mitochondriale a démontré que tous les ARNcr modifiés semblaient protégés du traitement par nucléase. Nous n'avons donc pas pu conclure sur l'importation mitochondriale des ARNcr chimiquement modifiés dans les conditions expérimentales utilisées.

Il est à noter que cette stratégie a été initiée lors de mes travaux de thèse mais n'a pas été finalisée. Nous pensons que l'obtention de preuves concrètes concernant l'importation mitochondriale de différents ARNcr ne peut être obtenue que grâce à une démonstration directe du clivage spécifique de l'ADNmt *in vivo*.

2.3. Évaluation de la fonctionnalité du système mitoAsCas12a *in vivo*

La partie la plus importante du projet, représentant la preuve de concept, consistait en la détection du clivage spécifique de l'ADNmt induit par le système mitoCRISPR.

Pour commencer, nous avons étudié le nombre de copies de l'ADNmt dans la lignée cellulaire stable développée. En utilisant l'analyse qPCR de l'ADN total isolé de cellules traitées avec Su9-AsCas12a et son ARNcr ciblant un site d'ADNmt spécifique, nous n'avons observé aucune diminution du nombre de copies d'ADNmt. Ce résultat est resté le même lorsque les cellules ont été traitées avec la nucléase en complexe avec deux ARNcr ciblant l'ADNmt, contrairement à ce qui avait été précédemment rapporté pour la nucléase SpCas9 avec deux ARNg (**Loutre, R. *et al.*, 2018**).

Nous émettons l'hypothèse que l'efficacité du système est limitée par l'importation de composants ARN dans les mitochondries. Si un clivage se produisait, il n'était pas suffisant pour provoquer un changement mesurable du nombre de copies de l'ADNmt. Il est certain que les conditions de cette expérience nécessitent des ajustements et des optimisations supplémentaires. Par exemple, nous pouvons évaluer le nombre de copies d'ADNmt après plusieurs cycles de traitement des cellules avec le système mitoCRISPR, en utilisant des ARNcr qui ciblent différents sites de l'ADNmt, incorporant potentiellement les modifications chimiques. Le test de plusieurs concentrations d'ARNcr pendant la transfection peut également améliorer l'effet, ainsi que l'utilisation de variantes AsCas12a plus efficaces qui possèdent également moins d'activité hors cible (**Kleinstiver, B. P. *et al.*, 2019**; **Zhang, L. *et al.*, 2021**).

Bien que nous n'ayons pas détecté auparavant de réduction des niveaux d'ADNmt suite à l'application du système mitoCRISPR nouvellement développé, notre objectif était d'établir une preuve de concept en confirmant des événements de clivage spécifiques dans l'ADNmt humain induits par l'activité nucléase Su9-AsCas12a ex vivo. Nous avons essayé d'y parvenir en utilisant des approches plus sensibles.

Afin de confirmer l'activité nucléase spécifique programmée par l'ARNcr, nous avons appliqué une stratégie publiée pour la détection des extrémités libres de l'ADNmt consistant en un séquençage de nouvelle génération de l'ADNmt ligaturé avec un linker (**Peeva, V. *et al.*, 2018**). Pour inhiber la dégradation rapide de l'ADNmt linéarisé, l'exonucléase mitochondriale (MGME1) a été inactivée avec du siARN (**Peeva, V. *et al.*, 2018**) avant de transfecter la lignée cellulaire stable, exprimant le mitoAsCas12a, avec le crRNA.

Avant de procéder au NGS, nous avons effectué un test de clivage *in vitro* dans des mitochondries lysées, isolées des cellules traitées. Ce test a révélé un clivage spécifique d'un fragment d'ADNmt, confirmant la présence de la nucléase et de son ARNcr à l'intérieur des mitochondries. Cette expérience devrait être répétée, avec l'étape supplémentaire consistant à traiter les mitochondries isolées avec des RNases pour éliminer la possibilité de contamination par des molécules d'ARNcr adhérant aux mitochondries à partir du cytosol.

Pour l'analyse NGS, l'ADNmt isolé a été ligaturé à un lieur asymétrique double brin avec une séquence connue pour marquer les cassures de l'ADNmt. Après la préparation de la bibliothèque et le NGS, les lectures obtenues ont été alignées sur des séquences mitochondriales de référence spécifiques à l'échantillon et criblées pour la séquence de liaison. L'analyse a révélé une augmentation de 2 à 4 fois de la fragmentation de l'ADNmt dans les échantillons traités avec la nucléase et l'ARNcr par rapport aux échantillons témoins. Malheureusement, en raison du faible enrichissement en ADNmt (1 à 3 %) dans les échantillons, la couverture en ADNmt était insuffisante pour identifier le clivage spécifique à la position attendue dans l'ADNmt.

Nous avons ensuite répété NGS de l'ADNmt ligaturé à un lieur dans les mêmes conditions, mais cette fois, les cellules ont été traitées avec des ARNcr ciblant une région différente de l'ADNmt, spécifiquement MT-COX1. Pour détecter les extrémités libres de l'ADNmt, nous avons effectué une PCR médiée par un lieur sur l'ADN total isolé des cellules avant NGS. Suite à la LM-PCR, nous avons effectué une hybridation par Southern blot avec une sonde d'ADNmt, révélant des fragments PCR de la taille attendue dans les échantillons traités avec la nucléase et les ARNcr, confirmant ainsi le clivage.

Lors de l'analyse des données NGS, nous avons une fois de plus observé une augmentation significative des cassures de l'ADNmt par rapport aux témoins. Malheureusement, malgré le pourcentage légèrement plus élevé d'ADNmt dans les échantillons (2 à 8 %), nous n'avons pas pu visualiser les sites de clivage aux positions attendues dans l'ADNmt. Par conséquent, une optimisation plus poussée des techniques de purification des mitochondries et de l'ADNmt serait nécessaire. Une approche potentielle consiste à utiliser des billes magnétiques recouvertes d'anticorps contre TOMM20 pour l'isolement des mitochondries, ce qui peut améliorer la pureté des mitochondries et de l'ADNmt tout en minimisant la contamination de l'ADN nucléaire.

Pour évaluer davantage l'activité du mitoAsCas12a dans les mitochondries, la lignée cellulaire stable a été transfectée avec deux crRNA conçus pour laisser des extrémités collantes compatibles afin de détecter une délétion induite par le système mitoCRISPR-AsCas12a. Nous pensions que cette conception expérimentale faciliterait la détection de l'impact du système sur l'ADNmt.

Grâce à NGS après LM-PCR, nous avons réussi à détecter le clivage induit par l'un des crRNA. Malheureusement, pour le deuxième ARNc, nous avons observé la même cassure dans l'échantillon témoin, ce qui suggère qu'elle pourrait s'être produite lors de la procédure d'isolement de l'ADNmt ou en raison de l'activité non spécifique de la nucléase AsCas12a. Pour résoudre ce problème, nous prévoyons de répéter l'expérience en incluant des cellules traitées avec AsCas12a mort par DNase, servant de contrôle négatif.

Les PCR de l'ADN isolé avec les amorces flanquant la délétion ont été analysées par hybridation par transfert de Southern, révélant la bande attendue correspondant à la molécule d'ADNmt portant la délétion dans les échantillons contenant le système mitoCRISPR. Pour augmenter la sensibilité de la PCR, nous avons conçu et réalisé une Nested PCR. L'ADN obtenu était suffisant pour effectuer le séquençage Sanger qui a confirmé la présence d'une délétion de l'ADNmt induite par le système. Le NGS ultérieur a confirmé les données de séquençage de Sanger obtenues. Nous avons pu constater une nette différence entre les échantillons témoins et l'ADNmt provenant de cellules exprimant la nucléase mitoAsCas12a et transfectées avec des ARNcr. De plus, grâce à l'analyse des sites de clivage des crRNA, nous avons pu identifier précisément les positions de clivage induites par le système.

Dans l'échantillon provenant des cellules traitées avec la nucléase Su9-AsCas12a, les crRNA et les siRNA contre MGME1, les extrémités de clivage ont été cartographiées précisément aux positions attendues des nucléotides pour le crRNA-45 et le crRNA-34, confirmant ainsi la délétion anticipée. Cependant, une analyse plus approfondie des séquances adjacentes de a

délétion a révélé une duplication des surplombs collants formés par AsCas12a dans 20 % des cas. Dans la majorité des lectures (80 %), nous avons observé qu'il manquait deux nucléotides.

On ne sait pas encore quels mécanismes moléculaires peuvent être impliqués dans ces réarrangements. Nous pouvons émettre l'hypothèse du rôle de l'activité exonucléase 3'-5' de PolG ou de la réparation des cassures double brin par un mécanisme de jonction des extrémités médié par la micro-homologie, connu de provoquer des délétions de nucléotides (**Fontana G. A., Gahlon H. L., 2020**). En ce qui concerne la duplication observée, elle pourrait éventuellement se produire par remplissage des extrémités adhésives par l'ADN polymérase puis par ligation les extrémités franches. Une analyse plus approfondie des répliques biologiques de cette expérience nous permettra de comprendre le sort de l'ADNmt après le clivage CRISPR/Cas12a. Certes, un contrôle essentiel, y compris l'utilisation de l'AsCas12a sans l'activité DNase, devrait être inclus pour garantir la fiabilité de nos résultats.

Nous supposons également que l'approche PCR que nous avons initialement sélectionnée pour détecter les délétions de l'ADNmt, qui impliquait un temps d'élongation minimisé, n'était peut-être pas optimale car elle entraînait une amplification de délétions préexistantes dans l'ADNmt qui s'étaient produites spontannément. Pour résoudre ce problème, nous prévoyons d'effectuer un NGS sans PCR de l'ensemble de l'ADNmt. Cette approche éliminera non seulement le problème de l'amplification des délétions naturelles, mais nous permettra également de quantifier avec précision les molécules d'ADNmt portant les délétions induites par le mito-AsCas12a. De plus, nous envisageons d'utiliser la qPCR avec des amorces spécifiques à l'ADNmt soit à l'intérieur de la région de délétion, soit à côté de celle-ci, comme autre approche pour estimer l'efficacité de la formation de délétions.

Au cours de l'analyse de l'ADNmt humain, nous avons identifié 30 paires d'ARNcr capables de générer des extrémités collantes compatibles, quatre situées sur le brin lourd de l'ADNmt et 26 sur le brin léger. Ces ARNcr seront utilisés pour induire diverses délétions. En outre, il serait particulièrement intéressant d'étudier si une délétion de l'ADNmt peut être induite par AsCas12a en complexe avec des ARNcr qui ne produisent pas d'extrémités cohésives ou par la nucléase SpCas9 qui introduit des extrémités d'ADN franches double brin.

Le système CRISPR-Cas12a de type V a montré son potentiel en tant qu'outil pour créer des délétions dans l'ADNmt. Cette capacité ouvre des opportunités pour générer des lignées cellulaires ou même des modèles animaux portant des délétions induites dans l'ADNmt, ce qui peut permettre d'étudier leur dynamique et leur effet physiologique.

2. CONCLUSIONS

- Il a été prouvé que le Su9 MTS fournit la meilleure localisation mitochondriale pour la nucléase AsCas12a;

- En utilisant le système recombinant Flp-In, nous avons créé une lignée cellulaire stable exprimant Su9-AsCas12a de manière inductible par la tétracycline, qui s'est révélée être active et parfaitement localisée dans les mitochondries;

- Nous avons démontré que l'importation mitochondriale d'ARNcr ne nécessite pas de MLS supplémentaire, tandis que l'importation des ARNcr ciblants différentes régions de l'ADNmt humain varie en fonction de leur structure secondaire;

- L'ARNcr partitionné (*split*) a dirigé un clivage hautement spécifique et efficace de l'ADN cible, et au moins une partie espaceur de l'ARNcr split s'est avérée importée dans les mitochondries;

- Le séquençage de nouvelle génération de l'ADNmt a démontré une augmentation des cassures de l'ADNmt dans les cellules, exprimant le système mitoAsCas12a-crRNA;

- Dans les cellules exprimant mitoAsCas12a et transfectées avec des ARNcr, nous avons détecté, par LM-PCR couplé avec Southern blot et NGS, un clivage spécifique de l'ADNmt;

- Pour la première fois, nous avons démontré, en utilisant le séquençage Sanger et le NGS des amplicons de l'ADNmt, la présence d'une délétion dans l'ADNmt humain induite par un système CRISPR.

3. PERSPECTIVES

- Évaluer l'efficacité de la formation de délétions d'ADNmt induite par le système mitoCRISPR en utilisant qPCR et NGS;

- Analyser les effets hors cible de mitoCRISPR-AsCas12a sur l'ADN mitochondrial et nucléaire à l'aide du séquençage complet de l'ADNmt;

- Améliorer l'efficacité du clivage de l'ADNmt du système mitoCRISPR par : 1) Optimisation de l'importation mitochondriale des ARNcr en introduisant des modifications chimiques et en utilisant des molécules d'ARNc fractionnées ; 2) Utiliser des versions modifiées de nucléases Cas12a avec une activité et une spécificité de clivage accrues;

- Appliquer des stratégies d'induction de délétions d'ADNmt pour générer des modèles cellulaires et animales afin d'étudier la distribution des délétions, leurs effets pathogènes et les approches thérapeutiques possibles;

- Appliquer le système mitoCRISPR-AsCas12a pour modifier le niveau d'hétéroplasmie dans les cellules humaines portant des mutations pathogènes dans l'ADNmt.

LA LISTE D'ARTICLES:

1) "Future of human mitochondrial DNA editing technologies", Verechshagina, N., **Nikitchina, N.**, Yamada, Y., Harashima, H., Tanaka, M., Orishchenko, K., &

Mazunin, I. (2019). Mitochondrial DNA Part A, 30(2), 214-221. **DOI:** 10.1080/24701394.2018.1472773 **(Publié)**

2) "Efficient target cleavage by Type V Cas12a effectors programmed with split CRISPR RNA", Shebanova, R. & **Nikitchina, N.**, Shebanov, N., Mekler, V., Kuznedelov, K., Ulashchik, E., Vasilev, R., Sharko, O., Shmanai, V., Tarassov, I., Severinov, K., Entelis, N., Mazunin, I. (2022). Nucleic acids research, 50(2), 1162-1173. **DOI:** 10.1093/nar/gkab1227 **(Publié)**

3) "Targeted Modification of Mammalian DNA by a Novel Type V Cas12a Endonuclease from *Ruminococcus bromii*", Vasilev, R., Gunitseva, N., Shebanova, R., Korzhenkov, A., Vlaskina, A., Evteeva, M., Polushkina, I., **Nikitchina, N.**, Toschakov, S., Kamenski, P., Patrushev, M., Mazunin, I. (2022). International Journal of Molecular Sciences, 23(16), 9289. **DOI:** 10.3390/ijms23169289 **(Publié)**

4) "Targeting of CRISPR-Cas12a crRNAs into human mitochondria", **Nikitchina, N.**, Ulashchik, E., Shmanai, V., Heckel, A. M., Tarassov, I., Mazunin, I., Entelis, N. (2023). Biochimie **DOI:** 10.1016/j.biochi.2023.09.006 **(Publié)**

5) "Use of the type V CRISPR-Cas system to induce a deletion in human mitochondrial DNA", **Nikitchina, N.**, Heckel, A. M., Smirnova, A., Shebanov, N., Ulashchik, E., Shmanai, V., Tarassov, I., Mazunin, I., Entelis, N. **(En cour)**

LA LISTE DES COMMUNICATIONS:

1) *The 11th World Congress on Targeting Mitochondria 2020*, 28 – 30 October 2020, online conference: «Use Of The Type 2 Crispr-Cas System For Human

Mitochondrial Genome Editing», **Natalia Nikitchina**, Ilya Mazunin, Nina Entelis, Ivan Tarassov **(Orale)**

2) *"The Doctoral School Days 2021" (ED Days 2021)*, organized by the University of Strasbourg, 1 – 2 April 2021, Strasbourg, France: «Efficient target cleavage by Type V Cas12a effector programmed with split CRISPR RNA», **Natalia Nikitchina**, Nina Entelis, Konstantin Severinov, Ilya Mazunin **(Par affiche)**

3) *CRISPR and Translational Medicine Congress*, organized by the University of Bordeaux, March 31 – 1 April 1 2022, Bordeaux, France: «Efficient target cleavage by Type V Cas12a effector programmed with split CRISPR RNA», **Natalia Nikitchina**, Regina Shebanova, Nikita Shebanov, Ivan Tarassov, Konstantin Severinov, Nina Entelis, Ilya Mazunin **(Orale)**

CRISPR CONFERENCE 2023, June 27 – July 1 2023, Würzburg, Germany: «Use of the type V CRISPR-Cas system to induce a deletion in human mitochondrial DNA», **Natalia Nikitchina**, Anne-Marie Heckel, Ilya Mazunin, Ivan Tarassov, Nina Entelis **(Par affiche)**

Natalia NIKITCHINA

Mise au point d'un système CRISPR-Cas12a ciblant l'ADN mitochondrial humain

Résumé

Les maladies neuromusculaires chez l'homme sont souvent causées par des mutations de l'ADNmt. La gravité de ces maladies dépend du niveau d'hétéroplasmie, où l'ADNmt mutant et sauvage coexistent dans la même cellule. Le développement d'approches expérimentales permettant la manipulation de l'ADNmt est crucial pour mettre au point des nouvelles thérapies. Ici, nous avons adapté le système CRISPR-AsCas12a de type V, qui reconnaît les séquences PAM riches en AT, pour une importation efficace dans les mitochondries humaines. La nucléase AsCas12a, portant le MTS de la sous-unité ATPase 9 de *Neurospora crassa*, exprimée dans une lignée cellulaire stable, a montré une localisation mitochondriale. Nous avons démontré que l'importation d'ARNcr ne nécessite pas de signaux de localisation mitochondriaux supplémentaires, mais dépend de sa structure secondaire. L'ARNcr peut être divisé en parties d'échafaudage et d'espacement, préservant ainsi la fonctionnalité du système, et l'espaceur peut être importé dans les mitochondries. Pour la première fois, en utilisant à la fois le séquençage Sanger et le séquençage de nouvelle génération, nous avons démontré qu'une délétion dans l'ADNmt humain peut être induite par un système CRISPR/Cas mitochondrial.

Mitochondries humaines, ADN mitochondrial, mutations, MitoCRISPR, Cas12a, importation mitochondriale

Summary

Neuromuscular diseases in humans often stem from mutations in mtDNA. The severity of these diseases depends on the level of heteroplasmy, where both mutant and wild-type mtDNA coexist in the same cell. Developing methods to model mtDNA dysfunction is crucial for experimental therapies. Here, we adapted Type V CRISPR-AsCas12a, which recognizes AT-rich PAM sequences, for efficient import into human mitochondria. The AsCas12a nuclease, bearing MTS from *Neurospora crassa* ATPase subunit 9, expressed in a stable cell line, showed mitochondrial localization. We demonstrated that crRNA import doesn't require additional mitochondrial localization signals, but depends on its secondary structure. We successfully split crRNA into scaffold and spacer parts, preserving functionality, with the spacer capable of being imported into mitochondria. For the first time, using both Sanger and next-generation sequencing, we demonstrated that a deletion in human mtDNA can be induced by a CRISPR/Cas system targeted to mitochondria.

Human mitochondria, mitochondrial DNA, mutations, MitoCRISPR, Cas12a, targeting mitochondria